



UNIVERSITY OF
LIVERPOOL

School of architecture

**Outdoor thermal comfort and airflow in relation to urban form
in Amman, Jordan: A residential setting analysis**

Yara Ayyad

BSc, MSc

A Thesis Submitted in Accordance with the Requirements of
The University of Liverpool for the Degree of
Doctor in Philosophy (PhD)

University of Liverpool

Liverpool, UK

August 2020

Title Page

Thesis Title: Outdoor thermal comfort and airflow in relation to urban form in Amman, Jordan: A residential setting analysis

Full name: Yara Nehrow Ibrahim Ayyad

Qualification: Doctor of Philosophy

School: School of Architecture

Supervisor: Prof. Stephen Sharples

Submission Date: August 2020

Contact: Yara_nehrow@hotmail.com

Declaration

I certify that this thesis constitutes my own work/investigation, except where otherwise stated; other sources are acknowledged by explicit references.

I declare that this thesis describes original work that has not previously been presented for the award of any other degree of any institution.

Signed: Yara Nehrow Ibrahim Ayyad

Date: August 2020

ABSTRACT

Rapid urbanisation and economic growth have put a significant pressure on urban planners to create layouts and buildings' forms that are sustainable, healthy, and thermally comfortable for urban occupants. In the context of semi-arid climate, the built environment is often afflicted with high pedestrian comfort levels due to the increase in phenomena such as urban heat islands (UHI).

The main aim of this research is to identify the key elements for enhancing the outdoor thermal comfort and airflow for pedestrians in a residential setting in the semi-arid climate of Amman in Jordan, through studying the urban geometrical parameters and their effects on the urban microclimate. The study followed an optimisation process that allowed a different variation of the designed proposals to be tested and simulated in terms of airflow and thermal comfort. The process analysed the urban elements on three different levels, the mesoscale (street grid layout), the microscale (compound layout) and the urban canyon scale.

ENVI-met is a computational fluid dynamics (CFD) model that assesses the effect of meteorological parameters (e.g., air temperature, wind speed and relative humidity) on the built environment, in which it is used to simulate and evaluate proposed scenarios to find out the best configuration in terms of thermal comfort and airflow. A validation study was performed on ENVI-met using Amman configurations to test the model's sensitivity and accuracy in predicting the microclimatic parameters change in the urban environment.

The research proposed five different common street layouts to test out the geometrical aspect of the street grid. The results showed that wind speed values were found to change greatly for different orientations. However, Physiological Equivalent Temperature (PET) levels were more sensitive to the different grid geometries rather than their orientation. The research also proposed two grid designs for an empty plot in Amman based on the findings of the street grid analysis which comprised of a layout with streets oriented in the wind direction and an adjusted version of the wind flow proposal with perpendicular intersections for better land distribution. The results showed that the adjusted layout produced better PET values due to better shading geometry.

Wind direction analysis showed that PET levels across the plot increased when the approaching wind angle was parallel to the streets and showed a significant decrease when directed at 45°. Compound design proposals showed that compound 1's design with the wind flow transition produced higher PET levels when compared to strips of buildings design that allowed for better ventilation and controlled shading.

The urban canyon scale analysis showed that increasing the buildings height enhanced the PET and airflow, while orienting the design in the (West-East) direction showed lower PET values when compared to the (North-South) orientation. The vegetation analysis showed airflow is enhanced with lower Leaf Area Density (LAD) values, due to less resistance from trees' foliage.

RELATED ACADEMIC PUBLICATIONS

- Ayyad, Y., & Sharples, S. (2017). Outdoor thermal comfort in a hot urban climate: Analysing the impact of creating wind passageways in Al-Moski, Egypt using ENVI-met. In Proceedings of 33rd PLEA International Conference: Design to Thrive, PLEA 2017 Vol. 1 (pp. 997-1004).
- Ayyad, Y. N., & Sharples, S. (n.d.). Envi-MET validation and sensitivity analysis using field measurements in a hot arid climate. In IOP Conference Series: Earth and Environmental Science Vol. 329 (pp. 012040). IOP Publishing. doi:10.1088/1755-1315/329/1/012040.

ACKNOWLEDGEMENTS

I would like to express my deepest gratitude to my supervisor Professor Steve Sharples, who has given me a continuous support throughout my study, by providing me with countless constructive feed-back and materials to build my thesis, and without his guidance and support reaching this point would never have been possible. I would like to thank all of my friends, especially Omar Arram, for giving me support in my most stressful times and helping me in staying focused and sharp.

Finally, I have no way to express my gratitude to my family, especially my sister Yusra Ayyad who was there for me since day one, supporting and encouraging me. I would like to dedicate this thesis to my mother Ihsan Rimawi, her support, warmth, strength, and unconditional love have carried me throughout the last 29 years, Thank you mom.

To Ihsan M. Rimawi

TABLE OF CONTENTS

ABSTRACT	III
RELATED ACADEMIC PUBLICATIONS	IV
ACKNOWLEDGEMENTS	V
TABLE OF CONTENTS	VI
LIST OF TABLES	XI
LIST OF FIGURES	XIII
CHAPTER 1 : INTRODUCTION	1
1.1 AMMAN, JORDAN AS A CASE STUDY	3
1.1.1 URBAN CONTEXT	3
1.2 CLIMATE OF AMMAN	6
1.3 OUTDOOR THERMAL COMFORT AND AIRFLOW IN AN URBAN SETTING	9
1.4 AIMS AND OBJECTIVES	11
1.5 RESEARCH APPROACH	12
1.5.1 CONTEXT OF THE RESEARCH	12
1.6 RESEARCH QUESTIONS	14
1.6.1 MAIN RESEARCH QUESTION	14
1.6.2 SUBSIDIARY RESEARCH QUESTIONS	15
1.7 RELEVANCE OF THE RESEARCH	15
1.8 STRUCTURE OF THE THESIS	16
CHAPTER 2 : LITERATURE REVIEW OF OUTDOOR THERMAL COMFORT	18
2.1 INTRODUCTION	19
2.2. BACKGROUND	19
2.3 THERMAL COMFORT IN CONTEXT OF INDOOR AND OUTDOOR ENVIRONMENTS	21
2.4 INDICES FOR ASSESSING THE OUTDOOR THERMAL STRESS- THE PREDICTIVE MODELS	23
2.5 THE PHYSIOLOGICALLY EQUIVALENT TEMPERATURE MICROCLIMATIC FACTORS	28
2.5.1 Air Temperature	28
2.5.2 Mean Radiant Temperature	30
2.5.3 Wind Speed	31
2.5.4 Relative Humidity	34
2.6 VEGETATION	35
2.6.1 Vegetation effects on solar radiation and thermal comfort	36
2.6.2 Vegetation effects on air temperature	37
2.6.3 Vegetation effects on wind flow	37
2.6.4 Vegetation effects on air humidity	37
2.7 PREVIOUS STUDIES ON OUTDOOR THERMAL COMFORT	38

2.8	SUMMARY	44
CHAPTER 3 : LITERATURE REVIEW ON THE AIRFLOW INSIDE AN URBAN SETTING.....		45
3.1	INTRODUCTION	46
3.2	THE URBAN SURFACE	46
3.3	AIRFLOW.....	48
3.3.1	STANDALONE BUILDINGS (ISOLATED).....	48
3.3.2	ARRAYED BUILDINGS WITH UNIFORM HEIGHTS.....	50
3.3.3	STREET CANYON AND INTERSECTIONS	52
3.4	URBAN CANYONS CONFIGURATIONS TO REDUCE THERMAL STRESS.	55
3.5.	THE RELATIONSHIP BETWEEN AIRFLOW AND TEMPERATURE.....	62
3.6	PREVIOUS STUDIES ON THE URBAN MICROCLIMATE USING NUMERICAL AND COMPUTATIONAL (CFD) METHODS.....	65
3.7	SUMMARY	69
CHAPTER 4 : METHODOLOGY		70
4.1	INTRODUCTION	71
4.2	RESEARCH WORK PROCESS	71
4.3	ENVI-MET VALIDATION METHODOLOGY	73
4.3.1.	SENSITIVITY TESTING	73
4.3.2	WIND SPEED SENSITIVITY TESTING.....	75
4.3.3	RELATIVE HUMIDITY SENSITIVITY TESTING.....	77
4.3.4	ALBEDO SENSITIVITY TESTING	79
4.3.5	GRID RESOLUTION SENSITIVITY TESTING.....	79
4.4	VALIDATION OF ENVI-MET MODEL.....	80
4.4.1	SITE SELECTION AND DATA COLLECTION.....	80
4.4.2	ENVI-MET MODELLING OF THE AL AHLIYYA AMMAN UNIVERSITY SITE.....	83
4.5	STREET GRID.	89
4.5.1	PET SUMMER RANGE.....	93
4.6	AMMAN, JORDAN CASE STUDY.	94
4.6.1	STREET GRID'S ANALYSIS.	94
4.6.2	SUMMER AND WINTER ANALYSES.....	95
4.6.3	ENVI-MET CONFIGURATION FILE.	96
4.6.4	WIND DIRECTION RELATION TO THE PET VALUES, ANALYSIS FOR LAYOUT-2 PROPOSAL.	99
4.6.5	BUILDINGS' CLUSTER ANALYSIS.	100
4.6.6	ENVI-MET CONFIGURATION FILE.	103
4.6.7	COMPOUND 2 SHADING ADDITION AND THEIR EFFECT ON PET.	104
4.6.8	BUILDINGS CLUSTER MICRO ANALYSIS.	105
4.6.9	GEOMETRICAL MODIFICATION; DESIGNING THE BUILDINGS PATHWAYS.....	106

4.6.10	BUILDINGS' HEIGHT MODIFICATION EFFECTS ON PET.....	106
4.6.11	TREE LEAF AREA DENSITY (LAD) AND ITS EFFECT ON PET AND WIND FLOW.....	108
4.6.12	SITE ORIENTATION AND ITS EFFECT ON PET AND WIND FLOW.....	109
4.7	THE CALCULATION OF THE PHYSIOLOGICAL EQUIVALENT TEMPERATURE INDEX USING RAYMAN.	109
4.8	SUMMARY.....	111
CHAPTER 5 : ENVI-MET MODEL VALIDATION		5-112
SECTION ONE: ENVI-MET: MODEL OVERVIEW.....		113
5.1	INTRODUCTION	114
5.2	SPACES: GRID LAYOUT	114
5.3	THE ATMOSPHERIC MODEL	116
5.3.1	WIND FIELD.....	116
5.3.2	TEMPERATURE (T_a) AND HUMIDITY.....	117
5.3.3	ATMOSPHERIC TURBULENCE	118
5.3.4	THE RADIATIVE FLUXES.....	119
5.4	THE SOIL MODEL.....	122
5.5	THE VEGETATION MODEL.....	123
5.6	SURFACES: GROUND AND BUILDINGS	124
5.7	NUMERICAL METHODS.....	126
5.8	SUMMARY	127
SECTION TWO: ENVI-MET VALIDATION		129
5.8	INTRODUCTION	130
5.9	PREVIOUS ENVI-MET VALIDATION STUDIES.	130
5.9.1	ELNABAWI, HAMZA AND DUDEK, 2014.....	130
5.9.2	SALATAA, GOLASIA, R. DE LIETO VOLLARO AND A. DE LIETO VOLLARO, 2016	133
5.10	ENVI-MET MODEL SENSITIVITY TESTING.....	135
5.10.1	SUMMARY.....	135
5.10.2	WIND SPEED SENSITIVITY.....	136
5.10.3	RELATIVE HUMIDITY SENSITIVITY.....	137
5.10.4	ALBEDO SENSITIVITY	137
5.10.5	GRID SIZE.....	138
5.10.6	CONCLUSION	139
5.11	CALIBRATION TESTING.....	140
5.11.1	SITE AND MODEL PARAMETERS.....	140
5.11.2	THE LOGGERS' READINGS FOR LOCATION A AND B.	142
5.11.3	SITE MODELLING IN ENVI-MET.....	143
5.11.4	MODEL VALIDATION TEST OF THE OBSERVED DATA AND THE PREDICTED DATA.	143
5.11.5	COMPARISON OF THE SIMULATED DATA VS THE OBSERVED DATA.	144

5.11.6 CONCLUSIONS	150
CHAPTER 6 RESULTS AND DISCUSSION	151
SECTION ONE: STREET GRID	153
6.1 STREET GRID (SUMMARY)	154
6.2 STREET GRID LAYOUT A	154
6.2.1 SCENARIO A.1.....	154
6.2.2 SCENARIO A.2.....	156
6.2.3 COMPARISON BETWEEN GRID A'S DIFFERENT ORIENTATION SCENARIOS.....	158
6.3 STREET GRID LAYOUT B.....	159
6.3.1 SCENARIO B.1.....	159
6.3.2 SCENARIO B.2.....	161
6.3.3 COMPARISON BETWEEN GRID B'S DIFFERENT ORIENTATION SCENARIOS.....	163
6.4 STREET GRID LAYOUT C.....	164
6.4.1 SCENARIO C.1.....	164
6.4.2 SCENARIO C.2.....	166
6.4.3 COMPARISON BETWEEN GRID C'S DIFFERENT ORIENTATION SCENARIOS.....	167
6.5 STREET GRID LAYOUT D.....	170
6.5.1 SCENARIO D.1.....	170
6.5.2 SCENARIO D.2.....	171
6.5.3 COMPARISON BETWEEN GRID D'S DIFFERENT ORIENTATION SCENARIOS.....	173
6.6 STREET GRID LAYOUT E.....	177
6.6.1 SCENARIO E.1.....	177
6.6.2 SCENARIO E.2.....	179
6.6.3 COMPARISON BETWEEN GRID E'S DIFFERENT ORIENTATION SCENARIOS.....	181
6.7 CONCLUSION.....	185
SECTION TWO: AMMAN CASE STUDY	187
6.8 AMMAN, JORDAN CASE STUDY.....	188
6.9 METHODOLOGY (SUMMARY).....	188
6.10 RESIDENTIAL LAYOUTS - STREET GRID (SUMMARY).....	190
6.10.1 PHYSIOLOGICAL EQUIVALENT TEMPERATURE ANALYSIS.....	190
6.10.2 SUMMER ANALYSIS.....	191
6.10.3 WINTER ANALYSIS.....	195
6.10.4 WIND DIRECTION RELATION TO PET VALUES, ANALYSIS FOR LAYOUT-2 (SUMMARY).....	200
6.10.5 PHYSIOLOGICAL EQUIVALENT TEMPERATURE (SUMMARY).....	201
6.11 CONCLUSIONS.....	203
SECTION THREE: BUILDINGS CLUSTER ANALYSIS.....	206
6.12 BUILDINGS CLUSTER ANALYSIS.....	207

6.12.1	<i>METHODOLOGY BRIEF</i>	207
6.12.2	<i>RESULTS</i>	208
6.13	COMPOUND 2 SHADING ADDITIONS AND THEIR EFFECT ON PET	214
6.14	BUILDINGS CLUSTER MICRO ANALYSIS.....	218
6.14.1	<i>GEOMETRICAL MODIFICATION; DESIGNING THE BUILDINGS PATHWAYS.</i>	218
6.15	BUILDINGS' HEIGHT MODIFICATION EFFECTS ON PET.....	221
6.16	TREE LEAF AREA DENSITY (LAD) AND ITS EFFECT ON PET AND WIND FLOW.....	224
6.17	SITE ORIENTATION AND ITS EFFECT ON PET AND WIND FLOW.	227
6.18	CONCLUSION	232
CHAPTER 7 CONCLUSION AND RECOMMENDATIONS		235
7.1	INTRODUCTION	236
7.2	MAIN CONCLUSIONS	236
7.3	RESEARCH IMPLICATIONS FOR FUTURE WORK AND GENERAL RECOMMENDATIONS.....	252
REFERENCES.....		254
APPENDICES.....		291

LIST OF TABLES

Table 2.1. Outdoor thermal comfort indices. Modified from Monteiro and Alucci (2006) - 1920s to 1970s.....	23
Table 2.2. Outdoor thermal comfort indices. Modified from Monteiro and Alucci (2006) – 1980s to 2000s.....	24
Table 2.3. PET thermal scale (Matzarakis, et al., 1999).....	26
Table 2.4. PET scale for different climates (Lin & Matzarakis, 2008; Pantavou, et al., 2014; Matzarakis, et al., 1999).....	27
Table 2.5. Wind effects. source Penwarden, 1973.....	33
Table 2.6. Wind comfort and danger criteria. Source Willemsen and Wisse (2007).	34
Table 2.7. Air relative humidity for Beijing from 1971-2003. Source Lui, et al (2009).....	35
Table 2.8. Previous studies on outdoor thermal comfort.	38
Table 2.9. Air temperature values for the University of Jordan. Source (Al-Azhari, et al., 2014).	41
Table 2.10. Base model and the parameters of the suggested scenario. Source (Al-Kurdi & Awadallah, 2015).	42
Table 3.1. Classification of urban morphological units based on a 1-million inhabitant. Source (Oke, et al., 2017).....	46
Table 3.2. Previous studies on the urban canyons.	58
Table 3.3. The UHI intensity in °C for all the studied urban canyons with eight wind directions. Source (Sen & Roesler, 2019).	64
Table 3.4. Past studies on Urban Microclimate using a CFD tool. Modified from (Toparlar, et al., 2017).	66
Table 4.1. Walls material's Albedo configuration for the model runs.....	79
Table 4.2. Pavement material's Albedo configuration for the model runs.	79
Table 4.3. The grid resolution configuration for the three model runs.	80
Table 4.4. Sensors Specifications for Kestrel 5400 Heat Stress tracker.	83
Table 4.5. S factor $S = V_H / V_{10}$	84
Table 4.6. Air temperature and relative humidity values for the 1st of October.....	85
Table 4.7. The PET index comfort levels.	96
Table 5.1. Grid sensitivity.....	134

Table 5.2. Model evaluation tests.	135
Table 5.3. Sensitivity test model parameters.	136
Table 5.4. Model validation for location A.	144
Table 5.5. Model validation for location B.....	144
Table 5.6. Average Model validation values for locations A and B.	150
Table 6.1. Area percentage of the areas that are receiving less than 0.5m/s of wind speed at 1.5m height.	186
Table 6.2. Averaged PET values for all layouts.	186
Table 6.3. Parameters used in the modelling phase.	191
Table 6.4. Layout-1 results for PET ranges (slightly warm, comfortable, and slightly cool).	205
Table 6.5. Layout-2 results for PET ranges (slightly warm, comfortable, and slightly cool).	205
<i>Table 6.6. Receptors detailed data analysis for compound 1.</i>	<i>209</i>
<i>Table 6.7. Receptors detailed data analysis for compound 2.</i>	<i>212</i>
Table 7.1. Area percentage of the areas that are receiving less than 0.5m/s of wind speed at 1.5m height.	242
Table 7.2. Averaged PET values for all layouts.	243
Table 7.3. Recommendations for layouts A, B, C, D and E.	244
Table A6. 1. Detailed microclimatic data for street grid layout C.1.	292
Table A6. 2. Detailed microclimatic data for street grid layout C.2.	295
Table A6. 3. Detailed microclimatic data for street grid layout D.1.	299
Table A6. 4. Detailed microclimatic data for street grid layout D.2.	305
Table A6. 5. Detailed microclimatic data for layout 1 summer analysis.	310
Table A6. 6. Detailed microclimatic data for layout 1 winter analysis.	313
Table A6. 7. Detailed microclimatic data for 0.5 LAD scenario.	335
Table A6. 8. Detailed microclimatic data for 1.0 LAD scenario.	340
Table A6. 9. Detailed microclimatic data for 1.5 LAD scenario.	345

LIST OF FIGURES

Figure 1.1. A view of the downtown area in Amman. Source, Photographer: Rachel Lewis...	3
Figure 1.2 Amman's increasing growth. Source: Greater Amman Comprehensive Development Plan, executive summary.	4
Figure 1.3 Amman's residential lands categories. Courtesy of GAM adapted from Potter, et al (2009).....	5
Figure 1.4 Amman's expansion plans. Source (Potter, et al., 2009).....	6
Figure 1.5 Amman's rainfall through the year of 2015. Source Department of Statistics, Jordan.	7
Figure 1.6 Air temperature values for Amman. Source Meteonorm.	8
Figure 1.7 Relative humidity values for Amman. Source Meteonorm.	8
Figure 1.8. Wind speed values for Amman. Source Meteonorm.	9
Figure 1.9 Research work process.	13
Figure 1.10 The Jordan Gate Towers project. Source: Abu-Hamid, 2017.	16
Figure 2.1. Comfortable air temperature in relation to wind speed. Modified from Huang, 2007.	29
Figure 2.2. Comfortable air temperature in relation to time spent outdoors. Modified from Huang, 2007.....	29
Figure 2.2.3. Comfort conditions, unshaded (Left), shaded (Right). Source Penwarden, 1973.	32
Figure 2.4. The air temperature for the summer conditions for all of the scenarios. Source (Al-Kurdi & Awadallah, 2015).	43
Figure 2.5. The air temperature for the winter conditions for all of the scenarios. Source (Al-Kurdi & Awadallah, 2015).	43
Figure 3.1. Urban cover parameters. Source (Oke, et al., 2017).	47
Figure 3.2. The airflow behaviour around a cubic building. A is the approaching wind flow, B is the displacement zone, C is the cavity zone and D is the wake zone. Above, approaching wind direct at the face of the building. Below, approaching wind directed 45° at the edge of the building. Source (Oke, et al., 2017).	49
Figure 3.3 Airflow characteristics. Source (Oke, et al., 2017).....	49

Figure 3.4. Wind flow behaviour on different H/W in an urban environment. Source (Oke, et al., 2017). (Modified after: (Oke, 1988; Hussain & Lee, 1980)).....	51
Figure 3.5. Airflow interactions inside an urban canyon. Source (Oke, et al., 2017). (Modified after: (Oke, 1997; Belcher, 2005)).	52
Figure 3.6. Airflow behaviour with street intersections. Source (Oke, et al., 2017). (Modified after: (Soulhac, et al., 2009)).	55
Figure 3.7. The studied cases. Source (Ali-Toudert & Mayer, 2007).....	57
Figure 3.8. The hypothetical urban area studied. Source (Sen & Roesler, 2020).....	63
Figure 4.1. Validating ENVI-met process.	72
Figure 4.2. Urban elements testing process.	72
Figure 4.3. sensitivity testing base model configurations.	73
Figure 4.4. Rendering of the site showing the monitored locations.	81
Figure 4.5. Kestrel 5400 heat stress tracker.	82
Figure 4.6. Pearson's correlation values diagram.....	87
Figure 4.7. RMSError diagram.....	88
Figure 4.8. Street grid layouts.....	90
Figure 4.9. The modified PET range for different climate zones in summer, source (Elnabawi, et al., 2016; Kruger, et al., 2012; Lin & Matzarakis, 2008; Sharmin, et al., 2019; Höppe, 1999).	93
Figure 4.10. Satellite image of the site chosen in the south of Amman.....	94
Figure 4.11. Main plot street grid layouts: proposal 1 (left) proposal 2 (right).	95
Figure 4.12. Wind direction histogram. Source: Meteonorm.	100
Figure 4.13. Location of the proposed compounds.....	101
Figure 4.14. Compound 1 (top) and compound 2 (bottom) diagram design.	102
Figure 4.15. Proposal 2 with shading devices additions.....	104
Figure 4.16. The area investigated for the microanalysis with the section cuts.	105
Figure 4.17. Pedestrian pathway through the row buildings.	106
Figure 4.18. 12-metre high analysis.....	107
Figure 4.19. 18-metre high analysis (Right) 24-metre high analysis (Left).....	107
Figure 4.20. Interface of RayMan software.	110
Figure 5.1. ENVI-met's basic model layout.	115
Figure 5.2. ENVI-met's vertical grids.....	116

Figure 5.3. Davies Vantage VUE.....	131
Figure 5.4. Air temperature values for both observed and predicted.	131
Figure 5.5. Relative humidity values for both observed and predicted.	132
Figure 5.6. Mean radiant Temperature values for both observed and predicted.	132
Figure 5.7. St. Peter in chain location.	133
Figure 5.8. Instrumentation used in the study.	134
Figure 5.9. The model used in the sensitivity testing.	135
Figure 5.10. Wind speed sensitivity testing.	136
Figure 5.11. Relative humidity sensitivity testing.....	137
Figure 5.12. Albedo sensitivity testing.....	138
Figure 5.13 Grid size sensitivity testing.	139
Figure 5.14. The location of Amman Ahliyya University.....	140
Figure 5.15. Trees labels in the site.	141
Figure 5.16. Trees labels in site 2.....	141
Figure 5.17. The loggers' readings for air temperature.....	142
Figure 5.18. The loggers' readings for relative humidity.....	142
Figure 5.19. The loggers' readings for wind speed.....	143
Figure 5.20. Data comparison between the observed and the predicted air temperature values, location A.....	145
Figure 5.21. Data comparison between the observed and the predicted air temperature values, location B.....	146
Figure 5.22. Data comparison between the observed and the predicted for relative humidity, location A.....	147
Figure 5.23. Data comparison between the observed and the predicted for relative humidity, location B.....	148
Figure 5.24. Data comparison between the observed and the predicted for wind speed, location A.....	149
Figure 5.25. Data comparison between the observed and the predicted for wind speed, location B.....	149
Figure 6.1. Wind speeds in scenario A.1.....	155
Figure 6.2. Wind flow in Scenario A.1.....	156
Figure 6.3. Wind speed in scenario A.2.....	157

Figure 6.4. Wind flow in scenario A.2.	157
Figure 6.5. Wind speed distribution for scenario A.1.	158
Figure 6.6. Wind speed distribution for scenario A.2.	158
Figure 6.7. PET values for receptor 1 for scenarios A.1 and A.2.	159
Figure 6.8. PET values for receptor 2 for scenarios A.1 and A.2.	159
Figure 6.9. Wind speed in scenario B.1.	160
Figure 6.10. Wind flow in Scenario B.1.	161
Figure 6.11. Wind speed in scenario B.2.	162
Figure 6.12. Wind flow in Scenario B.2.	162
Figure 6.13. Wind speed distribution for scenario B.1.	163
Figure 6.14. Wind speed distribution for scenario B.2.	163
Figure 6.15. PET values for receptor 1 for scenarios B.1 and B.2.	163
Figure 6.16. PET values for receptor 2 for scenarios B.1 and B.2.	164
Figure 6.17. Wind speed in scenario C.1.	165
Figure 6.18. Wind flow in Scenario C.1.	165
Figure 6.19. Wind speed in scenario C.2.	166
Figure 6.20. Wind flow in Scenario C.2.	167
Figure 6.21. Wind speed distribution for scenario C.1.	167
Figure 6.22. Wind speed distribution for scenario C.2.	167
Figure 6.23. PET values for receptor 1 for scenarios C.1 and C.2.	168
Figure 6.24. PET values for receptor 2 for scenarios C.1 and C.2.	169
Figure 6.25. PET values for receptor 3 for scenarios C.1 and C.2.	169
Figure 6.26. PET values for receptor 4 for scenarios C.1 and C.2.	169
Figure 6.27. PET values for receptor 5 for scenarios C.1 and C.2.	170
Figure 6.28. Wind speed in scenario D.1.	170
Figure 6.29. Wind flow in Scenario D.1.	171
Figure 6.30. Wind speed in scenario D.2.	172
Figure 6.31. Wind flow in Scenario D.2.	173
Figure 6.32. Wind speed distribution for scenario D.1.	173
Figure 6.33. Wind speed distribution for scenario D.2.	173
Figure 6.34. PET values for receptor 1 for scenarios D.1 and D.2.	174
Figure 6.35. PET values for receptor 2 for scenarios D.1 and D.2.	175

Figure 6.36. PET values for receptor 3 for scenarios D.1 and D.2.	175
Figure 6.37. PET values for receptor 4 for scenarios D.1 and D.2.	175
Figure 6.38. PET values for receptor 5 for scenarios D.1 and D.2.	175
Figure 6.39. PET values for receptor 6 for scenarios D.1 and D.2.	176
Figure 6.40. PET values for receptor 7 for scenarios D.1 and D.2.	176
Figure 6.41. PET values for receptor 8 for scenarios D.1 and D.2.	176
Figure 6.42. Ladd's Addition, courtesy of National Register Historic District.....	177
Figure 6.43. Wind speed in scenario E.1.....	178
Figure 6.44. Wind flow in Scenario E.1.	178
Figure 6.45. Wind speed in scenario E.2.....	179
Figure 6.46. Wind flow in Scenario E.2.	180
Figure 6.47. Wind speed distribution for scenario E.1.	181
Figure 6.48. Wind speed distribution for scenario E.2.	
Figure 6.49. PET values for receptor 1 for scenarios E.1 and E.2.	182
Figure 6.50. PET values for receptor 2 for scenarios E.1 and E.2.	183
Figure 6.51. PET values for receptor 3 for scenarios E.1 and E.2.	183
Figure 6.52. PET values for receptor 4 for scenarios E.1 and E.2.	183
Figure 6.53. PET values for receptor 5 for scenarios E.1 and E.2.	184
Figure 6.54. PET values for receptor 6 for scenarios E.1 and E.2.	184
Figure 6.55. PET values for receptor 7 for scenarios E.1 and E.2.	184
Figure 6.56. PET values for receptor 8 for scenarios E.1 and E.2.	185
Figure 6.57. Aerial view of the site.	188
Figure 6.58. Boundaries of the site... ..	
Figure 6.59. Layout-1 (left) and layout-2 (right).	189
Figure 6.60. PET values for receptor 1 under summer conditions on the 23 rd of June.....	192
Figure 6.61. Direct solar radiation for receptor 1 under summer conditions on the 23 rd of June.	192
.....	
Figure 6.62. PET values for receptor 2 under summer conditions on the 23 rd of June.....	193
Figure 6.63. Direct solar radiation for receptor 2 under summer conditions on the 23 rd of June.	193
.....	
Figure 6.64. PET values for receptor 3 under summer conditions on the 23 rd of June.....	194
Figure 6.65. Direct solar radiation for receptor 3 under summer conditions on the 23 rd of June.	194
.....	

Figure 6.66. PET values for receptor 4 under summer conditions on the 23 rd of June.....	195
Figure 6.67. Direct solar radiation for receptor 4 under summer conditions on the 23 rd of June.	195
Figure 6.68. PET values for receptor 1 under winter conditions on the 22 nd of December...	196
Figure 6.69. Direct solar radiation for receptor 1 under winter conditions on the 22 nd of December.....	197
Figure 6.70. PET values for receptor 2 under winter conditions on the 22 nd of December...	198
Figure 6.71. Direct solar radiation for receptor 2 under winter conditions on the 22 nd of December.....	198
Figure 6.72. PET values for receptor 3 under winter conditions on the 22 nd of December...	199
Figure 6.73. Direct solar radiation for receptor 3 under winter conditions on the 22 nd of December.....	199
Figure 6.74. PET values for receptor 4 under winter conditions on the 22 nd of December...	200
Figure 6.75. Direct solar radiation for receptor 4 under winter conditions on the 22 nd of December.....	200
Figure 6.76. Amman's all year wind rose. Source: Meteonorm.	201
Figure 6.77. Different wind direction PET values.	202
Figure 6.78. Summer simulation on the 23 rd of June comparison between layout-1 and layout- 2.	203
Figure 6.79. Winter simulation on the 22 nd of December for layout-1 comparison with comfort level.....	204
Figure 6.80. Winter simulation on the 22 nd of December for layout-2 comparison with comfort level.....	204
Figure 6.81. Buildings clusters, A) compound 1, B) location of the clusters, C) compound 2.	207
Figure 6.82. Compounds hourly average PET values for the entire plot.....	208
Figure 6.83. Original compound 2 design (left), compound 2 with the added shading (right).	215
Figure 6.84. Receptor 2 PET results with and without shading.....	215
Figure 6.85. Receptor 3 PET results with and without shading.....	216
Figure 6.86. Receptor 5 PET results with and without shading.....	216
Figure 6.87. Receptor 6 PET results with and without shading.....	216

Figure 6.88. Receptor 8 PET results with and without shading.....	217
Figure 6.89. Receptor 9 PET results with and without shading.....	217
Figure 6.90. The average change in PET values after the shading addition for compound 2.	217
Figure 6.91. The area investigated for the microanalysis with the section cuts.....	218
Figure 6.92. Receptor 8 PET results.....	219
Figure 6.93. Receptor 8 wind speed results.....	219
Figure 6.94. Receptor 9 PET results.....	220
Figure 6.95. Receptor 9 wind speed results.....	220
Figure 6.96. Receptor 1 PET levels for the height's scenarios.....	221
Figure 6.97. Receptor 3 PET levels for the height's scenarios.....	222
Figure 6.98. Receptor 5 PET levels for the height's scenarios.....	222
Figure 6.99. Receptor 7 PET levels for the height's scenarios.....	222
Figure 6.100. Wind speed cross-section through the receptors for scenario 12m high buildings.	223
Figure 6.101. Wind speed cross-section through the receptors for scenario 18m high buildings.	223
Figure 6.102. Wind speed cross-section through the receptors for scenario 24m high buildings.	223
Figure 6.103. The averaged PET values for all the receptors in the different LAD scenarios.	225
Figure 6.104. The averaged wind speed values for all the receptors in the different LAD scenarios.....	225
Figure 6.105. Wind speed plan section for the 0.5 m ⁻¹ LAD scenario.....	226
Figure 6.106. Wind speed plan section for the 1.0 m ⁻¹ LAD scenario.....	226
Figure 6.107. Wind speed plan section for the 1.5 m ⁻¹ LAD scenario.....	226
Figure 6.108. Average PET value for the scenario wind direction (West) and scenario with wind direction (North).....	228
Figure 6.109. Sun path for the different orientation scenarios.....	228
Figure 6.110. PET differences for individual receptors.....	229
Figure 6.111. wind flow inside the original orientation.....	230
Figure 6.112. wind flow inside the 90-degree orientation off north.....	230

Figure 6.113. Wind speed distribution for the 90-degrees orientation off north scenario. .	231
Figure 6.114. Wind speed distribution for the original orientation scenario.....	231
Figure 6.115. Wind speed distribution for the 45-degrees orientation off north scenario. .	232
Figure 7.1. Amman's wind rose. Source: Meteonorm.....	237
Figure A6. 1. Wind speed values for wind direction 150° at 11:00 am.	317
Figure A6. 2. Wind speed values for wind direction 135° at 11:00 am.	318
Figure A6. 3. Wind speed values for wind direction 120° at 11:00 am.	318
Figure A6. 4. Wind speed values for wind direction 105° at 11:00 am.	319
Figure A6. 5. Wind speed values for wind direction 90° at 11:00 am.	319
Figure A6. 6. Wind speed values for full gap scenario- At 11:00 am plan section.	320
Figure A6. 7. Wind speed values for full gap scenario- At 11:00 am A-A section.	321
Figure A6. 8. Wind speed values for full gap scenario- At 11:00 am B-B section.....	322
Figure A6. 9. Wind speed values for full gap scenario- At 11:00 am C-C section.....	322
Figure A6. 10. Wind speed values for half gap scenario- At 11:00 am plan section.	323
Figure A6. 11. Wind speed values for half gap scenario- At 11:00 am A-A section.	324
Figure A6. 12. Wind speed values for half gap scenario- At 11:00 am B-B section.....	325
Figure A6. 13. Wind speed values for half gap scenario- At 11:00 am C-C section.....	325
Figure A6. 14. Wind speed values for 12-meters buildings' height scenario- At 11:00 am plan section.....	326
Figure A6. 15. Wind speed values for 12-meters buildings' height scenario- At 11:00 am B-B section.....	327
Figure A6. 16. Wind speed values for 12-meters buildings' height scenario- At 11:00 am C-C section.....	327
Figure A6. 17. Wind speed values for 12-meters buildings' height scenario- At 11:00 am A-A section.....	328
Figure A6. 18. Wind speed values for 18-meters buildings' height scenario- At 11:00 am plan section.....	329
Figure A6. 19. Wind speed values for 18-meters buildings' height scenario- At 11:00 am A-A section.....	330
Figure A6. 20. Wind speed values for 18-meters buildings' height scenario- At 11:00 am B-B section.....	331

Figure A6. 21. Wind speed values for 18-meters buildings' height scenario- At 11:00 am C-C section.....	331
Figure A6. 22. Wind speed values for 24-meters buildings' height scenario- At 11:00 am plan section.....	332
Figure A6. 23. Wind speed values for 24-meters buildings' height scenario- At 11:00 am A-A section.....	333
Figure A6. 24. Wind speed values for 24-meters buildings' height scenario- At 11:00 am B-B section.....	334
Figure A6. 25. Wind speed values for 24-meters buildings' height scenario- At 11:00 am C-C section.....	334
Figure A6. 26. Receptor 1 PET values comparison for 90° and 0° orientation.	350
Figure A6. 27. Receptor 2 PET values comparison for 90° and 0° orientation.	350
Figure A6. 28. Receptor 3 PET values comparison for 90° and 0° orientation.	351
Figure A6. 29. Receptor 4 PET values comparison for 90° and 0° orientation.	351
Figure A6. 30. Receptor 5 PET values comparison for 90° and 0° orientation.	352
Figure A6. 31. Receptor 6 PET values comparison for 90° and 0° orientation.	352
Figure A6. 32. Receptor 7 PET values comparison for 90° and 0° orientation.	353

Chapter 1 :

Introduction

Content

1. Introduction.
- 1.1 Amman, Jordan as a case study.
 - 1.1.1 Urban context.
- 1.2 Climate of Amman
- 1.3 Outdoor thermal comfort and airflow in an urban setting
- 1.4 Aims and objectives
- 1.5 Research approach
 - 1.5.1 Context of the research
- 1.6 Research questions
 - 1.6.1 Main research question
 - 1.6.2 Subsidiary research questions
- 1.7 Relevance of the research
- 1.8 Structure of the Thesis

1. INTRODUCTION

Greenhouse gas (GHGs) emissions have been rising for the last 100 years, ever since the time of the Industrial Revolution. According to the UN Intergovernmental Panel on Climate Change (IPCC), GHGs are connected to the rising global temperatures. This increase of GHGs —CO₂ in particular— has happened in recent years and has made global warming inevitable for years to come, with a temperature increase of 0.85 °C from 1880 to 2012 (IPCC, 2014). The increase in the mean global temperature is especially alarming for cities, as it has been recorded that urban areas are warmer than rural areas, which risks human health and increase pollution - this phenomenon is called Urban Heat Island (UHI) (Gartland, 2008).

Urban heat islands occur in urban areas for two main reasons, surface materials and urban geometry (Gartland, 2008). Modification to the built environment has shown a mitigating effect to UHI, for example, shading and vegetation can play a crucial role in reducing the sun exposure, and light-coloured materials can reduce the amount of sun absorption. Though the addition of vegetation and light-coloured material has its benefits, it is not without problems, as trees can limit the night-time radiation cooling and light-coloured materials can cause glare and discomfort.

The thesis aims to examine the effect of urban geometry on pedestrians' thermal comfort and urban airflows in a residential setting in the semi-arid climate of Amman, Jordan. The analysis followed an optimisation process to a proposed urban design to a plot of land located in the south of Amman. The process consisted of three main design scales: mesoscale, microscale, and urban canyon scale. The thesis addresses the main geometrical aspects of the built environment, which consisted of street grid formation for the mesoscale analysis and the airflow-based design for the microscale. The urban canyon scale analysed different geometrical parameters as well as vegetation's Leaf Area Density (LAD) to achieve the best design in terms of pedestrians' thermal comfort. This research used ENVI-met as the main CFD programme to simulate the different built scenarios for the analysis, where a validation study was performed on ENVI-met in Amman to test its sensitivity and accuracy in predicting the microclimatic parameters in the urban environment .

1.1 AMMAN, JORDAN AS A CASE STUDY

1.1.1 URBAN CONTEXT

Jordan is considered a young country, and it was founded on the 11th of April 1921 under the name Emirate of Transjordan while being under the British protectorate. It went on and gained its full independence on May 25, 1946, ending the British influence in the country (Schein, 2016). Shortly after its creation, the whole region entered an unstable period which resulted in a massive refugees' surge - the 1948 Palestinian exodus and the six-day war in 1967 doubled the population of Jordan and changed the urban layout (Kadhim & Rajjal, 1988).

In addition to the Palestinians refugees' crisis in the late 40's and 60's, the return of the Jordanians from Iraq and Kuwait during the Gulf War, the Iraq War in 2003, and the Syrian Civil War in 2011 added unexpected immediate population surge in Jordan. The Department of Statistics estimates the population of Jordan at 10.4 million in 2019, with 45% of the country's population living in the capital Amman.

The history of Jordan dictated the urban layout of the country. The now economic districts once were farmlands; the old city district once was the financial district and the low-income housing areas once were refugee camps. All these changes in the urban fabric of Jordan and its capital Amman happened in a relatively small period of time, and this resulted in an unplanned layout of Amman with narrow streets and overpopulated districts, as seen in Figure 1.1 (Al-Asad, 2004), while Figure 1.2 shows the urban expansion of Amman since 1956.



Figure 1.1. A view of the downtown area in Amman. Source, Photographer: Rachel Lewis.

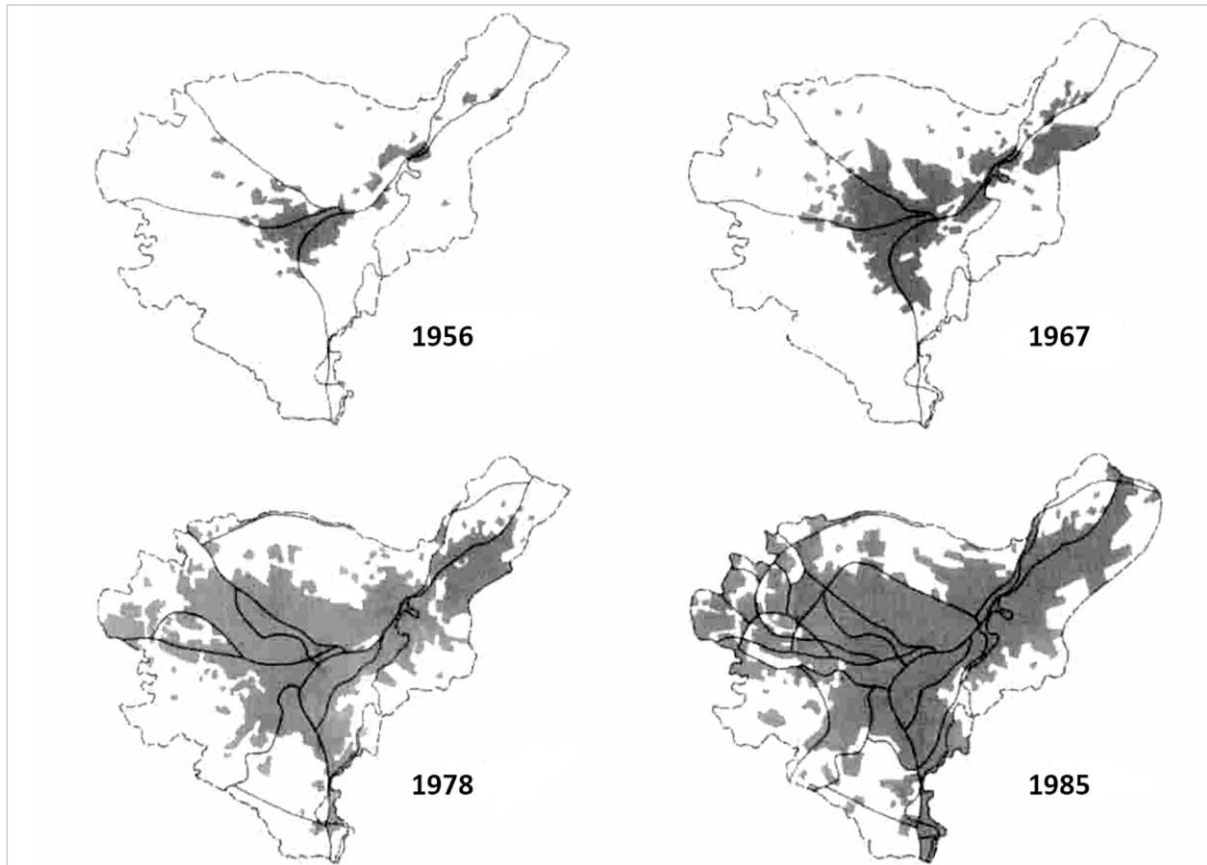


Figure 1.2 Amman's increasing growth. Source: Greater Amman Comprehensive Development Plan, executive summary.

Amman, compared to other oriental cities like Cairo and Damascus, is modern and has no relation to the ancient's roots of the land. The first laid plan to develop Amman as a city was proposed by the British mayor at the time, in 1938, as stated in the Department of Land Use (Kadhim & Rajjal, 1988; Malkawi & Abu-Dayyeh, 2004). Moving forward to 1985, a new plan called the Greater Amman Comprehensive Development Plan 1985-2005 (GACDP) was made. It was funded by USAID and developed by the municipality of Amman. The plan was heavily influenced by British urban ideology, with two satellite cities as the main focus (Abu-dayyeh, 2004). Though this plan promised to reshape the growth of Amman, it quickly became outdated and disregarded (Beauregard & Marpillero-Colomina, 2010).

In *Amman 2025: from Master Plan to Strategic Growth*, the planners initially designed the project to replace the GACDP and to regulate the city's future growth. However, due to the new large scale projects and their abundancy, the plan came to a halt, and the then-mayor, Omar Maani, instructed his team of planners to rethink the twenty-year master plan and to start shaping a plan based on strategic growth instead of the traditional urban planning.

Amman 2025, as described by its authors, is a process rather than a design, where it combines the design stage with the execution stage (Beauregard & Marpillero-Colomina, 2010).

The current layout of Amman displays a significant socio-spatial polarisation, with its mixed urban construct, the layout generally corresponds to the income of the families residing (Abu-dayyeh, 2004), where the wealthy areas are identified by wide streets and residential areas accompanied by leafy sidewalks, larger plot sizes, and low population density of 2500-6000 person/ km². On the other hand, the poor areas are identified by a narrow street grid, a compacted built environment, and small plot sizes, where the population can exceed 30000 person/ km² (Potter, et al., 2009). As described by the Department of Lands and Survey, Amman has a category system for residential lands that separate the buildable areas, in which the system is based on plot size, buildable area, and setbacks. Figure 1.3 shows the distribution of these lands throughout Amman. Grade A is mainly distributed in the eastern part of Amman with bigger plot sizes and setbacks when compared to grade D; located in downtown and western parts of Amman.

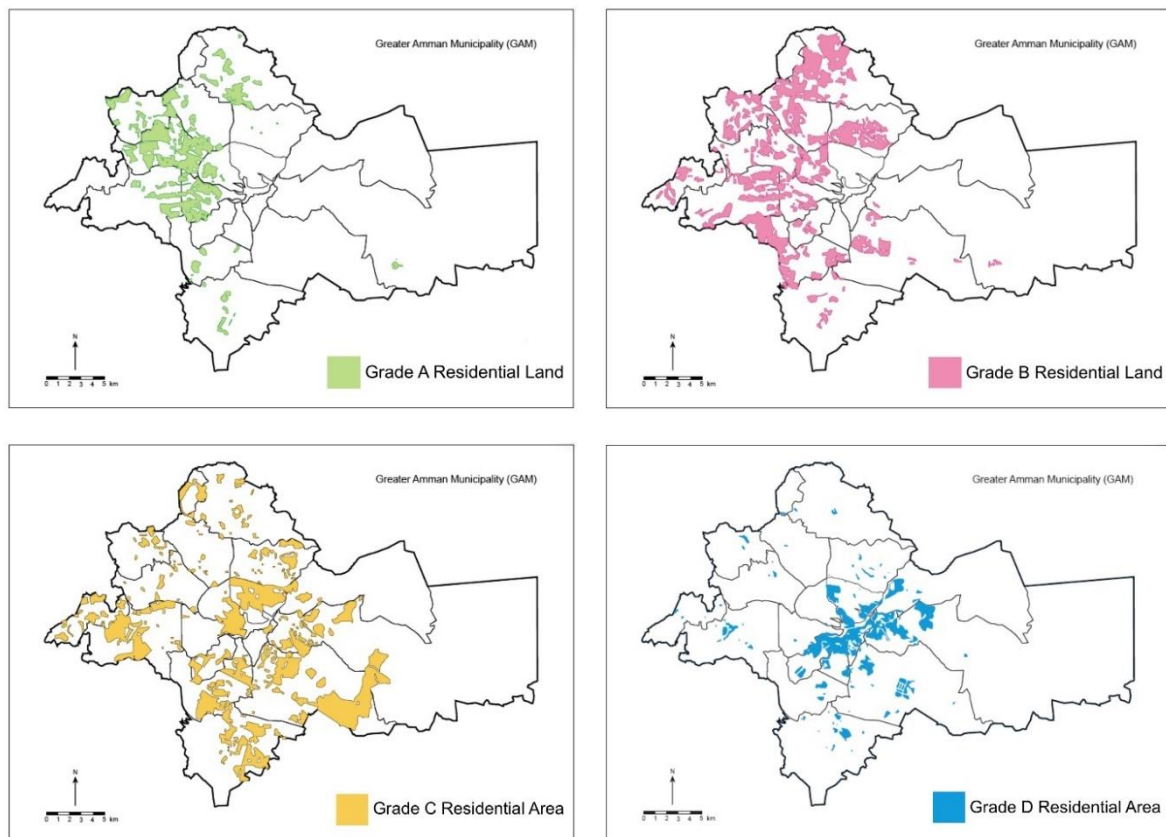


Figure 1.3 Amman's residential lands categories. Courtesy of GAM adapted from Potter, et al (2009).

Plans to expand Amman has been laid out to accommodate the population growth. Abu-Dayyeh, 2004, claims that the recommended plans for Amman's expansion were influenced by the British planning scheme, where the focus was on creating satellite towns to channel the population growth while preventing the growth of peri-urban and suburban areas. The expansion recommended the southern part of Amman near Queen Alia Airport, where two satellite towns were to be established (Figure 1.4). The present research takes into consideration these expansion plans, where the case study is located west of the airport.

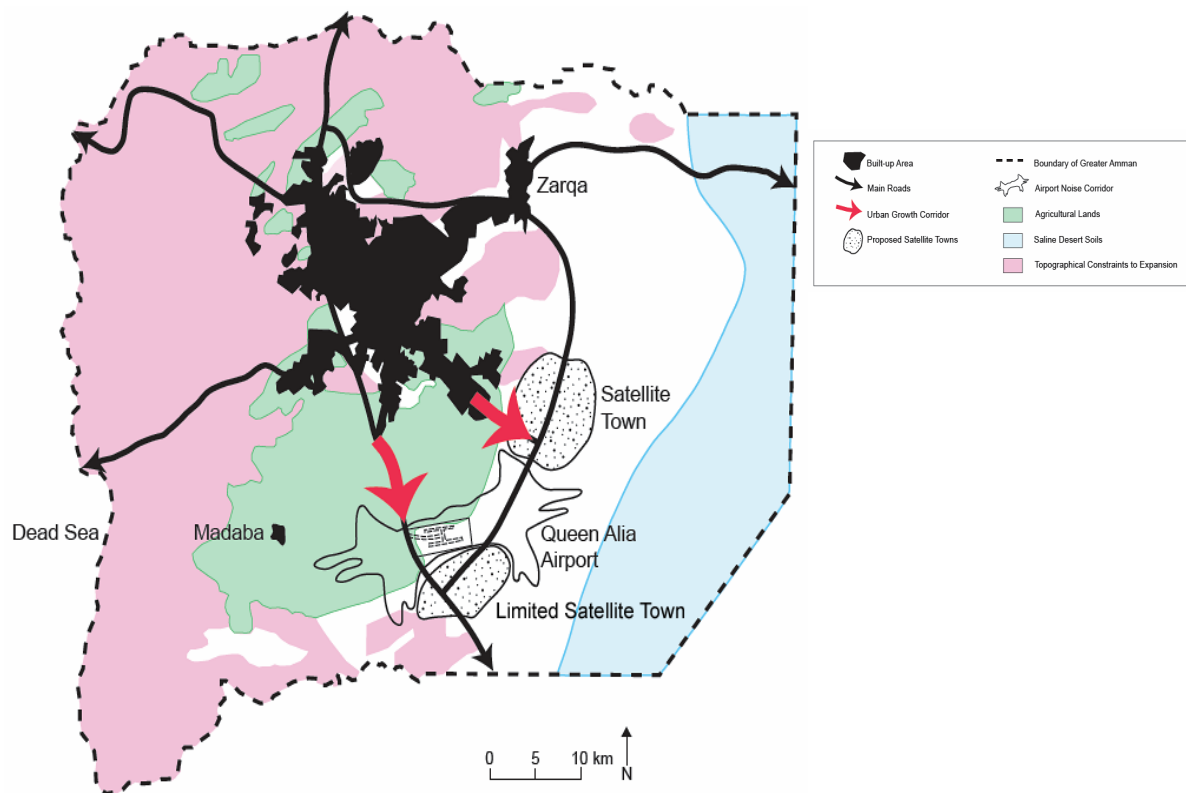


Figure 1.4 Amman's expansion plans. Source (Potter, et al., 2009).

1.2 CLIMATE OF AMMAN

Amman is characterised by hot summers and cold winters, as it is classified as semi-arid in the Köppen climate classification (Peel, et al., 2007). Jordan consists of three main geological features; upland Jordan Plateau, desert and Jordan rift regions (Abu Sada, et al., 2015), Amman lies in the highland part of Jordan where rainfall is concentrated between the months of November to April (see Figure 1.5). Air temperature varies throughout the year as Amman goes through the four seasons, summer's air temperature values tend to be the highest with July recording a high temperature of 32.1 °C, an average of 26.8 °C, and a low of 23 °C (Figure 1.6). January is the coldest month of the year in Amman, with a high temperature of 12.6 °C,

an average of 8.1 °C, and a low of 3.2 °C (Figure 1.6). Spring and autumn have shorter durations than summer and winter. However, they are locally recognised as the most comfortable seasons of the year (Potter, et al., 2009). Thus, the present research focuses on summer and winter analysis to test the urban parameters in the two extreme conditions, and it is applied to the grid analysis as wind flow is important in winter conditions; however, the winter analysis is not included in urban canyon level as the focus is on the solar access and thermal stress where most of the load lies in summer conditions.

Figures 1.7 and 1.8 show the relative humidity and the wind speed values in Amman. The humidity levels in Amman are moderate throughout the year, an increase can be seen in winter with values ranges around 65%, and a decrease is recorded in summer with values ranging from 37% to 45% (Figure 1.7). The wind speed average values vary throughout the year between 1.7 m/s to 3.1 m/s with a recorded high in June at 7.3 m/s, and a recorded low in September at 0.3 m/s (Figure 1.8).

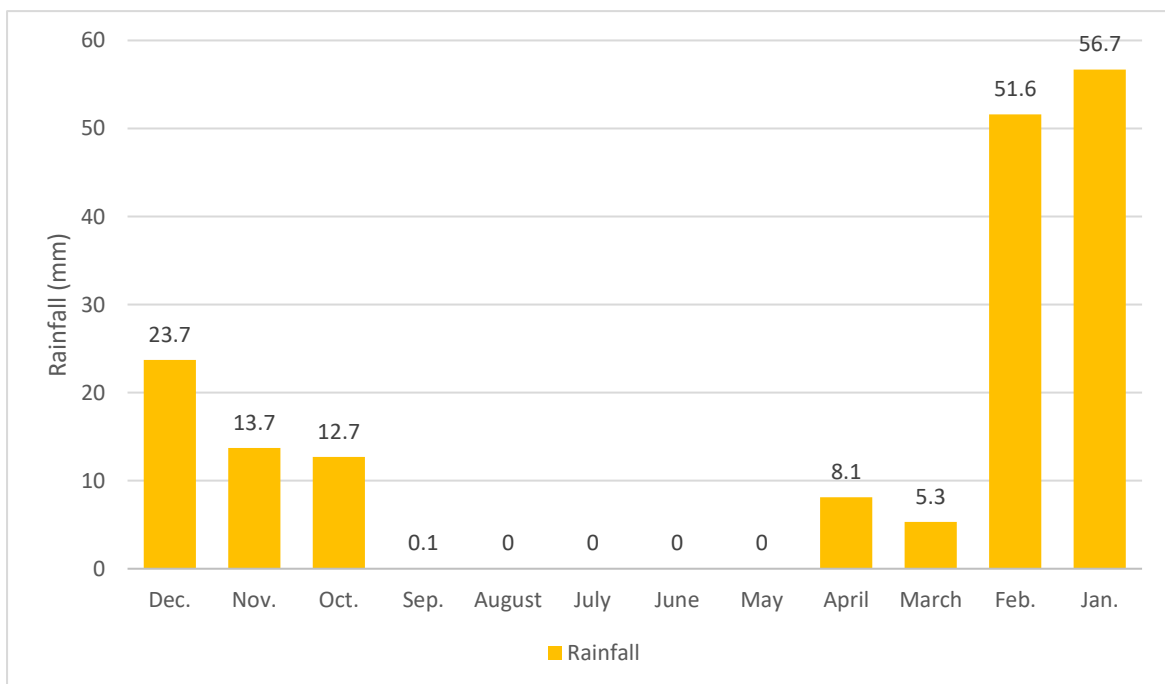


Figure 1.5 Amman's rainfall through the year of 2015. Source Department of Statistics, Jordan.

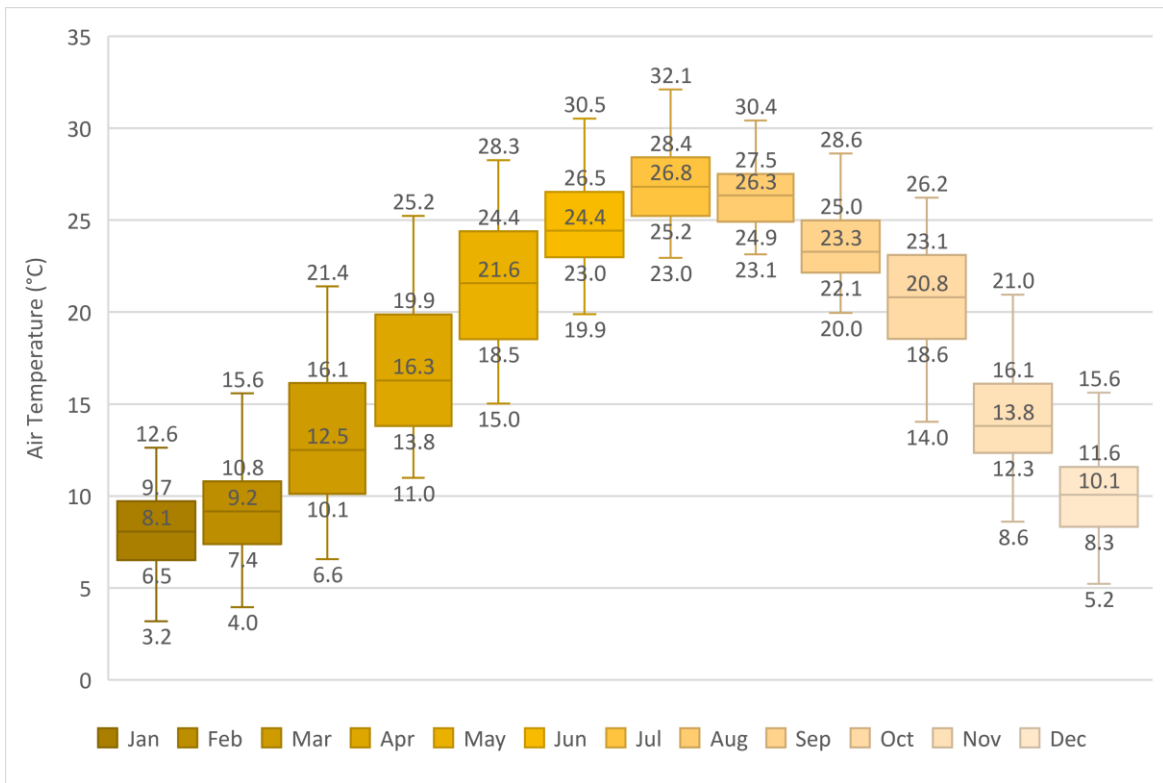


Figure 1.6 Air temperature values for Amman. Source Meteonorm.

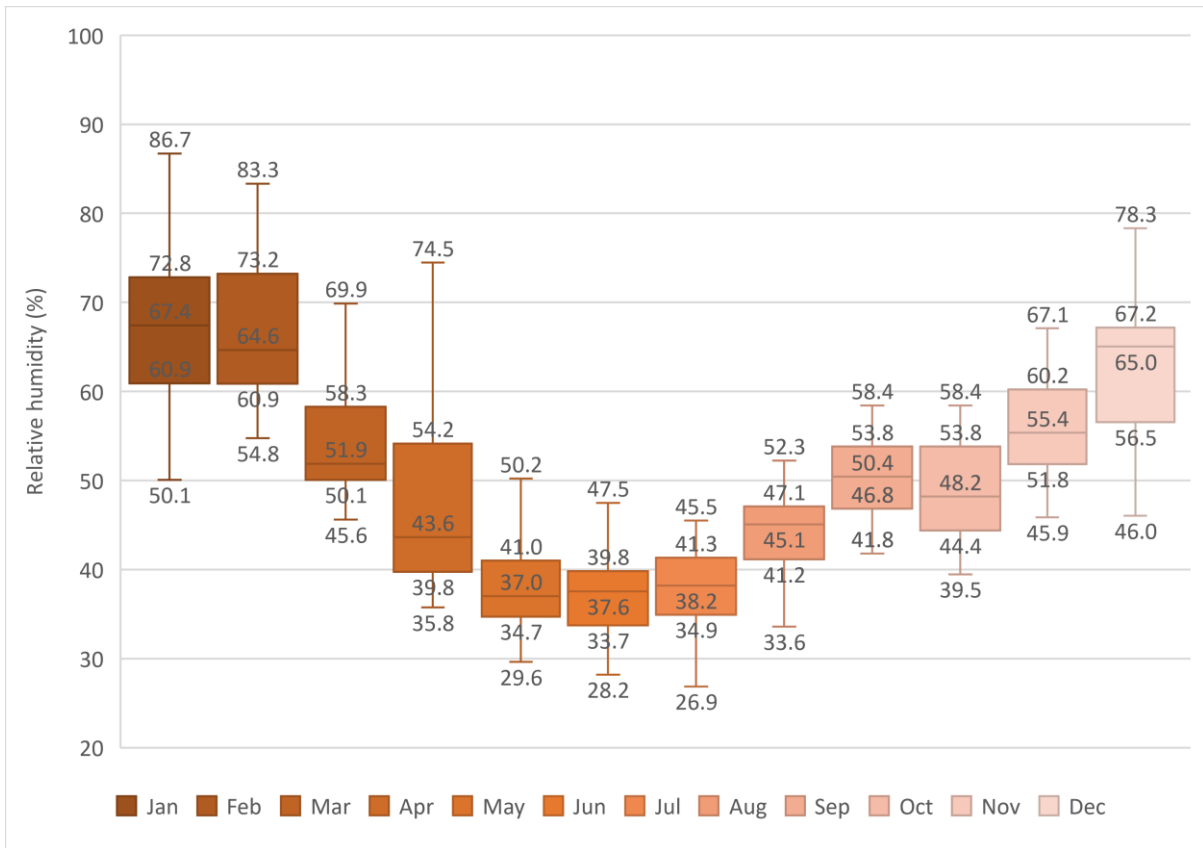


Figure 1.7 Relative humidity values for Amman. Source Meteonorm.

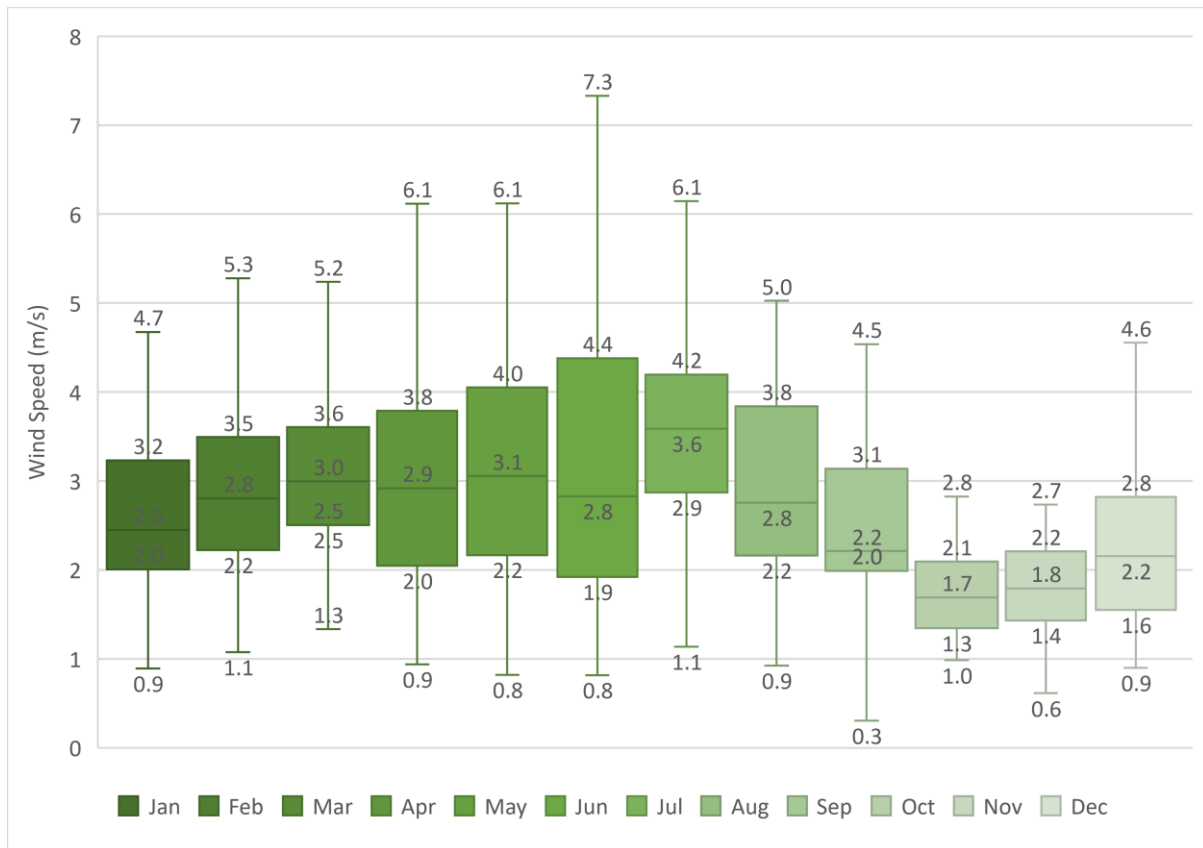


Figure 1.8. Wind speed values for Amman. Source Meteonorm.

1.3 OUTDOOR THERMAL COMFORT AND AIRFLOW IN AN URBAN SETTING

The study of urban spaces and their thermal implications have gained a special interest in research in the past few decades (Honjo, 2009). As more than half of the world's population are living in cities, the pressure of providing healthy and comfortable outdoor spaces has been increasing (Chen & Ng, 2012). This has led to a growing interest in the research of outdoor thermal comfort and made it essential in the urban planning field (Amit-Cohen & Maruani, 2007). According to Niachou, et al., 2008, the airflow inside the urban setting affects the thermal environment, where the favourable airflow can release some of the heat stress in the urban canyons and enhance the thermal stress on the pedestrians. The advances in computational sciences have pushed the study of the urban microclimate to numerical simulation approaches, e.g. Computational Fluid Dynamics (CFD) (Toparlar, et al., 2017; Moonen, et al., 2012), Erell et al., 2011, suggested that use of the CFD technology in the urban design field can advance the prediction possibilities of fluid fluxes and allow the study of urban geometry on thermal stress.

Morakinyo et al., 2020, have simulated the effects of Sky View Factor (SVF) and vegetation addition on the thermal comfort index, the Physiological Equivalent Temperature (PET). The study was conducted using a CFD method on different urban canyons height-to-width (H/W) ratios. The results showed that the simulations allowed for several recommendations for urban canyons geometry and trees placement to achieve higher thermal satisfaction. Moreover, Vallati et al., 2019, have studied the aspect ratio of urban canyons under Mediterranean conditions using CFD modelling and found that heat transfer inside the urban canyons is directly affected by the geometry of the canyons. The airflow in urban settings has been studied extensively (Oke, et al., 2017), and research of how airflows can be adjusted by controlling the urban geometry, this includes buildings heights, orientation and dimension of the urban canyons as well as the overall density of the urban sitting (Blocken & Carmeliet, 2008; Richards, et al., 2002; Oke, et al., 2017; Coceal, et al., 2006).

In order to study the urban geometry in the context of thermal stress, an appropriate approach needs to be selected and identified for a particular climatic condition. The study of outdoor thermal comfort is still limited when compared to the abundance of research on the indoor thermal comfort and especially in the area of study Amman, Jordan. The main climatic parameters that are generally addressed when studying the outdoor thermal comfort are air temperature, relative humidity, mean radiant temperature and wind speed. There have been many indices developed in regard to pedestrians' thermal comfort, such as the Physiological Equivalent Temperature (PET), the Universal Thermal Climate Index (UTCI) and Predicted Mean Vote (PMV). However, the PMV index is more used in the indoor thermal conditions than outdoors conditions, and it was found to give inaccurate results in predicting the thermal comfort for pedestrians (Potter & de Dear, 2000). The PET is the most used index in the recent studies regarding the outdoor thermal comfort (Gulyás & Matzarakis, 2009), and it was found to be the most suitable index to be used in the present research as it predicts the microclimate parameters and fluid flow accurately in response to the semi-arid climate of Jordan.

Literature has shown that the study of outdoor thermal comfort is limited in the arid climate and is even more scarce in the context of Jordan. The present research employs the urban simulations to fill the gap in the field of outdoor thermal comfort in Jordan, where different geometrical aspects of the built environment are investigated in order to achieve a lower thermal stress on pedestrians in harsh conditions of summer in Amman, Jordan. However,

this approach is not without limitation, where the urban environment has a large number of variables; this increases the computational time significantly and increase the cost of the devices and software.

1.4 AIMS AND OBJECTIVES

The research is going to focus on the outdoor thermal comfort and the effect of which prior planning of future urban development would have on Amman. The aim of this research is mainly to identify the key elements for enhancing the outdoor thermal for pedestrians in a residential setting. To achieve this aim, the study has the following subsequent objectives:

- To examine the case study of Amman in terms of urban context and climatic features (Chapter 1).
- To understand the main factors affecting the outdoor thermal comfort for pedestrians (Chapter 2).
- To review the effect of urban canyon configurations on airflow (Chapter 3).
- To consider the context of the urban environment and its implications on the microclimatic parameters and thermal stress (Chapter 3).
- To evaluate and assess ENVI-met, including the sensitivity to parameters' change and calibration testing through comparing the results to observed data (Chapter 5).
- To appraise the street grid layouts in terms of wind flow and thermal stress (Chapter 6 - Section 6.1).
- To review the mesoscale analysis which includes the grid design proposals for the studied site in Amman and the effect of different approaching wind angles on the thermal stress (Chapter 6 -Section 6.2).
- To assess the microscale analysis which included the buildings clusters design proposals based on the wind flow designs (Chapter 6 – Section 6.3).
- To evaluate the geometrical modification, orientation, and Leaf Area Density (LAD) of trees and their effects on airflow as well as thermal stress (Chapter 6 – Section 6.3).

- To make recommendation for future urban development regarding mitigating the thermal stress on pedestrians in residential areas based on Amman as a case study (Chapter 7).

Current research on urban design in Amman and Jordan in general is focused on how to manage the existing projects in terms of buildable areas and regulate the future ones in terms of urban expansion. Very little research is done on the outdoor thermal comfort and its implications. The latest paper in this area was published in 2018 and it assessed the use of plants to modify the microclimate of courtyards in Jordan (Alkhatib & Qrunfleh, 2018). Abdel-Aziz and Al-Kurdi, 2014, discussed the use of Envi-MET as a tool to evaluate the application of trees as a mean to reduce electricity use for air conditioning. These two papers are the latest paper published regarding outdoor thermal comfort and Envi-MET, which leaves a gap in literature for future urban development in Jordan.

1.5 RESEARCH APPROACH

1.5.1 CONTEXT OF THE RESEARCH

This research aims to identify the most efficient way to organise and create the urban elements to achieve the lowest thermal stress on the human body, especially on pedestrian who spent times outdoors. The main research method is to study the possible solutions for the selected parameters and then apply it into a comprehensive urban design on a selected site in Amman, Jordan. This should help the future urban development in Jordan through visualising the practical application of the research results' implementation in an urban design, whether be it a small-scale design as an urban canyon or on a larger scale e.g. neighbourhoods.

The research uses two approaches, empirical and Computational Fluid Dynamics (CFD) modelling, and since the research is heavily depended on CFD modelling, a validation process was needed to make sure that the outcomes were credible and sound. Envi-MET—the modelling software— was used to model and assess the urban elements studied in this research, e.g. the urban canyon orientation and the height of buildings. For that, data from the empirical phase were used to validate Envi-MET through calibration and variables sensitivity testing. Figure 1.9 shows the work process and how it connects to the research objective.

Research Work Process

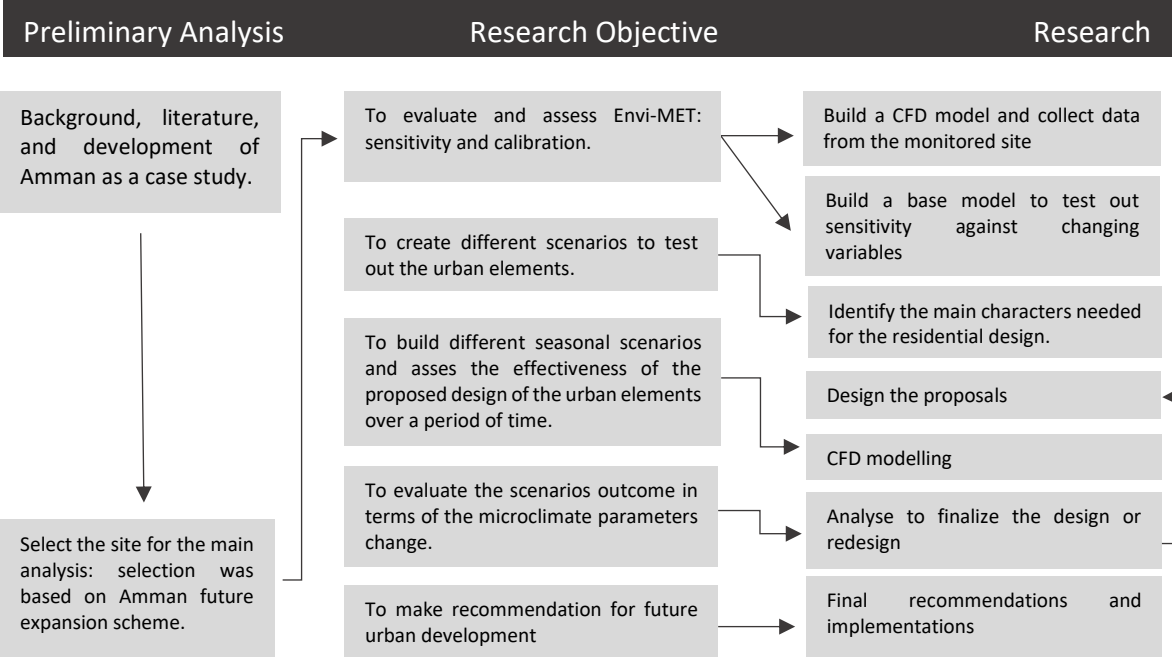


Figure 1.9 Research work process.

While the idea of modelling the urban environment and changing the microclimate is very promising, this method has its cons, with the main caveat being the large number of possibilities for changing the urban elements considered in the research and the uncontrollable variables, including the changes to the built environment and meteorological conditions. Due to this, most researchers will refer to the reductionist approach, as discussed in Byron, 2002, and used in Skelhorn,2013. The reductionists method is a quantitative data approach that assesses the connection between different components and returns a relationship between these components to build a unified outcome (Byron, 2002). Although the present research studies the effect of urban elements on pedestrians’ thermal comfort - by definition, the thermal stress felt by the human body in response to external factors - it could be considered as a reductionist approach as multiple parameters can be quantified, e.g. the meteorological parameters; but this cannot be said for all the parameters involved in the research as the human perception of thermal stress is not easily measured. All of this should be taken into consideration in later chapters where these quantitative and qualitative data are analysed and interpreted. Skelhorn, 2013, made a similar comparison in her work while studying the effect of vegetation on building energy consumption in an urban context, where

the research analysed the different variables including Leaf area density (LAD) of trees and trees' geometry.

Human perception of thermal stress, whether it be a cold or hot sensation, depends on two main factors: personal and environmental. In this research, the thermal comfort index that is used to assess the changes in the urban environment is the Physiological Equivalent Temperature (PET), since it evaluates the outdoor conditions' effect on the human body and sets the human variables — clothing insulation and metabolic rate— to fixed values in order to unify the results. It also uses an assessment scale system of 10 stages to express a wide range of thermal stress level. PET was first presented in 1999 by Peter Höppe, and it is based on the Munich Energy-balance Model for Individuals (MEMI) that was first developed by Höppe in the early 1980s (Höppe, 1999). The PET is one of the most cited thermal index in publications in outdoor thermal comfort, it is also recommended by the German Engineers Association and is used widely to evaluate the thermal stress on the human body in open spaces (Jendritzky & Höppe, 2017). The PET has a wide implementation in software such as ENVI-met and RayMan, which models the mean radiant temperature in an urban context and calculates of thermal indices.

1.6 RESEARCH QUESTIONS

1.6.1 MAIN RESEARCH QUESTION

Having the need to adapt to the global rise in temperatures, the study of the urban environment in terms of reducing the thermal stress is essential. Keeping this in mind, the study needs some specificity to regulate the research and find the relationships between microclimate and the urban elements in question. In view of the aforementioned, the research main question is:

How does the urban geometrical parameters affect the urban microclimate and pedestrians' thermal comfort in a residential setting in the semi-arid climate of Amman?

1.6.2 SUBSIDIARY RESEARCH QUESTIONS

To answer the research main question, the following subsidiary questions were addressed:

- How well does ENVI-met simulate the microclimatic parameters of Amman and is it sensitive to variables' change?
- How do different street grid layouts of Amman affect thermal stress and airflow?
- What is the most suitable grid layout for the proposed residential site in Amman?
- What are the effects of the geometrical modification, orientation, and Leaf Area Density (LAD) of trees at the proposed residential site in Amman on airflow and thermal stress?

1.7 RELEVANCE OF THE RESEARCH

For many years urban development has been disconnected from the other fields of design and engineering. In Amman, the development plans are neglected and ignored, which has resulted in uncontrollable growth throughout the last 50 years. Beauregard and Marpillero-Colomina, 2010, explain how in the field of urban development, the planning stage is disconnected from the implementation stage, and how the 1987 comprehensive development plan did not succeed due to this disconnection. This resulted in delay and cancellation of projects or, in some cases, costly alternations. An example of a recent failed project in Amman is the Jordan Gate Towers project (Figure 1.10), which has been paused for construction for years since it was started in 2005. The project has been described as the worst decision that has been taken by the municipality of Amman (Beauregard & Marpillero-Colomina, 2010) with a disconnection from the social construct of Amman and a lack of infrastructure in the site. The project raised many problems regarding regulations and how the effect on the surrounding buildings and vehicle traffic was neglected during the planning phase (Abu-Hamdi, 2017).

In Amman 2025: from Master Plan to Strategic Initiative, the project team introduced a new method of handling the urban uncontrollable growth, avoiding the old approach of redesigning the city, but rather fixing what was broken. The initiative sought to discard the hierarchy and plan a communication strategy, where the municipality is connected to the

professional community and the analysis is connected to the legislative interventions (Beauregard & Marpillero-Colomina, 2010).



Figure 1.10 The Jordan Gate Towers project. Source: Abu-Hamid, 2017.

The urban sector is being managed for improvements to handle the massive growth in Amman, but in its wake, it has neglected the environmental impact this growth has caused. Amman's population density varies from 2500-6000 person/km² to 30,000 person/km² (Potter, et al., 2009). This has caused many issues, such as slums being created to house this number of residents and numerous health issues regarding air quality and thermal stress. Additionally, the literature on outdoor thermal comfort in Jordan is very sparse, where the new projects are designed without any environmental consideration to outdoor thermal comfort or urban heat islands. This is where this research's importance comes to light, due to Amman's overpopulation and many projects hint at an expansion plan to the south of Amman. This research explores the idea of designing a residential area with the least outdoor heat stress on pedestrians located to south of Amman, based on the impact of the urban elements analysis on microclimate, and in doing so giving the urban planners community a better understanding to outdoor thermal comfort and its applications.

1.8 STRUCTURE OF THE THESIS

This thesis is divided into seven chapters. The first chapter is the introduction chapter, where the main concepts of the thesis are briefly discussed. The second chapter reviews the relevant literature related to human thermal comfort; it presents the main factors affecting the

thermal comfort and reviews the indices used to assess the thermal comfort in the context of indoor and outdoor settings. The third chapter examines the main airflow interactions within the urban context and reviews the effect of urban streets geometry on wind flow and microclimate. The fourth chapter outlines the methodology used in this research, detailing the CFD data used in the simulations and main approaches used to assess the outdoor thermal comfort for pedestrians. The fifth chapter introduces the CFD modelling software that was used in the research, ENVI-met, detailing its main calculation approach and validating its results with calibration and sensitivity tests. The sixth chapter is the results chapter, and it is divided into three sections, where the main findings of the research are discussed. The seventh and final chapter is the conclusion chapter, which addresses the main research questions and summarizes the methodology used to assess the thermal stress in urban residential settings. It also discusses the main findings of the research and conclude recommendations for future work.

Chapter 2 : Literature

Review of Outdoor

Thermal Comfort

Content

- 2.1 Introduction.
- 2.2 Background.
- 2.3 Thermal comfort in context of indoor and outdoor environments.
- 2.4 Indices for assessing the outdoor thermal stress- The predictive models.
- 2.5 The physiologically equivalent temperature microclimatic factors.
 - 2.5.1 Air temperature.
 - 2.5.2 Mean radiant temperature.
 - 2.5.3 Wind speed.
 - 2.5.4 Relative humidity.
- 2.6 Vegetation.
- 2.7 Previous studies on outdoor thermal comfort.
- 2.8 Summary.

2.1 INTRODUCTION

In this chapter, the thermal stress in the context of pedestrians' comfort will be reviewed. The current literature is discussed in terms of the origins and history of the predictive models of thermal sensation. Thermal indices for indoor and outdoor thermal comfort are discussed with the focus leaning towards outdoor thermal comfort in general and, more specifically, the physiological equivalent temperature (PET).

2.2. BACKGROUND

The current layout of Amman displays an undeniably socio-spatial polarisation (Abu-dayyeh, 2004), with its mixed urban construct, and the layout divided into wealthy areas and poor areas. The wealthy areas are identified with wide street residential areas accompanied by leafy sidewalks, larger plot sizes, and low population density of 2500-6000 person/ km². The poor areas, on the other hand, are identified by a narrow street grid, compacted built environment and small plot sizes, and the population density can exceed 30,000 person/ km² (Potter, et al., 2009). The aforementioned factors played a big part in accumulating urban thermal discomfort in Amman, with an insufficient number of public parks and green areas accompanied with compact urban designs. Tomah, et al., (2017) and Zhang et al, (2009) stated that the improper design of urban spaces with their elements such structures and materials has worsened the thermal environment of cities. It should be noted that summer records high discomfort levels compared to winter as Jordan falls under the hot arid zone (BW) with winter precipitation in the Köppen climate classification system (Farhan & Alnawaiseh, 2018).

The American Society of Heating, Refrigerating and Air-Conditioning Engineers (ASHRAE), defines thermal comfort as *'the state of mind, which expresses satisfaction with the thermal environment'* (ASHRAE, 2017). The relationship between the environment and the human body is the basis for the thermal comfort, with its characterization that depends on the human psychology and the physiological parameters (van Hoof, et al., 2010). Different approaches have been adopted when studying thermal comfort. Höpfe (1993) and Taffé (1997) state that thermal comfort indices should be derived from the human energy balance, thus linking the thermal comfort with the physiological parameters, while Brager and Dear (2001) linked thermal comfort to behavioural and individual assessments, which suggests that thermal comfort should combine the aspects of individuals whether it be physical or behavioural.

The study of thermal comfort had shown great progress in the 1960s after the climatic or environmental chambers became more available for researchers, and the chambers allowed for more focused analysis for the four main parameters regarding the thermal comfort - air temperature, air velocity, radiant temperature and humidity (Mayer & Höppe, 1987). Several attempts to categorize thermal sensation into working indices started to emerge. Gagge et al, (1971) first introduced the Standard Effective Temperature (SET), which was based on physiological parameters, clothing insulation (Clo), metabolic rate (Met), air movement, dry bulb temperature and air humidity. One of the earliest models concerning the thermal comfort was the PMV-model (Predicted Mean Vote) developed by Fanger (Honjo, 2009). Fanger's model was developed by testing a large sample of individuals, the parameters of the study were controlled under indoor conditions with two changing variables, the clothing insulation (Clo) and the activity levels (Met) (Fanger, 1970). Following that, many other indices were developed, for example, the Physiological Equivalent Temperature (PET) (Höppe, 1999), which is considered to be most used model in assessing outdoor thermal comfort (Gulyás & Matzarakis, 2009), the Universal Thermal Climate Index UTCI (Jendritzky, et al., 2012) and (Jendritzky & Höppe, 2017), *inter alia*.

The need for indoor air conditioning, especially in a hot arid climate, is consuming a massive amount of energy that is mainly derived from fossil fuels. This has resulted in an exponential increase in greenhouse gas emissions (de Dear, et al., 2020). Studies have shown that due to the excessive use of cooling that is based on electricity consumption, the global CO₂ emissions have tripled since 1990, rising to 1130 million tonnes by the end of 2016 (IEA, 2018). The demand for solutions for this energy consumption has led researchers to think of the urban environment as a mitigating tool to lessen the impact of climate on the indoor spaces.

In the following sections the physiological and personal parameters concerning the outdoor thermal comfort will be discussed in details as they are the most crucial aspects of assessing and evaluating the thermal stress on pedestrians (Gaitani, et al., 2007; Ghaffarianhoseini, et al., 2019; Amindeldar, et al., 2017; Nikolopoulou & Lykoudis, 2007; Leng, et al., 2020; Ma, et al., 2020).

2.3 THERMAL COMFORT IN CONTEXT OF INDOOR AND OUTDOOR ENVIRONMENTS

Parsons (2003) described the importance of designing the environment to adapt to the human thermal comfort, and his work analysed the human interactions with the surrounding environment. This included the physiological responses as well the personal responses e.g. clothing and behaviour. Murakami (2006) expressed how vital it was to obtain the thermal comfort levels when designing spaces, generally by using thermal comfort indices. Most thermal indices, whether they be for indoor or outdoor spaces, have several parameters in common to calculate the thermal stress; however, the means and the approaches can vary from one model to the other depending on the use and the studied space.

The indoor thermal comfort in the built environment has mainly been studied in two disciplines: Engineering and Architecture. The HVAC engineers developed a heat balance model that takes into account the relationship between the individuals and their surroundings as the budget of their metabolic heat transferred into the indoor environment, with the metabolic heat fluxes transferred by means of radiation, convection, conductivity and latent heat fluxes (Fanger, 1970). The adaptive thermal comfort model, which is linked to built environment studies, claims that the individuals can be comfortable in temperatures lower or higher than the predicted values in the heat balance model, which indicates the ability of occupants to adapt to their environment in summer and winter (Nicol & Humphreys, 1973; de Dear & Brager, 1998; Nicol & Humphreys, 2002).

The steady-state model has been modified since the first publication of the Fanger's PMV model, and the literature shows that the modified models (e.g. the ePMV model, the aPMV model, the eSET model, the aSET model and the ATHB model) helped in reducing the gap between the predicted results of the models and the observed thermal comfort temperatures (Ole Fanger & Toftum, 2002; Gao, et al., 2015; Yao, et al., 2009; Schweiker & Wagner, 2015). The PMV model was investigated under outdoor conditions to test its viability in predicting the thermal comfort for pedestrians, and the results showed that the PMV model was not suitable for the outdoor condition, with a divergence of 3°C from the observed results (Potter & de Dear, 2000). A study conducted by the Architectural Research Centre Consortium (ARCC) and Florida Atlantic University (FAU) in 2011 found that the PMV model can be recalibrated. The results showed that the recalibrated PMV model produced a good agreement when

compared to the observed values, However, the recalibration consists of multiple methods and strategies that needs more testing and validating (Thitisawat, et al., 2011).

The literature shows that the thermal sensation for the outdoor scenarios differs from the indoor scenarios, and the human body is built to adapt to outdoor conditions better than indoors, where the metabolic rate and clothing are faced with different boundary conditions (Hwang & Lin, 2007; Oliveira & Andrade, 2007; Chen & Ng, 2012). Many studies have been conducted in regard to testing the limitation of the indoor adaptive model in outdoors scenarios, and the results showed an overestimation of the thermal stress, where the thermal indoor models fall short in accumulating the broader range of human factors and meteorological parameters that the outdoor scenarios possess (Spagnolo & de Dear , 2003; Zhang, et al., 2007).

The need for an outdoor thermal comfort assessment rose from the fact that 90% of individuals time is spent indoors, and this can sometimes be due to uncomfortable outdoor thermal conditions (Leech, et al., 2000). Höppe (2002) discussed the three general approaches for thermal comfort - the heat balance model, thermophysiological approach and the physiological approach. According to Mayer (1993), the thermophysiological approach is based on the skin receptors, which means that the comfort level can be reached when those receptors are sending less nerve signals to the brain. The shortcoming of this approach is the temporal aspect of the process, where it takes hours for the mean skin temperature to reach the steady-state (Höppe, 2002). The psychological approach is defined by ASHRAE, 1997 as *“a condition of mind which expresses satisfaction with the thermal environment”*. This approach is influenced by the individuals' preference and history with thermal sensation, which can differ greatly from one individual to the other (Rohles, 1980). Höppe (2002) describes a study conducted in 1984 on 250 individuals spending a day in sunny conditions, with the PMV index assessed at the comfort level to be at +3, which is at the hot level; however, most of the subjects reported a comfortable sensation because of their personal perception of the conditions around the studied day.

According to Fanger (1972), the thermal comfort in the heat balance model relies on the metabolic rates, and it is obtained when the heat budget of the human body is balanced with comfort ranges of sweat and skin temperature. The skin temperature is considered the most

prominent parameter in the thermophysiological approach as well as the heat balance model, where it can be calculated from the Munich Energy-Balance Model for Individuals (MEMI) or by predictive models (regression) (Höppe, 1993) and (Höppe, 2002). Researchers tend to use the MEMI for its climatic inclusivity as the regression model only handles a number of climatic zones (Höppe, 2002).

2.4 INDICES FOR ASSESSING THE OUTDOOR THERMAL STRESS- THE PREDICTIVE MODELS

This section discusses the predictive models that are used to predict the thermal stress in outdoor environments. Tables 2.1 and 2.2 display a summary for the outdoor thermal indices that are commonly used in the literature.

Table 2.1. Outdoor thermal comfort indices. Modified from Monteiro and Alucci (2006) - 1920s to 1970s

Year	Authors	Index	Abbreviation	Key features
1923	Houghten et al.	Effective Temperature	ET	Parameter used: Wind speed, dry bulb temperature and wet bulb temperature.
1932	Vernon and Warner	Corrected Effective Temperature	CET	Parameters used: Globe temperature, wind speed and wet bulb temperature.
1957	Yaglou and Minard	Wet Bulb Globe Temperature	WBGT	Used for direct sun radiation environments, and considers the air temperature, wind speed, air humidity and sun radiation.
1965	Siple and Passel	Wind Chill Temperature	WCT	Developed for cold environments.
1965	Belding and Hatch	Heat Stress Index	HSI	Based on heat balance model.
1967	Gagge	New Standard Effective Temperature	SET*	Parameters used: wind speed, relative humidity (equals to air temperature), mean radiant temperature, activity levels and clothing levels.
1969	Givoni	Index of Thermal Stress	ITS	The first proposal only included the heat exchanges, and clothing and activity levels.
1979	Masterton and Richardson	Humidex	-	The model includes only two parameters, the air temperature and relative humidity.
1979	Jendrizky et al	Klima Michel Model	KMM	Based on Fagner, 1970. With the modifications of the mean radiant temperature and the solar radiation model.

Table 2.2. Outdoor thermal comfort indices. Modified from Monteiro and Alucci (2006) – 1980s to 2000s.

Year	Authors	Index	Abbrev	Key features
1981	Vogt	the evaluation of thermal stress through the required sweat rate	Swreq	Calculates the sweat rate and temperature based on the working conditions.
1995	Aroztegui	Outdoor Neutral Temperature	Tne	The parameters included solar radiation and wind speed.
1994	Blazejczyk	Man-Environment Heat Exchange model	Menex	The model is based on the human heat exchange balance.
1997	DeFreitas	Potential Storage Index	PSI	Based on the Menex model.
1999	Höppe	Physiological Equivalent Temperature	PET	The parameters included are the mean radiant temperature, air temperature, wind speed and relative humidity. The clothing level is set at 0.9 clo and the activity rate is set as 80 W.
2000	Givoni and Noguchi	Thermal Sensation Index	TS	Based on regression models from data extracted from experimental research.
2002	Bluestein and Osczevski	New Wind Chill Temperature	NWCT	Several experiments were conducted to measure the thermal sensation to humans exposed to wind.
2004	Nikolopoulou	Actual sensation vote	ASV	Parameters that are included in the calculations are the mean radiant temperature, wind speed, air temperature, relative humidity, activity levels and clothing levels.
2012	ISB and WMO	Universal thermal climate index	UTCI	The parameters include the mean radiant temperature, wind speed, air temperature, relative humidity or the water vapour pressure, activity levels and clothing levels.

Several indices were considered in assessing the thermal comfort for the outdoor environments in this study, and these indices were the outdoors standard effective temperature OUT_SET^* (Pickup & de Dear, 1999), the physiological equivalent temperature (PET) (Höppe, 1999) and the universal thermal climate index (UTCI) that was developed by the ISB and WMO in 2012. Gagge's two-node model (1971) calculates the thermal stress through the use of energy balance equations, and the equations solve the body core temperature and the skin temperature (Holopainen, 2012; Gagge, et al., 1971). The two-node model was used to develop a new thermal index, the new standard effective temperature (SET^*), to calculate the indoor thermal stress (Gagge, et al., 1986), and later the (SET^*) was modified to the outdoor environment by adding the mean radiant temperature parameter to the calculations by using the $OUT-MRT$ model (Pickup & de Dear, 1999). Compared to other indices, the OUT_SET^* index models the clothing level based on the activity level; however, the heat exchange model is limited in calculating the radiant and convective heat exchanges, where it overestimate the absorbed radiation values due to shortcomings in the $OUT-MRT$ model (Binarti, et al., 2020; Pickup & de Dear, 1999).

The universal thermal climate index (UTCI) is the temperature of an imaginary setting with specific parameters as the actual setting. The parameters in the reference setting are: air temperature equals to the mean radiant temperature, relative humidity at 50%, wind speed at 0.5 m/s and the metabolic rate at 135 W/m^2 (Fiala, et al., 2001; Katić, et al., 2016; Binarti, et al., 2020). The UTCI index uses a complex model (UTCI-Fiala model) that comprises of a 343-node system to calculate the thermal stress on the human body in a certain environment. to form the basis of the model, multiple experiments were conducted to include different climatic scenarios as well as the different metabolic rate from sedentary to heavy exercising (Blazejczyk, et al., 2013; Chen & Matzarakis, 2014; Binarti, et al., 2020; Fiala, et al., 2012; Coccolo, et al., 2016).

The biggest advantage of the UTCI model is its accuracy in calculating the temporal mean radiant temperature as well as the changes in wind speed (Blazejczyk, et al., 2013; Coccolo, et al., 2016); however, studies have shown a limitation with the model in predicting the comfort values in extreme climatic conditions (Chen & Matzarakis, 2017; Fiala, et al., 2012). The model also showed some discrepancy in calculating the thermal stress when certain clothing insulations are included (Chen & Matzarakis, 2014). The PET model's human factors

include the clothing levels and activity levels, where they were fixed at 0.9 clo and 80 W respectively (Höppe, 1999). When the UTCI index was compared to the PET under a constant clothing value, the UTCI showed a divergence in the results whereas the PET showed better results (Fang, et al., 2018; Lucchese, et al., 2016).

Höppe (1999) defines the PET as *“the physiological equivalent temperature at any given place (outdoors or indoors) and is equivalent to the air temperature at which, in a typical indoor setting, the heat balance of the human body (work metabolism 80 W of light activity, added to basic metabolism; heat resistance of clothing 0.9 clo) is maintained with core and skin temperatures equal to those under the conditions being assessed.”* It is based on the Munich energy balance model for individuals (MEMI) (Höppe, 1993). The PET index is expressed in degrees Celsius, where the thermal sensation ranges from extreme heat stress to extreme cold stress as shown in Table 2.3 (Matzarakis, et al., 1999).

Table 2.3. PET thermal scale (Matzarakis, et al., 1999).

PET (°C)	Thermal perception	Grade of physiological stress
<4	Very cold	Extreme cold stress
4 to 8	Cold	Strong cold stress
8 to 13	Cool	Moderate cold stress
13 to 18	Slightly cool	Slight cold stress
18 to 23	Comfortable	No thermal stress
23 to 29	Slightly warm	Slight heat stress
29 to 35	Warm	Moderate heat stress
32 to 41	Hot	Strong heat stress
>41	Very hot	Extreme heat stress

The PET index is considered to be the most used index in the outdoor thermal comfort studies (Chen & Matzarakis, 2014; Coccolo, et al., 2016). Several reasons contribute to PET’s popularity among the other thermal comfort indices - the thermal scale is expressed in degrees Celsius which makes it easier to understand (Chen & Ng, 2012; Yahia, et al., 2017) and for many years the calculation of PET software was free to use in RayMan (Fang, et al.,

2018; Paramita, et al., 2018; da Silva & de Alvarez, 2015), where the UTCI was only recently added. Another factor that is worth mentioning is that the PET was officially included in the German Association of Engineers (GAE) guideline 3787 (Li, et al., 2016; Lucchese, et al., 2016). The main advantage of using the PET index in hot climates is the fixed values for the clothing and activity, where these clothing insulation values correlate with the values that exist in these climatic zones (Fang, et al., 2018; Li, et al., 2016).

Coccolo et al. (2016) state that the PET index scale is not fixed for different climates, therefore, calibrations for the PET scale is needed through questionnaires and observed meteorological data. A new scale was modified for the hot humid climate of Taiwan (Table 2.4) where the comfort range shifted by 7°C (Lin & Matzarakis, 2008). A study conducted in 2014 investigated the thermal perception in a coastal Mediterranean climate and found that the comfort range shifted by 3°C from the original PET scale (Table 2.4) (Pantavou, et al., 2014). Another study on calibrating the PET for a hot arid climate was conducted in Egypt in 2016, and the results showed that the comfort range shifted from 18-23°C to 23-32°C under summer conditions (Elnabawi, et al., 2016). That said, the PET comfort range that was proposed by Matzarakis et al. (1999) was used in numerous studies in different climatic ranges, and more specifically in hot arid climates (Elwy, et al., 2018; Setaih, et al., 2013; Xystrakis & Matzarakis, 2010; Abdel-Ghany, et al., 2013; Yahia & Johansson, 2014; Kariminia, et al., 2016; Mahmoud, 2011; Zakhour, 2015).

Table 2.4. PET scale for different climates (Lin & Matzarakis, 2008; Pantavou, et al., 2014; Matzarakis, et al., 1999)

Thermal perception	PET (°C)	PET - Hot humid climate (°C)	PET – Mediterranean climate (°C)
Very cold	<4	<14	<8
Cold	4 to 8	14 to 18	8 to 12
Cool	8 to 13	18 to 22	12 to 15
Slightly cool	13 to 18	22 to 26	15 to 19
Comfortable	18 to 23	26 to 30	19 to 26
Slightly warm	23 to 29	30 to 34	26 to 28
Warm	29 to 35	34 to 38	28 to 34
Hot	32 to 41	38 to 42	34 to 40
Very hot	>41	>42	>40

Walther and Goestchel (2018) suggest that the PET index has some limitations regarding the heat gains and losses through the skin, as the model does not take into account the clothing insulation when calculating the air humidity levels. This is particularly shown in the vapour diffusion models, where the values vary from -7K to 2.6K (Blazejczyk, et al., 2013; Chen & Matzarakis, 2014).

The index chosen for this study is the physiologically equivalent temperature (PET) as it has been proven to evaluate the thermal stress for hot arid climates. The original PET scale was chosen to assess the thermal comfort without any calibration as the literature is still low on calibrating the PET for the hot arid climate. Another reason for choosing the original scale is the context of the study, where it assesses the effect of urban elements on the thermal comfort for pedestrians in a residential setting in a hot arid climate. The PET, in this case, will mostly produce high thermal stress, and the question in evaluating the effect of the urban elements is “how much would these elements lower the PET levels compared to the original design?” - thus, the calibrated scale is not of significance in this case. The following section will identify the main parameters concerning the PET index, and this will include the environmental factors such as: the mean radiant temperature, wind speed, air temperature and air relative humidity. However, it will not include the individuals' personal factors, the clothing insulation levels and the activity level as they are fixed in the PET model at 0.9 clo for clothing insulation and 80 W for metabolic rate (Höppe, 1999).

2.5 THE PHYSIOLOGICALLY EQUIVALENT TEMPERATURE MICROCLIMATIC FACTORS

2.5.1 Air Temperature

Parsons (2003) defines the air temperature as “*the temperature of the air surrounding the human body which is representative of that aspect of the surroundings which determines heat flow between the human body and the air*”. The air temperature in a specified environment will fluctuate depending on the heat exchange budget between the elements of the said environment, this means that the heat flow around the human body is not affected by a mass of air at a great distance. The air temperature behaves differently based on the climate of the studied areas; for example, in a warm setting where temperatures reach up to 40°C, the air mass adjacent to the individual will be “colder” in reference to the environment’s mean temperature and vice versa for cold environments (Parsons, 2014).

A study to predict the air temperature levels for the thermal comfort (T_{comf}) (Huang, 2007), showed that, for a given clothing level and metabolic rate, T_{comf} is affected by the wind speed and time spent outdoors. The comfortable air temperature rises with an increase of wind speed, and this is due to the increased heat loss through evaporation and convection (Figure 2.1). The expected air temperature for thermal comfort is significantly sensitive to time spent outdoors (Figure 2.2), where an individual can spend 8 hours outside at a temperature of 24°C but it only takes an hour for an individual to start feeling uncomfortable under air temperature of 30°C (Huang, 2007).

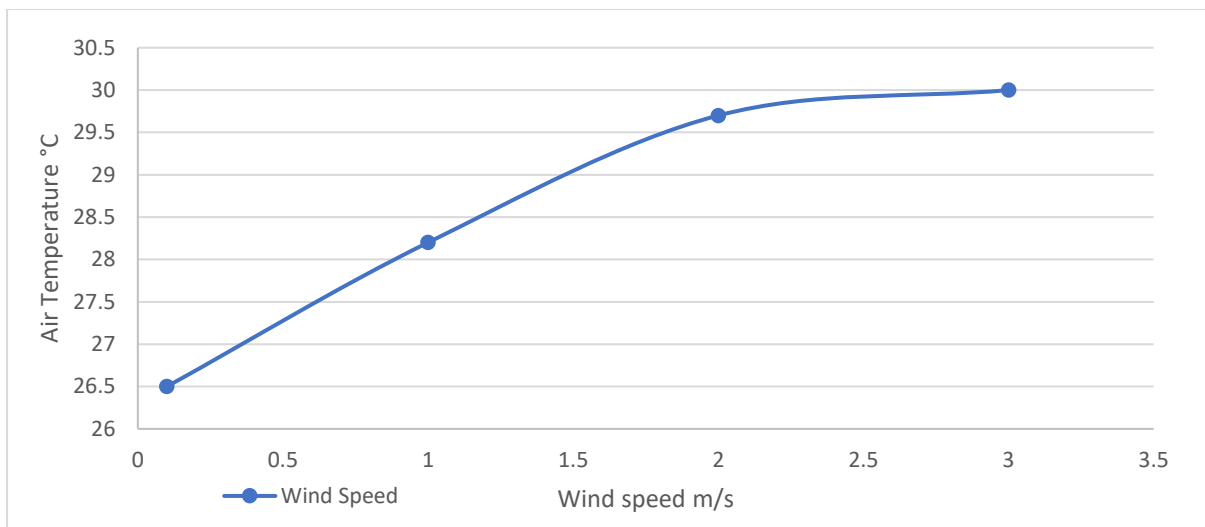


Figure 2.1. Comfortable air temperature in relation to wind speed. Modified from Huang, 2007.

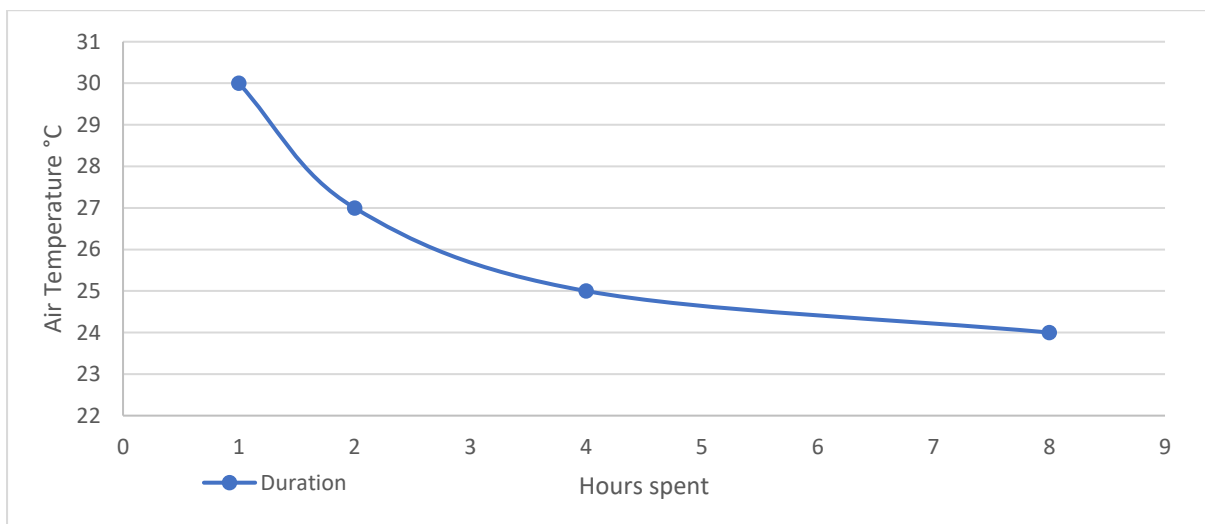


Figure 2.2. Comfortable air temperature in relation to time spent outdoors. Modified from Huang, 2007.

The rapid development of the urban environment has affected the water balance and microclimate of cities (Wang, et al., 2017; Bonacquisti, et al., 2006; Emmanuel & Krüger,

2012). The effect of urbanization on the global air temperature is relatively small (Bernstein, et al., 2008); however, the effect on the local air temperature is quite noticeable (Lan & Zhan, 2017; Taha, 1997; Mitchell, et al., 2001). The change in the local air temperature is particularly governed by the level of air pollution, the albedo of materials and the urban form (Masson, 2000; Yang, et al., 2017; Rizwan, et al., 2008). A study conducted by Erell and Williamson in 2007 measured the air temperature at sunrise in various locations in the city of Adelaide, Australia. The study was conducted in an open area outside the city, and a suburban location and inside the city in an urban canyon. The results showed an increase of the air temperature in the urban street canyon compared to the suburban area and the open area with a difference of 5.1°C and 7.6°C respectively (Erell & Williamson, 2007). The data used for this study in Amman were EPW files generated for the nearest weather station to the location as the area of study was located on the outskirts of Amman in an open space.

2.5.2 Mean Radiant Temperature

The mean radiant temperature is defined as the “uniform temperature of an imaginary enclosure in which the radiant heat transfer from the human body equals the radiant heat transfer in the actual non-uniform enclosure” (ASHRAE, 2017). The mean radiant temperature is regarded as the most important parameter in assessing the thermal comfort of individuals (Griffiths & McIntyre, 1972; Atmaca, et al., 2007). When compared, the air temperature within comfortable levels did not affect an individual’s sensation of discomfort when the subjects were close to warm surfaces (Fanger, 1977). According to Alfano et al. (2013), the mean radiant temperature has a direct relation to the materials of the surfaces it is emitting from, thus, the T_{mrt} can be calculated from the total sum of the radiation from all the surrounding surfaces based on the temperature of the material (Alfano, et al., 2013; Parsons, 2014) – see equation 2.1.

$$T_{mrt} = \sqrt[4]{\sum_i T_i^4 F_{p \rightarrow S_i}} \quad (2.1)$$

where, i is the desired surface, T_i is the temperature of said surface and F is the view factor.

To calculate the mean radiant temperature for the outdoor conditions the equations need to take into account the solar and atmospheric radiation (Huang, et al., 2014; ASHRAE, 2017; Hatefnia, et al., 2016).

$$T_{MRT} = \sqrt[4]{\left[\frac{1}{\sigma} (a_p \cdot e_{sol} \cdot F_{sol \rightarrow p} + \epsilon_{sky} \cdot e_{sky} \cdot F_{sky \rightarrow p} + \epsilon_{urb} \cdot e_{urb} \cdot F_{urb \rightarrow p}) \right]} \quad (2.2)$$

where, σ is the Stefan–Boltzmann constant ($5.67 \times 10^{-8} \text{ Wm}^{-2}\text{K}^{-4}$), for an individual a_p is the absorption coefficient, ϵ_{sol} is the sky emissivity, ϵ_{urb} is the solid surfaces emissivity, e_{sol} is the intensity of the sun radiation, e_{sky} is the intensity of the longwave radiation for the sky, e_{urb} is the intensity of the longwave radiation for the urban surfaces, $F_{sol \rightarrow p}$ is the shortwave view factor, $F_{sky \rightarrow p}$ is the visible sky view factor and $F_{urb \rightarrow p}$ urban surfaces view factor.

2.5.3 Wind Speed

Wind flow affects the human body in terms of comfort and discomfort depending on the activity level and the time spent in the wind conditions (Tsichritzis & Nikolopoulou, 2019). Studies show that the level of discomfort may vary for the same wind speed value in different climatic and personal situations, for example, in the case of a cold season wind speed would affect the discomfort levels more than if it was a normal season (Parsons, 2014). The human activities play a key role in the wind comfort sensation, where a certain wind speed may be acceptable if the individual is walking or exercising for a short period of time but might not be within comfort range if the individual is sitting or waiting for a long period of time (Tsichritzis & Nikolopoulou, 2019).

The wind flow inside an urban environment is primarily affected by the urban morphology at pedestrian level rather the upper wind layers over the buildings (Ricciardelli & Polimeno, 2006; Ng, 2009; Arnfield, 2003). The wind speed ratio is defined as the wind speed at the height of an individual to the unaffected wind speed at an open space (Tsichritzis & Nikolopoulou, 2019). Buildings heights, orientation and arrangements are the main parameters that govern the wind flow (Ng, et al., 2011; Ratti, et al., 2002). Other elements can affect the wind flow inside the urban fabric, and these include the vegetation and the orientation of the street. The street orientation controls the dynamics of the wind behaviour, where wind can flow either in a helical flow or a channelling flow, this is important for thermal and comfort and cities health in general as it regulates how wind speeds values are distributed in a city or an area of a city (Oke, et al., 2017).

Penwarden (1973) describes how the wind speed values are more significant when they are at low speeds, for example, if an individual is in unshaded open space and an increase of wind

speed occur from 0.5 m/s to 5 m/s, it will require an increase of 9°C in air temperature to maintain thermal comfort (thermal equilibrium). However, if wind speed increased from 5 m/s to 10 m/s it only requires an increase of 1.5°C to maintain thermal comfort. The wind and air temperature relationship can be seen in Figure 2.3. If an individual walked from an unshaded area with a wind speed of 5 m/s to a shaded area with the same wind speed, it will be equal to a drop in T_a of 3.6°C, while walking from an unshaded area with a wind speed of 0.5 to a shaded area with 5 m/s will equate to a drop in air temperature of 13°C (Penwarden, 1973). It should be noted that the variation in wind speed values throughout the duration of exposure is taken into account when assessing the wind comfort, where the acceptable range is estimated at 20% of exposure time for wind speed values greater than 5 m/s (Pendwarden & Wise, 1975).

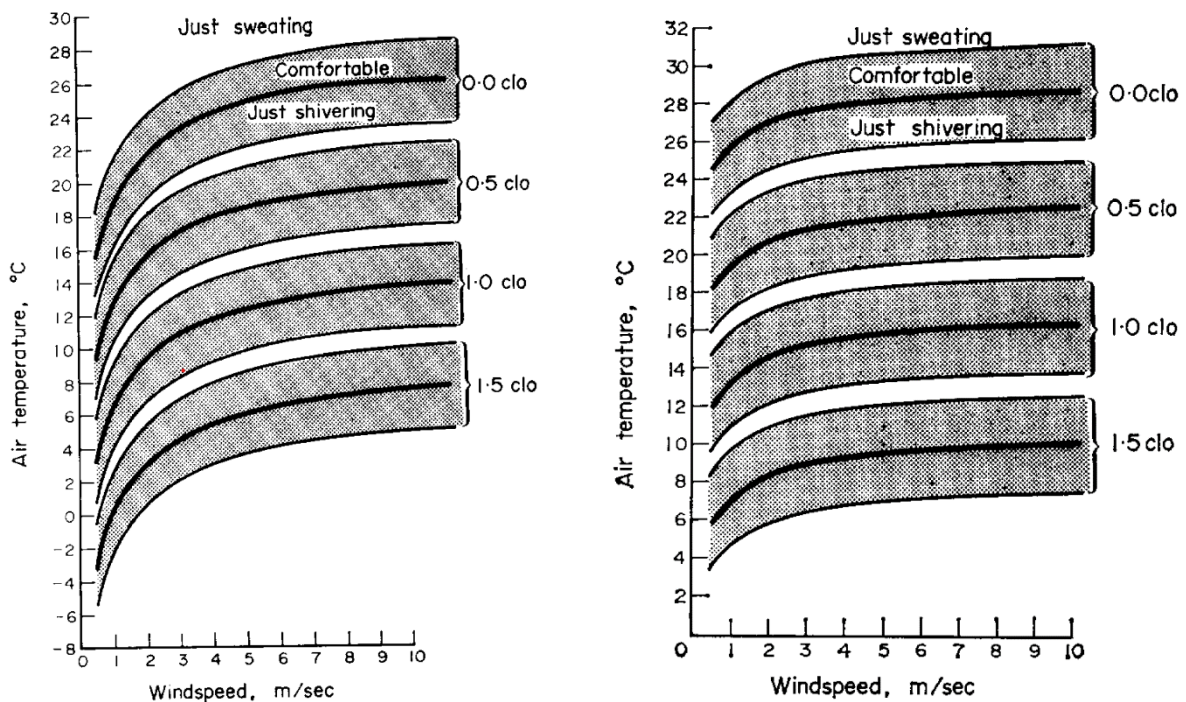


Figure 2.2.3. Comfort conditions, unshaded (Left), shaded (Right). Source Penwarden, 1973.

The wind effect on individuals has been studied in terms of mechanical effects and physiological effects, Penwarden (1973) describes an experiment conducted by the UK's Building Research Establishment (BRE) to measure the mechanical effects of wind speed on the human body. The study was coupled with literature from previous studies on soil erosion (Chepil, 1945), human physiology (Newburgh, 1949), gust speed effects (Melbourne & JouBerx, 1971)

and Beaufort land scale (Meteorological Office, 1969). Table 2.5 displays the main findings of the experiment.

Table 2.5. Wind effects. source Penwarden, 1973.

Beaufort Number	Speed in m/sec	Effects
0.1	0 - 1.5	Calm, no noticeable wind
2	1.6 – 3.3	Wind felt on face
3	3.4 – 5.4	Wind extends light flag, Hair is disturbed, Clothing flaps
4	5.5 - 7.9	Raises dust, dry soil and loose paper, Hair disarranged
5	8.0 – 10.7	Force of wind felt on body Drifting snow becomes airborne, Limit of agreeable wind on land
6	11.8 - 13.8	Umbrellas used with difficulty, Hair blown straight, Difficult to walk steadily, Wind noise on ears unpleasant, Windborne snow above head height (blizzard)
7	13.9 – 17.1	Inconvenience felt when walking
8	17.2 – 20.7	Generally impedes progress, Great difficulty with balance in gusts
9	20.8 – 24.4	People blown over by gusts

In 2007 the Netherlands developed a code to describe the human sensation of comfort and discomfort based on the mean wind speed. The threshold for wind comfort for no activity is 5 m/s while the threshold for danger was set at 15 m/s. Table 2.6 shows the comfort levels distributed between three different activities levels (Willemsen & Wisse, 2007).

Table 2.6. Wind comfort and danger criteria. Source Willemsen and Wisse (2007).

Wind comfort				
P ($V_{IS} > 5$ m/s) in % hours per year	Grade	Activity area		
		Traversing	Strolling	Sitting
< 2.5	A	good	good	good
2.5–5.0	B	good	good	moderate
5.0–10	C	good	moderate	poor
10–20	D	moderate	poor	poor
> 20	E	poor	poor	poor

Wind danger		
P ($V_{IS} > 15$ m/s)	Limited risk	0.05 - 0.3 % hours per year
	Dangerous	> 0.3 % hours per year

2.5.4 Relative Humidity

Relative humidity is defined as “the ratio of the prevailing partial pressure of water vapour to the saturated water vapour pressure” (Parsons, 2014). It is one of the basic parameters that governs thermal sensation (Li, et al., 2018; Djamila, et al., 2014; Li, et al., 2010) where it is responsible for the heat loss by means of vapour transfer (Parsons, 2014). Studies show that the effect of relative humidity on the thermal sensation could be negligible if the air temperature values are not exceeding the comfortable levels; however, in warm climates individuals have recorded the feeling of discomfort due to moisture on the skin (Fanger, 1970; Berglund, 1998; Fountain, et al., 1999; Jing, et al., 2013).

Ackerman (1987) recorded the values of relative humidity for an urban setting near an airport and a rural area in Chicago, USA. The results showed that relative humidity tended to be higher in rural areas compared to urban environments. Ackerman explained this phenomenon by the effect of the urban heat island as well as some natural weather occurrences (Ackerman, 1987). Similar results were found in London (Lee, 1991), and Edmonton, Canada (Hage, 1975).

Relative humidity variations of values can be seen throughout the day, this is because the relative humidity is primarily affected by the daily rise and fall of air temperature (Liu, et al., 2007). A study conducted in Beijing in an urban and a rural environment (Liu, et al., 2009), showed that the urban relative humidity is influenced by several factors: the surface roughness mixing with the thermal fields, reduced vegetation, the influence of industrial sources and pollution. Table 2.7 displays the relative humidity values for the period of (1971-2003), and the data show a noticeable drop in relative humidity in the urban area of Beijing compared to the rural area of Miyun in the recent years (Liu, et al., 2009).

Table 2.7. Air relative humidity for Beijing from 1971-2003. Source Lui, et al (2009).

	Period	Time				
		02:00	08:00	14:00	20:00	Average
Relative humidity for Beijing (A) (%)	1971 - 1980	71.45	68.43	43.18	61.67	61.18
	1981 - 1996	63.77	61.22	38.76	52.01	53.94
	1997 - 2003	67.05	64.33	41.06	55.46	56.97
Relative humidity for Miyun (B) (%)	1971 - 1980	71.61	65.32	40.58	60.83	59.59
	1981 - 1996	72.14	66.88	40.85	60.91	60.2
	1997 - 2003	70.35	66.1	39.56	58.92	58.73
Relative humidity difference (A - B) (%)	1971 - 1980	-0.16	3.11	2.59	0.85	1.6
	1981 - 1996	-8.37	-5.66	-2.09	-8.9	-6.26
	1997 - 2003	-3.3	-1.8	1.5	-3.46	-1.77

2.6 VEGETATION

Recent literature shows different mitigation approaches for enhancing the outdoor spaces. These have included changes to the urban geometry (Mahmoud & Ghanem, 2019; Galal, et al., 2020; Muniz-Gaal, et al., 2020); materials (Rosso, et al., 2016; Matias & Lopes, 2020;

Manni, et al., 2019); water features (Xu, et al., 2010) and vegetation (Ali-Toudert & Mayer, 2007; Lin, et al., 2008; Perini & Magliocco, 2014). Vegetation is implemented throughout urban spaces for various reasons, whether it be for city beautification or for shading effects. However, vegetation provides several contributions to urban environment, which include effects of solar and long-wave radiation, wind, and air temperature (Lai, et al., 2019).

2.6.1 Vegetation effects on solar radiation and thermal comfort

Trees, in general, can efficiently reduce the solar radiation in urban canyons. Trees either reflect or absorb radiation and may only transmit 30% of infrared radiation and 10% of visible light (Brown & Gillespie, 1995; Kotzen, 2003). Several studies analysed the effect of vegetation on the outdoor thermal comfort and mean radiant temperature. One study by Ali-Toudert and Mayer, 2007 showed that the addition of trees in an urban canyon that was oriented East-West with H/W of 2, reduced the PET values directly under the trees by 22K. Wang et al., 2015, measured the average difference of the mean radiant temperature in the Netherlands, and found a 7.4 K reduction in T_{mrt} in areas with trees when compared to open spaces. Moreover, PET and T_{mrt} usually show an increase in values during night periods, due to long-wave radiation being trapped by the trees. A study conducted on the effect of trees in a Nigerian university showed that the T_{mrt} values were 2.5K higher during night time but decreased significantly after sunrise (Morakinyo, et al., 2016).

The arrangement, geometry and species of vegetation can affect the thermal stress outcomes (Lai, et al., 2019). Lee et al., 2016 compared the PET value reductions for trees and grass and found that the trees produced less thermal stress by 3.0K while the grass only reduced the PET levels by 1.0K. Milosevic et al., 2107 studied different arrangements of tree placements throughout a parking space, and the results showed that increasing the number of trees and placing them strategically resulted in a 3.7°C decrease in the UTCI index and a 84% decrease in heat stress. Moreover, the geometry of the crowns showed different thermal stress results, with the cylinder shape having the most reduction in UTCI values of 3.9°C.

The leaf area density (LAD) and leaf area index (LAI) are indices used to define how dense the tree's foliage is (Oshio, et al., 2015). The LAD is the total of one side of the leaf surface area per unit volume of the tree and it is measured by (m^{-1}), and the LAI is the ratio of the total one-sided leaf surface area per unit of ground surface (Kong, et al., 2017). LAD and LAI are used to determine the trees' ability to intercept solar radiation, where the higher density of

leaves can block more solar radiation (Lai, et al., 2019). Fahmy et al., 2010, studied different LAI values for *F. elastica* and found that for LAI = 1 50% of the direct solar radiation was intercepted and when the LAI was adjusted to 3 the solar radiation interception increased to 84%. Moreover, Morakinyo and Lam, 2016, investigated the effect of LAI on solar radiation and PET levels and found that high LAI of 6 produced 4.3°C reduction of PET when compared to no trees and LAI of 1 only reduced the thermal stress of PET by 1.2°C.

2.6.2 Vegetation effects on air temperature

Vegetation reduces air temperature through transpiration and by providing shading (Lai, et al., 2019). Ali-Toudert and Mayer, 2007, found that planting trees in an urban canyon of H/W of 2 reduced the air temperature from 37.3°C to 38.8°C. Additionally, the use of vegetation as a tool to lower the air temperature has been found more beneficial in hot and dry climates, Alexandri and Jones, 2008, studied the effect of green roofs and green walls by using a two-dimensional modelling, and found that the air temperature was reduced significantly depending of the climate of the studied area. The study found the least air temperature change occurred in the continental cool summer conditions of Moscow, Russia, with air temperature change up to 3.5°C, and the highest was recorded in the hot arid climate of Riyadh, Saudi Arabia with a temperature change up to 11°C.

2.6.3 Vegetation effects on wind flow

Vegetation, unlike solid buildings, is porous by nature, and this can cause the wind velocity to be decreased and altered in direction (Oke, et al., 2017). Vegetation with high permeability was found to have the highest effect on wind flow (Frank & Ruck, 2005), and in order for the wind flow to be influenced by trees, the flows have to be in a close proximity of the tree, at a distance estimated at 5 times foliage diameter (Gromke & Ruck, 2008).

Studies have shown that trees can reduce the wind speed up to 50% in urban environments when compared to an open area (Morakinyo, et al., 2016; Park, et al., 2012). Leenders et al., 2007, studied the wind behaviour around small shrubs, and found that wind speed was reduced on the windward facing sides of the shrub to about 15%, and the effect reached up to 7 times the height of the shrub.

2.6.4 Vegetation effects on air humidity

Humidity in urban spaces is affected by vegetation by means of transpiration and soil irrigation (Broadbent, et al., 2018; Morakinyo, et al., 2016). Avissar, 1995, built a mesoscale

model to test the effect of vegetation on the urban environment, and the results showed a decrease in the air temperature but an increase in the specific humidity, where the an increase of 1 g/kg of specific humidity was recorded when raising the vegetation coverage from 33% to 67%. Morakinyo et al., 2016, found that the addition of trees had increased the relative humidity by an average of 6.1% over the months of September and October in the tropical climate of Nigeria.

2.7 PREVIOUS STUDIES ON OUTDOOR THERMAL COMFORT

Interest in studying the outdoor environment has been increasing rapidly in the past few decades (Honjo, 2009). The demand for comfortable urban spaces has been increasing, with the growing population of cities as more than half of the world’s population are now living in cities (Chen & Ng, 2012). This has made the research on the comfort for outdoor environments essential in urban planning and design (Amit-Cohen & Maruani, 2007).

The urban microclimate studies have been analysing the thermal comfort for pedestrians for a wide range of climates, including the temperate climate (Gulyas, et al., 2006; Nikolopoulou & Lykoudis, 2006; Nikolopoulou, et al., 2001; Thorsson, et al., 2004; Vasilikou & Nikolopoulou, 2020), subtropical climate (Lin, 2009; Spagnolo & De Dear, 2003; Cheng, et al., 2012), hot humid climates (Ahmed, 2003; Johansson & Emmanuel, 2006; Makaremi, et al., 2012; Yan, et al., 2020), cold climate (Stathopoulos, et al., 2004; Xi, et al., 2020) and hot arid climate (Ali-Toudert & Mayer, 2006; Yahia & Johansson, 2014; Yahia & Johansson, 2013; Zhao, et al., 2018; Barakat, et al., 2017; Atwa, et al., 2020). Table 2.8 shows a brief collection of the recent studies on the outdoor thermal comfort.

However, the literature on thermal comfort in Amman, Jordan is limited, and the studies conducted on the urban environment in Amman are explained further below.

Table 2.8. Previous studies on outdoor thermal comfort.

Year	Authors	Climate	Location	Thermal index
1996	Matzarakis and Mayer	Temperate	Freiburg, Germany	PET
2003	Ahmed, K. S	Hot humid	Dhaka, Bangladesh	Thermal Sensation

2003	Spagnolo and de Dear	Subtropical	Sydney, Australia	PET, PT, TOP, ET*, OUT-SET*
2004	Thorsson, et al.	Temperate	Göteborg, Sweden	PMV
2004	Stathopoulos, et al.	Cold	Montreal, Canada	Equivalent Temperature
2006	Gulyas, et al.	Temperate	Hungary	PET
2006	Nikolopoulou and Lykoudis	Temperate	Thessaloniki, Athens, Milan, Freiburg, Kassel, Sheffield, Cambridge	PET
2006	Johansson and Emmanuel	Hot humid	Colombo, Sri Lanka	PET
2006	Ali-Toudert and Mayer	Hot arid	Ghardaia, Algeria	PET
2007	Gaitani, et al.	Mediterranean	Athens, Greece	Comfa, Thermal Sensation
2009	Lin, T. P	Subtropical	Taiwan	PET
2010	Lin, et al.	Subtropical	Taiwan	PET
2011	Hwang, et al.	Subtropical	Taiwan	PET
2012	Cheng, et al.	Subtropical	Hong Kong	PMV, PET
2012	Makaremi, et al.	Hot humid	Malaysia	PET
2013	Yahia and Johansson	Hot arid	Damascus, Syria	PET
2013	Andreou, E	Mediterranean	Tinos, Greece	PET
2013	Yang, et al.	Hot humid	Singapore	Thermal Sensation

2014	Yahia and Johansson	Hot arid	Damascus, Syria	PET
2015	Sharmin, et al.	Hot humid	Dhaka, Bangladesh	Thermal Sensation Vote (TSV)
2016	Middel, et al.	Hot arid	Tempe, Arizona	PET
2017	Yang, et al.	Cold	Umeå, Sweden	Thermal Sensation Vote
2017	Barakat, et al.	Hot arid	Alexandria, Egypt	PMV
2018	Johansson, et al.	Hot humid	Guayaquil, Ecuador	PET, SET*
2018	Zhao, et al.	Hot arid	Phoenix, USA	PET
2019	Aminipouri, et al.	Temperate	Vancouver, Canada	TMRT
2019	Sharmin, et al.	Hot humid	Dhaka, Bangladesh	PET
2020	Vasilikou and Nikolopoulou	Temperate	Rome, Italy London, UK	Perceived Thermal Comfort (PTC)
2020	Yan, et al.	Hot humid- hot arid	Beihai, Turpan, china	Mean Thermal Sensation (MTS) vote
2020	Xi, et al.	Cold	Harbin, China	Thermal satisfaction votes
2020	Atwa, et al.	Hot arid	Alexandria, Egypt	PMV

Al-Azhari, et al. (2014) studied the effect of street orientation and buildings on the solar radiation accessibility in winter season in Amman, Jordan. Though thermal comfort indices were not used in this study, the effect of solar access in winter in Amman will enhance the thermal comfort sensation. The area chosen for the study was located in Dahiat Al Rasheed, an area characterized by streets of 12 metres width and maximum buildings heights of 15

metres according to the greater Amman municipality (Al-Azhari, et al., 2014). The street orientation parameter in the study included the following orientations: North to South, East to West, Northeast to Southwest, and Northwest to Southeast. The buildings height parameter was alternated between three heights (9, 12 and 15) metres on both sides of the street. The study was conducted in the coldest months of the year in Jordan (December, January, and February) as shown in Table 2.9 (Al-Azhari, et al., 2014).

Table 2.9. Air temperature values for the University of Jordan. Source (Al-Azhari, et al., 2014).

Temperatures (°C) Amman, University of Jordan (Located next to Dahiat Al Rasheed)												
	Jan	Feb	Mar	Apr	May	Jun	Jul	Aug	Sep	Oct	Nov	Dec
Extreme Max	24.0	25.1	26.3	33.0	39.0	38.3	39.0	41.5	39.0	34.6	28.0	24.8
Mean Max	10.1	11.5	15.0	20.2	25.2	28.1	29.5	29.6	28.3	25.1	18.2	12.4
Mean	6.4	7.4	10.2	14.6	18.9	21.9	23.6	23.6	22.2	19.0	13.1	8.4
Mean Min	2.7	3.2	5.4	8.9	12.5	15.7	17.7	17.6	16.0	12.8	8.0	4.3
Extreme Min	-8.3	-4.5	-6.5	-1.5	1.4	4.5	8.5	8.8	4.5	3.4	-2.0	-4.8

The results show that altering the heights of buildings was only beneficial when the street is oriented West to East and the buildings are facing South, but due to the sun angle, 9 metres and 12 metres proposals did not block the winter sun. The street orientation North to South did not yield any solar change when alternating the heights of the buildings. The Northwest to the Southeast orientation also did not have any effect on the change of solar access when the heights of buildings were changed. The aforementioned results have produced several recommendations to the Great Amman Municipality (GAM) when considering the solar access in winter, these recommendations included: the maximum height of buildings should be 12 metres when the streets are oriented West to East to guarantee solar access, the height of buildings can exceed the maximum set by GAM of 15 metres when the streets are oriented North to South as well as Northwest to Southeast (Al-Azhari, et al., 2014).

The study's results are limited to a single isolated street where the effect of the recommended heights do not take into account the effect on the adjacent streets and areas, also, the Northeast to Southwest orientation recommendation based on that the buildings facing the

Southeast would not affect the Northeast facing buildings is inaccurate as the height of the building will block the winter sun later in the evening after 14:00.

Al-Kurdi and Awadallah (2015) investigated the effect of streets parameters in reducing the urban heat island effect in Amman, Jordan. The study results are compared in terms of air temperature difference to indicate the effectiveness of the study against the urban heat islands. The study aimed to find a solution that would satisfy the summer and winter conditions through proposing different scenarios to a hypothetical street in the type C zoning areas, which is characterized by small sets backs and narrow streets. The base scenario's main parameters included: the street width, which was set to 12 metres, the finishing sidewalk materials, which was set to materials with a relatively high albedo, the height of buildings was set to 12 metres and the street orientation was set to West-East. Every parameter in the base model was individually changed to assess the isolated effect on the urban heat islands, where the receptor for data collection was placed in the middle of the streets (Al-Kurdi & Awadallah, 2015). The suggested scenarios were modelled in ENVI-met twice for each scenario, once in summer and once in winter. Table 2.10 shows a detailed description of the base model as well as the suggested scenarios.

Table 2.10. Base model and the parameters of the suggested scenario. Source (Al-Kurdi & Awadallah, 2015).

Case name	Type	Street width	Sidewalk finish	Buildings height	Street orientation
Base model	Residential type C	12 m	High Albedo	4 floors, 12 m	West- East
Case with 8 m street	Residential type C	8 m, H/W= 1.5	High Albedo	4 floors, 12 m	West- East
Case with North orientation	Residential type C	12 m	High Albedo	4 floors, 12 m	North-South
Case with vegetation	Residential type C- with trees on the sidewalk	12 m	High Albedo	4 floors, 12 m	West- East
Case with changed sidewalk materials	Residential type C	12 m	Higher Albedo	4 floors, 12 m	West- East
Case with changed buildings form	Residential type C	12 m	High Albedo	Arcades added	West- East

The results show that the scenarios with higher albedo and added vegetation produced better results in the summer in terms of air temperature, where the air temperature dropped 2-15°C due to less solar radiation and less absorbed heat (Figure 2.4). As for the winter conditions, the scenario with North-South oriented street yield the maximum air temperature, this can be explained by the increased solar access to the street especially at noon from the south direction (Figure 2.5). It should be noted the scenario with added vegetation was excluded from the winter simulation as it was assumed that the vegetation were deciduous trees (Al-Kurdi & Awadallah, 2015).

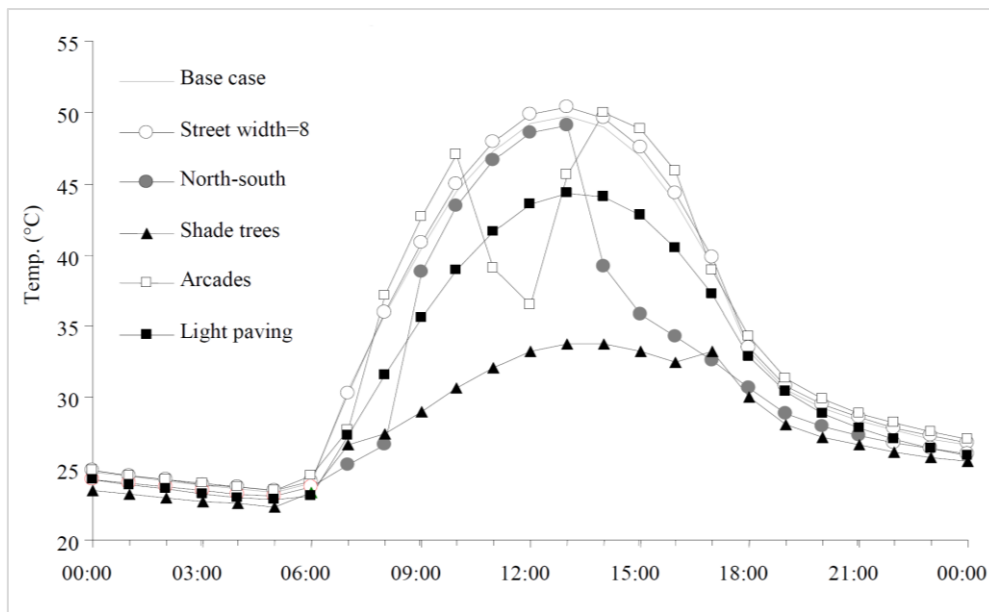


Figure 2.4. The air temperature for the summer conditions for all of the scenarios. Source (Al-Kurdi & Awadallah, 2015).

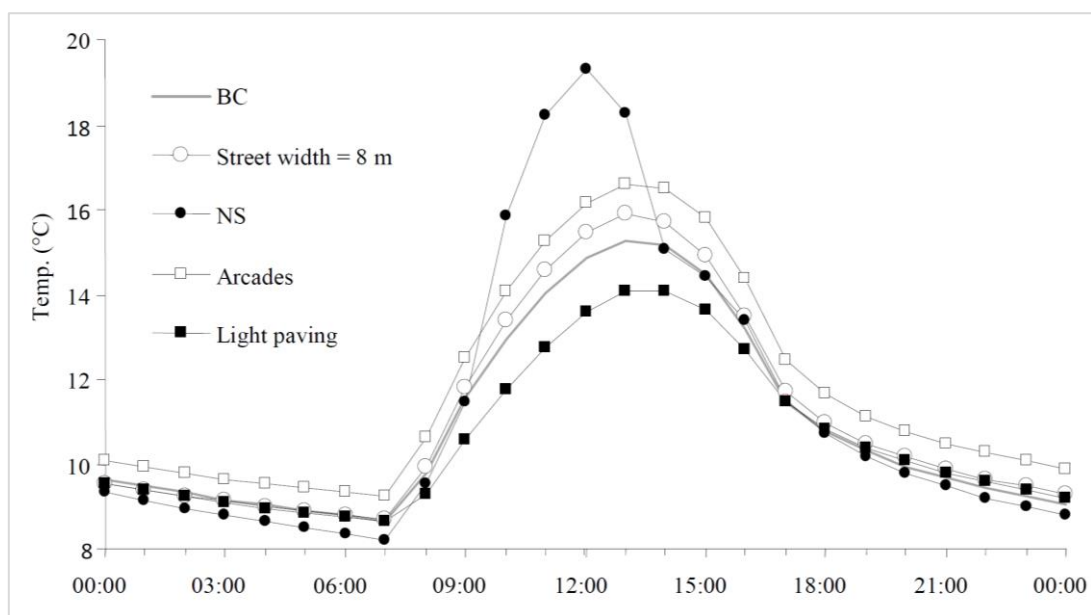


Figure 2.5. The air temperature for the winter conditions for all of the scenarios. Source (Al-Kurdi & Awadallah, 2015).

2.8 SUMMARY

This chapter has discussed thermal sensation in terms of comfort and discomfort effect on pedestrians in outdoors conditions. It presented the past and current literature related to the thermal comfort in the indoor environment and outdoor environment and their evolution throughout the past 50 years. The index chosen to assess the thermal stress in this study is the Physiological Equivalent Temperature (PET), which was used without a calibration to its comfort range as the current literature is not sufficient to ensure accurate results. The PET's main meteorological parameters have been discussed, which include air temperature, mean radiant temperature, wind speed and relative humidity. The software that was used to calculate the PET values was RayMan (discussed in Chapter 4: Methodology).

The recent literature shows a knowledge gap regarding the study of thermal comfort in Amman, Jordan, where the current limited research is focused on the change of air temperature and solar access rather than the study of the holistic elements and parameters of the outdoor environment. For this, the research focused on the main aspects of the urban environment. and their variations to test their impact on the outdoor thermal comfort (refer to Chapter 6).

Chapter 3 : Literature

Review on the Airflow

Inside an Urban Setting

Content

- 3.1 Introduction.
- 3.2 The urban surface.
- 3.3 Airflow.
 - 3.3.1 Standalone buildings (isolated)
 - 3.3.2 Arrayed buildings with uniformed heights.
 - 3.3.3 Street's canyons and intersections
- 3.4 Urban canyons configurations to reduce thermal stress.
- 3.5 The relationship between airflow and temperature.
- 3.6 Previous studies on the urban microclimate using numerical and computational (CFD) methods.
- 3.7 Summary.

3.1 INTRODUCTION

In this chapter, the main elements of the urban form are identified in terms of the effect they have on wind flow. The scale of the city is laid out from the microscale to the mesoscale to better understand the impact of the individual elements (e.g. buildings) compared to an array of buildings and eventually comparing it to the totality of the city.

3.2 THE URBAN SURFACE

Urban areas are estimated to cover only 0.05% of the Earth’s surface; however, their inhabitants are estimated to be more than half of the world’s population (Masson, 2006). The urban form has affected the climate of cities and changed it from the neighbouring countryside. Grimmond, et al., 1998, stated that the urban surface had changed the atmospheric parameters for the cities; this included the turbulences, the urban hydrology and pollution dispersion.

The urban environment is a combination of a smaller units arrayed and distributed across the city; these units include facets, elements, canyons, and blocks. They interact with each other to create the urban fabric A more detailed description of the units is displayed in Table 3.1 (Oke, et al., 2017).

Table 3.1. Classification of urban morphological units based on a 1-million inhabitant. Source (Oke, et al., 2017).

Urban units	Built features	Green and water features	Urban phenomena	climate	horizontal length scales	Climate scale
Facet	Roof, wall, road	Leaf, lawn, pond	Shadows, storage heat flux, dew, and frost patterns		10 x 10 m	Micro
Element	Residential building, high-rise, warehouse	Tree	Wake, stack plume		10 x 10 m	Micro
Canyon	Street, canyon	Line of street trees or gardens, river, canal	Cross-street shading, canyon vortex, pedestrian bioclimate, courtyard climate		30 x 200 m	Micro
Block	City block (bounded by canyons with interior courtyards), factory	Park, wood, storage pond	Climate of park, factory cumulus		0.5 x 0.5 km	Local
Neighbourhood or Local Climate Zone	City centre, residential (quarter), industrial zone	Greenbelt, forest, lake, swamp	Local neighbourhood climates, local breezes, air pollution district		2 x 2 km	Local
City	Built-up area	Complete urban forest	Urban heat island, smog dome, patterns of urban effects on humidity, wind		25 x 25 km	Meso
Urban region	City plus surrounding countryside		Urban ‘plume’, cloud and precipitation anomalies		100 x 100 km	Meso

Oke, et al., 2017, divide the urban surfaces into four categories based on their properties: the fabric of the urban environment, the surface cover, the structure of the urban environment and the urban emissions exchanges to the atmosphere (the urban metabolism). The urban surfaces affect the urban environment in different ways, where the urban fabric and cover affect the radiative fluxes with different materials properties on the ground level and the buildings height level (Figure 3.1). The wind flow is influenced by the geometry of the urban environment, and this includes the scale and structure of the urban elements, where the height, spacing and orientation of buildings significantly impact the local wind flow in terms of direction and magnitude (Figure 3.1). The following sections of this chapter will discuss the aforementioned geometry in the context of isolated buildings and groups, and their effect on the general wind flow behaviour.

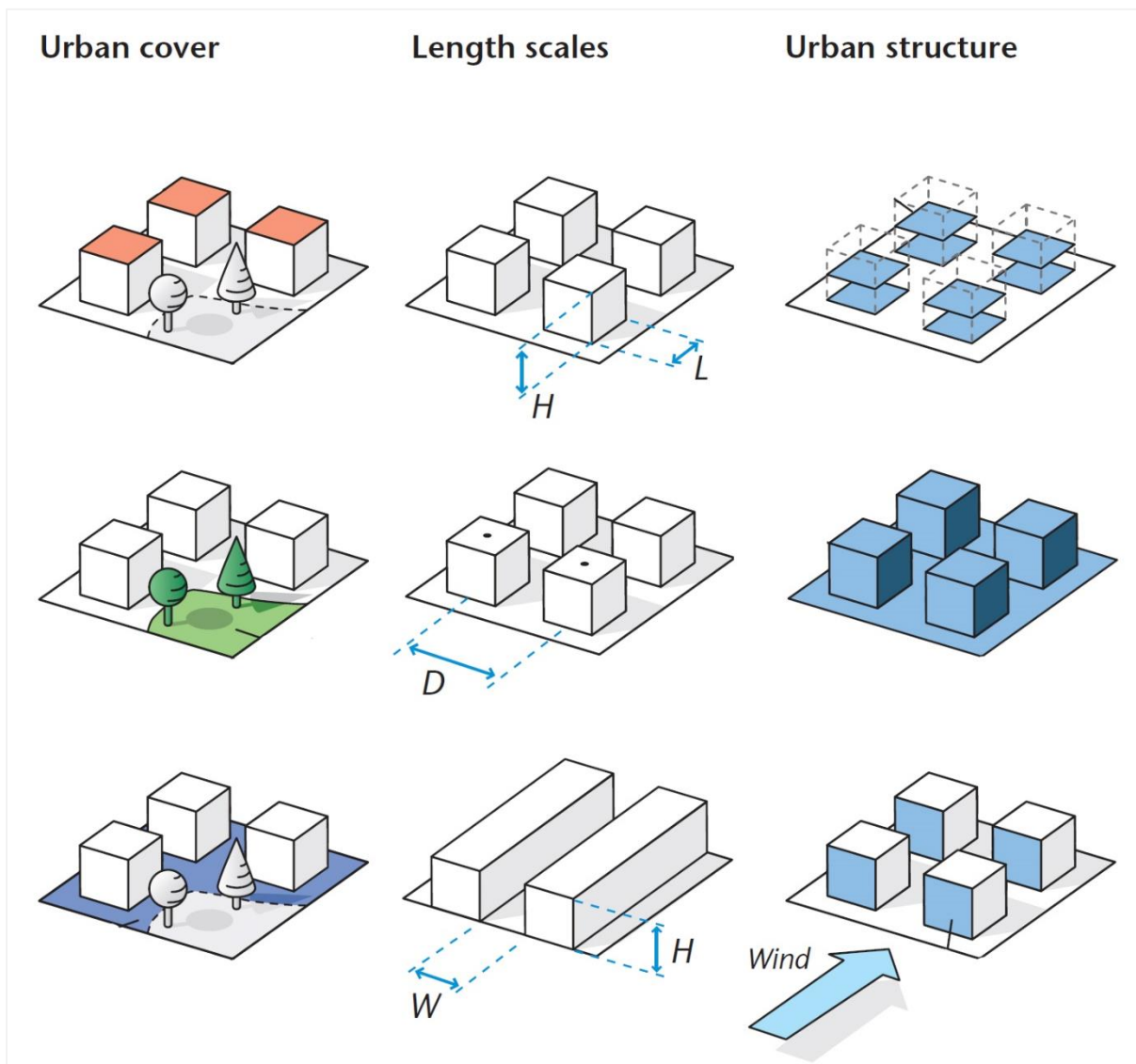


Figure 3.1. Urban cover parameters. Source (Oke, et al., 2017).

3.3 AIRFLOW

3.3.1 STANDALONE BUILDINGS (ISOLATED)

Obstacles in the urban environment dictate the airflow inside local microclimate; these interferences can be characterised by their attributes to thermal and mechanical effects (Sini, et al., 1996). In general, buildings tend to have a larger effect on the wind flow compared to vegetation as buildings are impermeable with, usually, sharp-edged shapes (Oke, et al., 2017). The airflow is perturbed through the drag forces and separation when coming in contact with buildings, and the mechanically formed turbulences are also influenced by the thermal characteristics of the buildings, where the radiative fluxes and moisture content also affect the production of turbulences (Paterson & Colin, 1986; Murakami, et al., 1987; Oke, et al., 2017).

The analysis of the airflow can be obtained by observation or by physical and numerical models. Most of the research on airflow is done using physical or computer models (Mathews, 1987; Razak, et al., 2013; Fuliotto, et al., 2010; Liu, et al., 2020); this is because the observation method is complex in nature, where the spatial and temporal parameters of the case studies require a significant number of sensors and time to operate these sensors with reliable data.

Oke, et al., 2017, describe in their book urban climates the interactions of airflow with an isolated building, which is studied in two directions. The first with the windward face is perpendicular to the approaching airflow, the second is the 45° rotation where the approaching airflow is facing the edge of the building. The approaching wind flow gets displaced due to the positive pressure on the windward surface of the building, indicated in Figure 3.2-B, the wind flow then proceeds and spreads vertically and horizontally above and around the building at the stagnation point which estimated about 60% of the height of the building as seen in Figure 3.3.

The vortices around the building are formed due to the zones of negative pressure which causes the wind to circulate in the opposite direction of the main wind flow, these zones are located on the roof, sides of the buildings and the backside of the building (leeward), as indicated in Figure 3.3 At the backside of the buildings, a cavity zone is formed due to the

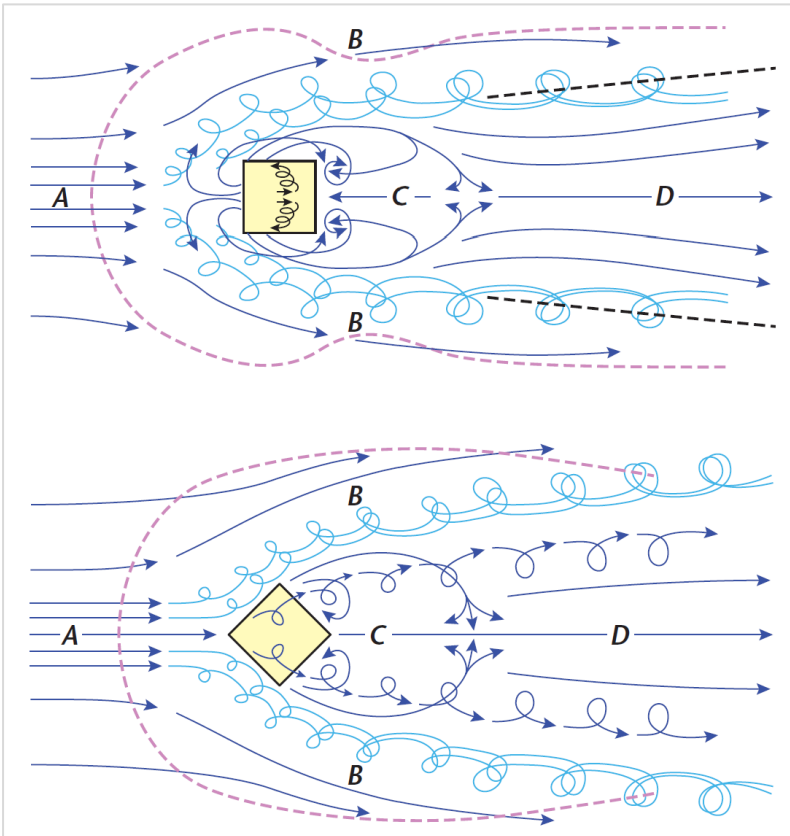


Figure 3.2. The airflow behaviour around a cubic building. A is the approaching wind flow, B is the displacement zone, C is the cavity zone and D is the wake zone. Above, approaching wind direct at the face of the building. Below, approaching wind directed 45° at the edge of the building. Source (Oke, et al., 2017).

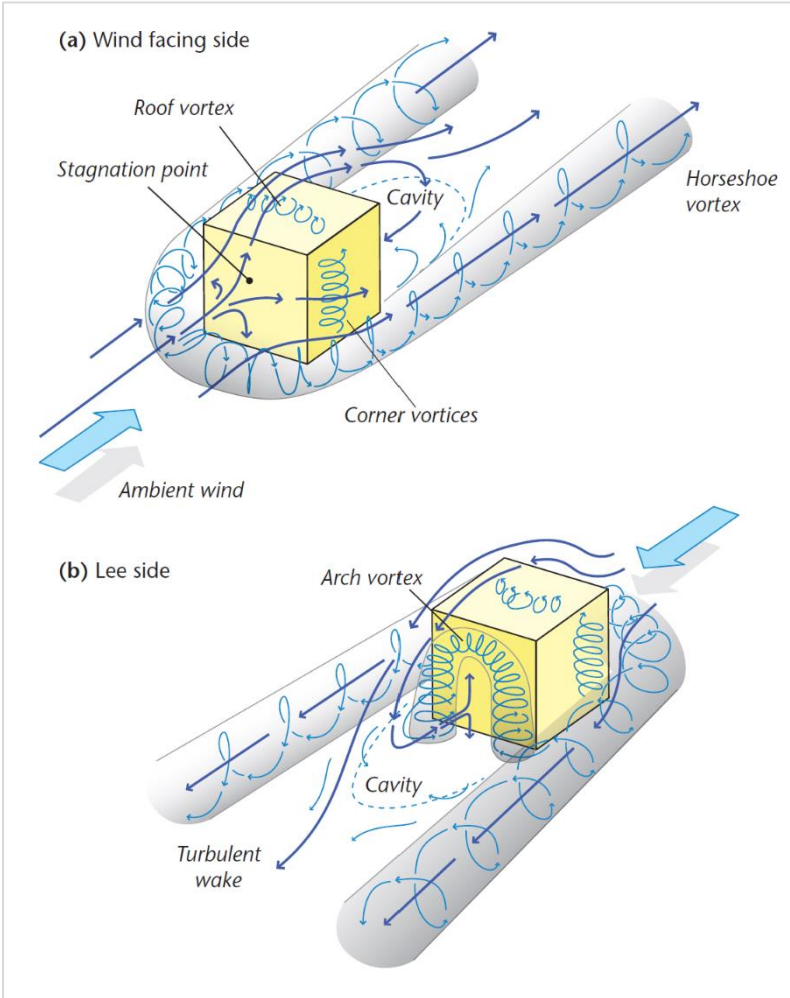


Figure 3.3 Airflow characteristics. Source (Oke, et al., 2017).

separation flow creating a suction zone (Figure 3.2-C), the cavity zone dimensions are controlled by three separation streams, these streams are: the stream over the roof along the direction of the mean wind flow, and two streams from both sides of the building (Meroney, 1982; Oke, et al., 2017; Tse, et al., 2017). The cavity dimensions spread as far as the building edges both vertically and horizontally. However, it spreads to 2-3 times the height of the building in the along-wind direction, and if the building height is shorter than its (Meroney, 1982) width, the cavity can reach up to 12 times the height of the building (Meroney, 1982). The cavity zone is responsible for the downwash phenomenon, where pollutants get sucked from the surrounding separation streams into the cavity. The wake zone, indicated in Figure 3.2-D, is where the mean kinetic energy is extracted, and turbulent kinetic energy is generated. The wake usually extends 3 to 4 the height of the building and can reach up to 30 times the building's height in the along-wind direction (Murakami & Mochida, 1989; Meroney, 1982; Oke, et al., 2017; Khanduri, et al., 1998).

Moreover, if the approaching wind is directed at 45° angle where it hits the edge of the building rather than the windward face (Figure 2), the flow would separate as it did in the first case; however, the main difference in the second case is the creation of two rotating streams that start at the two edges of the roof and continue down the building to join the downstream into the wake. The result is a smaller cavity zone and an increase in wake flow but a slower growth rate (Meroney, 1982; Oke, et al., 2017). The differences in shapes and heights of buildings will produce different results, but the main principles will still apply on isolated buildings, however, in an urban environment, the buildings are in close proximity to each other's, this causes the wakes to overlap and change the main principle discussed in an isolated building, the next section will discuss these changes in the form of arrayed buildings.

3.3.2 ARRAYED BUILDINGS WITH UNIFORM HEIGHTS.

The urban environment consists of multiple units, this means that the urban canyons would vary in height, length, and width. To simplify the wind analysis, the following description of the wind interactions inside an array of buildings will assume that the buildings have the same height. The wind flow is affected when the wake of the flow for two buildings are overlapping this sets three possible cases, the first case is when the buildings are too far apart so the wakes are not affecting each other's, the second case is when the buildings are close enough for the wakes to overlap, and the third case is when the buildings are too close so the mean

wind flow skips over the roofs of the buildings. Oke, et al., 2017 set these three cases at $H/W < 0.35$, $0.35 < H/W < 0.65$, and $H/W > 0.65$ consecutively as seen in Figure 3.4.

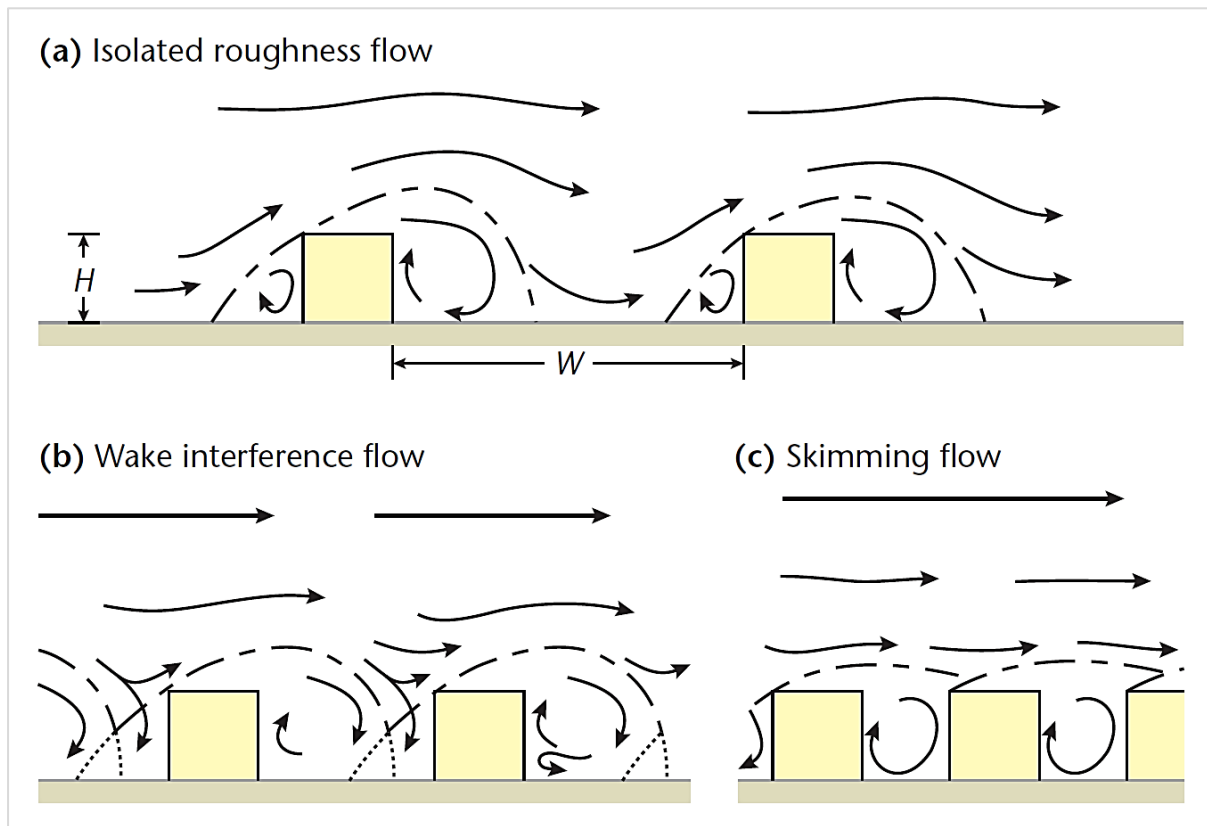


Figure 3.4. Wind flow behaviour on different H/W in an urban environment. Source (Oke, et al., 2017). (Modified after: (Oke, 1988; Hussain & Lee, 1980))

In the first case, the buildings' airflow interactions are treated like the isolated buildings, the only change occurs at the lateral wakes when the array of buildings is staggered or random. In the second case, the cavity of the upwind building starts to get disturbed by the downflow from the windward face of the adjacent building, this creates a fluctuation in the velocity of the vortices at small time intervals. In the third case, which is the closest to an urban environment, the airflow from the roofs skips over the street canyon to the next rooftop, this creates a vortex flow inside the street canyon circulating opposite to the above mean wind flow, which results in limited mixing between the street canyon air and the above mean airflow (Hussain & Lee, 1980; Oke, 1988; Oke, et al., 2017; Coceal, et al., 2006; Sini, et al., 1996).

3.3.3 STREET CANYON AND INTERSECTIONS

The street canyon configurations are an important aspect of the urban environment, due to their impact airflow and pollutants dispersion. The rate of dispersion is governed by the speed and angle of the approaching airflow, as well as the location in the urban canyons (Riain, et al., 1998). The airflow inside the street canyons can be summarized into three main interactions based on the angle of the approaching flow: (i) parallel to the street canyon or up to 30° entering angle; (ii) perpendicular to the street canyon and (iii) a flow angle between 30° and 90° (Oke, 1997) – see Figure 3.5. When the approaching wind is perpendicular to the street canyon, the flow skips the canyon at the roof level, and this creates a vortex in the cavity zone in the leeward face of the buildings reinforced with the downwind from the next building windward face (Louka, et al., 2000; Belcher, 2005; Oke, et al., 2017). In the case of pitched roofs, the vortex formation is weaker due to the geometry of the roofs that inhibits the formation of the shear layer at the roof level that feeds the vortex below (Kastner-Klein, et al., 2004).

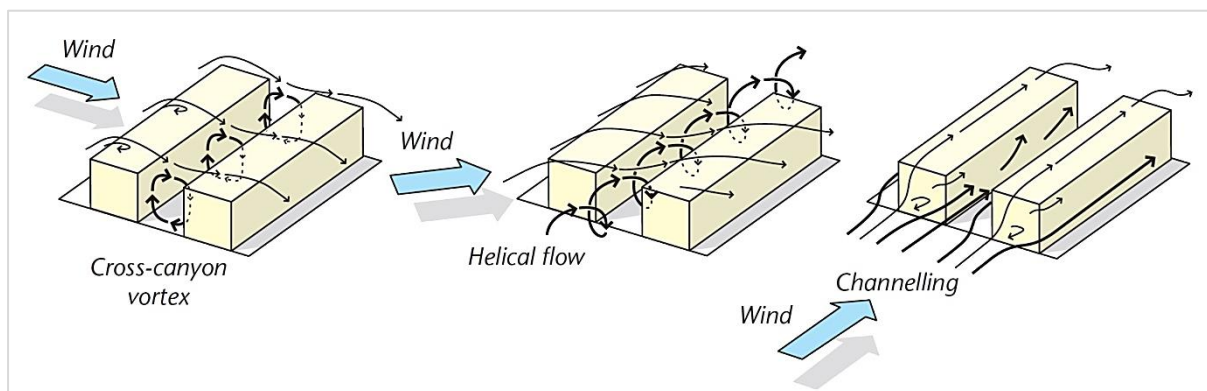


Figure 3.5. Airflow interactions inside an urban canyon. Source (Oke, et al., 2017). (Modified after: (Oke, 1997; Belcher, 2005)).

The approaching wind flow gets channelled in the street canyon when a strong transport is created, in this case, the angle of the flow is estimated between 0° and 30° and is depended on the dimensions of the canyon (Nakamura & Oke , 1988; Johnson & Hunter , 1999; Oke, 1997). When the flow enters the canyon in angle larger than 30° , the flow inside the canyon is a result of a superposition of the channelling flow and the cross-canyon vortex (Johnson & Hunter , 1999; Belcher, 2005). The flow is described as a helical flow that spirals down the canyon length (Oke, et al., 2017).

The airflow inside of a canyon is affected by other factors, this includes thermal masses and traffic (Oke, et al., 2017). The cross-canyon vortex is affected by the heated walls in its vicinity, where it can be reinforced or weakened depending on the location of the wall. The walls are heated by solar radiation where the adjacent air to these walls heats up and rise, the parcels of risen air reinforce the vortex when the heated wall is on the windward face of the building, and weakens the vortex when the heated wall is on the leeward face of the building (Sini, et al., 1996). Additionally, the night radiative cooling causes airflow mixing due to the Katabatic wind (Manins & Sawford, 1979), where it flushes the cooler rooftops air down to the warmer urban canyons. This negative buoyancy causes the warm air to flush up the urban canyon, reducing the pollutants concentrations and alleviating the canyon's sensible heat (Savijärvi & Jin, 2001; Nkemdirim, 1980). The airflow is also affected by the heavy vehicular traffic in urban canyons, where it causes a mechanical disturbance in the flow. This effect is mostly observed when the velocity of the approaching airflow is weak, where in one-way traffic the flow is governed by the speed and direction of the traffic (Oke, et al., 2017).

The street intersections are an important part of the urban geometry; however, they contain high concentrations of pollutants. The main reason the pollution rates are high in intersections is the nature of the urban use of the area, as vehicles slow down and repeatedly stop throughout the day resulting in a significant amount of pollutants emissions. Additionally, the urban canyons feed these areas with the flushed-out particle through the helical and channelling flow, increasing the pollutants count (Oke, et al., 2017). There have been several in situ studies on the vehicles' emissions near street intersections (Rosas , et al., 1980; Bullin, et al., 1982). Results showed that the concentrations of vehicle emissions vary at the intersections. Several empirical models were developed based on the data collected; however, they cannot be used in the urban environment as the settings that were used in the experiments were open areas and the models did not take into consideration the effect of the surrounding buildings (Soulhac, et al., 2009).

To study the flow interactions within an intersection, a numerical model of a symmetrical intersection was built to simplify the process. The geometry and aspect ratio of the streets are similar to each other, with streets direction denoted by the main cardinal directions (North, East, South and West). As seen in Figure 3.6, the main angles that were investigated were 0°, 15°, 30° and 45°. These four cases give a general representation of the wind

interactions inside a symmetrical intersection. Beyond the area of the intersection, Dobre et al., 2005 show that the airflow retains its behaviour into a channelling or helical flow at a short distance from the intersection.

When the approaching wind blows at 0° as seen in Figure 3.6, a channelling flow is generated along the (West-East) street; however, some of the flow escapes in to the side streets (North and South), where corner vortices are created. The corner vortices dimensions stretch to about half of the street's width and they are characterised with low air velocity which results in low dispersion of pollutants (Soulhac, et al., 2009; Oke, et al., 2017; Scaperdas & Colvile, 1999). In the case of 15° , the channelling flow is weakened a little and more of it is directed to the northern street, while a helical flow starts to form in the southern street that feeds the channelling flow in the (W-E) street (Oke, et al., 2017; Soulhac, et al., 2009). At 30° , the airflow in both of the streets (W-E) and (N-S) are helical flows, with (W-E) street having a stronger flow as per to the attacking angle. The flow from west to north is larger than the two previous cases which results in stronger corner vortices with higher velocity and larger dimensions (Soulhac, et al., 2009; Oke, et al., 2017). At 45° , both of the streets develop a helical flow of similar strength, where the western street feed the northern street and southern street feeds the eastern street and a conveyor-belt is created in the middle of the intersection that flows up and over the roof (Scaperdas & Colvile, 1999; Oke, et al., 2017; Soulhac, et al., 2009).

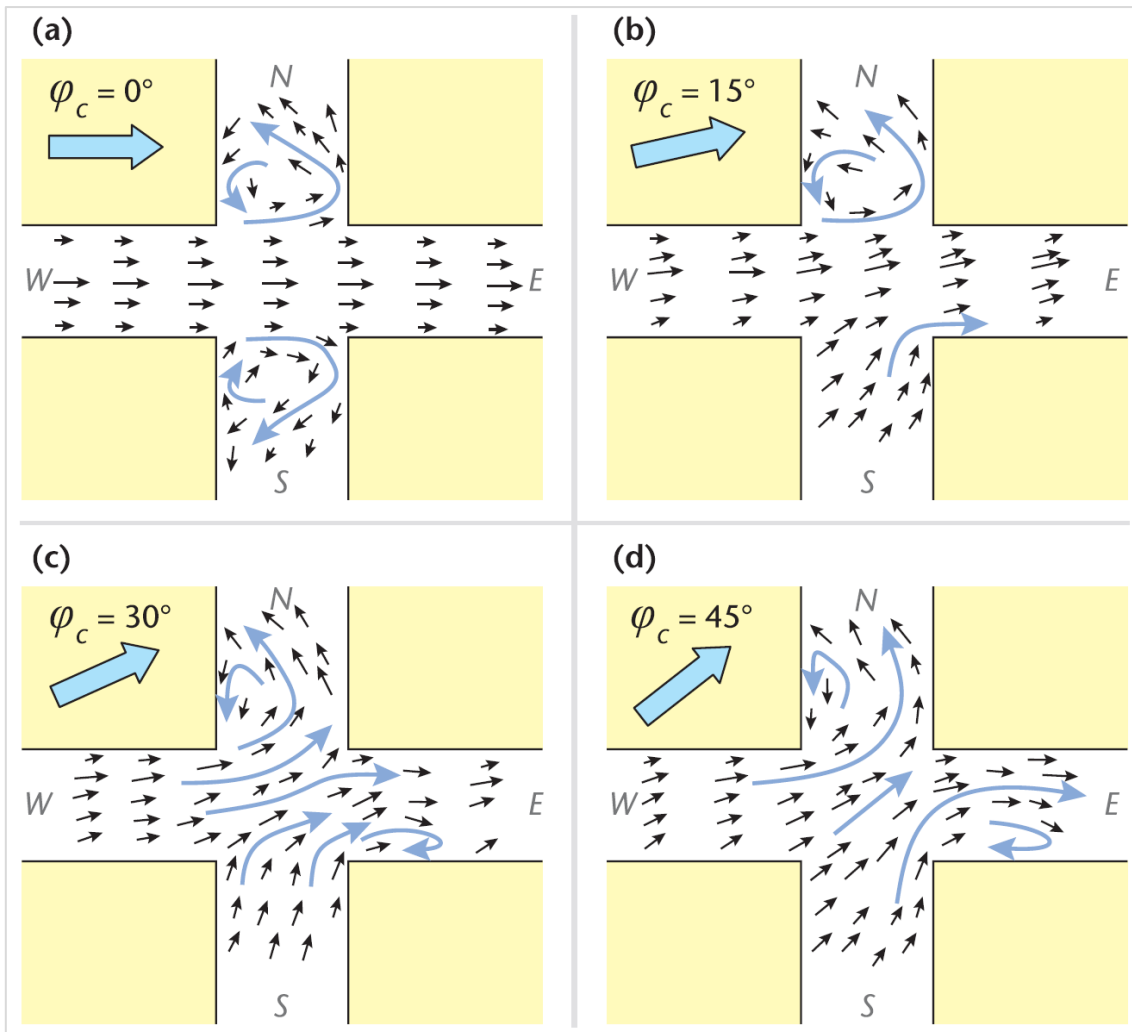


Figure 3.6. Airflow behaviour with street intersections. Source (Oke, et al., 2017). (Modified after: (Soulhac, et al., 2009)).

3.4 URBAN CANYONS CONFIGURATIONS TO REDUCE THERMAL STRESS.

The microclimate of the urban environment is affected by multiple factors, such as the vegetation, the water features, the urban geometry, the urban orientation, and materials (Francis & Jensen, 2017; Santamouris, 2014; Gago, et al., 2013; Aleksandrowicz, et al., 2017). If these factors are not appropriately implemented, the air temperature in the urban environment rises in comparison with its counterpart, the suburbs. This increase in air temperature is called the urban heat island (UHI) (Santamouris, et al., 2019; Oke, 1988; Oke, 1997). The urban heat island is a well-documented phenomenon, and it has been found that over 400 cities across different climatic zones have recorded an increase of air temperature in urban canyons between 5 °C to 10 °C (Santamouris, 2016).

Many studies were conducted in relation to the urban canyon and urban environment configuration. These studies analysed the urban canyon in two main configurations -

symmetrical (Akubue, 2019; Panagiotou, et al., 2013; Xi, et al., 2012; Ali-Toudert & Mayer, 2006; Santamouris, et al., 2019; Tominaga, et al., 2015) and asymmetrical canyons (Antoniou, et al., 2017; Todhunter, 1990; Ali-Toudert & Mayer, 2007). The parameters studied included the H/W ratio, orientation, and roof shapes. The aim of the present research is to analyse the geometrical aspects of a residential setting, where most of the canyons and street intersections tend to have symmetrical features. Moreover, the main objective of studying the symmetrical canyons is to establish a relation between the meteorological parameters of an area's microclimate and the built environment, where the possibility of building formation can be endless, with different heights and shapes. For this study, the analysis focused on the symmetrical canyons and their effects on pedestrians' thermal comfort where it could be applied in further complex formations.

Ali-Toudert and Mayer, 2007 studied five cases of urban canyons with different geometries to analyse their effects on thermal comfort, as seen in Figure 3.7. The buildings' heights were 16m, 8m, and 12m for H₁-H₃ consecutively, with street width of 8m. The study was conducted in Ghardaia, Algeria, which is characterized by a hot arid climate. The analysis compared a symmetrical canyon with H/W ratio of 2 (case 1) with two cases of asymmetrical canyons (cases 2 and 3 in Figure 3.7), the results showed that case two tended to have cooler air temperature around 17:00 when the area is shaded. Moreover, case 2 was more open to the sky with a sky view factor of 0.46 vs 0.39 in case 1. This indicates that the air was being cooled faster due to higher SVF. The same has been found in case 3 when compared to case 1, with faster cooling of the air at night due to higher SVF. In the case of vegetation addition, the study found that the air temperature was reduced significantly, where it changed from 38.8°C to 37.3 °C in the case of H/W =2 and showed a maximum change of air temperature of 2.6 °C in the case of H/W =1. The study included multiple parameters to study the proposed cases; however, the H/W ratio was not further investigated in relation to symmetrical or asymmetrical aspects of the canyons, which leaves a significant gap on the analysis of the urban canyons and their relation to thermal stress at the pedestrian level.

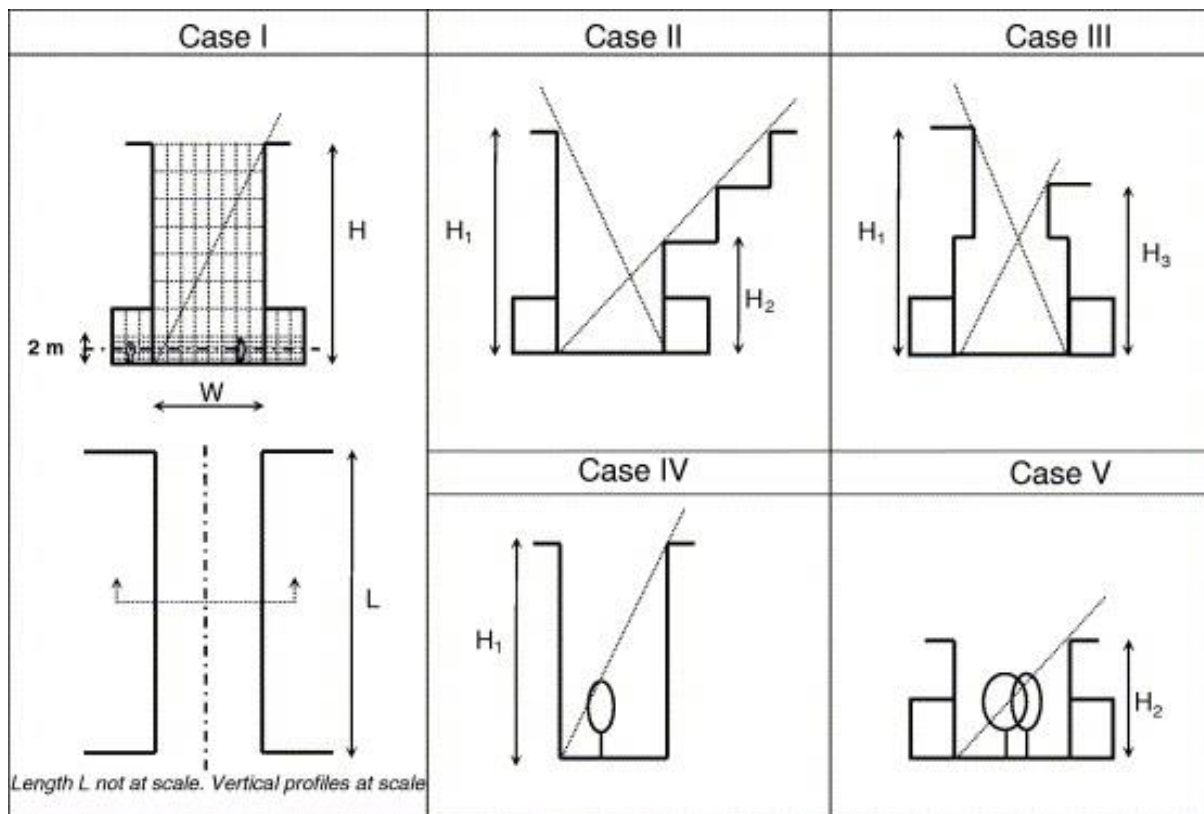


Figure 3.7. The studied cases. Source (Ali-Toudert & Mayer, 2007).

Air temperature in simple canyons is affected by the orientation of the canyons, where the west-east orientation tends to have higher air temperatures due to more early morning/late afternoon solar access, which increases the transferred sensible heat (Ali-Toudert & Mayer, 2006). Some field studies have shown that the geometry of an urban canyon as an isolated factor has a small effect on the air temperature compared to other factors such as wind speed and solar access (Nakamura & Oke, 1988; Yoshida, et al., 1990-1991).

Du et al., 2019 proposed an optimization method to design an ideal urban canyon that would produce the least thermal comfort stress. The study considered the canyons as uniform buildings, with variations of width, height, and spaces between the buildings. It also introduced the concept of the buildings lift-up as a mean of enhancing the wind flow inside the studied area. The results showed that for an ideal canyon, the most significant factor that influenced the thermal comfort was the gap between the buildings, and the H/W ratio. This study in concept correlates directly to the present research, however, the method of building the studied area was very general to the urban fabric, and this thesis is more focused on the residential setting of Amman, Jordan.

The literature shows an abundance of research done on urban canyons and their effects on thermal stress, and this included adjustment on the urban canyon’s geometry to enhance the thermal comfort (Mirzaei & Haghighat, 2011; Ali-Toudert & Mayer, 2006; Chatzidimitriou & Yannas, 2017; Mirzaei & Haghighat, 2010; Xi, et al., 2012). Other studies focused on improving the wind flow as a mitigating approach to reduce the UHI (Hang, et al., 2009; Ramponi, et al., 2015; Du & Mak, 2018; Kubota, et al., 2008; Ho, et al., 2015; Liu, et al., 2017). Moreover, the materials of the urban canyon have also been studied in terms of their solar reflectivity and absorption to reduce the thermal stress at the pedestrian level (Rossi, et al., 2016; Rosso, et al., 2016; Matias & Lopes, 2020; Manni, et al., 2019; Akbari, et al., 1992; Priyadarsini, et al., 2008; Sen & Roesler, 2019; Rosso, et al., 2018; Lobaccaro, et al., 2019). A summary of the previous studies on the urban canyon is listed in Table 2.

Table 3.2. Previous studies on the urban canyons.

Authors	Location	Climatic Zone	Main Findings
(Nunez & Oke, 1977)	Vancouver, Canada.	Temperate	The energy regime in the urban canyons are significantly affected by its geometry due to solar access. 70% of the radiative heat stored in the canyon is dissipated during the day through wind exchanges, and 30% is stored in the canyon’s materials. At night, the dissipation depends on the heat released from the materials.
(Mayer & Höppe , 1987)	Munich, Germany.	Temperate	The results showed that the lowest air temperature values were recorded near the trunk of the tree which was similar to the air temperature in canyon facing north, with an average air temperature difference of 4.6 K. while the highest air temperature values were recorded at the canyons facing north due to increased solar access.
(Nakamura & Oke , 1988)	Kyoto, Japan	Hot Humid	The wind flow inside the canyon is directly related to the flow above the buildings, air temperature values above and within the canyon are similar with an average difference of °C; however, significant air temperature values difference occur around surfaces that receive direct solar radiation.

(Golany, 1996)	-	Hot arid	The results showed that the orientation of the urban canyon could be used in different ways depending on the parameters of the area. Canyons oriented in the direction of the wind flow is more beneficial in increasing the wind speed through the channelling flow, however, if the studied area suffered from hot wind that carried dust throughout the day, a 90 degrees tilt in the urban canyon orientation would be more beneficial in reducing the thermal stress as well as dust. Moreover, the addition of vegetation in the direction of windward facades would help in reducing the solar access and reduce dusty wind.
(Johansson, 2006)	Fez, Morocco.	Hot Dry	The results showed that the maximum air temperature decreased with higher H/W ratio; however, the minimum air temperature increased with increased H/W ratio due to a restricted SVF. Deep canyons with H/W of 10 (alleyways) recorded lower air temperatures than shallow canyons, but it also recorded weak cooling effect at night.
(Alexandri & Jones, 2008)	London, UK. Montréal, Canada. Moscow, Russia. Athens, Greece. Beijing, China. Riyadh, KSA. Hong Kong, Mumbai, India. Brasilia, Brazil.	Temperate Subarctic Continental Mediterranean Steppe Desert Subtropical Rain forest Savanna	The addition of green roofs and green walls reduced the air temperature significantly in hot arid climates, where the results showed a maximum decrease in air temperature of 11.3 °C and an average of 9.1 °C. In a hot humid climate, the results showed a maximum decrease of 8.4 °C. The green walls strategy recorded its smallest effect on air temperature in wide canyons.
(Andreou, 2013)	Tinos, Greece.	Mediterranean	Vegetation added to the site in the traditional area produced better PET levels by 2 °C due to shading despite the fact that wind speed is lower than contemporary site. The albedo had a small effect on the thermal stress when compared to the urban geometry effect. Wind speed can affect the thermal stress if the orientation chosen for the urban canyon is favourable.

(Abreu-Harbich, et al., 2014)	Campinas, Brazil	Tropical	The results showed for the urban canyon studied that, orienting the streets in the northeast-southwest direction reduced the PET value the most. The Canyons with H/W ratio of 2 and higher provided shading, which helped in reducing the effect of solar radiation. The vegetation addition is better suited for canyons of H/W of 0.5 in order to introduce shading to the area.
(Perini & Magliocco, 2014)	Milan, Genoa, and Rome, Italy.	Mediterranean	The air temperature inside the canyons is affected by the addition of the vegetation, the amount of temperature change due to greenery is connected to several factors, where the results showed a higher impact on the air temperature with increased height of the building. However, increasing the density of the urban environment showed an increase in the air temperature, mean radiant temperature and PMV values. The vegetation cooling effect was found to be stronger when the relative humidity is low, and the air temperature is high.
(Morakinyo, et al., 2017)	Hong Kong	Subtropical	The study investigated eight trees species inside urban canyon. The result showed that the shade cast from the trees lowered the PET levels by a maximum value of 12 °C for a generic type of tree. The Leaf area index (LAI) has shown to be the most influential factor among the trees species in reducing the thermal stress in a canyon, where the high LAI showed a decrease in PET levels of 17.2 °C which changed the thermal sensation from “very hot” to “hot”.
(Lamarca, et al., 2018)	Concepción, Chile	Coastal Temperate	Canyons in a temperate climate are affected significantly by the orientation of the streets. Results showed that directing the urban canyon diagonally would benefit the thermal stress.
(Vallati, et al., 2019)	Milan, Italy.	Mediterranean	The paper addressed the urban canyons in a 3-D model. The results showed that the convection heat transfer coefficient (CHTC) is significantly affected by the canyon’s geometry (H/W) as well as the solar radiation.

			The CHTC is 50% higher in the windward facades when compared to the leeward facing façade. It was also found that the temperature of the walls increased with the increased H/W ratio.
(Deng & Wong, 2020)	Nanjing, China.	North subtropical monsoon	The results showed that the canyons with low H/W ratio displayed lower air temperature than canyons with high H/W ratio due to higher SVF. Air temperature values were at their minimum for all the canyons when the streets were oriented in the NE-SW direction. When the canyons were oriented in the NE-SW direction, the effect of the H/W ratio was less substantial.
(Morakinyo, et al., 2020)	Hong Kong	Subtropical	The study investigated the effect of SVF on the PET values in different canyons, where shallow canyons with high SVF recorded high PET values, and deep canyons with low SVF recorded low PET values, this was linked to the amount of solar radiation permitted into the canyons due to buildings heights, where deep canyons showed a significant PET levels improvement from “very hot” to “warm” when compared to open areas. The results of trees planting in different SVF canyons showed that the vegetation impact of the same trees’ species differed in the studied canyons, where canyons with SFV less than 0.45 had no significant influence on the thermal stress due to the building's shading outweighing the vegetation shading. However, trees planting showed substantial results in canyons with SVF higher than 0.6.

3.5. THE RELATIONSHIP BETWEEN AIRFLOW AND TEMPERATURE.

Airflow inside the urban setting affects the thermal environment, where the favourable airflow can release some of the heat stress in the urban canyons (Niachou, et al., 2008). For example, Müller et al., 2014 studied several elements to reduce the thermal stress through CFD modelling in Oberhausen, Germany. This included vegetation, water features and wind velocity. Their results have shown that the wind velocity factor was the most effective in reducing the thermal stress, where the vegetation recorded higher reductions than the water features due to the coupling effects of shading and evaporation. The airflow can be adjusted by controlling the urban geometry, this includes buildings heights, orientation and dimension of the urban canyons as well as the overall density of the urban sitting (Blocken & Carmeliet, 2008; Richards, et al., 2002; Oke, et al., 2017; Coceal, et al., 2006).

Ferreira et al., 2002 studied the effects of building structures on the airflow at the pedestrian's level. The study used a numerical (k-ε RNG model) and physical (1/175 scale) models to determine the extent of the buildings' influence. The study consisted of adding and removing two auxiliary buildings to an existing site in Lisbon, Portugal, where the wind velocity is described to be very high. The results have shown that the presence of the auxiliary buildings decreased the velocity of the wind, which in this specific location has increased the pedestrian level of comfort. Additionally, Zhang et al. 2012 have analysed the wind flow patterns around an under-construction isolated building in a university and concluded that the wind speed and thermal sensation could be adjusted with few changes to the buildings' façades and plan density.

The air temperature in the urban canyon is significantly influenced by the temperature of the surfaces of said canyons (Santamouris, 2014; Priyadarsini, et al., 2008; Sen & Roesler, 2020). The surfaces' temperatures are governed by the airflow inside the canyon, where airflow elevates the sensible heat trapped in the materials through the process of convection. Airflow can be adjusted through the proper planning of the canyon's orientation which depending on the location, can increase the speed of the airflow. Aliabadi et al., 2019 studied an existing urban canyon in Ontario, Canada, and analysed eight different directions of the wind flow. The results showed an increase in air temperature when the wind is perpendicular to the street canyon and a slight decrease when it is along the canyon axis.

Sen and Roesler, 2020, analysed the effect of wind directions on the urban heat island levels in Chicago, USA. The study investigated eight directions in a hypothetical urban scenario of nine buildings uniformly positioned in a 3x3 grid (Figure 3.8). The data were collected from 12 locations in the model which represented 12 different canyons with the same H/W ratio, this is important as the approaching wind angle will affect the different canyons based on their locations in the model. The results were analysed in term of the UHI intensity, which was calculated by finding the difference between air temperature in the studied canyons and the air temperature in the rural areas, as shown in Table 3. The results showed that, wind direction correlates directly with reducing the air temperature values, where the parallel directions to the street canyons showed the highest reduction in air temperature of 4.16 °C (highlighted in yellow in Table 3) with an average reduction of 4.41 °C.

The reduction in air temperature seen in Table 3 is due to the channelling flow generated in the canyons; however, the air temperature increased at the opposite end of the canyon away from the approaching wind due to wind speed decreasing along the canyons. The inner canyons (4,6,7 and 9) recorded the highest air temperatures due to their position, where wind speed was decreased (highlighted in red in Table 3.3). The study demonstrated the relationship between the wind speed and air temperature inside the urban environment, and how this relationship is governed by the location and orientation of the canyons. These results correlate with the present research of calibrating the street grid to produce the best airflow for pedestrians' comfort; however, the study did not investigate further buildings arrangement which would directly affect the wind speed values.

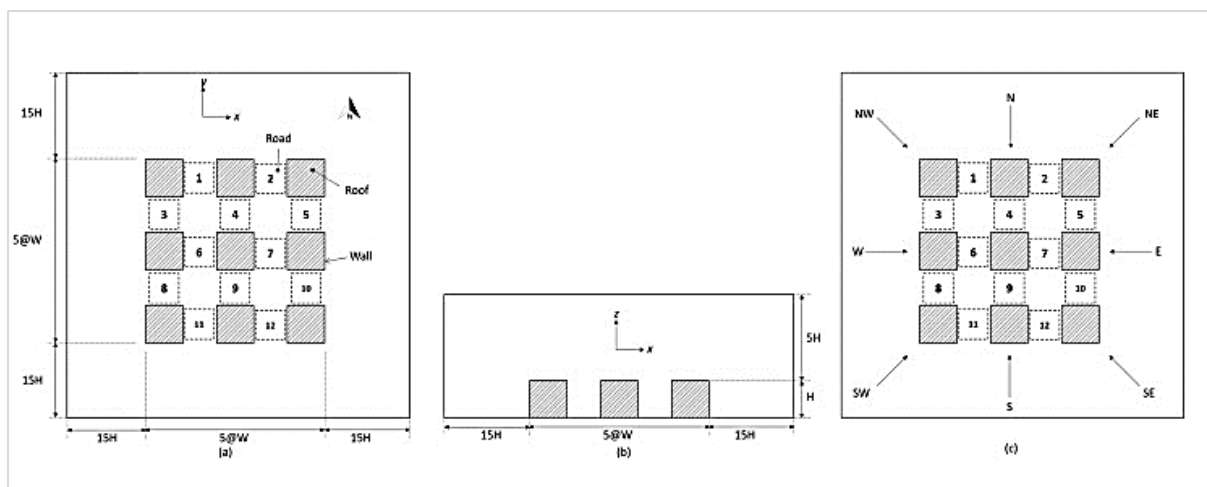


Figure 3.8. The hypothetical urban area studied. Source (Sen & Roesler, 2020).

Table 3.3. The UHI intensity in °C for all the studied urban canyons with eight wind directions. Source (Sen & Roesler, 2019).

Canyon	Wind direction							
	N	NE	E	SE	S	SW	W	NW
1	4.16	4.3	4.55	4.69	4.38	4.4	4.45	4.31
2	4.16	4.31	4.45	4.4	4.38	4.69	4.55	4.3
3	4.45	4.47	4.38	4.8	4.55	4.31	4.16	4.33
4	4.56	4.53	4.29	4.67	4.69	4.67	4.29	4.53
5	4.45	4.33	4.16	4.31	4.55	4.8	4.38	4.47
6	4.29	4.73	4.69	4.73	4.29	4.49	4.56	4.49
7	4.29	4.49	4.56	4.49	4.29	4.73	4.69	4.73
8	4.55	4.8	4.38	4.47	4.45	4.33	4.16	4.31
9	4.69	4.67	4.29	4.53	4.56	4.53	4.29	4.67
10	4.55	4.31	4.16	4.33	4.45	4.47	4.38	4.8
11	4.38	4.69	4.55	4.3	4.16	4.31	4.45	4.4
12	4.38	4.4	4.45	4.31	4.16	4.3	4.55	4.69
Average	4.41	4.5	4.41	4.5	4.41	4.5	4.41	4.5

Al-Sallal and Al-Rais, 2011 and 2012 analysed the urban environment in a traditional and a modern context in a hot arid climate of Dubai, UAE. The results showed that, in the traditional urban areas, airflow was restricted due to the curved nature of the streets. This was more noticeable when wind speed was lower than 3 m/s. However, the airflow showed better results in reaching deeper parts of the traditional area when speeds exceeded 5 m/s. In the case of the modern urban area in Dubai, the airflow moved freely due to wide streets and high buildings, this flow was increased with canyons with an aspect ratio of 1.75. Additionally, the built fabric of the modern areas consisted of elements that did not exist in the traditional areas, such as open spaces and parking lots. The airflow in these areas was unobstructed, where wind speed reached a maximum of 4.55 m/s; however, the airflow in the long canyons of Dubai recorded low wind speed of 0.51 m/s in winter and 1.52 m/s in summer. The study gives a valuable insight towards the uniformed modern urban fabric vs the traditional more organic fabric, however, the study did not consider any modification on the analysis of the modern area to test the effect of urban geometry on the thermal stress.

3.6 PREVIOUS STUDIES ON THE URBAN MICROCLIMATE USING NUMERICAL AND COMPUTATIONAL (CFD) METHODS.

Studying the airflow in a three-dimensional manner from on-site data collected through observation is a complicated procedure (Zajic, et al., 2003; Santamouris, et al., 1999; Arnfield & Mills, 1994; Nielsen, 2000). The task of analysing the wind behaviour in an urban environment requires the use of multiple sensors that would record over long periods of time due to the wind's temporal variability (Oke, et al., 2017; Moonen, et al., 2012; Blocken, 2014). As a result, the majority of the knowledge on wind behaviour is obtained from numerical models and CFD simulations (Aishe, et al., 2005; Johnson & Hunter, 1998; Deng & Wong, 2020; Blocken & Persoon, 2009) and physical models (Scaperdas, et al., 1999; Ferreira, et al., 2002; Tsonis, et al., 1987; Zhou & Zhou, 2020; Ferreira, et al., 1998). The CFD method is a very effective method for analysing the complex interactions inside the urban environment, it reduces the time needed to test limitless urban configurations with few restrictions to spatial or temporal variables as in the in-situ observation method or wind tunnel tests.

In recent years, the advances in computational resources has pushed the study of the urban microclimate to numerical simulation approaches (Toparlar, et al., 2017; Moonen, et al., 2012). The two main approaches that has been used in numerical simulations are the Energy Balance Modelling (EBM) and the Computational Fluid Dynamics (CFD) (Mirzaei & Haghighat, 2010). The EBM approach's main advantage is that it is very quick and does not need large computational power. However, the EBMs have a significant weakness where they decouple the airflow from the temperature model, which may result in inaccurate data. Moreover, the studied parameters in the model may vary in time-steps, which make the model results unreliable. This can be corrected by reducing the time-step, however, by doing the running time will increase, which defeats the main advantage of using EBMs (Mirzaei & Haghighat, 2010). CFD modelling simulates all of the urban microclimate parameters in the same domain, unlike the EBM, the CFD approach generates more accurate results that can be simulated in different scales, microscale, mesoscale and indoor settings. However, the CFD approach demands very high computational power when compared to other approaches, e.g. EBM (Murakami, 2006; Mirzaei & Haghighat, 2010). The present research uses the CFD approach through simulations performed using ENVI-met software. The use of ENVI-met was mainly for its wide range of output data - for example, it generates the airflow field with high

accuracy using the Reynolds Averaged Navier Stokes (RANS) equations and Yamada & Mellor E-ε turbulence model. It also calculates the thermal comfort index PET and provides data for air temperature and relative humidity. It should be noted that the ENVI-met interface has been adjusted in the past few years to be user-friendly, with individual extensions to build the model.

There have been multiple CFD tools used in the recent research to study the urban microclimate, with different turbulent modelling approaches. Table 3.4 represents an overview of the research done on urban microclimates, indicating the turbulent model used.

Table 3.4. Past studies on Urban Microclimate using a CFD tool. Modified from (Toparlar, et al., 2017).

Authors	Location	Climate	Model	CFD tool	Parameters investigated
(Fang, et al., 2004)	Beijing, China	Warm temperate	RANS ¹ / MEE ²	Not specified	Surface temperature and wind speed
(Robitu, et al., 2006)	Nantes, France	Temperate	RANS ¹ / STKE ³	SOLENE and ANSYS Fluent	Mean radiant temperature, predicted mean vote, and surface temperature
(Yu & Hien, 2006)	Singapore	Hot humid	RANS ¹ / YMEE ⁴	ENVI-met and TAS	Air temperature
(Wong, et al., 2007)	Singapore	Hot humid	RANS ¹ / YMEE ⁴	ENVI-met and TAS	Air temperature
(Huang, et al., 2008)	Kawasaki, Japan	Humid	RANS ¹ / STKE ³	Not specified	Air temperature, surface temperature and wind speed
(Fahmy & Sharples, 2009)	Cairo, Egypt	Hot arid	RANS ¹ / YMEE ⁴	ENVI-met	Predicted mean vote
(Fahmy, et al., 2010)	Cairo, Egypt	Hot arid	RANS ¹ / YMEE ⁴	ENVI-met	Air temperature, mean radiant temperature and relative humidity

(Al-Sallal & Al-Rais, 2011)	Dubai, United Arab Emirates	Subtropical desert	RANS ¹ / STKE ³	PHOENICS	Air temperature and wind speed
(Bouyer, et al., 2011)	Lyon, France	Semi-continental	RANS ¹ / STKE ³	SOLENE and ANSYS Fluent	Air temperature and building energy consumption
(Boukhabla & Alkama, 2012)	Biskra, Algeria	Subtropical desert	RANS ¹ / YMEE ⁴	ENVI-met	Air temperature, relative humidity, solar radiation, and wind speed
(Al-Sallal & Al-Rais, 2012)	Dubai, United Arab Emirates	Subtropical desert	RANS ¹ / STKE ³	PHOENICS	Air temperature and wind speed
(Dütemeyer, et al., 20113)	Gelsenkirchen, Germany	Temperate	RANS ¹ / YMEE ⁴	ENVI-met	Air temperature, wind speed and PET
(Declat-Barreto, et al., 2013)	Phoenix, USA	Subtropical desert	RANS ¹ / YMEE ⁴	ENVI-met	Air temperature and surface temperature
(Radhi, et al., 2013)	Bahrain	Hot arid	RANS ¹ / RNGKE ⁵	PHOENICS	Air temperature, wind speed and PMV
(Ambrosini, et al., 2014)	Teramo, Italy	Warm temperate	RANS ¹ / YMEE ⁴	ENVI-met	Air temperature, relative humidity, and wind speed
(Gros, et al., 2014)	Nantes, France	Mediterranean	RANS ¹ / STKE ³	EnviBatE	Air temperature, building energy consumption and surface temperature
(Gromke, et al., 2015)	Arnhem, Netherlands	Temperate	RANS ¹ / RKE ⁶	ANSYS Fluent	Air temperature and wind speed

(Girgis, et al., 2015)	Cairo, Egypt	Hot arid	RANS ¹ / YMEE ⁴ STKE ³	ENVI-met and ANSYS Fluent	Air temperature and surface temperature
(Lobaccaro & Acero, 2015)	Bilbao, Spain	Mediterranean	RANS ¹ / YMEE ⁴	ENVI-met	Air temperature, mean radiant temperature, PET, relative humidity, and wind speed
(Wang & Li, 2016)	Hong Kong	Subtropical	RANS ¹ / STKE ³	ANSYS Fluent	Air temperature and wind speed
(Cui, et al., 2016)	Shanghai, China	Humid subtropical	RANS ¹ / RKE ⁶ STKE ³	ANSYS Fluent	Airflow and pollutant dispersion
(Santiago, et al., 2017)	Pamplona and Madrid, Spain	Mediterranean	RANS ¹ / STKE ³	STAR- CCM+	Pollutant dispersion and wind speed
(Salata, et al., 2017)	Rome, Italy	Mediterranean	RANS ¹ / YMEE ⁴	ENVI-met	Air temperature and mean radiant temperature
(Karakounos, et al., 2018)	Serres, Greece	Humid subtropical	RANS ¹ / YMEE ⁴	ENVI-met	Air temperature, mean radiant temperature, surface temperature and PMV
(Wang, et al., 2018)	Wuhan, China	Humid subtropical	RANS ¹ / STKE ³	ANSYS Fluent	Pollutant dispersion and wind speed
(Farhadi, et al., 2019)	Tehran, Iran	Cold Semi-Arid	RANS ¹ / YMEE ⁴	ENVI-met	Air temperature and PET
(Mei, et al., 2019)	Not specified	Not specified	RANS ¹	OpenFOAM	Airflow and pollutant dispersion

1. Reynolds-averaged Navier-Stokes.

2. Miao E-ε turbulence model.

3. Standard k-ε turbulence model.

4. Yamada and Mellor E-ε turbulence model.

5. Re-Normalization Group k-ε turbulence model.

6. Realizable k-ε turbulence model.

3.7 SUMMARY

This chapter discussed the airflow in the urban environment, the strategies used in an urban setting to reduce the thermal stress and the approaches used in studying the urban microclimate. The first section focused on the airflow behaviour inside an urban context, where the effects of isolated buildings, urban canyons and street intersections were analysed in terms of their impact on wind speed and direction. The urban configurations were also discussed in terms of orientation, street aspect ratio (buildings' heights) and vegetation, which correlates directly to the present research.

The previous studies on the urban canyons showed that the orientation of urban canyons can help significantly in improving the airflow and consequently improving the thermal stress. It was also found that increasing the height of buildings can increase the wind speed which, depending on the case study, can increase or decrease pedestrian thermal comfort. Studies have shown that vegetation can improve the urban heat island effect if used appropriately, where the leaf area index (LAI) and tree geometry were found to be the most influential parameters in improving the thermal stress as they affect how much shade is added to the urban canyon. The literature mentioned urban optimization as a mean of finding the best urban canyon configuration. However, the current literature only analysed a simplified version of an urban setting, where the present research is optimizing a more complex residential design with different parameters, e.g. the vegetation, the orientation, and the heights of buildings.

In addition, the chapter discussed the different approaches that have been used in recent years in studying the urban microclimate; these can be summarised by observation and numerical and CFD models. The literature has shown that the most appropriate approach used in analysing the microclimate was the CFD modelling as it combines most of the parameters affecting the urban environment with reasonable accuracy.

Chapter 4 :

Methodology

Content

- 4.1 Introduction
- 4.2 Research work process
- 4.3 ENVI-met validation methodology
- 4.4 Validation of ENVI-met model
- 4.5 Street grid
- 4.6 Amman, Jordan case study
- 4.7 The calculation of the physiological equivalent temperature PET index
- 4.8 Conclusion

4.1 INTRODUCTION

In this chapter, the framework and the methodology of the thesis will be discussed and outlined. The thesis aims to identify the key elements for enhancing outdoor thermal comfort for pedestrians in a residential setting via using different urban design scenarios, where the computational fluid dynamics (CFD) modelling software ENVI-met is used to determine the best scenarios for several urban elements.

4.2 RESEARCH WORK PROCESS

The research goal was to identify the most efficient way to organize and create urban elements to achieve the least thermal stress on the human body. For this, the research's main method is to study the possible solutions for selected parameters (orientation, buildings heights, wind tunnel effect and vegetation's leaf area density) and then apply them into a comprehensive urban design on a selected site in Amman, Jordan. The end result should give an outline of the process of achieving an environmentally responsive urban plan for a residential setting.

The research used two approaches, empirical and computational fluid dynamics (CFD) modelling, and since the research is heavily depended on CFD modelling, a validation process was needed to ensure that the outcomes are credible and sound. Envi-MET—the modelling software— was used to model and assess the urban elements studied in this research. For that, the data from the empirical phase —which was obtained through the use of heat stress loggers that collected the necessary parameters— was used to validate ENVI-met through calibration testing and variables sensitivity testing.

Validating ENVI-met comprised of two phases - the first phase was the process's capability of simulating accurate real-life scenarios, and for this a site was selected in Jordan to test how responsive the software was in simulating in a hot arid climate. The second phase comprised of several tests to examine how sensitive ENVI-met was to the change of variables inside a hypothetical setting. The variables included in the test were: relative humidity, wind speed, albedo, and grid resolution. Figure 4.1 shows the framework of validate ENVI-met.

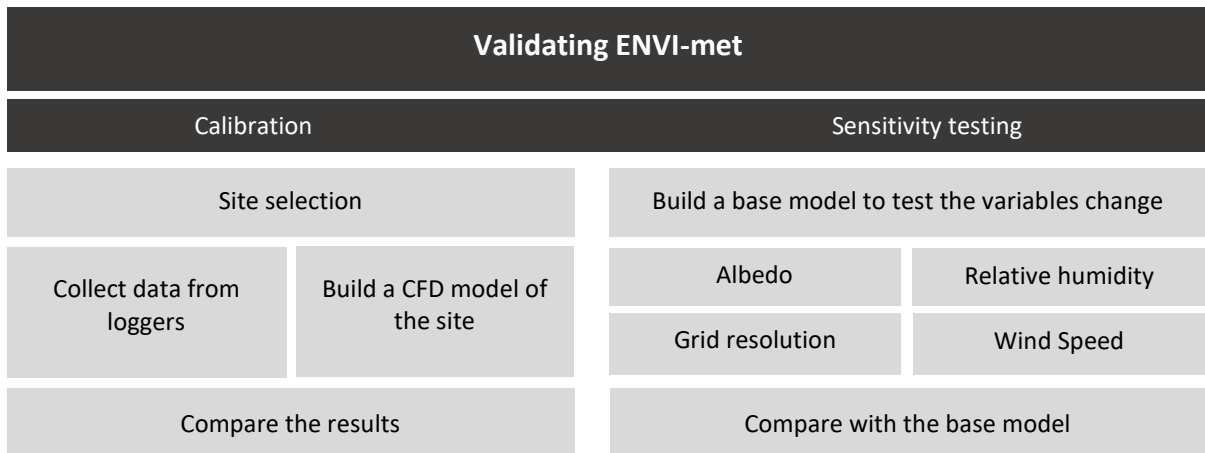


Figure 4.1. Validating ENVI-met process.

Testing the urban element phase was constructed to analyse the urban environment as a whole and then deconstruct its elements to further analyse different parameters on a micro-scale. The process consisted of selecting the site in Jordan based on the literature and background around Jordan’s future urban development scheme and then initiate the first macro analysis which comprised of the street grid. Following that, the analysis deconstructs the street grid into smaller compounds and row buildings to study various variables such as the height of the buildings and orientation (phases 1 and 2). Figure 4.2 shows the process of testing the urban environment.

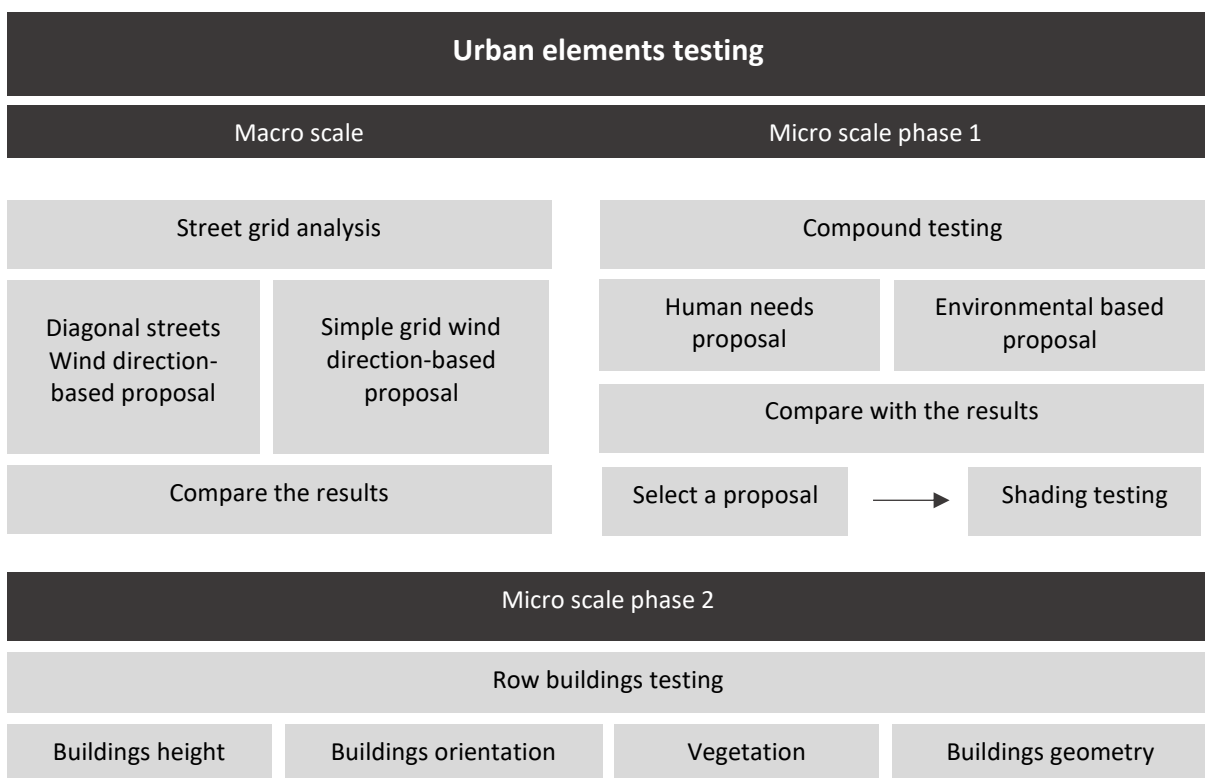


Figure 4.2. Urban elements testing process.

4.3 ENVI-MET VALIDATION METHODOLOGY

In order to validate ENVI-met version 4, a series of model runs was performed to ensure that the software was reliable to use as the simulation programme for the thesis. The process of validating ENVI-met was split into two phases, the first phase was to test how sensitive ENVI-met is to the change of variables and the second phase was the calibration phase, where it was tested on its accuracy in emulating real-life scenarios.

4.3.1. SENSITIVITY TESTING

A base model was used to test variables change in ENVI-met, and the base variable that was used to compare the change in the model runs' results was the air temperature (T_a). The base model comprised of six buildings spread out in a grid form in a 50 x 50 metre plot, the height of the buildings was set to 9 metres and the ground was tiled with grey tiles of an albedo of 50%. Two other models were built based on the original base model but with one variable changing either higher than the base or lower. These models were called the model high test and the model low test. The parameters that were tested were the relative humidity, wind speed, albedo, and grid resolution. A similar method was used to test ENVI-met's sensitivity by Skelhorn (2013). The following data shows the configuration of the base model that was used in sensitivity testing.

The base model parameters were set at 5 m/s for wind speed with a 90° counter-clockwise off north direction; a value of 65% for relative humidity; a 50% albedo of materials for both walls and ground, and the grid resolution was set to ($Dx=1,Dy=1,Dz=1$).

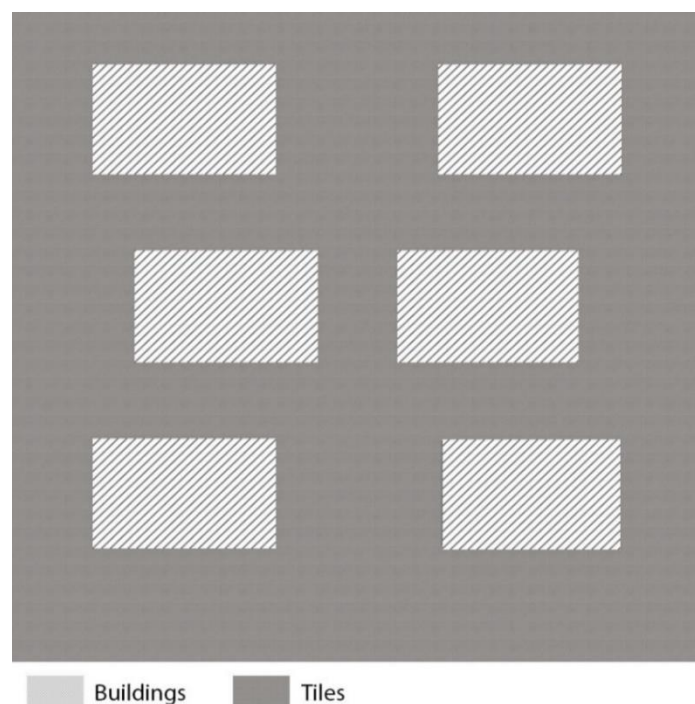


Figure 4.3. sensitivity testing base model configurations.

%---- ENVI-met V4 main configuration file -----

Fileversion =4.3

% Main data

Output Directory: =

Start Simulation at Day (DD.MM.YYYY): = 01.10.2017

Start Simulation at Time (HH:MM:SS): = 05:00:00

Total Simulation Time in Hours: = 26

Wind Speed in 10 m ab. Ground [m/s] = 5

Wind Direction (0:N..90:E..180:S..270:W..) = 270

Roughness Length z0 at Reference Point [m] = 0.01

Initial Temperature Atmosphere [K] = 298.150

Specific Humidity in 2500 m [g Water/kg air] = 7.0

Relative Humidity in 2m [%] = 65

% End main data

[OUTPUTTIMING]_____

Output interval main files (min) = 60.00

Output interval text output files (min) = 30.00

Include Nesting Grids in Output (0:n,1:y) = 0

[TIMING]_____

Update Surface Data each ? sec = 30.00

Update Wind field each ? sec = 900.00

Update Radiation and Shadows each ? sec = 600.00

Update Plant Data each ? sec = 600.00

[PARALLEL_CPU]_____

CPU usage settings =ALL

[IVSRADIATION]_____

Use IVS radiation transfer scheme (0:n,1:y) = 1

4.3.2 WIND SPEED SENSITIVITY TESTING

The following data are the configuration used in building the wind speed low model test, with the low wind speed set to 1 m/s.

```
%---- ENVI-met V4 main configuration file -----
Fileversion                =4.3
% Main data .....
Start Simulation at Day (DD.MM.YYYY):  =01.10.2017
Start Simulation at Time (HH:MM:SS):   =05:00:00
Total Simulation Time in Hours:        =26
Wind Speed in 10 m ab. Ground [m/s]    =1
Wind Direction (0:N..90:E..180:S..270:W..) =270
Roughness Length z0 at Reference Point [m] =0.01
Initial Temperature Atmosphere [K]     =298.150
Specific Humidity in 2500 m [g Water/kg air] =7.0
Relative Humidity in 2m [%]            =65
% End main data .....
[OUTPUTTIMING]_____
Output interval main files (min)       =60.00
Output interval text output files (min) =30.00
Include Nesting Grids in Output (0:n,1:y) =0
[TIMING]_____
Update Surface Data each ? sec        =30.00
Update Wind field each ? sec          =900.00
Update Radiation and Shadows each ? sec =600.00
Update Plant Data each ? sec          =600.00
[PARALLEL_CPU]_____
CPU usage settings                    =ALL
[IVSRADIATION]_____
Use IVS radiation transfer scheme (0:n,1:y) = 1
```


The wind speed high model test configuration is shown below with the high wind speed set to 10 m/s.

```
%--- ENVI-met V4 main configuration file -----
Fileversion                =4.3
% Main data .....
Start Simulation at Day (DD.MM.YYYY):  =01.10.2017
Start Simulation at Time (HH:MM:SS):   =05:00:00
Total Simulation Time in Hours:        =26
Wind Speed in 10 m ab. Ground [m/s]    =10
Wind Direction (0:N..90:E..180:S..270:W..) =270
Roughness Length z0 at Reference Point [m] =0.01
Initial Temperature Atmosphere [K]     =298.150
Specific Humidity in 2500 m [g Water/kg air] =7.0
Relative Humidity in 2m [%]            =65
% End main data .....
[OUTPUTTIMING]_____
Output interval main files (min)       =60.00
Output interval text output files (min) =30.00
Include Nesting Grids in Output (0:n,1:y) =0
[TIMING]_____
Update Surface Data each ? sec         =30.00
Update Wind field each ? sec           =900.00
Update Radiation and Shadows each ? sec =600.00
Update Plant Data each ? sec           =600.00
[PARALLEL_CPU]_____
CPU usage settings                    =ALL
[IVSRADIATION]_____
Use IVS radiation transfer scheme (0:n,1:y) = 1
```

The three models - the base, the high and the low - were compared together in terms of how they affected the base parameter, the air temperature.

4.3.3 RELATIVE HUMIDITY SENSITIVITY TESTING

The following data are the configuration used in building the relative humidity low model test, with the low relative humidity set to 40%.

```
%--- ENVI-met V4 main configuration file -----
Fileversion                =4.3
% Main data .....
Start Simulation at Day (DD.MM.YYYY):  =01.10.2017
Start Simulation at Time (HH:MM:SS):   =05:00:00
Total Simulation Time in Hours:        =26
Wind Speed in 10 m ab. Ground [m/s]   =5
Wind Direction (0:N..90:E..180:S..270:W..) =270
Roughness Length z0 at Reference Point [m] =0.01
Initial Temperature Atmosphere [K]     =298.150
Specific Humidity in 2500 m [g Water/kg air] =7.0
Relative Humidity in 2m [%]            =40
% End main data .....
[OUTPUTTIMING]_____
Output interval main files (min)       =60.00
Output interval text output files (min) =30.00
Include Nesting Grids in Output (0:n,1:y) =0
[TIMING]_____
Update Surface Data each ? sec        =30.00
Update Wind field each ? sec          =900.00
Update Radiation and Shadows each ? sec =600.00
Update Plant Data each ? sec          =600.00
[PARALLEL_CPU]_____
CPU usage settings                    =ALL
[IVSRADIATION]_____
Use IVS radiation transfer scheme (0:n,1:y) = 1
```

The relative humidity high model test configuration is shown below with the high relative humidity set to 90%. The three models are simulated and then compared in terms of the air temperature component.

```

%---- ENVI-met V4 main configuration file -----
Fileversion                =4.3
% Main data .....
Start Simulation at Day (DD.MM.YYYY):    =01.10.2017
Start Simulation at Time (HH:MM:SS):     =05:00:00
Total Simulation Time in Hours:          =26
Wind Speed in 10 m ab. Ground [m/s]     =5
Wind Direction (0:N..90:E..180:S..270:W..) =270
Roughness Length z0 at Reference Point [m] =0.01
Initial Temperature Atmosphere [K]      =298.150
Specific Humidity in 2500 m [g Water/kg air] =7.0
Relative Humidity in 2m [%]              =90
% End main data .....
[OUTPUTTIMING]_____
Output interval main files (min)         =60.00
Output interval text output files (min)  =30.00
Include Nesting Grids in Output (0:n,1:y) =0
[TIMING]_____
Update Surface Data each ? sec          =30.00
Update Wind field each ? sec             =900.00
Update Radiation and Shadows each ? sec  =600.00
Update Plant Data each ? sec             =600.00
[PARALLEL_CPU]_____
CPU usage settings                       =ALL
[IVSRADIATION]_____
Use IVS radiation transfer scheme (0:n,1:y) = 1

```

4.3.4 ALBEDO SENSITIVITY TESTING

For the albedo testing the site ground and buildings were covered with grey materials with the same surface roughness and albedo of 50% as the base model, 10% as the low model and 90% for the high model. Table 4.1 and 4.2 show the detailed configurations for the materials used in the model runs.

Table 4.1. Walls material's Albedo configuration for the model runs.

Parameters	Low Albedo Test	Base Albedo Test	High Albedo Test
Thickness	0.3 M	0.3 M	0.3 M
Absorption	90%	50%	10%
Reflection	10%	50%	90%
Emissivity	90%	90%	90%
Specific Heat	650 J/(Kg*K)	650 J/(Kg*K)	650 J/(Kg*K)
Thermal Conductivity	0.5 W/(M*K)	0.5 W/(M*K)	0.5 W/(M*K)
Density	1500 Kg/M ³	1500 Kg/M ³	1500 Kg/M ³

Table 4.2. Pavement material's Albedo configuration for the model runs.

Parameters	Low Albedo Test	Base Albedo Test	High Albedo Test
Z0 Roughness Length	0.01	0.01	0.01
Albedo	0.1	0.5	0.9
Emissivity	0.9	0.9	0.9
Surface Irrigation	None	None	None

4.3.5 GRID RESOLUTION SENSITIVITY TESTING

ENVI-met operates on a pixel system, where each pixel represents a metric volume in the design. The grid resolution is an indication of the accuracy of the design, where the small size of the grid cells in meters produce more accurate results than the larger ones. For the grid

resolution sensitivity testing the base model was chosen with the most accurate configuration (Dx=1,Dy=1,Dz=1), whereas the second and third model runs were set at (Dx=2,Dy=2,Dz=2) and (Dx=3,Dy=3,Dz=3) respectively – see Table 4.3.

The comparison was based on the results of the base model with the most accurate configuration, the purpose of this test is to minimize the model run with the most accurate results due to ENVI-met high computational needs where a single run can take up to 14 days.

Table 4.3. The grid resolution configuration for the three model runs.

Model Test	Model Geometry					
	Model Dimensions			Size of Grid Cell in Meters		
	X-Grid	Y-Grid	X-Grid	Dx	Dy	Dz
Base Model Test	50	50	30	1	1	1
2 M/ Pixel Model Test	25	25	30	2	2	2
3 M/ Pixel Model Test	17	17	17	3	3	3

4.4 VALIDATION OF ENVI-MET MODEL.

The process of calibrating ENVI-met consisted of two stages, the first was the site selection to install loggers and the second stage was modelling the site as accurate as possible in order to compare the two sets of data.

4.4.1 SITE SELECTION AND DATA COLLECTION.

The site selected was Al Ahliyya Amman University in Jordan. This site offered a range of different urban elements, such as a wide variety of vegetation, tiled pathways, buildings, and a car park (see Figure 4.4). The area surrounding the university is a hillside with empty plots and some scattered buildings. Trees at the edges acted as wind blockers. In addition, the University has 24-hour security that ensured the safety of the monitoring equipment. The Köppen climate classification system puts Jordan in two classifications - hot arid desert (BWh) and cold arid desert (BWk) (KOTTEK, et al., 2006) - with a maximum temperature in August of 41.5°C and a minimum in February -4.5°C, precipitation mostly occurs in winter, with an average of 55 rainy days.

The cladding of most University buildings is white limestone with an average albedo of 60%, and the pathways that link the buildings have different material. However, the area where the loggers were placed was tiled with grey cement tiles with an average albedo of 30%. The locations of A and B allowed for different conditions, with B being near to sprinklers and A being under larger thicker trees. The vegetation at the site is mostly local and coniferous in nature - the only deciduous tree is *Populus nigra*. other coniferous are *Pinus halepensis*, Mediterranean cypress (*Cupressaceae*), *Phoenix dactylifera* and *Cupressus macrocarpa* 'Goldcrest'.

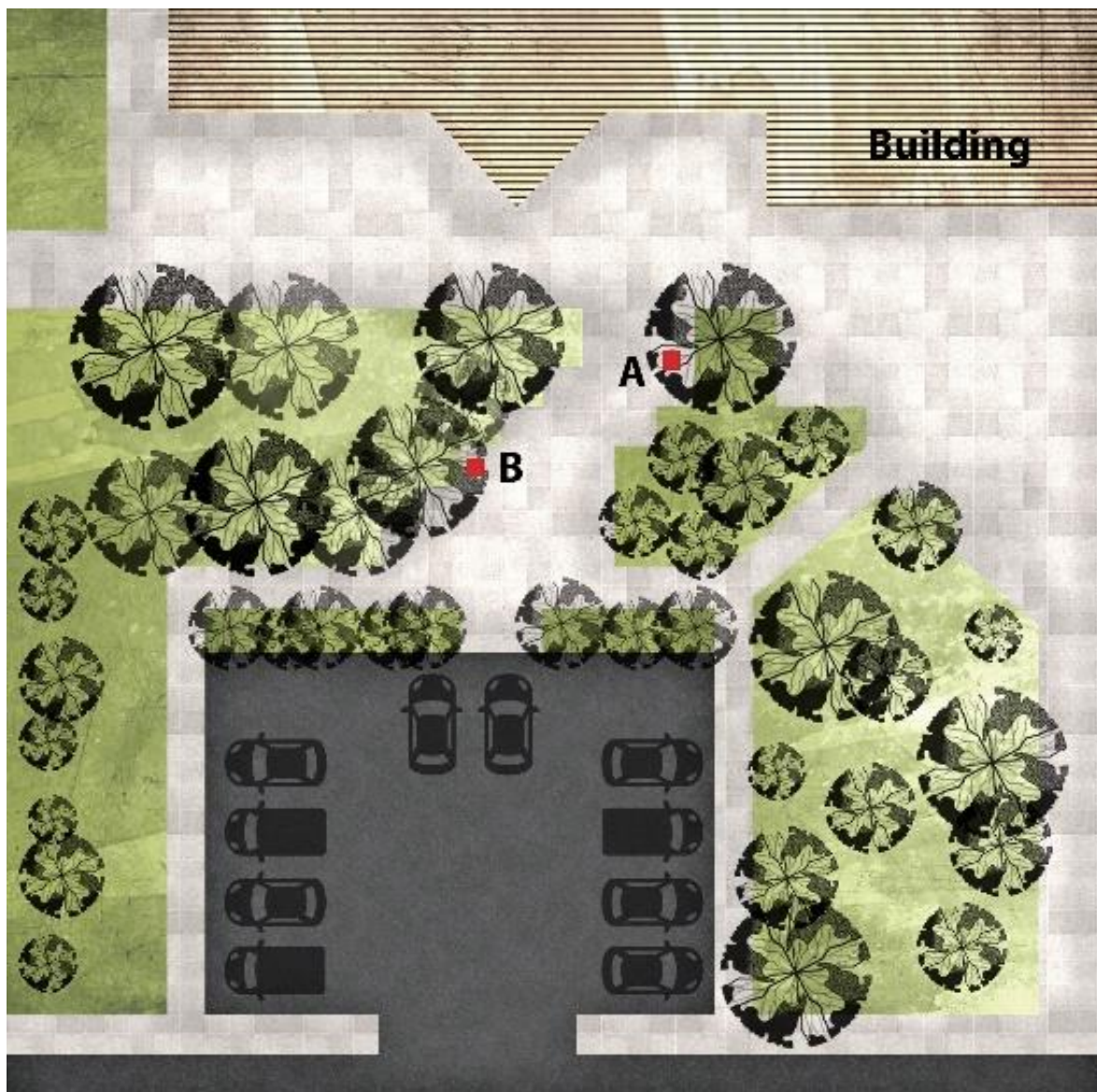


Figure 4.4. Rendering of the site showing the monitored locations.

The date chosen for the test was the 1st of October 2017, the loggers were set in location A and B for 24 hours. The loggers for the data collection phase were Kestrel 5400 Heat Stress

Trackers that were chosen for their capability of recording the parameters that are needed for the study i.e. parameters were wind speed, relative humidity, air temperature and mean radiant temperature. The loggers were new and unused and so factory calibrations were accepted. The loggers used were equipped with several sensors to measure different parameters. The 1-inch black globe is installed with a sensor inside of it to measure temperature. This temperature measurement is affected by the ambient air temperature, solar radiation, and wind speed. The globe data is usually used to calculate mean radiant temperature, however, in this analysis, the device had some technical difficulties which impaired the device in measuring the globe temperature. Two other sensors are installed in the device to measure the air temperature and relative humidity, and these sensors are located inside of a hollowed piece of the device to protect the sensors from any outside influences. Table 4.5 shows these sensors specifications. The loggers also come with a replaceable impeller to measure wind speed and a rotatable stand that would measure wind direction (Kestrel, 2015).

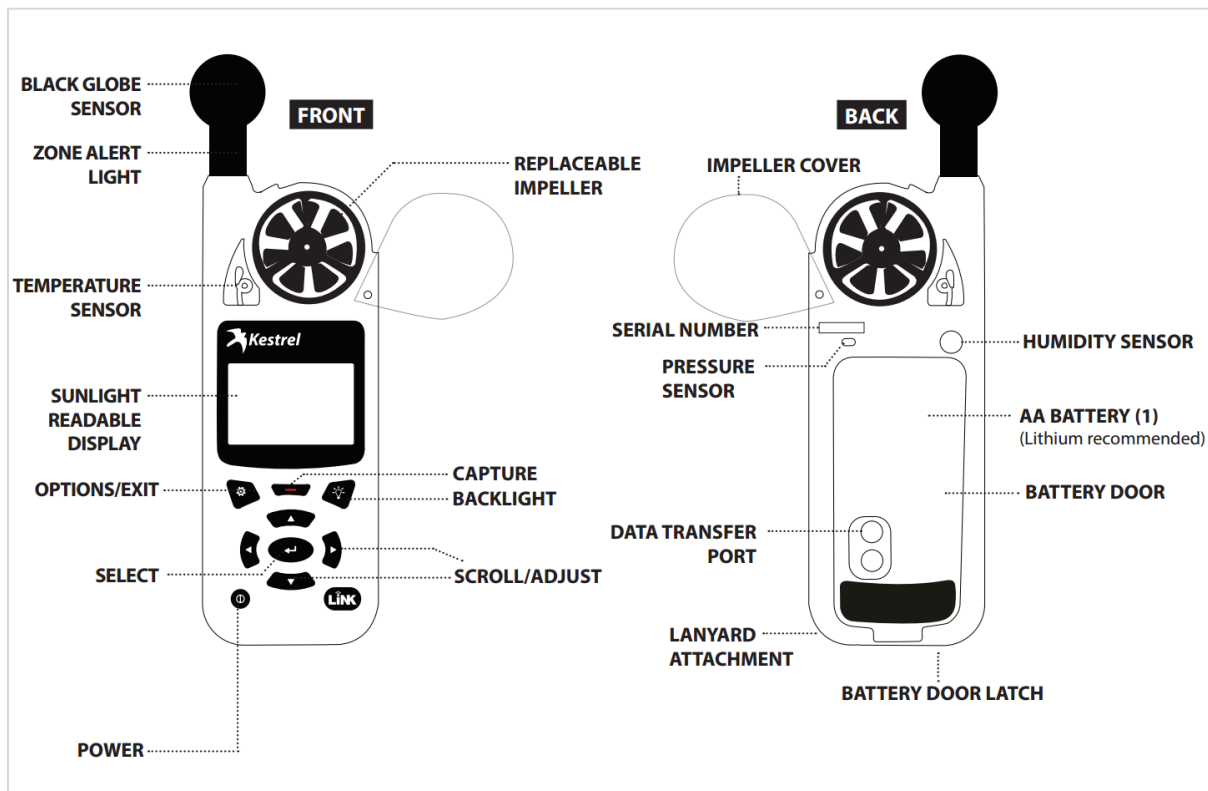


Figure 44.5. Kestrel 5400 heat stress tracker.

Table 4.4. Sensors Specifications for Kestrel 5400 Heat Stress tracker.

SENSOR	ACCURACY (+/-)	RESOLUTION	SPECIFICATION RANGE
Wind Speed Air Speed	Larger of 3% of reading, least significant digit or 20 ft/min	0.1 m/s 1 ft/min 0.1 km/h 0.1 mph 0.1 knots 1 B 0.1 F/S	0.6 to 40.0 m/s 118 to 7,874 ft/min 2.2 to 144.0 km/h 1.3 to 89.5 mph 1.2 to 77.8 knots 0 to 12 B 2-131.2
Ambient Temperature	0.9 °F 0.5 °C	0.1 °F 0.1 °C	-20.0 to 158.0 °F -29.0 to 70.0 °C
Globe Temperature	2.5 °F 1.4 °C	0.1 °F 0.1 °C	-20.0 to 140.0 °F -29.0 to 60.0 °C
Relative Humidity	2%RH	0.1 %RH	10 to 90% 25°C non-condensing
Pressure	1.5 hPa mbar 0.044 inHg 0.022 PSI	0.1 hPa mbar 0.01 inHg 0.01 PSI	25°C/77°F 700-1100 hPa mbar 20.67-32.48 inHg 10.15-15.95 PSI
Compass	5°	1° 1/16th Cardinal Scale	0 to 360°

4.4.2 ENVI-MET MODELLING OF THE AL AHLIYYA AMMAN UNIVERSITY SITE.

i. Spaces

A 3D model of the site was built using spaces - one of ENVI-met's components, where initial AutoCAD format drawings were used as a base for the model. Modelling in spaces is a grid system modelling with a default resolution of 2 metres. The 3D resolution was changed to dx=1 dy=1 dz=1 since the site in question is small enough to fit in the 60x60-pixel grid. Equidistant was chosen as the method of vertical grid generation as the highest point of the buildings only reaches 18 metres, which is enough to avoid any boundary issues that might occur due to the proximity to the upper limit of the model.

ii. Vegetation

Envi-MET allows its users to create their own vegetation database through Albero. To be able to use Albero in Envi-MET, the leaf area density (LAD) must be determined. However, in this study, there was no need to construct new vegetation since Envi-MET's library had similar trees to those on the site, and only some modifications on the existing Envi-MET's database were made.

iii. Wind

The wind speed values for the given simulated day at the monitoring site were extracted from an EPW file generated using Meteonorm. Usually, weather readings are taken in an open field 10 metres above ground level, which makes the readings potentially unreliable for an urbanized setting. It has been suggested that the wind speed values from a weather station can be adjusted to suit an urban setting by using a ratio S - the ratio between the wind speed at a height H above the urban area (VH) and the wind speed at 10m height in open flat country ($V10$), where $10\text{ m} \leq H \leq 150$ (Nikolopoulou, 2004). Table 4.5 shows the S factor values for urban and suburban areas.

Table 4.5. S factor $S = VH / V10$

Height	10	20	30	40	50	60	70	
S (suburban)	0.6	0.73	0.82	0.89	0.94	0.99	1.04	
S (urban)	0.36	0.47	0.55	0.62	0.68	0.73	0.77	
Height	80	90	100	110	120	130	140	150
S (suburban)	1.08	1.11	1.14	1.18	1.21	1.24	1.27	1.29
S (urban)	0.82	0.86	0.89	0.93	0.96	0.99	1.02	1.05

Al Ahliyya Amman University is situated outside of the city Amman on a hillside; therefore, it does not fall under urban or suburban areas regarding wind speed. The average wind speed was calculated as 4 m/s from a north-westerly direction (291°).

iv. Meteorological settings

The day chosen for the simulation was the 1st of October 2017- chosen for the mild conditions of the month, with average meteorological parameters. The values for air temperature and relative humidity were obtained from the EPW file, as shown in Table 4.6.

Table 4.6. Air temperature and relative humidity values for the 1st of October.

Hour	01:00	02:00	03:00	04:00	05:00	06:00	07:00	08:00	09:00	10:00	11:00	12:00
Air temperature	17.4	16.2	15	14.3	13.8	13.8	15.3	17.4	19.5	21.4	22.9	24.1
Relative humidity	47	49	50	52	50	50	50	41	34	28	24	22

Hour	13:00	14:00	15:00	16:00	17:00	18:00	19:00	20:00	21:00	22:00	23:00	24:00
Air temperature	24.9	25.2	25.1	24.3	23	21.5	20.3	19.1	17.9	16.8	15.6	14.4
Relative humidity	21	23	22	24	28	30	37	41	46	50	55	60

v. ENVI-met configuration file.

The model run needed more detailed input data when compared to the previous runs, and simple force was used to enter the exact air temperature and relative humidity for each hour of the day at the simulation date. The data were extracted from the EPW file generated using Meteonorm.

The following data is the configuration file used in the model run that imitates the site chosen in Jordan.

%---- ENVI-met V4 main configuration file -----

Fileversion =4.3

% Main data

Start Simulation at Day (DD.MM.YYYY):
=01.10.2017

Start Simulation at Time (HH:MM:SS):
=05:00:00

Total Simulation Time in Hours: =26

Wind Speed in 10 m ab. Ground [m/s] =4

Wind Direction (0:N..90:E..180:S..270:W..) =291.00

Roughness Length z0 at Reference Point [m] =0.01

Initial Temperature Atmosphere [K] =295.940

Specific Humidity in 2500 m [g Water/kg air] =7.0

Relative Humidity in 2m [%] =50

% End main data

[OUTPUTTIMING]_____

Output interval main files (min) =60.00

Output interval text output files (min) =30.00

Include Nesting Grids in Output (0:n,1:y) =0

[TIMING]_____

Update Surface Data each ? sec =30.00

Update Wind field each ? sec =900.00

Update Radiation and Shadows each ? sec =600.00

Update Plant Data each ? sec =600.00

[SIMPLEFORCE]

Hour 00h [Temp, rH] = 292.15, 50.00

Hour 01h [Temp, rH] = 291.15, 48.00

Hour 02h [Temp, rH] = 291.15, 47.00

Hour 03h [Temp, rH] = 291.15, 43.00

Hour 04h [Temp, rH] = 289.15, 43.00

Hour 05h [Temp, rH] = 291.15, 44.00

Hour 06h [Temp, rH] = 291.15, 41.00

Hour 07h [Temp, rH] = 292.15, 37.00

Hour 08h [Temp, rH] = 294.15, 37.00

Hour 09h [Temp, rH] = 295.15, 28.00

Hour 10h [Temp, rH] = 297.15, 28.00

Hour 11h [Temp, rH] = 298.15, 29.00

Hour 12h [Temp, rH] = 299.15, 28.00

Hour 13h [Temp, rH] = 300.15, 25.00

Hour 14h [Temp, rH] = 301.15, 21.00

Hour 15h [Temp, rH] = 302.15, 18.00

Hour 16h [Temp, rH] = 301.15, 20.00

Hour 17h [Temp, rH] = 300.15, 22.00

Hour 18h [Temp, rH] = 299.15, 23.00

Hour 19h [Temp, rH] = 299.15, 24.00

Hour 20h [Temp, rH] = 298.15, 25.00

Hour 21h [Temp, rH] = 297.15, 26.00

Hour 22h [Temp, rH] = 296.15, 30.00

Hour 23h [Temp, rH] = 295.15, 34.00

[PARALLEL_CPU]_____

CPU usage settings =ALL

[IVSRADIATION]_____

Use IVS radiation transfer scheme (0:n,1:y) = 1

vi. MODEL VALIDATION METHODS.

Four validation methods were used to compare the observed and the predict data in the study to show the different approaches that can be used to test/validate the simulated data.

a) Pearson correlation coefficient

One of the most used methods of model validation is Pearson's correlation coefficient developed by Karl Pearson (Erell & Williamson, 2006) and it is defined as "the measure of the strength of the linear relationship between two variables" (Lane, et al., 2013). Pearson's formula (Equation 4.1) consists of the covariance of the data sets given and their standard deviations, the results lie between -1 to 1 where the sign indicates the linear relationship Behavior and 0 shows no correlation within the data sets – see Figure 4.6 (Lane, et al., 2013).

$$r = \frac{\sum (x - \bar{x})(y - \bar{y})}{\sqrt{\sum (x - \bar{x})^2} \sqrt{\sum (y - \bar{y})^2}} \quad (4.1)$$

where \bar{x} = mean of X variable and \bar{y} = mean of Y variable

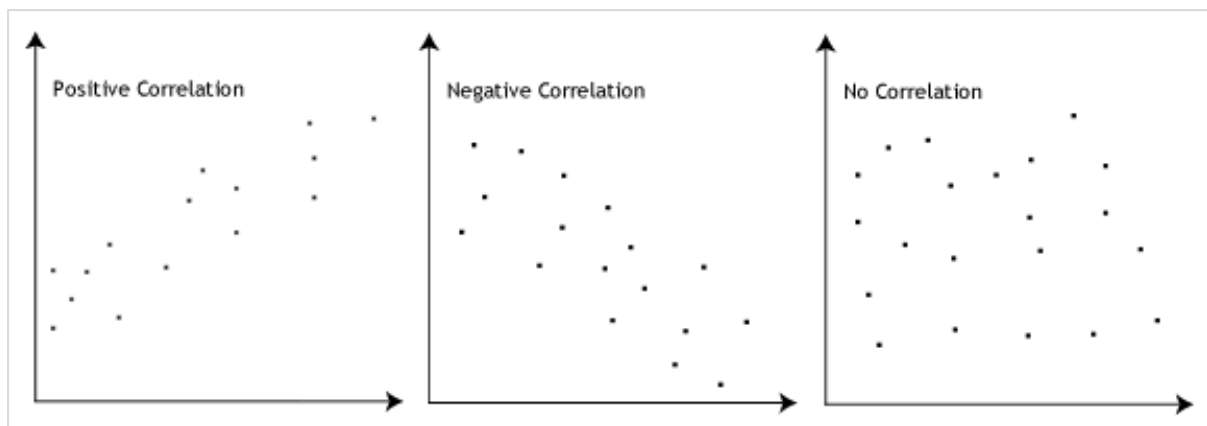


Figure 4.6. Pearson's correlation values diagram.

b) RMSError and MAE

RMSError (Root Mean Squared Error) is a dimensional metric used to identify how large the difference is between the observed and the predicted values, to indicated how spread out the predicted data are from the observed ones (see Figure 4.7). The formula consists of the square root of the sum of the squared variables difference divided by the number of the variables as shown in Equation 4.2 (Chai & Draxler , 2014).

$$RMSE = \sqrt{\frac{1}{n} \sum_{i=1}^n (p - o)^2} \quad (4.2)$$

where p = predicted values and o = observed values

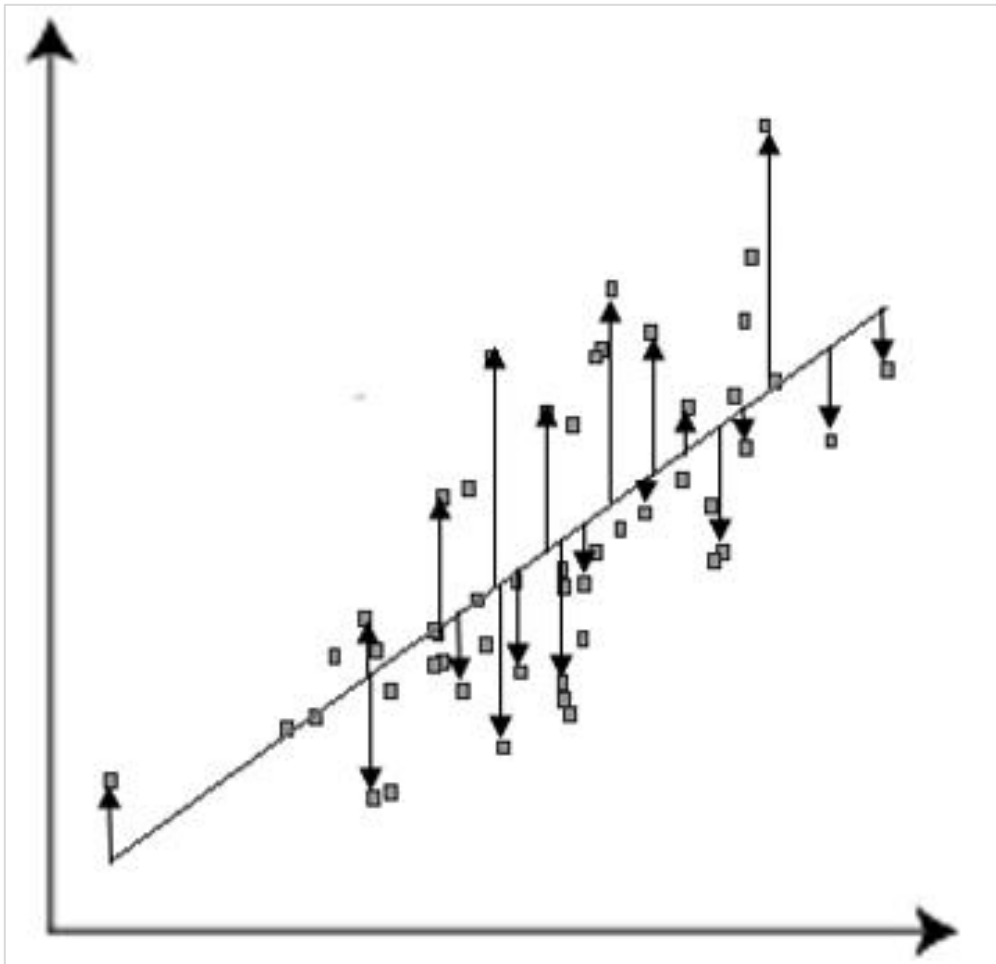


Figure 4.7. RMSE Error diagram.

MAE (Mean Absolute Error) is a dimensional metric used to measure the error between two sets of data, the formula consists of the sum of the absolute difference of the predicted and observed values over the number of variables as shown in Equation 4.3.

$$MAE = \frac{1}{n} \sum_{i=1}^n |P - O| \quad (4.3)$$

where p = predicted values and o = observed values

RMSE and MAE are also largely used among researchers to validate their predicted values. However, it has been suggested by Willmott and Matsuura (2005) that using RMSE Error is not

appropriate and replacing it with the MAE should give a more accurate description of the model validation. In recent years Chai and Draxler (2014) argued that the replacement of RMSE with MAE is not an accurate representation of the model validation process, especially when there is a Gaussian error distribution. Chai and Draxler (2014) advice the use of a combination of model verification methods to reach accurate results.

c) Index of Agreement

The formula for this index was originally developed by Willmott in the 1980s, the original form is listed in Equation 4.4 (Willmott, 1981).

$$\rho = 1 - \delta / \mu \quad (4.4)$$

where δ = the sum of the squared errors and μ = the overall sum of the squares of sums of the absolute values.

The formula can be simplified and written as shown in Equation 4.5.

$$d = 1 - \frac{\sum_{i=1}^n (P - O)^2}{\sum_{i=1}^n (|P - \bar{O}| + |O - \bar{O}|)^2} \quad (4.5)$$

where P is the predicted value and o is the observed value

An Index of Agreement ranges between 0 and 1, with 1 being a perfect correlation and 0 showing no relationship between the predicted and observed values.

4.5 STREET GRID.

This section will explore the street grid system as a single aspect of the urban layout that can affect wind flow and thermal stress. Five scenarios were introduced to the study and simulated under the same conditions in the CFD modelling software Envi-MET. The analyses included different orientations for the designed plot to assess the effect of the sun angle and wind direction. The results are compared in terms of average wind speed and physiological equivalent temperature (PET). A similar approach was used to test the impact of building layout on wind speed and air temperature in Wuhan, China and assessed using the Universal Thermal Index Climate Index (UTCI) (Jiang, et al., 2020). Moreover, several notable studies analysed the buildings layouts and their relations to microclimate and thermal stress using a

comparable method (Gao, et al., 2012), (Chan, 2011), (Yang, et al., 2010) and (Hong & Lin, 2015).

Five common urban layouts were modelled to quantify the effect of street grid form and street orientation on wind flow and PET. The streets were digitally located in Amman, Jordan. The grids were simulated twice, once facing north, and then after rotating the grid by 45° counter clockwise, to create two different wind directions. The data were extracted based on the average human height. Figure 4.8 shows the five layouts discussed in the street grids' analysis, labelled from A to E.

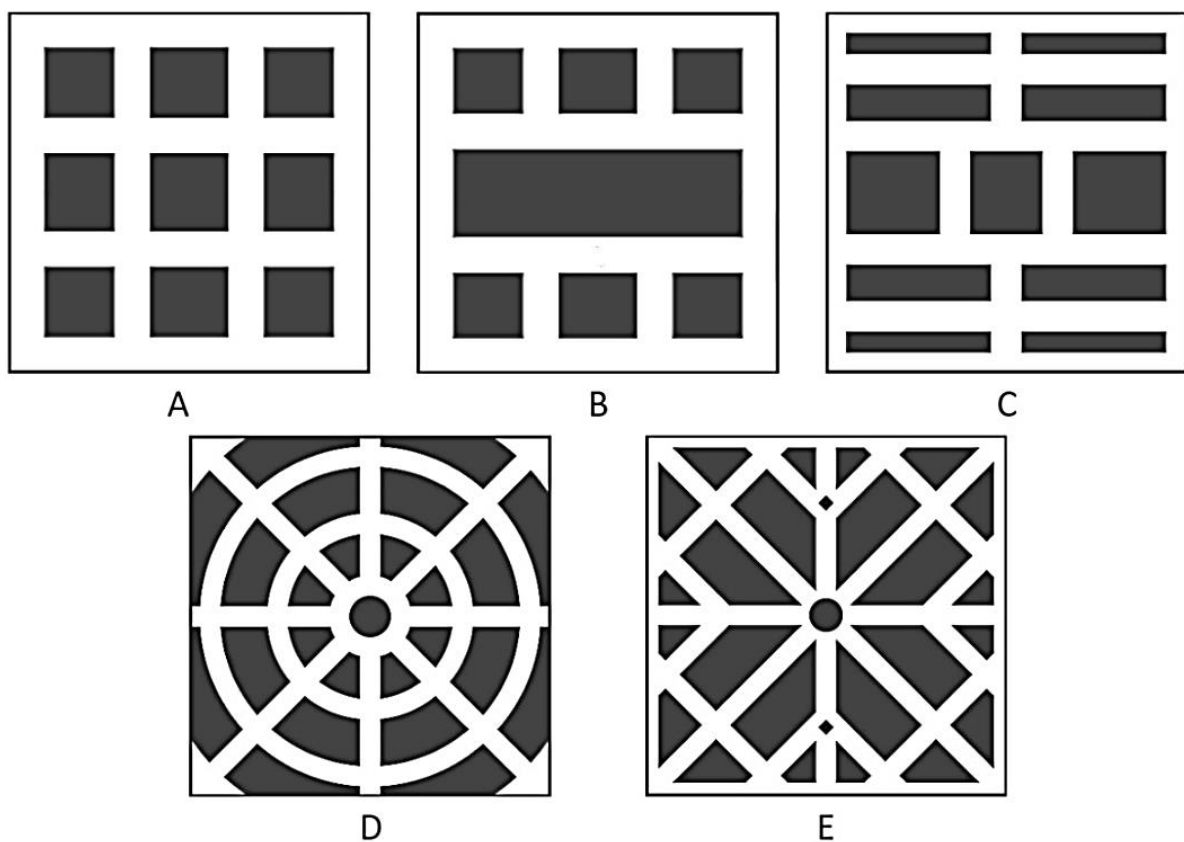


Figure 4.8. Street grid layouts.

All the Envi-MET simulations kept the at same conditions (apart from the grid layout), which were:

- The building height to street width ratio was set as 1.
- The buildings' cladding material was limestone (the most common choice in Jordan).
- Street albedo was 10% (asphalt).
- The dominant wind direction was westerly for all the layouts.

- Each street's orientation was rotated through 45° counter clockwise for a second simulation.

The results of the simulations were compared in terms of wind speed distribution for each layout at 11:00 am, and thermal comfort over a 24-hour period for two receptors positioned around the streets. The date for the simulation was 23rd September as it is the most optimal use of the space with mild conditions rather than extreme summer or winter.

The meteorological factors were averaged for all the scenarios with the following parameters:

- Air temperature was set to a minimum of 18 °C and a maximum of 28.7 °C.
- Wind speed was set to 4 m/s.
- The relative humidity was set to a minimum of 35% and a maximum of 70%.

All the previously mentioned ENVI-met's extensions were used to build the layouts and their different scenarios, the simulation configuration file remained the same for all the scenarios as the orientation of the site is set in the SPACES extension for each individual model. The models that were built in SPACES are then inserted into the final simulation run.

The following data are the configuration file used into the model and run the simulation for the grid layouts analysis, the data for the meteorological parameters were extracted from an EPW file generated using Meteonorm.


```

%---- ENVI-met V4 main configuration file ----
%---- generated with ProjectWizard -----
Fileversion                =4.3
% Main data .....
Start Simulation at Day (DD.MM.YYYY):
=23.09.2018
Start Simulation at Time (HH:MM:SS):
=05:00:00
Total Simulation Time in Hours:      =26
Wind Speed in 10 m ab. Ground [m/s]  =4
Wind Direction (0:N..90:E..180:S..270:W..)
=270
Roughness Length z0 at Reference Point [m]
=0.01
Initial Temperature Atmosphere [K]
=296.250
Specific Humidity in 2500 m [g Water/kg air]
=7.0
Relative Humidity in 2m [%]          =50
% End main data .....

[OUTPUTTIMING]_____
Output interval main files (min)      =60.00
Output interval text output files (min)
=30.00
Include Nesting Grids in Output (0:n,1:y) =0

[TIMING]_____
Update Surface Data each ? sec        =30.00
Update Wind field each ? sec          =900.00
Update Radiation and Shadows each ? sec
=600.00
Update Plant Data each ? sec          =600.00

```

[SIMPLEFORCE]

```

Hour 00h [Temp, rH] = 294.05, 69.00
Hour 01h [Temp, rH] = 292.15, 71.00
Hour 02h [Temp, rH] = 291.45, 71.00
Hour 03h [Temp, rH] = 291.35, 72.00
Hour 04h [Temp, rH] = 291.25, 71.00
Hour 05h [Temp, rH] = 291.15, 72.00
Hour 06h [Temp, rH] = 291.25, 73.00
Hour 07h [Temp, rH] = 292.35, 68.00
Hour 08h [Temp, rH] = 294.35, 61.00
Hour 09h [Temp, rH] = 296.25, 53.00
Hour 10h [Temp, rH] = 298.05, 45.00
Hour 11h [Temp, rH] = 299.55, 39.00
Hour 12h [Temp, rH] = 300.75, 38.00
Hour 13h [Temp, rH] = 301.45, 35.00
Hour 14h [Temp, rH] = 301.85, 35.00
Hour 15h [Temp, rH] = 301.75, 36.00
Hour 16h [Temp, rH] = 301.15, 39.00
Hour 17h [Temp, rH] = 299.95, 45.00
Hour 18h [Temp, rH] = 298.55, 47.00
Hour 19h [Temp, rH] = 297.75, 54.00
Hour 20h [Temp, rH] = 297.05, 58.00
Hour 21h [Temp, rH] = 296.25, 59.00
Hour 22h [Temp, rH] = 295.55, 61.00
Hour 23h [Temp, rH] = 294.75, 63.00

```

[PARALLEL_CPU]_____

CPU usage settings =ALL

[IVSRADIATION]_____

Use IVS radiation transfer scheme (0:n,1:y) = 1

4.5.1 PET SUMMER RANGE.

Studies have shown that thermal sensation in urban environments can differ in different climates, where the experiences of individuals directly affect their expectations of the microclimate (Nikolopoulou, et al., 2001; de Dear & Brager, 1998). Ruiz and Correa, 2015, studied six different thermal comfort indices in the city of Mendoza, Argentina. The results showed 75% discrepancies with the thermal indices ability to predict thermal sensation when compared to the Actual Sensation Vote (ASV).

Several studies have modified the PET range to fit the climatic zone. Kruger et al., 2012, have calculated the correlation factor between the PET and the thermal sensation vote in the Oceanic climate of Glasgow, UK, and found that the comfort range was between 9°C and 18°C, which falls under the cool range in the universal PET range. Lin and Matzarakis, 2007, have also calculated the PET comfort range for the tropical region of Taiwan, and found that the acceptable comfort range was 8°C higher than the universal range, the new range was estimated at 26°C to 30°C. Figure 4.9 displays the modified PET ranges for different climate zones in summer compared with the universal range.

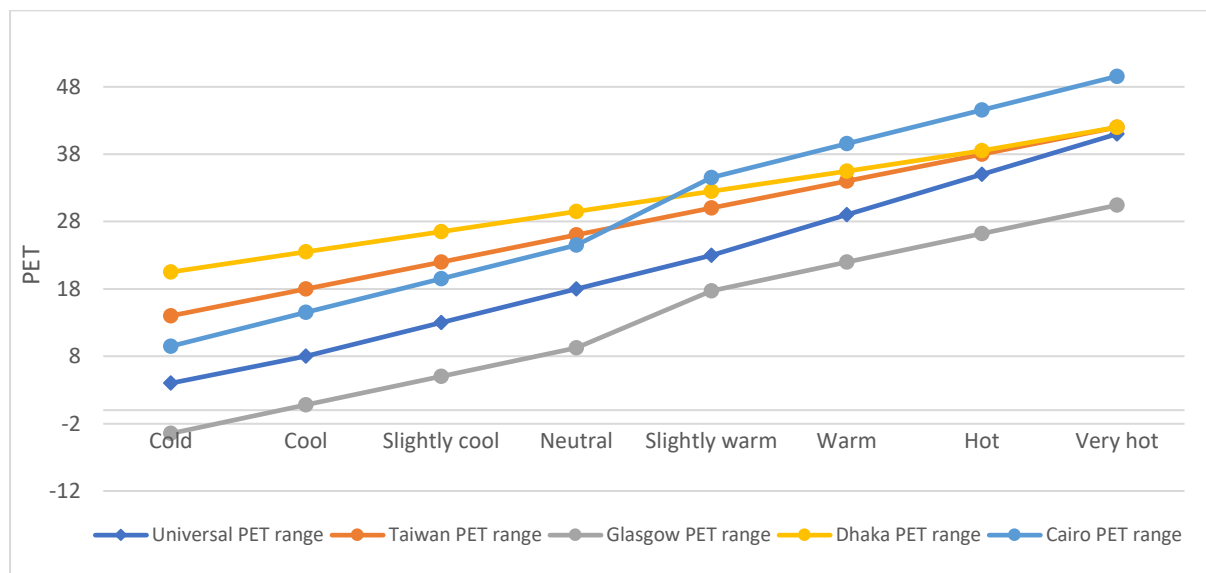


Figure 4.9. The modified PET range for different climate zones in summer - source (Elnabawi, et al., 2016; Kruger, et al., 2012; Lin & Matzarakis, 2008; Sharmin, et al., 2019; Höppe, 1999).

The modified PET ranges that were used in this research were calculated in the city of Anatolia, Turkey. Amman and Anatolia are under the cold semi-arid climate classification, according to the Köppen climate classification. Canan et al., 2019, calculated the modified PET

summer range using questionnaire surveys and in-situ monitoring. The results show that neutral or comfort range for the cold semi-arid climate is between 21.6 °C and 32 °C.

4.6 AMMAN, JORDAN CASE STUDY.

4.6.1 STREET GRID'S ANALYSIS.

Jordan has been developing fast in the past decades and this rapid growth has resulted in overcrowding and high rates of population in the capital of Jordan Amman. This has led Amman to extend to the southern areas of the capital to relieve the overpopulation issues. The area of the site chosen for the study is 282,600 m², with an incline estimated to be not more than 1%. The site is adjacent to satellite cities and located next to empty plots that are left unused – see Figure 4.10.



Figure 4.10. Satellite image of the site chosen in the south of Amman.

The study utilized a systematic procedure to plan the most efficient urban design for a residential setting in terms of pedestrians' thermal comfort. After studying the effect of street grids (results presented in Chapter 6), it was concluded that using the radial system was not effective in terms of thermal comfort nor particle dispersion. This has led the study to propose a grid system based on uniform shapes and spaces, to reinforce the wind flow and lower the thermal stress in the harsh summers.

The rectilinear nature of the proposed design for the site is derived from the most common streets grids chosen by urban planners, as seen in Manhattan in 1811, where it unified the city plan to ensure public convenience and health (Rose-Redwood, 2005) and San Francisco, where Viogets and O'Farrel planned the now-iconic grid system that laid the grid on the entirety of the area despite the harsh topography (Mawn, 1972).

The first proposal for the street grid layout is based on the wind direction with diagonal streets stretching from the main roads for a smoother wind flow (Figure 4.11-left). The second wind-based layout has the streets joining at 90 degrees angle (Figure 4.11-right). The decision was made for a realistic residential plot layout (more convenient for design purposes) with the main roads stretching in the direction of the predominant wind.

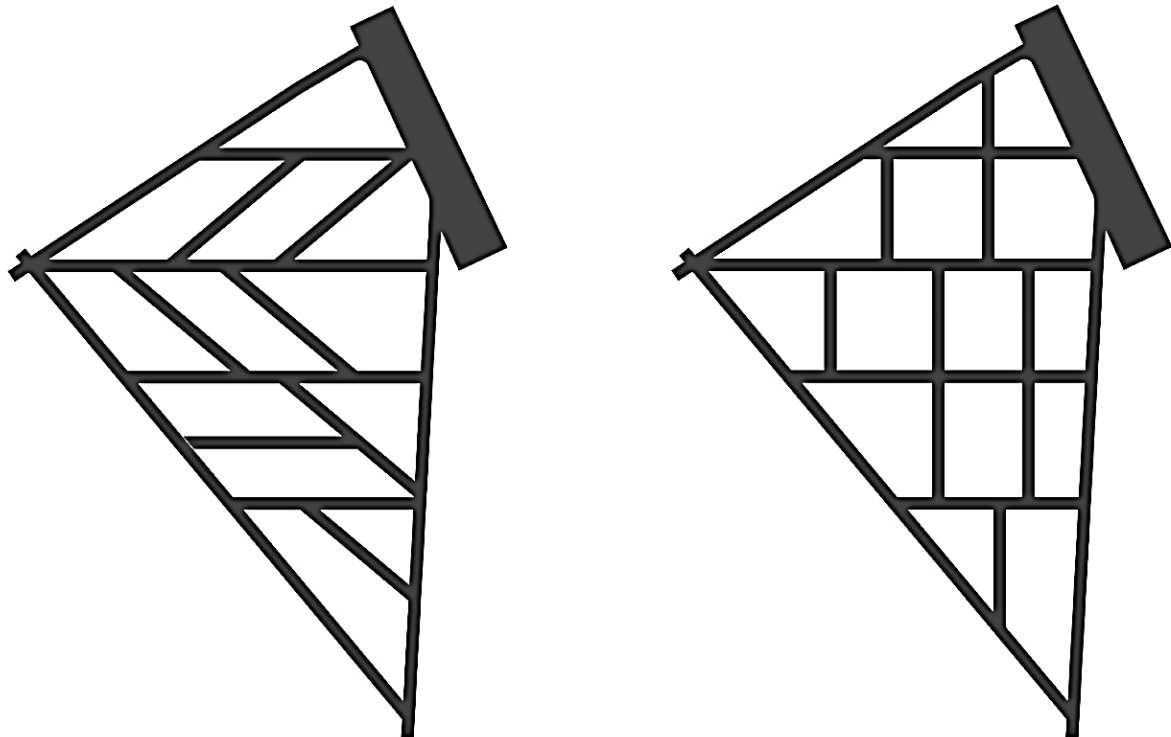


Figure 4.11. Main plot street grid layouts: proposal 1 (left) proposal 2 (right).

4.6.2 SUMMER AND WINTER ANALYSES.

PET is heavily influenced by solar radiation - more specifically, the mean radiant temperature. This means the shading patterns across the layouts determine the intensity of the PET levels. Looking at PET, it should be pointed out that it has weighted parameters, which means that some parameters can influence the results more than others, and the absence - or lower values - of the most influential parameter opens the chance to the other factors to play a

bigger part in the results. This case is seen when the mean radiant temperature is low - for example at night, wind speed controls the increase or decrease of the PET values.

The analysis for the streets grid is divided between summer and winter to find out the effect of different street pattern of changing weather, and the dates chosen for the simulations were 23rd June and 22nd December as they are a good examples of the seasons they are representing.

In order to calculate PET, four meteorological parameters must be present; wind speed, air temperature, relative humidity and mean radiant temperature. Envi-MET was used to obtain these parameters through modelling the layouts and using the EPW files as initial data for the simulation. Table 4.3 shows the data used for the modelling phase.

It should be noted that the comparison between the PET levels for layout 1 and 2 varies in approach between summer and winter scenarios, as under summer conditions it is near to impossible to reduce the PET levels to the comfort level. Instead, the PET is assessed on the increase or decrease of the values in reference to the results of the layout. In the case of winter scenarios, the PET levels are assessed on the proximity of the layout's results to the comfort levels shown in Table 4.7.

Table 4.7. The PET index comfort levels.

PET	Thermal perception	Physiological stress
< 4.1	Very cold	Extreme cold stress
4.1 – 8.0	Cold	Strong cold stress
8.1 -13.0	Cool	Moderate cold stress
13.1 -18.0	Slightly cool	Slight cold stress
18.1 – 23.0	Comfortable	No thermal stress
23.1 -29.0	Slightly warm	Slight heat stress
29.1 -35.0	Warm	Moderate heat stress
35.1 -41.0	Hot	Strong heat stress
> 41.0	Very hot	Extreme heat stress

4.6.3 ENVI-MET CONFIGURATION FILE.

The model run needed the hourly values for air temperature and relative humidity, and these data were extracted from an EPW file generated using Meteonorm. Simple force was used to enter the mentioned parameters while averaging out the wind speed parameter for the initial wind speed. The following data are the configuration files used in the model run for the street grid proposals in summer and winter.

SUMMER ANALYSIS ON THE 23RD OF JUNE.

```
%---- ENVI-met V4 main configuration file -----
%---- generated with ProjectWizard -----
Fileversion                =4.3
% Main data .....
Start Simulation at Day (DD.MM.YYYY):
=23.06.2018
Start Simulation at Time (HH:MM:SS):
=05:00:00
Total Simulation Time in Hours:      =26
Wind Speed in 10 m ab. Ground [m/s]  =3.0
Wind Direction (0:N..90:E..180:S..270:W..)
=255
Roughness Length z0 at Reference Point [m]
=0.01
Initial Temperature Atmosphere [K]
=301.580
Specific Humidity in 2500 m [g Water/kg air]
=7.0
Relative Humidity in 2m [%]          =50
% End main data .....
```

```
[OUTPUTTIMING]_____
Output interval main files (min)      =60.00
Output interval text output files (min)
=30.00
Include Nesting Grids in Output (0:n,1:y) =0

[TIMING]_____
Update Surface Data each ? sec        =30.00
Update Wind field each ? sec          =900.00
Update Radiation and Shadows each ? sec
=600.00
Update Plant Data each ? sec          =600.00
```

```
[SIMPLEFORCE]
```

```
Hour 00h [Temp, rH] = 297.55, 47.00
Hour 01h [Temp, rH] = 296.85, 41.00
Hour 02h [Temp, rH] = 296.45, 41.00
Hour 03h [Temp, rH] = 296.15, 41.00
Hour 04h [Temp, rH] = 296.15, 42.00
Hour 05h [Temp, rH] = 297.15, 42.00
Hour 06h [Temp, rH] = 298.65, 39.00
Hour 07h [Temp, rH] = 300.25, 37.00
Hour 08h [Temp, rH] = 301.75, 34.00
Hour 09h [Temp, rH] = 303.25, 31.00
Hour 10h [Temp, rH] = 304.55, 27.00
Hour 11h [Temp, rH] = 305.65, 26.00
Hour 12h [Temp, rH] = 306.45, 25.00
Hour 13h [Temp, rH] = 306.95, 24.00
Hour 14h [Temp, rH] = 307.05, 25.00
Hour 15h [Temp, rH] = 306.85, 26.00
Hour 16h [Temp, rH] = 306.25, 26.00
Hour 17h [Temp, rH] = 305.25, 27.00
Hour 18h [Temp, rH] = 304.05, 28.00
Hour 19h [Temp, rH] = 302.75, 30.00
Hour 20h [Temp, rH] = 301.45, 35.00
Hour 21h [Temp, rH] = 300.15, 36.00
Hour 22h [Temp, rH] = 298.85, 38.00
Hour 23h [Temp, rH] = 297.55, 41.00
```

```
[PARALLEL_CPU]_____
CPU usage settings          =ALL
[IVSRADIATION]_____
Use IVS radiation transfer scheme (0:n,1:y) =
1
```

WINTER ANALYSIS ON THE 22ND DECEMBER.

```

%---- ENVI-met V4 main configuration file -----
%---- generated with ProjectWizard -----
Fileversion                =4.3
% Main data .....
Start Simulation at Day (DD.MM.YYYY):
=22.12.2018
Start Simulation at Time (HH:MM:SS):
=05:00:00
Total Simulation Time in Hours:      =26
Wind Speed in 10 m ab. Ground [m/s]  =2
Wind Direction (0:N..90:E..180:S..270:W..)
=255
Roughness Length z0 at Reference Point [m]
=0.01
Initial Temperature Atmosphere [K]
=284.310
Specific Humidity in 2500 m [g Water/kg air]
=7.0
Relative Humidity in 2m [%]          =50
%      End      main      data
.....
[OUTPUTTIMING]_____
_____
Output interval main files (min)      =60.00
Output interval text output files (min)
=30.00
Include Nesting Grids in Output (0:n,1:y) =0
[TIMING]_____
_____
Update Surface Data each ? sec        =30.00
Update Wind field each ? sec          =900.00
Update Radiation and Shadows each ? sec
=600.00
Update Plant Data each ? sec          =600.00

```

[SIMPLEFORCE]

```

Hour 00h [Temp, rH] = 282.65, 71.00
Hour 01h [Temp, rH] = 280.25, 78.00
Hour 02h [Temp, rH] = 280.35, 75.00
Hour 03h [Temp, rH] = 280.45, 74.00
Hour 04h [Temp, rH] = 280.55, 72.00
Hour 05h [Temp, rH] = 280.65, 72.00
Hour 06h [Temp, rH] = 280.75, 71.00
Hour 07h [Temp, rH] = 280.85, 69.00
Hour 08h [Temp, rH] = 282.15, 65.00
Hour 09h [Temp, rH] = 283.95, 58.00
Hour 10h [Temp, rH] = 285.45, 55.00
Hour 11h [Temp, rH] = 286.95, 54.00
Hour 12h [Temp, rH] = 287.95, 51.00
Hour 13h [Temp, rH] = 288.65, 47.00
Hour 14h [Temp, rH] = 288.95, 47.00
Hour 15h [Temp, rH] = 288.75, 51.00
Hour 16h [Temp, rH] = 288.05, 52.00
Hour 17h [Temp, rH] = 287.05, 54.00
Hour 18h [Temp, rH] = 286.45, 57.00
Hour 19h [Temp, rH] = 285.75, 62.00
Hour 20h [Temp, rH] = 285.15, 63.00
Hour 21h [Temp, rH] = 284.55, 64.00
Hour 22h [Temp, rH] = 283.95, 65.00
Hour 23h [Temp, rH] = 283.25, 69.00

```

[PARALLEL_CPU]_____

CPU usage settings =ALL

[IVSRADIATION]_____

Use IVS radiation transfer scheme (0:n,1:y) = 1

4.6.4 WIND DIRECTION RELATION TO THE PET VALUES, ANALYSIS FOR LAYOUT-2 PROPOSAL.

The wind direction in Jordan varies with each month and season. Figure 4.12 shows the frequency of the wind direction over a one-year period. The wind direction was divided into 4 zones: north to east, east to south, south to west and west to north with each occupying 90°. The area highlighted in red represents the direction of the wind from south to west with the highest percentage of wind flowing from that direction of 46.1%, while the other quarters showed a much smaller percentage with 14.4%, 28.3% and 11.2% respectively. The previous analysis for the street grid dealt with seasonal simulations for summer and winter and the wind direction was determined for the exact days the simulation was performed at. However, the wide range of wind direction needed to be addressed in a different manner to determine a holistic street grid layout that would produce the best wind flow throughout the majority of the year. The analysis moves forward in this regard and introduces a wide range of wind direction analysis to study the full effect of plot orientation and its relation to wind flow.

This section analysed 5 directions starting with westerly direction to mid-way between the west-south quarter, these directions were 270°, 255°, 240°, 225° and 210°. The choice to simulate these directions only and not the entirety of the 90° quarter was taken to minimise the simulation time as every file took up to 6 days of simulation time and these directions give the needed information for the different angles as the effect will be repeated every 45° to a different street direction. A study conducted in Kuala Lumpur, Malaysia analysing the different street orientation and its effect on PET, used a similar approach to study the different wind inlet directions and solar radiation (Zaki, et al., 2020).

The five scenarios shared the same configuration file where the meteorological factors were set to the harshest conditions of high thermal stress of summer, but with different wind direction values. The analysis studies the data in terms wind flow and thermal comfort index, however, due to the usage of the same meteorological factors some parameters will not be discussed -such as direct sun radiation- in terms of raising or lowering the PET values. The focus will be the wind speed parameter inside the streets and how it affects the PET values extracted from four receptors laid in the plot.

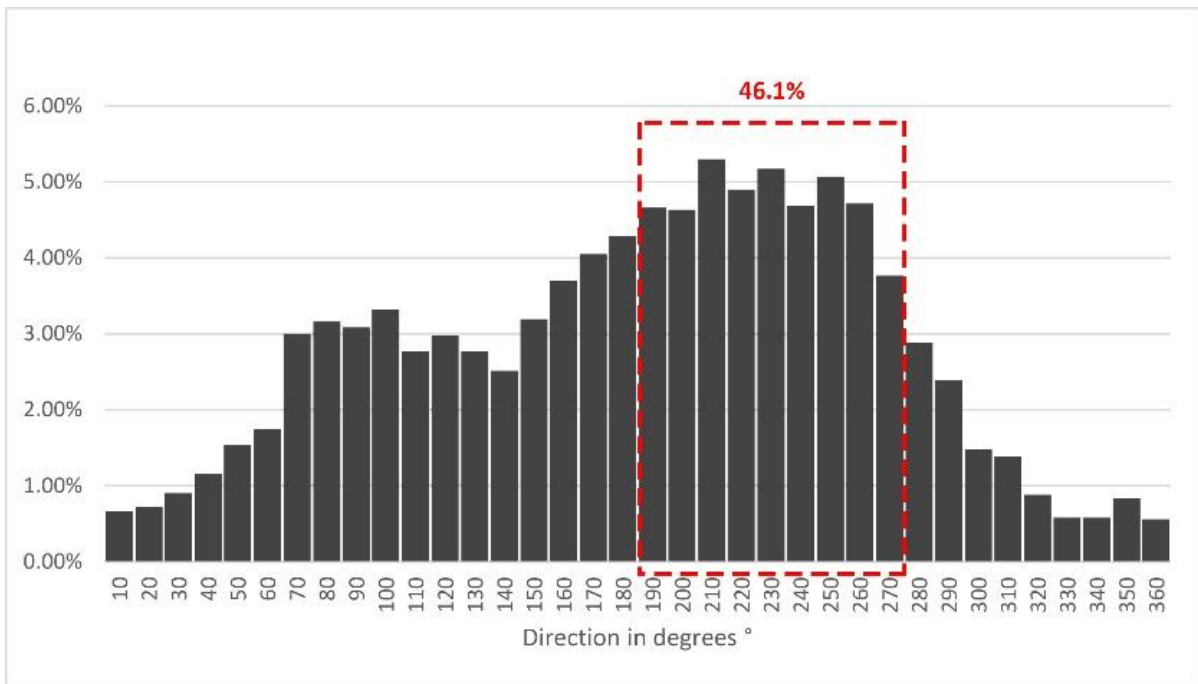


Figure 4.12. Wind direction histogram. Source: Meeonorm.

4.6.5 BUILDINGS' CLUSTER ANALYSIS.

This section will address the smaller scale analysis, the buildings' clusters analysis. The study proposes two main layouts for the analysis based on the common practice of designing residential layouts (Figure 4.13). The first proposal was called compound 1 and consisted of 16 buildings with vegetative entrances and vegetative pathways, the design maximizing on the built-up area. The second proposal was named compound 2 and consisted of 8 buildings aligned with the wind flow direction. The design was based on the basic environmentally responsive design with ventilated areas and vegetation that does not obstruct the wind flow.

Compound 1 shows a residential complex with a transition from the main street to the inner parts of the compound, as seen in Figure 4.14 The design consisted of three main areas, and they are characterised by air flow. In area 1 (the main street) wind flows without restrictions around the buildings, while in area 2 (main pathway) wind flows through the vegetative area with resistance caused by the trees, but due to wind tunnel effect, the effect is tolerated, and in area 3 wind flow is restricted due to the geometry of the buildings and the addition of trees. Compound 2, on the other hand, was designed to be more sensitive to the climatic parameters around the site. The compound was designed with strips of buildings rather than the C-shape conventionally used in residential compounds, and the buildings and pathways were oriented in the direction of the prevailing wind. This allowed for better wind ventilation,

reinforced with access points marked 6 in Figure 4.13. Each strip of buildings was connected 6 metres above ground to allow the creation of a roofed pathway that would connect the northern parts of the site with southern parts without wasting all of the vertical built-up area.

To test out the two mentioned designs, ten receptors were placed across the two compounds and then the site was simulated in Envi-MET to calculate the PET levels. The analysis was made under the summer conditions (23rd of June) because summer has the harshest conditions on the human thermal perception in Amman, Jordan. The results for the analysis are displayed between the hours of 05:00 to 16:00 for the purpose of reducing simulation time without compromising the results. The results of the simulations were analysed in terms of PET and wind flow.

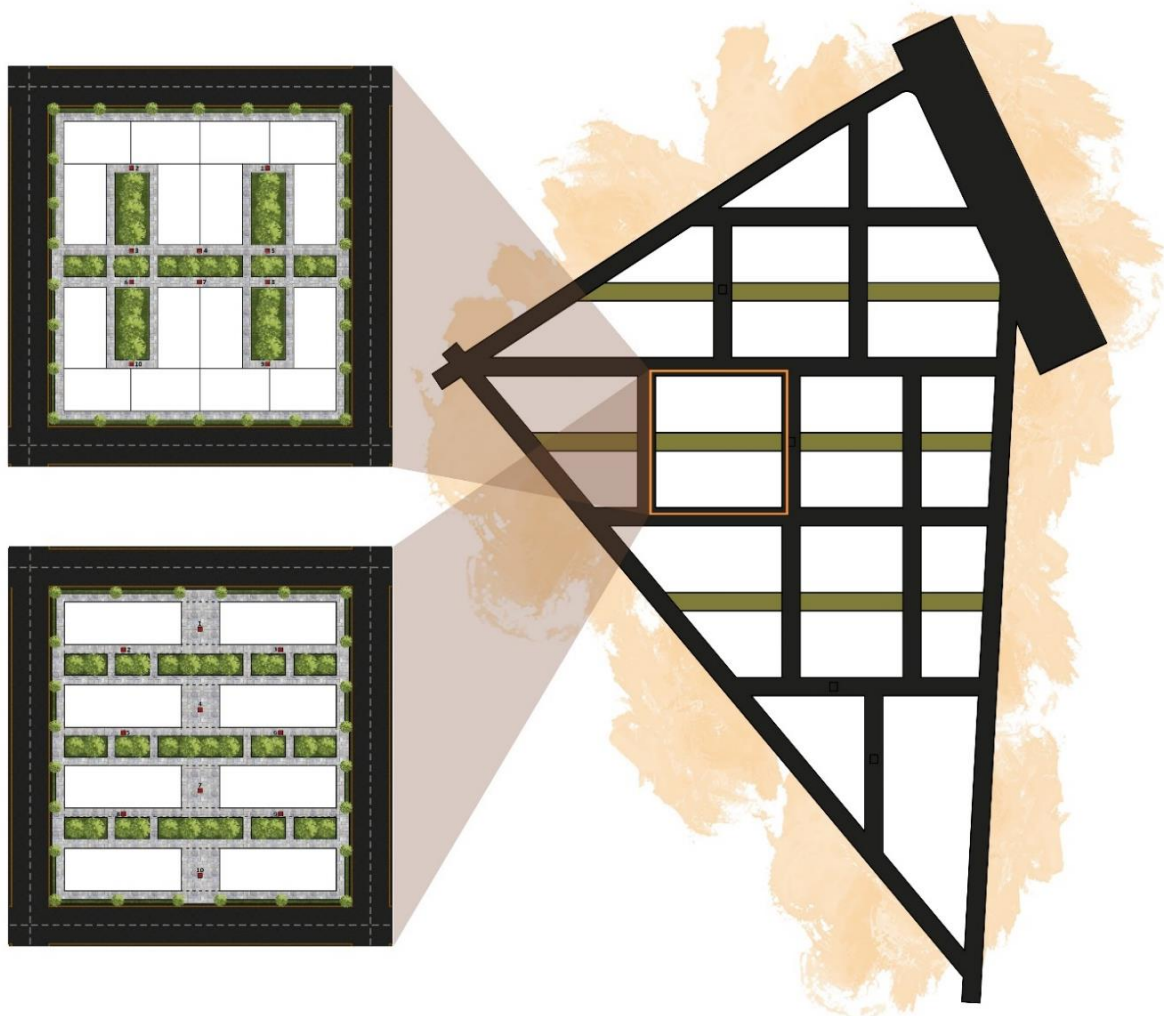


Figure 4.13. Location of the proposed compounds.

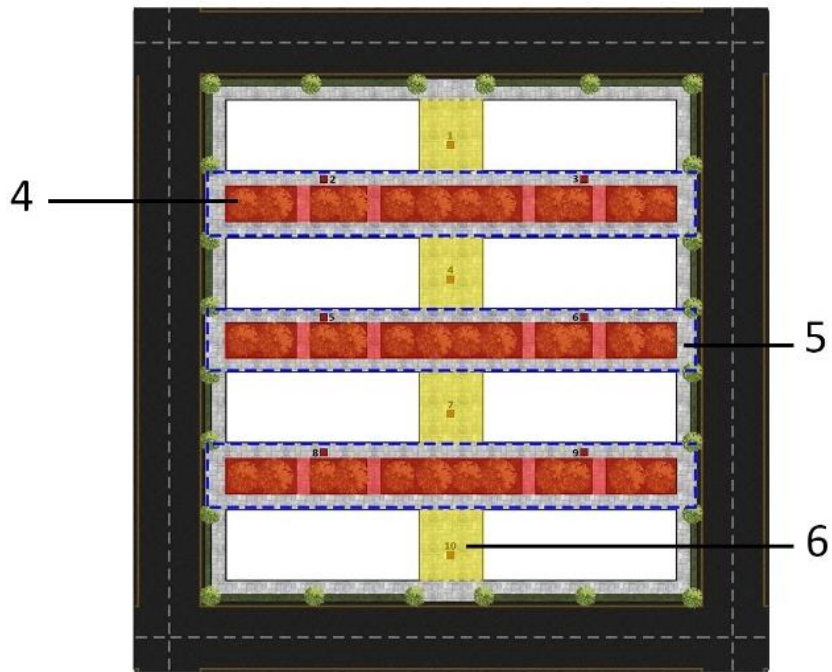
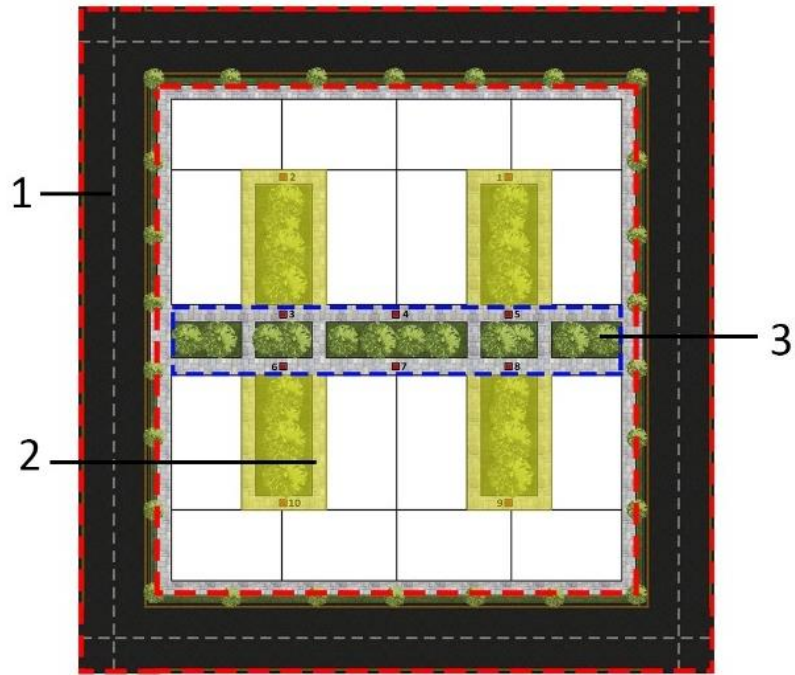


Figure 4.14. Compound 1 (top) and compound 2 (bottom) diagram design.

1. Main street- wind flows freely.
2. Pathway- wind flow is somewhat restricted.
3. Main buildings' entrance- wind flow is restricted.
4. Vegetation placed in the direction of prevailing wind and facing south facade.
5. Pathways in the direction of prevailing wind.
6. Access points for better ventilation.

4.6.6 ENVI-MET CONFIGURATION FILE.

The simulation time for this model run was limited to the day hours when direct solar radiation was present, and so the total simulation time in hours was set to 11. The meteorological parameters were extracted from an EPW file generated using Meteonorm.

```

%---- ENVI-met V4 main configuration file ----
%---- generated with ProjectWizard -----
Fileversion                =4.3
% Main data .....
Start Simulation at Day (DD.MM.YYYY):
=23.06.2018
Start Simulation at Time (HH:MM:SS):
=05:00:00
Total Simulation Time in Hours:      =11
Wind Speed in 10 m ab. Ground [m/s]  =3.0
Wind Direction (0:N..90:E..180:S..270:W..)
=270
Roughness Length z0 at Reference Point [m]
=0.01
Initial Temperature Atmosphere [K]
=301.580
Specific Humidity in 2500 m [g Water/kg air]
=7.0
Relative Humidity in 2m [%]          =50
% End main data .....
[OUTPUTTIMING]_____
Output interval main files (min)      =60.00
Output interval text output files (min)
=30.00
Include Nesting Grids in Output (0:n,1:y) =0
[TIMING]_____
Update Surface Data each ? sec        =30.00
Update Wind field each ? sec          =900.00
Update Radiation and Shadows each ? sec
=600.00
Update Plant Data each ? sec          =600.00

[SIMPLEFORCE]
Hour 00h [Temp, rH] = 297.55, 47.00
Hour 01h [Temp, rH] = 296.85, 41.00
Hour 02h [Temp, rH] = 296.45, 41.00
Hour 03h [Temp, rH] = 296.15, 41.00
Hour 04h [Temp, rH] = 296.15, 42.00
Hour 05h [Temp, rH] = 297.15, 42.00
Hour 06h [Temp, rH] = 298.65, 39.00
Hour 07h [Temp, rH] = 300.25, 37.00
Hour 08h [Temp, rH] = 301.75, 34.00
Hour 09h [Temp, rH] = 303.25, 31.00
Hour 10h [Temp, rH] = 304.55, 27.00
Hour 11h [Temp, rH] = 305.65, 26.00
Hour 12h [Temp, rH] = 306.45, 25.00
Hour 13h [Temp, rH] = 306.95, 24.00
Hour 14h [Temp, rH] = 307.05, 25.00
Hour 15h [Temp, rH] = 306.85, 26.00
Hour 16h [Temp, rH] = 306.25, 26.00
Hour 17h [Temp, rH] = 305.25, 27.00
Hour 18h [Temp, rH] = 304.05, 28.00
Hour 19h [Temp, rH] = 302.75, 30.00
Hour 20h [Temp, rH] = 301.45, 35.00
Hour 21h [Temp, rH] = 300.15, 36.00
Hour 22h [Temp, rH] = 298.85, 38.00
Hour 23h [Temp, rH] = 297.55, 41.00
[PARALLEL_CPU]_____
CPU usage settings                =ALL
[IVSRADIATION]_____
Use IVS radiation transfer scheme (0:n,1:y) =
1

```

4.6.7 COMPOUND 2 SHADING ADDITION AND THEIR EFFECT ON PET.

Pedestrians' thermal comfort is immensely affected by solar radiation in the summertime in a hot arid climate. For that reason, the main approach for reducing the thermal stress is shading, whether it be by using vegetation or fixed shading devices. Shading as a mean of reducing PET is the case in multiple studies, such as (Yin, et al., 2019), where they analysed three cases of streets configurations: an alley, an arcade and a boulevard. Other studies also investigated the effect of shading and found a huge improvement in thermal stress indices (Jamei, et al., 2016), (Lai, et al., 2017), (Zhao, et al., 2018) (Morakinyo, et al., 2017) and (Jamei & Rajagopalan, 2017).

The analysis of the two compounds proposals showed that proposal 2 as hypothesized with the environmentally responsive design performed better in terms of PET levels (see Chapter 6- section 2). However, there were a few critical areas with high predicted PET levels. This section will address these areas and attempt to enhance the PET levels with horizontal shading added to the buildings as the targeted area face the south sun with high radiation.

Figure 4.14 shows the second proposal before and after the addition of the horizontal shading devices. The shading dimensions were calculated to protect from the harsh summer sun where the solar altitude is 82° in June. The height of the device was set to 3 metres with a 3 metre depth to cover the receptors that were placed 2.5 metres away from the edge of the building. Receptors 2, 3, 5, 6, 8 and 9 were re-examined after the site has been modified and the PET levels were calculated and compared to the original proposal.

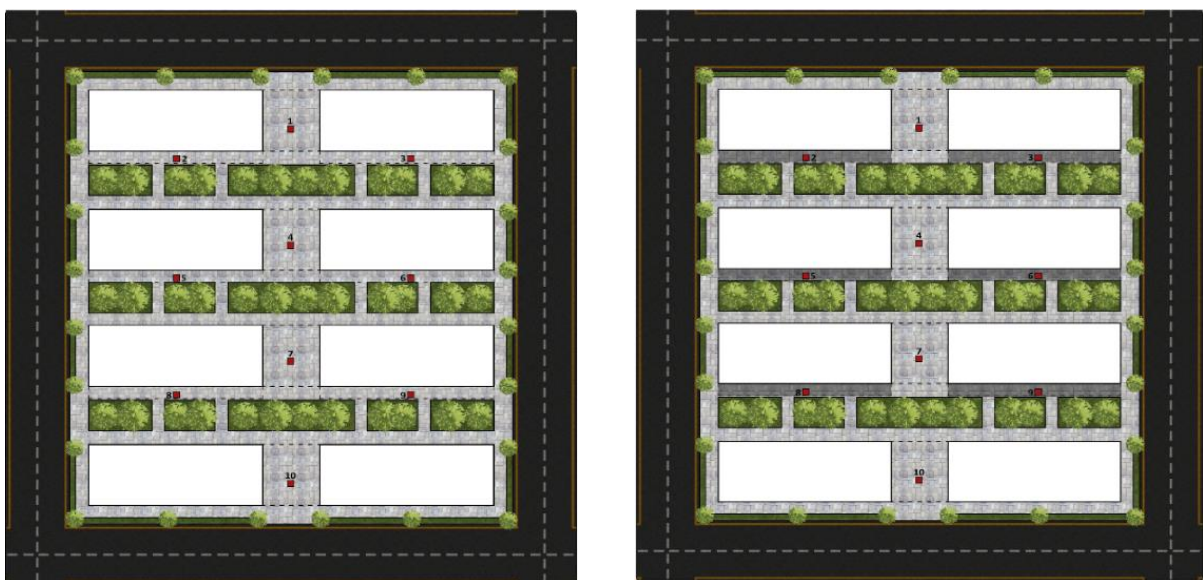


Figure 4.15. Proposal 2 with shading devices additions.

4.6.8 BUILDINGS CLUSTER MICRO ANALYSIS.

In this section, the study zooms in to two strips of buildings and examines the geometrical and vegetation variation effects on the PET levels at the pedestrian level. This section will address the effect of the geometrical modifications such as cutting a pathway all the way up the buildings instead of a tunnel-like structure. The hypothesis is that by leaving the initial tunnel between the buildings, wind speed would increase in that area which will feed the internal wind flow of the studied area.

The study also addresses the effect of changing the heights of the buildings without changing the width of the streets - in other words, changing the height to street width ratio. The heights of the buildings that were introduced into the study were 24m, 18m and 12m, with a pathway width of 9m. These heights reflect some extreme cases in which urban environments suffer, as studies have shown (Bakarman & Chang, 2015), (Jamei, et al., 2017) and (Achour-Younsi & Kharrat, 2016). The study also investigates the effect of changing the leaf area density (LAD) of the trees added to the site as well as changing the orientation with keeping the initial wind direction the same.

Figure 4.15 shows the area that will be further investigated for this analysis, three vertical sections were made to show the wind behaviour in the z-axis as well as the pedestrians level cut at 1.5 meters. The area includes two strips of buildings with a walking area between them that has 12 trees added for shading. The base model parameters are set to 12 meters for buildings height, 1.5 for LAD of trees, 90° counter-clockwise off north for wind direction and the gap between the buildings is roofed at 6 meters height.

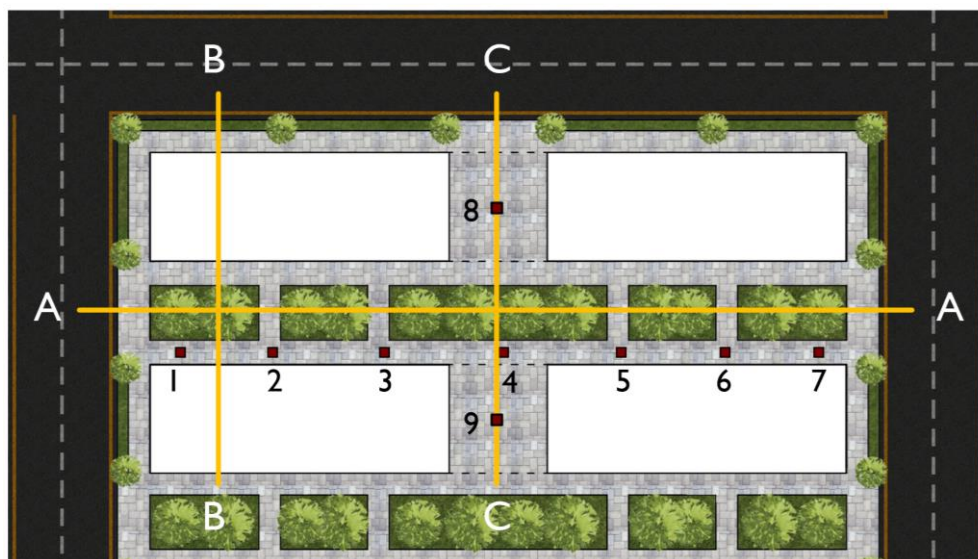


Figure 4.16. The area investigated for the microanalysis with the section cuts.

4.6.9 GEOMETRICAL MODIFICATION; DESIGNING THE BUILDINGS PATHWAYS

Compound's 2 design started with a row of buildings arranged towards the wind direction four times, then a pedestrian pathway was added between the buildings throughout the compound on its North-South axis. The initial instinct as an architect was to preserve as much built-up area as possible when designing the compound, so the pathway was constructed as a 6-metre high tunnel with the upper part of the buildings connected - highlighted in pink in Figure 4.16.

In this section the alternative to the tunnel was introduced as a full cut in the buildings separating the row buildings into two masses. This geometrical change should answer the question of whether it would be beneficial for the wind flow and PET at the pedestrians level to have a tunnel pathway or an open gap. Many studies have suggested the benefits of wind tunnels in creating better wind flow if it was deployed under a favourable condition such as the direction of the wind (Sharples & Bensalem, 2001), (Castelli, et al., 2018) and (Blackman, et al., 2015).

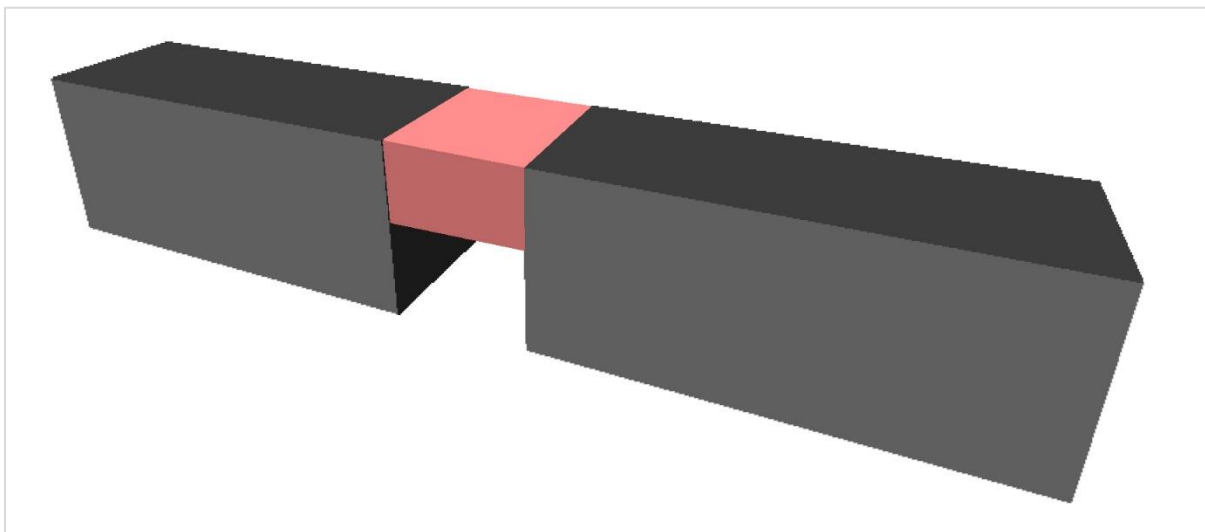


Figure 4.17. Pedestrian pathway through the row buildings.

4.6.10 BUILDINGS' HEIGHT MODIFICATION EFFECTS ON PET.

This section will continue studying the plot segment taken from compound 2 in terms of buildings' height and its effect on PET and wind flow at the pedestrians' level. The analysis kept the initial meteorological parameter as in the compound 2 simulation file to keep a

cohesive comparable data. The width of the buildings was also kept at the same value of 10 metres for all the simulation process.

Three scenarios were designed with buildings heights of 12, 18 and 24 metres. The width between the buildings remained constant at 9 metres, which made the height to width ratios for the scenarios 1.3, 2 and 2.6, respectively. The ratios 2 and 2.6 are on the high end of the spectrum when urban canyons are discussed, but they are not unheard of in the urban environment. The configurations are shown in Figures 4.17 and 4.18. The results of the simulation will be analysed in term of PET levels and wind flow effectivity.

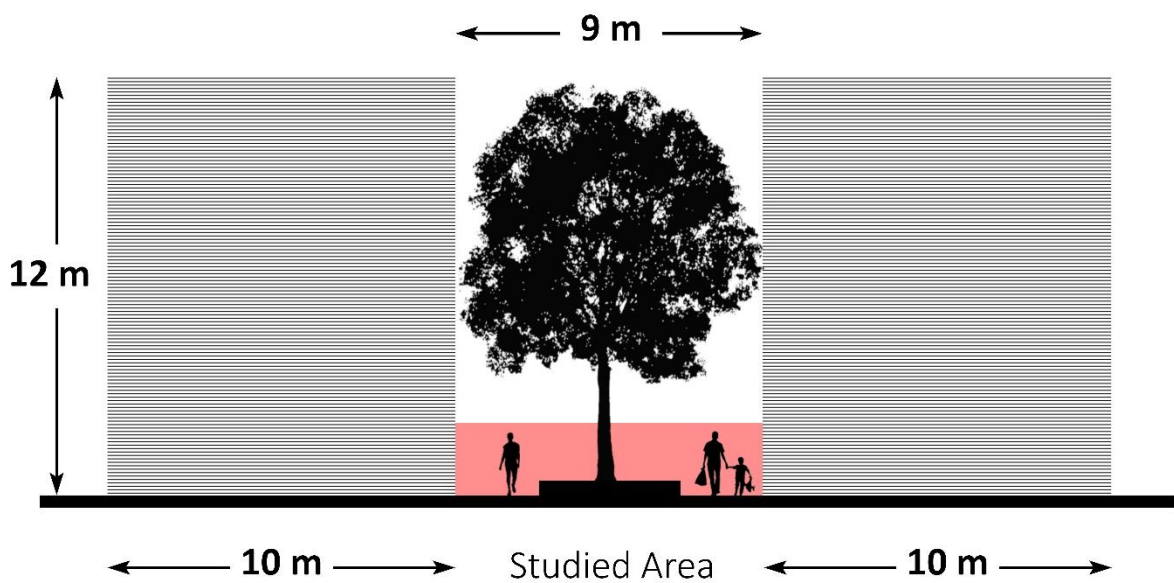


Figure 4.18. 12-metre high analysis.

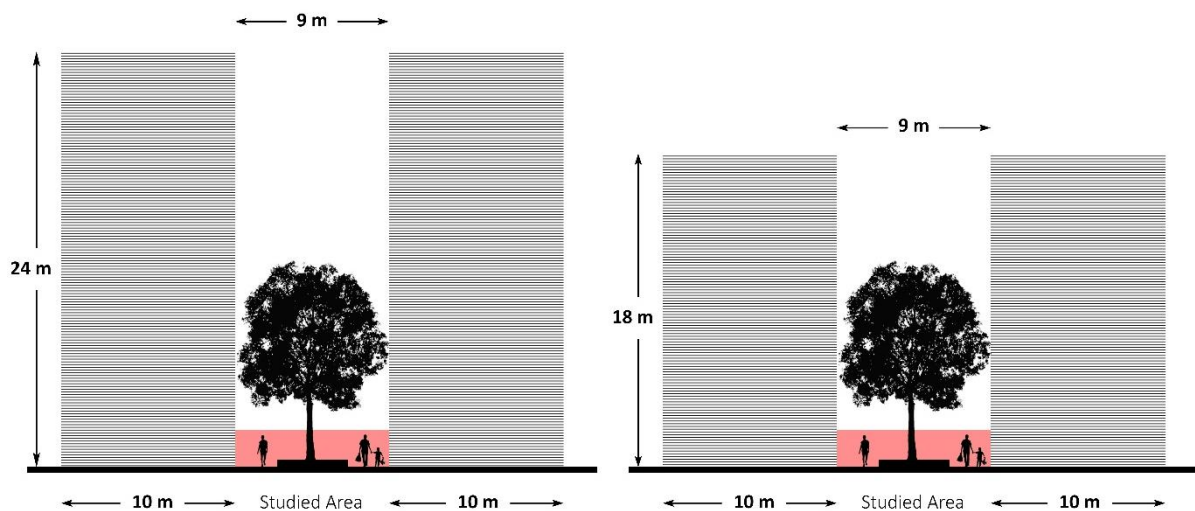


Figure 4.19. 18-metre high analysis (Right) 24-metre high analysis (Left).

4.6.11 TREE LEAF AREA DENSITY (LAD) AND ITS EFFECT ON PET AND WIND FLOW.

Vegetation can play a key role in reducing the thermal stress in an urban environment, whether it be by providing shading or by evapotranspiration cooling (Fahmy, et al., 2016), (Zhao, et al., 2018), (Lee & Mayerb, 2018), (Zheng, et al., 2016), (Wu & Chen, 2017) and (Abreu-Harbich, et al., 2015). In this section, the study will discuss the different leaf area densities (LAD) of the vegetation added to the site and their effect on wind flow and thermal comfort at pedestrian level.

The study of trees placement is effective when the subject in hand is a wide court or a square in a city for instance. However, in this study the space that is being studied is a long strip between buildings. The walkability inside this strip was considered while placing the trees, and the end result of placing the trees is seen in figure 4.18. The study leaned closer to analysing the tree shading coverage as well as its cooling effect on the surrounding pedestrian level rather than the location, and this demanded the study of the LAD effect of different trees. The determination of a tree species' LAD is a more difficult process that uses imaging methods (Meir, et al., 200) or numerical calculation (Stadt & Lieffers, 2000). For this reason, the LAD was estimated based on the work of Stadt and Lieffers (2000), where they list multiple tree species LAD ranging from 0.124 m^{-1} to 1.98 m^{-1} . Future studies are needed to estimate Jordan's local vegetation LAD, as they are detailed in works, such as (Al- Eisawi, 1986), (Boulos & Lahham, 1977) and (Al-Eisawi, 1987).

ENVI-met's vegetation tool Albero was used to edit the profile of the tree. In a study conducted in 2018 to validate the vegetation model in ENVI-met, it was found that the correlation factor between the simulated and observed data were within the acceptable ranges. However, there is room for improvement as the leaf area density, relative humidity, air temperature and vapour flux show underestimation (Liu, et al., 2018). The site was kept at its original parameters with 12-metre high buildings and a 9-metre gap between the buildings. The trees were chosen to be a deciduous type and they were spread out along the one axis with the same foliage structure to limit the variables that could affect the outcome of the PET levels and wind flow.

The simulation process consisted of three scenarios with different LAD values for the trees. The first scenario's LAD was set to 0.5 m^{-1} , the second at 1.0 m^{-1} and the third at 1.5 m^{-1} . The

meteorological factors were kept the same as in the previous sections to test out the effect of different leaf area densities on the thermal stress on pedestrians as well as wind speed.

4.6.12 SITE ORIENTATION AND ITS EFFECT ON PET AND WIND FLOW.

The orientation of buildings is one of the study's aspects of the urban geometry analysis, and this includes the heights and shapes of the build-up areas (Deng & Wong, 2020), (Guo, et al., 2019) and (Krüger, et al., 2011). In this section the focus is on the effect of different orientations to the same design. This method allows the study to identify the effect of wind direction as well as the sun angle on an elongated buildings design, and this method can be applied to different urban elements such as streets design and alleyways (Hong & Lin, 2015) and (Ali-Toudert & Mayer, 2006).

This section will discuss two different orientation to the designed scenarios for this study, the original design was kept with 12-meter high buildings, pathway width at 9 meters and trees LAD at 1.5 m^{-1} . The analysis will discuss the original orientation versus the 90- degrees rotation counter clockwise from north, this will show how wind flow is affected by the geometry change in the site as well as the PET values due to the change of geometry shading.

4.7 THE CALCULATION OF THE PHYSIOLOGICAL EQUIVALENT TEMPERATURE INDEX USING RAYMAN.

Literature has shown that several methods are used to calculate the thermal stress on the human body, e.g. questionnaires (Zamanian, et al., 2017), (Salata, et al., 2016), (Yang, et al., 2017) and (Vasilikou & Nikolopoulou, 2020) as well as micrometeorological measurements (Abaas, 2020), (Wai, et al., 2020), (Fröhlich, et al., 2019) and (Sodoudi, et al., 2018). The pedestrian thermal comfort in this study has been expressed by the PET index, by using the micrometeorological measurement method. The data that were gathered from ENVI_met simulations were collected in terms of four meteorological parameters: air temperature, wind speed, relative humidity and mean radiant temperature. These aforementioned data were used to calculate the PET using RayMan software.

RayMan is time-independent computer model that operates for one point in space e.g. Receptors. It was developed to calculate the radiation fluxes in an urban environment (Matzarakis, et al., 2006) and (Matzarakis, et al., 2009). The model calculates the mean radiant temperature (T_{mrt}), which is the most weighted factor in calculating thermal comfort indices

like PET and UTCI. RayMan is widely used to calculate the T_{mrt} and the thermal indices (PET and UTCI) (Fröhlich, et al., 2019), (Li, et al., 2020), and (Lee, et al., 2020). The model does not need high computational capability to operate and it is user friendly. However, RayMan falls short in the spatial analysis as it only calculates one point of interest (Matzarakis, et al., 2009). The physiological equivalent temperature in definition does not accommodate a change of clothing insulations or activity as it is described by Höppe (1999) as “*a real climatic index describing the thermal environment in a thermo physiologically weighted way*”. Thus, the only way to change the parameters inserted into RayMan was via the meteorological parameters: air temperature, wind speed, relative humidity and mean radiant temperature, whereas the human parameters were fixed at 0.9 clo for clothing insulation and 80 W for activities. The process of calculating PET in RayMan is a straightforward process, where the meteorological data is saved with their respective headings in a tab-delimited text file, and then inserted into RayMan through the input portal. The PET values are generated in a text file to be saved and used for further analysis and comparison. Figure 4.19 shows the interface for RayMan.

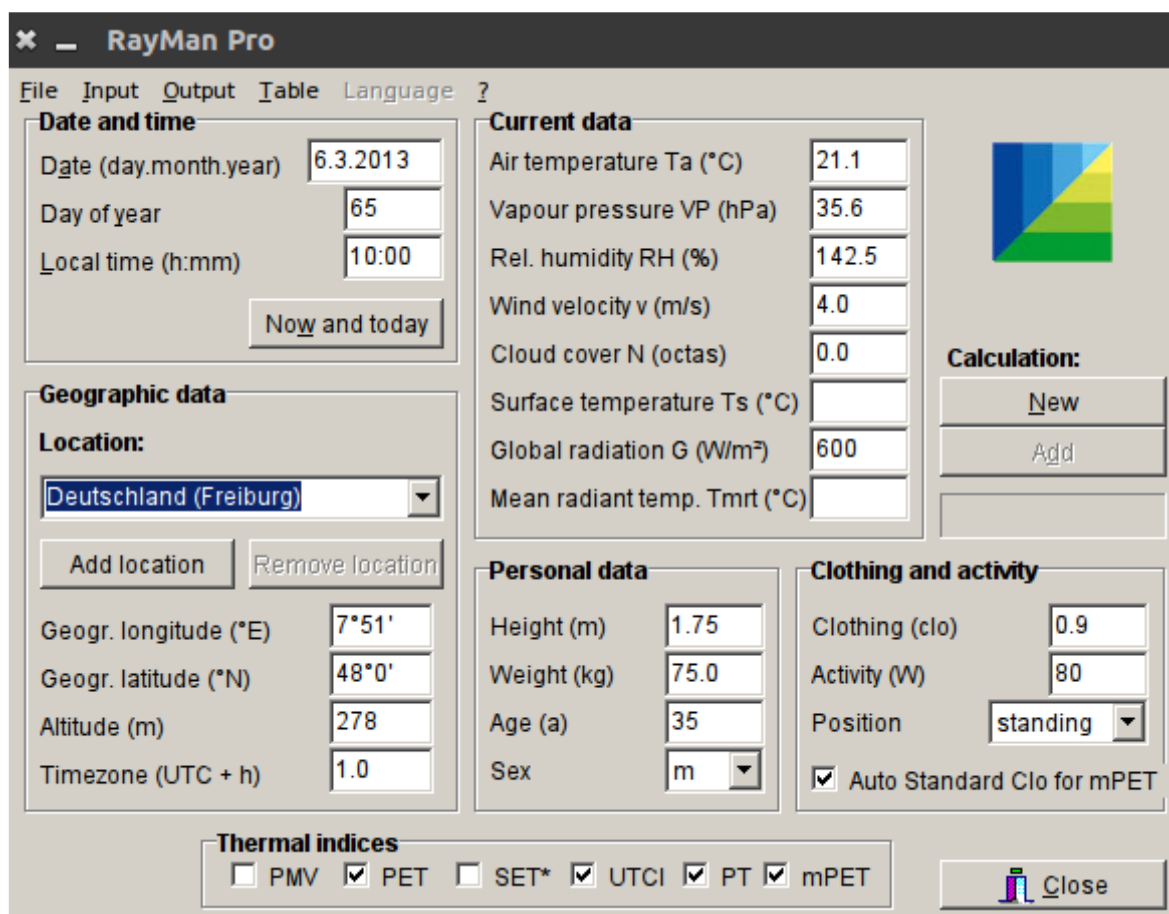


Figure 4.20. Interface of RayMan software.

4.8 SUMMARY

This chapter has outlined the framework and the general methodological approaches that have been adopted in this study. The arrangements for the validation of the ENVI-met model were illustrated and the statistical means by which the validation results will be checked were described (see Section 4.3)

The extensive range of urban parameters to be analysed by the model have been itemised, and the reasons for their choice have been justified. The aim is to use ENVI-met to identify the best scenarios for the specific urban factors.

In the next chapter, the results of the ENVI-met validation are presented and discussed.

Chapter 5 : ENVI-met model validation

Content

1. Section one: ENVI-met: model overview.
2. Section two: ENVI-met validation.

SECTION ONE: ENVI-MET: MODEL OVERVIEW

Content

- 5.1 Introduction.
- 5.2 Spaces: grid layout.
- 5.3 The atmospheric model.
- 5.4 The soil model.
- 5.5 The vegetation model.
- 5.6 Surfaces: ground and buildings.
- 5.7 Numerical methods.
- 5.8 Summary.

5.1 INTRODUCTION

ENVI-met is a computational fluid dynamics software that assesses the effect of meteorological parameters on the urban environment. The software takes into consideration multiple elements of the urban environment, such as water features, vegetation, and the built environment. ENVI-met was developed by Bruse and Fleer in 1998. They established the main models that ENVI-met operated on, which included the atmospheric model, the soil model, the vegetation model, the numerical aspects and the built environment (Bruse & Fleer, 1998). Since then ENVI-met has been used in numerous investigations of which some of the most recent ones are (Liu, et al., 2020), (Abdallah, et al., 2020), (Fabbri, et al., 2020) and (Galal, et al., 2020), and also validation studies (Bande, et al., 2019) and (Gál & Kántor, 2020).

In this section, the main models of the CFD software ENVI-met will be explained based on the existing documentation of version 3.0, published by Bruse, 2004.

5.2 SPACES: GRID LAYOUT

The model in ENVI-met is comprised of three sub-models that work simultaneously in the same boundary setting. These sub-models are

The boundary model, the soil model, and the atmospheric model (Figure 5.1). The boundary model is a one-dimensional model that is used as a boundary condition for the atmospheric model, it is also used as the preliminary step to start the model.

The grid layout in the atmospheric model in ENVI-met is the area where all the physical objects are constructed. The three-dimensional model system consists of pixel-based geometry where the rectangular pixel is either filled with an object or empty, this is considered as a shortcoming of the construction of the object in ENVI-met, as any object that is not parallel to the main axis of Y and Z is roughly estimated with rough and sharp outlines. By the end of 2018, ENVI-met added a new vector-based system called MONDE, in this new tool users can import vector-based files like Shapefiles to MONDE and export them to SPACES, which reduced the modelling error for the built environment.

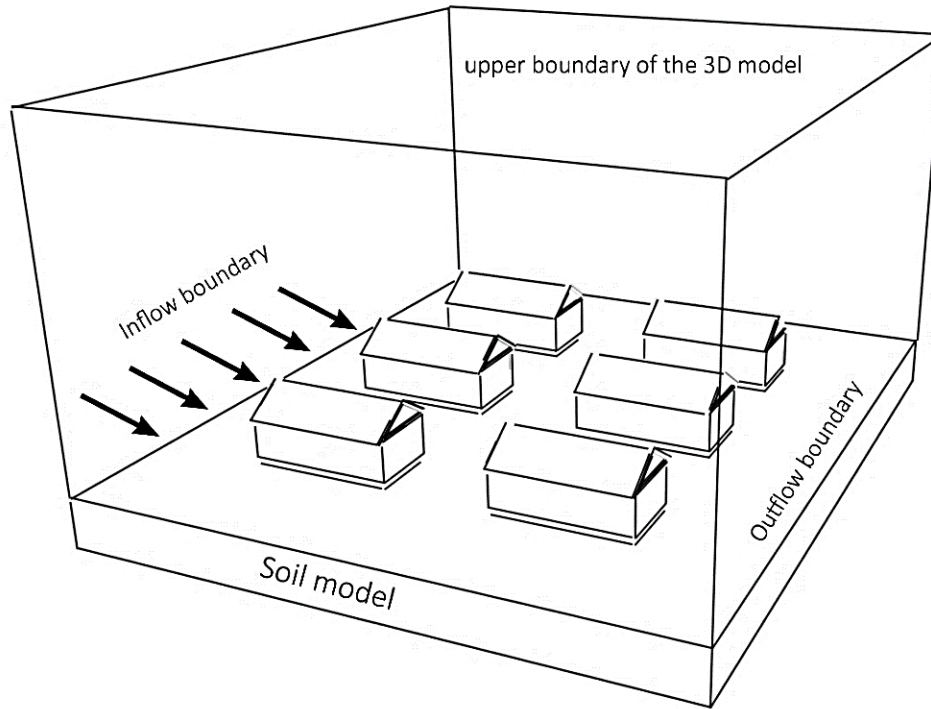


Figure 5.1. ENVI-met's basic model layout.

The dimensions of the grid cells are expressed with x , y and z , the spacing for x and y are always constant and expressed with dx and dy , the vertical spacing however has two methods of vertical grid generation: Equidistant and telescoping (Figure 5.2). The Equidistant dz mode splits the lowest gridbox into five sub-cells with size $dz_g = 0.2 * dz$ (Bruse & Fleer, 1998). This enhances the model's interaction on the ground level with more detailed pedestrians level environment. The telescoping mode allows the modelling of high-rise buildings where dz increases with increased height, this ensures that the lower levels of the buildings are modelled in a high resolution as they are the most crucial areas when studying the meteorological effect on humans. The telescoping option is set by a factor which is limited to a maximum of 20% and a start point which gives flexibility to the user of ENVI-met based on the study needs.

Equation 5.1 is used to calculate the grid size of a box (k) for the telescoping option after setting the main dimensions of the first box above the surface and the extension factor (s).

$$\Delta z(k) = \left[1 + \frac{s}{100} \right]^{k-1} \Delta z_{\text{start}} \quad (5.1)$$

where, s is the percentage of the telescoping factor, Δz_{start} is the size of the first box from the surface and k is the box after the first initial box.

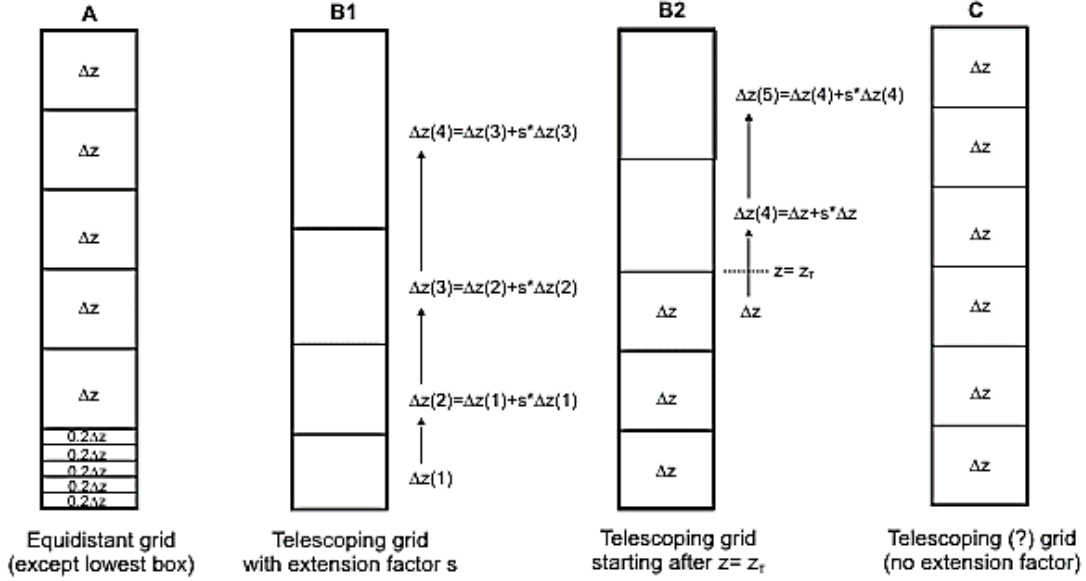


Figure 5.2. ENVI-met's vertical grids.

5.3 THE ATMOSPHERIC MODEL

5.3.1 WIND FIELD

ENVI-met uses the Reynolds-averaged non-hydrostatic Navier-Stokes equations to solve the wind flow for each time interval and for each grid cell in the built model space, and it takes into consideration the vegetation aspect as obstacles that would generate drag forces to the wind flow. The wind flow is calculated near the built surfaces for roofs and façades to ensure a detailed accurate representation of the wind flow. ENVI-met offers the wind analysis inside complex structures or semi-opened buildings with its single wall feature (ENVI-met, 2019). Equations 5.2 to 5.5 are used to calculate the wind flow based on the Reynolds-averaged non-hydrostatic Navier-Stokes equations (Bruse, 2004):

$$\frac{\partial u}{\partial t} + u_i \frac{\partial u}{\partial x_i} = - \frac{\partial p}{\partial x} + k_m \left[\frac{\partial^2 u}{\partial x_i^2} \right] + f(v - v_g) - s_u \quad (5.2)$$

$$\frac{\partial v}{\partial t} + u_i \frac{\partial v}{\partial x_i} = - \frac{\partial p}{\partial y} + k_m \left[\frac{\partial^2 v}{\partial x_i^2} \right] + f(u - u_g) - s_v \quad (5.3)$$

$$\frac{\partial w}{\partial t} + u_i \frac{\partial w}{\partial x_i} = - \frac{\partial p}{\partial z} + k_m \left[\frac{\partial^2 w}{\partial x_i^2} \right] + g \frac{\theta(z)}{\theta_{ref}(z)} - s_w \quad (5.4)$$

$$\frac{\partial u}{\partial x} + \frac{\partial v}{\partial y} + \frac{\partial w}{\partial z} = 0 \quad (5.5)$$

where, p is the pressure perturbation, θ the potential temperature at level z and f is the Coriolis parameter that equals 10^4 sec^{-1} . θ_{ref} represents the reference temperature and it is calculated using the average temperature for the empty cells in the grid reaching the upper boundary limit. It should be noted that, though the Coriolis parameter is implemented in ENVI-met, it is disabled in the default settings (Huttner, 2012) and the air density parameter was removed from the initial Reynolds-averaged non-hydrostatic Navier-Stokes equation by using the Boussinesq-Approximation (Bruse, 2004).

Vegetation in ENVI-met is characterised by its leaf area density (LAD) and its occupying geometry. As an obstacle vegetation create drag forces that affect the wind flow and decreases its velocity. Equation 5.6 describes this interaction based on Liu (1996) and Yamada (1982) work:

$$S_{u(i)} = \frac{\overline{\partial p'}}{\partial x_i} = c_{d,f} \text{ LAD}(z) \cdot W \cdot u_i \quad (5.6)$$

where, $c_{d,f}$ is the vegetation mechanical drag coefficient and it is set at 0.2, $\text{LAD}(z)$ is the leaf area density for the vegetation at the required height z and W is the mean wind speed at the required height z .

ENVI-met sets several conditions for the model boundaries to deal with the wind flow. To obtain the wind inflow and outflow two different conditions were implemented, the 1D reference model for the inflow and a zero-gradient Neumann condition for the outflow, while motions between layers at the top boundary are assumed to be zero. It is worth noting that all objects with solid surfaces are implemented with a no-slip condition (Bruse, 2004).

5.3.2 TEMPERATURE (T_a) AND HUMIDITY

ENVI-met calculates the air temperature and specific humidity based on different elements inside the model domain. These elements act as sources and sinks for the content of water vapour and sensible heat, which are affected by the wind flow by means of advection and diffusion. Inside the atmospheric model, the ground surface and vegetation affect the air temperature and humidity by either increasing or reducing the parameters. The built environment affects the parameters through heat exchange with the air surrounding it, and it can also affect the humidity if green walls and roofs are applied (ENVI-met, 2019).

Equations 5.7 and 5.8 are used to calculate the air temperature by combining the advection and diffusion equations. These equations use internals of the sources and sinks inside the model domain.

$$\frac{\partial \theta}{\partial t} + u_i \frac{\partial \theta}{\partial x_i} = k_h \left[\frac{\partial^2 \theta}{\partial x_i^2} \right] + \frac{1}{c_p \rho} \frac{\partial R_{n,lw}}{\partial z} + Q_h \quad (5.7)$$

$$\frac{\partial q}{\partial t} + u_i \frac{\partial q}{\partial x_i} = k_q \left[\frac{\partial^2 q}{\partial x_i^2} \right] + Q_q \quad (5.8)$$

where θ is the distribution of air temperature, q is the specific humidity, Q_h and Q_q relate to the vegetation effect on the atmospheric model, and their exact values are extracted from the vegetation model. The term $\left(\frac{1}{c_p \rho} \frac{\partial R_{n,lw}}{\partial z} \right)$ is used to express the change of air temperature as a result of the longwave radiation divergence (Bruse, 2004).

5.3.3 ATMOSPHERIC TURBULENCE

Turbulence is generally generated when the wind flow is sheared, and this is caused by several factors, such as temperature inversions and surface obstructions. In ENVI-met, the airflow changes directions and speed when facing obstacles e.g. buildings and vegetation, and this causes the creation of turbulences that usually do not dissipate but rather travel in the form of eddies by the mean wind flow.

To simulate turbulences, ENVI-met introduced a turbulence closure with 1.5 order to contain the exchanges. E-epsilon model was used to add two additional variables: (E) the turbulence and the turbulence dissipation rate (ϵ) (Mellor & Yamada, 1975). Equations 5.9 and 5.10 represent the turbulence distribution in the model:

$$\frac{\partial E}{\partial t} + u_i \frac{\partial E}{\partial x_i} = k_E \left[\frac{\partial^2 E}{\partial x_i^2} \right] + Pr - Th + Q_E - \epsilon \quad (5.9)$$

$$\frac{\partial \epsilon}{\partial t} + u_i \frac{\partial \epsilon}{\partial x_i} = k_\epsilon \left[\frac{\partial^2 \epsilon}{\partial x_i^2} \right] + c_1 \frac{\epsilon}{E} Pr - c_3 \frac{\epsilon}{E} Th - c_2 \frac{\epsilon^2}{E} + Q_\epsilon \quad (5.10)$$

where Q_E and Q_ϵ are the turbulences due to vegetation, and Pr and Th are the turbulences due to wind shearing at buildings surface and thermal stratification. C_1 , C_2 and C_3 were set to 1.44, 1.92 and 1.44 respectively (Launder & Spalding, 1974); however, these values could change depending on the model.

Pr and Th are calculated using Equations 5.11 and 5.12:

$$Pr = k_m \left[\frac{\partial u_i}{\partial x_j} + \frac{\partial u_j}{\partial x_i} \right] \frac{\partial u_i}{\partial x_j} \quad \text{with } i, j = 1, 2, 3 \quad (5.11)$$

$$Th = \frac{g}{\theta_{ref}(z)} k_h \frac{\partial \theta}{\partial z} \quad (5.12)$$

Turbulences are formed due to vegetation in the model, and transferred eddies also affect the local turbulences, where larger eddies transfer to smaller eddies thus weakening it. For this, Q_E and Q_ε were added to the E-epsilon model (Liu, et al., 1996) and (Wilson, 1988). Q_E and Q_ε are calculated using Equations 5.13 and 5.14:

$$Q_E = c_{d,f} LAD(z) \cdot W^3 - 4 c_{d,f} LAD(z) \cdot |W| \cdot E \quad (5.13)$$

$$Q_\varepsilon = 1.5 c_{d,f} LAD(z) \cdot W^3 - 6 c_{d,f} LAD(z) \cdot |W| \cdot \varepsilon \quad (5.14)$$

The turbulence exchange coefficients K_m , K_q , K_E and K_ε are calculated using Equations 5.15 and 5.18, with $c_\mu=0.09$, $\sigma_E=1$ and $\sigma_\varepsilon=1.3$.

$$K_m = c_\mu \frac{E^2}{\varepsilon} \quad (5.15)$$

$$K_H, K_q = 1.35 \cdot K_m \quad (5.16)$$

$$K_E = \frac{K_m}{\sigma_E} \quad (5.17)$$

$$K_\varepsilon = \frac{K_m}{\sigma_\varepsilon} \quad (5.18)$$

5.3.4 THE RADIATIVE FLUXES

The radiative fluxes in ENVI-met include the shortwave and the longwave radiation. These fluxes are calculated inside the model, which contains complex elements. ENVI-met considers several model components that would affect the radiative fluxes, including the vegetation's leaf area index (LAI), the visibility of the sky and reflections by various elements.

The calculation of the shortwave and the longwave in ENVI-met is based on the work of Taesler and Anderson, 1984, and Günter Gross, 1991. The longwave was calculated using a two-stream approximation and the shortwave was given by several empirical formulae. The

atmospheric radiation depends on the coefficients that are denoted by the gases and water vapour in the atmosphere different layers (Huttner, 2012), to accurately calculate the radiation fluxes all of the aerosols, water vapour and greenhouse gases that resides in the atmospheric layers must be taken into account. However, ENVI-met's approximation to calculate the radiative fluxes only considers the water vapour in its calculation.

The longwave can be calculated using Equation 5.19 (Paltridge & Platt, 1976):

$$Q_{lw}^{\downarrow}(z) = \sum_{n=1}^N \sigma T^4(n) [\epsilon_n(m + \Delta m) - \epsilon_n(m)] \quad (5.19)$$

where ϵ_n is the emissivity, m is the water vapour and T is the absolute temperature.

The shortwave can be calculated using Equation 5.20 and 5.21.

$$Q_{sw}^* = \int_{0.29}^{4.0} I_0(\lambda) \exp\{-\sigma_R(\lambda)m + \sigma_M(\lambda)m\} d\lambda \quad (5.20)$$

$$m = \begin{cases} \frac{1}{\sin h} & , \text{ if } h > 10 \\ 1.22 \left(\frac{1.0144}{\sin(h + 1.44)} - 0.49 \right) & , \text{ if } h \leq 10 \end{cases} \quad (5.21)$$

where I_0 is the radiation intensity of the sun, $\sigma_R(\lambda)$ and σ_M are Rayleigh and Mie coefficients and are given as $0.00816 \cdot \lambda^{-4}$ and $\lambda^{-1.3} \beta_{tr}$ respectively, and β_{tr} is the opacity coefficient.

Furthermore, direct and diffuse shortwave radiation are calculated as absolute values and are given Equations 5.22 to 5.25.

$$Q_{sw,dir}^0 = Q_{sw}^* - Q_{sw,abs} \quad (5.22)$$

$$Q_{sw,abs} = 70 + 2.8 \cdot e_{2m} \cdot m$$

$$Q_{sw,dif}^0 = R_{sw,dir}^0 \sin h \left(\frac{\gamma(h)}{1 - \gamma(h)} \right), \quad \text{for cloudless skies} \quad (5.23)$$

$$Q_{sw,dir}^0(\text{clouds}) = Q_{sw,dir}^0 \left(1 - \frac{N}{8} \right), \quad \text{clouds are present} \quad (5.24)$$

$$Q_{sw,dif}^0(\text{clouds}) = \left(\frac{Q_{sw,dir}^0 \sin h}{1 - \gamma(h)} \right) \left(\frac{a_s - 1}{a_s a_c - 1} \right) - Q_{sw,dir}^0(\text{clouds}) \sin h \quad (5.25)$$

where $Q_{sw, abs}$ is the radiation related to water vapour (Liljequist & Cehak, 1984), $R_{sw,dir}^0$ is the absolute direct shortwave, e_{2m} is the water vapour pressure, $Q_{sw,dif}^0$ is the diffuse shortwave radiation with $Y(h) = \frac{1}{1 + 8 (\sin h)^{0.7}}$, a_s and a_c are the albedo of the soil and clouds respectively and N is the cloud cover (Taesler & Andersson, 1984).

The reduction coefficient σ is used to describe the effect that vegetation and buildings have on the fluxes of radiation. The coefficients range from 0 to 1 depending on the characteristic of the materials or vegetation, where 0 stands for complete absorption and 1 stands for unaffected fluxes (Bruse, 1995).

$$\sigma_{sw,dir}(z) = \exp(-F \cdot LAI^*(z)) \quad (5.26)$$

$$\sigma_{sw,dif}(z) = \exp(-F \cdot LAI(z, z_p)) \quad (5.27)$$

$$\sigma_{1w}^\downarrow(z) = \exp(-F \cdot LAI(z, z_p)) \quad (5.28)$$

$$\sigma_{1w}^\uparrow(z) = \exp(-F \cdot LAI(0, z)) \quad (5.29)$$

$$\sigma_{svf}(z) = \frac{1}{360} \sum_{\pi=0}^{360} \cos \lambda(\pi) \quad (5.30)$$

Equations 5.26 and 5.27 represent the effect of vegetation on the shortwave for both the diffuse and direct radiation. Equations 5.28 and 5.29 describe the effect of vegetation on the longwave radiation in the upward and downward fluxes. Equation 5.30 relates to buildings' effects on the sky view factor, where 1 is the unobstructed visible sky and 0 is no visibility.

The leaf area index (LAI) is calculated through the leaf area density (LAD), and it is given by Equation 5.31

$$LAI(z, z + \Delta z) = \int_{z'}^{z' + \Delta z} LAD(z') dz' \quad (5.31)$$

The shortwave fluxes are calculated in terms of diffuse and direct radiation using Equations 5.32 and 5.33.

$$R_{sw,dir}(z) = \sigma_{sw,dir}(z) R_{sw,dir}^0 \quad (5.32)$$

$$R_{sw,dif}(z) = \sigma_{sw,dif}(z) \sigma_{svf}(z) R_{sw,dif}^0 + \left(1 - \sigma_{svf}(z)\right) R_{sw,dif}^0 \cdot \bar{a} \quad (5.33)$$

where, $R_{sw,dif}$ is the direct shortwave fluxes, $R_{sw,dif}$ is the diffused shortwave fluxes. \bar{a} is the albedo of the walls.

The longwave radiative fluxes are calculated using the reduction coefficient method based on Equations 5.34 to 5.36.

$$R_{lw}^{\downarrow}(z) = \sigma_{lw}^{\downarrow}(z) R_{lw}^{\downarrow,0} + \left(1 - \sigma_{lw}^{\downarrow}(z)\right) \varepsilon_f \sigma_B \bar{T}_{f+}^4 \quad (5.34)$$

$$R_{lw}^{\uparrow}(z) = \sigma_{lw}^{\uparrow}(z) \varepsilon_s \sigma_B T_0^4 + \left(1 - \sigma_{lw}^{\uparrow}(z)\right) \varepsilon_f \sigma_B \bar{T}_{f-}^4 \quad (5.35)$$

$$R_{lw}^{\leftrightarrow}(z) = \left(1 - \sigma_{svf}(z)\right) \varepsilon_w \sigma_B \bar{T}_w^4 \quad (5.36)$$

where σ_B is the Stefan-Boltzman constant, ε is the emissivity for ground surface, foliage, and walls.

5.4 THE SOIL MODEL

ENVI-met takes into consideration several properties of the soil when modelling the soil layers. These properties include the soil surface temperature and the temperature of the soil layers. These are calculated for artificial materials as well as natural soils. The model also includes the water content for the soil layers, where it solves the hydraulic state based on Darcy's law (ENVI-met, 2019).

ENVI-met handles the grid system for the soil profile as 14 layers system, where the thickness of these layers gradually increases with depth. The top layer has a thickness of 0.01 metres while the bottom layer has a thickness of 0.5 metres. The overall thickness of the soil profile is 2 metres. The soil profile modelling is divided into a one-dimensional profile and three-dimensional heat transfer calculation in the top layer. The temperature (T_s) and the soil water content (η) are calculated using the following equations:

$$\frac{\partial T_s}{\partial t} = k_s \frac{\partial^2 T_s}{\partial z^2} \quad (5.36)$$

$$\frac{\partial \eta}{\partial t} = D_\eta \frac{\partial^2 \eta}{\partial z^2} + \frac{\partial K_\eta}{\partial z} - S_\eta(z) \quad (5.37)$$

where

k_s = thermal diffusivity.

S_η = water content taken up by the roots.

K_η = hydraulic conductivity.

D_η = hydraulic diffusivity.

5.5 THE VEGETATION MODEL

ENVI-met models the vegetation as a one-dimensional column, and each vegetation species is identified by the geometry, the leaf area density (LAD) and the root area density (RAD). This system of identifying the vegetation allows for a variety of greenery, from grass and crops to large trees, as long as the properties are adjusted in Albero. Vegetation affects the air around it through the leaves' profile, and this interaction is summed up with three main fluxes: sensible heat, evaporation, and transpiration, which is mainly caused by the stomata of the leaves.

$$J_{f,h} = 1.1 r_a^{-1} (T_f - T_a) \quad (5.38)$$

$$J_{f, \text{evap}} = \frac{\Delta q \delta_c f_w + (1 - \delta_c) \Delta q}{r_a} \quad (5.39)$$

$$J_{f, \text{trans}} = \frac{(1 - \delta_c) \Delta q}{\delta_c (r_a + r_s)} \quad (5.40)$$

where $J_{F,h}$ are the sensible heat fluxes, $J_{f, \text{evap}}$ are the evaporation fluxes and $J_{F, \text{trans}}$ are the transpiration fluxes. T_A is the air temperature, T_F is the foliage temperature, Q_A is air specific humidity, Δq is humidity difference, q is the saturation at leaf's surface, Δ_c is the possibility of evaporation (0 for not possible and 1 for possible), r_s is the stomata resistance and r_a is the aerodynamic resistance, calculated from:

$$r_a = A \sqrt{\frac{D}{\max(W, 0.05)}} \quad (5.41)$$

where D is the diameter of the leaf and W is the wind velocity.

Following Deardorff, 1978, in typical vegetation there can be wet parts and dry parts where the wet parts evaporate, and the dry parts transpire. This might leave some grid boxes in

ENVI-met's model with a mixture of wet and dry parts. Therefore, a fraction of the wet parts is needed and is calculated using Equation 5.42.

$$f_w = \left(\frac{W_{dew}}{W_{dew,max}} \right)^{2/3} \quad (5.42)$$

where, W_{dew} is the amount of dew on the leaves and $W_{dew,max}$ is the maximum value of dew on the leaves.

The stomatal resistance is calculated based on Deardorff, 1978, and the equation considers the shortwave radiation in the actual and maximum fluxes as well as the water content in the root area.

$$r_s = r_{s,min} \left[\frac{R_{sw,max}}{0.03 R_{sw,max} + R_{sw}} + \left(\frac{\eta_{wilt}}{\eta} \right)^2 \right] \quad (5.43)$$

where R_{sw} and $R_{sw,max}$ are the shortwave radiation, and η is the water content around the roots.

ENVI-met models the transpiration process from the roots to the leaves the roots take the water content from the soil and transfer it up to the plant, and this results in a decrease in the water content in the soil. If the water content in the soil is not enough for the plant, this will affect the resistance of the stomata and the transpiration rate, the following equations are used to calculate the mass of water (m_{trans}) taken up by the plant.

$$m_{trans} = \rho \int_0^{z_p} LAD(z) J_{f,trans}(z) dz \quad (5.44)$$

$$S_\eta(-z) = \frac{m_{trans}}{\rho_w} \left(RAD(-z) D_\eta(-z) \right) \left(\int_{-z_r}^0 RAD(-z) D_\eta(-z) dz \right)^{-1} \quad (5.45)$$

5.6 SURFACES: GROUND AND BUILDINGS

To calculate the ground surface temperature the following energy balance equation is used.

$$0 = R_{sw,net} + R_{lw,net} - c_p \rho J_h^0 - \rho L \cdot J_v^0 - G \quad (5.46)$$

where $R_{sw,net}$ is the net shortwave radiative energy fluxes, $R_{lw,net}$ is the net longwave radiative energy fluxes, J_h is the heat turbulent fluxes, J_v is the vapour turbulent fluxes and G is the soil heat flux.

To accurately calculate the net longwave radiation energy fluxes, ENVI-met includes in the longwave modelling the effect of vegetation and the reflection of buildings. The budget used to calculate the longwave is divided into two parts - a part where the area is shaded by the buildings and another part where the area is unshaded by a building.

$$R_{lw,net}(T_0) = \sigma_{svf} R_{lw,net}^{us}(T_0) + (1 - \sigma_{svf}) R_{lw,net}^s \quad (5.47)$$

where σ_{svf} is the sky view factor, (T_0) is the temperature of the ground surface, $R_{lw,net}^s$ is the longwave budget that is shaded by buildings and $R_{lw,net}^{us}$ is the longwave budget that is unshaded by buildings.

The following equations describe the relationship between the vegetation with the longwave ($R_{lw,net}^{us}$), as well as the buildings with the longwave ($R_{lw,net}^s$) (Deardorff, 1978):

$$R_{lw,net}^{us} = \sigma_{lw}^{\downarrow}(0) (R_{lw}^{\downarrow,0} - \varepsilon_s \sigma_B T_0^4) + (1 - \sigma_{lw}^{\downarrow}(0)) \frac{\varepsilon_f \varepsilon_s}{\varepsilon_f + \varepsilon_s - \varepsilon_f \varepsilon_s} (\sigma_B \bar{T}_f^4 - \sigma_B T_0^4) \quad (5.48)$$

$$R_{lw,net}^s = \frac{\varepsilon_w \varepsilon_s}{\varepsilon_w + \varepsilon_s - \varepsilon_w \varepsilon_s} \{ \max(\sigma_B \bar{T}_w^4, \sigma_B T_0^4) - \sigma_B T_0^4 \} \quad (5.49)$$

where T_w the building's walls average temperature and ε_w is the emissivity of the walls.

ENVI-met calculates the turbulent fluxes near the building walls and ground surface for the heat fluxes (J_h^0) and water vapour (J_v^0).

$$J_h^0 = -K_h^0 \left. \frac{\partial T}{\partial z} \right|_{z=0} = -K_h^0 \left. \frac{\theta(k=1) - T_0}{0.5 \Delta z(k=1)} \right| \quad (5.50)$$

$$J_v^0 = -K_v^0 \left. \frac{\partial q}{\partial z} \right|_{z=0} = -K_v^0 \left. \frac{q(k=1) - q_0}{0.5 \Delta z(k=1)} \right| \quad (5.51)$$

where, K_h^0 is the heat exchange coefficient, K_v^0 is the vapour exchange coefficient and $K=1$ represents the first layer in the calculations whether it be adjacent to the surface or above it.

Following Deardorff, 1978, the calculation of the humidity at the ground surface level, the water content of the soil is used at ($z = -1$):

$$q_0 = \beta q * (T_0) + (1 - \beta) q (z = 1) \quad (5.52)$$

$$\beta = \min (1, \eta (z = -1) / \eta_{fc}) \quad (5.53)$$

where η is the volumetric water content in the soil and η_{fc} is the soil water content at the field capacity.

To calculate the water fluxes, ENVI-met links the parameter to the soil model, where the ground surface evaporation is added to the calculation.

$$S_{\eta,0} (k = -1) = -\frac{\rho}{\rho_w} J_V^0 \frac{1}{\Delta z (k = -1)} \quad (5.54)$$

where ρ_w is the water density, Δz is the thickness of the layer in the soil model and $S_{\eta,0}$ is evaporation on the ground surface.

ENVI-met calculates the heat fluxes of the soil from two parameters, the ground surface temperature, and the temperature of the soil first layer using Equation 5.55.

$$G = \lambda_s (k = -1) \frac{T_0 - T (k = -1)}{0.5 \Delta z (k = -1)} \quad (5.55)$$

where λ_s is the soil heat conductivity.

The buildings heat fluxes are calculated using the following equation:

$$Q_w = k (T_w - T_{a,i}) \quad (5.56)$$

where $T_{a,i}$ buildings internal temperature and k is the walls different materials heat transmission coefficient.

5.7 NUMERICAL METHODS

The numerical methods that are used in ENVI-met were mainly chosen to lessen the computational strain on the users. ENVI-met's large number of differential equations are solved using the finite difference method. In regards to the advection and diffusion equations, ENVI-met uses a fully implicit scheme that ensures accurate results with quick model solutions (ENVI-met, 2019).

The following method is used to solve the Navier-Stokes equations:

$$\frac{\partial u_i^{t+\Delta t}}{\partial t} = \frac{\partial u_i^{aux}}{\partial t} + \frac{1}{\rho} \nabla p \quad (5.57)$$

where $u_i^{t+\Delta t}$ is wind field, u_i^{aux} is the auxiliary wind field and ρ is the field pressure.

The following equations are used to calculate the auxiliary wind flow:

$$\frac{\partial u^{aux}}{\partial t} + u_i \frac{\partial u^{aux}}{\partial x_i} = K_m \left(\frac{\partial^2 u^{aux}}{\partial x_i^2} \right) + f(v - v_g) - S_u \quad (5.58)$$

$$\frac{\partial u^{aux}}{\partial t} + u_i \frac{\partial u^{aux}}{\partial x_i} = K_m \left(\frac{\partial^2 v^{aux}}{\partial x_i^2} \right) - f(u - u_g) - S_v \quad (5.59)$$

$$\frac{\partial w^{aux}}{\partial t} + u_i \frac{\partial w^{aux}}{\partial x_i} = K_m \left(\frac{\partial^2 w^{aux}}{\partial x_i^2} \right) + g \frac{\theta(z)}{\theta_{ref}(z)} - S_w \quad (5.60)$$

The pressure field can be calculated using the following equation:

$$\nabla^2 p = \frac{\rho}{\Delta t} \nabla u_i^{aux} \quad (5.61)$$

To calculate the mass-conserving wind speed more accurately, ENVI-met uses the Simultaneous Over Relaxation method:

$$u_i^{t+\Delta t} = u_{aux}^i - \frac{\Delta t}{\rho} \frac{\partial p}{\partial x_i} \quad (5.62)$$

5.8 SUMMARY

This chapter discussed the CFD modelling software (ENVI-met) that was used in this study. This section outlined the equations and models used to investigate different variables inside the urban environment. The following were outlined in terms of ENVI-met's algorithms:

- ENVI-met uses the Reynolds-averaged non-hydrostatic Navier-Stokes equations to solve the wind flow for each time interval and for each grid cell in the built model space.
- Vegetation in ENVI-met is characterised by its leaf area density (LAD) and its occupying geometry, as an obstacle vegetation creates drag forces that affect the wind flow and decreases its velocity.

- The air temperature is calculated by combining the advection and diffusion equations.
- ENVI-met uses the K-epsilon model to simulate the turbulence.
- ENVI-met considers several factors that would affect the radiative fluxes, e.g. the vegetation's leaf area index (LAI), the visibility of the sky and reflections by various elements.
- The soil model analyses several soil properties, this included surface temperature, layers temperature, and water content. The soil hydraulic state is solved by Darcy's law.

SECTION TWO: ENVI-MET VALIDATION

Content

- 5.8 Introduction.
- 5.9 Previous ENVI-met validation studies.
- 5.10 ENVI-met model sensitivity testing.
- 5.11 Calibration testing.

5.8 INTRODUCTION

ENVI-met, as previously mentioned, is a computational fluid dynamic modelling (CFD) software through which urban conditions are tested and simulated. In this chapter, a series of simulations were performed and compared to collected data from loggers to test the accuracy of the software. The site used for the validation process is located in Al-salt Jordan, for the reason of testing the capability of ENVI-met's performance in a hot arid climate.

To test the sensitivity of ENVI-met, a hypothetical site was constructed and modelled in three low, base, and high key terms. The tested meteorological parameters were wind speed, relative humidity, the albedo of the surrounding surfaces and grid size. The evaluation of the data was based on the change in air temperature for the different scenarios mentioned above.

5.9 PREVIOUS ENVI-MET VALIDATION STUDIES.

5.9.1 ELNABAWI, HAMZA AND DUDEK, 2014

The study submitted was carried out in Cairo, Egypt, in Al-Muizz street located 5 kilometres to the east of downtown. The area lies under the arid hot climate zone, with minimal rainfall and high air temperature (Elnabawi, et al., 2014). The instruments used in the study included a DAVIS Vantage VUE station (Figure 5.3), and the station recorded outside conditions such as biometric pressure, relative humidity, air temperature and wind speed with accuracies ranging from $\pm 0.5^\circ\text{C}$ for air temperature and $\pm 5\%$ for wind speed (DAVIS, 2011). The simulation program used in this study was ENVI-met.

ENVI-met predicted values showed a good proximity to the ones collected by the Vantage Vue station. The highest recorded reading for the observed values occurred at 14:30 with a value of 37.5°C (Figure 5.4), while ENVI-met simulation recorded the highest value at 14:30 with a value of 35.2°C . Both values underwent a statistical analysis that calculated the correlation coefficient R^2 with a value of 0.942, which states a good relationship between the observed values and ENVI-met's predicted values. Based on these results, ENVI-met can be considered as a reliable CFD software for computing air temperature (Elnabawi, et al., 2014).



Figure 5.3. Davies Vantage VUE.

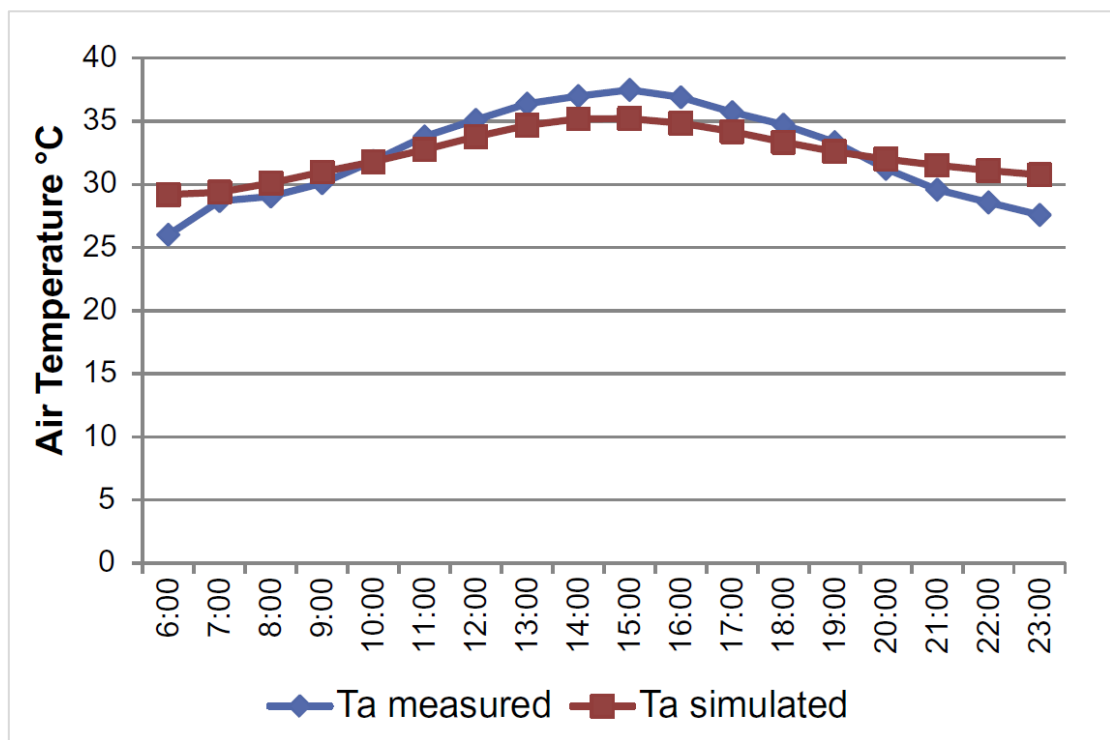


Figure 5.4. Air temperature values for both observed and predicted.

As for the relative humidity, Figure 5.5 shows the compared data for the observed and the predicted values. The two graphs behave in a similar manner with a slight shift of approximately 6%. Both reach their minimum and maximum values at the same time intervals 14:00-18:00 and 06:00-10:00 respectively (Elnabawi, et al., 2014).

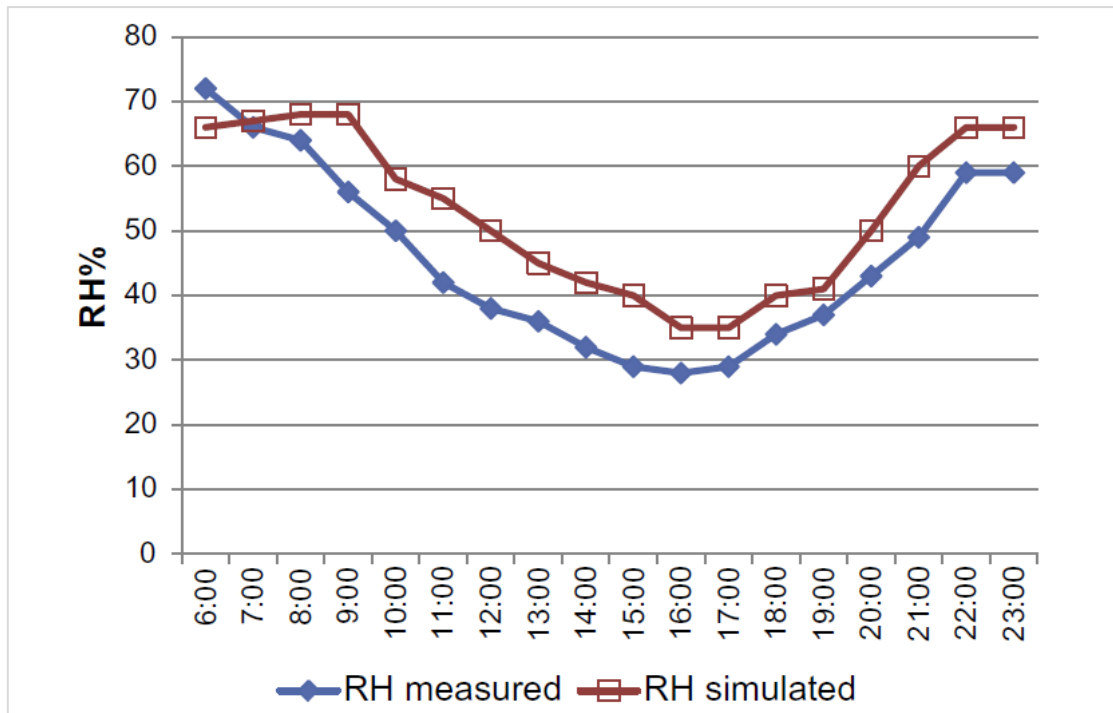


Figure 5.5. Relative humidity values for both observed and predicted.

ENVI-met behaved in a close approximation to the measured T_{mrt} values (Figure 5.6) with a 0.916 calculated R2 correlation coefficient. However, in the time interval (16:00-23:00) ENVI-met values has a significant drop with an average of 8°C. This could be explained by ENVI-met’s algorithm that does not include material heat storage in the simulation process. ENVI-met bases its heat storage calculation on the U-value of walls and roofs, which neglects a material’s heat capacity (Elnabawi, et al., 2014).

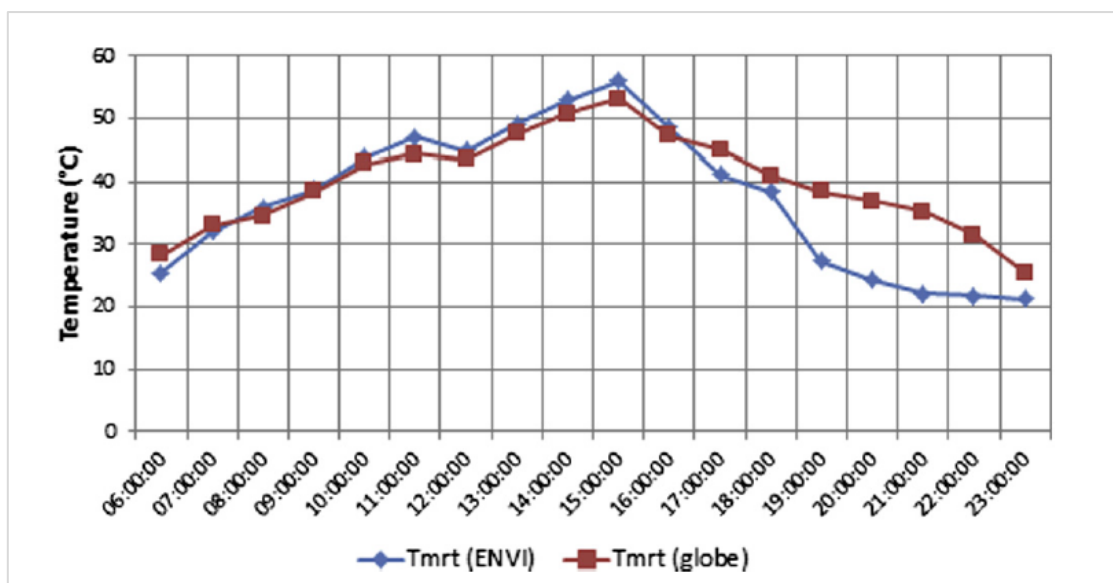


Figure 5.6. Mean radiant Temperature values for both observed and predicted.

5.9.2 SALATAA, GOLASIA, R. DE LIETO VOLLARO AND A. DE LIETO VOLLARO, 2016

The site chosen for the study was a part of the historical side of Rome, the cloister of St. Peter in chains (San Pietro in Vincoli). It is now considered as a part of the School of Engineering in Sapienza University where this study took place (Salata, et al., 2016). The site has different features, including an orange tree, a fountain and a well (Figure 5.7).

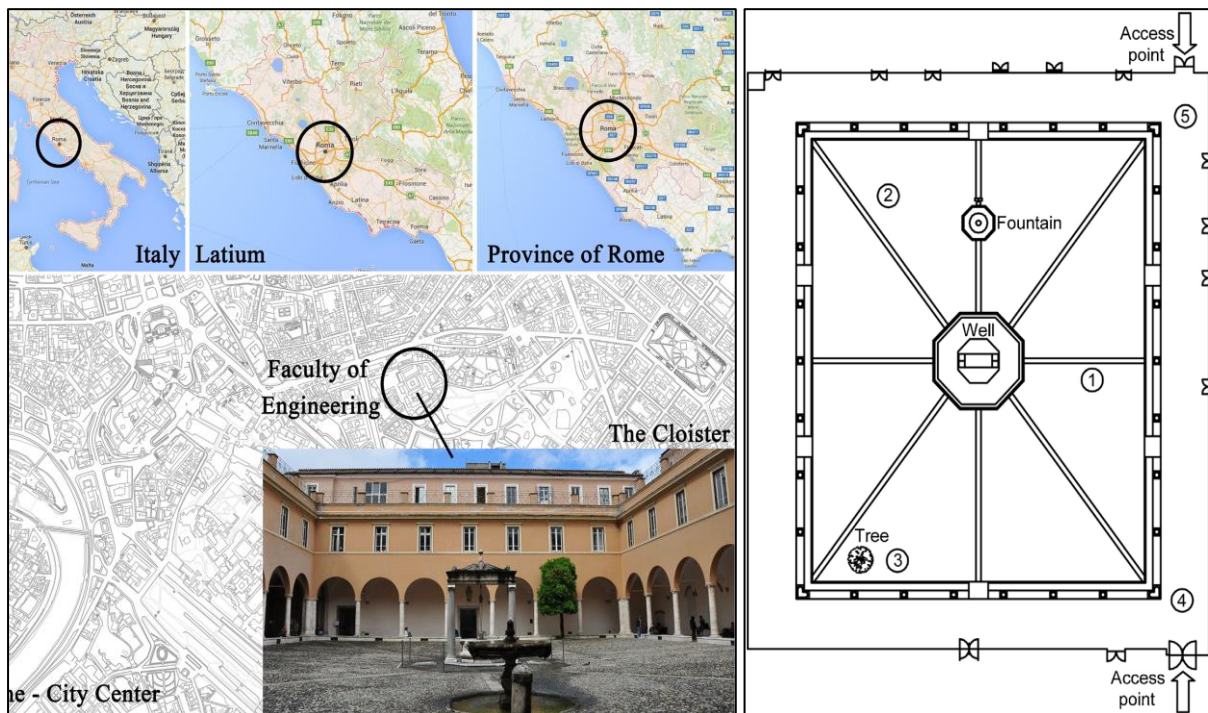


Figure 5.7. St. Peter in chain location.

The instruments that were used were a combination of a microclimate control unit (LSI Babuc/A 11) and loggers (Delta OHM HD 2102.2) attached to different probes (Figure 5.8). The probes were added to measure air temperature, relative humidity, wind speed and globe temperature (Salata, et al., 2016). The simulation process was performed for a whole day (February 13th, 2014), and to show ENVI-met capabilities, the simulation process was split into three simulations, each with different grid resolutions (1m, 2m, 3m). The study compared the following parameters for the three cases respectively: air temperature, relative humidity, mean radiant temperature and global temperature (Salata, et al., 2016).



Figure 5.8. Instrumentation used in the study.

The simulation results were compared to the observed values. As shown in Table 5.1, the accuracy of the parameters differs from one resolution to the other, keeping in mind the increasing computing time that each simulation takes with a higher resolution. The compared data show that the most suitable grid size was $2 \times 2 \text{ m}^2$ with suitable accuracy rates and an acceptable simulation time (Salata, et al., 2016).

Table 5.1. Grid sensitivity.

	T_A	T_{MR}	UR	I_G
Cell size of $3 \times 3 \text{ m}^2$	0.81%	1.33%	2.79%	11.25%
Cell size of $2 \times 2 \text{ m}^2$	0.58%	0.85%	2.01%	9.33%
Cell size of $1 \times 1 \text{ m}^2$	0.47%	0.69%	1.76%	8.89%

The study evaluated the two parameters that most affect the human's thermal comfort - air temperature and mean radiant temperature (Salata, et al., 2016). With the use of model validation methods (RMSE, Pearson's correlation coefficient, index of agreement) these two parameters were evaluated and are shown in Table 5.2.

Table 5.2. Model evaluation tests.

	R ² [-]	RMSE [K]	d [-]
T _A	0.88	1.89	0.91
T _{MR}	0.96	2.79	0.87

Table 5.2 shows a good correlation between the observed and predicted values in air temperature and mean radiant temperature, with Pearson’s coefficients of 0.88 and 0.96 (where 1 would be a perfect correlation) (Salata, et al., 2016).

5.10 ENVI-MET MODEL SENSITIVITY TESTING.

5.10.1 SUMMARY

For the purpose of testing ENVI-met’s sensitivity, this study undertook a series of model runs with a range of different parameters. The tested area comprised of 50x50 metre plot, with six 9-metre-high buildings (Figure 5.9). The model was run three times for every parameter, testing the base case, and the low and high values of the parameters including relative humidity, wind speed, albedo, and grid resolution (Table 5.3).

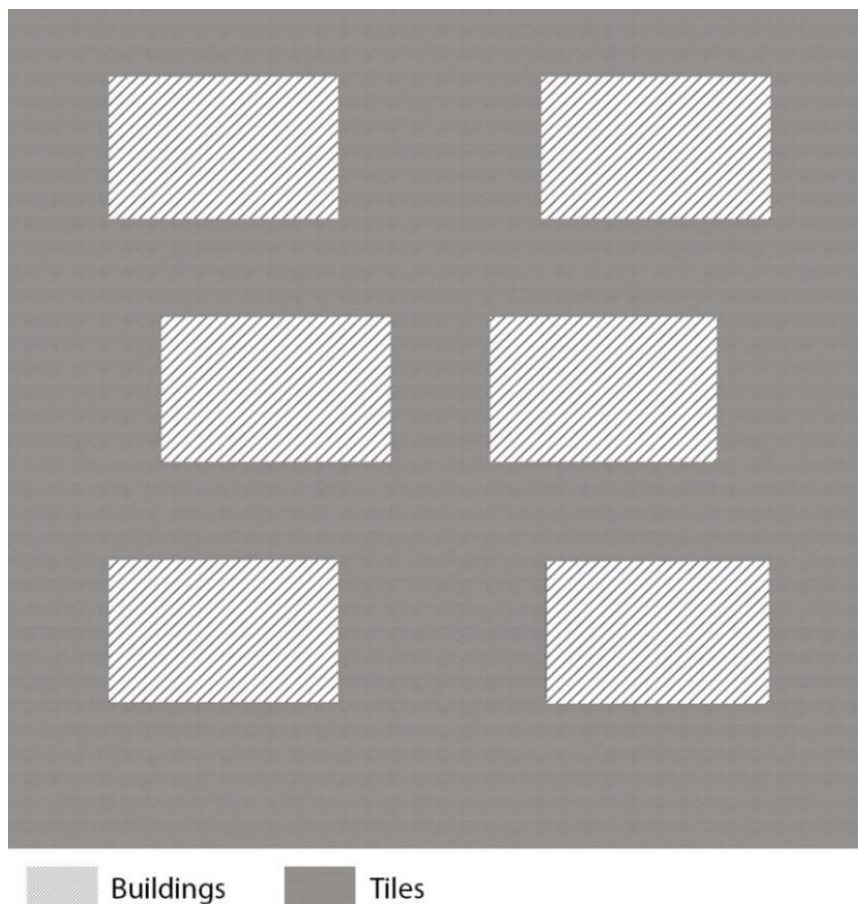


Figure 5.9. The model used in the sensitivity testing.

Table 5.3. Sensitivity test model parameters.

PARAMETERS	LOW TEST MODEL	BASE MODEL	HIGH TEST MODEL
RELATIVE HUMIDITY	40	65	90
WIND SPEED	1	5	10
ALBEDO	10	50	90

5.10.2 WIND SPEED SENSITIVITY.

Figure 5.10 shows the plotted data from the ENVI-met model testing for the wind speed. Low winds of 1 m/s tended to lower the base case model air temperature for the interval of 06:00 pm -08:00 am by an average value of 1.5°C, a maximum value of 2.3°C and a minimum of 0.5°C due to reduced air movement in the modelled area. However, through the time interval of 09:00 am – 05:00 pm the low wind speed showed a significant increase in air temperature by an average of 1.8°C, a maximum value of 2.9°C and a minimum of 0.3°C. High wind speeds, on the other hand, showed a slight increase of air temperature for the same time intervals in the night time by an average of 0.4°C, a maximum value of 0.8°C and a minimum of 0.1°C. By daytime it showed lower air temperature values by an average of 1.1°C, a maximum value of 1.4°C and a minimum of 0.5°C. All three models experienced the same time intervals for the highest predicted air temperature values.

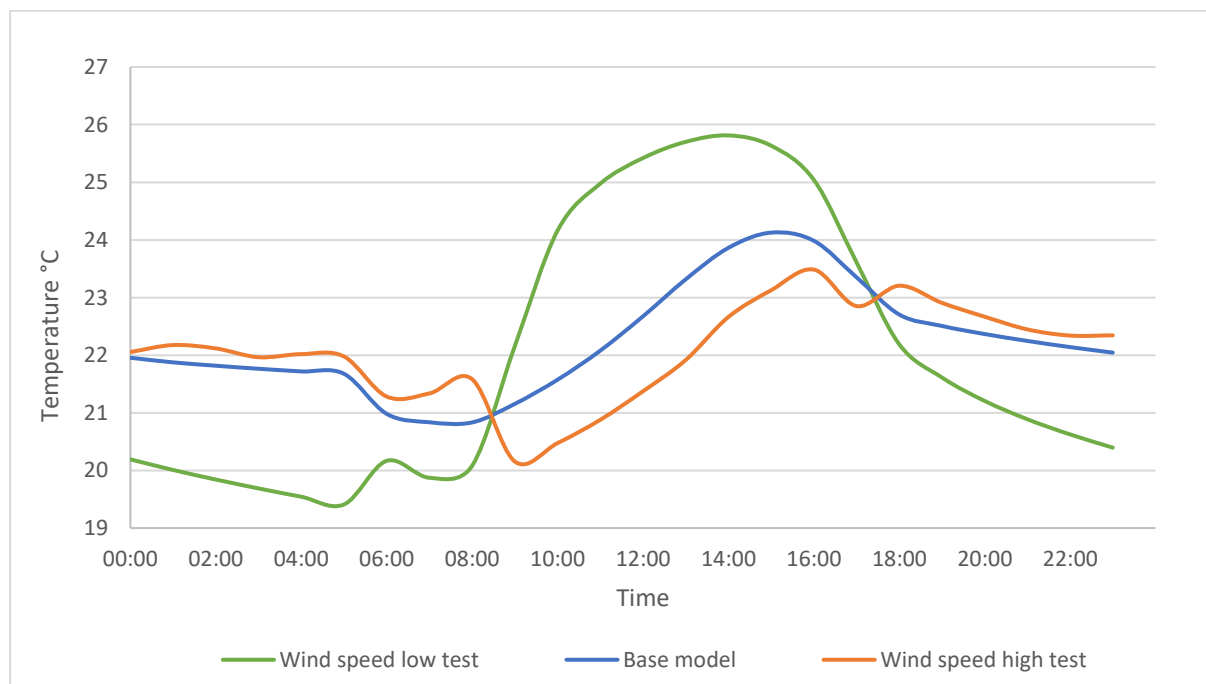


Figure 5.10. Wind speed sensitivity testing.

5.10.3 RELATIVE HUMIDITY SENSITIVITY.

Figure 5.11 shows the plotted data from the ENVI-met model testing for the relative humidity. The low test of 40% relative humidity shows higher air temperature values compared to the base model for the time interval of 11:00 am - 05:00 pm, with the average change value is 0.3°C, while the maximum value is 1.0°C and the minimum value is 0.1°C. The low RH tends to lower the air temperature values for the time interval of 05:00 am - 10:00 am due to solar radiation, with an average change value of 1.0°C, a maximum value of 1.3°C and a minimum of 0.4°C. The air temperature values for the 90% relative humidity high test showed an average increase of 0.9°C for the time interval of 06:00 am- 01:00 pm, a maximum value of 1.3°C and a minimum of 0.0°C. For the rest of the day, the high relative humidity tended to lower the base model's air temperature by an average value of 0.4°C, a maximum value of 0.8°C and a minimum of 0.3°C.

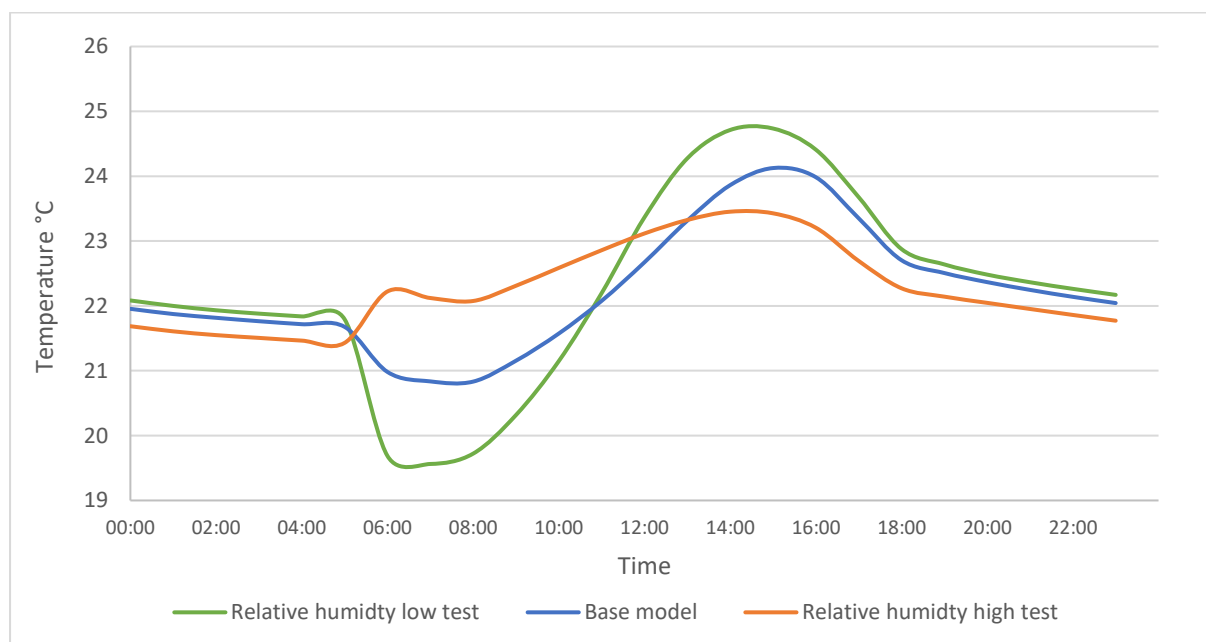


Figure 5.11. Relative humidity sensitivity testing.

5.10.4 ALBEDO SENSITIVITY

Figure 5.12 shows the plotted data from the ENVI-met model testing for the albedo. The albedo of the buildings' cladding and the pavement area were modified as a low albedo of 10%, a base model value of 50% and high albedo of 90%. The high albedo test shows virtually no change in the air temperature compared to the base model, the highest recorded value of change is less than 0.01°C. However, the low albedo test showed a slightly higher change in

air temperature values compared to the high albedo test, with an average change of 0.18°C and a maximum value of 0.25°C.

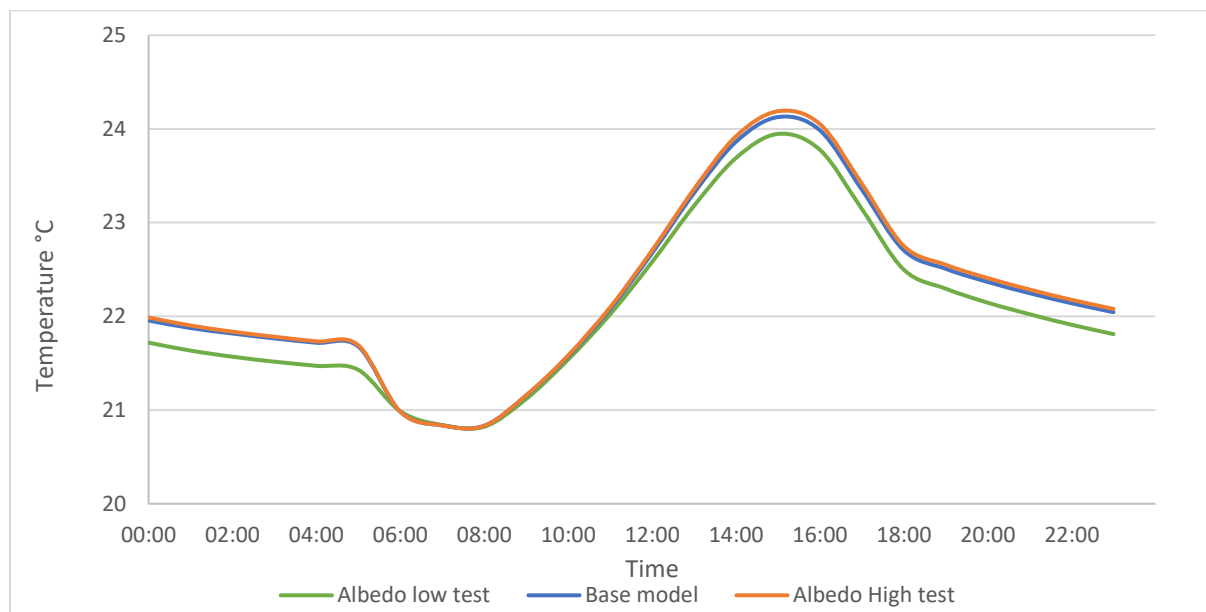


Figure 5.12. Albedo sensitivity testing.

5.10.5 GRID SIZE.

Simulating in ENVI-met relies heavily on the size of the actual project and in some cases the studied parameter. A higher resolution grid or a thicker mesh would give more accurate results, that is if the site is relatively small. However, increasing the resolution of the grid will raise the hardware requirement and the simulation time. The base model that was used in the testing was a 50 x 50 metre plot with a resolution of 1 x 1 metres, which is the most accurate mesh count. In order to test ENVI-met sensitivity, two other mesh counts were introduced: 2 x 2m and 3 x 3m. As Figure 5.13 shows, the 3 x 3 grid's air temperature values had a large increase compared to the base model for the time interval of 01:00 pm-03:00 am, with an average change value of 4.8°C, a maximum change value of 12.2°C and a minimum change value of 0.4°C. For the rest of the day the variations showed a decrease in air temperature values of an average change value of 2.8°C, a maximum change value of 4.2°C and a minimum change value of 0.1°C. The 2 x 2 grid had a better accuracy than the previously mentioned grid. However, as seen in Figure 5.13, air temperature values showed a decrease from the base model for the time interval of 02:00 pm- 09:00 am, with an average change value of 1.9°C, a maximum change value of 2.9°C and a minimum change value of 0.1°C. for

the time interval of 10:00 am – 01:00 pm the graph shows a slight increase in air temperature values of an average change value of 0.5°C, a maximum change value of 0.7°C and a minimum change value of 0.5°C.

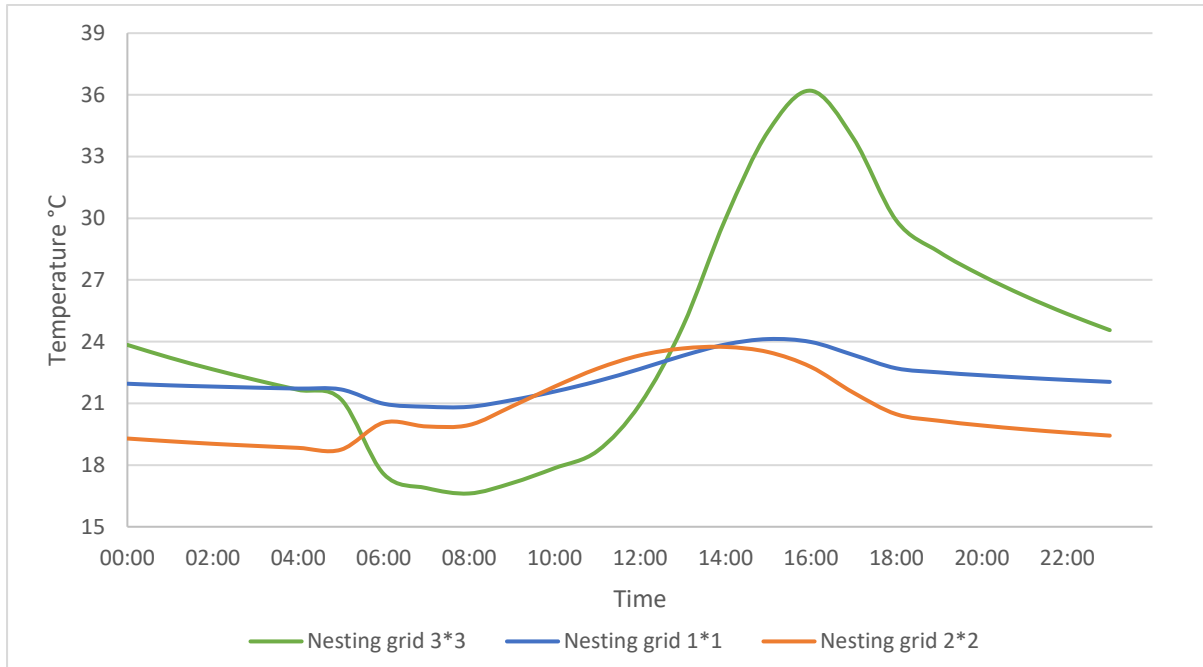


Figure 5.13 Grid size sensitivity testing.

5.10.6 CONCLUSION

Envi-MET showed different sensitivity levels across the tested parameters. The relative humidity change showed a good response to air temperature, especially at the highest value of the day, where the rise in relative humidity produced lower a lowering effect on air temperature values and vice versa. For the wind speed, Envi-MET also showed an effect in changing the air temperature compared to the base model. Air temperature had a significant increase when reducing the wind speed to a minimum with an average of 1.8°C, a maximum value of 2.9°C and a minimum of 0.3°C. However, it showed a smaller change in Ta when increasing the wind speed to double the value of the base model (from 5m/s to 10m/s).

Lowering the grid count was shown to produce inaccurate results compared to the base model, particularly when simulating small urban plots in Envi-MET using a small resolution, as seen for the 3 x 3 meters grid, which produced a maximum 50.83% deviation from the base model’s results. However, the 2 x 2 masters grid showed less error percentage of 13.38% compared to the base model. The albedo test had the least impact on air temperature

compared to the other parameters where it only showed a slight decrease in values in the low test.

5.11 CALIBRATION TESTING.

5.11.1 SITE AND MODEL PARAMETERS.

Several issues were taken into consideration when choosing the site for the ENVI-met validation process. Al Ahliyya Amman University provided the most suitable setting for the study. The site provided different elements, like a wide range of vegetation, tiled pathways, adjacent buildings, parking lot and 24-hour security for the protection of instruments (Figure 5.14).



Figure 5.14. The location of Amman Ahliyya University.

The buildings' cladding in the university are mostly white limestone with different variations of texture roughness and an average an albedo of 60%. The pathways that link the buildings have different material. However, the area where the loggers were placed is tiled with grey cement tiles with an average albedo of 30%. The trees and shrubs used in the site are mostly of local origins and coniferous in nature. The only deciduous tree is *Populus Nigra*, while the conifers are *Pinus Halepensis*, Mediterranean Cypress (*Cupressaceae*), *Phoenix Dactylifera* and *Cupressus Macrocarpa* 'Goldcrest' (Figures 5.15 and 15.16).

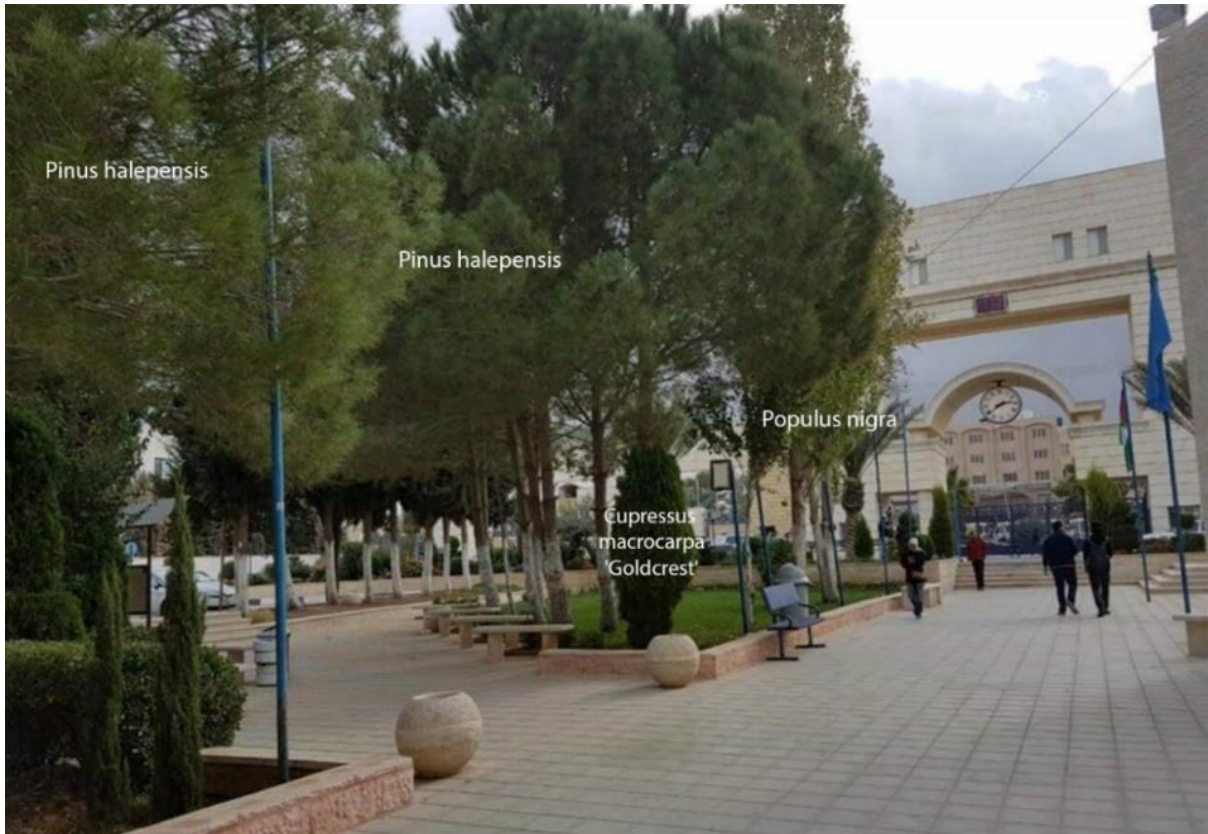


Figure 5.15. Trees labels in the site.



Figure 5.16. Trees labels in site 2.

5.11.2 THE LOGGERS' READINGS FOR LOCATION A AND B.

The initial study was to compare thermal comfort indices such as PET, but the Kestrel loggers had one usability fault that was not described in the manual. This was that global temperature cannot be recorded unless the time intervals for the readings are more than 10 minutes, which is a large interval for the validation. Therefore, the validation process focused on three main parameters wind speed, air temperature and relative humidity. Figures 5.17, 5.18 and 5.19 show the readings for 1st October 2017. The two loggers show significant similarities in recorded values. The shift in values in location B in the early morning hours to mid-day was due to the added water vapour in the air caused by the sprinkles next to location B.

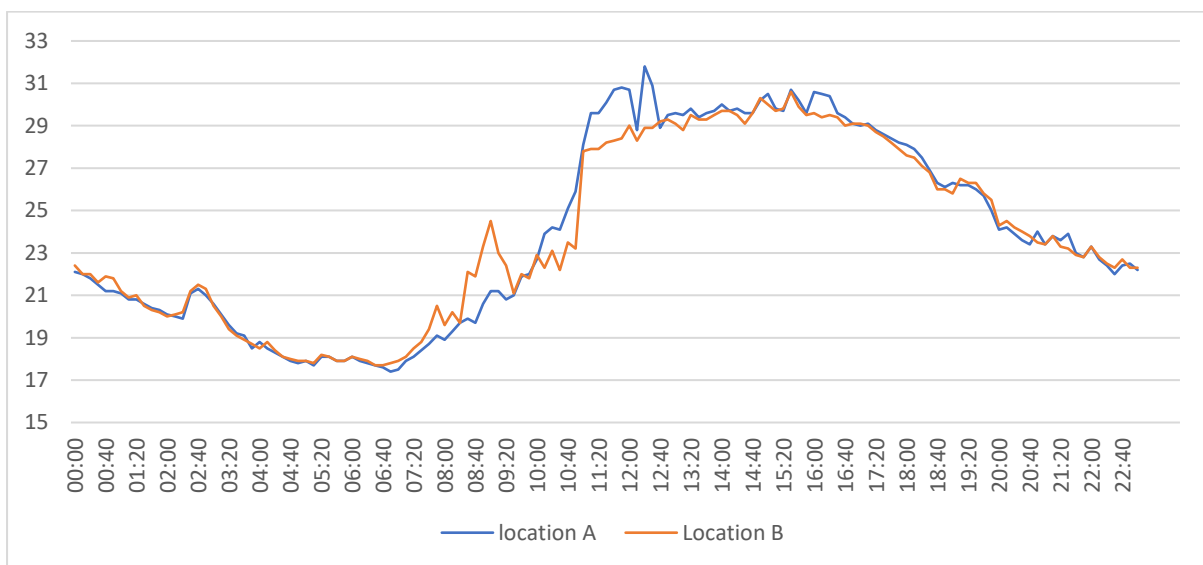


Figure 5.17. The loggers' readings for air temperature.

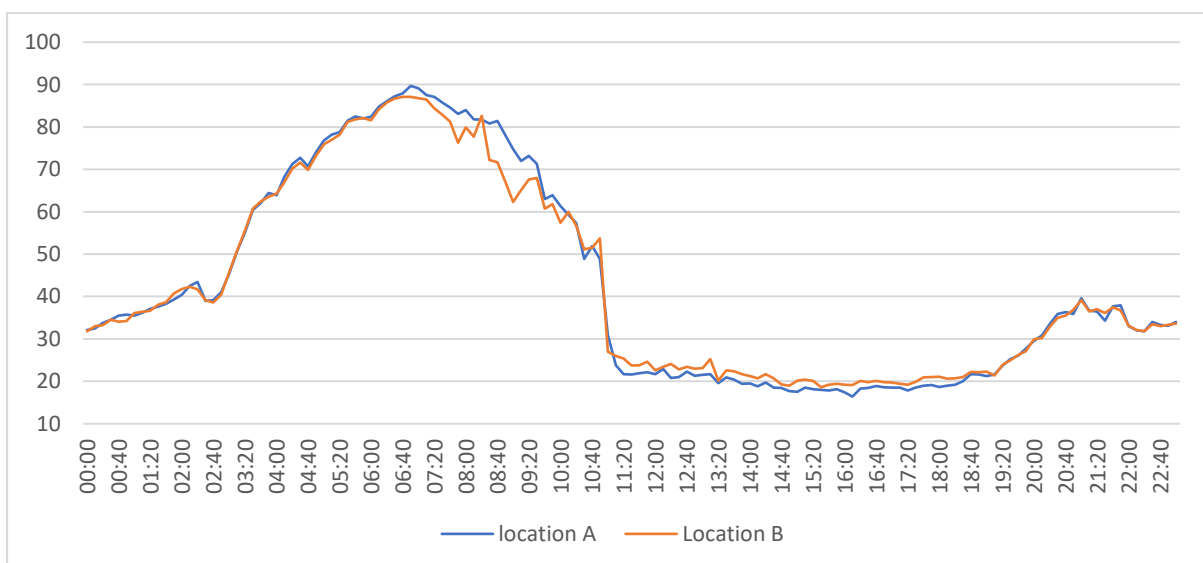


Figure 5.18. The loggers' readings for relative humidity.

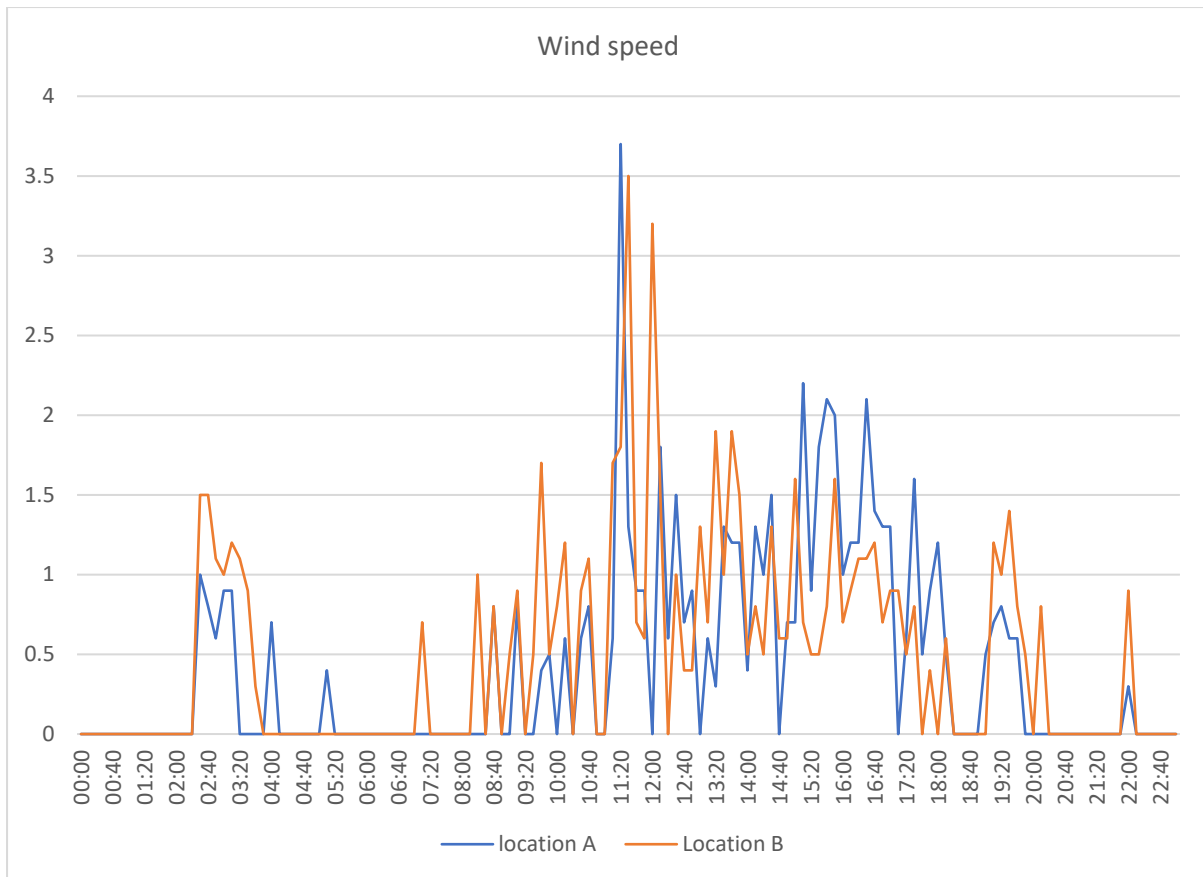


Figure 5.19. The loggers' readings for wind speed.

5.11.3 SITE MODELLING IN ENVI-MET.

The site was modelled in ENVI-met using the SPACES extension, and the data were modified using DBManager extension to fit the chosen site. This included the material used for the ground tiles, the buildings' cladding, and the car park's asphalt paving. The meteorological data were extracted from an EPW file from the nearest weather station to the site.

5.11.4 MODEL VALIDATION TEST OF THE OBSERVED DATA AND THE PREDICTED DATA.

For this section four different model validation methods were used to compare the results of the ENVI-met simulation of the site observed data collected from the loggers (as mentioned in the Methodology chapter). Tables 5.4 and 5.5 show the different validation tests for both of the locations A and B, and these data will be further investigated in the next section for each of the parameters.

Table 5.4. Model validation for location A.

Validation method	Temperature	Relative humidity	Wind Speed
Index of agreement	0.886	0.646	0.104
RMSError	2.602	18.797	0.424
MAE	1.974	14.436	0.362
Pearson correlation coefficient	0.933	0.743	0.102

Table 5.5. Model validation for location B.

Validation method	Temperature	Relative humidity	Wind Speed
Index of agreement	0.890	0.688	0.168
RMSError	2.455	16.624	0.819
MAE	1.889	12.814	0.593
Pearson correlation coefficient	0.934	0.768	-0.325

5.11.5 COMPARISON OF THE SIMULATED DATA VS THE OBSERVED DATA.

Figure 5.20 shows the predicted and measured values of air temperature at monitoring point A. Envi-MET values are generally lower than the logged ones by an average difference of 2.8°C between the time intervals of 09:00 am - 07:00 pm and 00:00 - 04:00 am. However, the

predicted values show a slight increase for the time intervals 08:00 pm - 11:00 pm and 05:00 am – 08:00 am, with an average difference of 0.3°C. Overall, the two sets of data show a good correlation, with an index of agreement value of 0.886 and Pearson correlation coefficient of 0.933, as shown in Table 5.3.

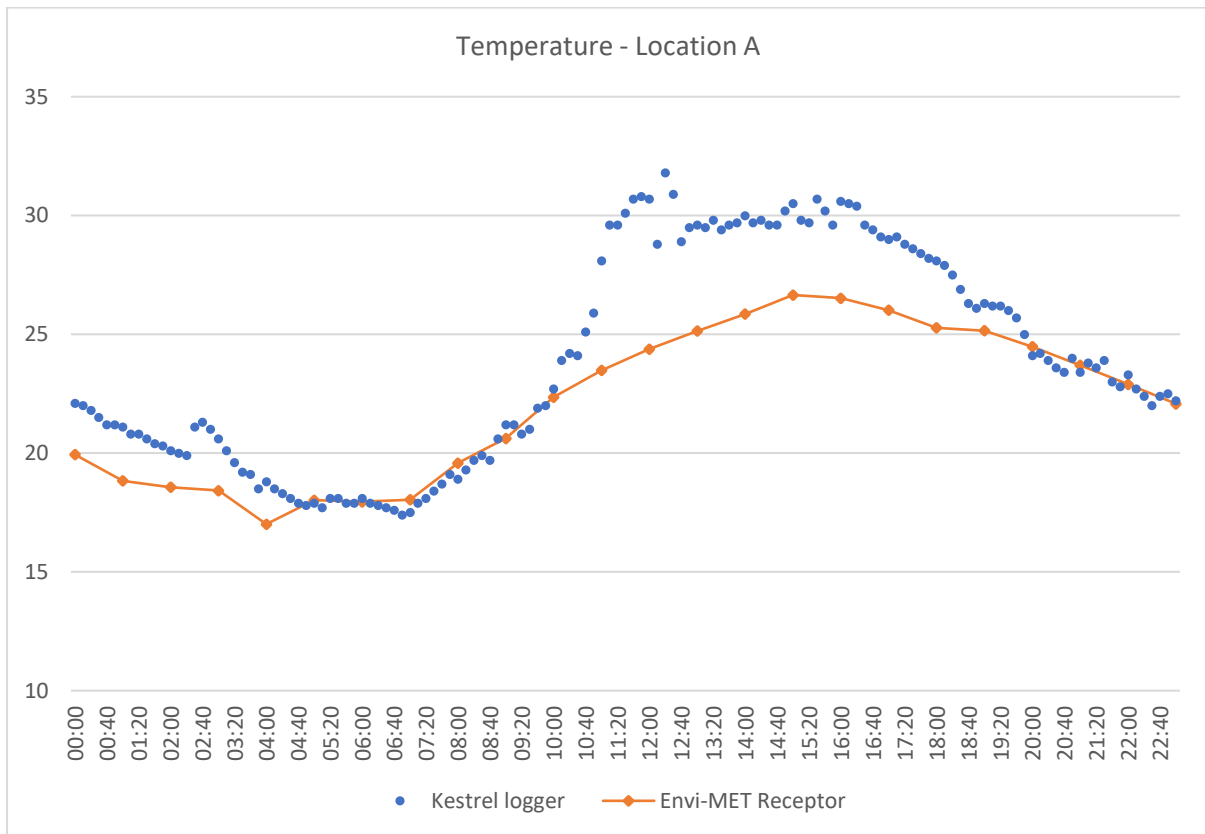


Figure 5.20. Data comparison between the observed and the predicted air temperature values, location A.

Figure 5.21 shows, for location B, that the predicted temperature values for the time intervals of 09:00 am - 07:00 pm and 00:00 – 04:00 am are lower compared to the loggers’ readings with an average change value of 2.9°C. For the rest of the day, the predicted values are similar to the observed ones, with a slight increase of an average change value of 0.2°C. Overall, the two sets of data show a good correlation, with an index of agreement value of 0.890 and Pearson correlation coefficient of 0.934 (see Table 5.4).

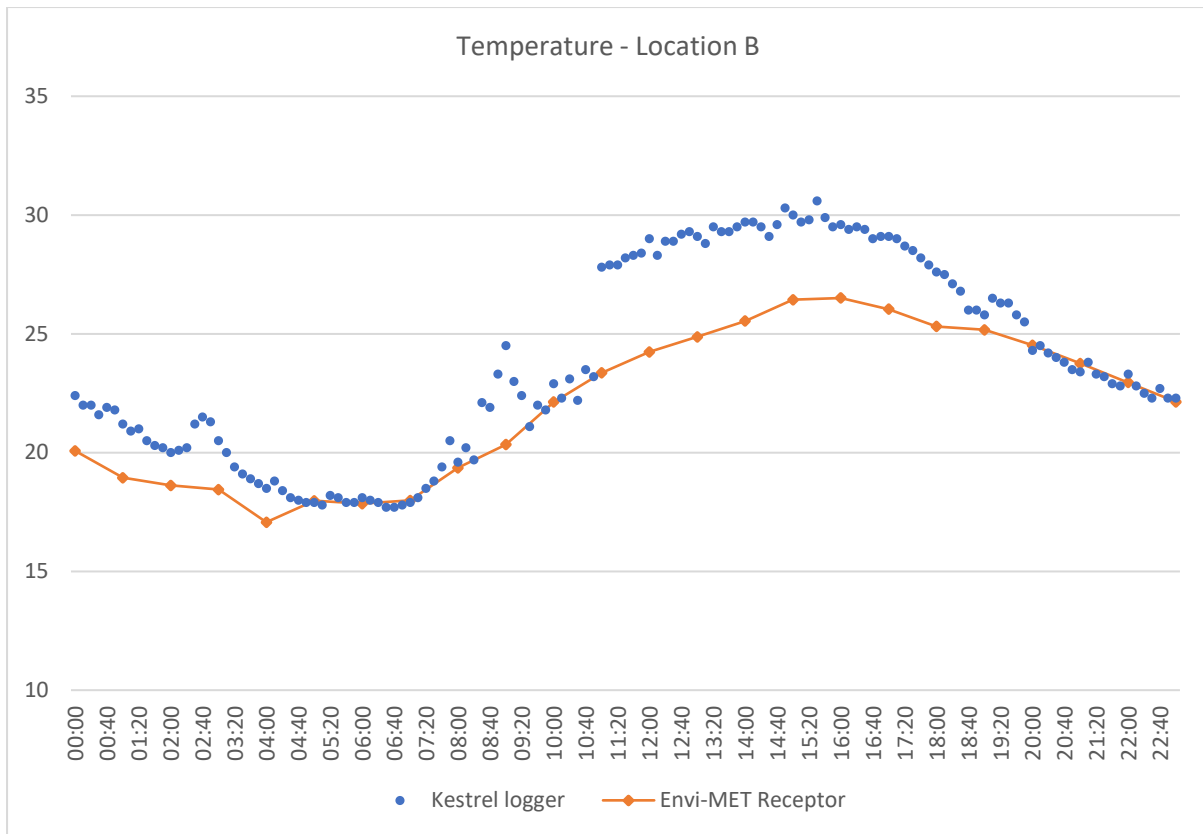


Figure 5.21. Data comparison between the observed and the predicted air temperature values, location B.

Figure 5.22 shows the predicted and measured values of relative humidity at monitoring point A. The predicted values do not have the same air temperature impact on its value compared to the observed values, and the divergence can be seen clearly for the time interval of 03:00 am- 10:00 am, where the relative humidity of observed values rise to its daily maximum due to the lower air temperature values at night. However, this impact is much smaller in the predicted values. For the rest of the day, the predicted values seem to have a closer pattern behaviour to the observed ones, with an average change value of 8.8%. Overall, the two sets of data present an adequate correlation, with an index of agreement value of 0.646 and Pearson correlation coefficient of 0.743 as shown in Table 5.3.

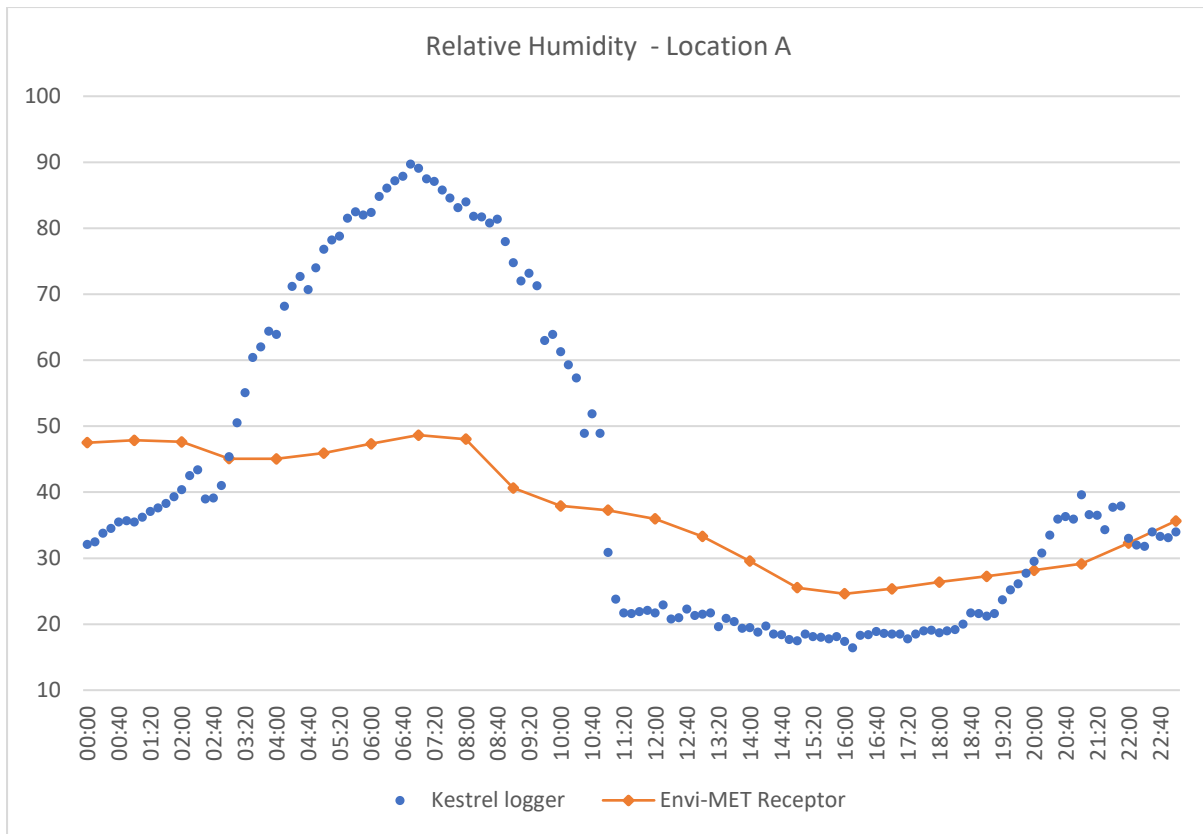


Figure 5.22. Data comparison between the observed and the predicted for relative humidity, location A.

As shown in Figure 5.23 for location B, ENVI-met behaves in a similar fashion as in location A, with predicted values having a large divergence between 03:00 am and 10:00 am, with an average change value of 18.4%. For the rest of the time intervals, the average change in values is 8.11%, which is closer in value to the observed values. The sets of data have an adequate correlation with an index of agreement value of 0.688 and Pearson correlation coefficient of 0.768 as shown in table 4.

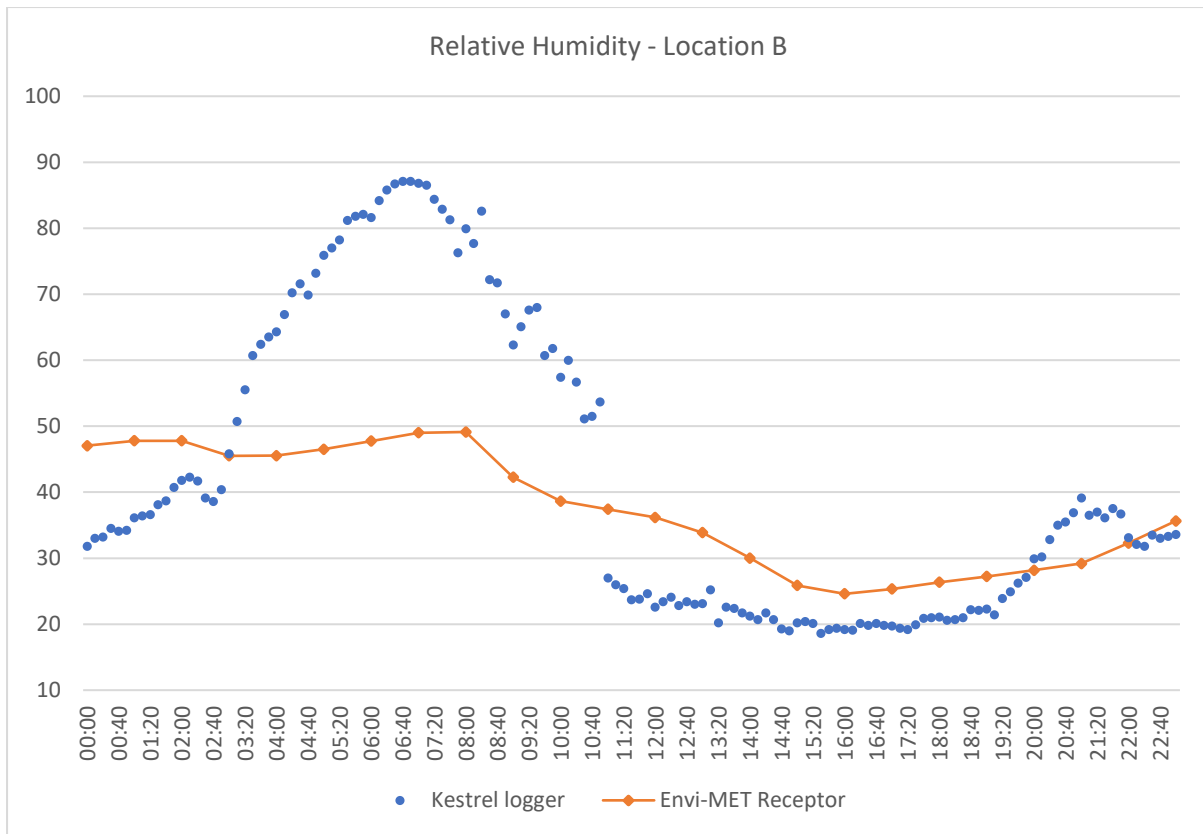


Figure 5.23. Data comparison between the observed and the predicted for relative humidity, location B.

Figures 5.24 and 5.25 indicate the predicted and observed values for wind speed; however, the predicted values for wind speed are averaged over an hourly basis, whereas the observed values were recorded every 10 minutes. The trend line shows great similarities with the predicted values, although there are large individual differences. In this case, even though the model validation methods in Tables 5.3 and 5.4 show a very low correlation, Envi-MET's results are still valid. This example shows the difficulty of trying to validate Envi-MET with a rapidly fluctuating parameter like the wind.

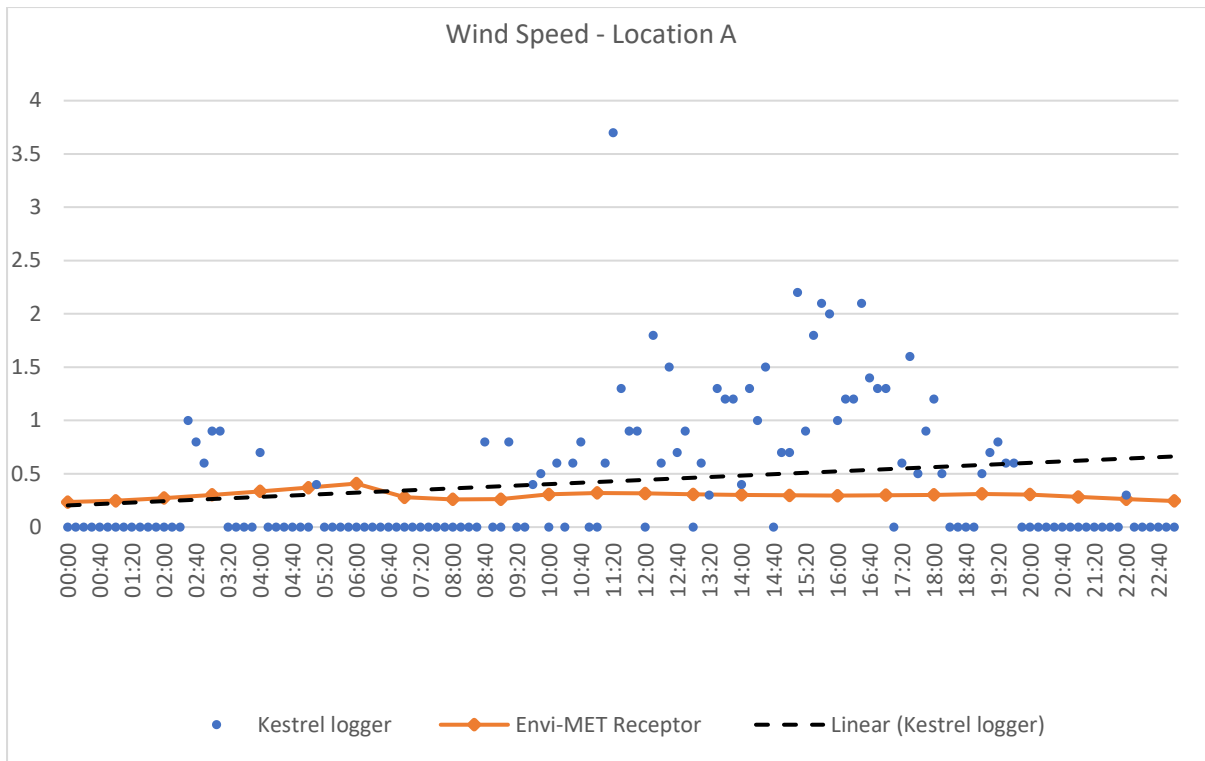


Figure 5.24. Data comparison between the observed and the predicted for wind speed, location A.

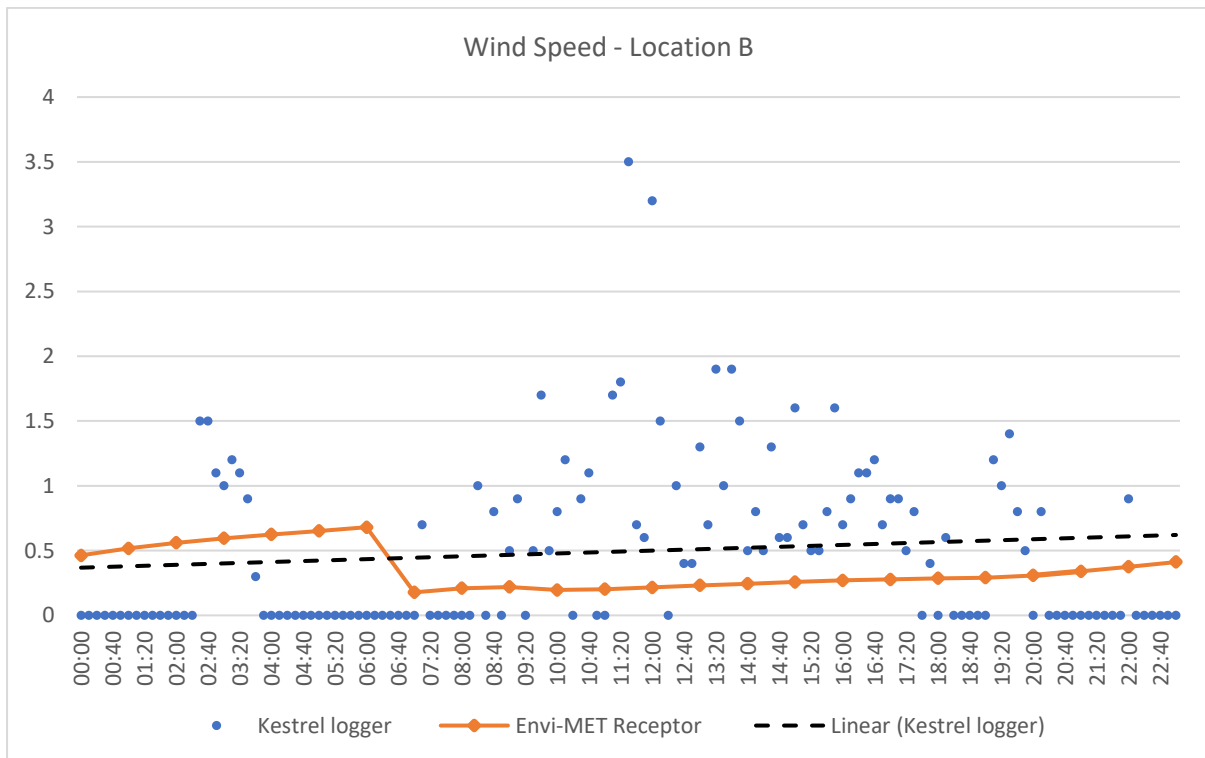


Figure 5.25. Data comparison between the observed and the predicted for wind speed, location B.

5.11.6 CONCLUSIONS

Although Envi-MET gave some unsatisfactory results, as with the relative humidity testing with an index of agreement of 0.667, and Pearson correlation coefficient of 0.7555 (Table 5.6), it showed that the data reacted to air temperature changes for night time to some extent, and it had a good correlation value for the rest of the day, with an index of agreement of 0.888, and Pearson correlation coefficient of 0.9335 (Table 5.6). The air temperature testing showed the most accurate results with the highest index of agreement values.

As for the wind speed, Envi-MET showed a very good correlation with the trend line of the observed values. The validation methods used in Table 5.6 were not sufficient enough to use as a tool to compare the observed and simulated results due to ENVI-met averaging the wind speed values on an hourly basis. As a result, the trend line for the observed data was used to compare the results. Overall, the study showed that Envi-MET as a simulation software is better suited to analysing the relative change in parameters rather than the change in absolute values, as it shows a great response to the modification of microclimatic parameters.

Table 5.6. Average Model validation values for locations A and B.

Validation method	Temperature	Relative humidity	Wind Speed
Index of agreement	0.888	0.667	0.136
RMSError	2.5285	17.7105	0.6215
MAE	1.9315	13.625	0.4775
Pearson correlation coefficient	0.9335	0.7555	-0.1115

Chapter 6 Results and Discussion

Content

Section One: Street Grid.

Section Two: Amman Case Study.

Section three: Buildings Cluster Analysis.

This chapter focusses on the results of the research, through studying the outdoor thermal comfort and the effects informed prior planning of future urban developments would have on Amman, the capital of Jordan. The aim of this chapter is to identify the key elements for enhancing the outdoor thermal comfort for pedestrians in a residential setting. The computational fluid dynamics (CFD) modelling software ENVI-met was used to create several scenarios to analyse street patterns, vegetation displacement and building forms to determine which scenario plays best in terms of pedestrian thermal comfort, with PET being used to quantify the comfort levels.

SECTION ONE: STREET GRID

Content

- 6.1 Street grid results.
- 6.2 Street grid layout A.
- 6.3 Street grid layout B.
- 6.4 Street grid layout C.
- 6.5 Street grid layout D.
- 6.6 Street grid layout E.
- 6.7 Conclusion.

6.1 STREET GRID (SUMMARY).

Different street grids were analysed to study the effect of buildings placement in an urban setting. The scenarios were built with the following properties:

- The buildings height-to-street width ratio was constant for all the scenarios, with a value of 1.
- The materials used for building cladding was limestone, as it is the most used material for building exteriors in Jordan.
- The streets were covered with asphalt having an albedo of 10%.
- The meteorological factors were averaged for all the scenarios with mild conditions as would be the case in early autumn in Jordan for the purpose of comparison.
- The same scenario was simulated twice with different layout orientation – original and twisted 45° counter-clockwise.
- The dominant wind direction was West for all the scenarios.

The meteorological factors were averaged for all the scenarios with the following parameters:

- Minimum air temperature of 18°C and maximum temperature of 30°C.
- 4 m/s starting wind speed.
- Minimum relative humidity of 35% and a maximum of 70%.
- The date of the simulation was the 23rd September.

6.2 STREET GRID LAYOUT A

6.2.1 SCENARIO A.1

Figure 6.1 shows scenario A.1 for the street grids analysis. The grid is a classic grid with perpendicular streets with 45° orientation from the North. The Figure also shows wind speed at 11:00 am, as well as the placement of receptors 1 and 2 (shown in red).

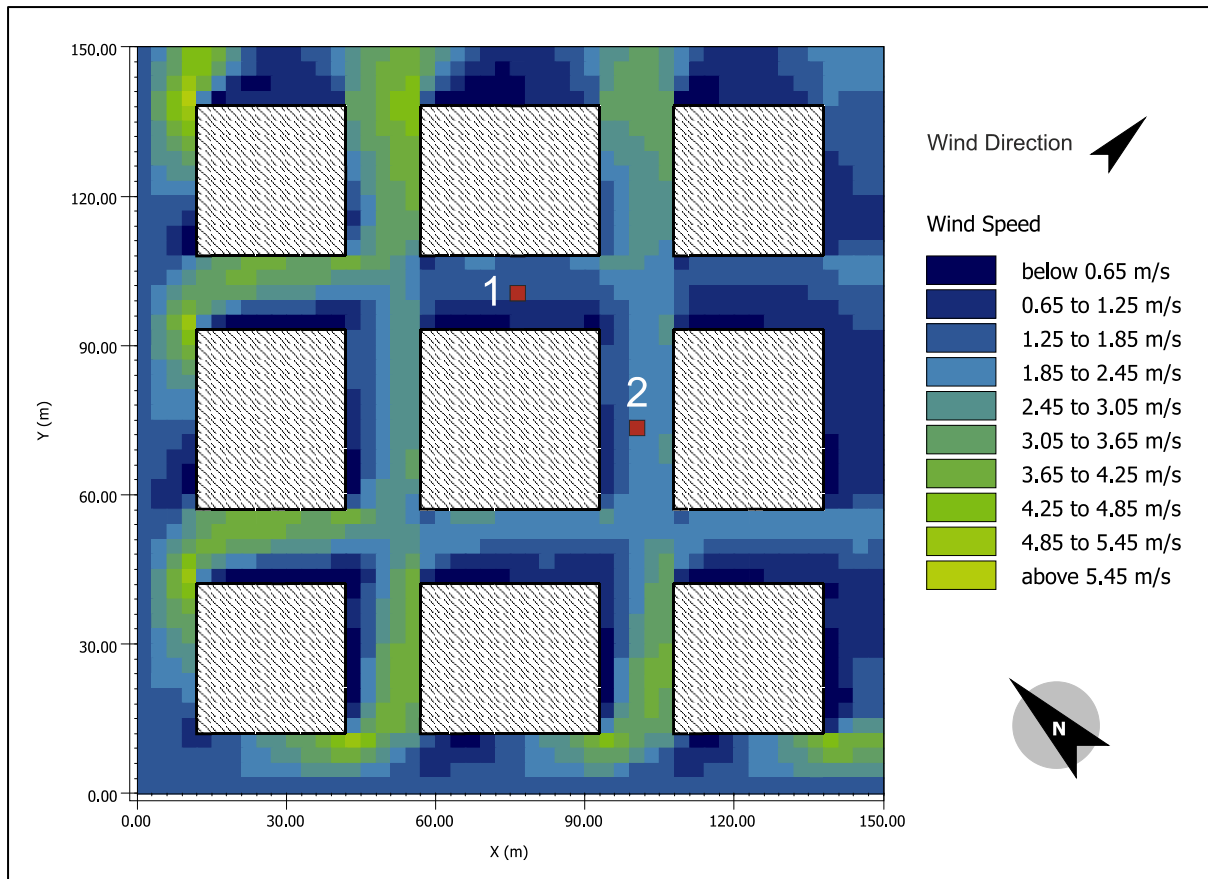


Figure 6.1. Wind speeds in scenario A.1.

The 135° angle that wind is entering the plot is creating a flow separation when it reaches the sharp edge of the buildings as shown in Figure 6.2. Because of this, the mean wind flow is displaced, and vortices are formed in the cavity zone at the backside facades of the buildings due to the lower surface pressure. This causes the wind speed to be reduced significantly compared to the mean flow in the streets. This is shown in Figure 6.1 in dark blue for all the buildings in the plot. As wind flow progresses into the plot, a helical wind flow is created throughout the streets of the plot, this phenomenon is the vector sum of the vortices and the channelling flow created by the external wind flow.

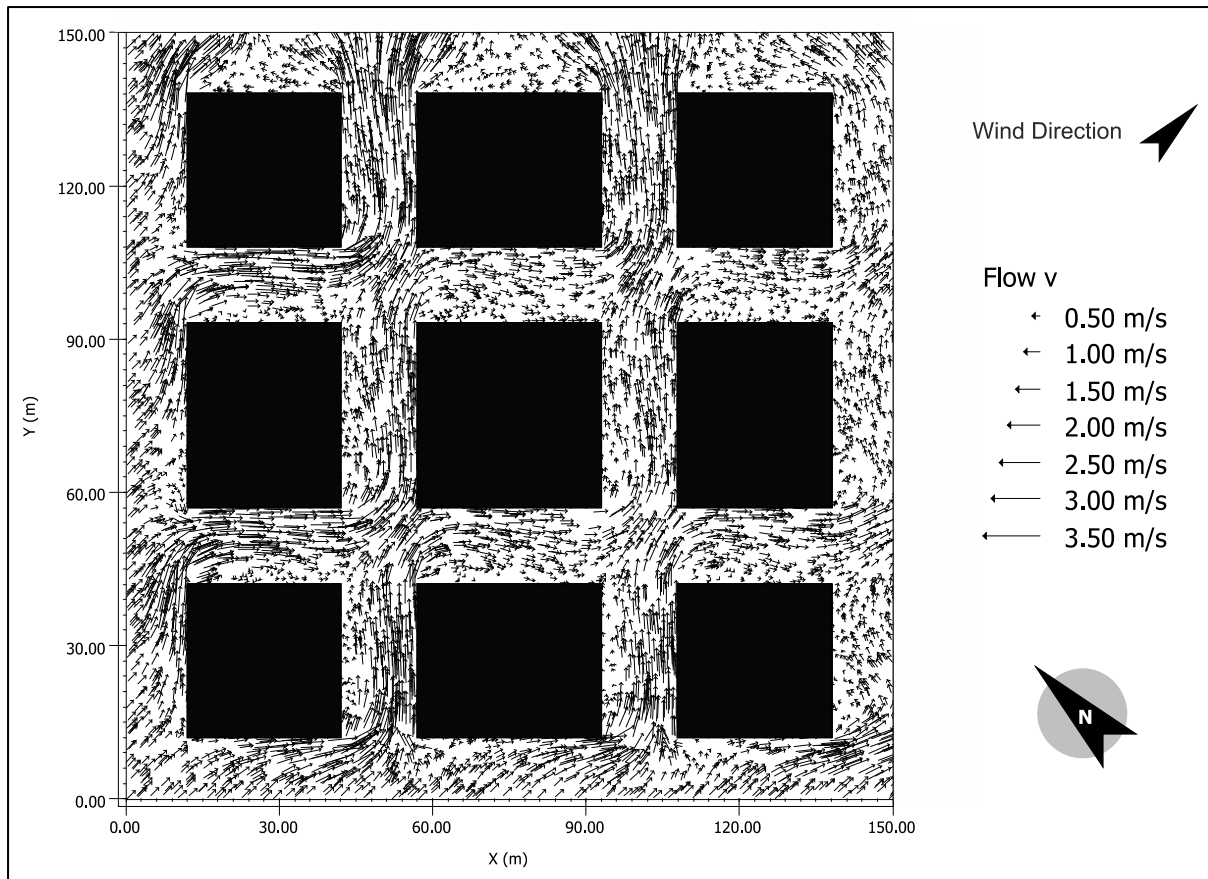


Figure 6.2. Wind flow in Scenario A.1.

6.2.2 SCENARIO A.2.

Figure 6,3 shows scenario A.2 for the street grids analysis; the grid is a classic grid with perpendicular streets and 0°angle orientation from the North. The Figure also shows wind speed at 11:00 am, as well as the placement of receptors 1 and 2 (shown in red).

The wind is entering the plot at a 90° angle, and this is creating what is called a channelling flow (Figure 6.4). This flow is causing a high pressure in the streets that are oriented in the flow path, which in turn, restricts the wind to flow to the streets oriented perpendicular to the flow. The high wind speed flow coming from the West in the (West-East) oriented streets form corner vortices in (North-South) streets, these vortices have low velocity and spread out to a less than the street width, this is shown in dark blue in Figure 6.3. It should be noted that in the (North-South) streets, there are two vortices created with opposite rotating directions, but because they have low velocities, they do not affect each other.

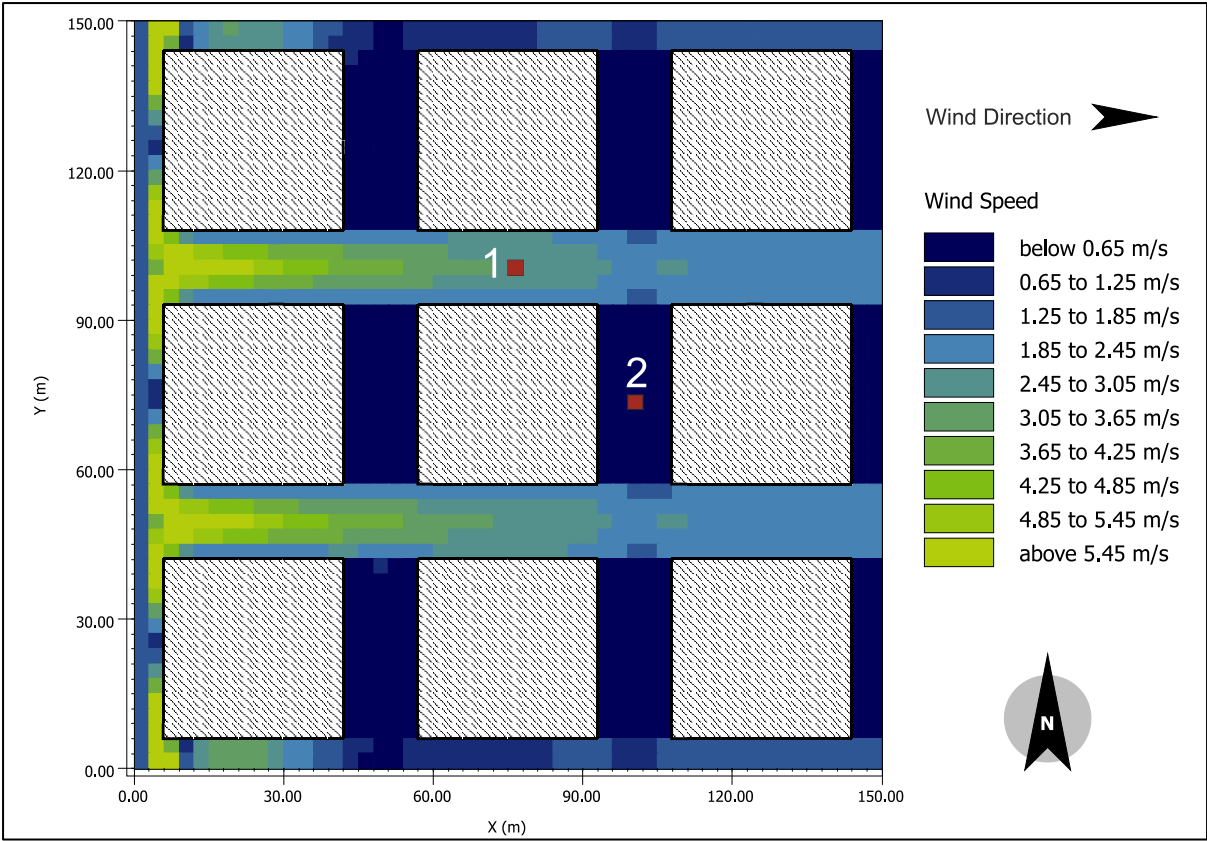


Figure 6.3. Wind speed in scenario A.2.

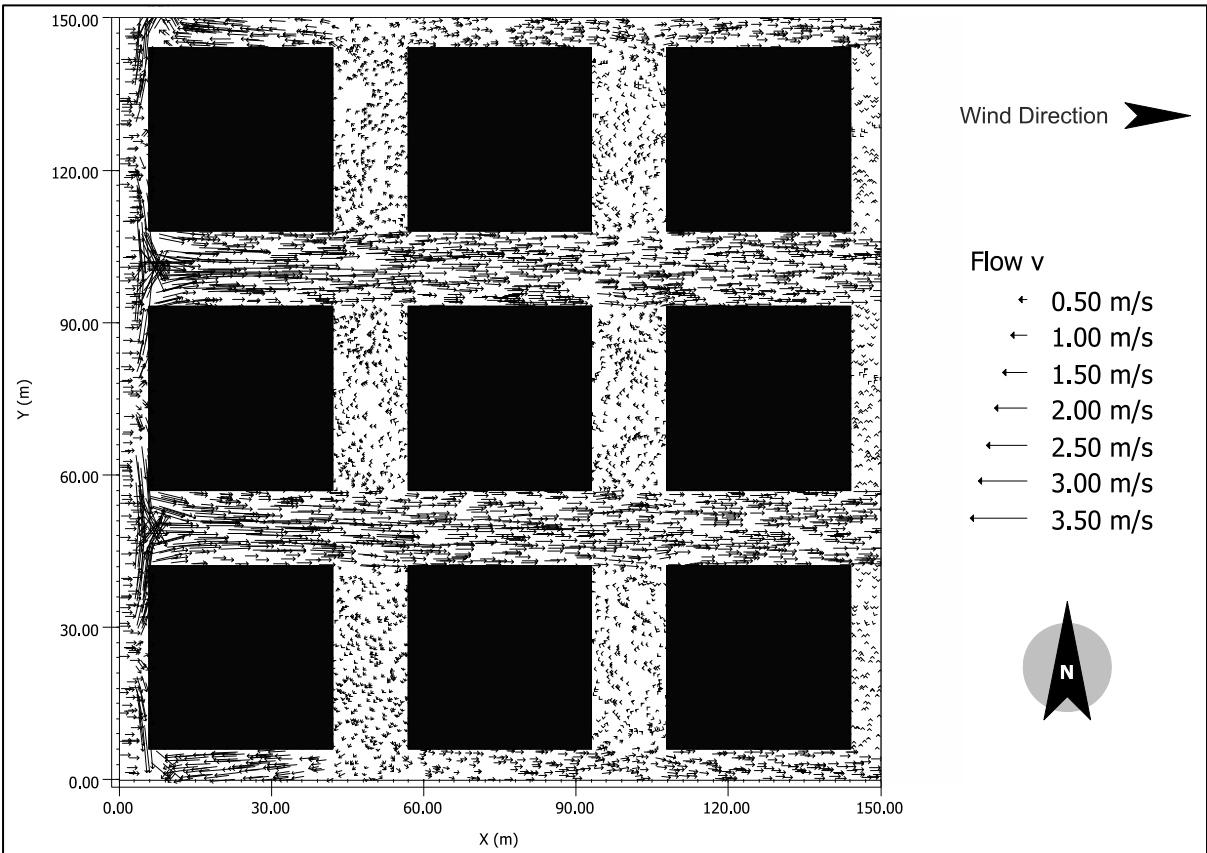


Figure 6.4. Wind flow in scenario A.2.

6.2.3 COMPARISON BETWEEN GRID A'S DIFFERENT ORIENTATION SCENARIOS.

Having the street grid geometrically designed is not sufficient to determine the optimal design in terms of wind flow or physiological equivalent temperature (PET). For that reason, every scenario for the street grid was simulated in two orientations to test out the wind behaviour when mean wind flow changes as well as the direct sun radiation direction. As shown in Figure 6.6, scenario A.2 shows a higher percentage of distribution for high wind speeds than scenario A.1 (Figure 6.5), but it has an equal high percentage of low wind speeds. This means that some parts of the plot would get a strong wind flow and in some other parts a stale air where pollution particles can gather in high concentrations. Scenario A.1, with its normal distribution, has a better chance of comfort with more suitable wind flow for pedestrians.

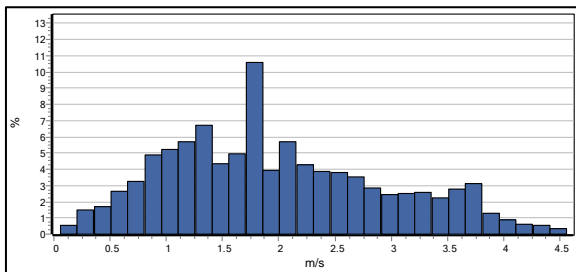


Figure 6.5. Wind speed distribution for scenario A.1.

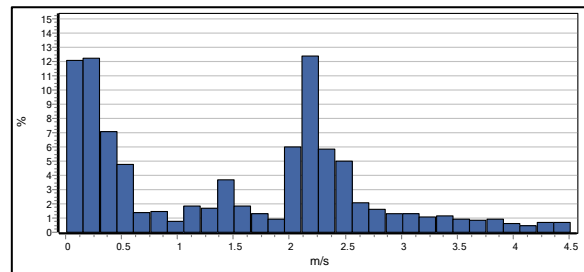


Figure 6.6. Wind speed distribution for scenario A.2.

To compare the PET levels in both scenarios, two receptors were placed in the inner part of the plot, shown in red in Figure 6.1 and Figure 6.3. Both scenarios differ in PET levels, with this depending hugely on the direct solar radiation access duration throughout the day. This is determined by the geometry of the design and, in this case particularly, the orientation. As seen in Figure 6.7, scenario A.2 has higher PET values than scenario A.1 during the early hours of the day and later on between the hours of 15:00 and sunset. The rise in PET values in this situation is due to the location of receptor 1, where it is situated on the west-east axis with no shading from the morning and evening sun. The opposite can be seen in A.1, where higher PET levels were recorded during midday, due to the location of the receptor on the north-western- south-eastern axis, which means it would not be shaded from the high sun in the south. The change of orientation of the plot changed the areas that the sun would reach in different times of the day, and when inspecting the shadows cast by the buildings for both of the scenarios, it was concluded that scenario A.1 had the least time duration of direct solar radiation. Having reduced time duration of sun radiation, like in scenario A.1, would reduce PET levels in the summertime, and would make these pedestrian areas more comfortable

and more walkable with less additional shading devices. It should be noted that, for scenario A.1 both receptors recorded 7 hours in the comfortable range while scenario A.2 recorded 6 and 9 hours for receptor 1 and 2, respectively.

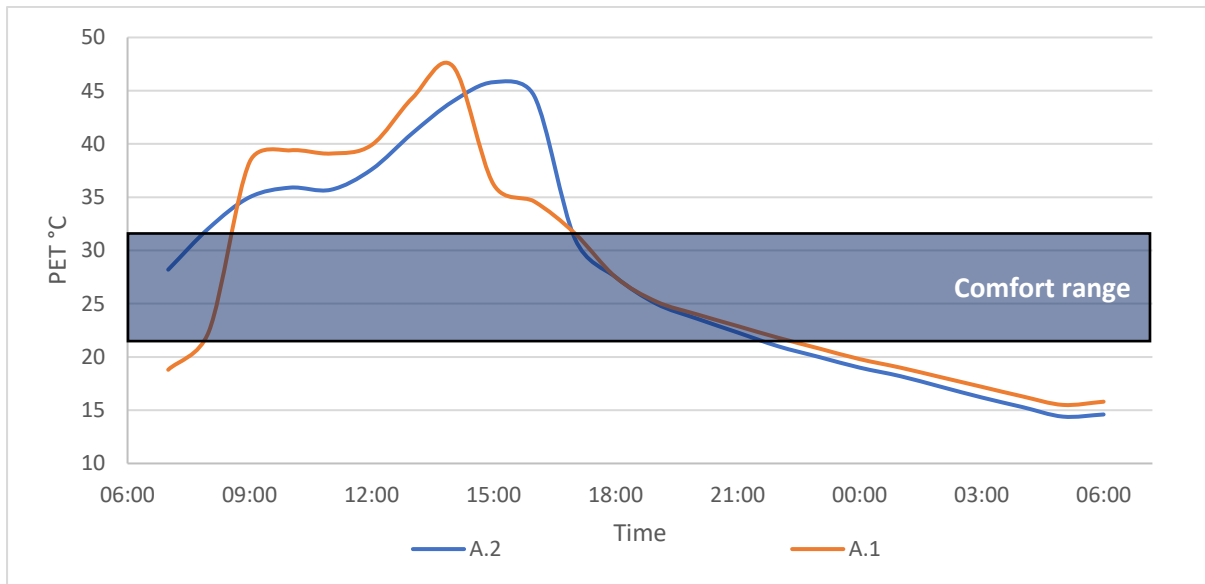


Figure 6.7. PET values for receptor 1 for scenarios A.1 and A.2.

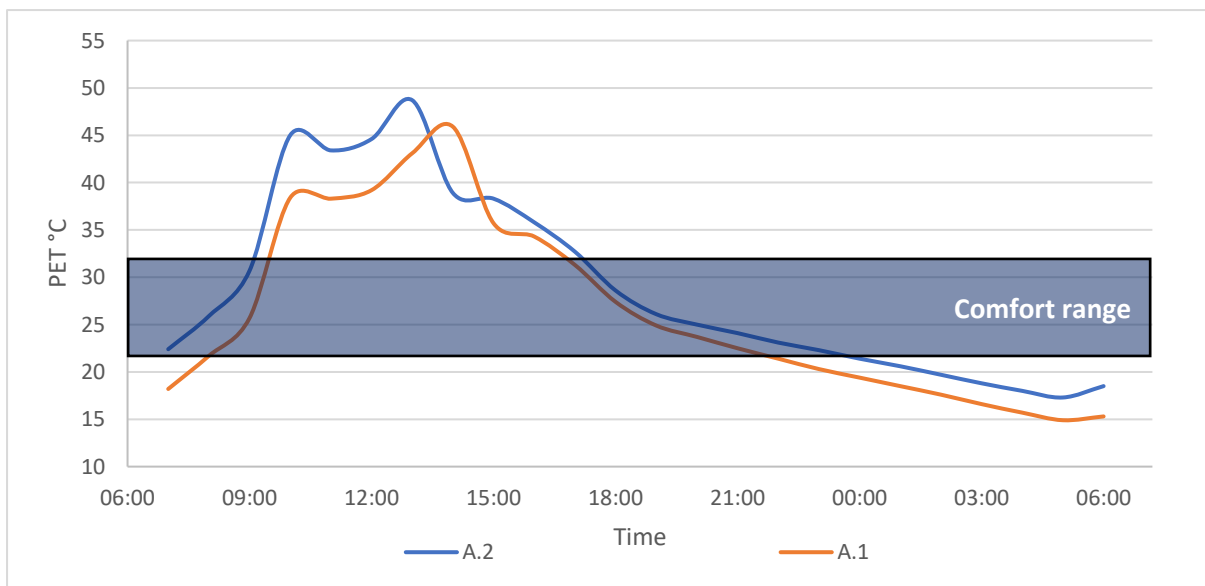


Figure 6.8. PET values for receptor 2 for scenarios A.1 and A.2.

6.3 STREET GRID LAYOUT B.

6.3.1 SCENARIO B.1.

Figure 6.9 shows scenario B.1 for the street grids analysis - this grid is an altered version of scenario A, with perpendicular streets and 45° angle orientation from the North. Scenario B has an attached row of buildings obstructing the wind flow inside the plot. Figure 6.9 displays the wind speed at 11:00 am, as well as the placement of receptors 1 and 2 (shown in red).

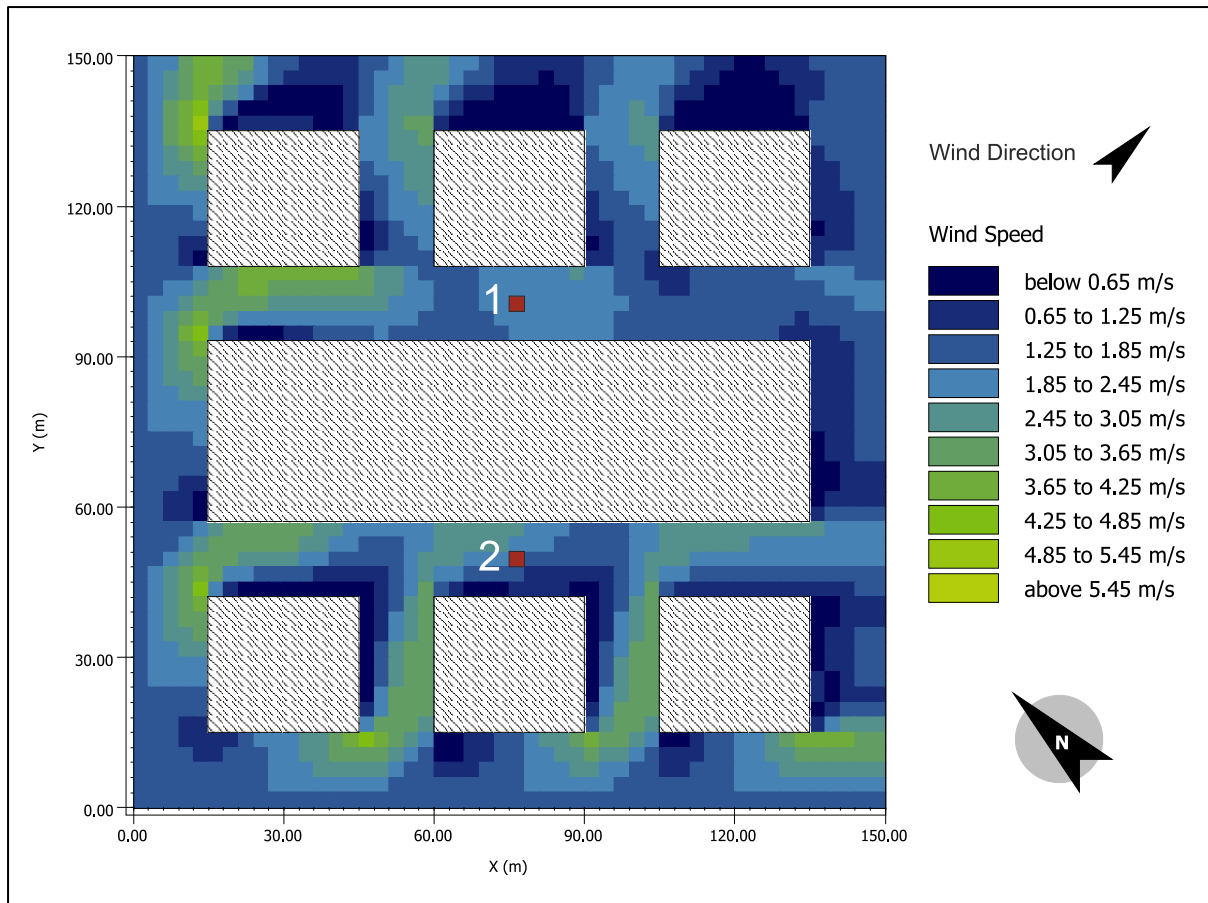


Figure 6.9. Wind speed in scenario B.1.

As in the previous scenario, the inlet angle is creating a flow separation when it reaches the sharp edge of the buildings as shown in Figure 6.10. This causes the mean wind flow to be displaced and forms vortices in the cavity zone located at the backside of the buildings, where wind speed is lower than the rest of the plot, shown in dark blue in Figure 6.9. As wind flow progresses into the plot, it gets disturbed by the attached row of buildings and forms a stream that gets fed by the wind coming from the detached buildings while maintaining a high speed. On the other side of the row buildings, the wind flow is strong when it enters the street, but it gets weaker as it loses its intensity moving forward due to its flow direction that allows flow separation when it hits the edges of the detached buildings.

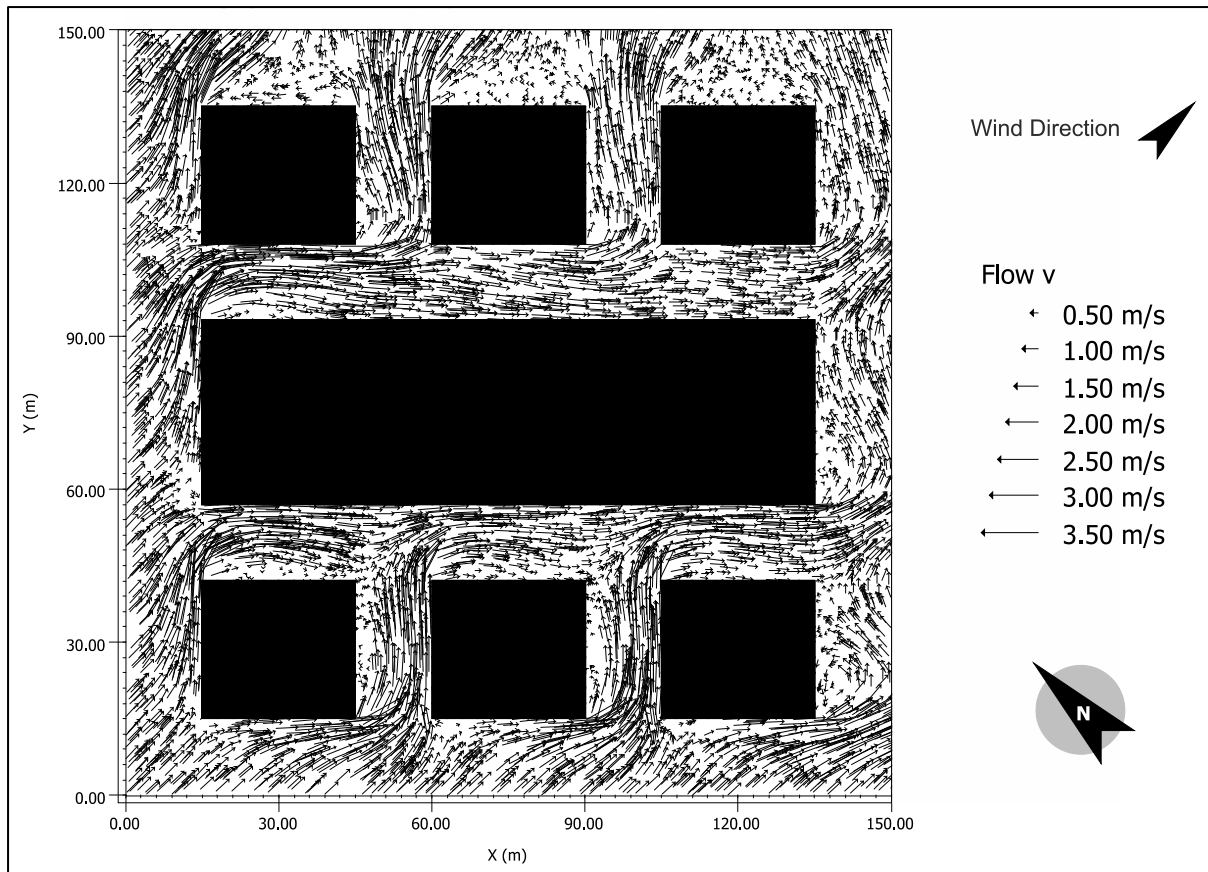


Figure 6.10. Wind flow in Scenario B.1.

6.3.2 SCENARIO B.2.

Figure 6.11 shows scenario B.2 for street grid analysis, where the grid is a classic take of the grid system with attached row buildings in the middle of the plot. For scenario B.2 the plot was kept with its original orientation, 0° angle from the North. Figure 6.11 shows the wind speed at 11:00 am, as well as the placement of receptors 1 and 2 (shown in red).

As in Scenario A.2, the wind is entering the plot at a 90° angle, which causes a channelling effect inside the streets that face (West-East). Because of the continuous non-infiltrating nature of the attached row buildings, the stream formed on both sides of the row buildings have higher velocities than Scenario A.2, though the difference doesn't exceed 0.1 m/s. The high intensity of the channelling flow does not allow much air to escape to the streets facing (North-South), and this leaves these areas with poor air quality. Figure 6.12 shows the wind flow behaviour in the plot, where it displays the high intensity of the channelling flow, and the weak vortices formed in the (North-South) facing streets.

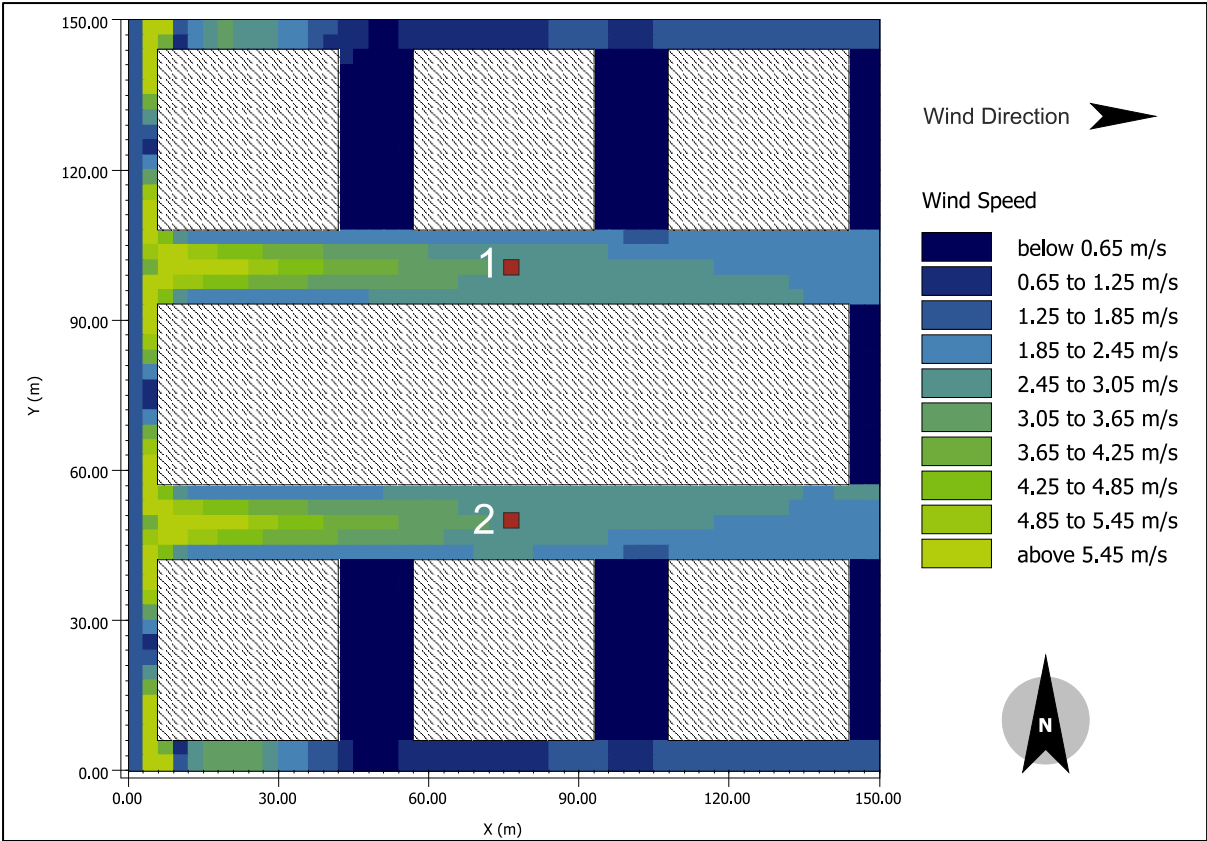


Figure 6.11. Wind speed in scenario B.2.

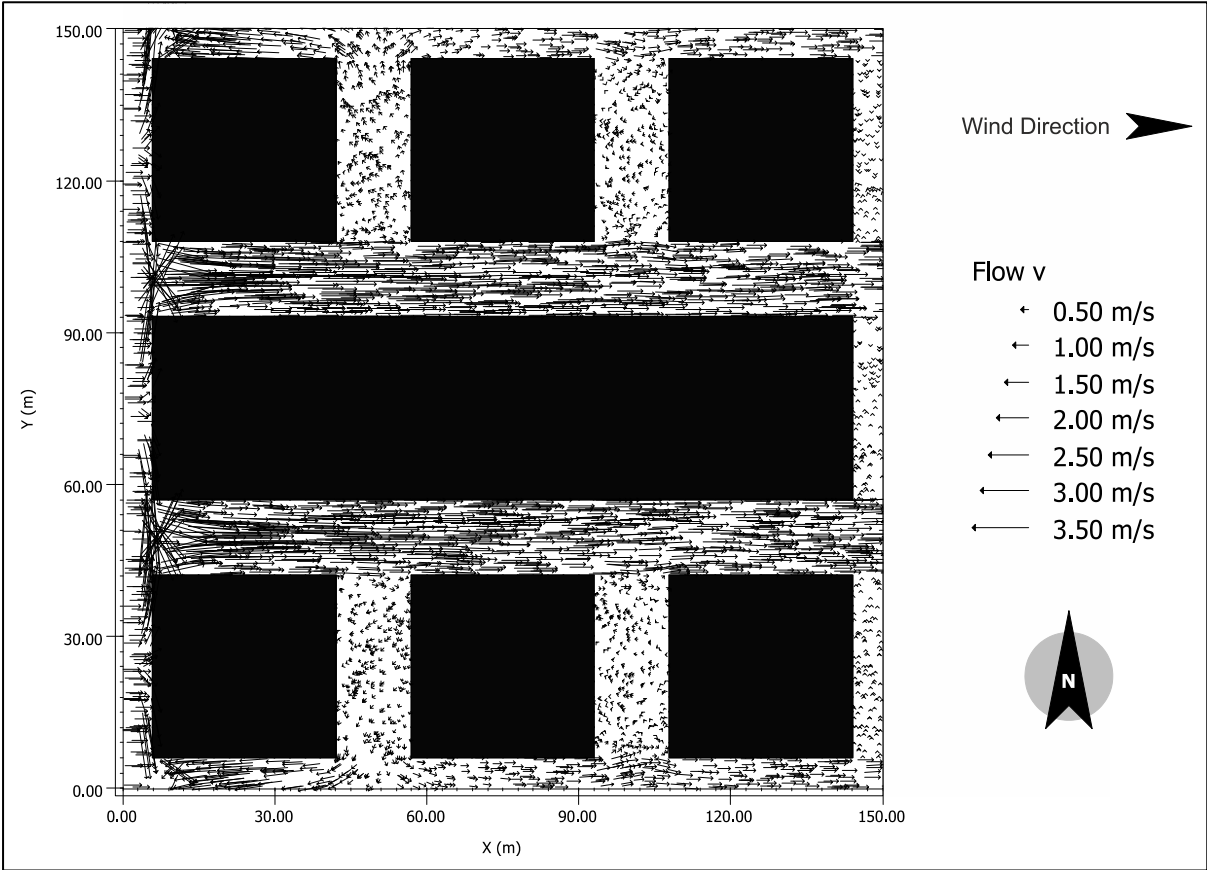


Figure 6.12. Wind flow in Scenario B.2.

6.3.3 COMPARISON BETWEEN GRID B'S DIFFERENT ORIENTATION SCENARIOS.

As shown in Figure 6.14, scenario B.2 shows a high percentage of low wind speed due to the high pressure caused by the channelling flow, compared to scenario B.1 (Figure 6.13), where wind speed values show a better distribution, with 13% of the plot having 2 m/s wind speed.

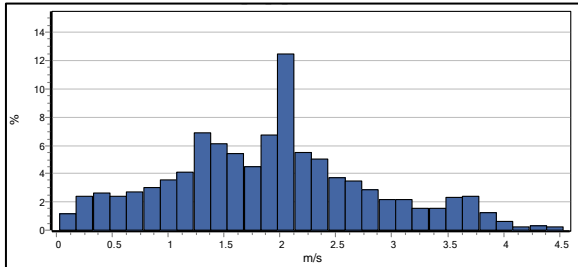


Figure 6.13. Wind speed distribution for scenario B.1.

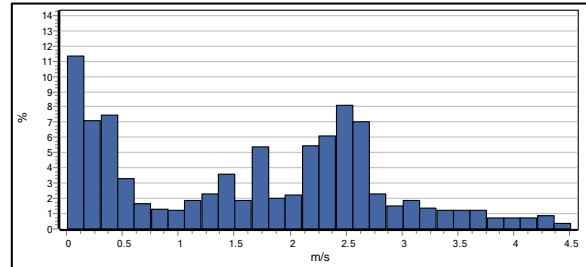


Figure 6.14. Wind speed distribution for scenario B.2.

To compare the PET levels in both scenarios, two receptors were placed in the inner part of the plot, shown in red in Figure 6.9 and Figure 6.11. PET is heavily affected by solar radiation, and this can be seen for both receptors in Figure 6.15 and Figure 6.16, between the hours of 18:00-06:00. The spike of PET levels is also explained by the sun's position at the time of day, where the receptors have lower PET values whenever they are shaded by the surrounding buildings. It should be noted that wind speed in both scenarios are close in value, with approximately 0.1 m/s difference, and that is the reason why no effect is noticed in the night-time. Scenario B.2 recorded 2 hours of comfortable range more than B.1 due to the presence of solar radiation in the early hours of the day in scenario B.2, which raised the PET values to the comfort range of (21.6 - 32) °C between the hours of 07:00 and 08:00.

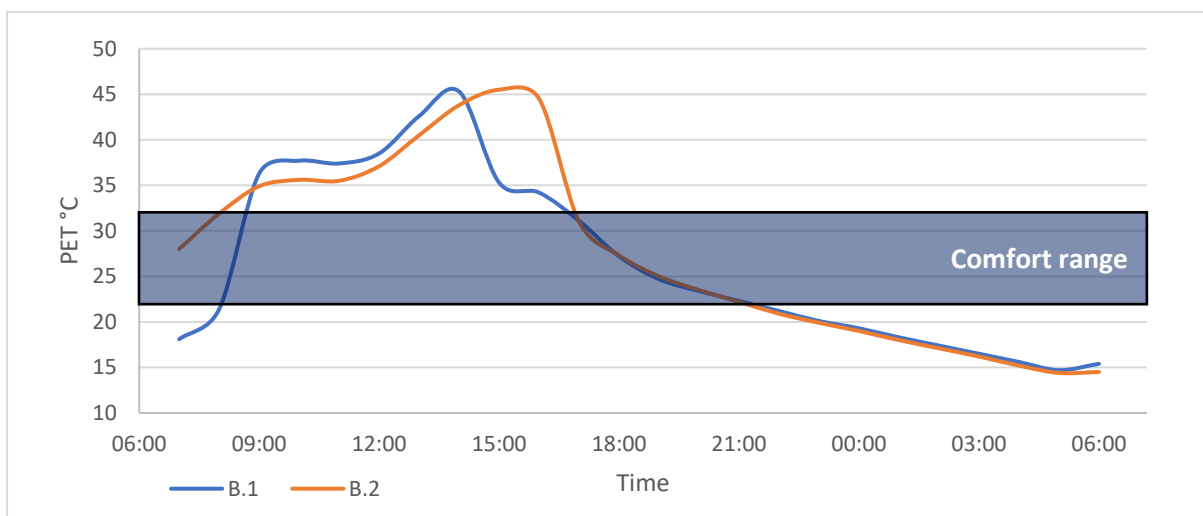


Figure 6.15. PET values for receptor 1 for scenarios B.1 and B.2.

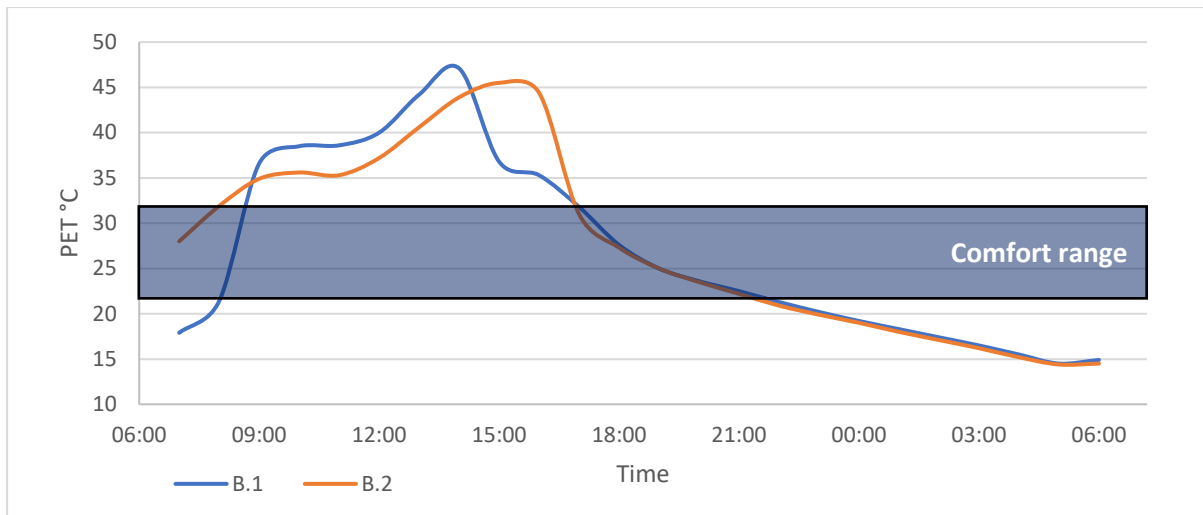


Figure 6.16. PET values for receptor 2 for scenarios B.1 and B.2.

6.4 STREET GRID LAYOUT C.

6.4.1 SCENARIO C.1.

Figure 6.17 shows scenario C.1 for the street grids analysis, where this grid is an altered version of the Oglethorpe Plan— a grid consisting of cellular city blocks. Savannah, Georgia was designed following the Oglethorpe plan with four residential buildings in the corner and civic buildings in the middle. Scenario C.1 has the basic geometrical shape of an Oglethorpe plan but was altered to conform with the grid properties mentioned in Section 6.1. The scenario has perpendicular streets and 45° angle orientation from the North. Figure 6.16 displays the wind speed at 11:00 am, as well as the placement of receptors 1-5 (shown in red). The geometry in scenario C.1 introduces the effect of linear buildings against the square cluster of buildings. Figure 6.17 shows how wind flow enters the plot from the bottom left corner, and immediately gets split into two streams, with the left stream free from obstacles accelerating while the right stream decelerates facing the buildings. As wind flows deeper into the plot, it is noticeable that wind speed increases in between the linear buildings compared to the big cluster of buildings in the middle of the plot. This is explained by the size of the cavity area cast by the bigger cluster of buildings where vortices are formed, and wind speed is reduced. Low wind speed can be seen at receptor 1 in Figure 6.17, and this is due to the strong wind flow coming from street opening, which gets reinforced by the helical vortex from the adjacent canyon, all of this create strong pressure that would not allow wind to escape into the area where receptor 1 is placed. Figure 6.18 displays the wind vortices and wind flow around the buildings, where it clearly shows the cavity areas behind the buildings.

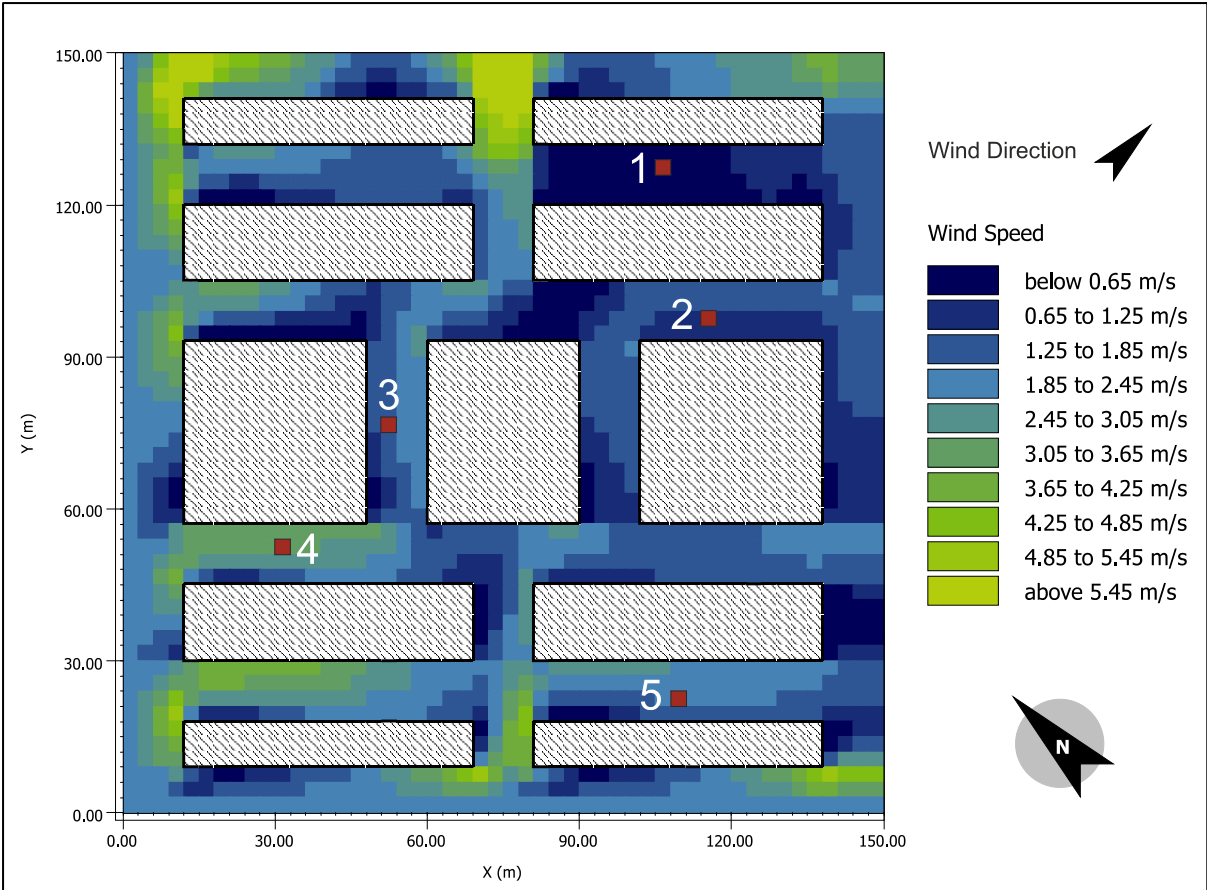


Figure 6.17. Wind speed in scenario C.1.

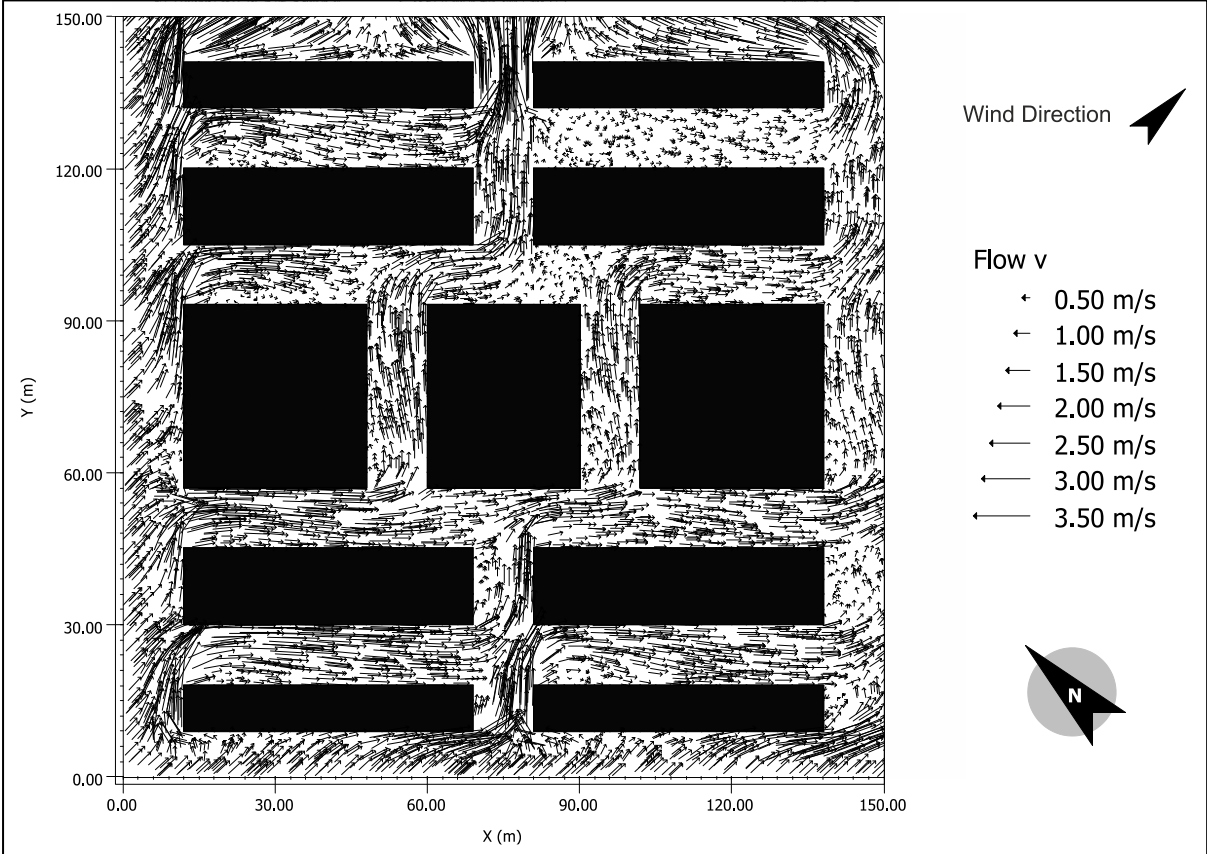


Figure 6.18. Wind flow in Scenario C.1.

6.4.2 SCENARIO C.2.

Figure 6.19 shows scenario C.2 for street grid analysis, and it is a modified version of the Oglethorpe Plan as in scenario C.1. For this scenario, the plot was kept with its original orientation, 0° angle from the North. Figure 6.19 shows the wind speed at 11:00 am, as well as the placement of receptors 1-5 (shown in red).

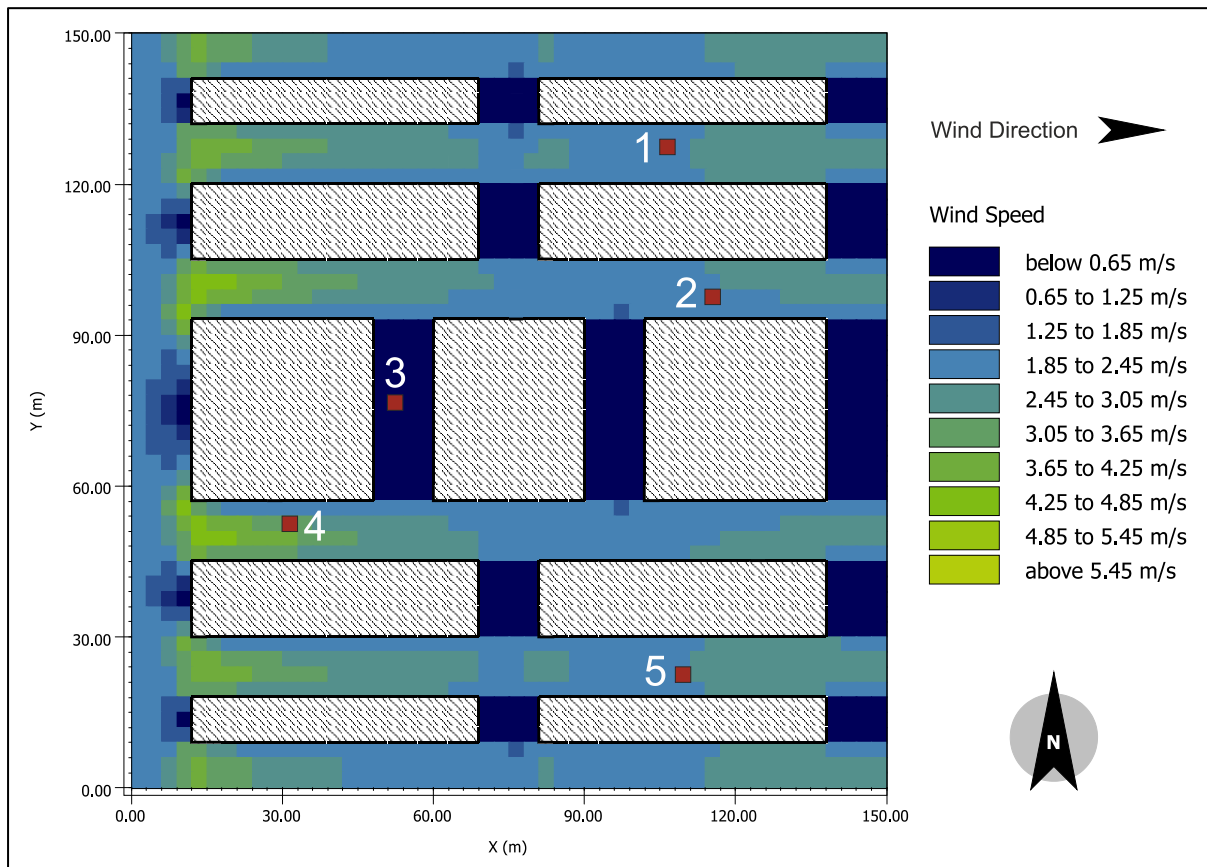


Figure 6.19. Wind speed in scenario C.2.

The effect of linear buildings shows in scenario C.2 through the channelling effect. As seen in Figure 6.19, wind enters the plot from the West parallel to the (West-East) streets, and wind flow in these streets generates high velocity due to the entering angle. This causes high pressure that limits wind penetration to (North-South) streets. Figure 6.20 shows the wind flow behaviour in the plot, where it displays the low-speed vortices formed in the (North-South) streets. Longer (N-S) streets, however, have two vortices forming from each end with opposite rotations. Having this orientation for the plot may raise the overall wind speed, but it produces areas with very low wind movement, this may cause bad ventilation which would result in minimal particle dispersion.

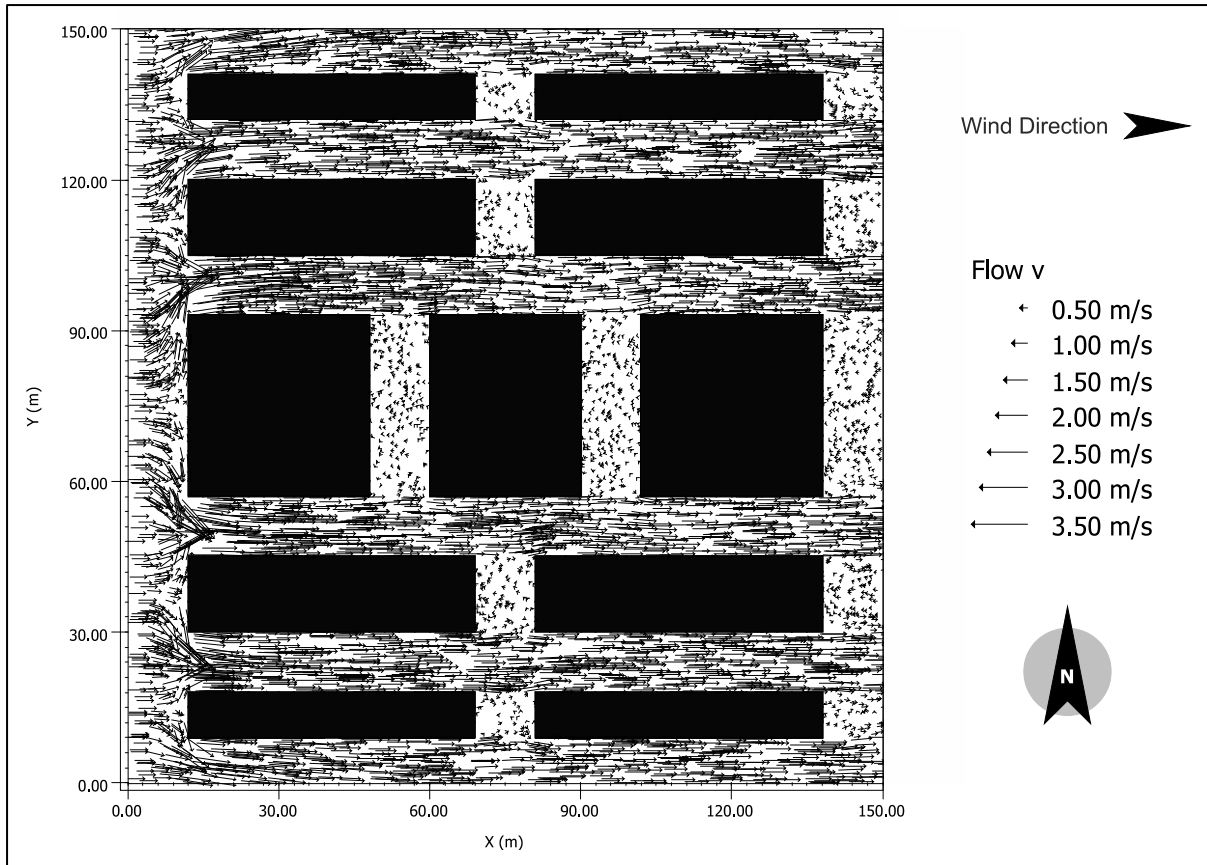


Figure 6.20. Wind flow in Scenario C.2.

6.4.3 COMPARISON BETWEEN GRID C'S DIFFERENT ORIENTATION SCENARIOS.

As seen in Figure 6.21, wind speed shows a normal distribution for the plot, and this means a lower count for high wind speed areas and a lower count for low wind speed areas too. In scenario C.2 the plot shows high wind speed distribution for (2-2.5) m/s velocity; however, it also shows a higher count for low speeds than scenario C.1, which means more stale air in poorly ventilated areas than C.1.

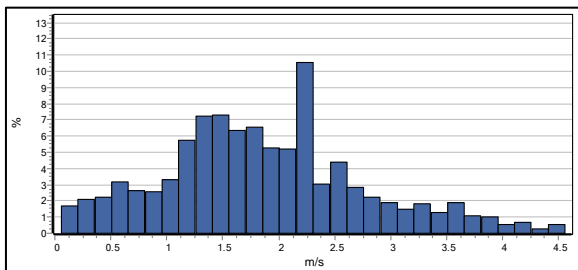


Figure 6.21. Wind speed distribution for scenario C.1.

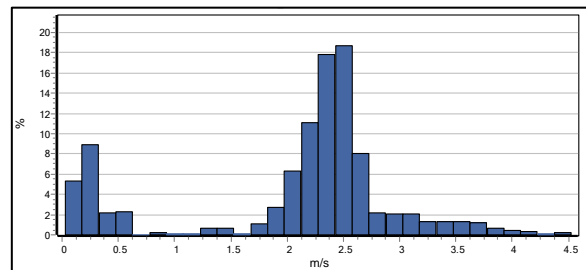


Figure 6.22. Wind speed distribution for scenario C.2.

PET levels at night are drastically reduced due to the lack of solar radiation. The absence of solar radiation shows how PET levels are affected by wind speed change, and this can be seen in Figures 6.23 and 6.24 for receptors 1 and 2, where scenario C.1 has higher PET values than

scenario C.2 due to lower wind speed values as a result of wind channelling in scenario C.2. The opposite is seen in receptor 3 in Figure 6.25, as the location for this receptor is in a (North-South) oriented street for scenario C.2 with low wind speed values, and higher wind speed values for scenario C.1. Figures 6.26 and 6.27 show that PET has similar levels for receptors 4 and 5, due to similar wind speed values.

PET levels in the daytime are heavily influenced by solar radiation, and for this reason, orientation is crucial in determining the shaded areas and consequently PET. In receptors 1,2,4 and 5 the PET values for scenario C.2 spike in the morning between (06:00-09:00) and again before sundown between (14:00-18:00). This can be explained by the position of the buildings in regard to North, where direct solar radiation irradiates these receptors through the (West-East) oriented streets. However, these receptors are shaded when the sun is facing South between the hours of (09:00-14:00). As for receptor 3, the location is shaded throughout the morning and evening period but receives strong direct sun radiation mid-day, which raises the PET levels higher than Scenario C.1. Scenario C.1, on the other hand, provides a wider range of shading throughout the plot which helps in lowering down the PET values compared to scenario C.2. Scenario C.1 recorded 36 comfortable hours throughout the five receptors while Scenario C.2 recorded 34 hours, with scenario C.1 having average PET values of 26.7 °C and Scenario C.2 having an average of 28.3 °C.

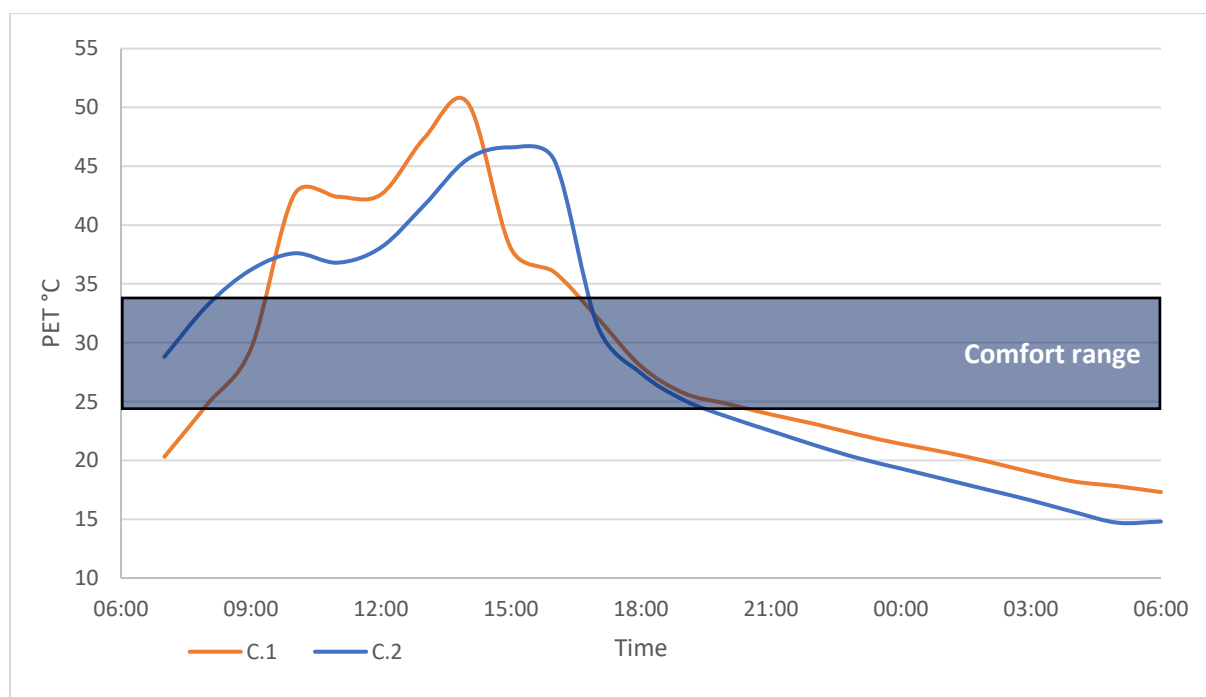


Figure 6.23. PET values for receptor 1 for scenarios C.1 and C.2.

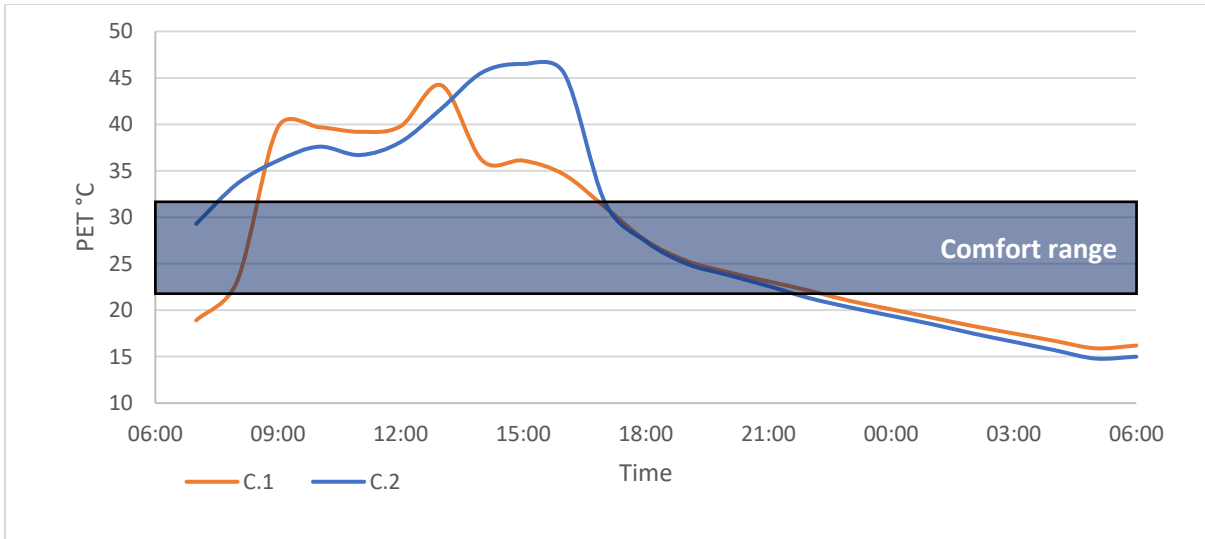


Figure 6.24. PET values for receptor 2 for scenarios C.1 and C.2.

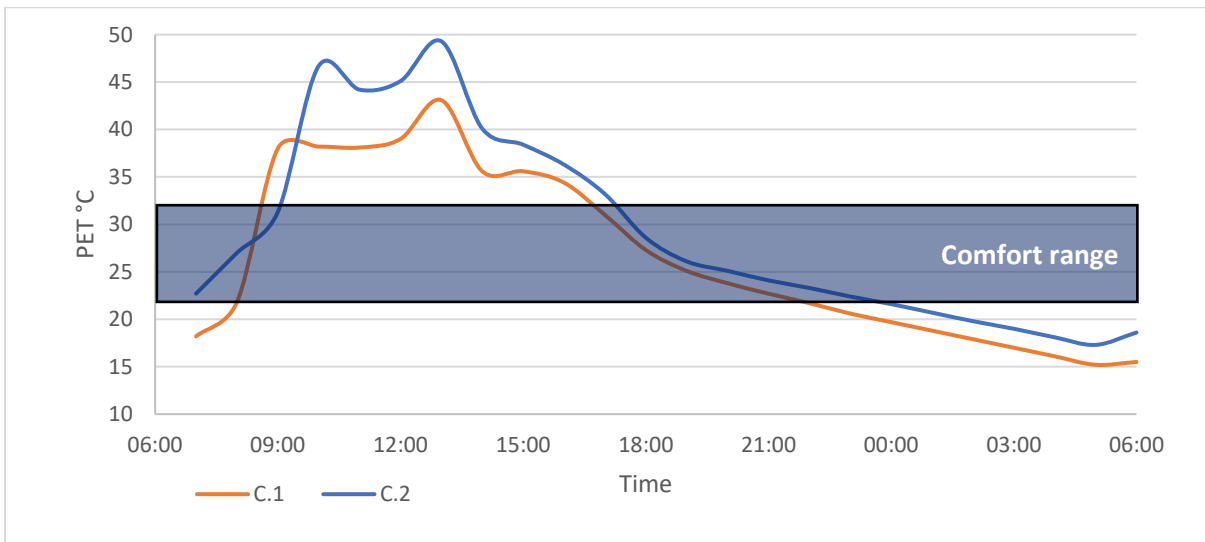


Figure 6.25. PET values for receptor 3 for scenarios C.1 and C.2.

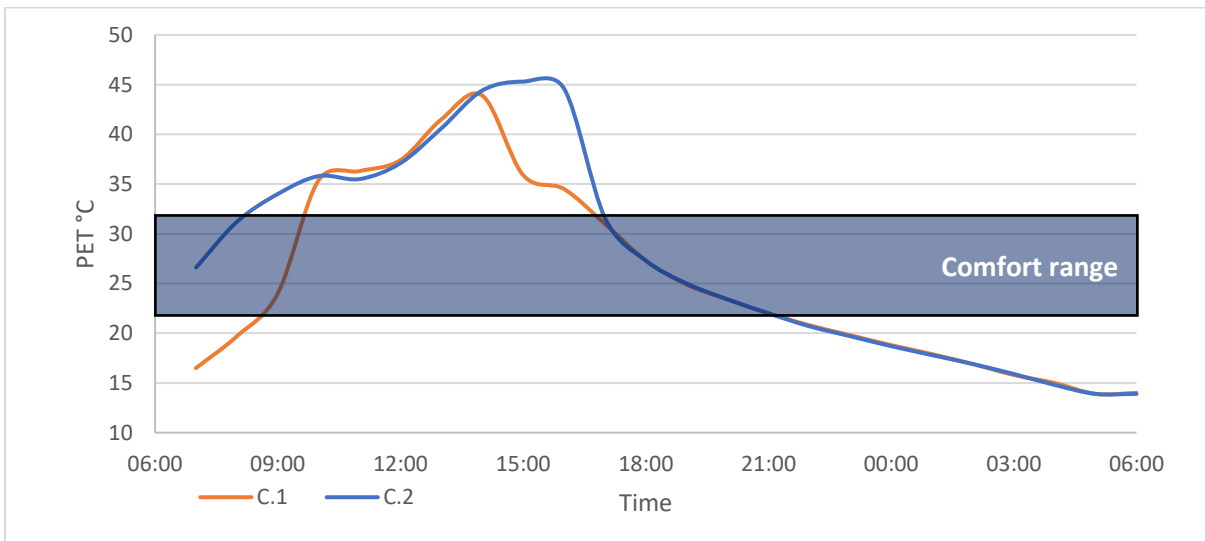


Figure 6.26. PET values for receptor 4 for scenarios C.1 and C.2.

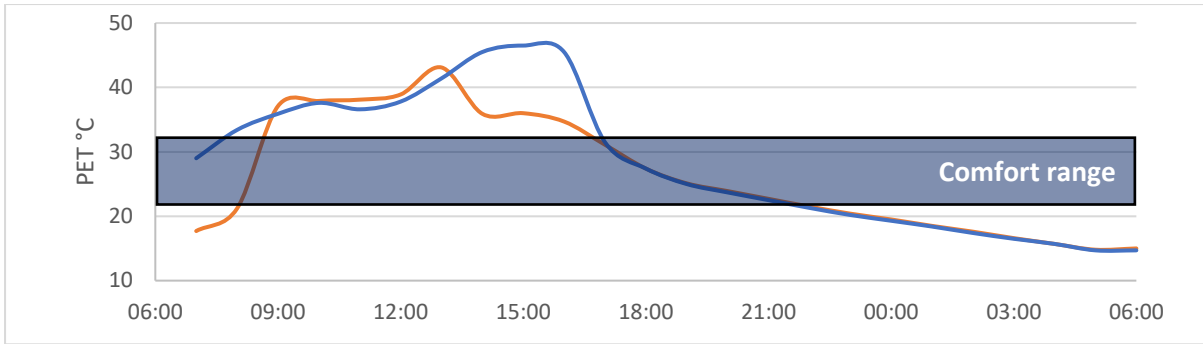


Figure 6.27. PET values for receptor 5 for scenarios C.1 and C.2.

6.5 STREET GRID LAYOUT D.

6.5.1 SCENARIO D.1.

Figure 6.28 shows scenario D.1 for the street grids analysis, and this scenario is the simplest form of radial grids, with the centre being a landmark e.g. monuments, civic buildings, worshipping institutes. The radial grid system is usually used in combination with other grid systems but for the sake of comparing the grid systems, this layout is using only radial streets to test the effects of this urban form. Scenario D.1 has a 45° angle orientation from the North and West wind directions. Figure 6.29 displays the wind speed at 11:00 am, as well as the placement of receptors 1-8 (shown in red).

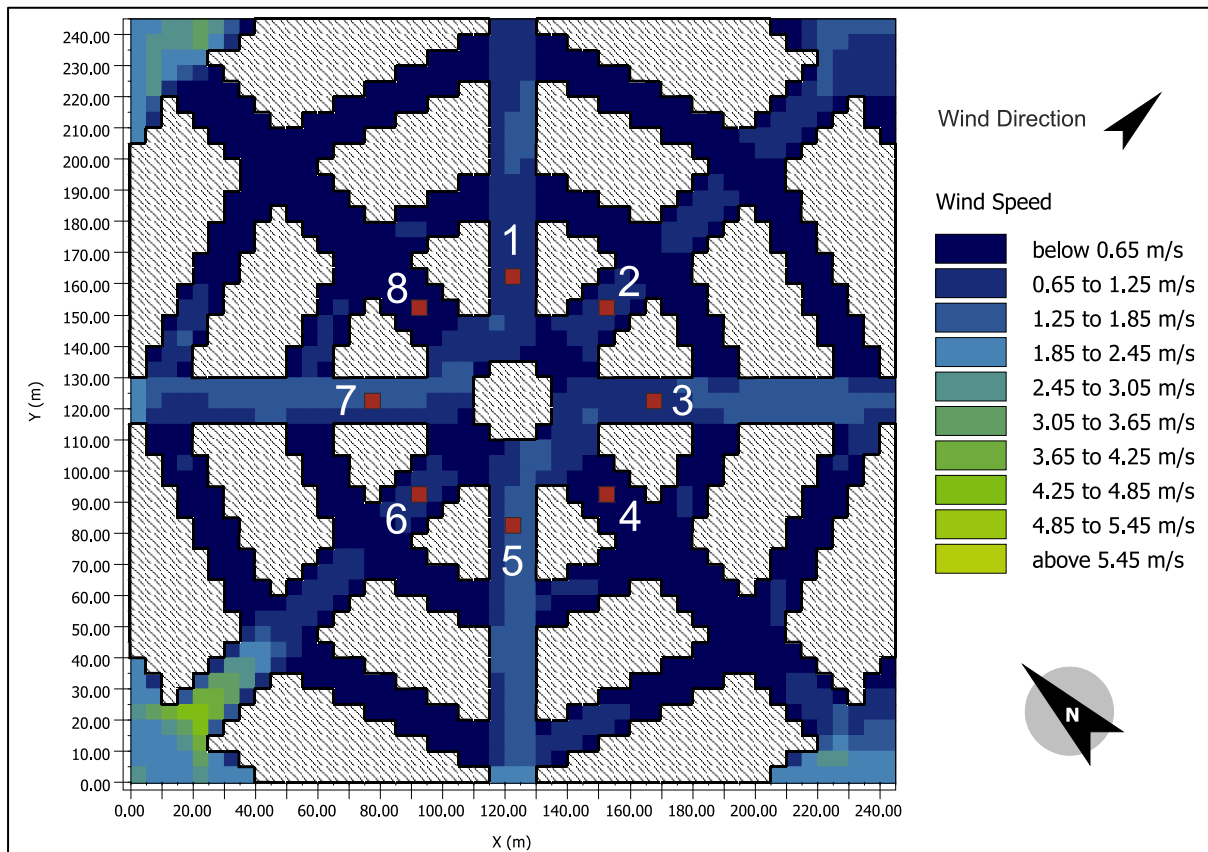


Figure 6.28. Wind speed in scenario D.1.

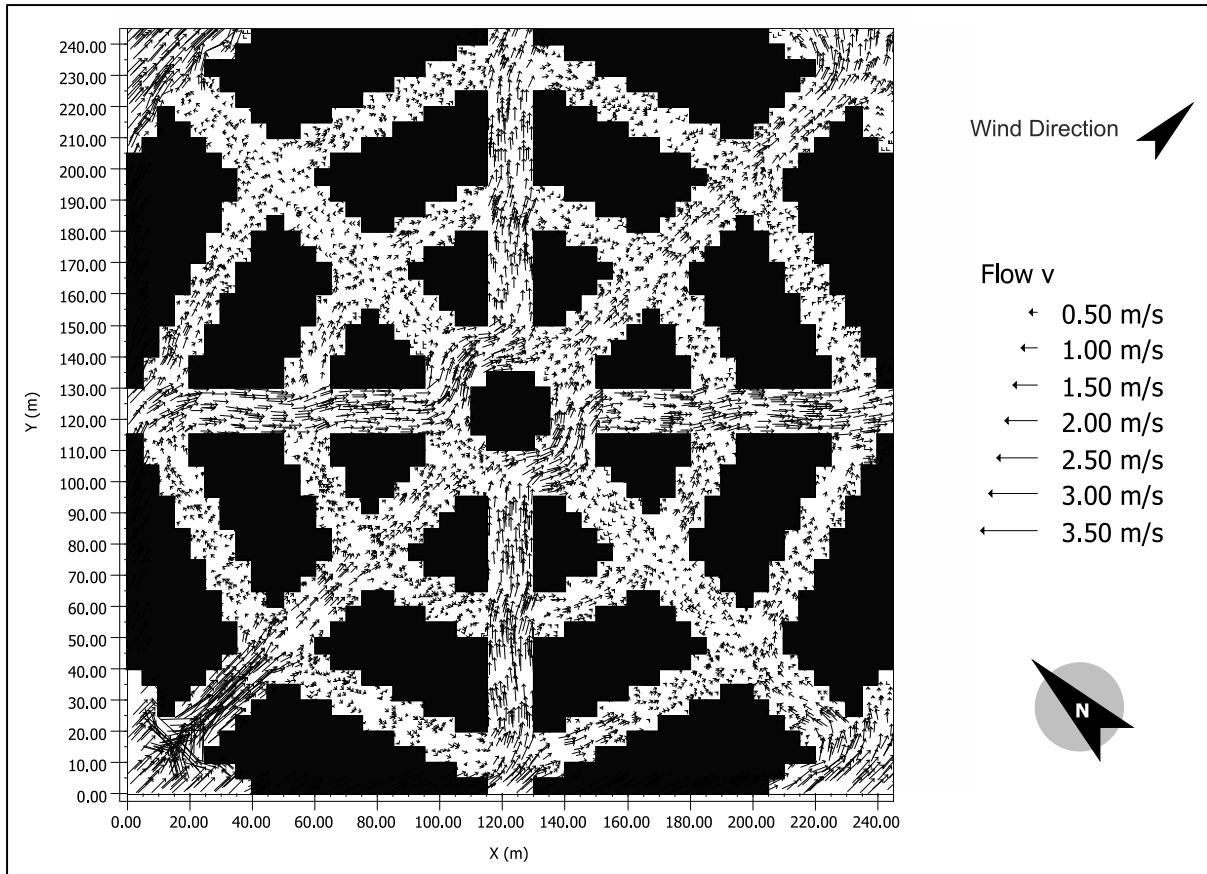


Figure 6.29. Wind flow in Scenario D.1.

The geometry of a radial grid has various street orientations, and this disturbs wind flow and limits the movement of the air inside the plot. As seen in Figure 6.28, wind flow enters the plot from the bottom left corner, and as it progresses inside the plot, wind speed decelerates rapidly from a lack of reinforcement geometry. The geometry that enhances wind flow is the one with gathering different streams into one main flow without facing obstacles. Figure 6.29 shows how the main wind flow reaches the centre of the plot passing through receptor 6 with low velocity and splitting into two streams. The two streams have higher wind speed values because it is being fed from the two streams passing through receptors 7 and 5 and exiting through streets where receptors 1 and 3 are placed. It should be noted wind speed inside the plot averages between 0.15-1.4 m/s and the entering speed is 4 m/s.

6.5.2 SCENARIO D.2.

Figure 6.30 shows scenario D.2 for street grid analysis. As with scenario D.1, this is a simple radial grid system with the centre being a landmark. For this scenario, the plot was kept with its original orientation, 0° angle from the North. Figure 6.29 shows the wind speed at 11:00 am, as well as the placement of receptors 1-8 (shown in red).

Wind flow enters the plot from the West side of the plot (Figure 6.30), and as it progresses into the plot passing through receptor 7, the wind maintains its velocity until it reaches the centre of the plot, where the flow is split into two streams moving around the centre of the plot and exiting through the opposite street passing through receptor 3. In the case of scenario D.1, the flow exited the plot through two streets passing through receptor 1 and 3, but in Scenario D.2 the flow separated and gathered itself in the same line of motion; this might have happened as a shortcoming of ENVI-met, where the simulation software read the edges of the building as small ridges rather than a continuous line. The average wind speed inside the plot is between 0.1-1.25 m/s.

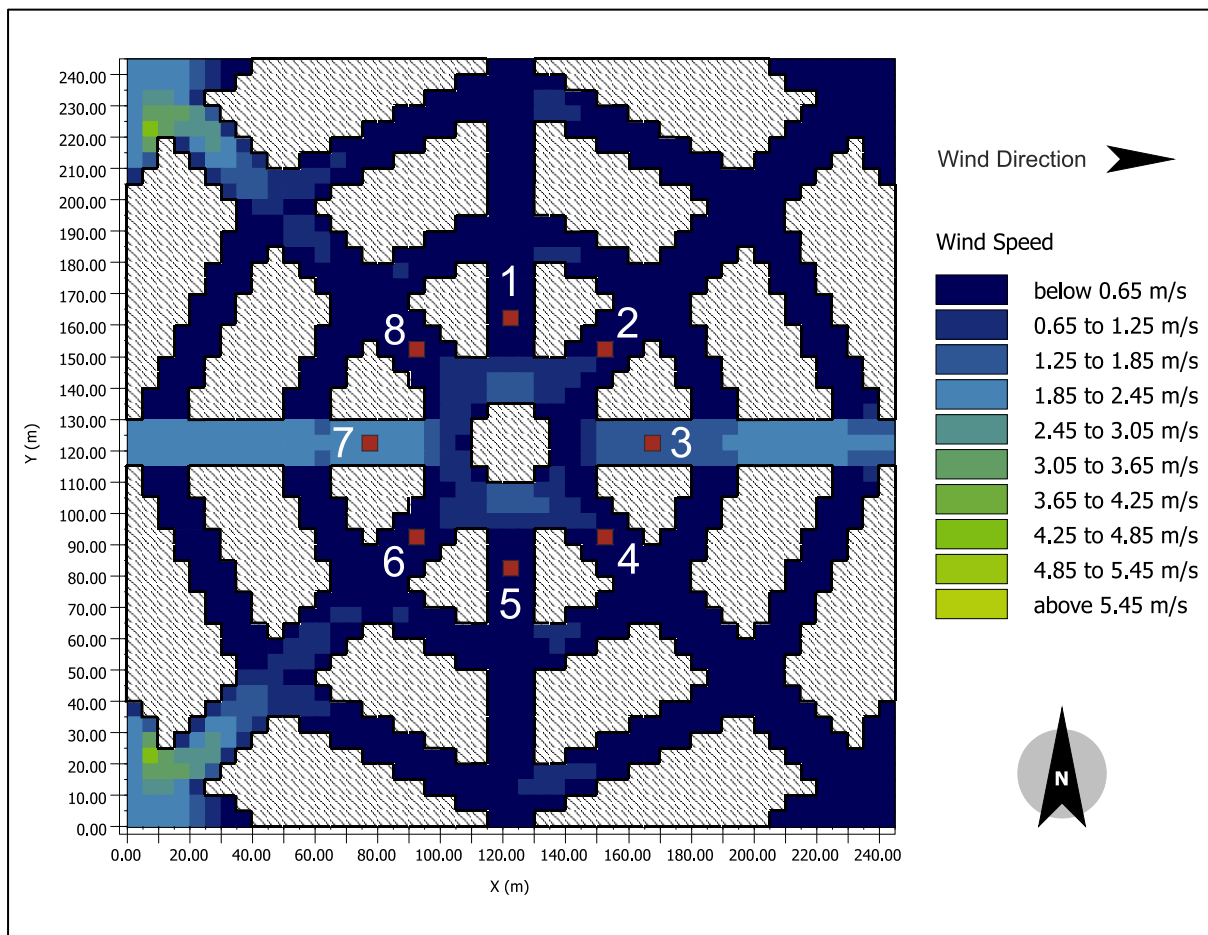


Figure 6.30. Wind speed in scenario D.2.

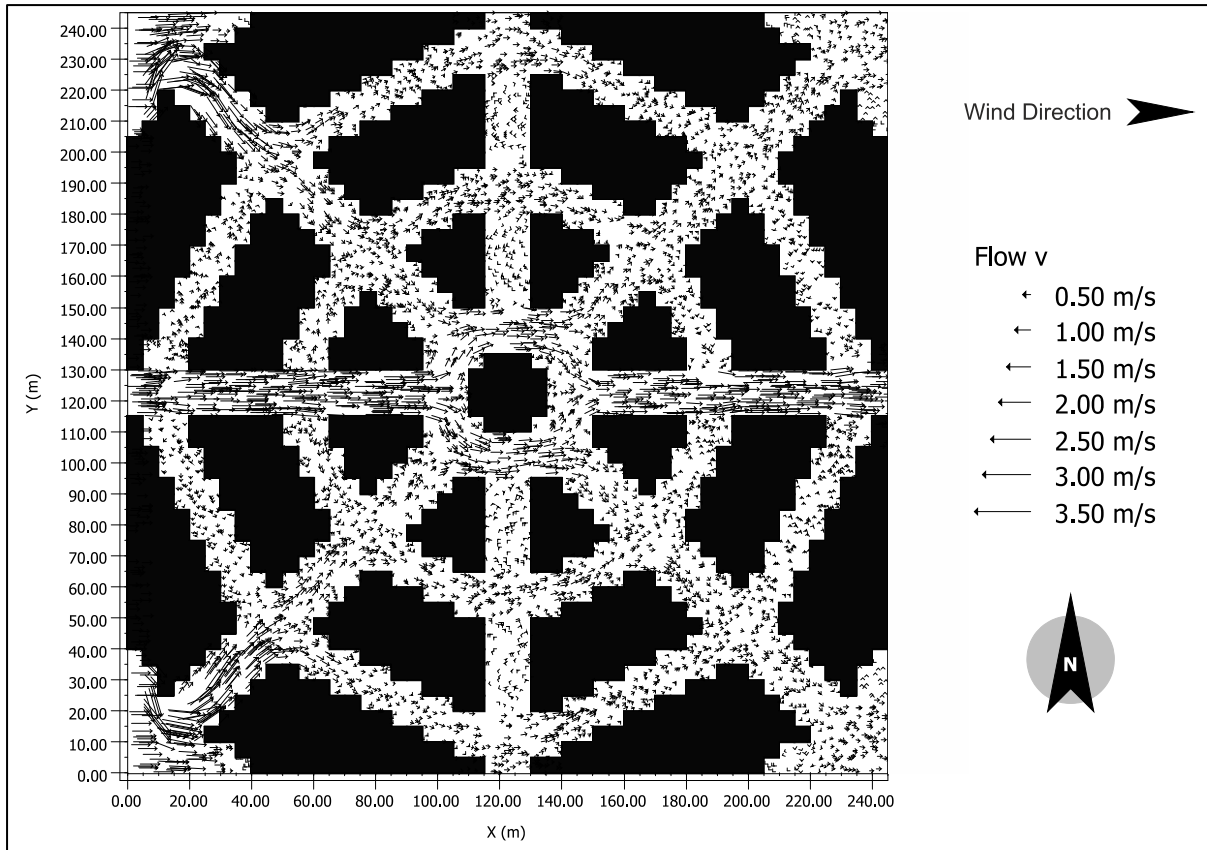


Figure 6.31. Wind flow in Scenario D.2.

6.5.3 COMPARISON BETWEEN GRID D'S DIFFERENT ORIENTATION SCENARIOS.

As seen in Figures 6.32 and 6.33, wind speed distribution is centred around the lower values compared to the previous grid layouts. However, scenario D.1 has areas with wind speeds of 0.5-1.5 m/s more than Scenario D.2, with the majority of the areas having wind speed values between 0-0.75 m/s. Both scenarios show low air ventilation which raises the risk of poor particle dispersion.

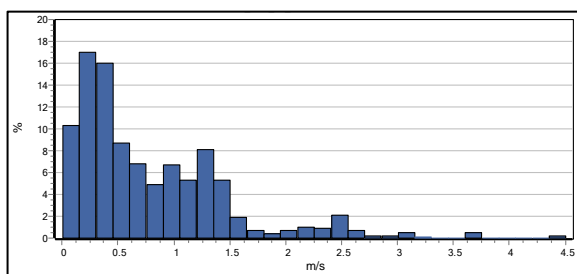


Figure 6.32. Wind speed distribution for scenario D.1.

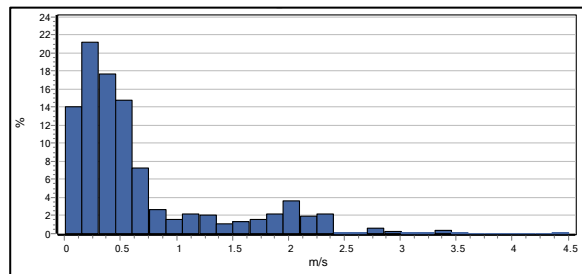


Figure 6.33. Wind speed distribution for scenario D.2.

As mentioned previously, PET is heavily influenced by solar radiation, and for this reason a spike in PET levels is noticed each time the receptor is hit by direct solar radiation. Figure 6.37 shows this rise in PET levels at 17:00 for receptor 4 in scenario D.2. A drop in PET values can be noticed in Figure 6.35 and 6.39 for receptors 2 and 6 in scenario D.2, and this happens

when the receptor is being shaded for a brief period of time after being exposed to direct sun radiation.

Streets holding receptors 2,4,6 and 8 in scenario D.1 are affected by direct solar radiation more than the other streets due to their location. In Figures 6.35 and 6.39 between (06:00-09:00) and (15:00-18:00), PET for scenario D.1 is noticeably higher than scenario D.2. This is due to their location being on the line of (West-East) axis where direct sun reaches the receptors in the morning and evening. It should be noted the exact case is seen in receptors 3 and 7 for scenario D.2 where PET levels are higher than scenario D.1 for the exact time intervals, shown in Figures 6.36 and 6.40. Figures 37 and 41 show the receptors that are being receiving midday solar radiation for Scenario D.1, due to their location being on the line of (North-South) axis. Thus, receptors 4 and 8 in scenario D.1 have higher PET levels between the hours of 10:00 and 16:00, compared to Scenario D.2. Similarly, in Figures 6.34 and 6.38, PET is higher in Scenario D.2 for receptors 1 and 5 as they lay on the (North-South) axis.

PET levels for both scenarios are reduced at night and have very close values, as seen throughout the previous layouts. This can be explained by the close value of the meteorological factors - air temperature, wind speed, mean radiant temperature and relative humidity. It has been noticed that some of the meteorological factors, like the air temperature and relative humidity, are difficult to affect in an urban layout through geometrical modification, but other meteorological factors, like wind speed and mean radiant temperature, vary significantly from one urban form to the other, which creates the big difference in PET values at day and the small difference at night. Scenario D.1 recorded 67 comfortable hours throughout the eight receptors while Scenario D.2 recorded 62 hours, with D.1 having average PET values of 28.6 °C and D.2 having an average of 29.3 °C.

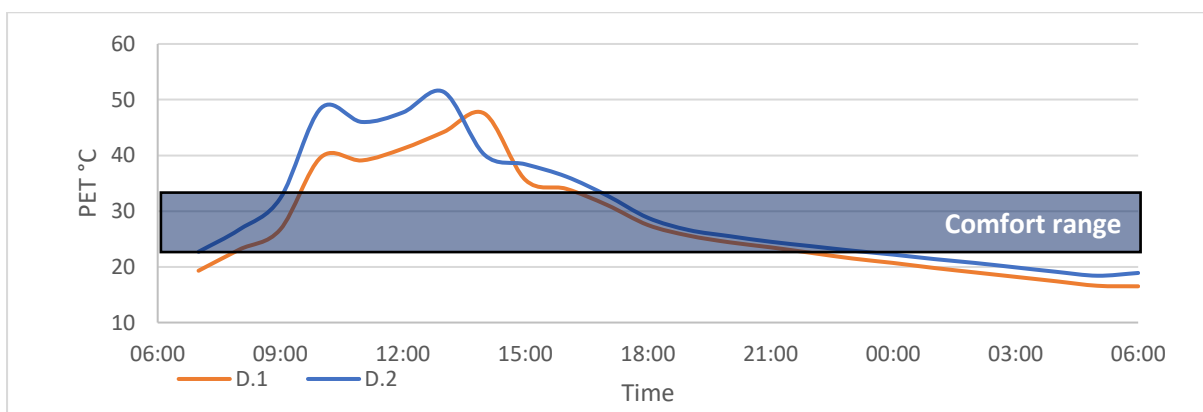


Figure 6.34. PET values for receptor 1 for scenarios D.1 and D.2.

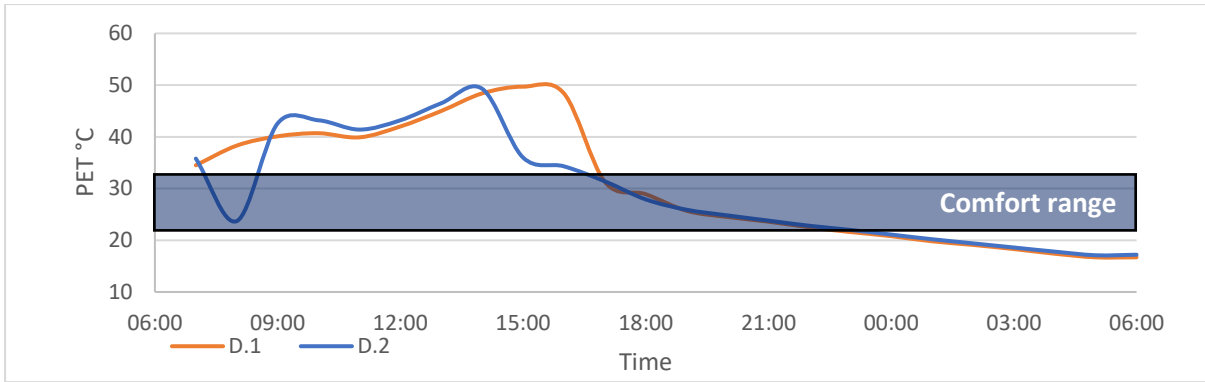


Figure 6.35. PET values for receptor 2 for scenarios D.1 and D.2.

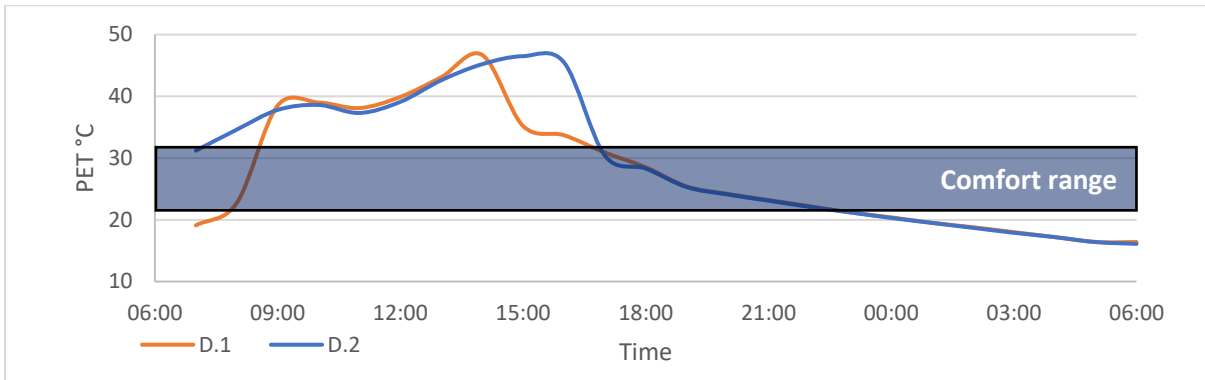


Figure 6.36. PET values for receptor 3 for scenarios D.1 and D.2.

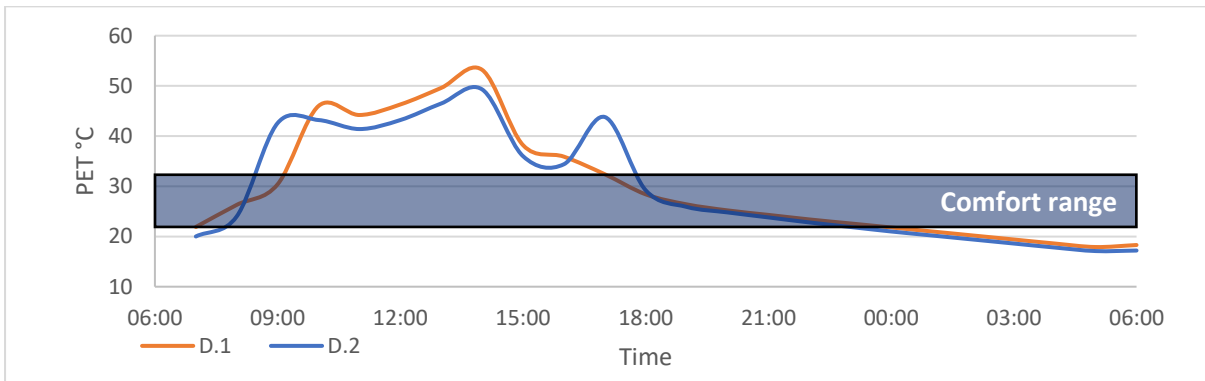


Figure 6.37. PET values for receptor 4 for scenarios D.1 and D.2.

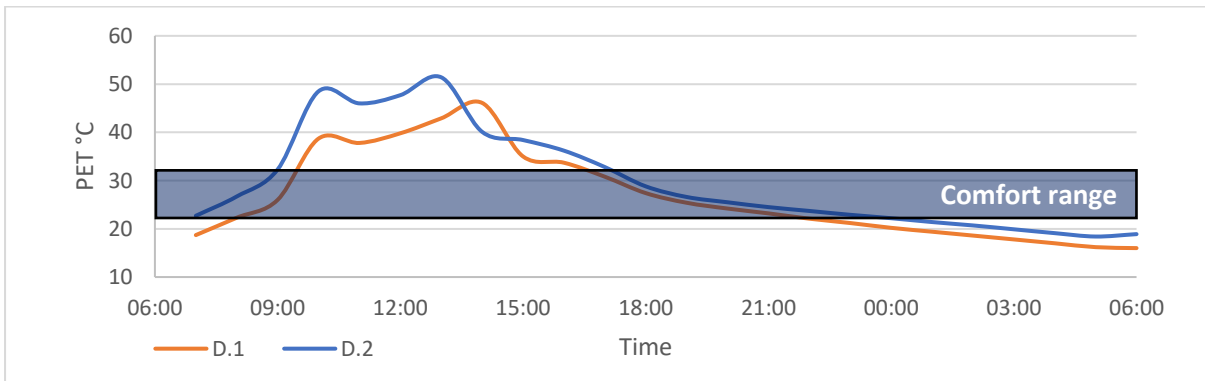


Figure 6.38. PET values for receptor 5 for scenarios D.1 and D.2.

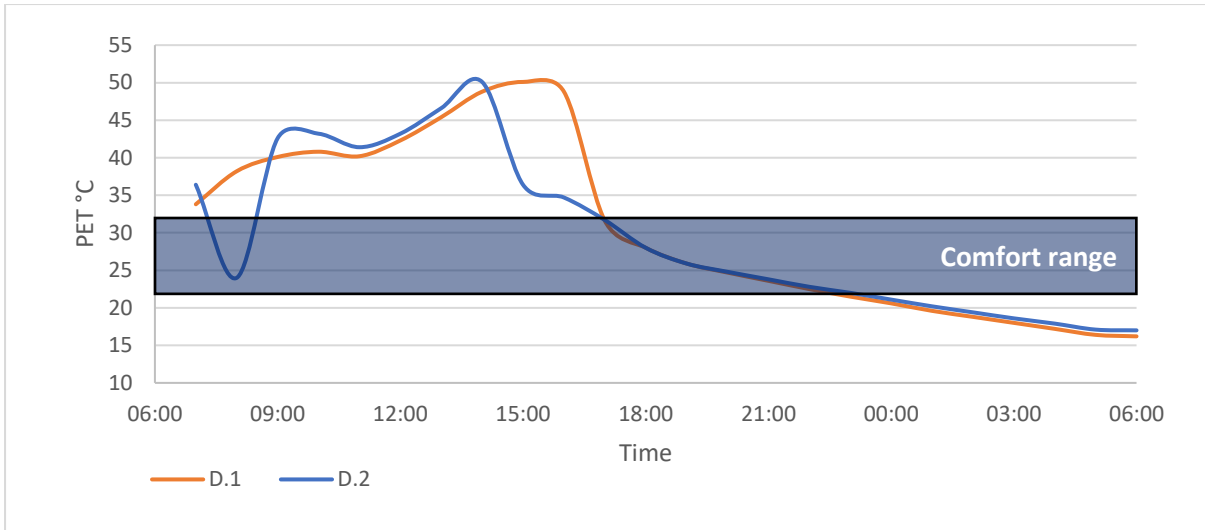


Figure 6.39. PET values for receptor 6 for scenarios D.1 and D.2.

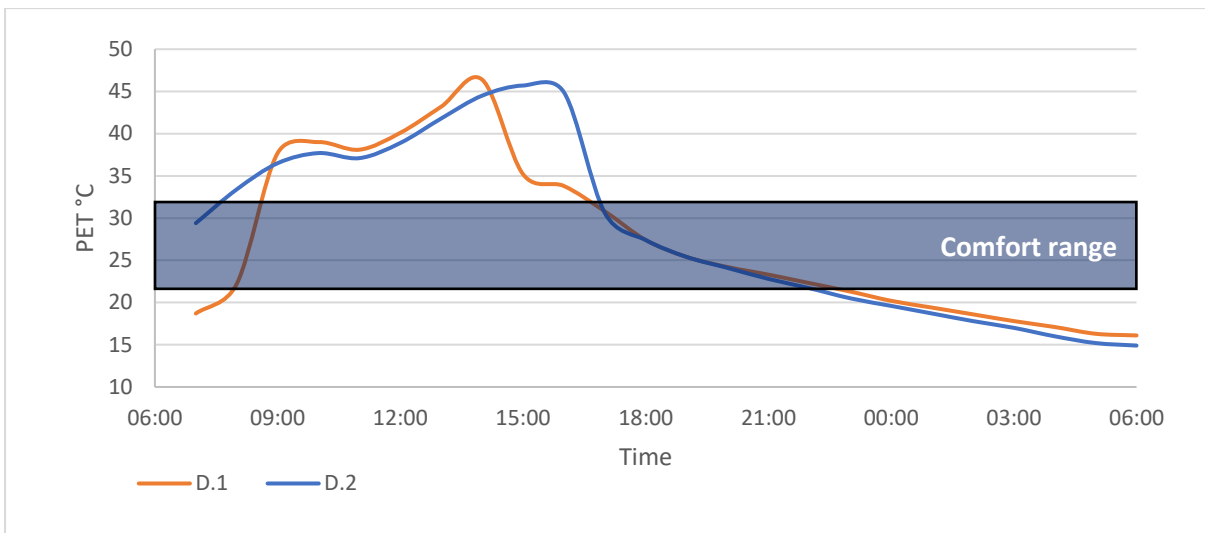


Figure 6.40. PET values for receptor 7 for scenarios D.1 and D.2.

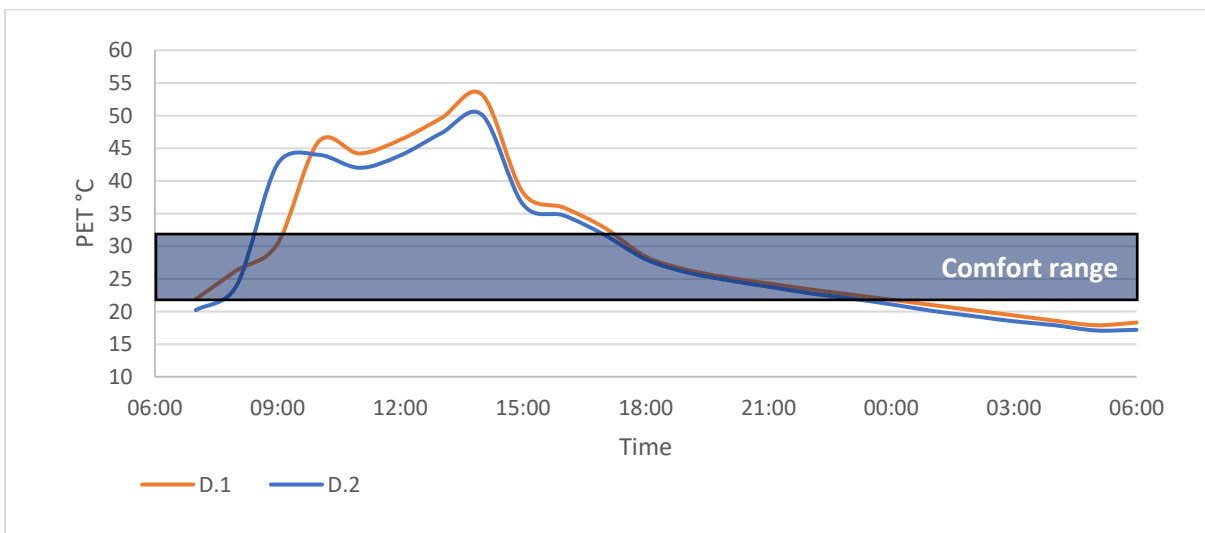


Figure 6.41. PET values for receptor 8 for scenarios D.1 and D.2.

6.6 STREET GRID LAYOUT E.

6.6.1 SCENARIO E.1.

Figure 6.42 shows scenario E.1 for the street grid analysis, where the layout was inspired by the Ladd's Addition in Portland in the United States (Figure 6.42). Ladd's Addition consisted of two main boulevards and radial grid system of streets and alleyways, but the main element in the layout was kept at Ladd circle (Bureau of Planning 1988). Layout E is not an exact translation of Ladd's addition as it contains gardens and alleyways that would not conform to this analysis with strict parameters. For that reason, the main grid for Ladd's additions was maintained but the vegetation was removed, and streets were normalised at the same width. Scenario E.1 has a 45° angle orientation from the North and West wind direction. Figure 6.43 displays the wind speed at 11:00 am, as well as the placement of receptors 1-8 (shown in red).

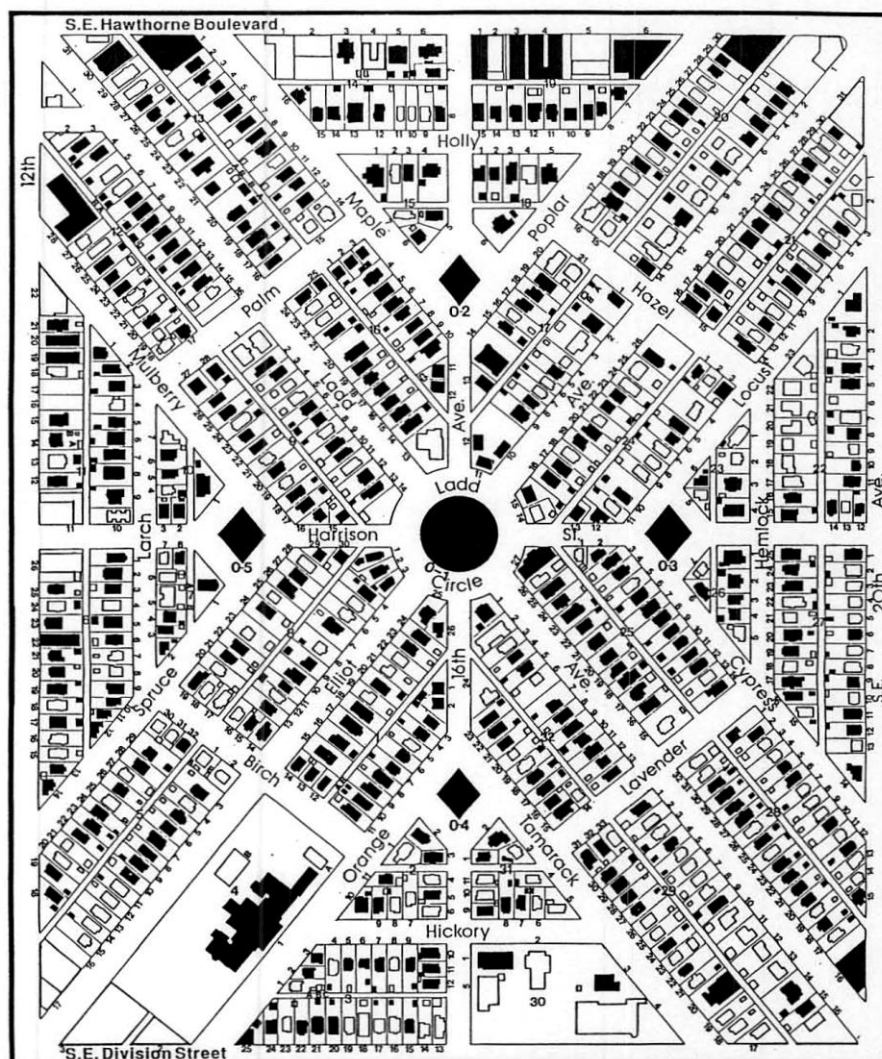


Figure 6.42. Ladd's Addition, courtesy of National Register Historic District.

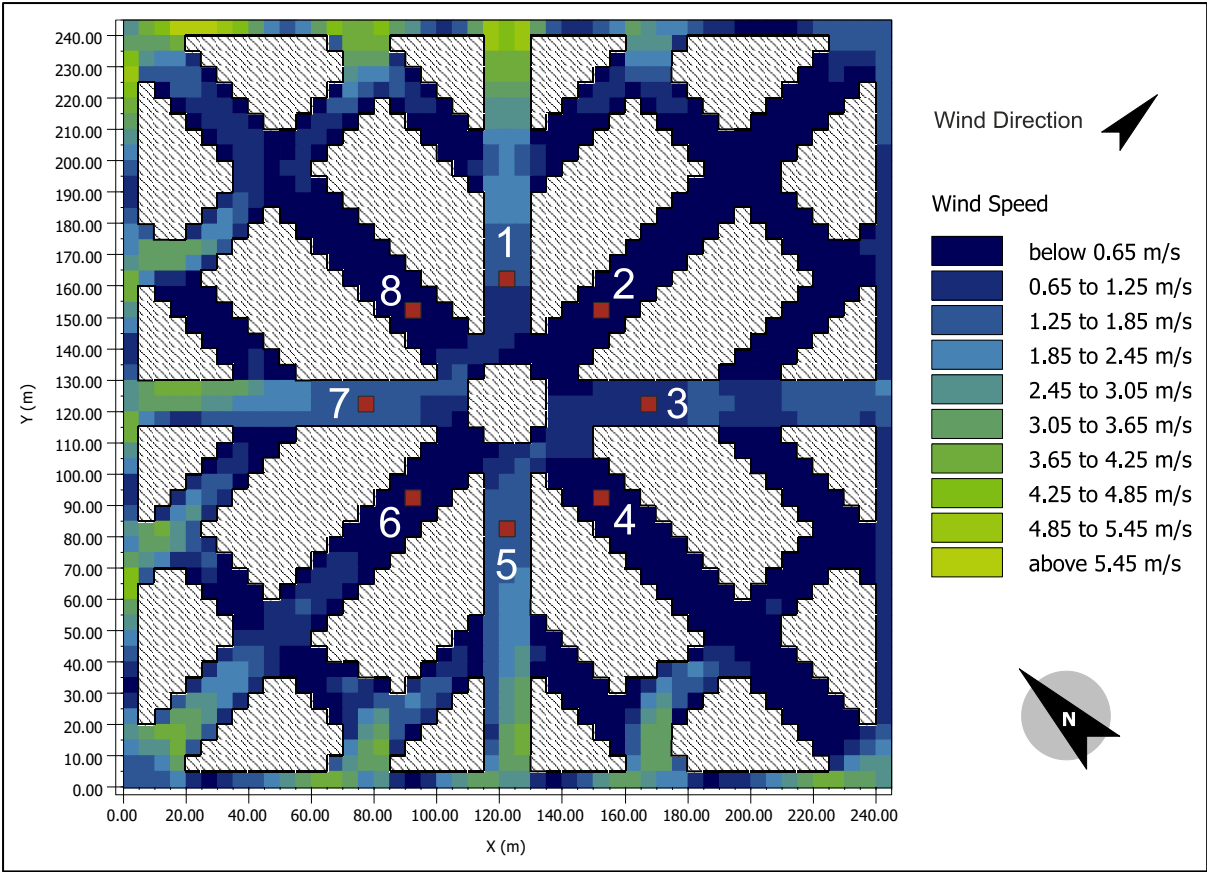


Figure 6.43. Wind speed in scenario E.1.

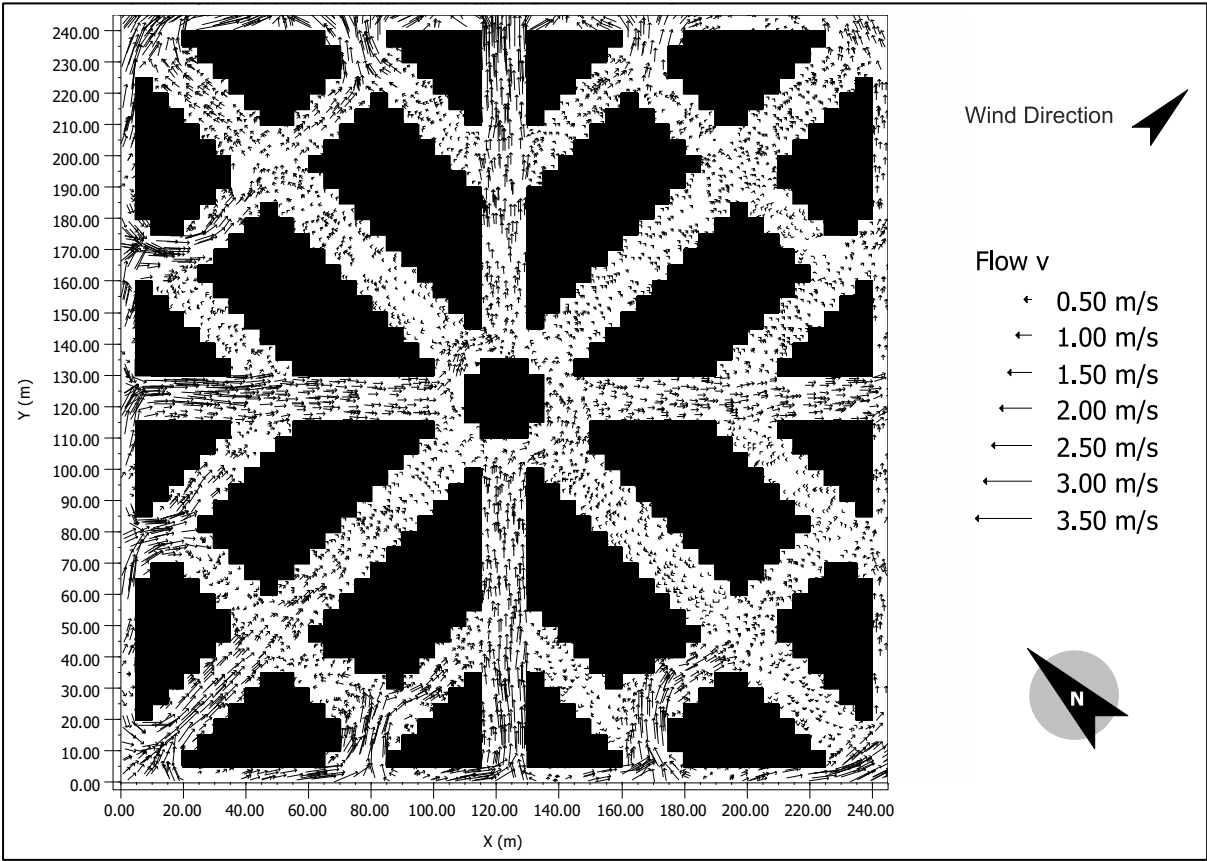


Figure 6.44. Wind flow in Scenario E.1.

As in the street grid layout D layout, the flow of wind is disturbed by the multiple street orientations, and this has caused a decrease in the wind speed in the deeper parts of the plot. As seen in Figure 6.43, wind flow enters the plot from the bottom left corner and as it progresses deeper inside the plot, the wind speed decreases. It should be noted that the level of wind speed reduction in layout E.1 is less than layout D.1 due to the replacement of curved streets with straight streets that helps in keeping the wind momentum going. Figure 6.44 displays the flow of wind inside the plot, streets with receptors (7,3) and (1,5) show better wind flow, due to the entering angle of wind being 45° that enhances the wind flow by gathering the streams from other streets into itself. The wind speed inside the plot averages between 0.65-2.45 m/s and the entering speed is 4 m/s.

6.6.2 SCENARIO E.2.

Figure 6.45 shows scenario E.2 street grid analysis, and as for E.1 this is a rendition of Ladd's Addition with the same parameters except for the orientation.

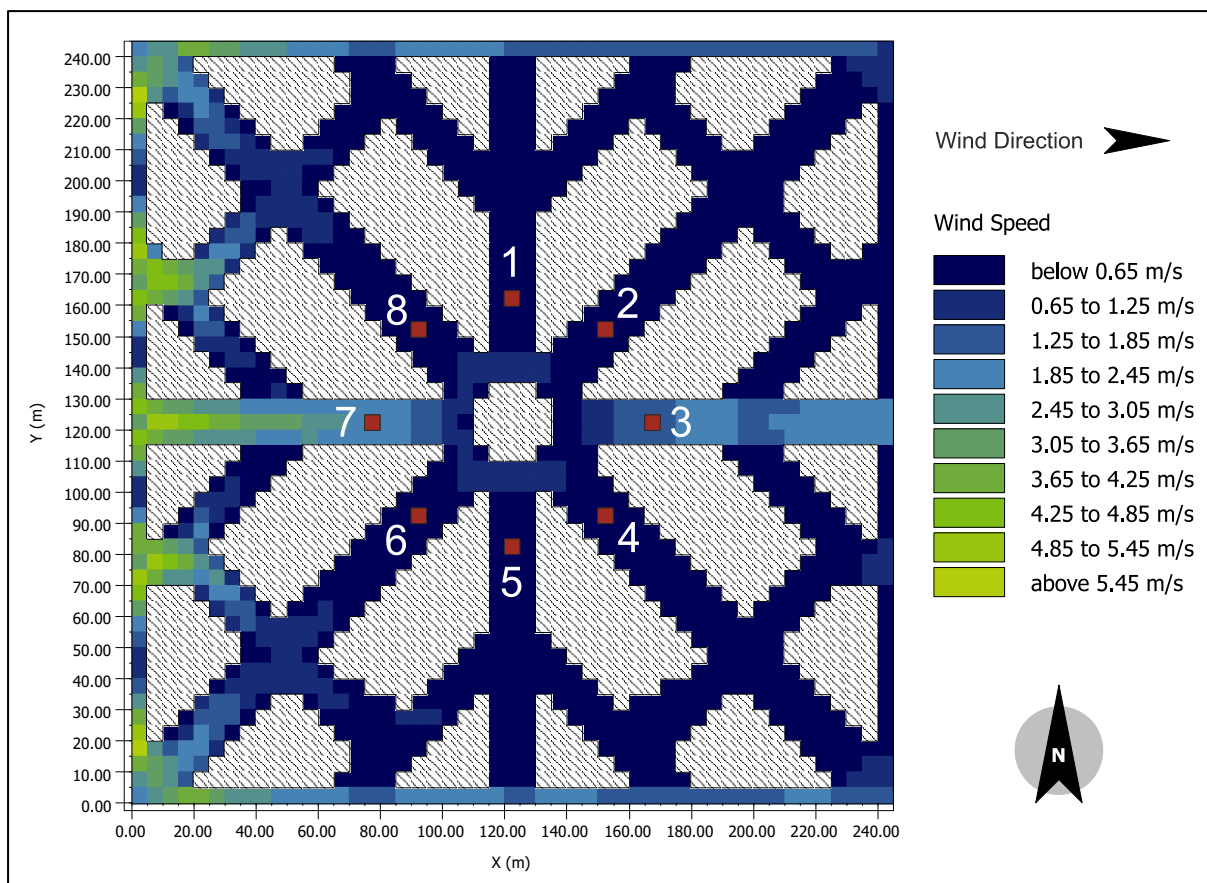


Figure 6.45. Wind speed in scenario E.2.

For this scenario, the plot was kept with its original orientation, 0° angle from the North. Figure 6.45 shows the wind speed at 11:00 am, as well as the placement of receptors 1-8 (shown in red).

Wind flow enters the plot from the west side of the plot (Figure 6.45), and for this reason most of the high wind speed values are concentrated on the west side of the plot. As in layout D.2, the only street with high wind speed values is the street that passes through receptor 7 where the wind maintain its velocity until it reaches the centre of the plot, then the flow splits around the circle losing some of its momentum to two streets that pass through receptor 2 and 4. The wind flow continues with through the street that passes through receptor 3 with less wind speed than the entering speed but with higher values than the streets adjacent to it (Figure 6.46). The average wind speed inside the plot is between 0.65-1.85 m/s.

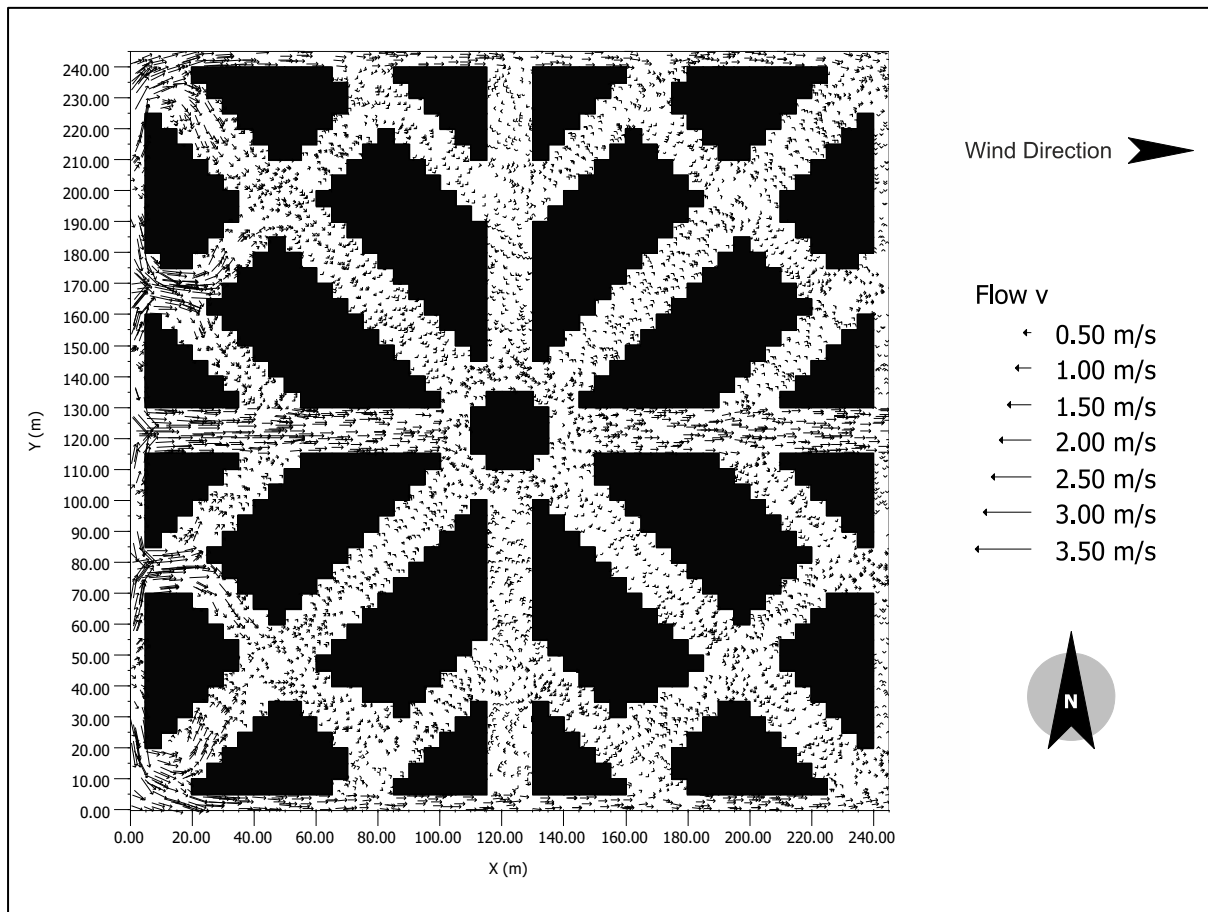


Figure 6.46. Wind flow in Scenario E.2.

6.6.3 COMPARISON BETWEEN GRID E'S DIFFERENT ORIENTATION SCENARIOS.

Figure 6.47 and 6.48 show how wind speed values are distributed around the plot in both scenarios E.1 and E.2. Both scenarios show a high tendency for slow wind speed values, however, 60% of scenario E.2's area have wind speed values of 0.5 m/s or less while for the same wind speed range of (0-0.5) m/s scenario E.1 have only 42%.

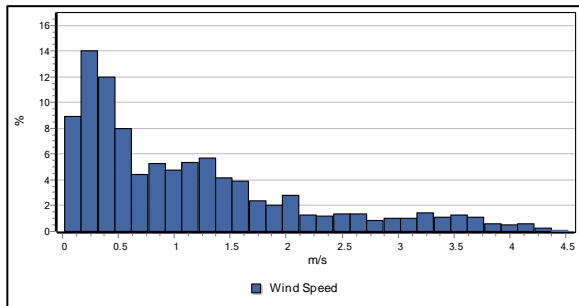


Figure 6.47. Wind speed distribution for scenario E.1.

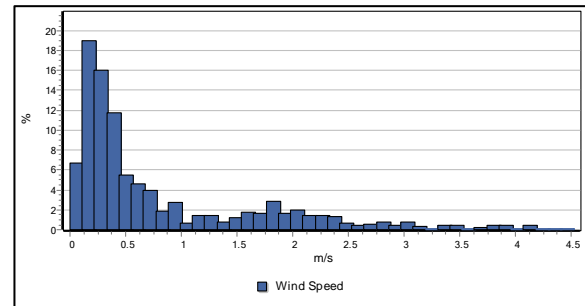


Figure 6.48. Wind speed distribution for scenario E.2.

In this radial layout, the main streets act like axes that cross through the centre of the plot, and for this reason, 4 different results for the 8 receptors that are placed in layout E can be seen, as every two receptors that are placed on the same axis will have fairly similar conditions contributing to their PET analysis. It should be noted that a small difference is expected between every corresponding receptor due to the different wind speed values that are affected by the distance from the inlet source for the wind flow. Receptors 1 and 5 (Figures 6.49 and 6.53) show high PET levels for scenario E.2 between the hours of 10:00 to 13:00 due to the direct sun gain between these hours, while scenario E.1 shows a spike in PET values between the hours of 10:00- 14:00. Scenario E.2 shows lower PET values compared to E.1, and this can be explained by the higher wind speed values observed in scenario E.2; the average wind speed in E.2 is 1.7 m/s and the average wind speed in E.1 is 0.23 m/s. Another contributing factor in this PET difference is the lower relative humidity values compared to E.1 results.

Receptor 2 and 6 (Figures 6.50 and 6.54) show a spike in the PET values for scenario E.1 early in the morning between the hours of 07:00 and 16:00, due to the position of the receptor to the north, where the high summer sun reaches the area during noon. E.2 shows a spike in the PET levels between the hours of 09:00 and 14:00 due to direct sun radiation between those hours.

Receptor 3 and 7 (Figures 6.51 and 6.55) show a spike in the PET values for E.1 between the hours of 09:00 and 14:00 due to the area being affected by direct solar radiation in these hours. E.2 shows a spike in the PET values early in the morning between the hours of 07:00 and 16:00, as seen in receptors 2 and 6 for E.1, as the location of the receptor caused the long direct sun exposure.

Receptor 4 and 8 (Figures 6.52 and 6.56) show a spike in the PET values for E.1 between the hours of 09:00 and 14:00 and E.2 between the hours of 10:00 and 14:00. Receptors 4 and 8 are placed in the (North-South) axis in scenario E.2 and for that reason the area receives the mid-day sun radiation and shaded for the rest. For scenario E.2 the axis that receptor 4 and 8 lay on is tilted 45° counter clockwise of the north, which creates the variation in the direct sun duration between the two scenarios.

As mentioned before, PET values fall during the night, and the absence of solar radiation causes these results, while leaving other parameters in control of the PET values. Receptors 1 and 5 present a slight difference in the PET values between scenario E.1 and E.2, and this difference is caused by the big difference in wind speed values in the scenarios, where scenario E.1 has an average wind speed of 1.7 m/s and scenario E.2 has an average speed of 0.23 m/s. Scenario E.1 recorded 62 comfortable hours throughout the eight receptors while Scenario E.2 recorded 57 hours, with E.1 having average PET values of 28.8 °C and E.2 having an average of 29.6 °C.

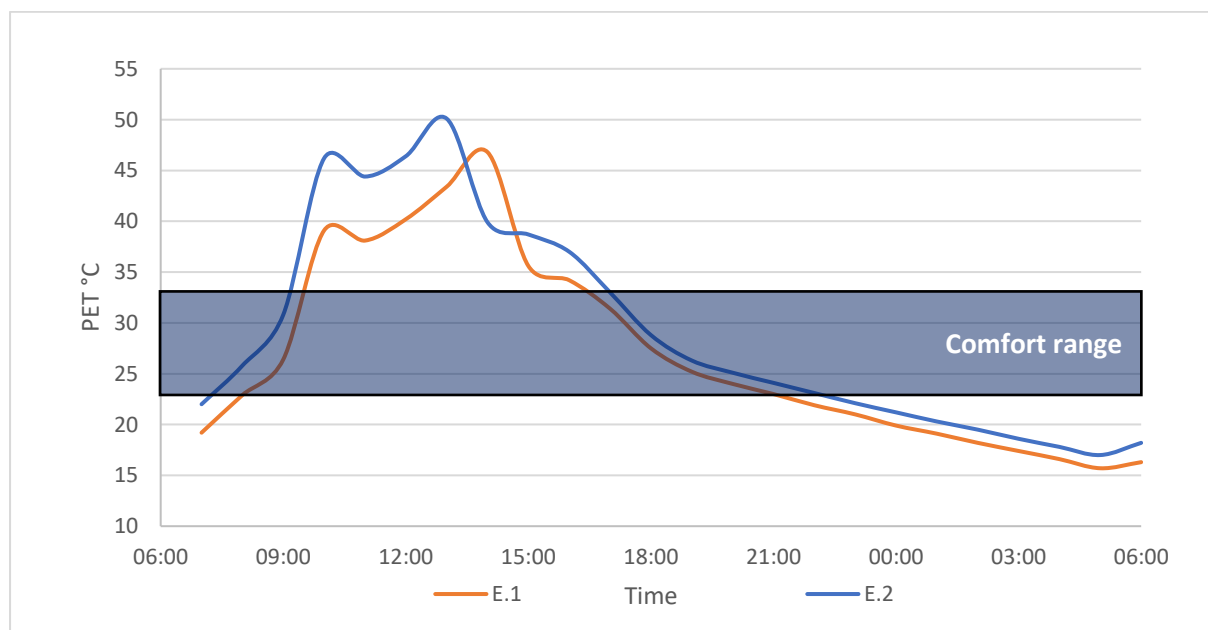


Figure 6.49. PET values for receptor 1 for scenarios E.1 and E.2.

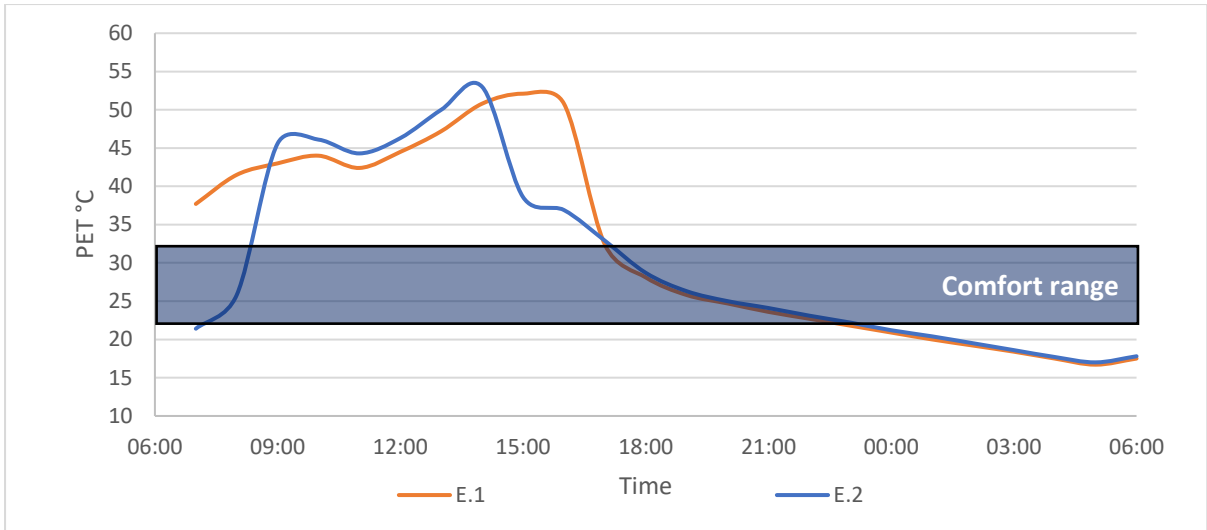


Figure 6.50. PET values for receptor 2 for scenarios E.1 and E.2.

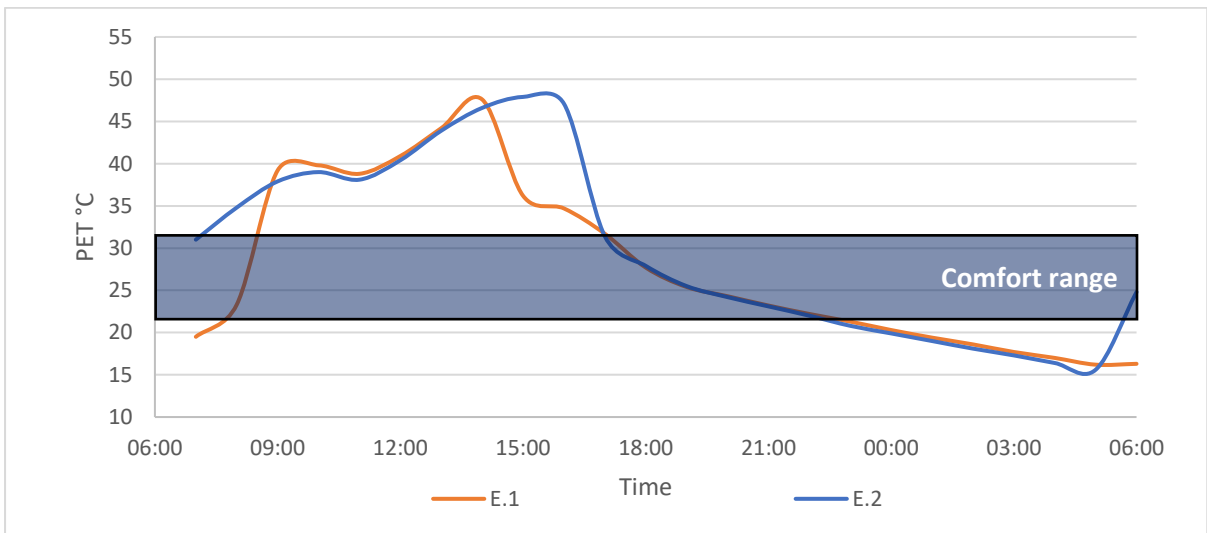


Figure 6.51. PET values for receptor 3 for scenarios E.1 and E.2.

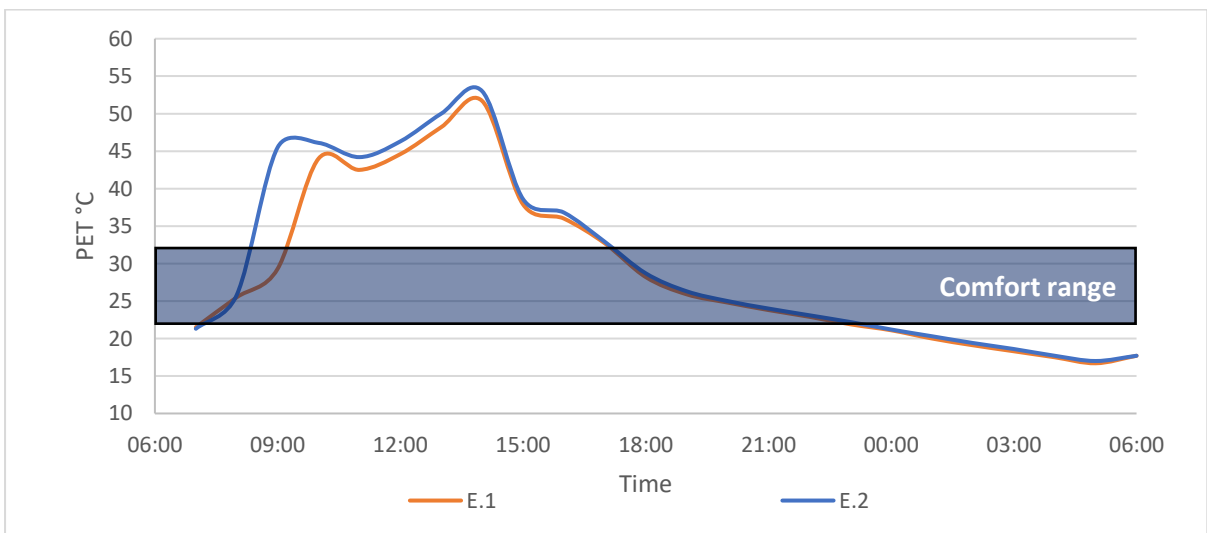


Figure 6.52. PET values for receptor 4 for scenarios E.1 and E.2.

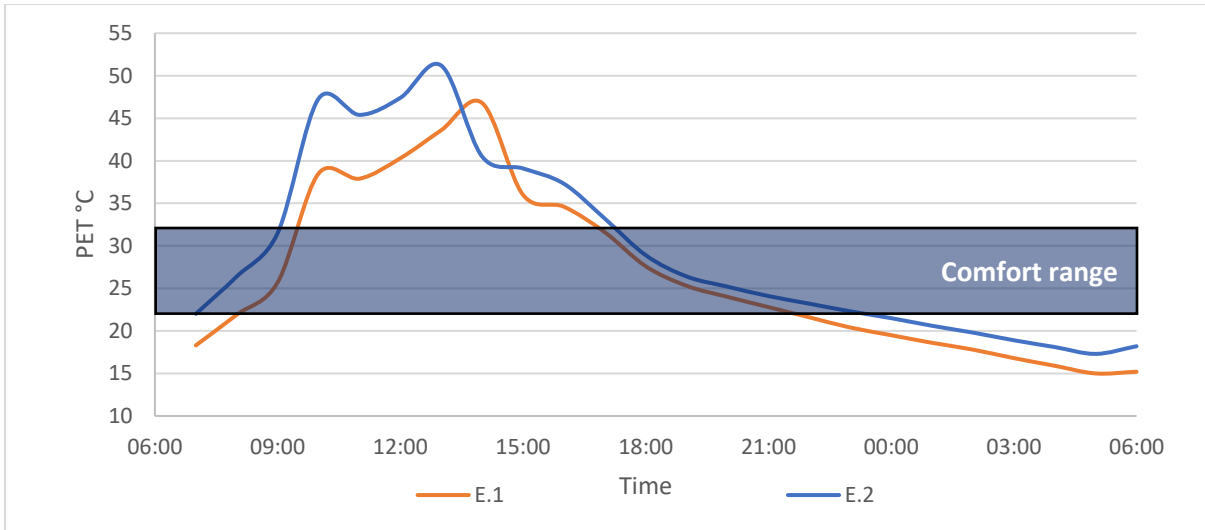


Figure 6.53. PET values for receptor 5 for scenarios E.1 and E.2.

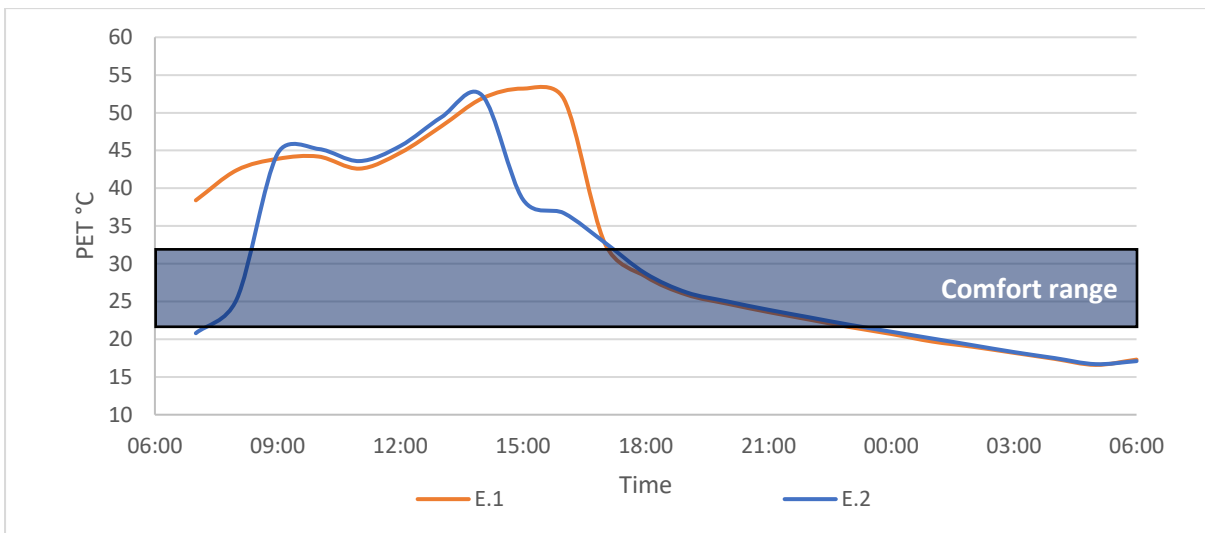


Figure 6.54. PET values for receptor 6 for scenarios E.1 and E.2.

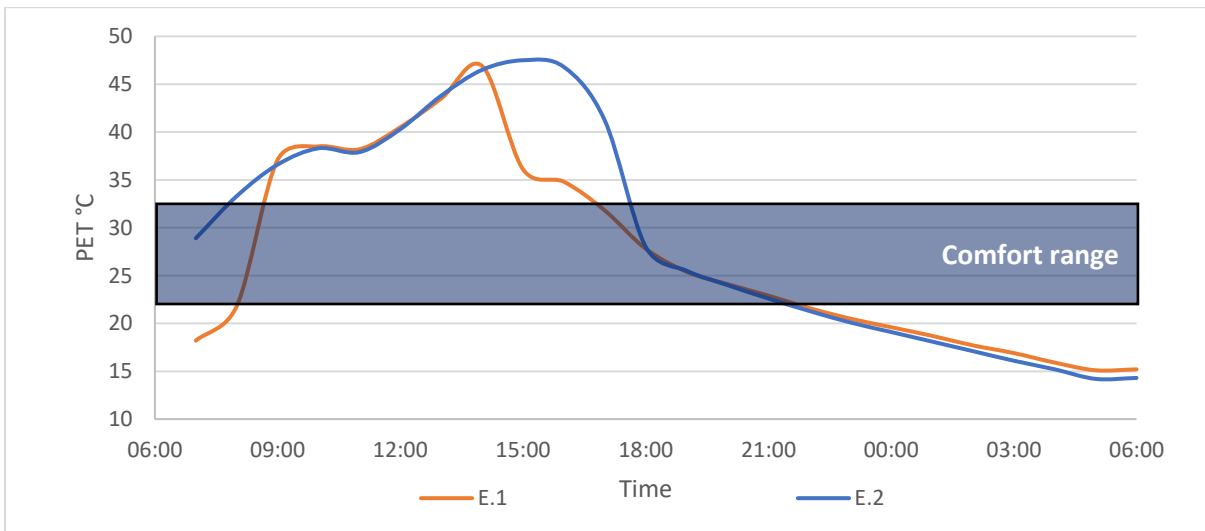


Figure 6.55. PET values for receptor 7 for scenarios E.1 and E.2.

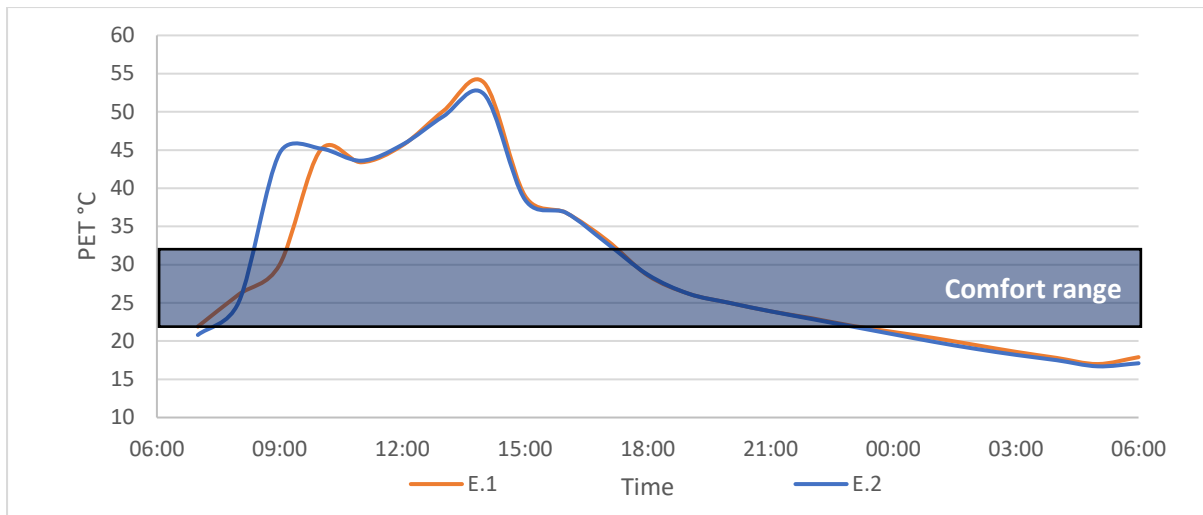


Figure 6.56. PET values for receptor 8 for scenarios E.1 and E.2.

6.7 CONCLUSION.





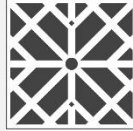




















The street grid layouts are comprised of a multitude of variables controlling their design, including orientation, wind direction, height to width ratio and many more. For the sake of narrowing down the results, some variables were assumed at a fixed state, like initial meteorological factors and height to width ratio. The street grid analysis covered the geometrical composition of five designs— containing orthogonal and radial grids, with every grid restricted to exact several properties to ensure all results are calibrated in the same conditions.

The street grid analysis showed interesting results throughout the different layouts. Wind speed was affected greatly by the change of orientation, where the 45° counter clockwise rotation from North showed a major improvement in wind flow distributions. However, the change in orientation did not play a key part in the PET levels even though the change in orientation changed the shadow patterns. The main reason behind the rise and fall of PET levels was the geometry of the plot, whether it was rotated from the original orientation or not. Understanding the geometry of the site is a key component in determining the thermal stress on the human body.

Table 6.1 shows how geometrical layouts distribute wind flow differently. Scenarios 1 with a 45° orientation counter-clockwise of north showed improved results when compared to scenario 2 with no tilt from north. Layout A scenario 1 showed better results across all layouts and scenarios with only 6% of the area having low wind speed of (0- 0.5) m/s, while layout D

showed the worst results across layouts due to its curved streets that obstructed wind flow, with 68% of the area having low wind speeds.

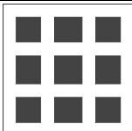
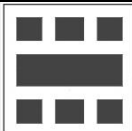


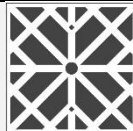




















Table 6.1. Area percentage of the areas that are receiving less than 0.5m/s of wind speed at 1.5m height.

LAYOUTS	A		B		C		D		E	
ICONS										
NORTH DIRECTION										
WIND DIRECTION										
SCENARIOS	A.1	A.2	B.1	B.2	C.1	C.2	D.1	D.2	E.1	E.2
AREA PERCENTAGE	6%	36%	8%	29%	9%	18%	52%	68%	42%	60%

The averaged PET values showed in Table 6.2 do not convey how well the layouts present their comfort level, but rather they show how in the same layout the different orientation shifts the comfort levels - scenarios 1 and 2. An increase in PET values is noticed in all of the layouts in scenario 2, this is caused by the (North-South) orientation streets that receive the highest solar radiation throughout the day.

Designing an urban layout needs to take into consideration the specification of the project. This is apparent when comparing two layouts with different PET levels and wind speed distributions. For an example, scenario D.2 has 68% of area under 0.5m/s wind speed. However, the average PET value was 29.3°C, which is 0.3°C less than scenario E.2, which had a better wind speed distribution of 60%. This is explained by the shading patterns in D.2, with a more compact design (radial) and solar radiation levels are minimized throughout the day.

Table 6.2. Averaged PET values for all layouts.

LAYOUTS	A		B		C		D		E	
ICONS										
NORTH DIRECTION										
WIND DIRECTION										
SCENARIOS	A.1	A.2	B.1	B.2	C.1	C.2	D.1	D.2	E.1	E.2
PET	26.1	27.2	26.6	27.7	26.7	28.3	28.2	29.3	28.4	29.6

SECTION TWO: AMMAN CASE STUDY

Content

- 6.8 Amman, Jordan case study.
- 6.9 Methodology (summary)
- 6.10 Residential layouts - street grid.
- 6.11 Conclusion

6.8 AMMAN, JORDAN CASE STUDY.

This section is going to explore different ways an empty plot can be designed, based on the previous section and thermal sensitivity to its occupants. The aim of this section is to identify the key elements for enhancing the outdoor thermal comfort for pedestrians in a residential setting. The site chosen for the study is located to the South of Amman, with an area of 282,600 m², and an incline estimated to be not more than 1% (Figures 6.57 and 6.58). The analysis will include street grid layouts, compound design, buildings heights and vegetation Leaf Area Density (LAD, m²/m³).



Figure 6.57. Aerial view of the site.



Figure 6.58. Boundaries of the site

6.9 METHODOLOGY (SUMMARY)

Looking into the urban environment in a holistic manner, the design starts with identifying the main components of the plot, setting the main orientation layouts based on predominant wind direction and geographic North, then setting the street grids layout and main residential zones (Figure 6.59). The approach moves into a smaller scale recommending two layouts for the residential zones based on wind flow. The study explores further the effect of vegetation and building heights in terms of wind behaviour and thermal stress inside the residential zones.

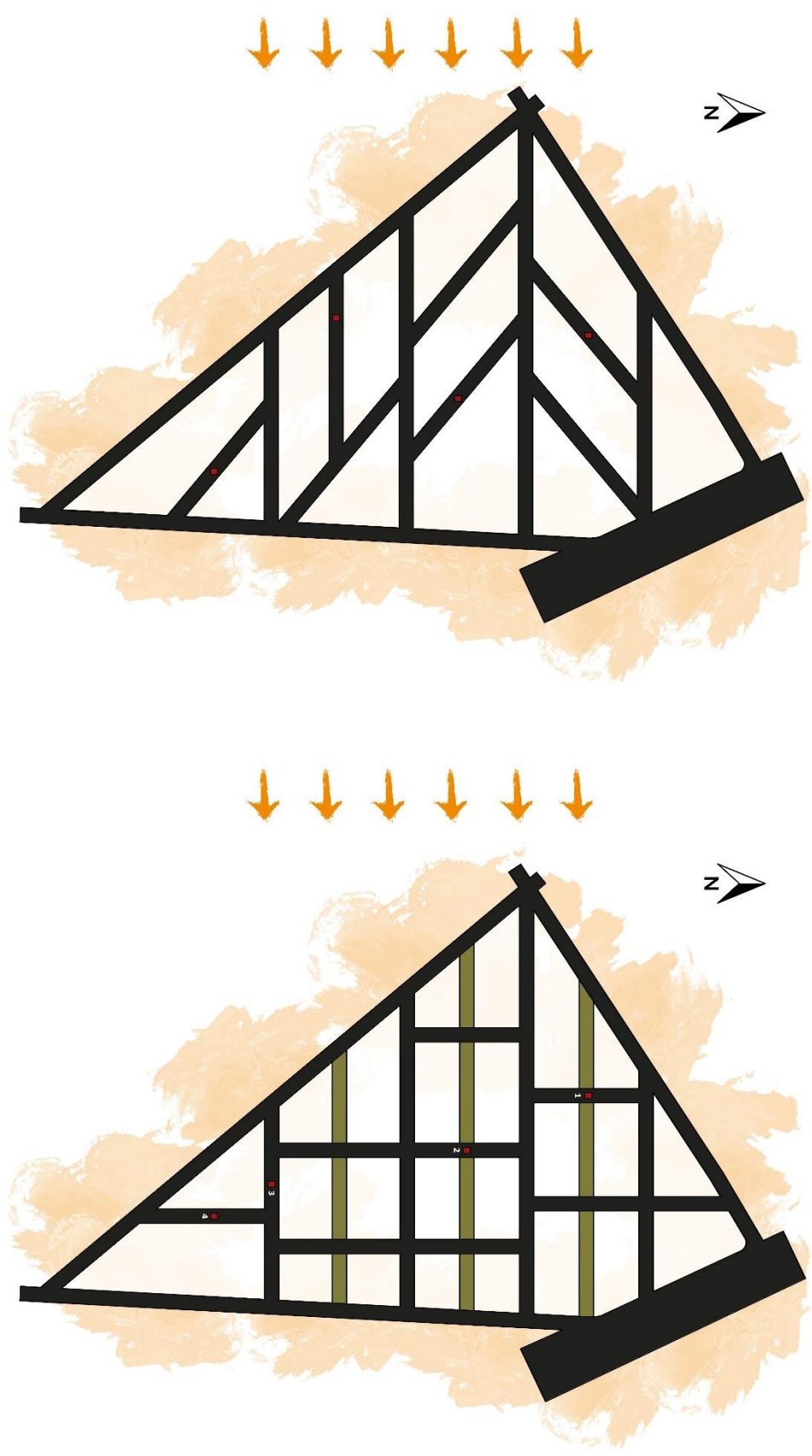


Figure 6.59. Layout-1 (left) and layout-2 (right).

6.10 RESIDENTIAL LAYOUTS - STREET GRID (SUMMARY).

In this section, the focus is on the thermal stress analysis, and wind behaviour. The two layouts will be compared in terms of physiological equivalent temperature (PET), in two conditions - summer and winter, through multiple receptors placed throughout the simulated plot. The analysis will continue to study the wind flow from a different angle and how it affects the overall wind speed inside the simulated plot.

The proposed grids had similar straight streets in the direction of the prevailing winds to ensure best ventilation but differed with the crossed streets' directions, as proposal 1 directed the streets with diagonal crossed streets for a smoother wind flow and proposal 2 had peduncular intersections

6.10.1 PHYSIOLOGICAL EQUIVALENT TEMPERATURE ANALYSIS.

The analysis for the PET was divided into summer analysis and winter analysis, to assess the thermal layout behaviour under different meteorological parameters. The dates chosen for the simulations were the 21st of June - for summer modelling, and the 22nd of December - for winter modelling.

In order to calculate PET, four meteorological parameters must be present; wind speed, air temperature, relative humidity and mean radiant temperature. Envi-MET was used to obtain these parameters through modelling the layouts and using the EPW files as initial data for the simulation. Table 6.3 shows the data used for the modelling phase. The aforementioned four-parameter concerning the PET is then extracted from ENVI-met and inserted into RayMan to calculate the PET values.

Table 6.3. Parameters used in the modelling phase.

TIME	WINTER			SUMMER		
	Air temperature	Relative humidity	Wind speed	Air temperature	Relative humidity	Wind speed
01:00	7.1	78	2.3	24.5	41	5.2
02:00	7.2	75	3	23.7	41	5
03:00	7.3	74	2.5	23.3	41	4.4
04:00	7.4	72	3	23	42	2.7
05:00	7.5	72	1.7	23	42	1.9
06:00	7.6	71	2.1	24	39	2.4
07:00	7.7	69	1.9	25.5	37	1.6
08:00	9	65	1.7	27.1	34	2.4
09:00	10.8	58	1.2	28.6	31	3.1
10:00	12.3	55	2.3	30.1	27	4
11:00	13.8	54	1.7	31.4	26	3.8
12:00	14.8	51	1.9	32.5	25	3.3
13:00	15.5	47	3.3	33.3	24	2.9
14:00	15.8	47	2.1	33.8	25	2.7
15:00	15.6	51	0.9	33.9	26	1.6
16:00	14.9	52	1.7	33.7	26	2.2
17:00	13.9	54	1.7	33.1	27	2.4
18:00	13.3	57	1	32.1	28	1.7
19:00	12.6	62	1.3	30.9	30	1.6
20:00	12	63	1.4	29.6	35	2
21:00	11.4	64	1.2	28.3	36	3.3
22:00	10.8	65	1.3	27	38	2.6
23:00	10.1	69	1.7	25.7	41	1.4
00:00	9.5	71	2.1	24.4	47	2

6.10.2 SUMMER ANALYSIS.

Receptor 1 shows higher PET values for layout-1 compared to layout-2 (Figure 6. 60). Although the average change in wind speed between layout-1 and layout-2 is 0.75 m/s in favour of layout-1, a higher PET levels in layout-1 is observed, and this can be explained by the geometry of the layouts - the different orientation of the streets - and how they allow access to direct solar radiation (DSR) throughout the day. Figure 6.61 shows the times when the receptor is hit by direct sun radiation, where in layout-1 the receptor is affected by DSR for 9 hours - from 07:00 to 15:00, and Layout-2 is only affected by DSR for 7 hours - from 07:00 to 13:00. This increase in solar radiation raised the MRT values which in terms raised the PET for layout-1.

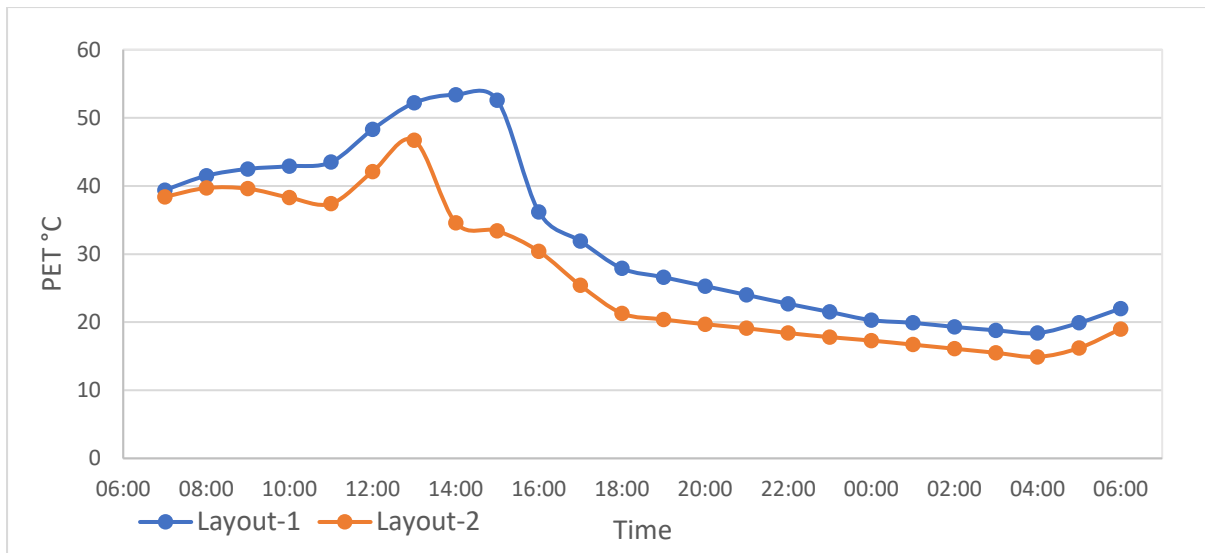


Figure 6.60. PET values for receptor 1 under summer conditions on the 23rd of June.

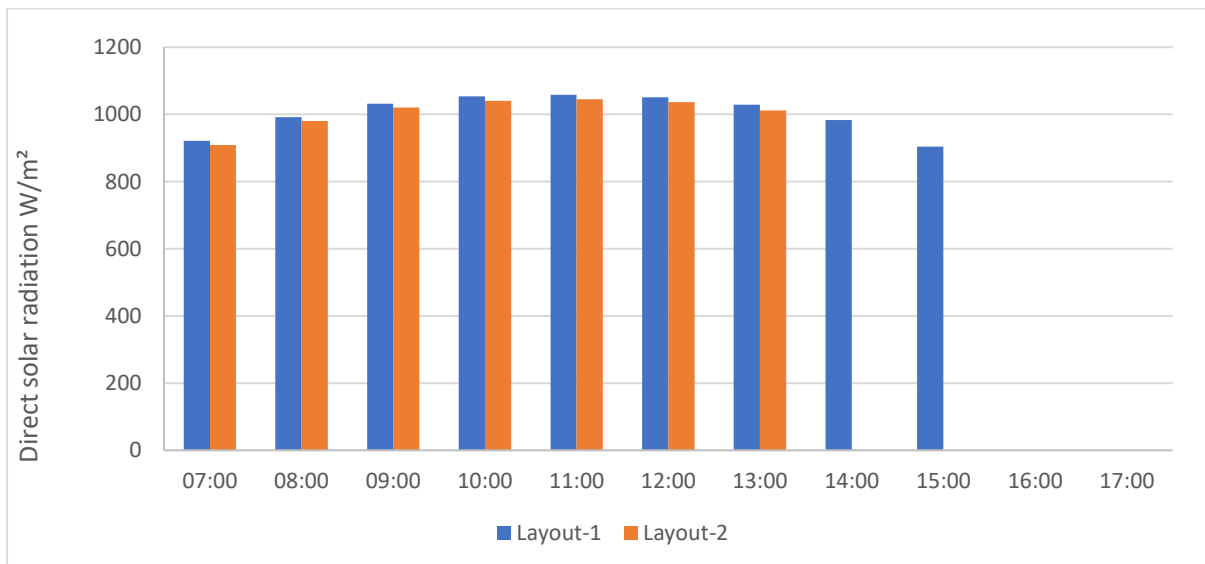


Figure 6.61. Direct solar radiation for receptor 1 under summer conditions on the 23rd of June.

As in receptor 1, receptor 2 shows higher PET values for layout-1 compared to layout-2 (Figure 6.62). Layout-1 has higher wind speed values of an average change of 0.25 m/s. However, the solar radiation is cast on the receptors for a longer period of time compared to layout-2, Figure 6.63 shows the times when the receptor is hit by direct sun, where in layout-1 the receptor is affected by DSR for 10 hours - from 06:00 to 15:00, and Layout-2 is only affected by DSR for 7 hours - from 09:00 to 15:00. For this reason, layout-2 has better PET values early in the morning compared to layout-1. This increase in solar radiation raised the PET values for layout-1.

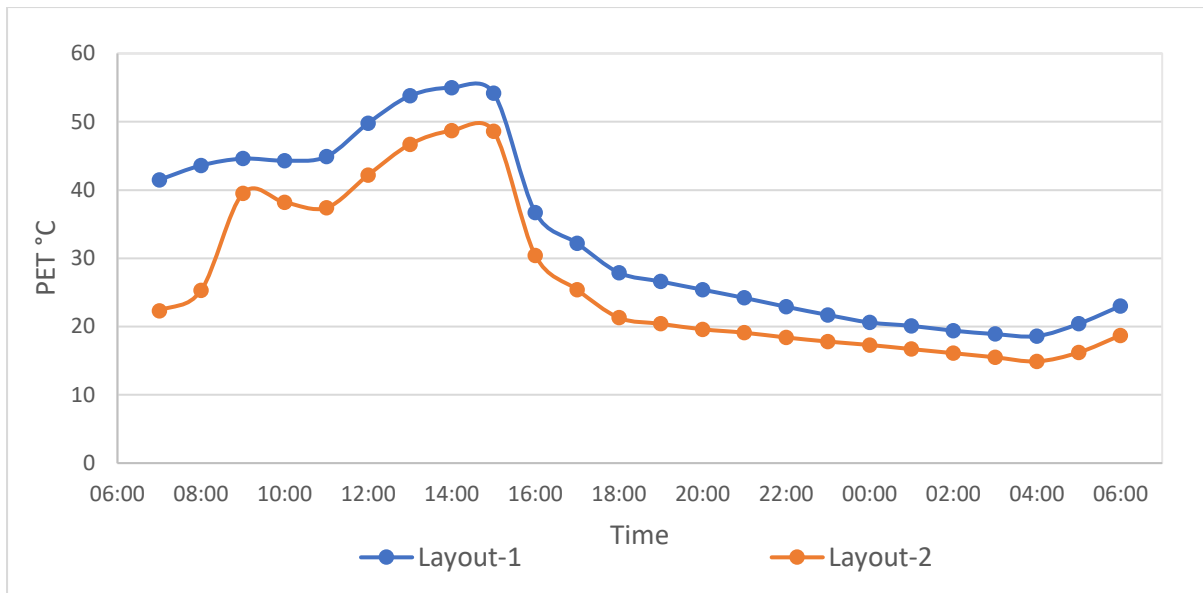


Figure 6.62. PET values for receptor 2 under summer conditions on the 23rd of June.

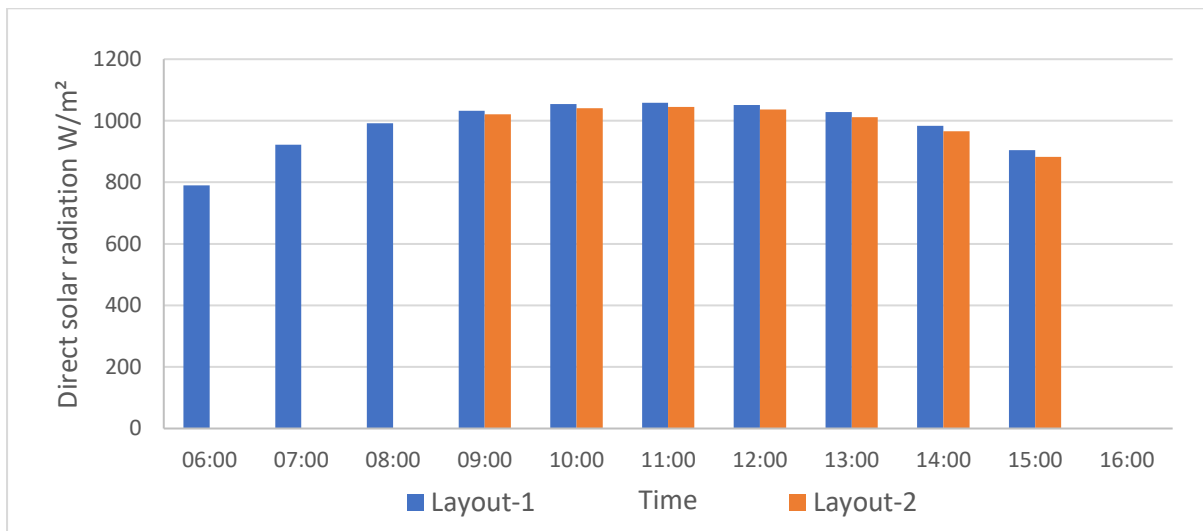


Figure 6.63. Direct solar radiation for receptor 2 under summer conditions on the 23rd of June.

Receptor 3 is located in a (West-East) facing street in both layouts. Layout-1 has the receptor placed between two buildings with wide facades, and in layout-2 the receptor is placed between two buildings with narrower facades. This variation in geometry caused a change in shadow casting that resulted in more solar radiation time in layout-2 - not to be confused with the previous receptors that were placed in different orientation streets. For the most part, the PET values are higher in layout-1 compared to layout-2 (Figure 6.64), due to higher solar radiation values when the hourly values are compared. Figure 6.65 shows the times where the receptor was hit by direct sun radiation, where in layout-1 the receptor is affected by DSR for 10 hours - from 06:00 to 15:00, and Layout-2 is affected by DSR for 12 hours - from

05:00 to 16:00. For this reason, layout-2 shows two spikes in PET values at hour 05:00 and 16:00, whereas layout-1 has 0 direct solar radiation and layout-2 has 440 W/m² at 05:00 and 722 W/m² at 16:00.

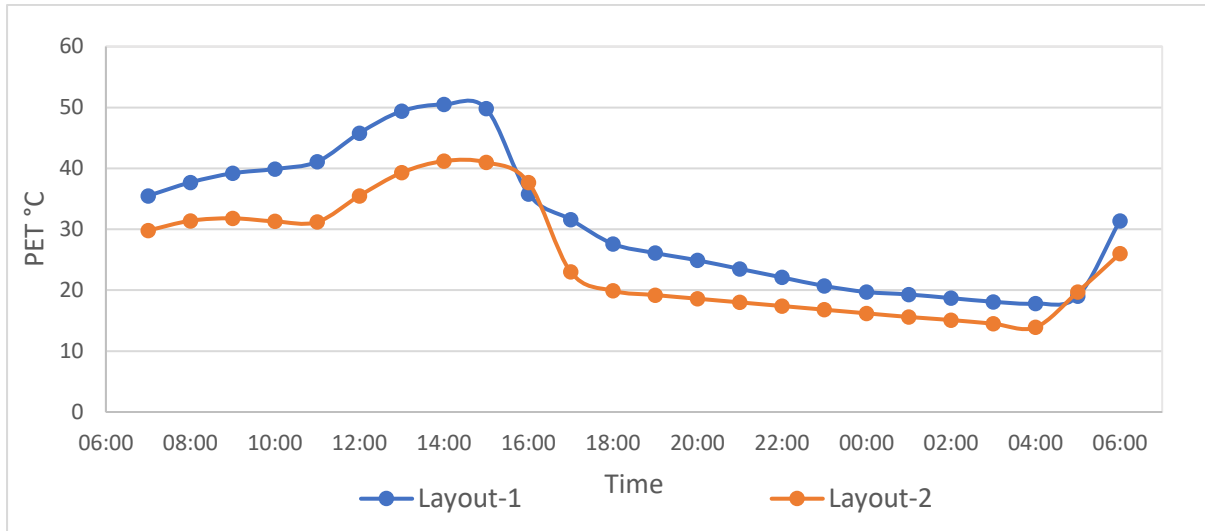


Figure 6.64. PET values for receptor 3 under summer conditions on the 23rd of June.

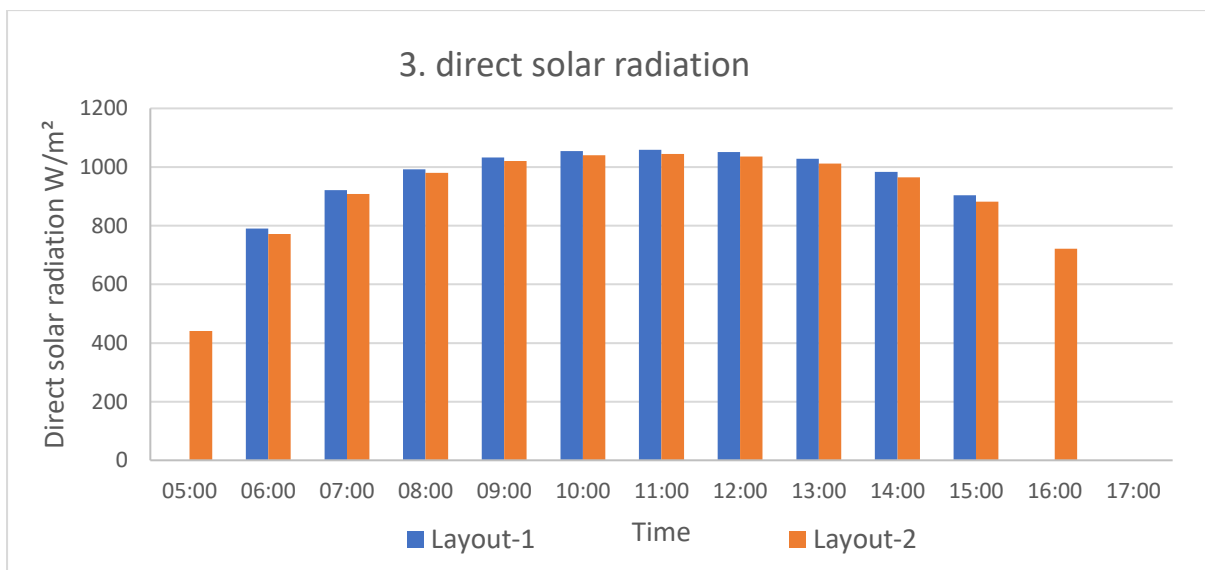


Figure 6.65. Direct solar radiation for receptor 3 under summer conditions on the 23rd of June.

Receptor 4 and 2 have similar results as they are located at similar conditions. Whereas in layout-1 receptor 2 and 4 are located in a street rotated 50° degrees counter-clockwise from the South, and in layout-2 they are located in a street oriented of the (North-South) axis. Receptor 4 shows higher PET values for layout-1 compared to layout-2 (Figure 6.66). The average change of wind speed is 0.26 m/s in favour of Layout-1 but due to the longer sun exposure compared to layout-2, layout-1 suffers from higher PET values. Figure 6.67 shows

the times where the receptor was hit by direct sun radiation, where in layout-1 the receptor is affected by DSR for 10 hours - from 06:00 to 15:00, and Layout-2 is only affected by DSR for 7 hours - from 09:00 to 15:00, for this reason, layout-2 have better PET values early in the morning compared to layout-1.

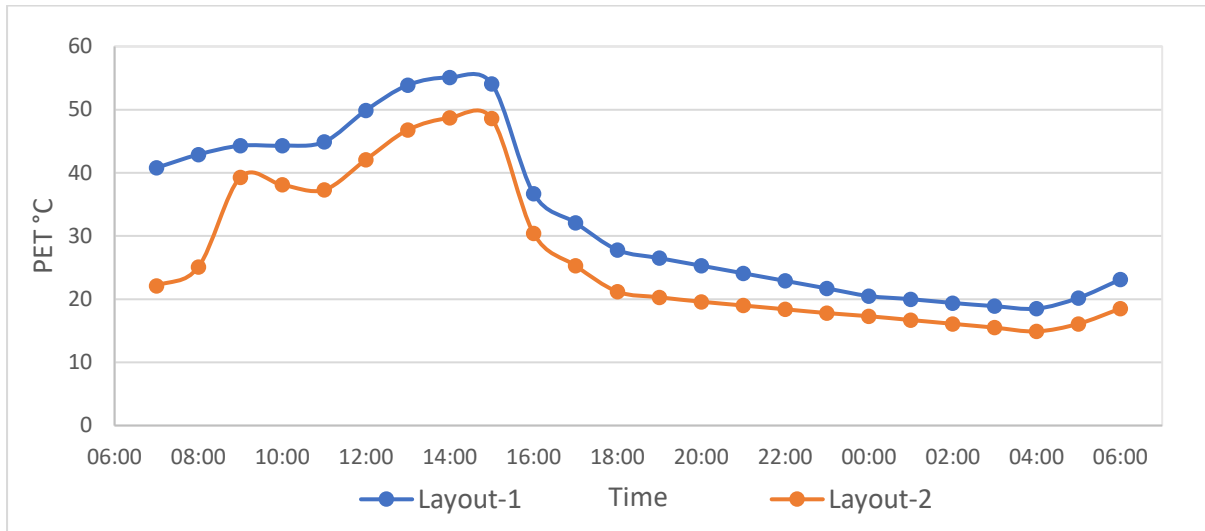


Figure 6.66. PET values for receptor 4 under summer conditions on the 23rd of June.

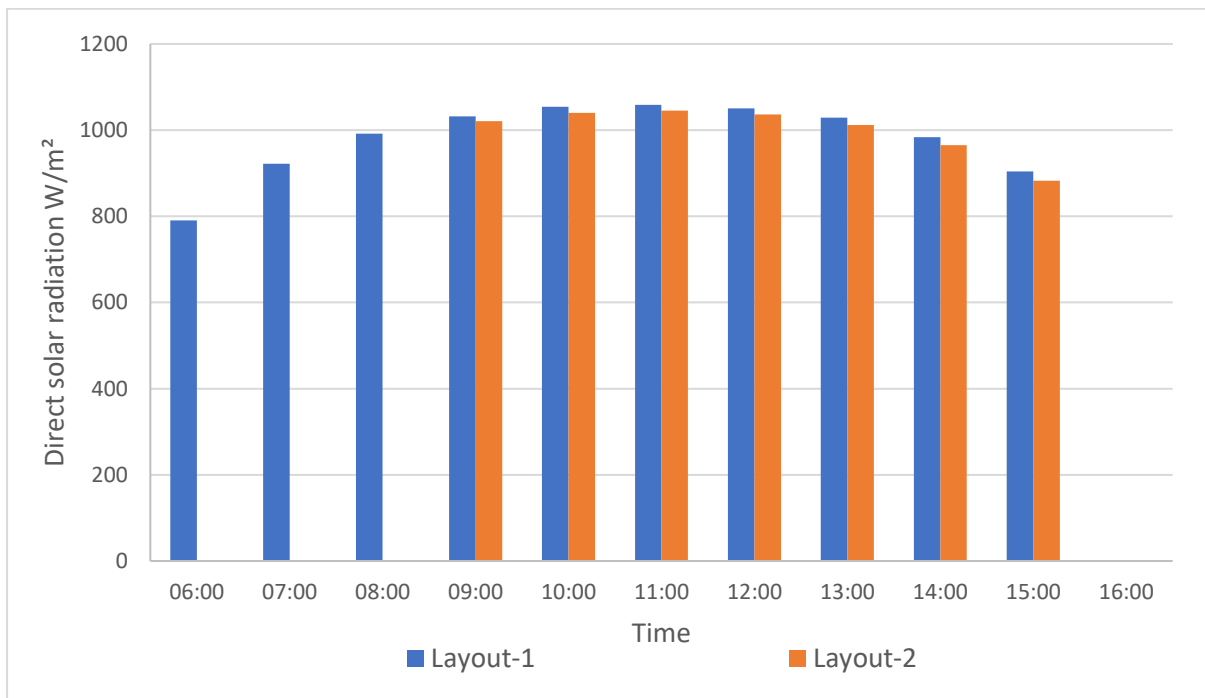


Figure 6.67. Direct solar radiation for receptor 4 under summer conditions on the 23rd of June.

6.10.3 WINTER ANALYSIS.

Air temperatures fall drastically in Amman in December compared to June, and it records a minimum of 2°C, an average of 10°C and a maximum of 21°C. This drop in air temperature

brings with it several changes in the comfort levels, as the drop in air temperature will increase wind density, therefore, changing the comfort sensation for the same wind speed in July.

Figure 6.68 shows the PET levels for receptor one for both layout 1 and 2, and the receptor in layout-1 is located in a street that is rotated 50° degrees counter clockwise off East, whereas in layout-2 the receptor is located in a street oriented in the (North-South) axis. Per to the location, the PET levels rise for layout-2 early in the morning between the hours of 08:00 and 12:00, as it receives direct sun radiation at that exact time (Figure 69). Similarly, layout-1 has an increase in the PET levels shown between the hours of 10:00 and 14:00 and it receives direct sun radiation at the same time intervals.

It should be noted that the PET results for layout-2 with an index of agreement value of 0.44 are closer to the PET comfort range 18-23°C, compared to layout-1 index of agreement of 0.41.

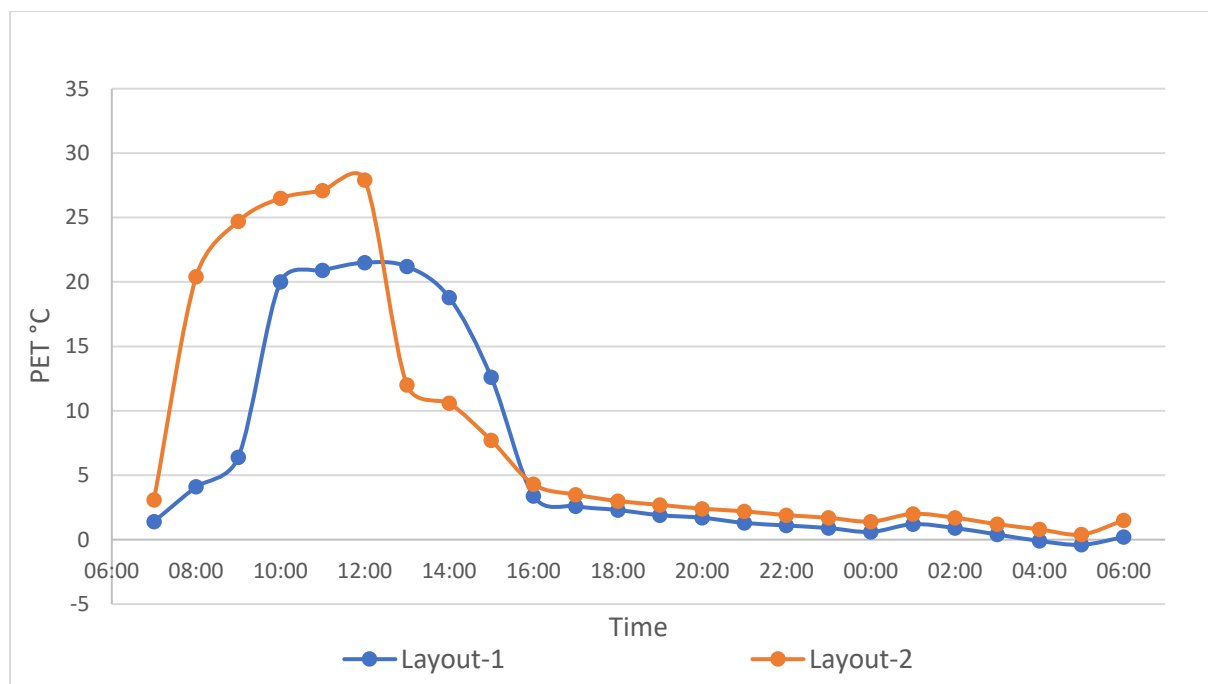


Figure 6.68. PET values for receptor 1 under winter conditions on the 22nd of December.

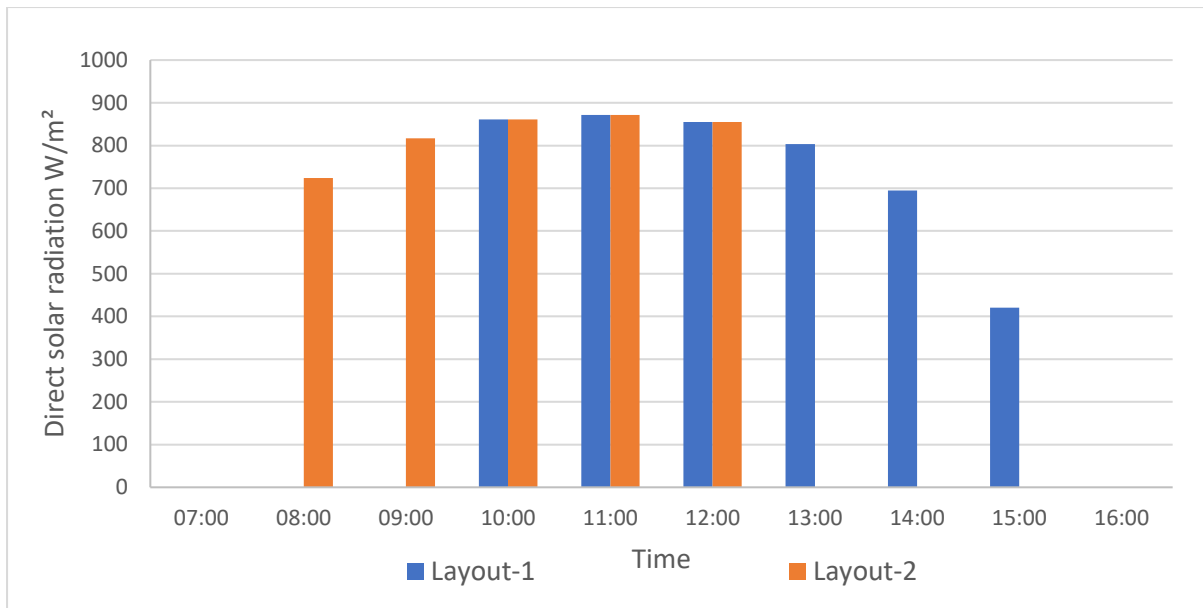


Figure 6.69. Direct solar radiation for receptor 1 under winter conditions on the 22nd of December.

Figure 6.70 shows the PET levels for receptor two for both layouts, and similar to the previous receptor, receptor 2 is located in a street oriented in the (North-South) axis in layout-2, and in layout-1 it is located in a street that is rotated 50° degrees clockwise off East. Due to the change of orientation, both receptors have different direct solar radiation times. Layout-1 has 6 hours of direct sun starting from 07:00 to 12:00 (Figure 71) - an increase of PET levels is noticed in this time interval. Layout-2 has 4 hours of direct sun starting from 10:00 to 13:00 and, similar to the other receptors, an increase in PET is recorded at those times.

Receptors 1 and 2 in layout-2 lay in the same street orientation, and they are expected to have the same results during the solar radiation time intervals, but this is not the case as can be seen in Figures 6.54 and 6.56. This can be explained by the horizontal placement of the receptors; the model in ENVI-met was built using the exe file SPACES, and this exe file uses pixels as its core model building technique, which in this case divided the street into 2 pixels, each pixel with a resolution of 10 m. The placement of receptor 1 was on the left side of the two pixels street and receptor 2 was on the right side. This resulted in different shading patterns from the adjacent buildings to the receptors, which eventually caused the different solar radiation patterns seen in the results.

Due to reduced solar exposure, the PET results for layout-2 display a colder sensation compared to layout-1 PET results between the hours of 07:00 to 09:00, while it shows higher

values of PET deviating from the comfort zone 18-23°C, and this can be seen between the hours of 10:00 to 13:00. The index of agreement test shows that layout-1 is closer to the PET comfort zone 18-23 °C with a value of 0.43 compared to layout-2 value of 0.41.

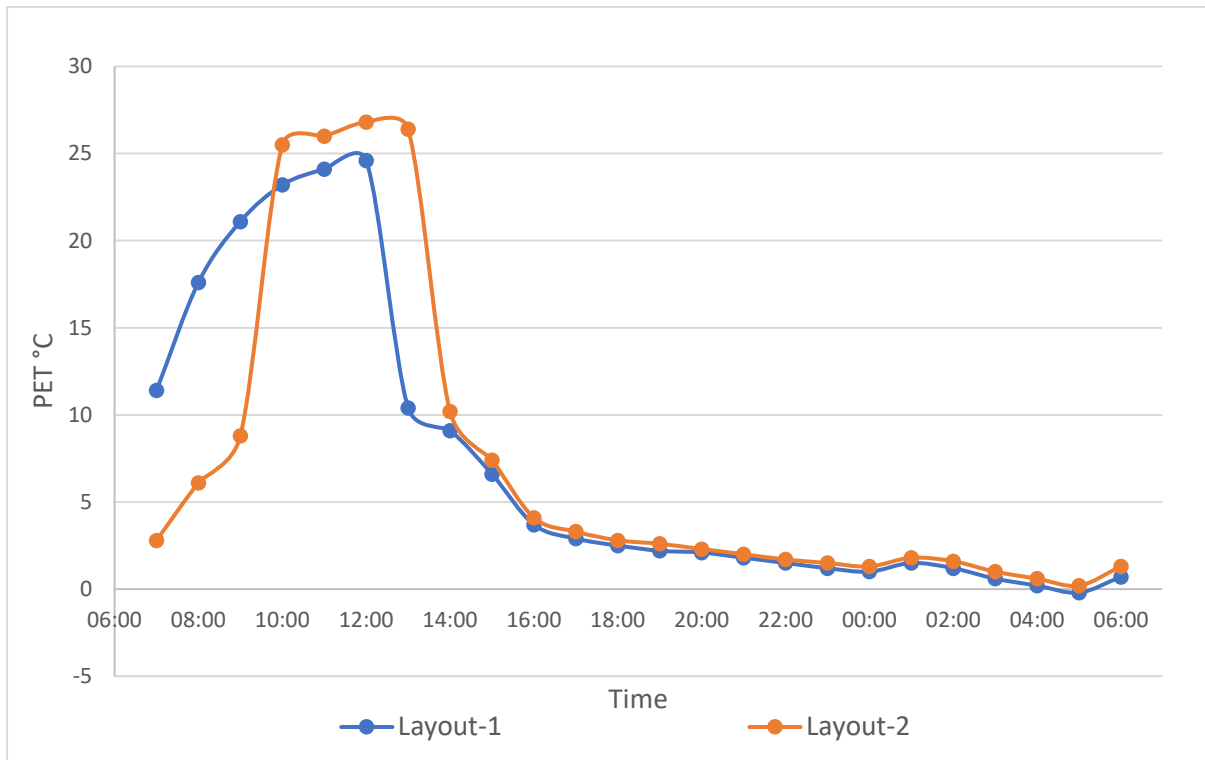


Figure 6.70. PET values for receptor 2 under winter conditions on the 22nd of December.

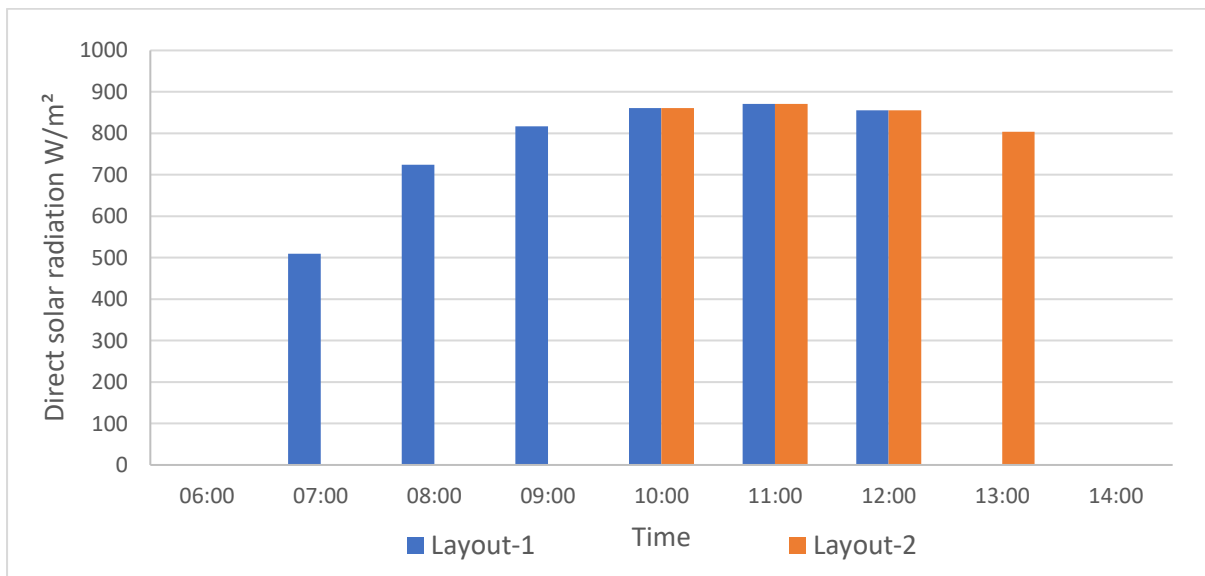


Figure 6.71. Direct solar radiation for receptor 2 under winter conditions on the 22nd of December.

Figure 6.72 shows the PET values for receptor 3 in both layout-1 and layout-2, receptor 3 lays in a street oriented on the (West-East) axis on both layouts, which meant that the receptor

received the similar parameters' values of air temperature, wind speed, relative humidity, mean radiant temperature and direct sun radiation (Figure 6.73). This similarity in values resulted in a very close PET level. It should be noted that in studying receptor 3 under summer condition, the results had different behaviour, and this can be explained by the variation of sun angle between summer and winter, where the summer sun reached the receptor earlier in the morning and remained later in the day.

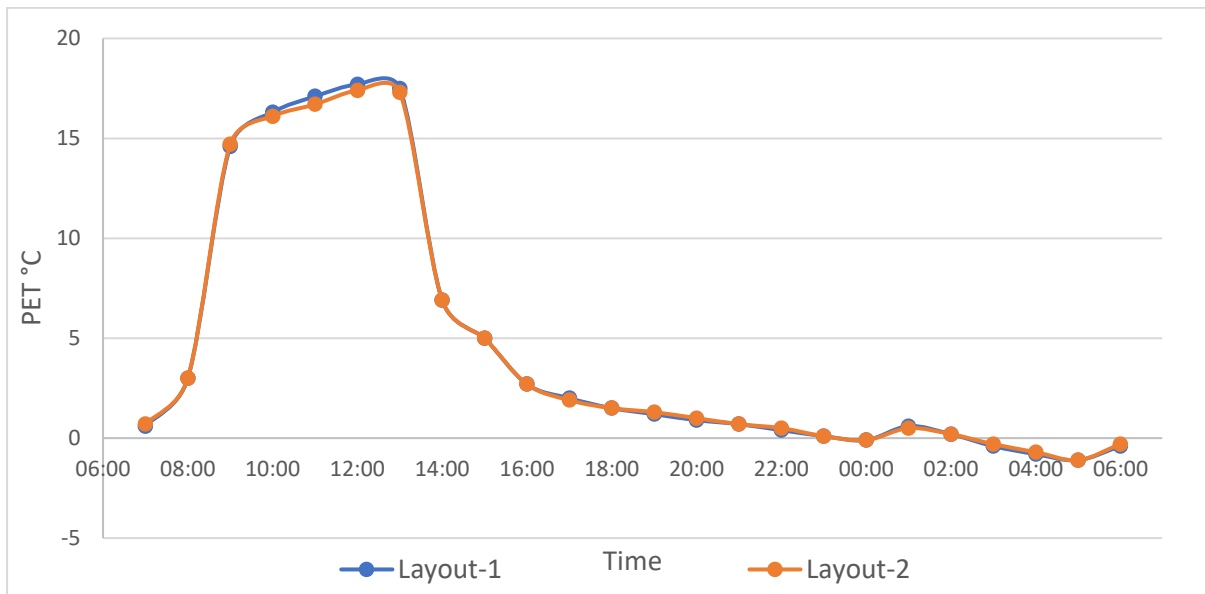


Figure 6.72. PET values for receptor 3 under winter conditions on the 22nd of December.

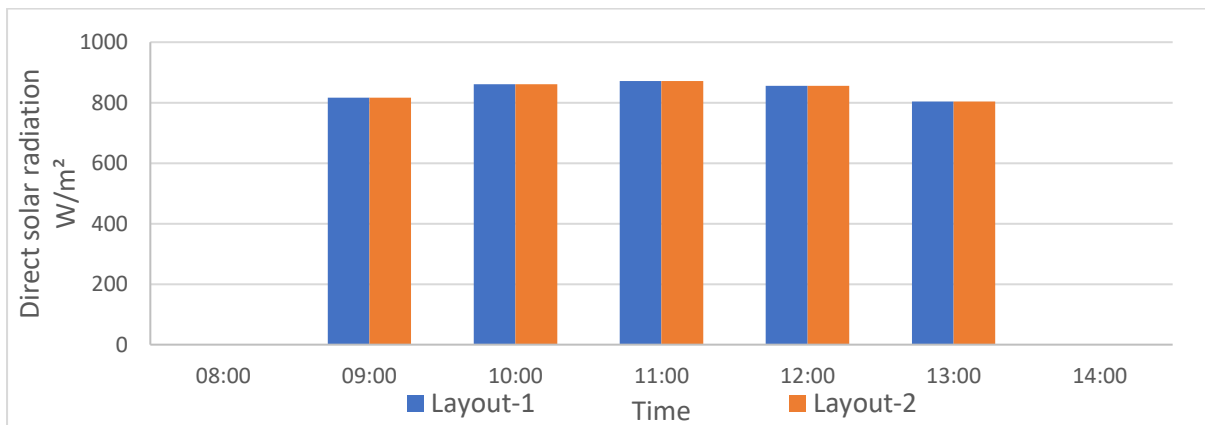


Figure 6.73. Direct solar radiation for receptor 3 under winter conditions on the 22nd of December.

Figure 6.74 shows the PET values for receptor 4 for layout-1 and layout-2. Receptor 4 is located in similar conditions as receptor 2, and for this reason, the results show a good agreement to each other's values. Receptor 4 is located in a street rotated 50° degrees clockwise off East, and in layout-2 it is located in a street oriented in the (North-South) axis. The change of orientation produced different solar radiation times, and Figure 6.75 shows the

direct solar radiation values and time intervals for both scenarios and these time intervals correlate to the spike in PET values for both layouts, as shown in Figure 6.74.

The PET results for layout-2 show an overall colder sensation in the time intervals where there is no solar radiation. However, they show high values with warm sensation when solar radiation is present, and in both cases, the PET values are either under or above the comfort zone of 18-23°C. This deviation of values away from the comfort zone created an index of agreement of 0.41 which measured less than layout-1's value of 0.43. Both of the values are less than favourable; however, this analysis is a comparative analysis and, in this case, layout-1 behaves better in terms of thermal comfort compared to layout-2.

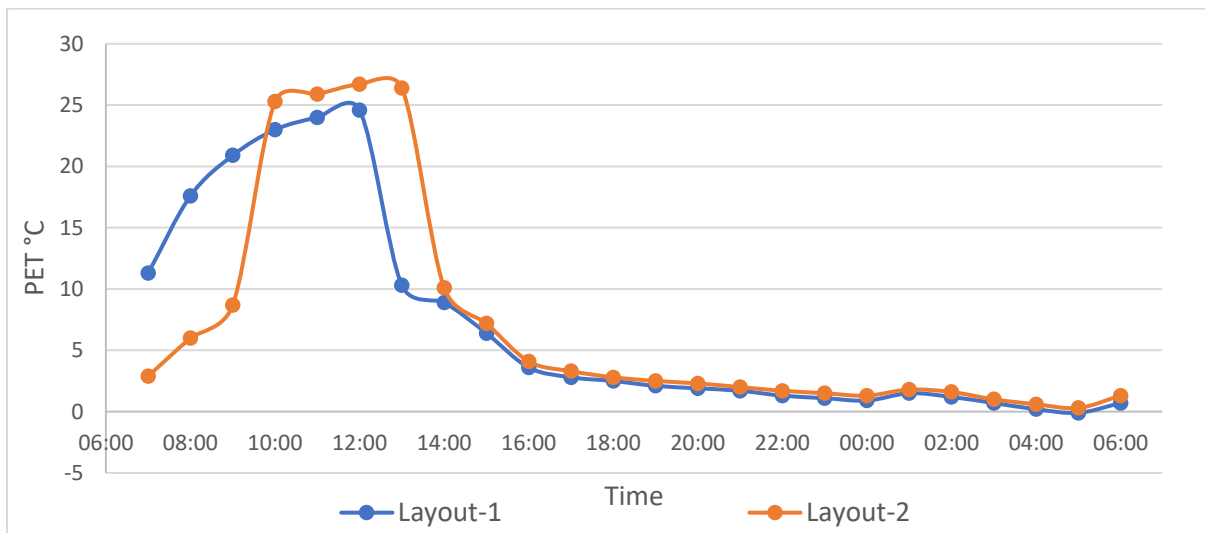


Figure 6.74. PET values for receptor 4 under winter conditions on the 22nd of December.

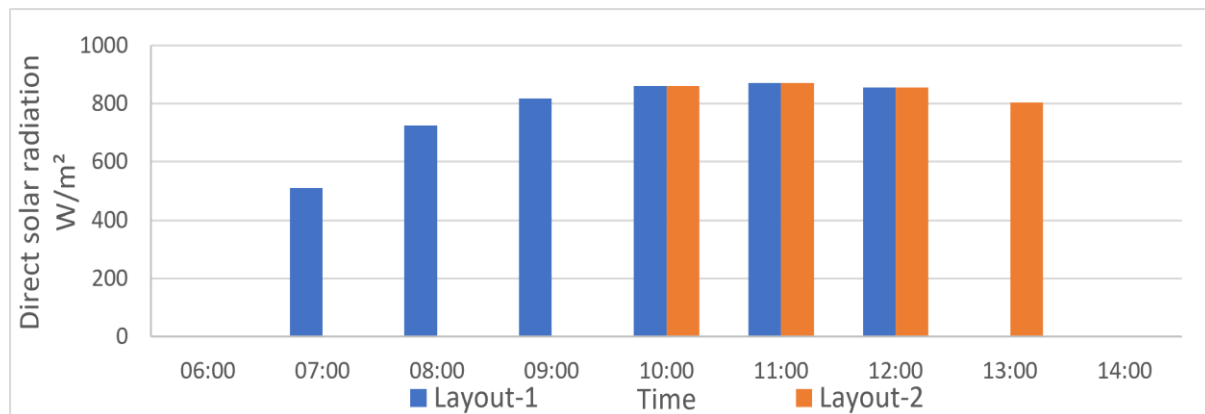


Figure 6.75. Direct solar radiation for receptor 4 under winter conditions on the 22nd of December.

6.10.4 WIND DIRECTION RELATION TO PET VALUES, ANALYSIS FOR LAYOUT-2 (SUMMARY).

Amman's wind rose (Figure 6.76) shows that wind direction is mostly distributed around west and south directions. The previous section focused on the summer and winter analysis, where

wind direction was 105° counter-clockwise from north. This section is going to analyse the different wind directions and how they affect PET. The conditions that were chosen for this analysis were summer conditions as they are the harshest throughout the year in Jordan. A comparison between the different angles will be carried out in terms of wind distribution and PET levels.

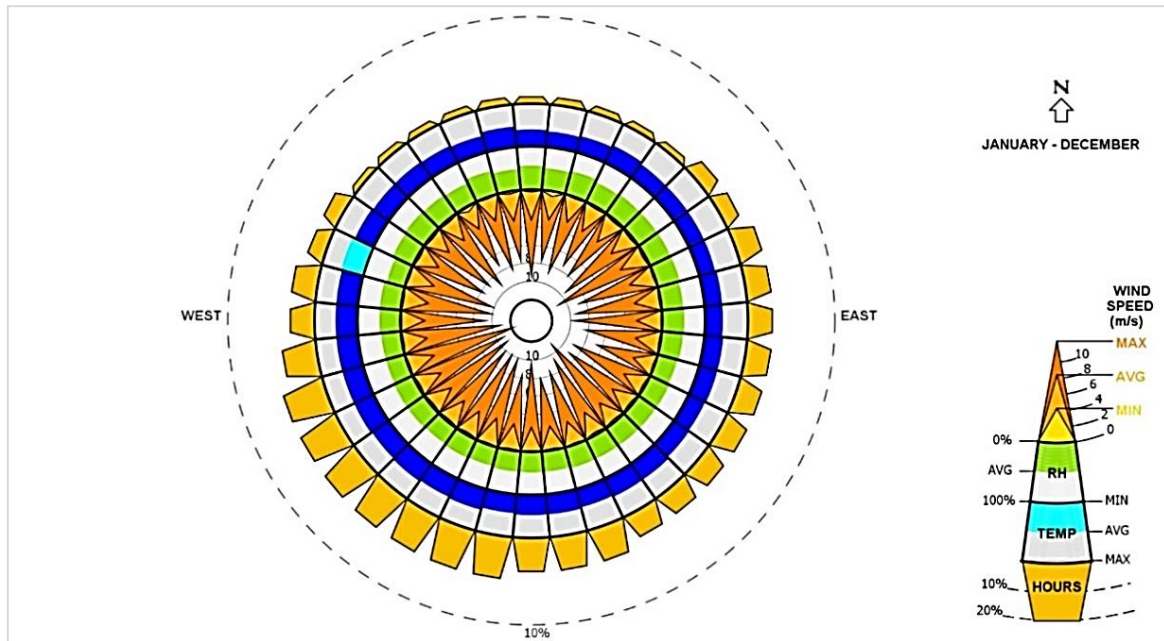


Figure 6.76. Amman's all year wind rose. Source: Meteonorm.

Five scenarios were created with different wind directions: 90°, 105°, 120°, 135° and 150° counter-clockwise from north. Each scenario was simulated under the same conditions and the layouts were kept at the same original layout-2 configuration.

6.10.5 PHYSIOLOGICAL EQUIVALENT TEMPERATURE (SUMMARY).

Since all the scenarios have the same parameters except for wind direction, the direct solar radiation and other parameters will not be included in the discussion as they were discussed in the previous section.

As seen in Figure 6.77, the highest PET values were recorded when the wind direction was parallel to the (West-East) streets when the wind direction was at 90°. This has caused wind flow to move in one direction and create channelling flow which, in turn, limited the wind flow to the (North-South) streets. The high percentage of low wind speed values across the layout has reproduced high PET levels, while the other wind flow directions are noticeably lower in PET values. However, the results produced from directing the approaching wind

parallel to the main streets were lower than the PET values produced in the empty plot, and this is due to the continuous high sun exposure throughout the day.

The angle of which the approaching wind is directed at plays a key role in distributing the wind flow evenly in the urban layouts. Literature has shown that creating helical flows inside the urban canyons improves the wind speed values (discussed in Chapter 2), and this is observed in Figure 6.77, where PET values show a significant drop with an average of 10.5°C. Helical flows are created when the approaching wind enters the plot and separates at the edges of the buildings and the mean flow is displaced, a helical flow is then created throughout the inner streets of the plot by combing the vector sum of the vortices and the channelling flow created by the external wind flow. However, the helical flow is best seen when the approaching wind is directed at 45° from the main streets or the targeted urban canyons.

Although the helical flow produced a higher mean wind speed value, it should be noted that the channelling flow produced higher wind speed values in the main streets of the plot or any urban canyon in the direction of the approaching wind. This might be beneficial in certain designs where high wind speed is desired in certain areas and vice versa.

(Appendix A.6 shows the wind speed maps for the scenarios through Figures A6.1-A6.5).

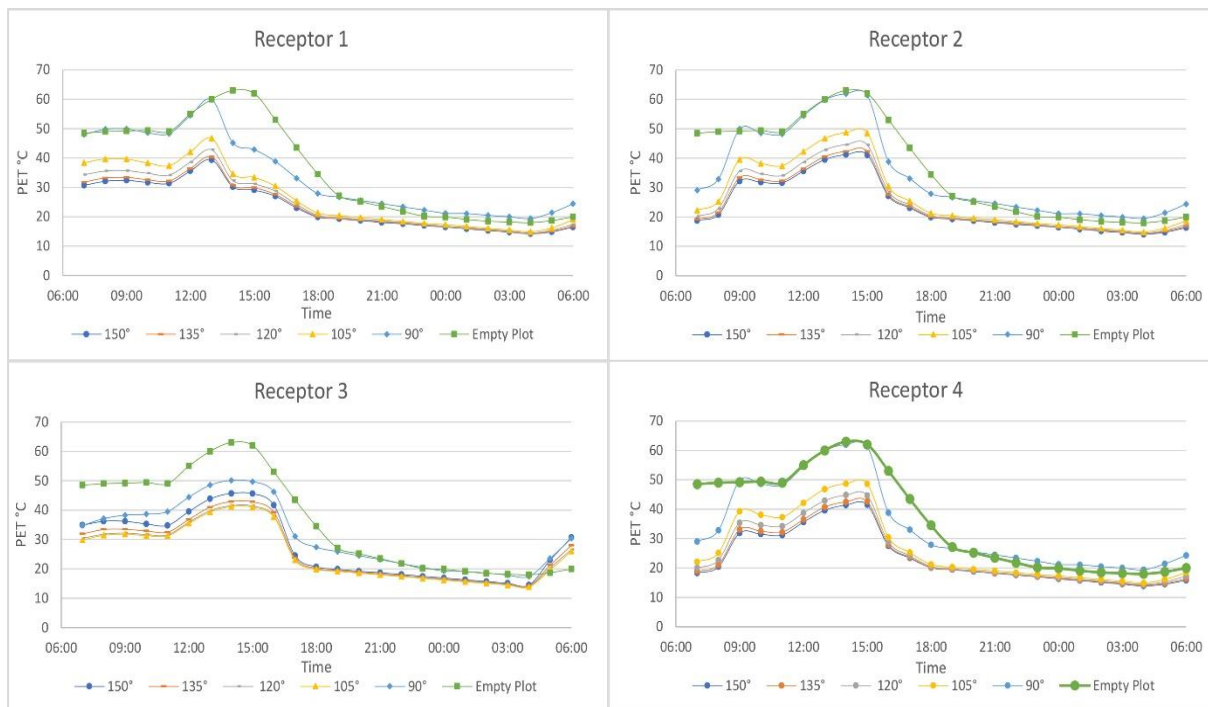


Figure 6.77. Different wind direction PET values.

6.11 CONCLUSIONS

The study of Amman was based on a detailed analysis of the environmental factors that would affect the urban planning, and the study looked at this analysis from a broad point of view and started analysing the best suited street grid system for a selected site located in Amman. The designs that were proposed for the grid system connected the wind flow with the design, where the first design was proposed to orient the streets to help wind flow and the second was an adjusted version of the wind flow proposal with perpendicular intersections for better land distribution.

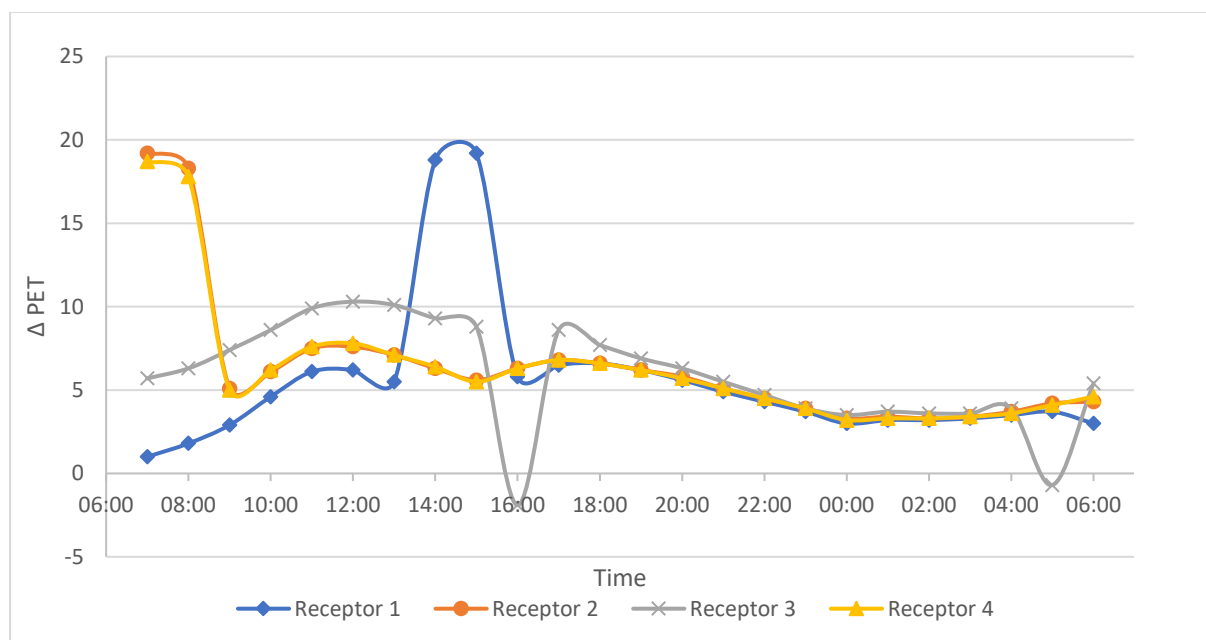


Figure 6.78. Summer simulation on the 23rd of June comparison between layout-1 and layout-2.

The analysis included winter and summer simulations, to test out the grid systems in both thermal stress scenarios hot and cold. The results show that layout-2 produced better PET values than layout-1 due to several factors mainly the direct sun radiation parameter, where layout-1 crossed streets were directed on the (Northeast – Southwest) and (Northwest – Southeast) axis which allowed for more solar access when compared to layout-2 that had the crossed streets directed at the (North-South) axis. Figure 6.78 shows the PET level differences between layout-1 and layout-2 for all the receptors. The positive values indicate higher values of PET in layout-1 and the negative values indicate higher PET values in layout-2. The two instances where receptor 3 has higher PET values in layout-2 are due to longer exposure to direct solar radiation, where in layout-1 receptor 3 is affected by direct solar radiation from 06:00 to 15:00, and layout-2 is affected by direct solar radiation from 05:00 to 16:00. As A

Result, receptor 3 in layout-2 was exposed to 722 W/m² of direct solar radiation for the hours 05:00 and 16:00, while layout-1 was shaded.

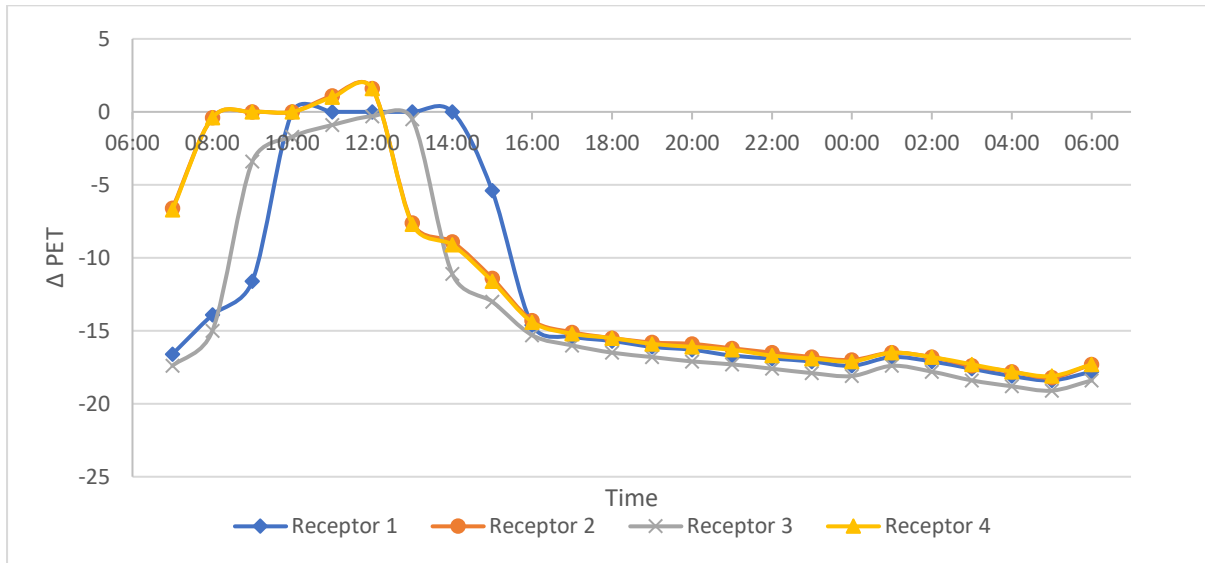


Figure 6.79. Winter simulation on the 22nd of December for layout-1 comparison with comfort level.

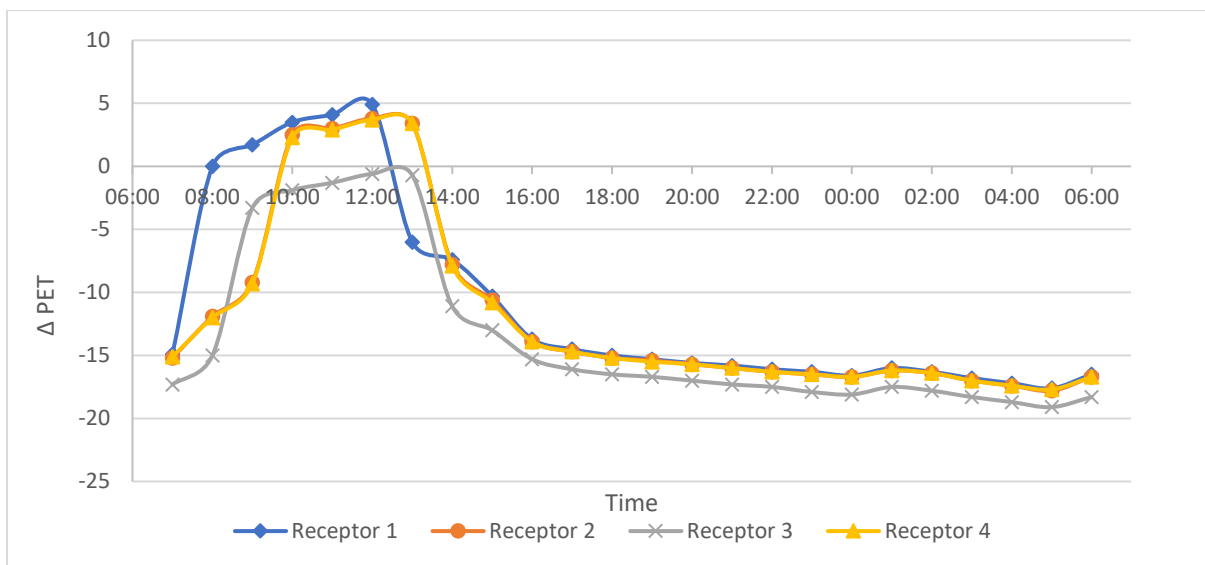


Figure 6.80. Winter simulation on the 22nd of December for layout-2 comparison with comfort level.

The winter analysis produced much lower PET levels than the summer analysis, where most of the PET results were below the comfort range. As a result, the data were analysed based on the resultant PET levels' closeness to the comfort level rather than compare them against each other as in the summer simulation. Figure 6.79 and 6.80 show the receptors PET levels' closeness to the comfort range of (18 °C -23 °C), which in this case is indicated by the 0 X-axis.

Both layouts produced values that are considered as cold sensation on the human body, especially at night-time. However, layout-1 produced more PET values that are within the

comfort range when compared to layout-2. Layout-1 produced (5,1,0 and 1) hours of comfortable sensation for receptors 1,2,3 and 4 respectively which is higher than layout-2 with only one hour in the comfort range in receptor 1 at 08:00 am. The duration of time in the comfort range for each layout is reflected in the index of agreement analysis, where Layout-1 scored an average value of 0.43 and layout-2 scored an average of 0.41.

Table 6.4 and 6.5 show the time duration for both layouts under the comfort range, slightly warm range, and slightly cool range, where it should be noted that, layout-2 recorded more hours in the slightly warm range which might be preferable in winter time when compared to layout-1 with more hours in the slightly cool range.

Table 6.4. Layout-1 results for PET ranges (slightly warm, comfortable, and slightly cool).

Ranges	Duration in hours			
	1	2	3	4
Receptors				
Slightly cool range (13-18)	0	1	5	1
comfort range (18-23)	5	1	0	1
Slightly warm range (23-29)	0	3	0	3

Table 6.5. Layout-2 results for PET ranges (slightly warm, comfortable, and slightly cool).

Ranges	Duration in hours			
	1	2	3	4
Receptors				
Slightly cool range (13-18)	0	0	5	0
comfort range (18-23)	1	0	0	0
Slightly warm range (23-29)	4	4	0	4

The wind direction analysis tests showed that the PET levels were affected by the approaching wind angle, where a significant decrease in the PET values was seen when the wind direction was tilted away from the direction of the streets and, conversely, showed high PET levels when the approaching wind was parallel to the streets. The analysis showed that directing the approaching wind away from the direction of the main streets (15° - 45°) created a helical flow effect, which increased the mean wind value inside the plot. However, directing the wind flow in the direction of the main streets might be beneficial if the design requires high wind speeds in those streets. The final decision on the orientation of design should take into account the position of the targeted area in relation to sun angle as well as approaching wind direction.

SECTION THREE: BUILDINGS CLUSTER ANALYSIS.

Content

- 6.12 Buildings cluster analysis.
- 6.13 Compound 2 shading additions and their effect on PET
- 6.14 Building cluster micro analysis
- 6.15 Building height modification effects on PET.
- 6.16 Tree leaf area density (LAD) and it effect on PET and wind flow.
- 6.17 Site orientation and its effect on PET and wind flow
- 6.18 Conclusion

6.12 BUILDINGS CLUSTER ANALYSIS.

6.12.1 METHODOLOGY BRIEF

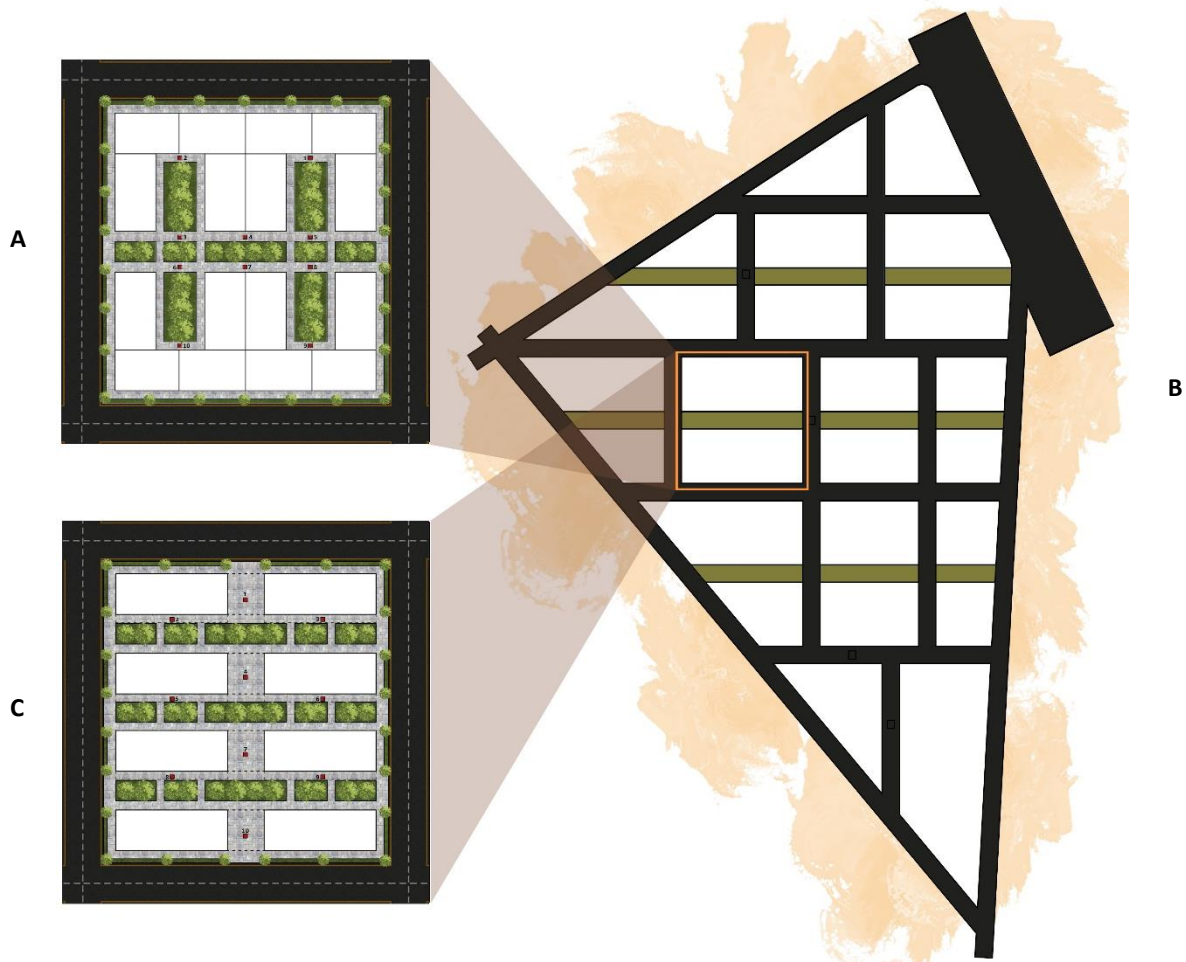


Figure 6.81. Buildings clusters, A) compound 1, B) location of the clusters, C) compound 2.

The analysis moves forward to study the physiological equivalent temperature on a smaller scale (Figure 6.81-B). The buildings clusters proposed for this analysis is based on wind flow (Figure 6.81-A and C).

To test out the two designs mentioned, ten receptors were placed across the two compounds and then the site was simulated in Envi-MET to calculate the PET levels. The analysis was made under the summer conditions, due to summer having the harshest conditions on the human thermal perception in Amman, Jordan. The results for the analysis are displayed between the hours of 05:00 to 16:00 for the purpose of reducing simulation time.

6.12.2 RESULTS

Compound 1 shows higher PET values compared to compound 2's results, as the compact design of compound 1 prevented air movement inside the private zones, and this has caused low wind speed values combined with high solar radiation values on the south-facing zones.

Compound 2 was designed to answer three questions; would orienting the main pathways in the direction of wind flow benefits the overall PET? Would placing the vegetation in the direction of wind flow enhance the thermal stress? And how beneficial is it to create perpendicular openings to the overall ventilation? As concluded in the first section of this chapter, creating roads parallel to wind flow would constrict the wind flow into one direction due to the high pressure created. This helps in answering the first and third questions where the majority of the plot is getting high wind speeds that help in flushing out the heat during night-time. The problematic areas in compound 2 - which question three is addressing – which has limited wind speed values due to the perpendicular orientation to the wind flow. To solve this problem the entirety of the compound needs to be oriented at least 15° off the wind flow. The vegetation played a key role in providing shading to the south-facing areas but not sufficient enough to lower the PET values.

Receptors without shading have higher PET values compared to the shaded receptors (Tables 6.6 and 6.7). The south-facing receptors receive high solar radiation throughout the day which in terms raises the mean radiant temperature resulting in high PET values. Compound 2 has higher wind speeds compared to compound 1, which means under the same metrological conditions compound 2 will result in lower PET values, as shown in Figure 6.82.

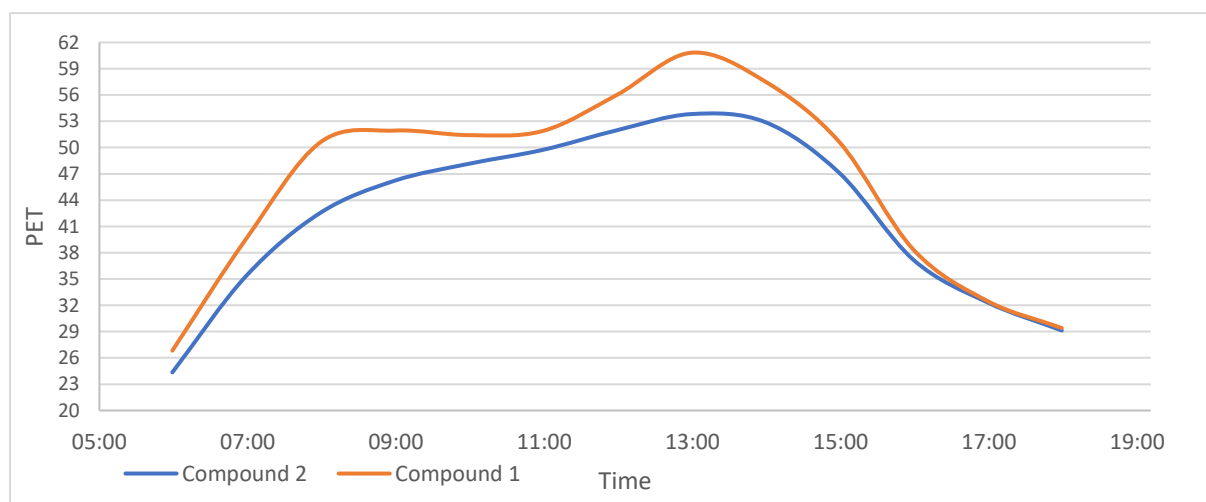


Figure 6.82. Compounds hourly average PET values for the entire plot.

Table 6.6 shows the detailed results for compound 1 PET simulations, and the highlighted data represent the highest PET recorded throughout the day. Receptors 1,2,9 and 10 have the highest PET values compared to the rest of the receptors, and, has been mentioned before, this is due to the air restricted movement and high solar radiation, especially in receptors 1 and 2 with south facing zones.

Table 6.6. Receptors detailed data analysis for compound 1.

time	Receptor 1					Receptor 2				
	Ta	RH	v	T _{mrt}	PET	Ta	RH	v	T _{mrt}	PET
h:mm	°C	%	m/s	°C	°C	°C	%	m/s	°C	°C
06:00	24	49.4	0.1	34.1	29.5	23.8	50.7	0.1	34	29.4
07:00	25.4	47.1	0.1	44.5	36.1	25.4	48	0.1	44.4	36.1
08:00	27	43.6	0.1	76.5	57.7	27.1	44.1	0.1	76.5	57.8
09:00	28.6	38.7	0.1	73.2	56.1	28.7	38.9	0.2	73.2	54.6
10:00	30	33.2	0.1	67.7	52.9	30.1	32.8	0.2	67.7	51.6
11:00	31.2	29.9	0.1	69.8	54.8	31.4	29.5	0.2	69.7	53.5
12:00	32.1	27.3	0.1	74.6	58.4	32.5	26.8	0.2	74.5	57.3
13:00	32.9	25.5	0.1	85.9	66.9	33.3	24.9	0.2	85.9	65.5
14:00	33.2	24.4	0.1	85.4	66.7	33.6	23.8	0.2	85.3	65.2
15:00	33.1	23.7	0.1	53.3	44.8	33.5	23	0.2	53.3	44.3
16:00	32.8	23.9	0.1	43.4	38.7	33.1	23.3	0.2	43.3	38.4
17:00	32	24.7	0.1	33.8	33	32.3	24.3	0.2	33.8	32.9
18:00	25	46.3	0.1	34	30	25.3	46.5	0.2	34.5	30
time	Receptor 3					Receptor 4				
	Ta	RH	v	T _{mrt}	PET	Ta	RH	v	T _{mrt}	PET
h:mm	°C	%	m/s	°C	°C	°C	%	m/s	°C	°C
06:00	22.8	55.3	1.4	32.9	23.3	22.9	55.1	1.8	33.7	22.9
07:00	24.8	51.2	1.4	71.5	42.6	24.9	51.1	1.8	72.2	41.5
08:00	27	45.8	1.3	75.5	47.1	27.1	45.5	1.8	76.2	45.5
09:00	29.1	39	1.3	76.9	49.5	29.3	38.5	1.7	77.5	48.5
10:00	30.9	31.4	1.4	75.1	49.6	31.1	31.2	1.8	75.5	48.7
11:00	32.4	27.9	1.4	71.5	49	32.6	27.8	1.8	71.8	48.2
12:00	33.7	24.7	1.4	77.6	53.2	33.8	24.7	1.8	78.2	52.4

13:00	34.6	22.6	1.4	85.1	58	34.7	22.6	1.8	85.7	57.2
14:00	34.9	21.7	1.5	84.6	57.6	35.1	21.7	1.8	85.2	57.2
15:00	34.7	21.2	1.5	79.7	54.8	34.8	21.2	1.8	80.2	54.3
16:00	34	21.8	1.5	42.6	36.9	34.1	21.9	1.8	43.1	37
17:00	32.9	23.3	1.5	33.2	32.3	32.8	23.5	1.8	33.6	32.3
18:00	25.4	46	1.4	34.2	29.5	25.9	46.5	1.8	34.9	29.4

time	Receptor 5					Receptor 6				
	Ta	RH	v	Tmrt	PET	Ta	RH	v	Tmrt	PET
h:mm	°C	%	m/s	°C	°C	°C	%	m/s	°C	°C
06:00	23	55.3	1.3	33	23.7	23	54.4	1.3	43.7	28.1
07:00	25	51.3	1.3	71.5	43.3	25	50.3	1.3	71.5	43.2
08:00	27.3	45.7	1.2	75.6	47.8	27.1	45.1	1.3	75.5	47.1
09:00	29.5	38.4	1.2	77	50.3	29.2	38.6	1.3	76.9	49.6
10:00	31.2	31.4	1.2	75.1	50.6	30.9	31.3	1.3	75.1	50
11:00	32.6	27.9	1.2	71.6	49.8	32.4	27.8	1.3	71.5	49.3
12:00	33.9	24.9	1.2	77.7	54.1	33.7	24.8	1.3	77.6	53.5
13:00	34.7	22.8	1.2	85.2	58.9	34.5	22.8	1.3	85.1	58.3
14:00	35.1	21.8	1.2	84.7	58.9	34.8	21.9	1.3	84.6	58.2
15:00	34.8	21.4	1.2	79.8	55.9	34.7	21.3	1.3	79.7	55.4
16:00	33.9	22.3	1.2	42.6	37.1	34	21.8	1.4	51.3	40.7
17:00	32.7	23.9	1.2	33.2	32.2	32.9	23.2	1.4	33.2	32.4
18:00	25	45.9	1.3	34	29.1	25.2	46.7	1.3	33	29.2
time	Receptor 7					Receptor 8				
	Ta	RH	v	Tmrt	PET	Ta	RH	v	Tmrt	PET
h:mm	°C	%	m/s	°C	°C	°C	%	m/s	°C	°C
06:00	23.2	54	1.9	47.8	28.5	23.3	53.5	1.3	38.8	26.3
07:00	25.1	49.9	1.9	71.8	41.1	25.2	49.6	1.3	71.4	43.4
08:00	27.3	44.7	1.8	75.8	45.5	27.4	44.6	1.3	75.5	47.4
09:00	29.4	38.2	1.8	77	48	29.3	38.1	1.3	76.8	49.6
10:00	30.9	31.5	1.8	75.5	48.5	30.9	31.7	1.3	75	49.9
11:00	32.5	27.9	1.8	76.5	50.4	32.3	28.3	1.3	71.4	49.2
12:00	33.8	24.8	1.8	82	54.4	33.5	25.3	1.3	77.6	53.4

13:00	34.5	22.9	1.8	85.2	56.9	34.3	23.3	1.3	85	58.1
14:00	34.9	21.9	1.8	84.8	56.8	34.6	22.4	1.3	84.6	58.1
15:00	34.7	21.4	1.8	79.8	54	34.5	21.8	1.3	79.7	55.3
16:00	34	22	1.8	51.5	40.3	33.8	22.4	1.3	45.7	38.2
17:00	32.8	23.6	1.8	33.5	32.2	32.6	23.9	1.3	33.1	32.1
18:00	25.8	46.2	1.8	34.5	29.5	25.3	45.9	1.3	34.9	29
time	Receptor 9					Receptor 10				
	Ta	RH	v	Tmrt	PET	Ta	RH	v	Tmrt	PET
h:mm	°C	%	m/s	°C	°C	°C	%	m/s	°C	°C
06:00	24.1	48.6	0.2	33.8	28.6	23.9	49.9	0.3	33.8	28
07:00	25.3	46.5	0.2	44.1	34.9	25.3	47.5	0.3	44.2	34.2
08:00	26.9	43.3	0.2	76.2	55.8	27	43.8	0.3	76.2	54.5
09:00	28.4	38.7	0.2	77.3	57.2	28.5	38.8	0.3	77.3	56
10:00	29.6	33.4	0.2	75.7	56.7	29.9	32.9	0.3	75.7	55.7
11:00	30.9	30.2	0.2	76.6	57.9	31.2	29.7	0.3	76.6	56.9
12:00	31.9	27.6	0.2	82.2	62.2	32.3	27	0.3	82.2	61.3
13:00	32.6	25.8	0.2	85.5	64.9	33	25.1	0.3	85.5	63.9
14:00	32.9	24.7	0.2	60.7	48.5	33.4	24.1	0.3	60.7	48.1
15:00	33	23.9	0.2	52.9	43.9	33.3	23.3	0.3	52.9	43.5
16:00	32.6	24	0.2	43.1	38.1	33	23.4	0.3	43.1	38
17:00	32	24.7	0.2	33.7	32.7	32.2	24.3	0.3	33.7	32.7
18:00	25.5	46	0.2	33.8	29.3	25.8	46.9	0.3	33.8	29.1

Table 6.7 shows the detailed results for compound 2 PET simulation, and the highlighted data shows a significant decrease in PET values compared to compound 1 due to better shading and air movement. However, it should be pointed out that the shaded receptors (1,4,7 and 10) have lower PET values with an average of 3.7 C decrease and receptors 3,6 and 9 have higher PET values than 2,5 and 8 due to lower wind speed.

Table 6.7.Receptors detailed data analysis for compound 2.

time	Receptor 1					Receptor 2				
	Ta	RH	v	Tmrt	PET	Ta	RH	v	Tmrt	PET
h:mm	°C	%	m/s	°C	°C	°C	%	m/s	°C	°C
06:00	22.8	55.7	0.2	32.7	27.4	22.7	55.6	1.8	32.8	22.4
07:00	24.6	52.3	0.2	42.9	33.9	24.6	52	1.8	71.3	40.8
08:00	26.7	47	0.2	51.2	39.8	26.7	46.5	1.8	74.8	44.4
09:00	28.8	40.1	0.2	58.5	45.2	28.8	39.6	1.8	75.8	46.8
10:00	30.5	32.8	0.2	63.1	48.9	30.6	31.8	1.8	73.7	47.4
11:00	32	29.1	0.2	65.8	51.3	32.2	28.2	1.9	70.1	46.8
12:00	33.3	26	0.2	66.1	51.5	33.5	24.9	1.9	76.5	51.1
13:00	34	24	0.2	63.6	51.9	34.4	22.8	1.9	84	55.6
14:00	34.4	23	0.2	59	48.2	34.8	21.9	1.9	83.9	55.2
15:00	34.2	22.5	0.2	51.7	43.8	34.6	21.4	1.9	79.3	53.4
16:00	33.5	23.1	0.2	42.5	38.2	33.9	22	1.9	42.4	36.5
17:00	32.3	24.6	0.2	33.5	32.8	32.8	23.4	1.9	33.3	32.1
18:00	29.8	38.1	0.2	33.1	29.5	28.1	37.9	1.8	33	29

time	Receptor 3					Receptor 4				
	Ta	RH	v	Tmrt	PET	Ta	RH	v	Tmrt	PET
h:mm	°C	%	m/s	°C	°C	°C	%	m/s	°C	°C
06:00	22.9	56.3	1.8	32.7	22.5	22.8	55.8	0.2	32.8	27.5
07:00	24.7	52.9	1.8	71.2	40.8	24.6	52.3	0.2	42.9	33.9
08:00	26.9	47.2	1.7	74.8	45	26.7	47	0.2	51.3	39.8
09:00	29.1	39.8	1.7	75.8	47.4	28.8	40.1	0.2	58.6	45.3
10:00	31	32.3	1.7	74.2	48.3	30.5	32.8	0.2	63.3	49
11:00	32.5	28.5	1.7	72.6	48.8	32.1	29	0.2	66	51.5
12:00	33.7	25.3	1.7	73.7	50.4	33.3	25.9	0.2	66.3	52.3
13:00	34.6	23	1.7	83.9	56.3	34.1	23.8	0.2	63.8	52.3
14:00	35	21.9	1.7	83.8	56.2	34.5	22.9	0.2	59.2	48.4
15:00	34.8	21.5	1.7	79.2	54	34.3	22.4	0.2	51.8	43.9
16:00	33.9	22.5	1.7	42.4	36.7	33.5	23.1	0.2	42.6	38.3

17:00	32.5	24.2	1.7	33.3	31.9	32.3	24.5	0.2	33.6	32.8
18:00	29.9	38.1	1.8	33.2	29.1	29.7	38.2	0.2	33.5	29
time	Receptor 5					Receptor 6				
	Ta	RH	v	Tmrt	PET	Ta	RH	v	Tmrt	PET
h:mm	°C	%	m/s	°C	°C	°C	%	m/s	°C	°C
06:00	22.7	55.6	1.9	32.5	22.1	22.8	56.3	1.8	32.7	22.4
07:00	24.6	51.9	1.9	71.1	40.3	24.7	52.9	1.8	71.2	40.8
08:00	26.8	46.4	1.8	74.6	44.4	26.9	47.2	1.8	74.8	44.6
09:00	28.9	39.5	1.8	75.6	46.8	29.1	39.9	1.7	75.8	47.4
10:00	30.7	31.7	1.9	73.9	47.3	31	32.2	1.7	74.2	48.3
11:00	32.4	27.8	1.9	75.2	49.4	32.5	28.5	1.8	72.7	48.6
12:00	33.7	24.6	1.9	80.6	53.2	33.7	25.2	1.7	73.7	50.4
13:00	34.5	22.6	2	83.7	55.3	34.6	22.9	1.7	84	56.4
14:00	34.8	21.9	2	83.7	55.1	35	21.9	1.7	83.9	56.1
15:00	34.6	21.4	2	79.1	53.1	34.8	21.5	1.7	79.2	54
16:00	33.9	22	2	42.3	36.4	33.9	22.5	1.7	42.4	36.7
17:00	32.8	23.4	2	33.2	32.1	32.5	24.2	1.7	33.3	31.9
18:00	29.6	37.9	1.9	33.2	29.3	29.1	38.9	1.8	32.9	28.9

time	Receptor 7					Receptor 8				
	Ta	RH	v	Tmrt	PET	Ta	RH	v	Tmrt	PET
h:mm	°C	%	m/s	°C	°C	°C	%	m/s	°C	°C
06:00	22.8	55.7	0.2	32.8	27.4	22.8	54.8	1.8	32.2	22.2
07:00	24.6	52.3	0.2	43	34	24.6	51.4	1.8	42	27.7
08:00	26.7	47	0.2	51.3	39.8	26.8	45.8	1.8	73.9	44.1
09:00	28.8	40.1	0.2	58.7	45.3	28.9	39	1.8	74.7	46.4
10:00	30.5	32.8	0.2	63.3	49	30.8	31.3	1.8	72.9	47.2
11:00	32.1	29.1	0.2	66.1	51.6	32.4	27.7	1.9	74.1	48.9
12:00	33.3	25.9	0.2	66.3	52.1	33.6	24.6	1.9	79.6	52.7
13:00	34.1	23.9	0.2	63.8	52.5	34.4	22.7	1.9	82.9	55.8
14:00	34.4	22.9	0.2	59.2	48.3	34.8	21.9	1.9	83	55.4
15:00	34.2	22.4	0.2	51.8	43.8	34.6	21.4	1.9	51	40.6
16:00	33.5	23.1	0.2	42.6	38.3	33.8	22	1.9	42	36.3

17:00	32.3	24.6	0.2	33.6	32.8	32.8	23.4	1.9	33.1	32.1
18:00	29.4	38.2	0.2	33.4	29.1	29.3	38.4	1.8	33.1	29.4
time	Receptor 9					Receptor 10				
	Ta	RH	v	Tmrt	PET	Ta	RH	v	Tmrt	PET
h:mm	°C	%	m/s	°C	°C	°C	%	m/s	°C	°C
06:00	22.9	55.9	1.8	32.1	22.3	22.9	54.4	0.2	32.5	27.3
07:00	24.7	52.7	1.8	42	27.9	24.7	51	0.2	42.7	33.8
08:00	26.9	47	1.8	73.8	44.1	26.7	46	0.2	51.1	39.7
09:00	29.2	39.5	1.8	74.6	46.6	28.7	39.6	0.2	58.3	45
10:00	31.1	31.8	1.8	72.9	47.4	30.4	32.6	0.2	62.9	48.7
11:00	32.7	27.9	1.8	74	49.4	31.9	29	0.2	65.6	51.1
12:00	34	24.7	1.8	79.6	53.3	33.1	26.1	0.2	65.9	51.9
13:00	34.8	22.7	1.8	82.8	56.7	33.8	24.2	0.2	63.4	52.7
14:00	35.1	21.8	1.8	82.9	56	34.1	23.3	0.2	58.8	47.9
15:00	34.8	21.5	1.7	51	40.9	34	22.7	0.2	51.5	43.5
16:00	33.8	22.5	1.7	41.9	36.4	33.3	23.2	0.2	42.3	38
17:00	32.6	24.1	1.7	33.1	31.9	32.3	24.5	0.2	33.5	32.8
18:00	29.1	38.1	1.8	32.1	28.9	29.7	38.6	0.2	32.5	29.1

6.13 COMPOUND 2 SHADING ADDITIONS AND THEIR EFFECT ON PET

The previous section analysed the two compounds in terms of thermal stress on pedestrians and showed that compound 2 performed better in terms of PET values. This section will focus on compound 2 and will address the problematic areas shown in the data results (Table 6.7). The receptors that were placed in the south-facing zones had the highest solar radiation values during the day, and this caused the PET levels to rise significantly compared to the receptors placed in the shaded areas. For this reason, a simple addition of horizontal shading was added to the designed compound and simulated under the same conditions. (Figure 6.83).



Figure 6.83. Original compound 2 design (left), compound 2 with the added shading (right).

Figures 6.84 to 6.89 show the PET results from adding shading devices to the south-facing zones, and it is apparent in all the graphs that removing the direct sun element produced a steady increase and decrease (Parabolic) of PET throughout the day - shown in orange. Figure 6.90 shows the average improvement of PET levels after adding the shading for each receptor as well as the maximum and minimum values. Receptor 6 had the highest improvement with an average of 7.8°C decrease in PET values and a maximum improvement value of 14°C, while receptor 8 had the least average improvement with a 7°C decrease in PET levels.

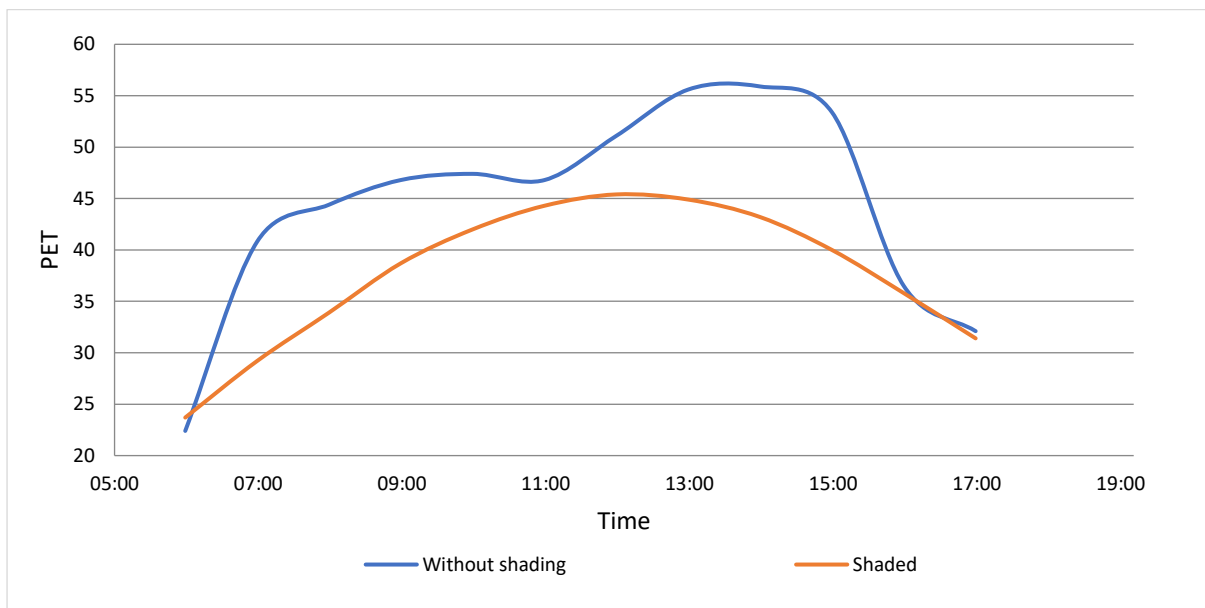


Figure 6.84. Receptor 2 PET results with and without shading.

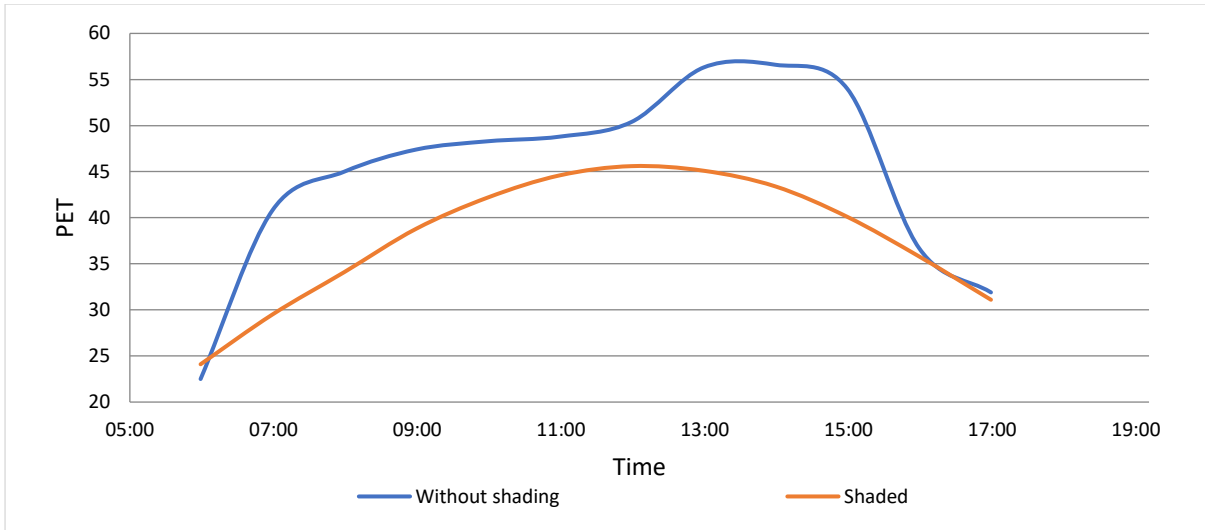


Figure 6.85. Receptor 3 PET results with and without shading.

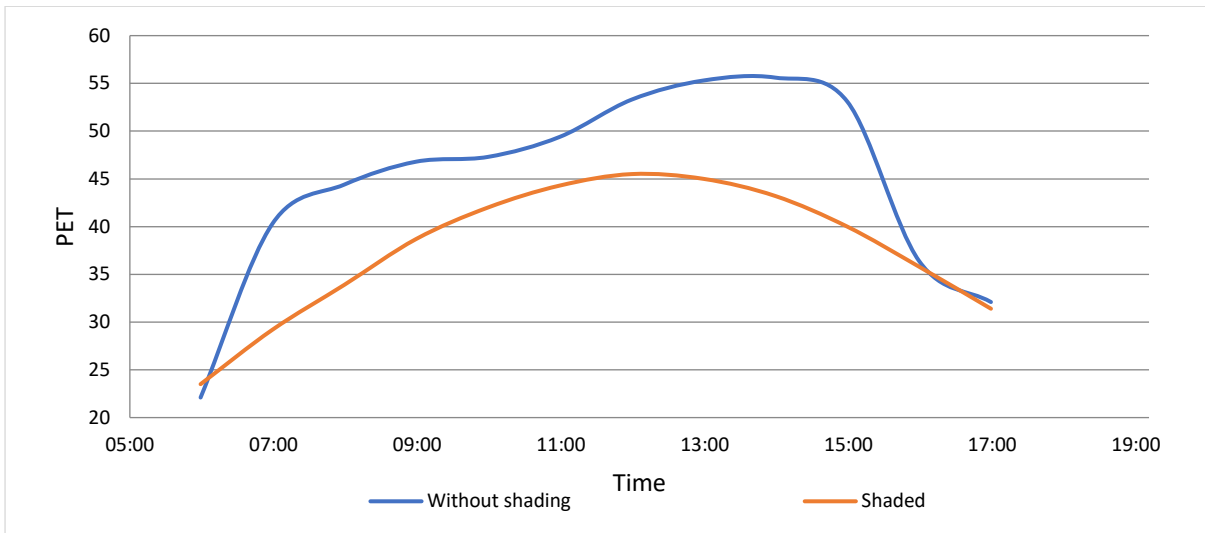


Figure 6.86. Receptor 5 PET results with and without shading.

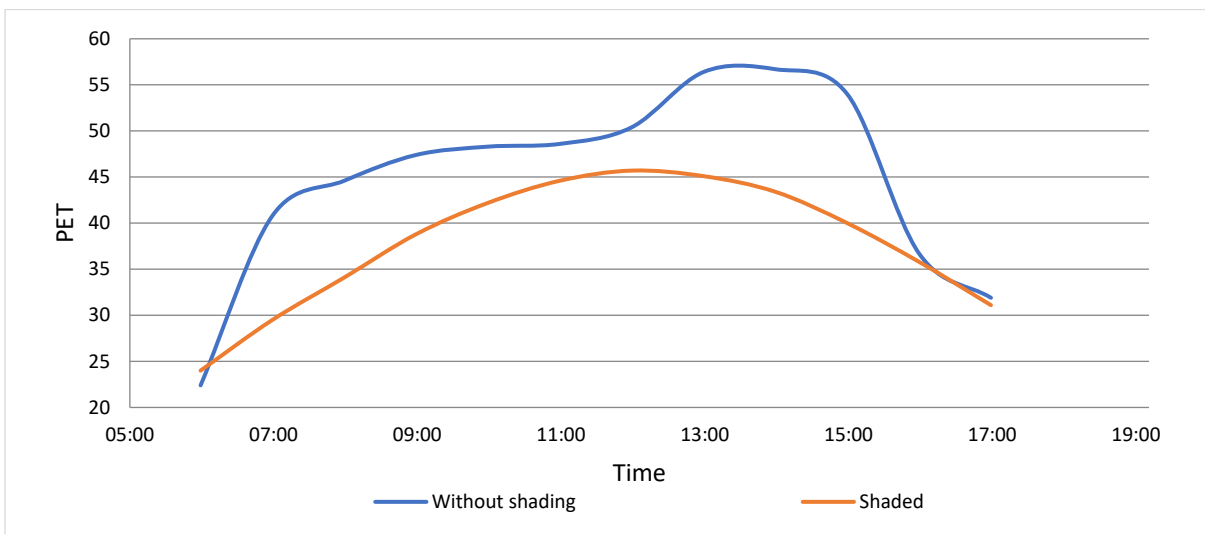


Figure 6.87. Receptor 6 PET results with and without shading.

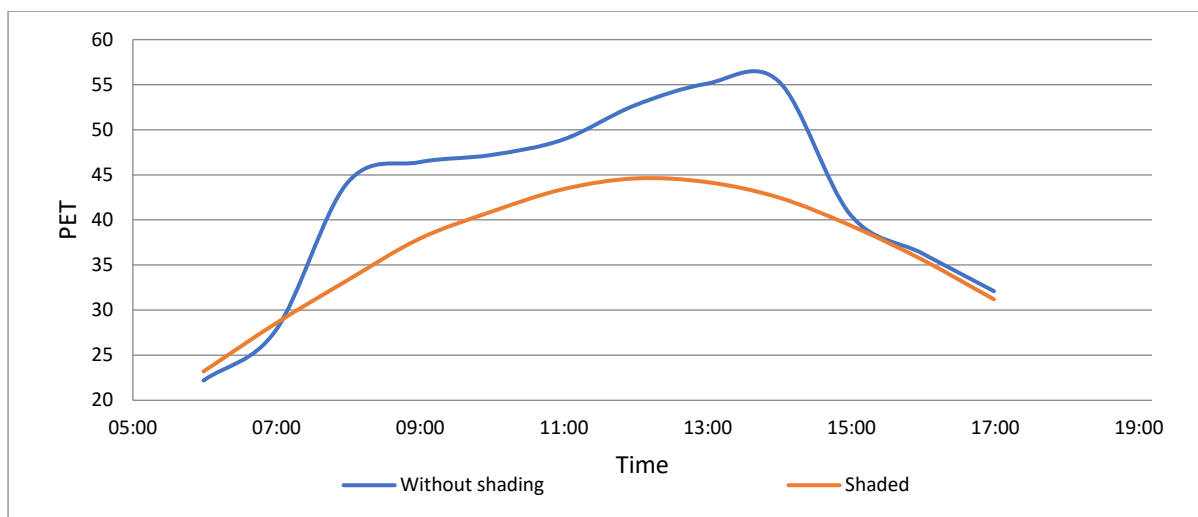


Figure 6.88. Receptor 8 PET results with and without shading.

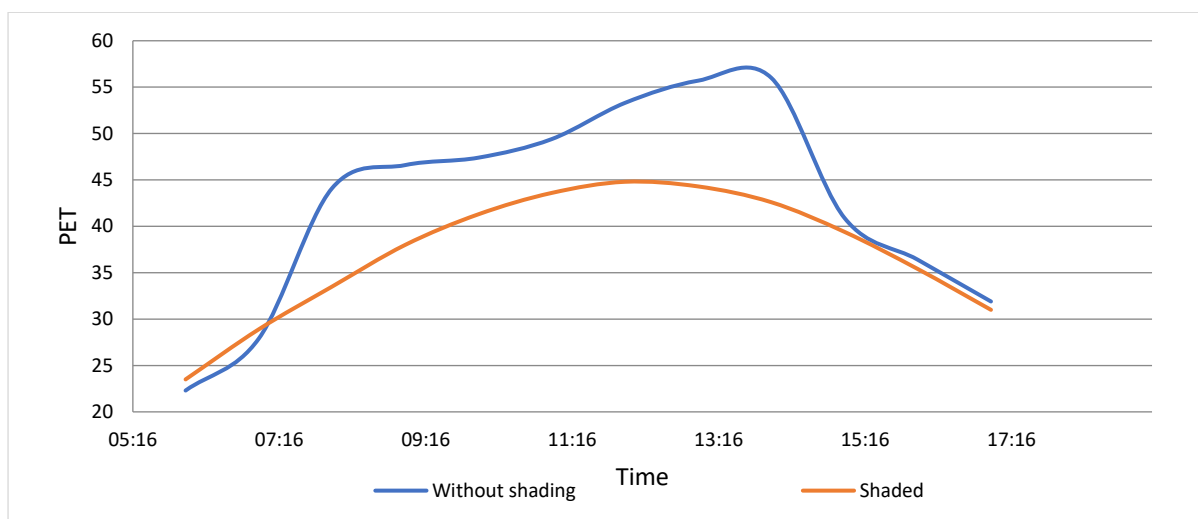


Figure 6.89. Receptor 9 PET results with and without shading.

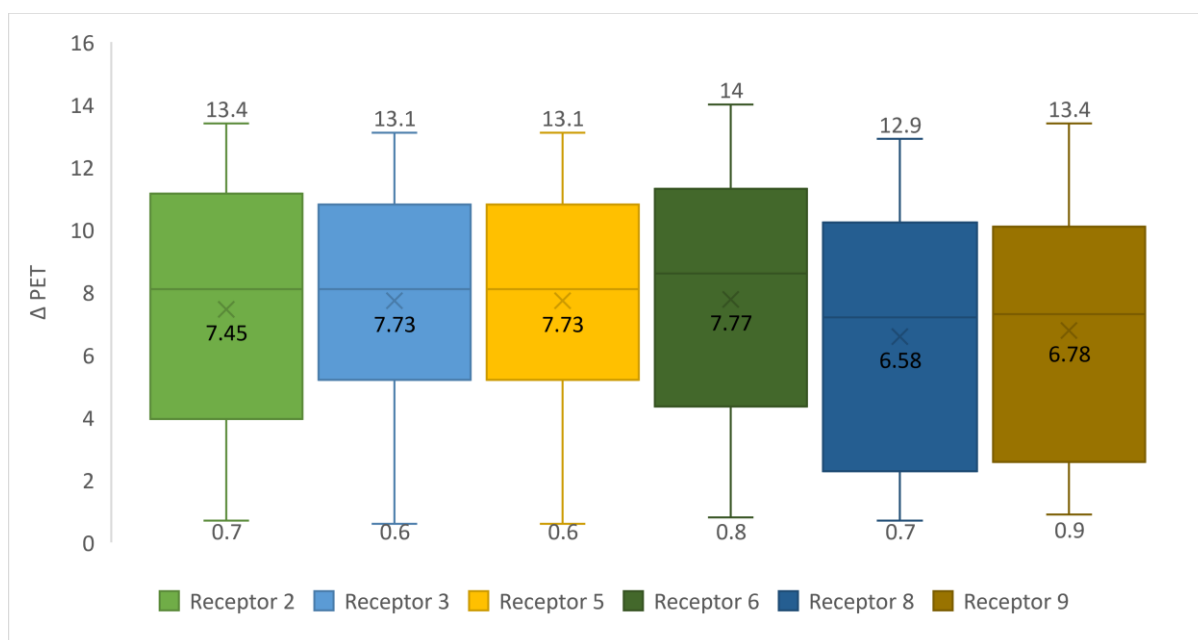


Figure 6.90. The average change in PET values after the shading addition for compound 2.

6.14 BUILDINGS CLUSTER MICRO ANALYSIS.

In this section, the study will analyse the two strips of buildings. It will investigate how geometrical and vegetation variations affect the PET at the pedestrian's level. This section will address the effect of the wind tunnel when the wind direction is perpendicular to the axis of the tunnel, it will also address the effect of changing the heights of the buildings without changing the width of the streets. the study also investigates the effect of changing leaf area density (LAD) of the trees added to the site as well as changing the orientation with keeping the initial wind direction the same.

Figure 6.91 shows the area that will be further investigated for this study, and it will serve as a reference for receptors placement and sections cuts for the upcoming sections.

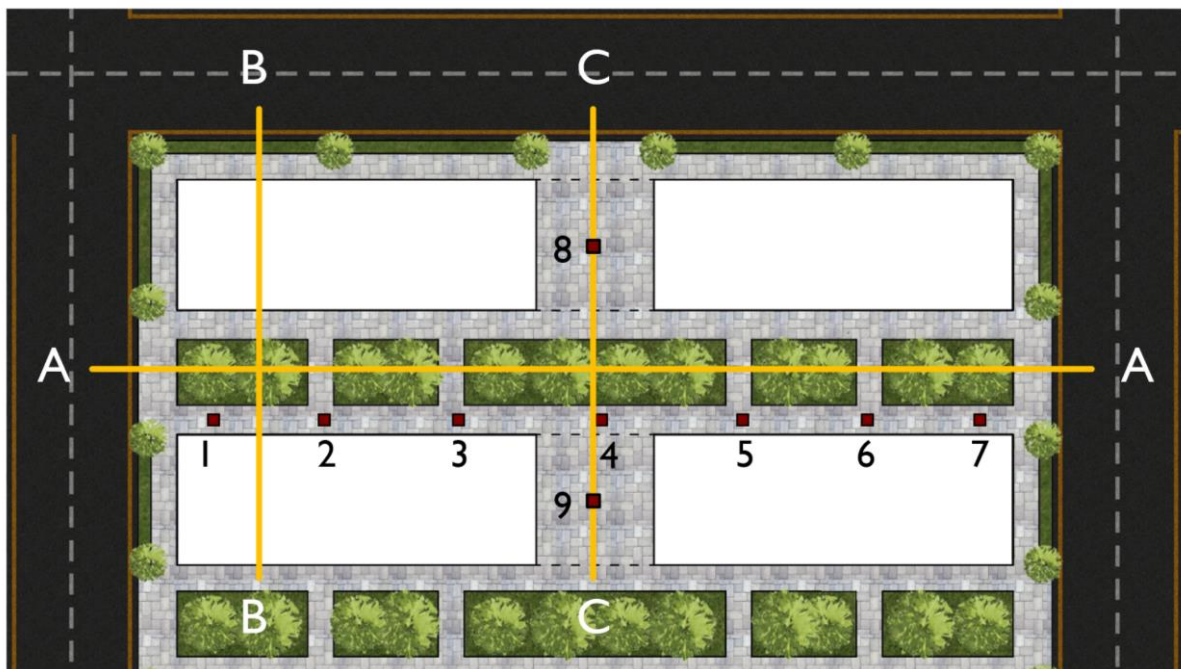


Figure 6.91. The area investigated for the microanalysis with the section cuts.

6.14.1 GEOMETRICAL MODIFICATION; DESIGNING THE BUILDINGS PATHWAYS.

This section will address the question: how beneficial is the wind tunnel design within an elongated design when the wind direction is perpendicular to the wind tunnel axis? The initial design was built with a wind tunnel-like structure, and a second scenario was built without the wind tunnel to test the wind behaviour in the two cases.

The scenarios were simulated under the same conditions with 12-metre high buildings placed 9 metres apart. Figure 6.92 shows the PET results for the two different scenarios, where the tunnel-like pathway (half gap) resulted in a slightly higher PET values throughout the day

compared to the full cut through the buildings scenario (full gap). Both scenarios did not receive direct sun radiation, due to the position of the receptors - where in the full gap scenarios the receptor is shaded by the surrounding buildings and the half gap scenario is shaded by the connection orange structure. The reason PET is higher in the wind tunnel scenario is that the structure produced more reflected solar radiation inside the tunnel where in the other scenario the reflected solar radiation is lower by an average 24.8 W/m² throughout the day.

The wind speed results for the half gap scenario showed a slight improvement compared to the full gap scenario (Figure 6.93) - this is due to the stronger wind tunnel effect with the confined space as in the half gap scenario.

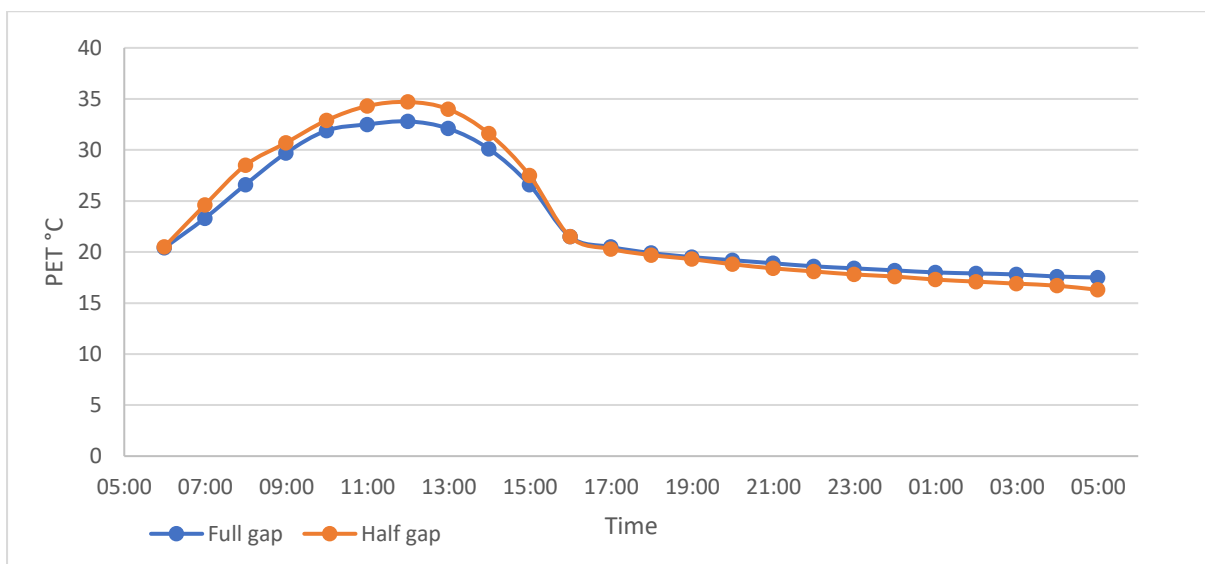


Figure 6.92. Receptor 8 PET results.

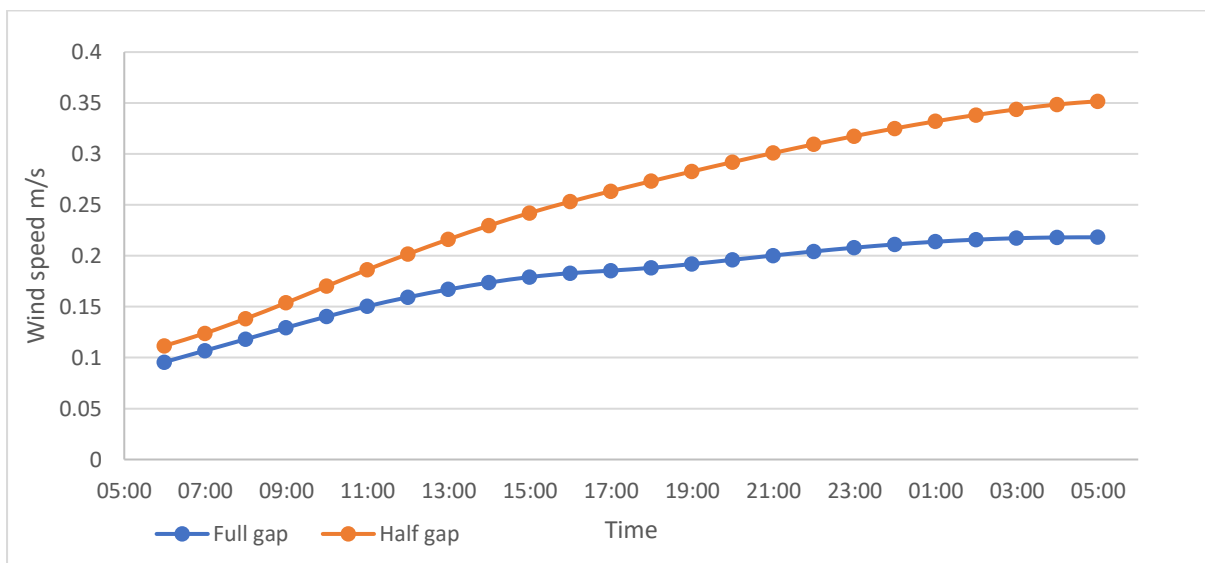


Figure 6.93. Receptor 8 wind speed results.

The simulation was performed on a segment of the compound, this eliminated some elements that would affect the outcome of the simulation. The placement of receptor 9 is adjacent to trees from the front and the back side, and this would have provided enough shading for the location so that the PET levels did not rise drastically like in the case of receptor 8. However, Receptor 9 had a spike in PET levels between the hours of 09:00 and 12:00 in the full gap scenario (Figure 6.94). This is, as mentioned above, due to the elimination of the trees in the back side. The situation is beneficial in showing how the south far end of the compound performs in terms of PET and wind speed as this segment of the compound is a representative of the compound as a whole.

The wind speed results for receptor 9 mirror the results of receptor 8, where the wind speed values for the half gap scenario were higher than the full gap scenario (Figure 6.95). The wind tunnel effect was also stronger in the half gap, as in receptor 8.

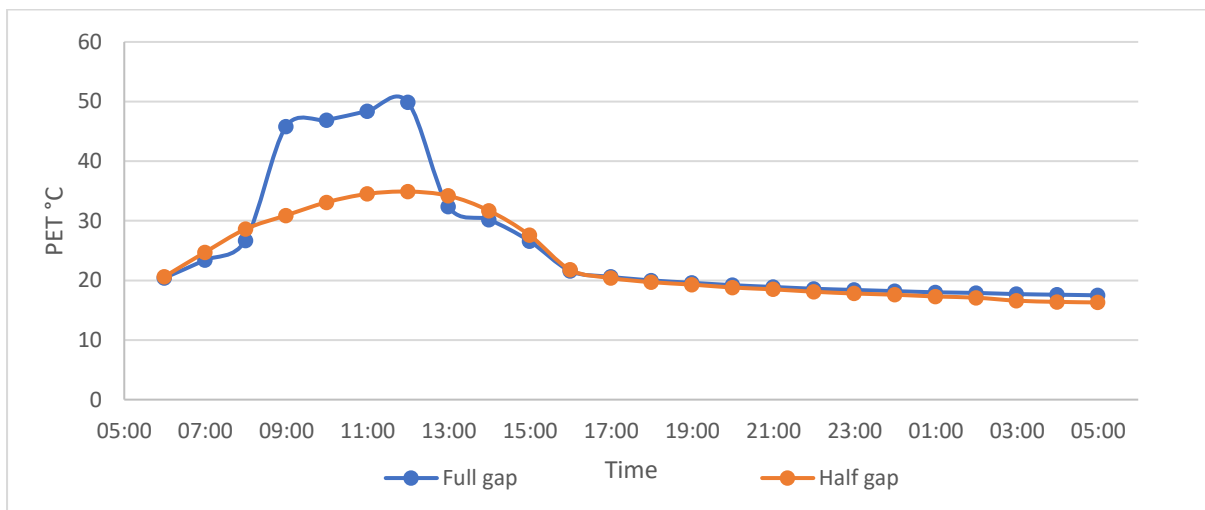


Figure 6.94. Receptor 9 PET results.

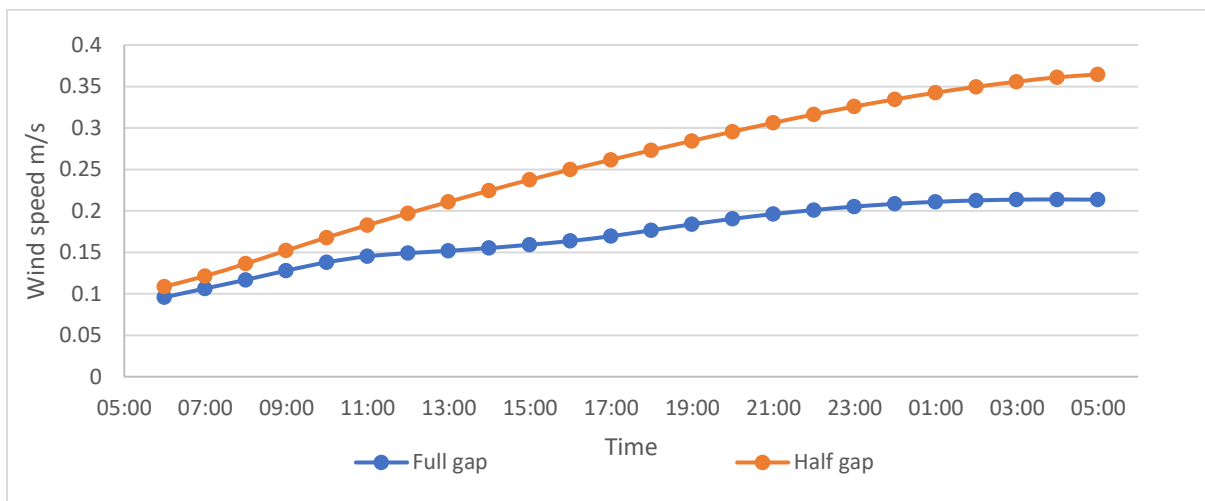


Figure 6.95. Receptor 9 wind speed results.

6.15 BUILDINGS' HEIGHT MODIFICATION EFFECTS ON PET.

This section will continue analysing the plot segment taken from compound 2 (Figure 6.91) in terms of building heights and their effect on PET and wind flow at the pedestrian level. The heights that were introduced to the design were: 12 metres, 18 metres and 24 metres. The meteorological parameters, as well as the design's geometry other than the heights, were kept the same. The results of the simulation will be analysed in term of PET levels and wind flow effectivity.

Figure 6.91 shows the placement of the receptors (1-7) along the (West-East) pathway. Only four receptors will be discussed in this section as all the receptors behaved fairly similarly in regards of PET and its reaction to the height change of the buildings. Figures 6.96 to 6.99 show the PET levels for the height scenarios, the 12mr high building scenario produced the highest PET levels followed by the 18m with the lowest PET levels being for the 24m high scenario. It should be noted that PET levels showed a significant drop from the 12m high buildings scenario to the 24m high buildings scenario with an average reduction of 3.3°C. This reduction was due to the higher wind speed produced in the 24m high buildings scenarios.

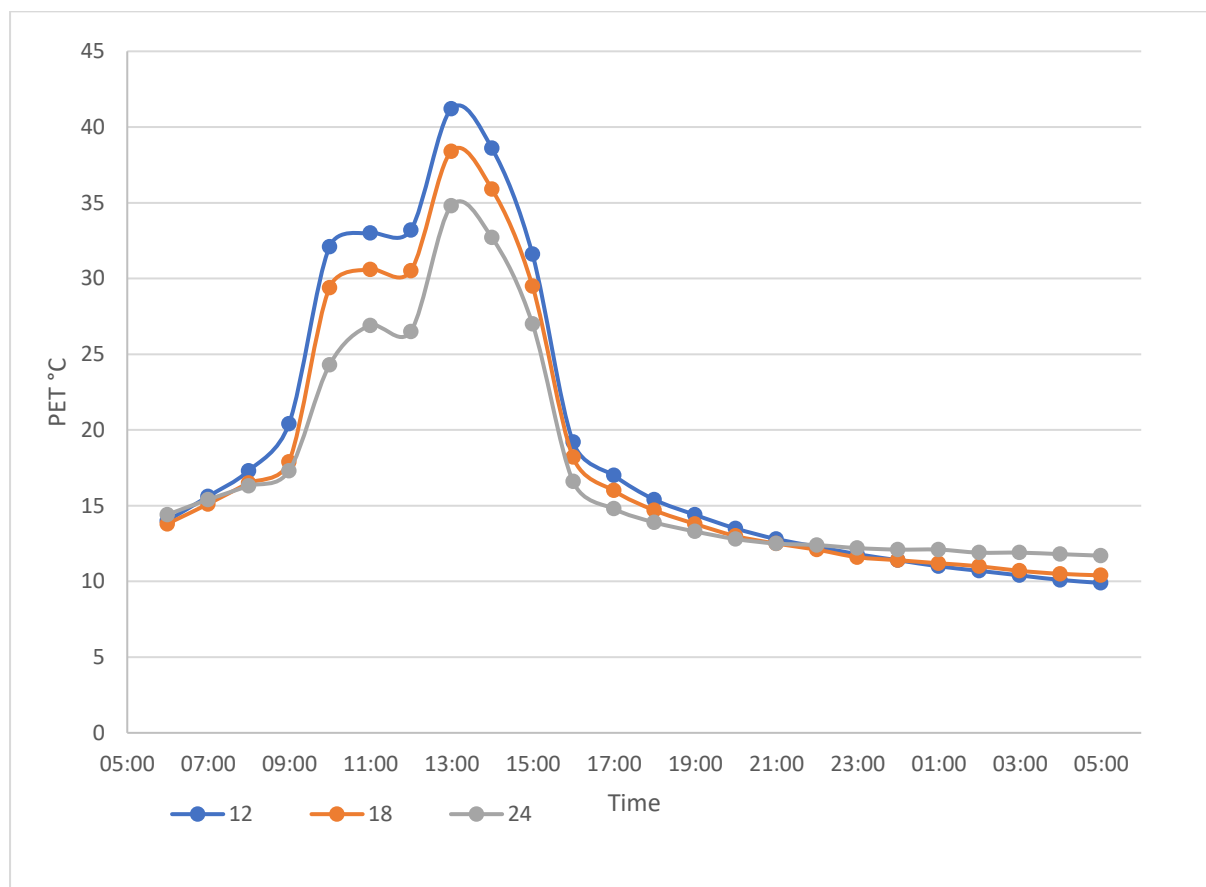


Figure 6.96. Receptor 1 PET levels for the height's scenarios.

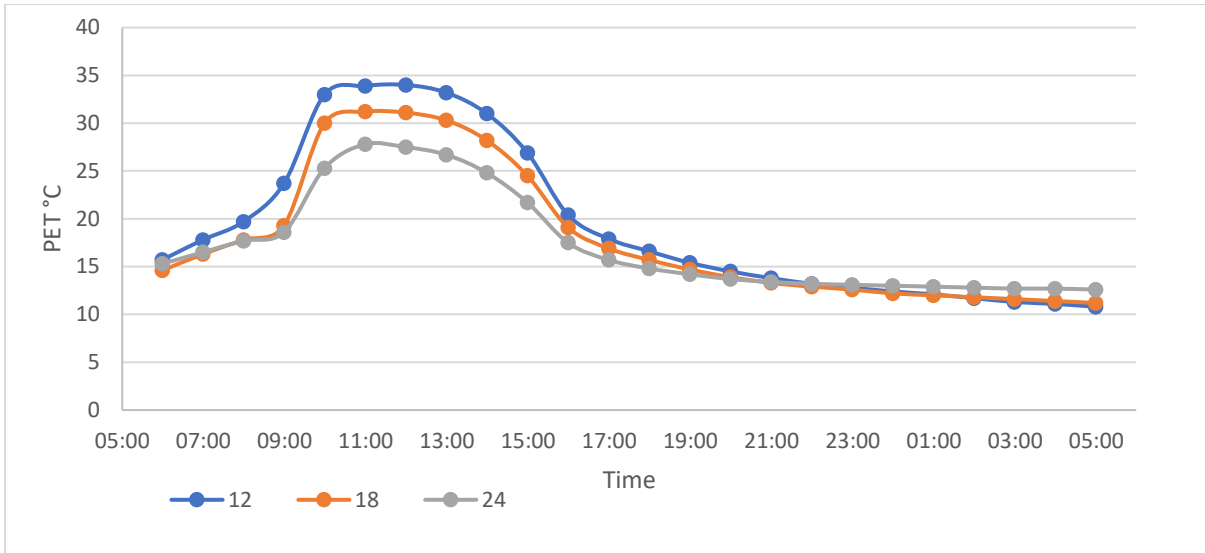


Figure 6.97. Receptor 3 PET levels for the height's scenarios.

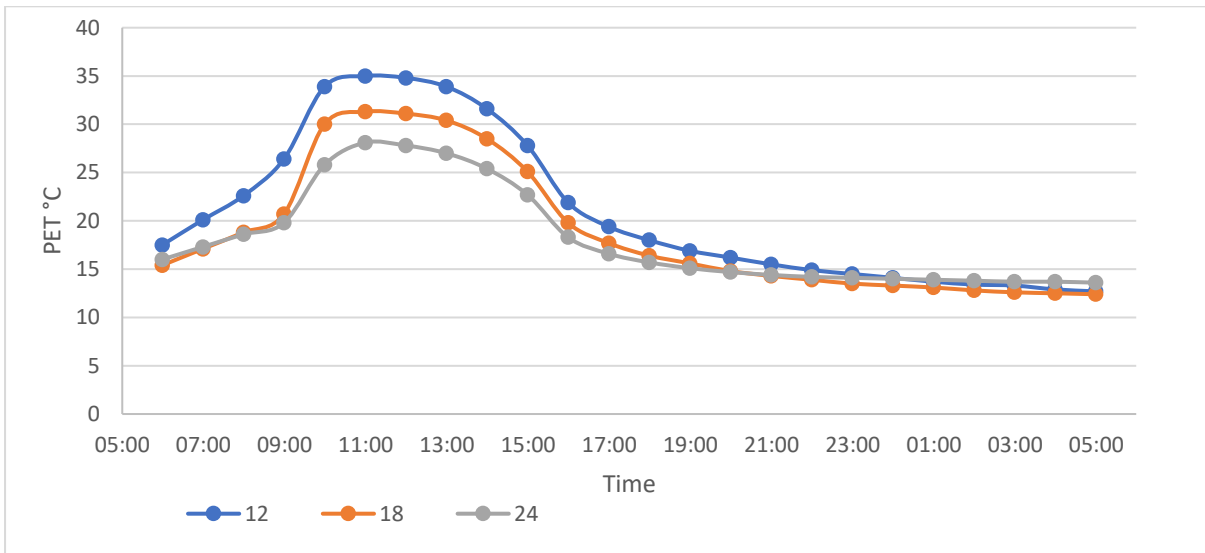


Figure 6.98. Receptor 5 PET levels for the height's scenarios.

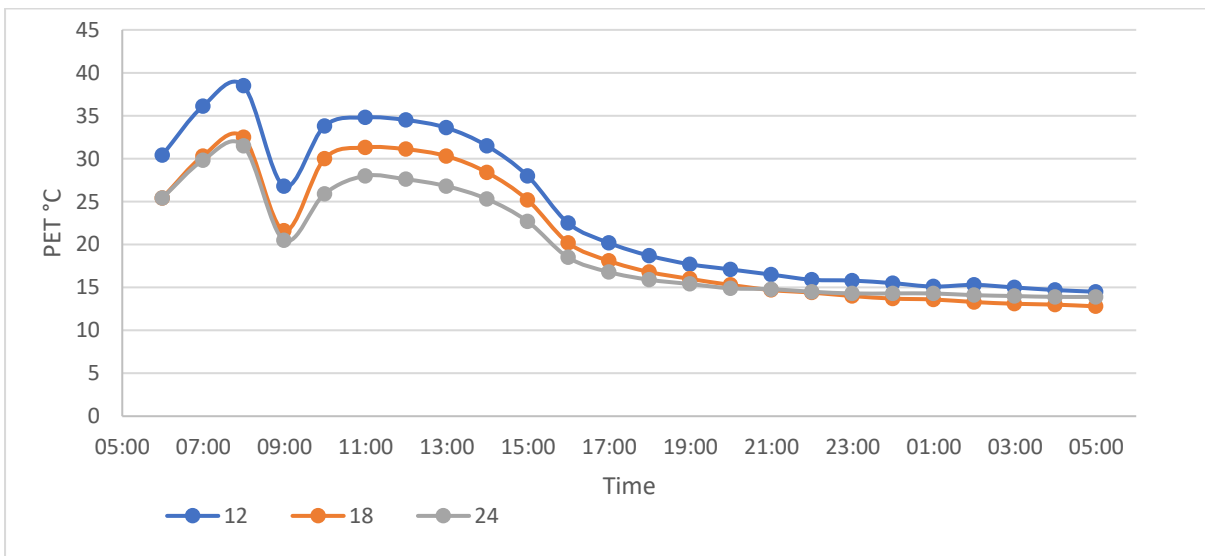


Figure 6.99. Receptor 7 PET levels for the height's scenarios.

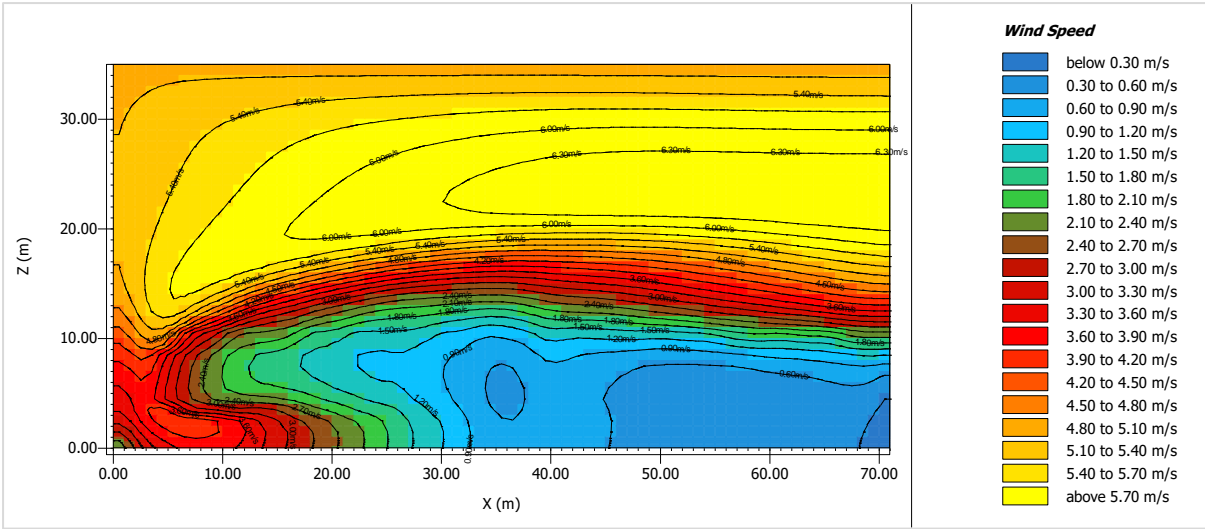


Figure 6.100. Wind speed cross-section through the receptors for scenario 12m high buildings.

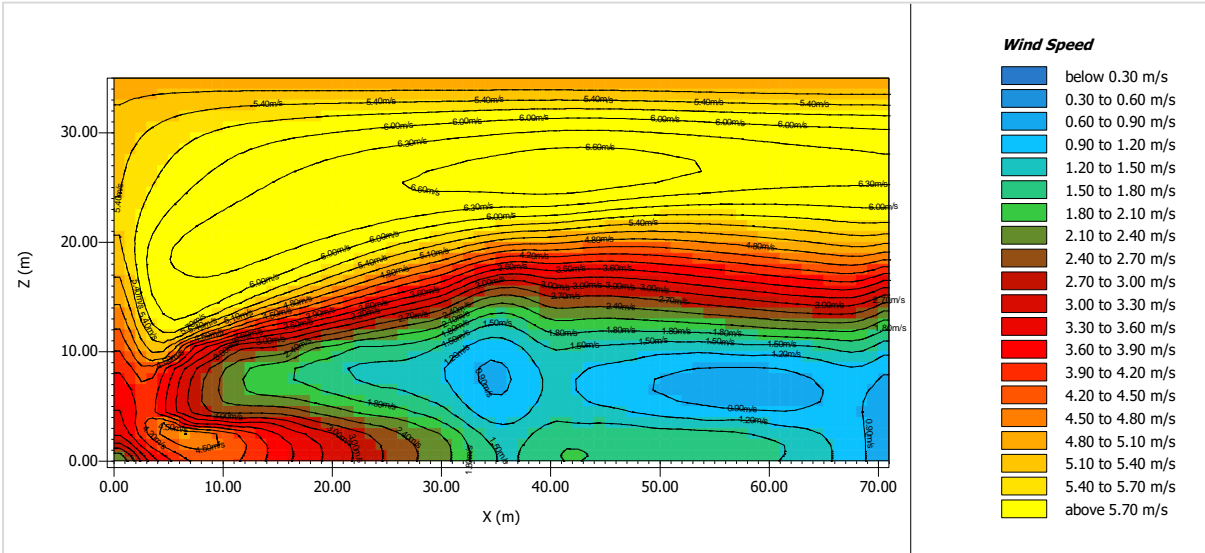


Figure 6.101. Wind speed cross-section through the receptors for scenario 18m high buildings.

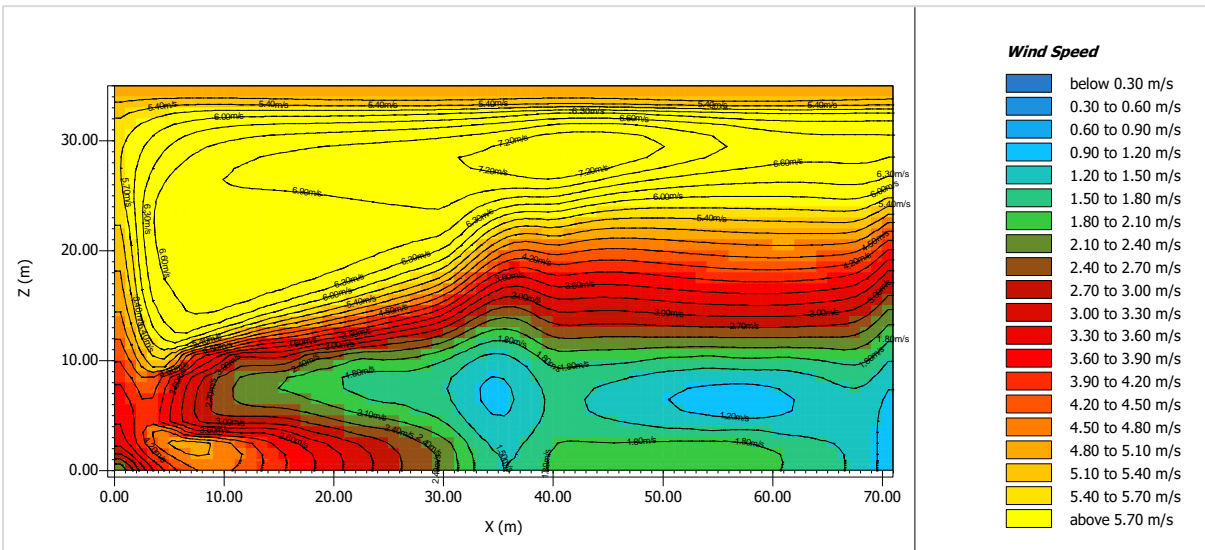


Figure 6.102. Wind speed cross-section through the receptors for scenario 24m high buildings.

Figures 6.100 to 6.102 show the wind speed cross-sections in the building height scenarios, and it is observed that wind speed is increased with the increase of buildings height. At the $x=30$ the wind speed is 1.2 m/s for the 12m scenario, 2.1 m/s for the 18m scenario and 2.4 m/s for the 24m scenario. This can be explained by the higher surface of the buildings that the wind profile effects. The wind is more constrained with higher buildings compared to shorter ones which, in turn, strengthens the wind tunnel effect that forms the channelling flow. Furthermore, with higher buildings heights the wind flow over the buildings tends to be greater, which creates higher negative pressure underneath it, and this pushes down the air underneath the main flow over the buildings and the trees which feeds the wind stream on the pedestrian's level. The downstream flow should accelerate between all the buildings compared to the mean wind speed due to venturi effect, however, in this case, the flow was obstructed by the trees in the passageway which caused the deacceleration. It should be noted that the stagnation point is higher in the vertical axis in the higher buildings, this also contributes to enhancing the wind speed inside the urban canyon.

6.16 TREE LEAF AREA DENSITY (LAD) AND ITS EFFECT ON PET AND WIND FLOW.

This section will discuss the different LAD of the vegetation added to the site. The site was kept at its original parameters with 12m high buildings and 9m gaps between the buildings. The trees were spread out along the same axis with the same geometry. The simulation process consisted of three scenarios with different LAD values for the trees. The first scenario's LAD was set to 0.5 m^{-1} , the second at 1.0 m^{-1} and the third at 1.5 m^{-1} . The meteorological factors were kept the same as the previous sections to test out the effect of different leaf area densities on the thermal stress on pedestrians as well as wind speed.

Figure 6.103 shows the PET results for the LAD analysis, and they show little to no change in the PET values, especially in the daytime when solar radiation was present. As discussed in previous sections, the PET has weighted parameters where the solar radiation holds the largest weight. The foliage of the trees as a geometrical shape was the same for the different scenarios so they cast the same shading to all the analysed receptors, and the different leaf area densities did not affect the casted shadows, and as a result the PET levels were not affected. The no trees scenario showed high wind speed values. However, the PET levels produced were high due to increased solar radiation with maximum PET increase of $24 \text{ }^{\circ}\text{C}$.

High leaf area density obstructs the wind flow, due to added surfaces that would drag the flow. Figure 6.104 shows the wind speed results for the three LAD simulated scenarios, the scenario where LAD was set to 0.5 m^{-1} showed higher wind speeds than the other two scenarios with 1.0 m^{-1} and 1.5 m^{-1} LAD. This is due to reduced resistance to the wind flow in the lower LAD trees. The no trees scenario showed an increase in wind speed with an average increase of 2.6 m/s due to the undisturbed flow of wind.

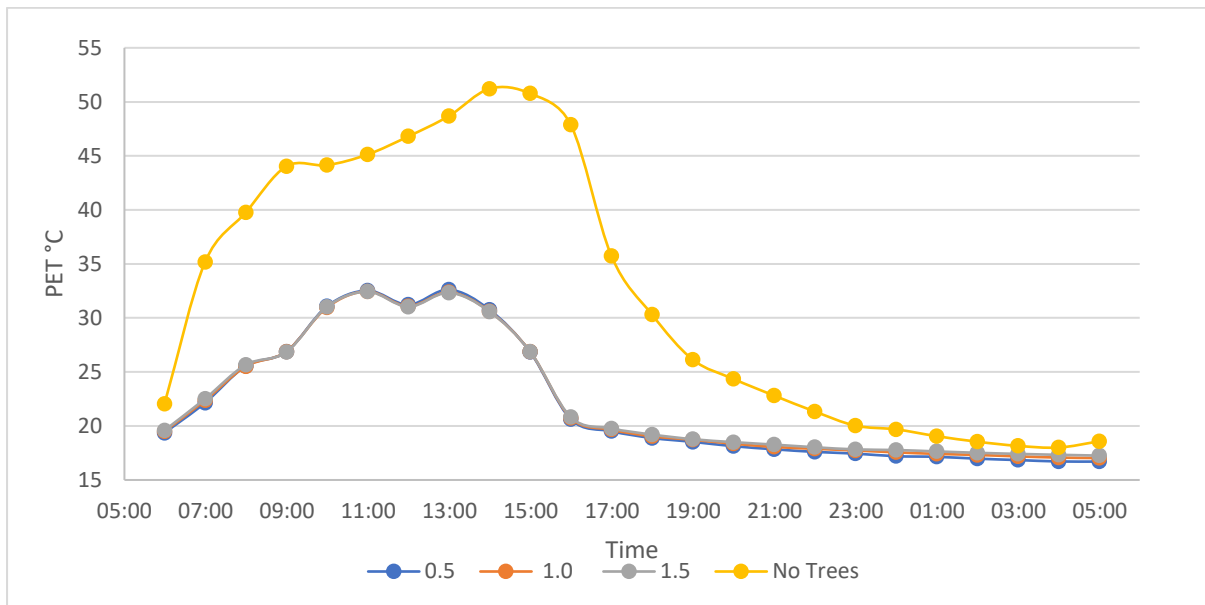


Figure 6.103. The averaged PET values for all the receptors in the different LAD scenarios.

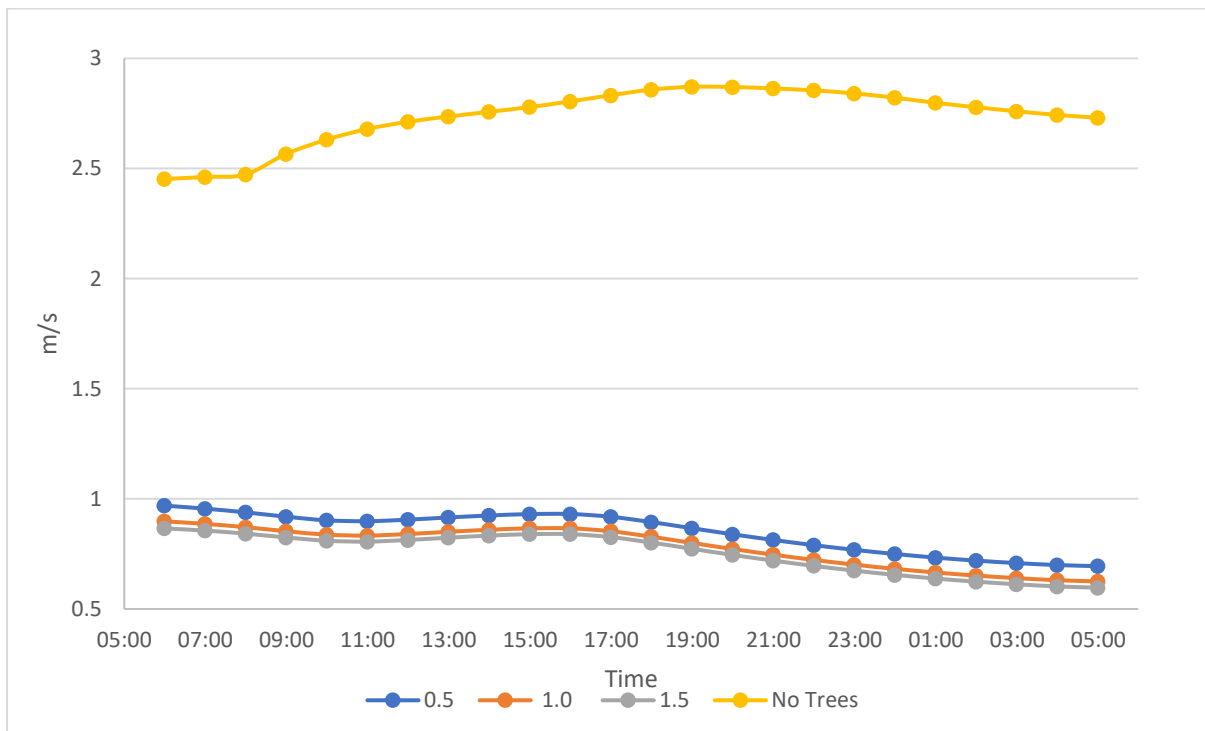


Figure 6.104. The averaged wind speed values for all the receptors in the different LAD scenarios.

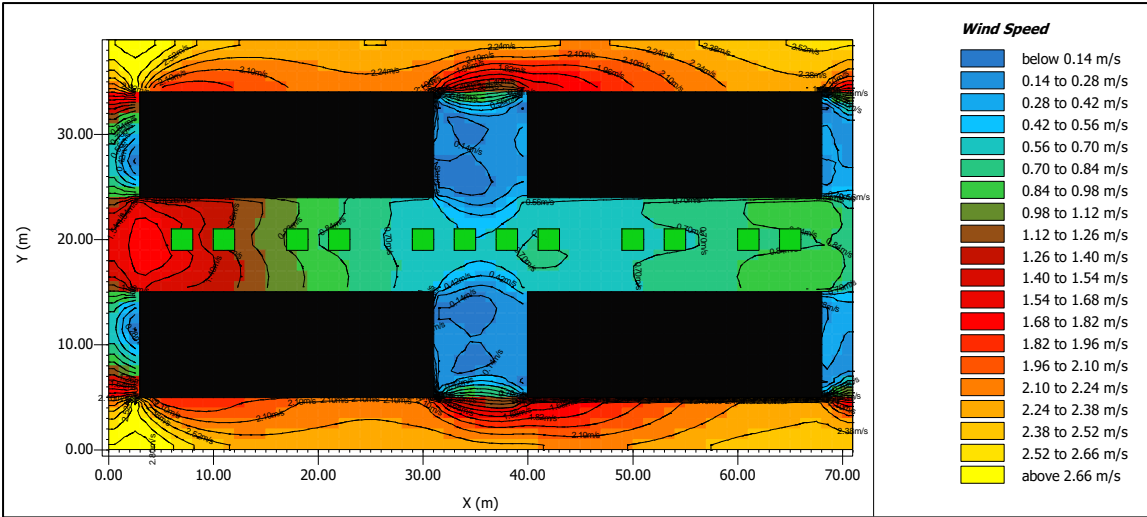


Figure 6.105. Wind speed plan section for the 0.5 m⁻¹ LAD scenario.

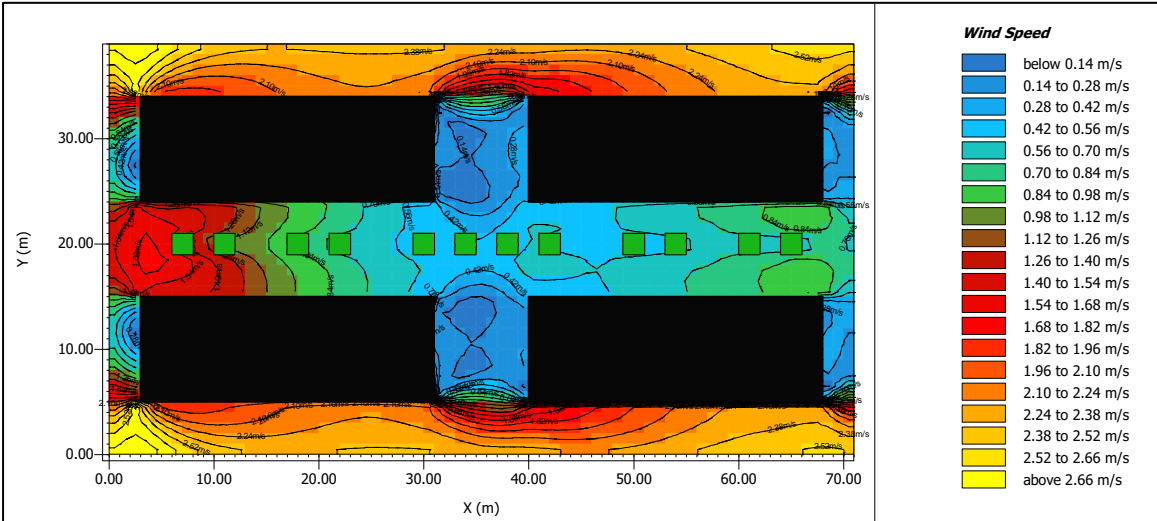


Figure 6.106. Wind speed plan section for the 1.0 m⁻¹ LAD scenario.

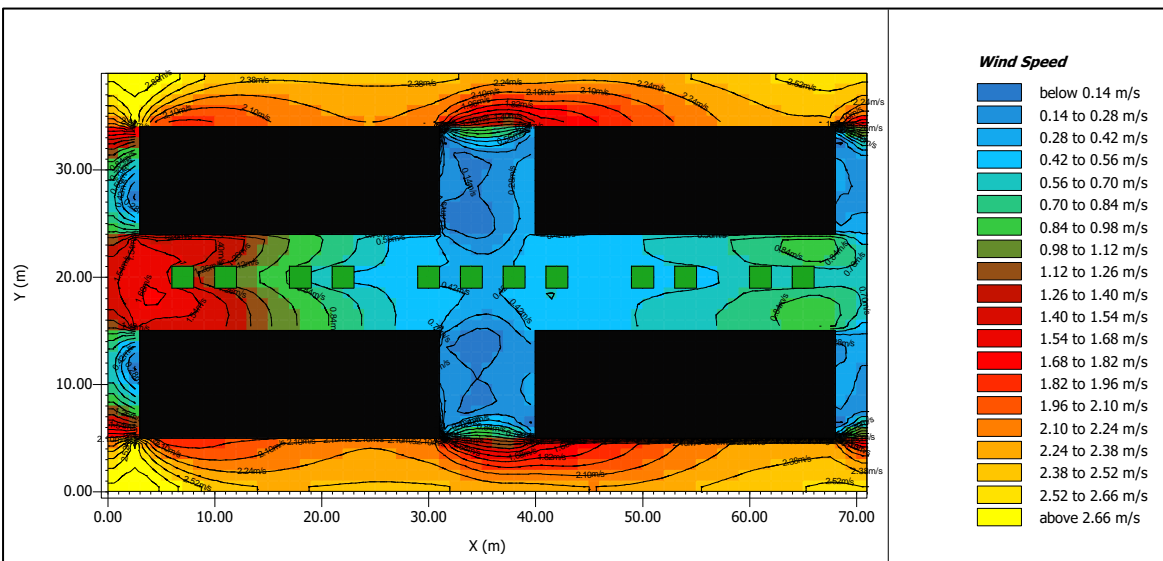


Figure 6.107. Wind speed plan section for the 1.5 m⁻¹ LAD scenario.

Figures 6.105 – 6.107 show the plan sections for the site and display the wind speed map at the pedestrians' level for all the scenarios. As the wind flow approaches the left of the site it squeezes through the buildings and gets obstructed by the trees, and this occurs in the three scenarios. However, there is a shift that can be noticed in wind speed values when LAD is higher, in Figure 6.107 at $x=14$ $y=20$, the wind speed contour lines indicate that the wind speed values are from 1.12 - 1.26 m/s, while in Figure 6.105 and 6.106, for the same coordinates, the values are 0.98 - 1.1 m/s.

The tunnel effect is a phenomenon that occurs when an approaching wind flow squeezes through a small gap between buildings where wind speed is accelerated, which creates the channelling flow. In this case, the wind flow is squeezed between the buildings from the left, but it is immediately hit by the trees which causes the deacceleration. Another contributing factor to the deacceleration is the gap between the row of buildings, as it acts as a diffuser where tunnel effect no longer exists, and the flow is at its lowest speed.

The flow continues through the second segment of the site after passing alongside the gap between the row buildings, and the flow then squeezes through and a tunnel effect is formed. It is noticed that despite the existence of obstacles (trees) the wind flow speed is accelerated, and this might be explained by the open space after the tunnel ends where the main flow of the site regathers and flow in the approaching wind directions. This would influence the wind inside the wind tunnel affected area in the second segment and from a pull force that would accelerate the flow speed.

6.17 SITE ORIENTATION AND ITS EFFECT ON PET AND WIND FLOW.

As in the previous analysis, the site parameters were kept the same for both the geometrical and meteorological parameters, with the base design being at 12-metre high buildings, a pathway width at 9 metres and a tree LAD at 1.5 m^{-1} . The original scenario will be compared against a 90° counter-clockwise off north rotated scenario. The results should display how wind flow is affected by the geometry change in the site as well as the PET values due to the change of geometry shading.

Figure 6.108 shows the averaged PET values for both orientation scenarios. PET levels show a significant drop in the original orientation where the long edge of the buildings is facing the south. The 90° orientation shifted the shading cast from the buildings away from the pathway

where in the original orientation it shaded the pathway. Figure 6.109 shows how the sun path affects the shaded areas when the entire site is rotated. In the case of the pathway directed on the (north-south) axis, the mid-day sun is shining through the pathway with high values of direct sun radiation, whereas when the pathway is oriented on the (west-east) axis the mid-day sun is obstructed by the long edge of the buildings. The 45° orientation produced better PET results when compared to the 90° orientation due to longer shading periods from the trees and buildings. However, the original orientation had lower PET values with a maximum decrease of 5 °C due to the sun path and trees' placement where it provided longer shaded durations periods of time.

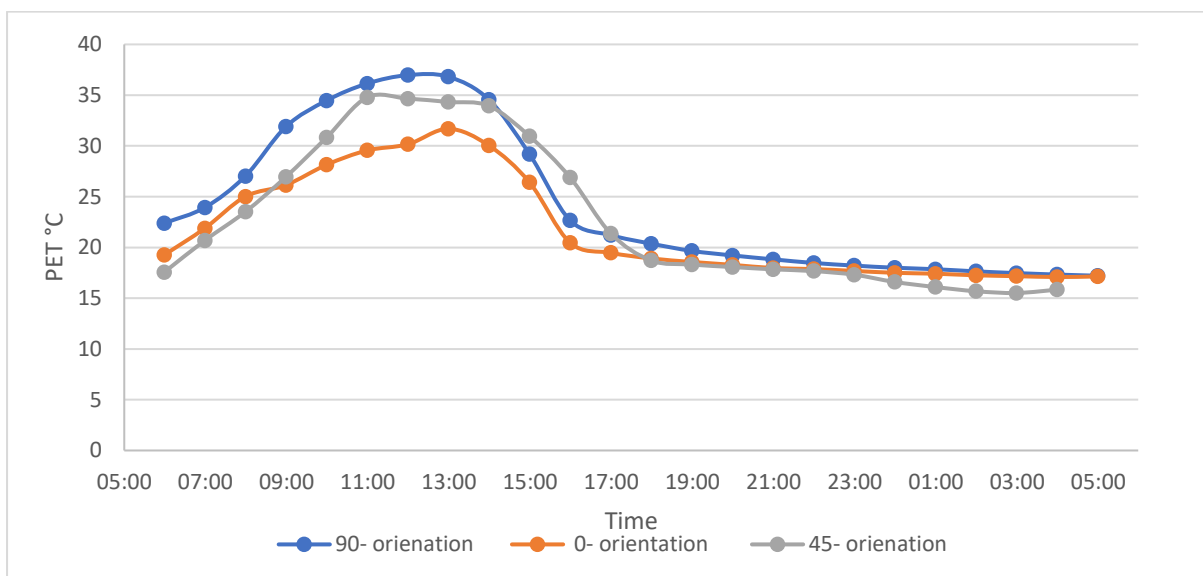


Figure 6.108. Average PET value for the scenario wind direction (West) and scenario with wind direction (North).

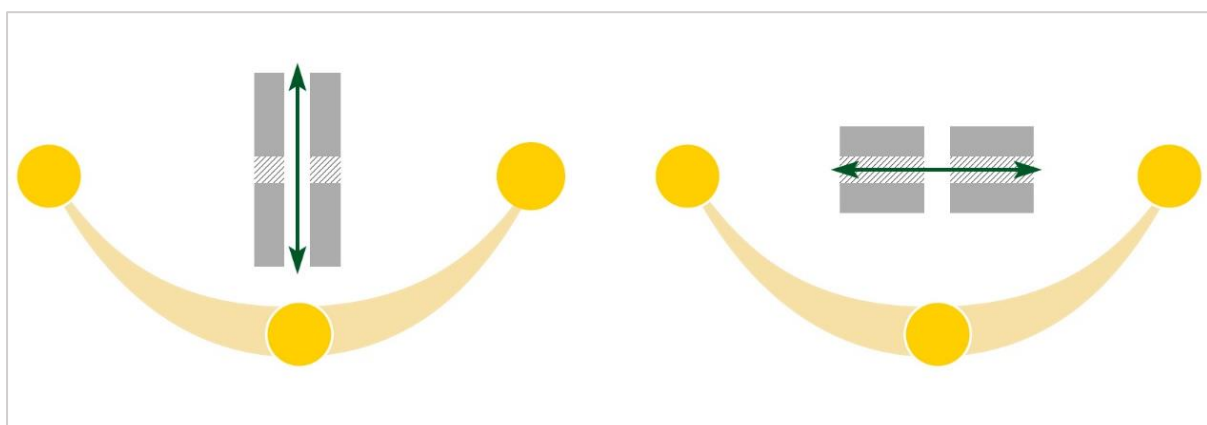


Figure 6.109. Sun path for the different orientation scenarios.

Figure 6.110 shows the differences between the individual receptor along the axis of the pathway for both of the scenarios. The graph shows that most of the data are above the 0 axis which means that scenario, where the site is rotated, had higher PET values, with a

difference as high as 21.8°C seen in receptor 1 in Figure 6.112. Some receptors behaved better in the 90° rotated scenario due to the position of the receptor on the east end of the pathway. As seen in receptor 7, in the early hours of the morning in the original orientation, the receptor received high direct solar radiation from the east whereas in the second scenario the 90° angle orientation shielded the receptor from the morning and evening sun.

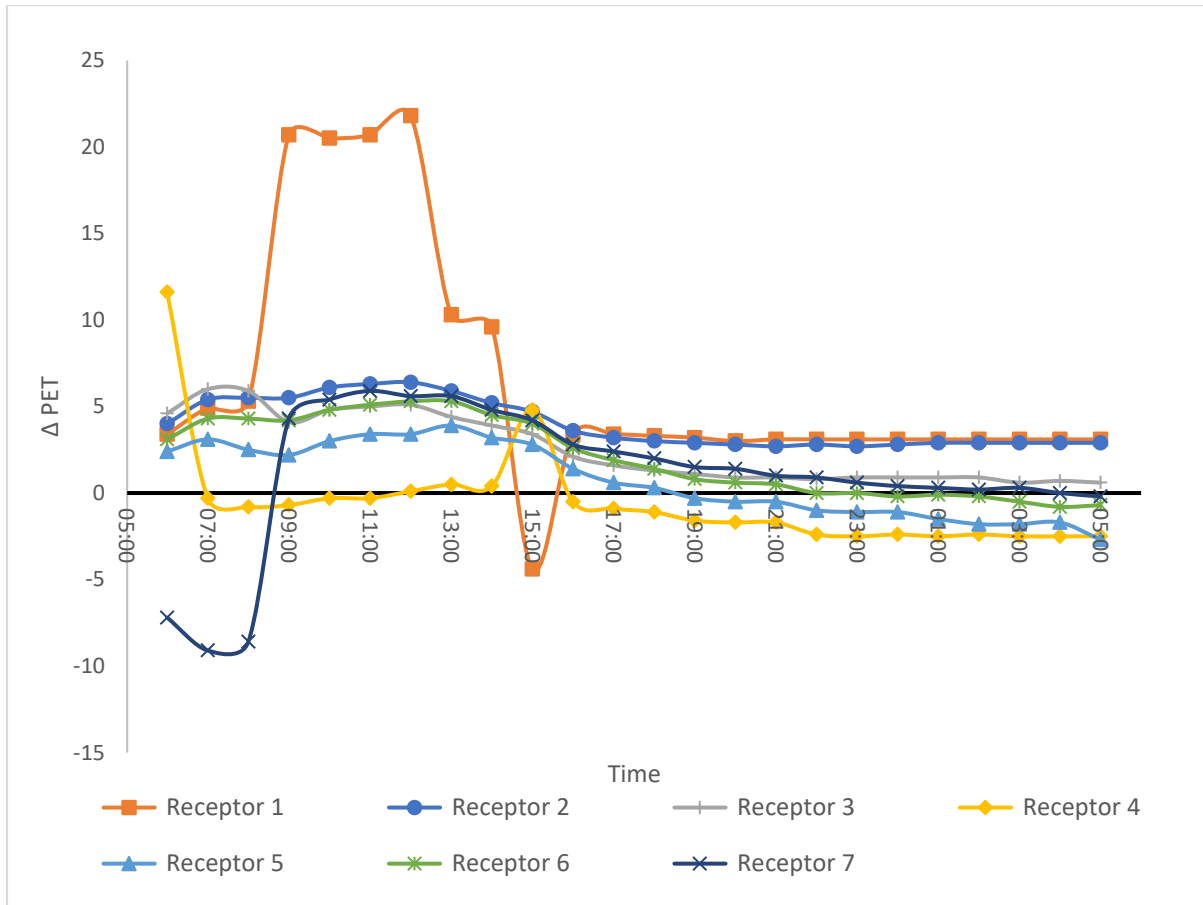


Figure 6.110. PET differences for individual receptors.

The wind approaching flow changed for the buildings with the change of orientation, and the inlet to the pathway shifted from the long pathway axis to the small gap between the buildings. This has changed the overall wind quality inside the residential plot. Figure 6.111 shows the original orientation wind flow, where wind speed inside the pathway was strong enough to discard any pollutants and disperse any lingering unwanted particles. The gap between the buildings suffers from slow wind flow where pollutants can be sucked into the two vortices formed and lingers there. Figure 6.112 shows the 90° orientation off north counter-clockwise scenario. The wind flow inlet inside the plot is from the gap between the buildings, and for that an increase in wind speed is noticed compared to the previous

scenario. However, the pathway wind speed was decreased drastically compared to the original scenario which lowers the wind quality and increases pollutants.

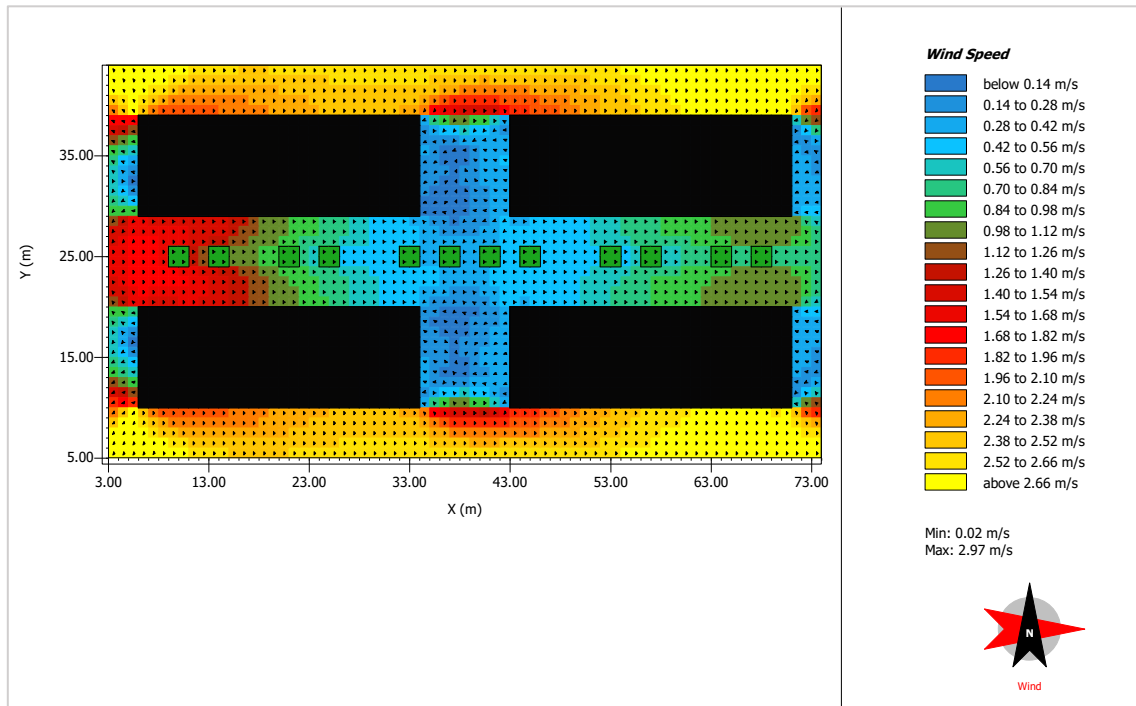


Figure 6.111. wind flow inside the original orientation.

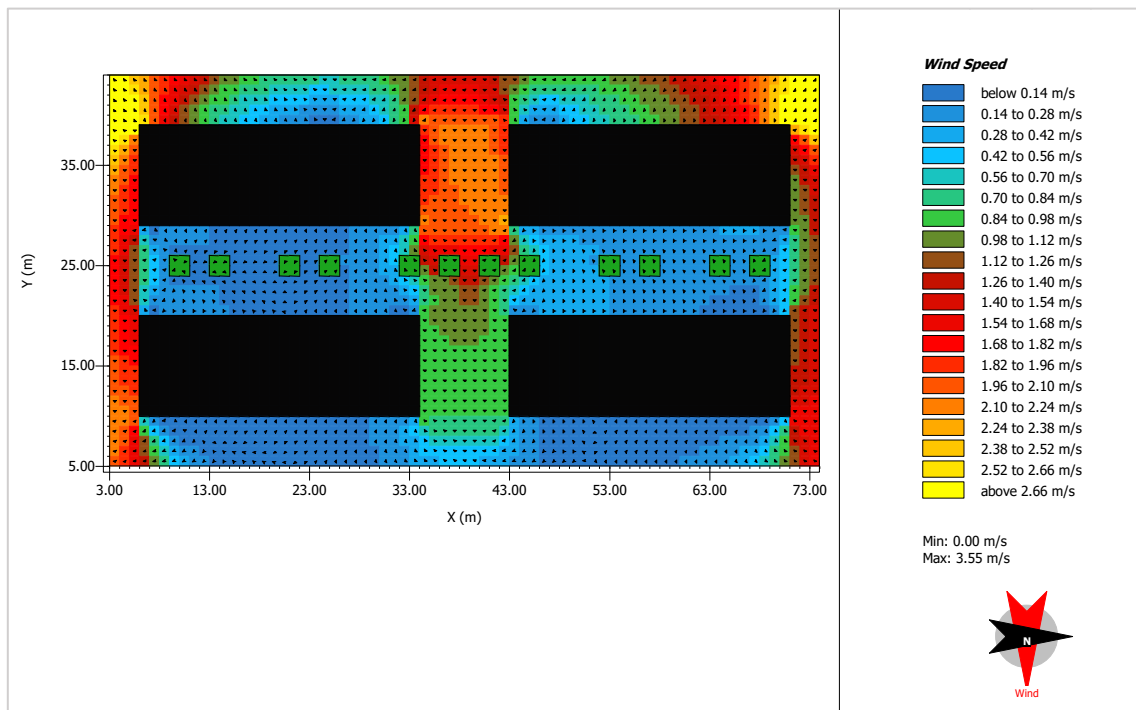


Figure 6.112. wind flow inside the 90-degree orientation off north.

Figure 6.113 shows the distribution of wind speed inside the plot for the 90° orientation off north scenario, and the chart shows the high count for low wind speed which can be expected

due to the direction of the approaching wind for this scenario. It should be noted that resulting wind speed for values of 0.4 m/s or less cover more than 55% of the plot whereas the mid wind speed values only cover about 25%.

Figure 6.114 shows the wind speed distribution inside the plot for the original scenario. Compared to the 90° scenario the wind speed in the original orientation did not reach as high a wind speed as the 90° oriented one. This is due to the smaller gap that wind squeezing through will strengthen due to the wind tunnel effect in that area. However, wind quality shows an increase in this scenario due to higher areas with mid-speed wind and less areas with wind speed of 0.4 m/s or less.

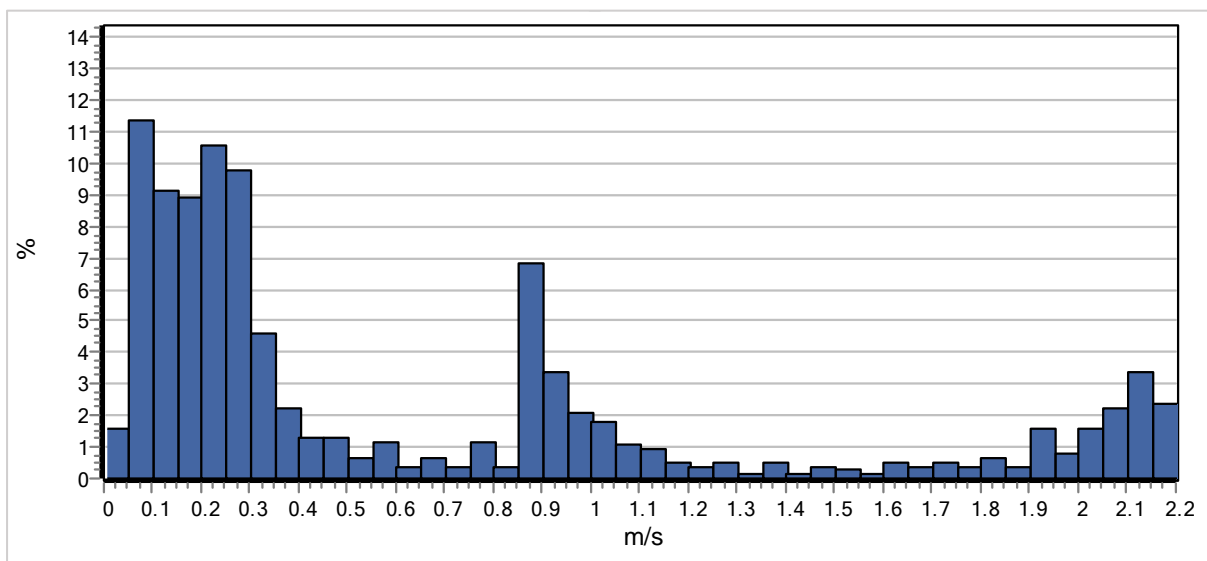


Figure 6.113. Wind speed distribution for the 90-degree orientation off north scenario.

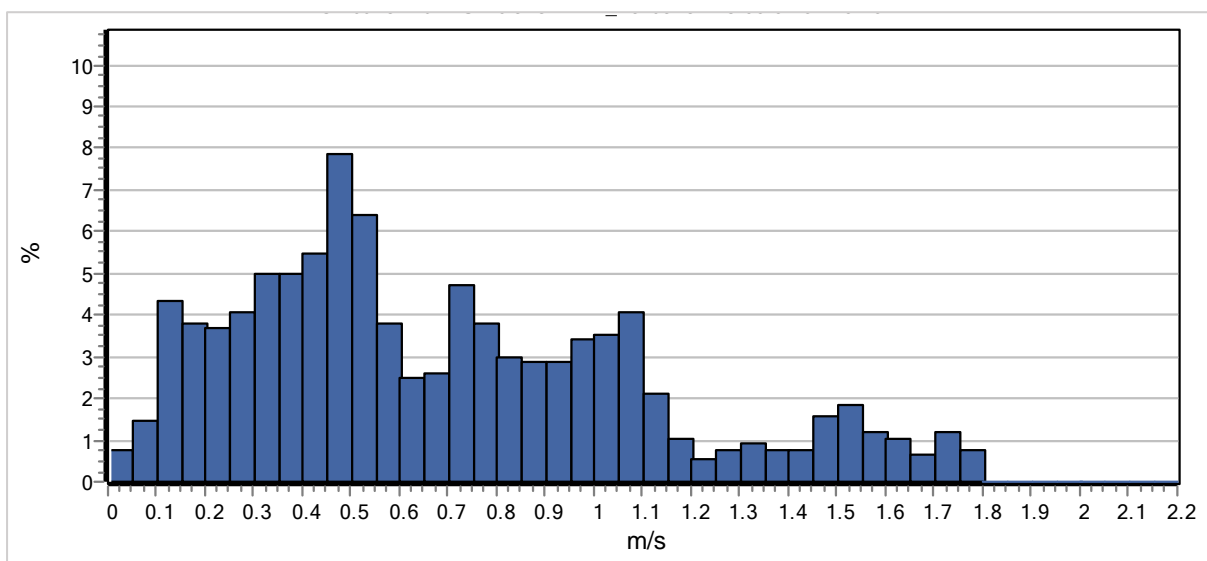


Figure 6.114. Wind speed distribution for the original orientation scenario.

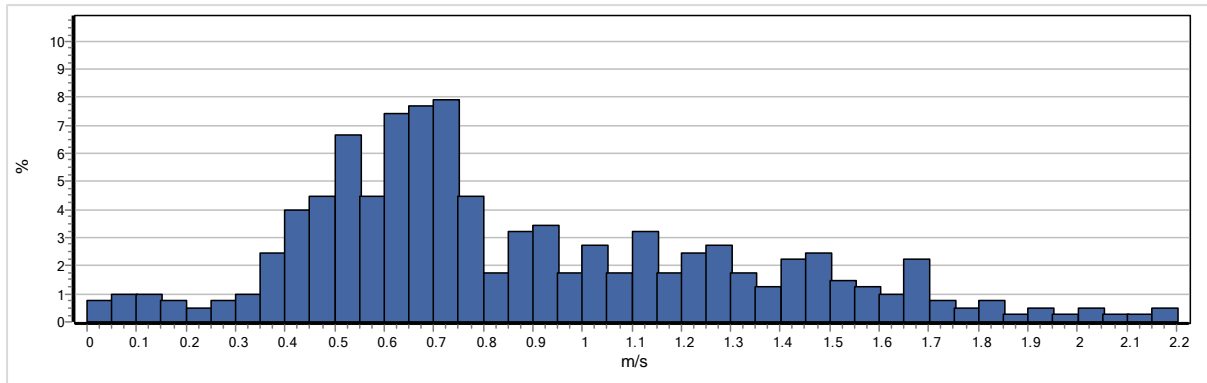


Figure 6.115. Wind speed distribution for the 45-degree orientation off north scenario.

Figure 6.113 shows the distribution of wind speed inside the plot for the 45° orientation off north scenario. Compared to the previous scenarios, the 45° orientation produced higher wind speed values across the plot, and 8% of area that recorded wind speed of 0.4 m/s or less. This can be explained by the helical flow created inside the canyon which produced an even flow of wind which raised the average wind speed values.

Scenarios 90° and the original resulted in problematic areas where the wind speed was very low, and this was caused by the inlet angle at which the wind was approaching the site. Both scenarios generated channelling flows due to the flow being parallel to the edges of the building which, in turn, caused high pressure in these areas with high wind speed that restricted the flow of air to the rest of the plot. The best solution to solve this flow issue is to orient the design to allow the wind flow to enter the plot in a 30-45° angle as this will create a helical flow inside the pathways that will spread out to the rest of the plot with even mid wind speed to ensure good particle dispersion and good air quality.

6.18 CONCLUSION

The analysis moved from the macro-scale analysis to a smaller segment of the layouts, which included the buildings cluster analysis and the micro buildings cluster analysis. The buildings cluster analysis (the compounds) consisted of two main design proposal, the first proposal was based on the wind flow transition zones and the second proposal was based on environmentally responsible design with buildings layout that reinforced wind flow. Both were simulated under the same conditions and the results showed that proposal-1 produced higher PET values than proposal-2 due to closed off areas where air movement was restricted and increased solar access in the south-facing facades. Directing the main pathway in the approaching wind direction has increased the wind speed values, which helped in reducing

the PET values, especially during the hours of night through night-flush effect. Adding trees to the design helped in lowering the PET values through reducing the solar access by shading the receptors. However, the effectiveness of trees in regard to reducing the PET values is limited beyond their shadow radius. Additionally, placing the trees in one line rather in a scattered manner and the height of the foliage contributed to keeping the wind flow at an acceptable level.

The analysis moves forward to the first modification on the proposal that produced the best PET with general horizontal shading devices that were placed in the problematic areas. The results showed a PET levels improvement when compared to the non-shaded design, where the maximum PET level recorded at 02:00 of 55 °C was reduced to 43 °C. The receptors showed an average decrease in the PET values of 7.5°C, a maximum reduction of 13.4°C, and a minimum reduction of 0.6°C throughout the day.

The buildings cluster micro analysis investigated the four main modifications on the design and studied the different effects each of them had on PET and wind flow. The first modification that was studied was the gap between the row buildings and how having it roofed and connected to the buildings affected the overall PET and wind flow of the site. The results showed that PET increased slightly when the gap was roofed with a maximum increase of 2.1 °C due to the increased reflected solar radiation inside the tunnel with an average increase throughout the day of 24.8 W/m². However, the wind flow was enhanced when the gap was roofed because the wind tunnel effect was stronger as the flow was constricted by four sides rather than three, with a maximum increase of 0.15 m/s. It should be noted that at receptor 8 in both cases the area was shaded by the adjacent buildings. However, receptor 9 showed an increase in direct solar radiation in the unroofed case from 09:00 -12:00, this is because the receptor lacked the shading from the trees from the backside of the buildings as it represents the southern far end of the compound design. The increase in PET was recorded at a maximum of 15 °C.

The buildings height modification showed that when increasing the height of the buildings the wind flow was strengthened at the pedestrian level. At X=30 in the vertical section of the canyon, the wind speed was observed to be 1.2 m/s for the 12-meters scenario, 2.1 m/s for the 18-meters scenario and 2.4 m/s for the 24-meters scenario, the effect of enhancing the wind speed is stronger between scenarios 12m and 18m with a 75% increase in wind speed,

while the effect is weaker between scenarios 18m and 24m with only a 14.2% increase in wind speed. The PET values showed a significant drop with higher buildings, where a 3.5 °C difference is seen between the 6 meters in height difference between the scenarios. The increased height of buildings produced more shading hours as well as better wind speed values which contributed to lowering the PET values.

As for the LAD analysis, the results showed that with different LAD (0.5,1.0,1.5) the PET was not affected due to the unaffected shading in the area as the foliage of the trees did not change. However, when studying the canyon without any vegetation addition the PET levels showed a significant increase in values with maximum PET increase of 24 °C. The wind flow was at its strongest when LAD was at its lowest, showing less resistance to airflow and allowing for better ventilation. When LAD was set to 0.5 at (X=14,Y=20), the wind speed values indicated that the wind speed is between (1.12 - 1.26) m/s, while in LAD 1.0 and 1.5, for the same coordinates, the values are between 0.98 - 1.1 m/s, which shows a 14.5% reduction in wind speed values. It should be noted that the gap between the buildings acted as a diffuser for wind flow and consequently lowered the wind speed values as the wind tunnel effect near the gaps was weak. All in all, the 14.5% change in wind speed was not high enough to affect the PET levels at the pedestrians' level.

The last modification tested in the microanalysis was the orientation of the site, changing the orientation resulted in the change of the approaching wind direction and the sun path, this changed the approaching wind direction from the long pathway to the short axis that goes through the gap between the row buildings. This resulted in high wind speed along this axis but resulted in a poorly ventilated area in the long pathway. The results show in the 90° orientation scenario that the designed plot had 55% of area with wind speed values of 0.4 m/s or less while the original orientation had only 35% of area under 0.4 m/s wind speed and the 45° scenario resulted in 8% area of low wind speed. As for the solar radiation, the site was exposed to more sun radiation when the orientation changed to 90° and 45°, this was at its maximum at noon where there was no shading from the buildings affecting the long pathway, which resulted in high PET levels. The averaged PET values showed a maximum increase of 7.5 °C at 12:00 between the original orientation and the 90° scenario.

Chapter 7 Conclusion and Recommendations

Content

- 7.1 Introduction
- 7.2 Main conclusions
- 7.3 Research implications for future work and recommendations

7.1 INTRODUCTION

This chapter discusses the results of the research. The main drive in conducting this study was to improve the urban design practices by directing it to a more thermally comfortable approach. As the city of Amman is being expanded to address the overpopulation concerns, the research offers an urban geometry study that analysed the effect of urban design choices on the thermal stress, and studied the factors that affect the thermal stress on pedestrians as well as the airflow behaviour in urban settings. The conclusions on the urban geometry adjustments to enhance the outdoor thermal comfort and the proposed future work are summarised in this chapter.

7.2 MAIN CONCLUSIONS

This research assessed the urban geometry effects on the pedestrian microclimate and thermal comfort in a proposed residential area in the semi-arid climate of Amman. It evaluated the optimisations applied to the proposed design in terms of thermal comfort on pedestrian's level and wind flow. The following conclusions are derived from the research findings to fulfil the research objectives.

Objective 1 (Understanding the case study of Amman in terms of urban context and climatic features - Chapter 1).

Chapter One discussed the main features concerning Amman; this included the climate characteristics, urban context, and the development plans. The main conclusions that were derived from the literature were:

- Air temperatures are high in the summer season ranging between 23°C to 32.1°C compared to the rest of the year.
- Summers are very dry with rainfall concentrated between the months of December to February.
- Jordan has many variations of topography where Amman is located in the upland plateau region, which gives it a milder climate compared to the desert region and the rift regions.
- The wind speed values are moderate in Amman, ranging between 1.7 m/s to 7.3 m/s.
- Amman suffers from overpopulation that affects the urban layout and the general health of the urban spaces.

- Amman's history dictated the urban layout with rapid growth and unplanned districts.
- Amman's urban layout is influenced by the British urban ideology e.g. the focus on satellite cities rather than suburban areas.
- Amman's future expansion plans are towards the south of Amman to alleviate the overpopulation problem, and this was the main reason for choosing the location of the proposed design.

Urban planners' recommendations:

Planners should make initial consideration regarding the climatic parameters in Amman, this includes the predominant wind direction, wind speed and solar radiation throughout the year in different seasons, the use of EPW files as shown in figure 7.1 is very beneficial in collecting and studying the microclimatic parameters of Amman. Additional recommendation regarding the design features will be further discussed in the following objectives. In regards to site selection as stated in the ligature it is advisable to consider locations on the outskirts of Amman to relief the overpopulation and high traffic issues in which Amman suffers from, please refer to the expansion proposals cited in Potter, et al., 2009.

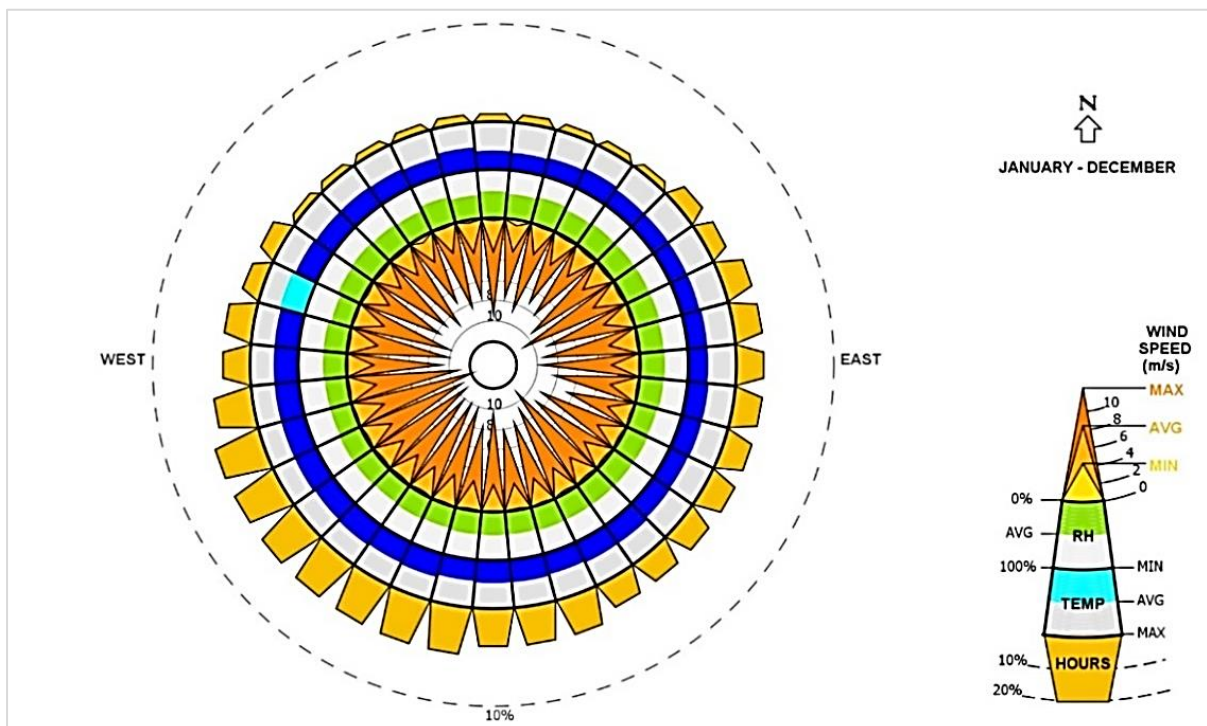


Figure 7.1. Amman's wind rose. Source: Meteonorm.

Objective 2 (Understanding the main factors affecting the outdoor thermal comfort for pedestrians - Chapter 2).

Chapter Two discussed the present literature on outdoor thermal comfort, outlining the main factors affecting the pedestrians' microclimate and thermal stress. The following are the main notes derived from the literature:

- It highlighted the main reasons why thermal stress is high in public spaces in Amman, e.g. high population, insufficient number of public parks, and compact urban design.
- It reviewed the literature relating to thermal comfort in the context of an indoor and an outdoor setting and outlined the main models used in each setting.
- It reviewed the previous studies relating to outdoor thermal comfort, citing the background and the optimisation that the thermal indices went through to the present day.
- It reviewed the most suitable outdoor thermal comfort indices that have been used in the previous studies and outlined their advantages and disadvantages.
- It outlined the main factors affecting the outdoor thermal comfort, and this included the air temperature, relative humidity, wind speed, and mean radiant temperature.
- It reviewed the studies related to the urban microclimate in Jordan and outlined the gaps in the current state of urban microclimate research in Jordan.

Objective 3 (Understanding and evaluating the effect of urban canyon's configurations on airflow - Chapter 3).

Chapter Three evaluated the airflow behaviour in the urban context, and it reviewed the urban setting in terms of isolated buildings, an array of buildings, urban canyons and street intersections and their effect on airflow patterns. The following was outlined:

- In isolated buildings:
 - When the approaching airflow is perpendicular to the windward face of the building, a part of the flow is displaced due to the positive pressure on the windward surface of the building, the rest of the flow spreads vertically and horizontally, as well as above and around the building at the stagnation point. Vortices are created around and

above the building due to negative pressure zones. At the backside of the buildings, a cavity zone is formed due to the separation flow creating a suction zone.

- When the approaching airflow is directed at 45° , two rotating streams are formed at the two edges of the roof where they flow down the building to join the downstream into the wake. This results in a smaller cavity zone and faster flow in the wake zone.
- The cavity zone is responsible for the downwash phenomenon, where pollutants get sucked from the surrounding separation streams into the cavity.
- In arrayed buildings:
 - The airflow is affected when the wake of the flow for two buildings are overlapping; this results in three cases based on the distance between the buildings. The first case is when H/W is less than 0.35, where the wakes do not overlap, and the buildings are assumed as isolated. The second case is when H/W is less than 0.65 but greater than 0.35, and this results in wakes overlapping. The third case is when H/W is greater than 0.65, where the buildings are too close, and the flow skips over the roofs.
- In street canyons:
 - The airflow is channelled along the canyon's length when the approaching wind angle is between 0° and 30° . The flow is characterised with strong wind speed compared to other approaching angles.
 - When the approaching wind angle is larger than 30° , the flow is a product of a superposition of the channelling flow and the cross-canyon vortex. The resultant flow is described as a helical flow that spirals down the canyon length.
 - When the approaching wind is perpendicular to the street canyon, the flow skips the canyon at the roof level, and this creates a vortex in the cavity zone in the leeward face of the buildings reinforced with the downwind from the next building windward face.
- In street intersections:
 - When the approaching wind is directed at an angle of 0° in one of the street intersection's axes, the flow is channelled along the street, and some of the flow

escapes to the perpendicular streets and form vortices that rotate on the opposite direction of the main flow.

- When the approaching wind is directed at an angle of 15° , the channelling flow is a bit weakened, and some of it is directed to the perpendicular street and a helical flow starts to form.
- When the approaching wind is directed at an angle of 30° , the airflow in both of the axis of the streets is a helical flow, with a stronger flow in the streets closer to the attacking angle.
- When the approaching wind is directed at an angle of 45° , a helical flow is formed in both axis streets of similar strengths. A conveyor belt is created in the middle of the intersection that flows up and over the roof.

Objective 4 (Understanding the context of the urban environment and its implications on microclimatic parameters and thermal stress - Chapter 3).

Chapter Four also discussed the configuration of the urban canyon and how it affects the thermal stress. This included the orientation, vegetation addition, Sky View Factor and H/W.

The following was outlined:

- The orientation of the urban canyon affects the amount of solar radiation and wind speed reaching the pedestrian level. The (West-East) orientation was found to have higher air temperature values due to higher solar access.
- High Sky View Factor (SVF) can provide a faster cooling effect when compared to low SVF.
- The addition of vegetation can improve the thermal stress levels as it provided shading and was found most useful in wide canyons. The Leaf Area Index (LAI) was found to be the most influential factor in reducing the thermal stress.
- Reducing the width of the canyon can reduce solar access. However, it also reduces the cooling effect at night.

The chapter also discussed the Computational Fluid Dynamics (CFD) and the Energy Balance Modelling (EBM) approaches as a method of studying the urban microclimate, outlining the advantages and disadvantages of both methods. It also lists the different tools that have been used in the recent research to study the urban microclimate.

Objective 5 (evaluating and assessing ENVI-met, including the sensitivity to parameters' change and calibration testing by comparing the results to observed data - Chapter 5).

Chapter Five discussed the CFD modelling software (ENVI-met) that was used in this study, and the first section outlined the equations and models used to solve different variables inside the urban environment. The second section validated ENVI-met results by calibration tests and sensitivity to change of variables tests.

Section two validated ENVI-met's and the following were concluded:

- The sensitivity test showed that ENVI-met is sensitive to the change of the following variables (Wind speed, relative humidity, and grid size). However, it showed a low effect on the change of albedo of ground and buildings materials.
- The grid size analysis showed that 2x2 grid resolution is best suited to be used in microscale urban simulations as it produced accurate results with less computational time.
- The air temperature calibration test showed that ENVI-met simulates air temperature with a reasonable accuracy, with an index of agreement of 0.886 and 0.89, and Pearson correlation coefficient of 0.933 and 0.934.
- The relative humidity calibration test showed that ENVI-met simulates relative humidity with unsatisfactory results, and the variation of relative humidity through the day is small compared to the observed data, with an index of agreement of 0.646 and 0.688, and Pearson correlation coefficient of 0.743 and 0.768.
- The wind speed calibration test showed that ENVI-met simulates wind speed with reasonable accuracy. The trend line for the observed data produced a good correlation with the simulated data.





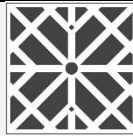




















Objective 6 (Evaluating and assessing the street grid layouts in terms of wind flow and thermal stress – Chapter 6, section 1)

Chapter Six discussed the results of the study. The chapter is divided into three sections, where chapter one discussed the street grid layouts and their effects on the airflow and thermal stress. The study was conducted by analysing five different street’s layouts through CFD numerical modelling, the analysis for each layout was conducted in two different wind directions (0° and 45° counter clockwise from north) and the results were compared in terms of wind speed distribution and PET levels. Findings can be summarised as follows:

- The results showed a significant improvement in wind speed in all layouts when the approaching wind was directed at 45° counter clockwise from the north due to the creation of helical flows inside the layouts rather than the channelling flow that was created in the 0° case.
- The change of PET levels varied between the layouts when they were simulated in a different orientation, this was because the shading patterns changed with the orientation. Though the wind speed was higher in the 45° case, it did not reduce the PET levels in a significant manner because solar radiation was present in some layouts.

The wind speed distribution was analysed for all the layouts, where the layouts were labelled from A to E and numbered 1 for 45° and 2 for 0°. The data were filtered based on the area percentage of low wind speed distribution 0 - 0.5 m/s. Table 7.1 summarises the area percentage of low wind speed in each layout.

Table 7.1. Area percentage of the areas that are receiving less than 0.5m/s of wind speed at 1.5m height.

LAYOUTS	A		B		C		D		E	
ICONS										
NORTH DIRECTION										
WIND DIRECTION SCENARIOS										
	A.1	A.2	B.1	B.2	C.1	C.2	D.1	D.2	E.1	E.2
AREA PERCENTAGE	6%	36%	8%	29%	9%	18%	52%	68%	42%	60%

The highest wind speed values were found in the classic grid layout A, with 6% of area having low wind speeds in the 45° case and 36% of the area in the 0° case. The lowest wind speed values were found in the radial street layout D, with 52% of area having low wind speed in the 45° case and 68% of the area in the 0° case. This is explained by the shape of the streets, where airflow moves unobstructed in straight streets when compared to curved ones.

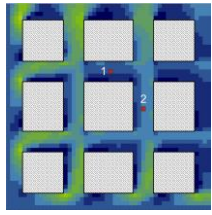
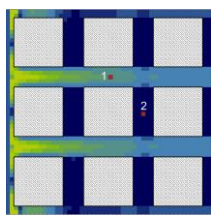
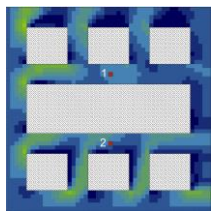
The averaged PET values in Table 7.2 do not convey how well the layouts present their comfort level, but instead they show how in the same layout the different orientations shift the comfort levels; scenarios 1 and 2. An increase in PET values is noticed in all of the layouts in scenario 2, this is caused by the (North-South) orientation streets that receive the highest sun radiation throughout the day.

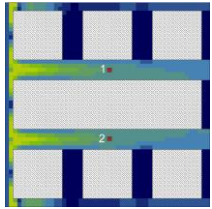
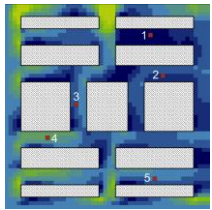
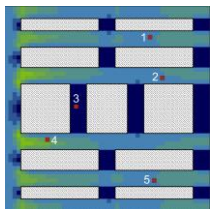
Table 7.2. Averaged PET values for all layouts.

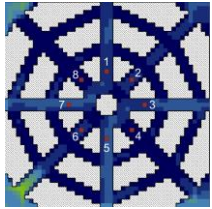
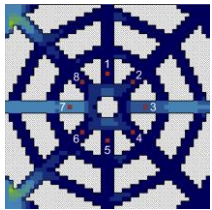
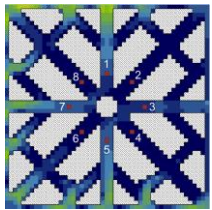
LAYOUTS	A		B		C		D		E	
ICONS										
NORTH DIRECTION										
WIND DIRECTION										
SCENARIOS	A.1	A.2	B.1	B.2	C.1	C.2	D.1	D.2	E.1	E.2
PET	26.1	27.2	26.6	27.7	26.7	28.3	28.2	29.3	28.4	29.6

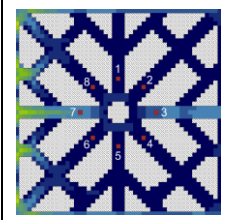
Recommendations for urban planners:

Table 7.3. Recommendations for layouts A, B, C, D and E.

Illustration of the grid layouts	Main results of the analysis	Recommendation for urban planners
Layout A		
A.1		
	<ul style="list-style-type: none"> - 6% of the area recorded wind speed values between (0-0.5) m/s. - The average PET value was 26.1 °C for the entire plot. - The approaching wind was displaced at the edge of the buildings creating a helical flow in the streets. 	<ul style="list-style-type: none"> - The orientation of the plot and the predominant wind direction is important to enhance the wind speed, the simple grid system of squares accompanied with the tilted wind direction away from the main streets would benefit the urban design with enhancing the wind speed. The thermal comfort in this case is heavily influenced by the solar radiation, where minimising south facing facades (the long edge of the street) will reduce the thermal stress.
A.2		
	<ul style="list-style-type: none"> - 36% of the area recorded wind speed values between (0-0.5) m/s. - The average PET value was 27.1 °C for the entire plot. - The approaching wind was parallel the main streets which created a channelling flow that raised the wind speed in the main streets. - The perpendicular streets to the approaching wind flow produced low wind speed of 0.5 m/s and below. 	<ul style="list-style-type: none"> - In layout A.1 the main street where receptor 1 was placed recorded lower wind speed than A.2, however the shading patterns covered more hours of the day in A.1 which lowered the thermal stress. Depending on the design objective and the targeted location, A.1 scenario presented an overall better result than A.2, while A.2 recorded better wind speed values in the main streets. It should be noted that layout A.1 produced the best results in terms of wind speed and thermal stress when compared to layouts B, C, D and E.
Layout B		
B.1		
	<ul style="list-style-type: none"> - 8% of the area recorded wind speed values between (0-0.5) m/s. - The average PET value was 26.6 °C for the entire plot. - The approaching wind was displaced at the edge of the buildings creating a helical flow in the streets. - The main street with receptor 1 produced less wind speed values than the main street with receptor 2. 	<ul style="list-style-type: none"> - Layout B is a modified version of layout A to explore more urban geometry in the built environment. Scenario B.1 showed better wind distribution across the layout when compared to layout B. However, the main streets in which the receptors were placed in had better wind speed values in B.2. If the objective of the design is to increase wind speed the main streets scenario B.2 is more beneficial due to the channelling flow, while scenario B.1 has better wind speed distribution across the layout because of the helical flow. - The attached buildings in the middle of the layout blocked the wind flow from reaching the top part of the design. However, the main street with receptor 2 has highest wind speed values when compared with layout A, where the attached buildings helped in gathering the wind flow in one direction and enforcing the wind speed.

B.2		
	<ul style="list-style-type: none"> - 29% of the area recorded wind speed values between (0-0.5) m/s. - The average PET value was 27.6 °C for the entire plot. - The approaching wind was parallel the main streets which created a channelling flow that raised the wind speed in the main streets. - The perpendicular streets to the approaching wind flow produced low wind speed of 0.5 m/s and below. - Layout B design comprised of less perpendicular streets with low wind speed when compared to layout A. 	<ul style="list-style-type: none"> - There isn't a significant difference in the PET values between layout A and B. However, the attached buildings helped in generating more shade throughout the day in the adjacent areas which lowered the PET levels in those said areas. It is worth mentioning that the reason the low wind distribution is higher in A.2 when compared to B.2 is because A.2 has more streets that are perpendicular to the approaching wind direction in which the attached buildings blocked in B.2.
Layout C		
C.1		
	<ul style="list-style-type: none"> - 9% of the area recorded wind speed values between (0-0.5) m/s. - The average PET value was 26.7 °C for the entire plot. - The approaching wind was displaced at the edge of the buildings creating a helical flow in the streets. - Buildings with small depth and longer sides along the canyon had smaller cavity zones in the leeward facades, which raised the wind speed values. 	<ul style="list-style-type: none"> - Layout C was designed to study the effect of designing the buildings with longer leeward facades or longer along canyon facades. Urban planners should take notice to the cavity zone in regard to the wind flow inside the design proposals. As demonstrated in this layout, the cavity zones (lower wind speed zones) were bigger with square shaped buildings, and the elongated buildings had smaller cavity zones. The elongated buildings also have an advantage when oriented in the direction of the approaching wind (scenario C.2), where the majority of designed area is subjected to the channelling flow.
C.2		
	<ul style="list-style-type: none"> - 18% of the area recorded wind speed values between (0-0.5) m/s. - The average PET value was 28.3 °C for the entire plot. - The approaching wind was parallel the main streets which created a channelling flow that raised the wind speed in the main streets. - The layout has smaller percentage of area of streets perpendicular to the approaching wind direction when compared to layout A and B. 	<ul style="list-style-type: none"> - There isn't a significant difference in the PET values between layout A, B and C. However, the elongated buildings generate shading throughout the day better than the square shaped buildings in layout A. - Depending on the objective of the design, layouts A, B and C have different advantage and disadvantages, where layout A preforms best in terms of PET and wind flow, the design compromises on the built-up area when compared to layout B. Moreover, layout C has the best results with wind speed when the layout is oriented in the direction of the approaching wind, but like layout A compromises on the built-up area.

Layout D		
	<p>D.1</p>	<ul style="list-style-type: none"> - 52% of the area recorded wind speed values between (0-0.5) m/s. - The average PET value was 28.2 °C for the entire plot. - The approaching wind was distributed with channelling flow in some streets and a helical flow in others due to the circular shaped design. - ENVI-met have some inaccuracy with simulating diagonal lines, which affected the wind speed results.
	<p>D.2</p>	<ul style="list-style-type: none"> - 68% of the area recorded wind speed values between (0-0.5) m/s. - The average PET value was 29.3 °C for the entire plot. - The approaching wind was distributed with channelling flow in some streets and a helical flow in others due to the circular shaped design. - ENVI-met have some inaccuracy with simulating diagonal lines, which affected the wind speed results.
Layout E		
	<p>E.1</p>	<ul style="list-style-type: none"> - 42% of the area recorded wind speed values between (0-0.5) m/s. - The average PET value was 28.4 °C for the entire plot. - The approaching wind was distributed with channelling flow in some streets and a helical flow in others due to the radial shaped design. - The streets' design was linear radial rather than the circular radial design like in layout D which improved the wind speed values.
<p>- Layout D was designed based on the radial grid system, this grid is usually used to indicate an important landmark in the middle of the grid and can be seen in urban layouts such as in Paris, France. Keeping in mind that ENVI-met underestimated the wind speed values, the nature of the radial system is filled with multidirectional streets, which hindered the wind flow inside the layout. Layout D showed the worst wind flow values and PET levels due to low wind speed values and shade pattern cast from the building. Further modification to the layout is needed to enhance the thermal stress and wind flow in the radial system, which is the case of layout E.</p> <p>- Layout E is a modified version of layout D, and it was designed to study the radial form without the circular shaped streets that hindered the wind flow in layout D. The wind speed values were improved significantly in layout E with 10% reduction of low speed areas in scenario E.1 when compared to scenario D.1, and 8% reduction in low wind speed areas in scenario E.2 when compared to D.2.</p> <p>- The PET levels showed a slight increase from layout D's PET values due to more solar access throughout the day. The compact design of layout D provided more shading than layout E.</p> <p>- Depending on the design objective, planners should take notice to advantages and disadvantages of both layouts D and E, where layout E produced lower PET values</p>		

E.2	
	<ul style="list-style-type: none"> - 60% of the area recorded wind speed values between (0-0.5) m/s. - The average PET value was 29.6 °C for the entire plot. - The approaching wind was distributed with channelling flow in some streets and a helical flow in others due to the radial shaped design. - The streets' design was linear radial rather than the circular radial design like in layout D which improved the wind speed values.
	<p>when the approaching wind was directed along the main street with receptors 7 and 3, and Layout E produced better wind flow especially when the approaching wind was directed along the main street with receptors 7 and 3.</p> <ul style="list-style-type: none"> - Thermal stress has weighted parameters, which in this case solar radiation affect the thermal stress more than improved wind flow. However, improved wind flow is crucial for better urban environment as it is important for particle dispersion and ventilation.

Objective 7 (Assessing the mesoscale analysis which includes the grid design proposals for the studied site in Amman, and the effect of different approaching wind angles on the thermal stress – Chapter 6, Section 2).

In chapter 6 - section 2, proposals for the street grid design were analysed based on the results of section 1. The proposal consisted of straight streets to enhance airflow in the direction of the prevailing wind, the cross streets in the first proposal were directed diagonally, and the second proposal had the crossed streets perpendicular to the streets along the wind direction. The rectilinear nature of the proposed designs for the site is derived from the most typical streets grids chosen by urban planners and serve the most efficient design in terms of wind flow and thermal stress. The main findings can be summarised as follows:

- In the summer analysis, the second proposal generated lower PET values compared to the first proposal, and this is due to different shading patterns produced by the crossed streets. The first proposal's crossed streets were directed on the (Northeast – Southwest) and (Northwest – Southeast) axis which allowed for more solar access when compared to the second proposal that had the crossed streets directed at the (North-South) axis.
- In the winter analysis, the PET values for both proposals were analysed based on the closeness of the values to the comfort level, as the PET values can get very low at night in the winter season for both proposals. The results showed that the first proposal showed a slightly closer PET values to the comfort range compared to the second proposal, this divergence can be seen between the hours of 08:00 – 14:00 where solar radiation was present.

- The approaching wind analysis showed that the PET levels are affected by the direction of the wind in the context of the proposed streets' design. The results showed a decrease in the PET levels when the approaching wind angle is larger than the parallel to streets direction, and this is due to the helical flow generated in the layout when the attacking angle is larger than the parallel angle. The helical flow directs more airflow deeper inside the street grid compared to the channelling flow. The channelling flow appears when the approaching wind is parallel to the streets, where the high wind speed values restrict the flow to escape to the crossed streets and lower the overall wind speed of the layout.

Recommendations for urban planners:

Depending on the microclimatic parameters for the chosen site, planners should make the appropriate decision of the grid system that will be used as a base for the design. The results for the street grid system showed different favourable results for summer and winter analysis, where layout-1 showed better thermal stress results in winter and layout-2 showed better thermal stress results in summer.

The decision for the grid system was based on the previous section results. The simple square-shaped buildings were chosen for a better wind flow and shading patterns, where the radial system would not have been beneficial especially in the harsh heat of summer in Amman. Planners should avoid the radial system but if they must, they should avoid the circular street shapes to enhance wind flow.

The orientation of the plot was also a crucial part of the design as to set a helical flow inside the designed area to create better overall wind speed values. It is preferable to orient the design (15° - 45°) away from the approaching wind direction to ensure better wind flow. It should be noted that improving the PET levels in the harsh conditions of summer is not sufficient enough to reduce the thermal stress from the very hot range to the comfortable range. However, reducing the PET will extend the duration of comfort in months prior to summer and extending the use of outdoor spaces throughout the year. Overall, urban planners should study the relevant parameters to their design's objective and chose the grid system that suits their targeted season or location based on the microclimatic parameters of the site.

Objective 8 (Assessing the microscale analysis, which included the buildings clusters design proposals based on the wind flow designs – Chapter 6, Section 3).

Section 3 analysed the cluster of buildings proposals (compound 1 and compound 2). The Compound 1's design was comprised of a residential complex with a transition of wind flow from unhindered flow to restricted flow around the buildings. Compound 2 was designed to be more sensitive to the climatic parameters around the site, the design comprised of strips of buildings rather than the C-shape conventionally used in residential compounds, the buildings and pathways were oriented in the direction of the prevailing wind, this allowed for better wind ventilation reinforced with access points in the middle of the strip of buildings. The main findings of the analysis are as follows:

- The compact design of compound 1 prevented air movement inside the private zones and this, plus the increased solar access due to south-facing facades, has increased the PET levels compared to compound 2, where air movement is unrestricted.
- Directing the main pathway in compound 2 in the approaching wind direction has increased the wind speed significantly, which helped in reducing the PET values, especially at night.
- The vegetation addition helped in reducing the PET levels with more shaded areas. However, their effect is limited beyond their casted shadows radius. Also, the position that the trees were placed in did not hinder the airflow due to the high position of the foliage above the pedestrian level.
- The addition of horizontal shading in the south-facing facades had helped in reducing the PET values from a maximum of 55°C at 2:00 to 43°C. The receptors showed an average decrease in the PET values of 7.5°C, a maximum reduction of 13.4°C, and a minimum reduction of 0.6°C throughout the day.

Recommendations for urban planners:

The general design of buildings compound should take into consideration the predominant wind direction as well as the south facing facades. Urban planners should avoid the clustering of buildings which restrict the flow of wind and reduce the wind speed values consequently. The first design while restricted the wind flow is seen to be used Widley for its visual privacy

aspects in architecture. However, the outdoor spaces that was created bore a significant heat stress rendering the spaces unusable in the summer thermal stress. It is advisable to design buildings that runs in one axis along the predominant wind or oriented at (15°-45°) to the predominate wind direction, this formation should create channelling flow (if along the wind direction) or helical flow (if oriented at 15°-45°) around the buildings while arrayed at the same angle.

Thermal stress is significantly influenced by solar radiation, and in order to create better outdoor spaces, it is advisable to create buildings formation that would provide the maximum shading duration throughout the day (please refer to objective 9 for buildings' heights and shading patterns). Avoid orienting the array of buildings on the (North-South) and (West-East) to minimise the overall solar access to the south-facing facades. Also, incorporating vegetation in the site would increase the shading patterns in the outdoor spaces and decrease the air temperature by means of transpiration, where it has been found that the use of vegetation as a tool to lower the air temperature is more beneficial in hot and dry climates (Alexandri & Jones, 2008). It should be noted that the use of external shading devices is also an effective tool to introduce more shading to the outdoor spaces. However, it is not advisable as it would block the sun in winter whereas trees would shed their leaves and allow for more solar access in winter.

Objective 9 (Evaluating the geometrical modification, orientation, and Leaf Area Density (LAD) of trees and their effects on airflow as well as thermal stress – Chapter 6, Section 3).

In chapter 6, section 3, the analysis showed that the proposal (compound 2) produced lower PET values than compound 1. The analysis continued by focusing on a smaller section of compound 2 and performed several adjustment assessments. The adjustments included geometrical modification, orientation, and Leaf Area Density (LAD) of trees. The following findings represent the effect of the urban adjustment on the thermal stress (PET) and airflow:

- The PET results for the auxiliary access in the middle of the strip of buildings showed that the airflow was enhanced when the access was roofed due to strengthened wind tunnel effect. However, the PET levels were higher compared to the unroofed case, this is due to the higher amount of reflected solar radiation introduced to the area. It should be noted that in both cases the area was shaded by the adjacent buildings.

- The buildings' height analysis showed that with increased height of the buildings, the wind flow is strengthened at the pedestrians' level, this allowed for better ventilation and enhanced the PET levels. The results showed an average decrease of PET levels at noon of 7 °C.
- The Leaf Area Density (LAD) analysis showed that the airflow was slightly enhanced with lower LAD due to less resistance from trees and allowing better ventilation. However, due to the small increase in wind speed, the PET levels did not show a significant change in their values.
- The results of changing the orientation caused a change in the approaching wind direction and the sun path, and this shifted the approaching wind direction from the long pathway to the short axis that went through the auxiliary access between the strip of buildings. This resulted in high wind speeds along this axis but caused a poorly ventilated area in the long pathway. As for the solar radiation, the site was exposed to more sun when the orientation changed, and this was at its maximum at noon where there is no shading from the buildings affecting the long pathway, which resulted in high PET levels. The averaged PET values showed a maximum increase of 7.5°C at noon.

Recommendations for urban planners:

In an urban canyon, several modifications can be performed to enhance the quality of the outdoor spaces, this includes modifications on buildings' height or H/W ratio, vegetation addition, geometrical modifications, and orientation. It is crucial to the urban planners to study the site's microclimatic parameter and decide the appropriate modifications accordingly.

The orientation of the site will dictate the amount of solar access and the intensity of the air flow inside the designed area. Creating helical flows inside the urban canyon is the most effective method is distributing the wind, especially if there was perpendicular pathways or streets around the studied area. The helical flow can be achieved by orienting the design (15°-45°) away from the approaching wind direction accompanied with elongated buildings' structure to help guide the flow, it should be noted that the helical flow is at its strangest when the design is oriented at 45°. The channelling flow can be beneficial to maximise the wind speed values if the inlet values of the predominate wind is low, but this means that perpendicular streets to the urban can will experience very low wind speed values in return.

The Height/Width ratio can impact the thermal stress levels as well as the wind flow inside the urban canyon. Higher ratios tend to cast more shade throughout the day which decrease the solar access and reduce the thermal stress. Higher ratios also improve the wind speed values, this occurs when the stagnation point is higher with higher buildings which results in stronger down stream that feeds the main flow in the urban canyon.

The vegetation can elevate some of the thermal stress by providing additional shading and lowering the air temperature by means of transpiration. The choice of vegetation should take into consideration the thickness of the trees' foliage described by the Leaf Area Density (LAD) or Leaf Area Index (LAI), where higher LAD and LAI might hinder the air flow. The placement of trees is also important, it is advisable to place the trees along side the south facing facades to minimise the harsh solar access especially during summer. Choosing deciduous species of trees is preferable as they allow for more solar access during winter and provide shading during summer.

7.3 RESEARCH IMPLICATIONS FOR FUTURE WORK AND GENERAL RECOMMENDATIONS

This study focused on designing an urban residential layout that produces the least thermal stress on pedestrians using different parameters at different scales. The results showed that choosing the right mitigation approach at the right circumstances would significantly impact the thermal outcomes of an urban project. The following mitigation strategies are general recommendation for Amman's future projects (refer to section 7.2 for detailed recommendations):

- The street grid design should avoid curved streets or radial grid system as it hinders airflow, and it should be directed 15° to 45° from the prevailing wind direction to enhance wind speed through avoiding channelling flow and enforcing helical flow.
- Avoid directing the streets on the (North-South) and (West-East) to minimise the overall solar access to the south-facing facades.
- Wind direction is vital for reducing the PET levels; however, increased wind speed is most effective with reduced solar access. Therefore, increased wind speed should be combined with shading through appropriate orientation, vegetation, or shading devices.
- Avoid C shaped pathways in residential areas as they limit airflow and particle dispersion.

- Avoid orientating the pedestrian's pathways along the direction of the prevailing wind to prevent channelling flow, as high wind speed can be uncomfortable and cause disturbances for pedestrians.
- Avoid orientating the pedestrian's pathways perpendicular to the approaching wind, to prevent the mean wind flow from skipping over the roofs of buildings and reducing wind speed significantly at pedestrians' level.
- Adding roofs to short pathways between buildings is not always beneficial in reducing the thermal stress, the location plays a crucial role in enhancing the effect of the roofs. If the pathway is exposed to solar radiation, roofs can help in reducing the thermal stress by providing shade and increasing wind speed with strengthened wind tunnel effect. However, if the pathway is in a south-facing façade and is shaded by the height of the buildings, adding a roof would increase the wind speed, but it will increase the reflected solar radiation while raising the level of discomfort. Roofing the pathways should consider, orientation, material used and surrounding structures.
- Raising the H/W ratio can reduce the thermal stress during the day by providing shading and enhancing airflow. However, increasing the H/W can reduce the SVF, which will reduce the night cooling effect.
- Choosing trees with low LAD values can slightly increase the wind speed.
- Avoid orienting the pathways along the (North-South) axis to minimise solar access.

This study investigated several parameters regarding the urban environment and thermal comfort. However, there are still many other factors and parameters that have not been studied in this research due to time limitation. The following are some recommendation for future studies:

- Different H/W ratios when investigating the street grid design.
- Different trees geometry and their effect on reducing the thermal stress.
- Asymmetrical street canyons analysis and their implications on airflow and thermal stress
- Adding water features to investigate the evaporative cooling effect in Amman's climate.

Further studies are needed to fill the gap in the urban design sector in Jordan. This is especially important for changing the current planning policies regarding urban expansion, while building a comprehensive guide for healthier open spaces in Amman and in Jordan as a whole.

REFERENCES

- Abaas, Z. R., 2020. Impact of development on Baghdad's urban microclimate and human thermal comfort. *Alexandria Engineering Journal*, 59(1), pp. 275-290.
- Abdallah, A. S. H., Hussein, S. W. & Nayel, M., 2020. The Impact of outdoor shading strategies on Student thermal comfort in Open Spaces Between Education Building. *Sustainable Cities and Society*, p. 102124.
- Abreu-Harbich, L. V., Labaki, L. C. & Matzarakis, A., 2014. Thermal bioclimate in idealized urban street canyons in Campinas, Brazil. *Theoretical and Applied Climatology*, Volume 115, p. 333–340.
- Abreu-Harbich, L. V., Labaki, L. C. & Matzarakis, A., 2015. Effect of tree planting design and tree species on human thermal comfort in the tropics. *Landscape and Urban Planning*, Volume 138, pp. 99-109.
- Al-Azhari, W., Haddadin, M. & Hiyasat, R., 2014. THE EFFECT OF STREET ORIENTATION AND SURROUNDING. *AMIT*, 4(29), pp. 29/14-09.
- Aliabadi, A. et al., 2019. Flow and temperature dynamics in an urban canyon under a comprehensive set of wind directions, wind speeds, and thermal stability conditions. *Environmental Fluid Mechanics*, Volume 19, pp. 81-109.
- Al-Sallal, A. & Al-Rais, A., 2012. Outdoor airflow analysis and potential for passive cooling in the modern urban context of Dubai. *Renewable Energy*, 38(1), pp. 40-49.
- Al-Sallal, K. A. & Al-Rais, L., 2011. Outdoor airflow analysis and potential for passive cooling in the traditional urban context of Dubai. *Renewable Energy*, 36(9), pp. 2494-2501.
- Galal, O. M., Mahmoud, H. & Sailor, D., 2020. Impact of evolving building morphology on microclimate in a hot arid climate. *Sustainable Cities and Society*, Volume 54, p. 102011.
- Gál, C. V. & Kántor, N., 2020. Modeling mean radiant temperature in outdoor spaces, A comparative numerical simulation and validation study. *Urban Climate*, Volume 32, p. 100571.

- Jamei, E., Rajagopalan, P., Seyedmahmoudian, M. & Jamei, Y., 2016. Review on the impact of urban geometry and pedestrian level greening on outdoor thermal comfort. *Renewable and Sustainable Energy Reviews*, Volume 54, pp. 1002-1017.
- KOTTEK, M. et al., 2006. World Map of the Köppen-Geiger climate classification updated. *Meteorologische Zeitschrift*, 15(3), pp. 259-263.
- Li, G., Ren, Z. & Zhan, C., 2020. Sky View Factor-based correlation of landscape morphology and the thermal environment of street canyons: A case study of Harbin, China. *Building and Environment*, Volume 169, p. 106587.
- Newburgh, L. H., 1949. *Physiology of heat regulation and the science of clothing*. 1st ed. Philadelphia: W. B. Saunders Co..
- Nikolopoulou, M., 2004. *Designing Open Spaces in the Urban Environment: a Bioclimatic Approach*. 1st ed. Greece: Centre for Renewable Energy Sources.
- Zaki, S. A. et al., 2020. Effects of Roadside Trees and Road Orientation on Thermal Environment in a Tropical City. *Sustainability*, 12(3), p. 1053.
- Abdel-Aziz, D. & Al-Kurdi, N., 2014. Estimating the Effect of Urban Trees on Summertime Electricity use and Air Quality Improvement in Urban Areas –Amman as a case Study. *Journal of Environment and Earth Science*, 4(23), pp. 37-47.
- Abdel-Ghany, A., Al-Helal, I. & Shady, M., 2013. Human Thermal Comfort and Heat Stress in an Outdoor Urban Arid Environment: A Case Study. *Advances in meteorology*, pp. 1-7.
- Abu Sada, A., Abu-Allaban, M. & Al-Malabeh, A., 2015. Temporal and Spatial Analysis of Climate Change at Northern Jordanian Badia. *Jordan Journal of Earth and Environmental Sciences*, Volume 7, pp. 87-93.
- Abu-dayyeh, N. I., 2004. Persisting vision: plans for a modern Arab capital, Amman, 1955–2002. *Planning Perspectives*, 17 May, pp. 79-110.
- Abu-Hamdi, E., 2017. Neoliberalism as a site-specific process: The aesthetics and politics of architecture in Amman, Jordan. *Cities*, Volume 60, pp. 102-112.
- Achour-Younsi, S. & Kharrat, F., 2016. Outdoor Thermal Comfort: Impact of the Geometry of an Urban Street Canyon in a Mediterranean Subtropical Climate – Case Study Tunis, Tunisia. *Procedia - Social and Behavioral Sciences*, Volume 216, pp. 689-700.

- Ackerman, B., 1987. Climatology of Chicago Area Urban-Rural Differences in Humidity. *J. Climate Appl. Meteor.*, Volume 26, p. 427–430.
- Ahmed, K. S., 2003. Comfort in urban spaces: Defining the boundaries of outdoor thermal comfort for the tropical urban environments. *Energy and Buildings*, 35(1), pp. 103-110.
- Aishe, Z., Cuilan, G. & Ling, Z., 2005. Numerical simulation of the wind field around different building arrangements. *Journal of Wind Engineering and Industrial Aerodynamics*, 93(12), pp. 891-904.
- Akbari, H. et al., 1992. *Cooling Our Communities. A Guidebook on Tree Planting and Light-Colored Surfacing*, Washington: Lawrence Berkeley National Laboratory.
- Akubue, J. A., 2019. Effects of Street Geometry on Airflow Regimes for Natural Ventilation in Three Different Street Configurations in Enugu City. In: A. B. Cakmakli , ed. *Different Strategies of Housing Design*. s.l.:IntechOpen..
- Al- Eisawi, D. M., 1986. Studies on the Flora of Jordan 12. Monocotyledons New to Jordan, with Notes on Some Interesting Species. *Kew Bulletin*, 41(2), p. 349.
- Al-Asad, M., 2004. Ever-growing Amman. *Jordan times*.
- Al-Eisawi, D. M., 1987. The Orchids of Jordan. *Kew Bulletin*, 41(2), p. 359.
- Aleksandrowicz, O., Vuckovic, M., Kiesel, K. & Mahdavi, A., 2017. Current trends in urban heat island mitigation research: observations based on a comprehensive research repository. *Urban Climate*, Volume 21, pp. 1-26.
- Alexandri, E. & Jones, P., 2008. Temperature decreases in an urban canyon due to green walls and green roofs in diverse climates. *Building and Environment*, 43(4), pp. 480-493.
- Alexandri, E. & Jones, P., 2008. Temperature decreases in an urban canyon due to green walls and green roofs in diverse climates. *Building and Environment*, 43(4), pp. 480-493.
- Alfano, F. R. et al., 2013. On the measurement of the mean radiant temperature and its influence on the indoor thermal environment assessment. *Building and Environment*, Volume 63, pp. 79-88.

Ali-Toudert, F. & Mayer, H., 2006. Numerical study on the effects of aspect ratio and orientation of an urban street canyon on outdoor thermal comfort in hot and dry climate. *Building and Environment*, 41(2), pp. 94-108.

Ali-Toudert, F. & Mayer, H., 2006. Numerical study on the effects of aspect ratio and orientation of an urban street canyon on outdoor thermal comfort in hot and dry climate. *Building and Environment*, 41(2), pp. 94-108.

Ali-Toudert, F. & Mayer, H., 2007. Effects of Asymmetry, Galleries, Overhanging Façades and Vegetation on Thermal Comfort in Urban Street Canyons. *Solar Energy*, 81(6), pp. 742-754.

Alkhatib, L. M. S. & Qrunfleh, M. M., 2018. Plants as an Element in Microclimate Modification in Jordan Landscape Courtyard Gardens. *Jordan Journal of Agricultural Sciences*, 14(1), pp. 50-78.

Al-Kodmany, K., 1999. Residential Visual Privacy: Traditional and Modern Architecture and Urban Design. *JOURNAL OF URBAN DESIGN*, pp. 283-312.

Al-Kurdi, N. & Awadallah, T., 2015. Role of Street-Level Outdoor Thermal Comfort in Minimizing Urban Heat Island Effect by Using Simulation Program, Envi-Met: Case of Amman, Jordan. *Research Journal of Environmental and Earth Sciences*, 7(3), pp. 42-49.

Ambrosini, D. et al., 2014. Evaluating mitigation effects of urban heat islands in a historical small center with the ENVI-Met® climate model. *Sustainability*, Volume 6, pp. 7013-7029.

Amineldar, S., Heidari, S. & Khalili, M., 2017. The effect of personal and microclimatic variables on outdoor thermal comfort: A field study in Tehran in cold season. *Sustainable Cities and Society*, Volume 32, pp. 153-159.

Aminipouri, M. et al., 2019. Urban tree planting to maintain outdoor thermal comfort under climate change: The case of Vancouver's local climate zones. *Building and Environment*, Volume 158, pp. 226-236.

Amit-Cohen, I. & Maruani, T., 2007. Open space planning models: A review of approaches and methods. Landscape and Urban Planning. *Landscape and Urban Planning*, 81(1-2), pp. 1-13.

Andreou, E., 2013. Thermal comfort in outdoor spaces and urban canyon microclimate. *Renewable Energy*, Volume 55, pp. 182-188.

Antoniou, N. et al., 2017. CFD and wind-tunnel analysis of outdoor ventilation in a real compact heterogeneous urban area: Evaluation using “air delay”. *Building and Environment*, 126(1), pp. 355-372.

Arnfield, A. J., 2003. Two decades of urban climate research: A review of turbulence, exchanges of energy and water, and the urban heat island. *International Journal of Climatology*, 23(1), pp. 1-26.

Arnfield, A. & Mills, G., 1994. An analysis of the circulation characteristics and energy budget. I. Circulation characteristics. *International Journal of Climatology*, Volume 14, pp. 119-134.

Arotegui, J. M., 1995. *Índice de Temperatura Neutra Exterior*. Gramado, ENCAC.

ASHRAE, 2017. *American Society of Heating, Refrigerating and Air-Conditioning Engineers handbook : fundamentals..* SI edition. ed. Atlanta, Georgia : ASHRAE.

ASHRAE, 2017. *Standard 55-2017 -- Thermal Environmental Conditions for Human Occupancy*. 5th ed. Atlanta: American Society of Heating, Refrigerating, and Air-conditioning Engineers.

Atmaca, I., Kaynakli, O. & Yigit, A., 2007. Effects of radiant temperature on thermal comfort. *Building and Environment*, 42(9), pp. 3210-3220.

Atwa, S., Ibrahim, M. G. & Murata, R., 2020. Evaluation of plantation design methodology to improve the human thermal comfort in hot-arid climatic responsive open spaces. *Sustainable Cities and Society*, Volume 59, p. 102198.

Avissar, R., 1996. Potential effects of vegetation on the urban thermal environment. *Atmospheric Environment*, 30(3), pp. 437-448.

Bakarman, M. A. & Chang, J. D., 2015. The Influence of Height/width Ratio on Urban Heat Island in Hot-arid Climates. *Procedia Engineering*, Volume 118, pp. 101-108.

Bande, L. et al., 2019. Validation of UWG and ENVI-Met Models in an Abu Dhabi District, Based on Site Measurements. *sustainability*, Volume 11,, p. 4378.

Barakat, A., Ayad, H. & El-Sayed, Z., 2017. Urban design in favor of human thermal comfort for hot arid climate using advanced simulation methods. *Alexandria Engineering Journal*, 56(4), pp. 533-543.

- Beauregard, R. & Marpillero-Colomina, A., 2010. *AMMAN 2025: From Master Plan to Strategic Initiative*, Amman: Greater Amman Municipality, the Amman Institute for Urban Development.
- Belcher, S. E., 2005. Mixing and transport in urban areas. *Philosophical Transactions of the Royal Society A*, Volume 363, p. 2947–2968.
- BELDING, H. & HATCH, T., 1955. Index for evaluating heat stress in terms of resulting physiological strain. *Heating, Piping, Air Conditioning*, Volume 27, pp. 129-142.
- Berglund, L. G., 1998. Comfort and humidity. *ASHRAE Journal*, 40(8), p. 35.
- Bernstein, L. et al., 2008. *IPCC, 2007: climate change 2007: synthesis report*, Geneva: Intergovernmental Panel on Climate Change.
- Binarti, F. et al., 2020. A review of outdoor thermal comfort indices and neutral ranges for hot-humid regions. *Urban Climate*, Volume 31, p. 100531.
- Blackman, K., Parret, L., Savory, E. & Piquet, T., 2015. Field and wind tunnel modeling of an idealized street canyon flow. *Atmospheric Environment*, Volume 106, pp. 139-153.
- Blazejczyk, K., Epstein, Y., Jendritzky, G. & Staig, H., 2013. Comparison of UTCI to selected thermal indices. *Int. J. Biometeorol.*, 56(3), pp. 515-535.
- Błażejczyk, K. & Kraawczyk, B., 1994. New climatological and physiological model of the human heat balance outdoor (MENEX) and its applications in bioclimatological studies in different scales. *Bioclimatic research of the human heat balance*, Volume 28, pp. 27-58.
- Blazejczyk, K., Tokura, H., Bortkucz, A. & Szymczak, W., 1999. Solar radiation and thermal physiology in man. *International Congress of Biometeorology & International Conference on Urban Climatology*, Volume 15, pp. 267-272.
- Blocken, B., 2014. 50 years of Computational Wind Engineering: past, present and future. *Journal of Wind Engineering and Industrial Aerodynamics*, Volume 129, pp. 69-102.
- Blocken, B. & Carmeliet, J., 2008. Pedestrian wind conditions at outdoor platforms in a high-rise apartment building: generic sub-configuration validation, wind comfort assessment and uncertainty issues. *Wind and Structures*, 11(1), pp. 51-70.

Blocken, B. & Persoon, J., 2009. Pedestrian wind comfort around a large football stadium in an urban environment: CFD simulation, validation and application of the new Dutch wind nuisance standard. *Journal of Wind Engineering and Industrial Aerodynamics*, Volume 97, pp. 255-270.

Bluestein, M. & Osceveski, R., 2002. *Wind chill and the development of frostbite in the face*. Kansas City, American Meteorological Society.

Bonacquisti, v., Casale, G., Palmieri, S. & Siani, A., 2006. A canopy layer model and its application to Rome. *Sci. Total Environ.*, 364(1), pp. 1-13.

Boukhabla, M. & Alkama, D., 2012. Impact of vegetation on thermal conditions outside, thermal modeling of urban microclimate, case study: the street of the republic, Biskra. *Energy Procedia*, Volume 18, pp. 73-84.

Boulos, L. & Lahham, J., 1977. Studies on the flora of Jordan: 4. *Candollea*, 32(1), pp. 81-98.

Bouyer, J., Inard, C. & Musy, M., 2011. Microclimatic coupling as a solution to improve building energy simulation in an urban context. *Energy Build*, Volume 43, pp. 1549-1559.

Brager, G. S. & de Dear, R., 2001. *Climate, Comfort & Natural Ventilation: A new adaptive comfort standard for ASHRAE Standard 55*, Berkeley: University of California.

Broadbent, A., Coutts, A., Tapper, N. & Demuzere, M., 2018. The cooling effect of irrigation on urban microclimate during heatwave conditions. *Urban Clim.*, Volume 23, pp. 309-329.

Brown, R. & Gillespie, T., 1995. *Microclimatic Landscape Design: Creating Thermal Comfort and Energy Efficiency*. 1st ed. New York: Wiley.

Bruse, M., 1995. *Development of a microscale model for the calculation of surface temperatures in structured terrain*. s.l.:Institute for Geography, Ruhr-University Bochum.

Bruse, M., 2004. *Bleeding edge: The most-recent doc you can have*. [Online] Available at: <http://www.envi-met.net/documents/papers/overview30.pdf> [Accessed 10 april 2020].

Bruse, M. & Fleer, H., 1998. Simulating surface-plant-air interactions inside urban environments with a three dimensional numerical model. *Environmental Modelling and Software*, Volume 13, p. 373–384.

- Bullin, J., Hinz, M. & Hinz, S., 1982. *Vehicle Emissions from Intersections*, Texas : Texas Transportation Institute.
- Bureau of Planning, L. A. D. A. C. P. H. L. C., 1988. *Ladd's Addition Conservation District Guidelines*, Portland: the Historic Landmarks Program.
- Byron, D., 2002. *interpreting quantitative data*. london: Sage publications Ltd.
- Canan, F. et al., 2019. Outdoor thermal comfort conditions during summer in a cold semi-arid climate. A transversal field survey in Central Anatolia (Turkey). *Building and Environment*, Volume 148, pp. 212-224.
- Castelli, S. et al., 2018. Validation of a Lagrangian particle dispersion model with wind tunnel and field experiments in urban environment. *Atmospheric Environment*, Volume 193, pp. 273-289.
- Chai, T. & Draxler , R. R., 2014. Root mean square error (RMSE) or mean absolute error (MAE)? – Arguments against avoiding RMSE in the literature. *Geosci*, 7(3), p. 1247–1250.
- Chan, A., 2011. Effect of adjacent shading on the thermal performance of residential buildings in a subtropical region. *Applied Energy*, pp. 516-522.
- Chatzidimitriou, A. & Yannas, S., 2017. Street canyon design and improvement potential for urban open spaces; the influence of canyon aspect ratio and orientation on microclimate and outdoor comfort. *Sustainable Cities and Society*, Volume 33, pp. 85-101.
- Cheng, V., Ng, E., Chan, C. & Givoni, B., 2012. Outdoor thermal comfort study in sub-tropical climate: A longitudinal study based in Hong Kong. *International Journal of Biometeorology* , Volume 56, p. 43–56.
- Chen, L. & Ng, E., 2012. Outdoor thermal comfort and outdoor activities: a review of research in the past decade. *Cities*, Volume 29, pp. 118-125.
- Chen, Y. & Matzarakis, A., 2017. Modified physiologically equivalent temperature—basics and applications for western European climate. *Theor. Appl. Climatol.*, Volume 128, pp. 1-15.
- Chen, Y. & Matzarakis, A., 2014. Modification of physiologically equivalent temperature. *J. Heat Island Inst. Int.*, Volume 9, pp. 26-32.
- Chepil, W., 1945. Dynamics of soil movement. *Soil Science*, Volume 60, pp. 305, 397, 475.

Coccolo, S., Kämpf, J., Scartezzini, J. & Pearlmutter, D., 2016. Outdoor human comfort and thermal stress: a comprehensive review on models and standards. *Urban Climate*, Volume 18, pp. 33-57.

Coceal, O., Thomas, T., Castro, I. & Belcher, S., 2006. Mean flow and turbulence statistics over groups of urban-like cubical obstacles.. *Boundary-Layer Meteorol*, Volume 121, p. 491–519.

Cui, P.-Y., Li, Z. & Tao, W.-Q., 2016. Buoyancy flows and pollutant dispersion through different scale urban areas: CFD simulations and wind-tunnel measurements. *Building and Environment*, Volume 104, pp. 76-91.

da Silva, F. T. & de Alvarez, C. E., 2015. An integrated approach for ventilation's assessment on outdoor thermal comfort. *Building and Environment*, Volume 87, pp. 59-71.

DAVIS, 2011. *Vantage VUE Integrated Sensor Suite Manual*. s.l.:DAVIS instruments.

de Dear, . R. & Brager, G., 1998. Developing an adaptive model of thermal comfort and preference. *ASHRAE Trans*, Volume 104 , pp. 1-18.

de Dear, R., Xiong, J., Kim, J. & Cao, B., 2020. A review of adaptive thermal comfort research since 1998. *Energy and Buildings*, Volume 214, p. 109893.

Deardorff, . J. W., 1978. Efficient prediction of ground surface temperature and moisture with inclusion of a layer of vegetation. *Journal of Geophysical Research*, 83(c4), pp. 1889-1903.

Declet-Barreto, J. et al., 2013. Creating the park cool island in an inner-city neighborhood: heat mitigation strategy for Phoenix, AZ. *Urban Ecosystems*, Volume 16, p. 617–635.

Deng, J.-Y. & Wong, N. H., 2020. Impact of urban canyon geometries on outdoor thermal comfort in central business districts. *Sustainable Cities and Society*, Volume 53, p. 101966.

Djamila, H., Chu, C.-M. & Kumaresan, S., 2014. Effect of Humidity on Thermal Comfort in the Humid Tropics. *Journal of Building Construction and Planning Research*, 2(2), pp. 109-117.

Dobre, A. et al., 2005. Flow field measurements in the proximity of an urban intersection in London, UK. *Atmospheric Environment*, Volume 39, pp. 4647-4657.

Dütemeyer, D., Barlag, A., Kuttler, W. & Axt-Kittner, U., 2011. Measures against heat stress in the city of Gelsenkirchen, Germany. *Urban climate and heat stress*, 144(3-4), pp. 181-201.

Du, Y. & Mak, C., 2018. Improving pedestrian level low wind velocity environment in high-density cities: A general framework and case study. *Sustainable Cities and Society*, Volume 42, pp. 314-324.

Elnabawi, M., Hamza, N. & Dudek, S., 2016. Thermal perception of outdoor urban spaces in the hot arid region of Cairo, Egypt. *Sustainable Cities and Society*, Volume 22, p. 136–145.

Elnabawi, M. H., Hamza, N. & Dudek, S., 2014. Numerical modelling evaluation for the microclimate of an outdoor urban form in Cairo, Egypt. *Housing and Building National Research Center*.

Elwy, I., Ibrahim, Y., Fahmy, M. & Mahdy, M., 2018. Outdoor microclimatic validation for hybrid simulation workflow in hot arid climates against ENVI-met and field measurements. *Energy Procedia*, Volume 153, pp. 29-34.

Emmanuel, R. & Krüger, E., 2012. Urban heat island and its impact on climate change resilience in a shrinking city: the case of Glasgow, UK. *Build. Environ. Times*, Volume 53, pp. 137-149.

ENVI-met, 2019. *ENVI-met: A holistic microclimate model*. [Online] Available at: <http://www.envi-met.net/hg2e/doku.php?id=intro:modelconcept#internals> [Accessed 9 April 2020].

Erell, E. & Williamson, T., 2006. Comments on the correct specification of the analytical CTTC model for predicting the urban canopy layer temperature. *Energy and Buildings*, 38(8), pp. 1015-1021.

Erell, E., Pearlmutter, D. & Williamson, T., 2011. *Urban Microclimate: Designing the Spaces Between Buildings*. 1 ed. London: Earthscan.

Erell, E. & Williamson, T., 2007. Intra-urban differences in canopy layer air temperature at a mid-latitude city. *International Journal of Climatology*, 27(9), pp. 1243-1255.

Fabbri, K., Gaspari, J., Bartoletti, S. & Antonini, E., 2020. Effect of facade reflectance on outdoor microclimate: An Italian case study. *Sustainable Cities and Society*, Volume 54, p. 101984.

- Fahmy, . M., El-Hady , H. & Mahdy , M., 2016. LAI and Albedo Measurements Based Methodology for Numerical Simulation of Urban Tree's Microclimate: A Case Study in Egypt. *International Journal of Scientific & Engineering Research*, 7(9), pp. 2229-5518.
- Fahmy, M. & Sharples, S., 2009. On the development of an urban passive thermal comfort system in Cairo, Egypt. *Building and Environment*, 44(9), pp. 1907-1916.
- Fahmy, M., Sharples, S. & Yahiya, M., 2010. LAI based trees selection for mid latitude urban developments: A microclimatic study in Cairo, Egypt. *Building and Environment*, 45(2), pp. 345-357.
- Fanger, P., 1977. Local discomfort to the human body caused by non-uniform thermal environments. *Annals of Occupational Hygiene*, 20(3), pp. 285-291.
- Fanger, P. O., 1970. *Thermal comfort. Analysis and applications in environmental engineering..* 1st ed. Copenhagen: Malabar, Fla. : R.E. Krieger Pub. Co..
- Fang, X. et al., 2004. The multi-scale numerical modeling system for research on the relationship between urban planning and meteorological environment. *Advances in Atmospheric Sciences*, 21(1), pp. 103-112.
- Fang, Z. et al., 2018. Investigation into sensitivities of factors in outdoor thermal comfort indices. *Build. Environ.*, Volume 128, pp. 129-142.
- Farhadi, H., Faizi, M. & Sanaieian, H., 2019. Mitigating the urban heat island in a residential area in Tehran: Investigating the role of vegetation, materials, and orientation of buildings. *Sustainable Cities and Society*, Volume 46, p. 101448.
- Farhan, Y. & Alnawaiseh, S., 2018. Spatio-Temporal Variation in Rainfall Erosivity over Jordan Using Annual and Seasonal Precipitation. *Natural Resources*, Volume 9, pp. 242-267.
- Ferreira, A., Sousa, A. & Viegas, D., 1998. Numerical and experimental simulation of the wind field in the EXPO '98 area. *Wind and Structures*, 1(4), pp. 337-349.
- Ferreira, A., Sousa, A. & Viegas, D., 2002. Prediction of building interference effects on pedestrian level comfort. *Journal of Wind Engineering and Industrial Aerodynamics*, 90(4-5), pp. 305-319.
- Fiala, D. et al., 2012. UTCI-Fiala multi-node model of human heat transfer and temperature regulation. *Int. J. Biometeorol.*, 56(3), pp. 429-441.

Fiala, D., Lomas, K. & Stohrer, M., 2001. Computer prediction of human thermoregulatory and temperature responses to a wide range of environmental conditions. *Int. J. Biometeorol*, 45 (3), pp. 143-159.

Fountain, M. et al., 1999. An Investigation of Thermal Comfort at High Humidities. *ASHRAE Transactions*, 105(2), pp. 94-103.

Francis, L. & Jensen, M., 2017. Benefits of green roofs: a systematic review of the evidence for three ecosystem services. *Urban Forestry and Urban Greening*, Volume 28, pp. 167-176.

Frank, C. & Ruck, B., 2005. Double-arranged mound-mounted shelterbelts: influence of porosity on wind reduction between the shelters. *Environmental Fluid Mechanics*, 5(3), pp. 267-292.

Fröhlich, D., Gangwisch, M. & Matzarakis, A., 2019. Effect of radiation and wind on thermal comfort in urban environments - Application of the RayMan and SkyHelios model. *Urban Climate*, Volume 27, pp. 1-7.

Fuliotto, R. et al., 2010. Experimental and numerical analysis of heat transfer and airflow on an interactive building facade. *Energy and Buildings*, 42(1), pp. 23-28.

Gagge, . A., Fobelets, A. & Berglund, L., 1986. A standard predictive index of human response to the thermal environment. *ASHRAE Transactions*, Volume 92, pp. 709-731.

Gagge, A., Stolwijk, J. A. J. & Hardy, J. D., 1967. Comfort and thermal sensations and associated physiological responses at various ambient temperatures. *Environ. Res.*, Volume 1, pp. 1-20.

Gagge, . A., Stolwijk, J. & Nishi, Y., 1971. An Effective Temperature Scale Based on a Simple Model of Human Physiological Regulatory Response. *ASHRAE Transactions*, Volume 77, pp. 247-257.

Gago, E., Roldan, J., Pacheco-Torres, R. & Ordóñez, J., 2013. The city and urban heat islands: a review of strategies to mitigate adverse effects. *Renewable and Sustainable Energy Reviews*, Volume 25, pp. 749-758.

Gaitani, N., Mihalakakou, G. & Santamouris, M., 2007. On the use of bioclimatic architecture principles in order to improve thermal comfort conditions in outdoor spaces. *Building and Environment*, 42(1), pp. 317-324.

- Galal, O. M., Sailor, D. J. & Mahmoud, H., 2020. The impact of urban form on outdoor thermal comfort in hot arid environments during daylight hours, case study: New Aswan. *Building and Environment*, Volume 184, p. 107222.
- Gao, J., Wang, Y. & Wargocki, P., 2015. Comparative analysis of modified PMV models and set models to predict human thermal sensation in naturally ventilated buildings. *Build. Environ.*, Volume 92, pp. 200-208.
- Gao, Y. et al., 2012. Field studies on the effect of built forms on urban wind environments. *Renewable Energy*, Volume 46, pp. 148-154.
- Gartland, L., 2008. *Heat islands: understanding and mitigating heat in urban areas..* London: Earthscan.
- Ghaffarianhoseini, A., Berardi, U., Ghaffarianhoseini, A. & Al-Obaidi, K., 2019. Analyzing the thermal comfort conditions of outdoor spaces in a university campus in Kuala Lumpur, Malaysia. *Science of The Total Environment*, Volume 666, pp. 1327-1345.
- Girgis, N., Elariane, S. & Razik, M., 2015. Evaluation of heat exhausts impacts on pedestrian thermal comfort. *Sustainable Cities and Society*, Volume 27, pp. 152-159.
- Givoni, B., 1969. *Man, climate and architecture*. New York: John Wiley & Sons.
- Givoni, B. & Noguchi, M., 2000. *Issues in outdoor comfort research*. London, J&J, pp. 562-565.
- Golany, G. S., 1996. Urban design morphology and thermal performance. *Atmospheric Environment*, 30(3), pp. 455-465.
- Griffiths, I. & McIntyre, D., 1972. *Radiant Temperature and Comfort*. Building Research, Watford, England, Symposium 'Thermal Comfort and Moderate Heat' CIB Commission W45.
- Grimmond, C., King, T., Roth, M. & Oke, T., 1998. Aerodynamic roughness of urban areas derived from wind observations. *Bound-Layer Meteor*, Volume 89, p. 1-24.
- Gromke, C. et al., 2015. CFD analysis of transpirational cooling by vegetation: Case study for specific meteorological conditions during a heat wave in Arnhem, Netherlands. *Building and Environment*, Volume 83, pp. 11-26.
- Gromke, C. & Ruck, B., 2008. Aerodynamic modelling of trees for small-scale wind tunnel studies. *Forestry*, Volume 81, pp. 243-258.

Gros, A., Bozonnet, E. & Inard, C., 2014. Cool materials impact at district scale—Coupling building energy and microclimate models. *Sustainable Cities and Society*, Volume 13, pp. 254-266.

Gross, G., 1991. On the application of mesoscale models with Darmstadt as an example. I: Wind and temperature. *Meteorol Rundsch*, 43(4), pp. 97-112.

Gulyás, Á. & Matzarakis, A., 2009. Seasonal and spatial distribution of physiologically equivalent temperature (PET) index in Hungary. *Quarterly Journal of the Hungarian Meteorological Service*, 113(3), p. 221–231.

Gulyas, A., Unger, J. & Matzarakis, A., 2006. Assessment of the microclimatic and human comfort conditions in a complex urban environment: Modelling and measurements. *Building and Environment*, Volume 41, pp. 1713-1722.

Guo, C., Buccolieri, R. & Gao, Z., 2019. Characterizing the morphology of real street models and modeling its effect on thermal environment. *Energy and Buildings*, Volume 203, p. 109433.

Gu, Z., Zhang, Y. & Lei, K., 2010. Large eddy simulation of flow in a street canyon with tree planting under various atmospheric instability conditions. *Science China Technological Sciences*, Volume 53, pp. 1928-1937.

Hage, K. D., 1975. Urban-Rural Humidity Differences. *J. Appl. Meteor.*, Volume 14, p. 1277–1283.

Hang, J., Sandberg, M. & Li, Y., 2009. Effect of urban morphology on wind condition in idealized city models. *Atmospheric Environment*, Volume 43, pp. 869-878.

Hatefnia, N., Barakati, A., Ghobad, M. & Panah, A. E., 2016. *A Novel Methodology to Assess Mean Radiant Temperature in Complex Outdoor Spaces*. Los Angeles, PLEA - 32th International Conference on Passive and Low Energy Architecture..

Holopainen, R., 2012. *A human thermal model for improved thermal comfort*. Finland: VTT Technical Research Centre of Finland.

Hong, B. & Lin, B., 2015. Numerical studies of the outdoor wind environment and thermal comfort at pedestrian level in housing blocks with different building layout patterns and trees arrangement. *Renewable Energy*, Volume 73, pp. 18-27.

- Honjo, T., 2009. Thermal Comfort in Outdoor Environment. *GlobEnvironment Res*, p. 43–47.
- Höppe, P., 1993. Heat balance modelling.. *Experientia*, Volume 49, p. 741–746.
- Höppe, P., 1999. The physiological equivalent temperature – a universal index for the biometeorological assessment of the thermal environment. *International Journal of Biometeorology*, Volume 43, p. 71–75.
- Höppe, P., 2002. Different aspects of assessing indoor and outdoor thermal comfort. *Energy and Buildings*, 34(6), pp. 661-665.
- Houghten, F. & Yaglou, C., 1923. Determining lines of equal comfort.. *ASHVE Transactions*, Volume 29.
- Ho, Y., Liu, C. & Wong, M., 2015. Preliminary study of the parameterisation of street-level ventilation in idealised two-dimensional simulations. *Building and Environment*, Volume 89, pp. 345-355.
- Huang, H. et al., 2008. CFD analysis on traffic-induced air pollutant dispersion under non-isothermal condition in a complex urban area in winter. *Journal of Wind Engineering and Industrial Aerodynamics*, Volume 96, pp. 1774-1788.
- Huang, J., 2007. Prediction of air temperature for thermal comfort of people in outdoor environments. *International Journal of Biometeorology*, Volume 51, p. 375–382.
- Huang, J., Cedeño-Laurent, J. & Spengler, J. D., 2014. CityComfort+: A simulation-based method for predicting mean radiant temperature in dense urban areas. *Building and Environment*, Volume 80, pp. 84-95.
- Hussain, M. & Lee, B., 1980. *An investigation of wind forces on three-dimensional roughness elements in a simulated atmospheric boundary layer flow. Part II. Flow over large arrays of identical roughness elements and the effect of frontal and side aspect ratio variations*, Sheffield: Department of Building Sciences, University of Sheffield.
- Huttner, S., 2012. *further development and application of the 3d microclimate simulation environment*. Mainz: Johannes Gutenberg-Universität Mainz.
- Hwang, R.-L., Lin, T.-P. & Matzarakis, A., 2011. Seasonal effects of urban street shading on long-term outdoor thermal comfort. *Building and Environment*, 46(4), pp. 863-870.

Hwang, R. L. & Lin, T. P., 2007. Thermal Comfort Requirements of Occupants of Semi-Outdoor and Outdoor Environments in Hot Humid Regions. *Architectural Science Review*, 50(4), pp. 357-364.

IEA, 2018. *The future of cooling*, IEA Publications France : Opportunities For Energy Efficient Air Conditioning.

IPCC, 2014. *Climate Change 2014: Synthesis Report*, Geneva: IPCC.

Jamei, E., Ossen, D. R. & Rajagopalan, P., 2017. Investigating the effect of urban configurations on the variation of air temperature. *International Journal of Sustainable Built Environment*, 6(2), pp. 389-399.

Jendritzky, G. & De Dear, R., 2009. *Biometeorology for Adaptation to Climate Variability and Change*. s.l.:Springer, Dordrecht.

Jendritzky, G., de Dear, R. & Havenith, G., 2012. UTCI—Why another thermal index?. *International Journal of Biometeorology*, Volume 56, p. 421–428.

Jendritzky, G. & Höppe, P., 2017. The UTCI and the ISB. *Int J Biometeorol* , pp. 23-27.

Jendritzky, G. & Nübler, W., 1981. A Model Analysing the Urban Thermal Environment in Physiologically Significant Terms. *ARCHIVES FOR METEOROLOGY, GEOPHYSICS, AND BIOCLIMATOLOGY*, pp. 313-326.

Jendritzky, G., Sönning, W. & Swantes, J., 1979. *Klimatologische Probleme – ein einfaches Verfahren zur Vorhersage der Wärmebelastung*, in *Zeitschrift für angewandte Bäder und Klimaheilkunde*, Freiburg: s.n.

Jiang, Y., Wu , C. & Teng, M., 2020. Impact of Residential Building Layouts on Microclimate in a High Temperature and High Humidity Region. *Sustainability*, 12(3), p. 16.

Jing, S., Li, B., Tan, M. & Lui, H., 2013. Impact of Relative Humidity on Thermal Comfort in a Warm Environment. *Indoor and Built Environment*, 22(4), p. 598–607.

Johansson, E., 2006. Influence of urban geometry on outdoor thermal comfort in a hot dry climate: A study in Fez, Morocco. *Building and Environment*, 41(10), pp. 1326-1338.

- Johansson, E. & Emmanuel, R., 2006. The influence of urban design on outdoor thermal comfort in the hot, humid city of Colombo, Sri Lanka. *International Journal of Biometeorology*, Volume 51, p. 119–133.
- Johansson, E., Yahia, M. W., Arroyo, I. & Bengs, C., 2018. Outdoor thermal comfort in public space in warm-humid Guayaquil, Ecuador. *International Journal of Biometeorology*, Volume 62, p. 387–399.
- Johnson, G. & Hunter, L., 1999. Some insights into typical urban canyon airflows. *Atmos. Environ.*, Volume 33, p. 3391–3399.
- Johnson, G. & Hunter, L., 1998. Urban wind flows: wind tunnel and numerical simulations—a preliminary comparison. *Environmental Modelling & Software*, 13(2-4), pp. 279-286.
- Kadhim, A. & Rajjal, Y., 1988. City profile: Amman. *Cities*, 5(4), pp. 318-325.
- Kadhim, M. & Rajjal, Y., 1988. City profile Amman. *cities*, November, 5(4), pp. 318-325.
- Karakounos, I., Dimoudi, A. & Zoras, S., 2018. The influence of bioclimatic urban redevelopment on outdoor thermal comfort. *Energy and Buildings*, Volume 158, pp. 1266-1274.
- Kariminia, S. et al., 2016. RETRACTED ARTICLE: Modelling thermal comfort of visitors at urban squares in hot and arid climate using NN-ARX soft computing method. *Theoretical and Applied Climatology*, Volume 124, p. 991–1004.
- Kastner-Klein, P., Berkowicz, R. & Britter, R., 2004. The influence of street architecture on flow and dispersion in street canyon. *Meteorology and Atmospheric Physics*, Volume 87, p. 121–131.
- Katić, K., Li, R. & Zeiler, W., 2016. Thermophysiological models and their applications: a review. *Build. Environ.*, Volume 106, pp. 286-300.
- Kestrel, 2015. *Kestrel 5400 Heat Stress Tracker Guide*. s.l.:kestrel meters.
- Khanduri, A., Stathopoulos, T. & Bédard, C., 1998. Wind-induced interference effects on buildings — a review of the state-of-the-art. *Engineering Structures*, 20(7), pp. 617-630.
- Kong, L. et al., 2017. Regulation of outdoor thermal comfort by trees in Hong Kong. *Sustainable Cities and Society*, Volume 31, pp. 12-25.

Kotzen, B., 2003. An investigation of shade under six different tree species of the Negev Desert towards their potential use for enhancing micro-climatic conditions in landscape architectural development. *Journal of Arid Environments*, Volume 55, pp. 231-274.

Kruger, E., Drach, P., Emmanuel, R. & Corbella, O., 2012. Assessment of daytime outdoor comfort levels in and outside the urban area of Glasgow, UK. *International Journal of Biometeorology*, Volume 57, pp. 521-533.

Krüger, E., Minella, F. & Rasia, F., 2011. Impact of urban geometry on outdoor thermal comfort and air quality from field measurements in Curitiba, Brazil. *Building and Environment*, 46(3), pp. 621-634.

Kubota, T., Miura, M., Tominaga, Y. & Mochida, A., 2008. Wind tunnel tests on the relationship between building density and pedestrian-level wind velocity: Development of guidelines for realizing acceptable wind environment in residential neighborhoods. *Building and Environment*, Volume 43, pp. 1699-1708.

Lai, A., Maing, M. & Ng, E., 2017. Observational studies of mean radiant temperature across different outdoor spaces under shaded conditions in densely built environment. *Building and Environment*, Volume 114, pp. 397-409.

Lai, D. et al., 2019. A review of mitigating strategies to improve the thermal environment and thermal comfort in urban outdoor spaces. *Science of The Total Environment*, Volume 661, pp. 337-353.

Lamarca, C., Qüense, J. & Henríquez, C., 2018. Thermal comfort and urban canyons morphology in coastal temperate climate, Concepción, Chile. *Urban Climate*, Volume 23, pp. 159-172.

Lane, D. M., Hebl, M. & Guerra, R., 2013. *Introduction to Statistics*, Houston: University of Houston.

Lan, Y. & Zhan, Q., 2017. How do urban buildings impact summer air temperature? The effects of building configurations in space and time. *Build. Environ.*, Volume 125, pp. 88-98.

Lauder, B. & Spalding, D. B., 1974. The numerical computation of turbulent flows. *Computer Methods in Applied Mechanics and Engineering*, 3(2), p. 269–289.

- Leech, A. et al., 2000. Outdoor air pollution epidemiologic studies. *American Journal of Respiration and Critical Care Medicine*, 161(3), p. A308.
- Lee, D., 1991. Urban rural humidity differences in London. *International Journal of Climatology*, 11(5), pp. 577-582.
- Lee, H. & Mayerb, H., 2018. Maximum extent of human heat stress reduction on building areas due to urban greening. *Urban Forestry & Urban Greening*, Volume 32, pp. 154-167.
- Lee, H., Mayer, H. & Chen, L., 2016. Contribution of trees and grasslands to the mitigation of human heat stress in a residential district of Freiburg, Southwest Germany. *Landscape and Urban Planning*, Volume 148, pp. 37-50.
- Lee, L. S. H., Cheung, . P. K., Fung, C. K. W. & Jim, . C. Y., 2020. Improving street walkability: Biometeorological assessment of artificial-partial shade structures in summer sunny conditions. *International Journal of Biometeorology* , Volume 64, p. 547–560.
- Leenders, J., van Boxel, J. & Sterk, G., 2007. The effect of single vegetation elements on wind speed and sediment transport in the Sahelian zone of Burkina Faso. *Earth Surface Processes and Landforms*, 32(10).
- Leng, H., Liang, S. & Yuan, Q., 2020. Outdoor thermal comfort and adaptive behaviors in the residential public open spaces of winter cities during the marginal season. *International Journal of Biometeorology*, Volume 64, p. 217–229.
- Li, B. et al., 2010. Occupant's perception and preference of thermal environment in free-running buildings in China. *Indoor Built Environ* , 19(4), p. 405–412.
- Li, K. & Yu, Z., 2008. Comparative and combinative study of urban heat island in Wuhan City with remote sensing and CFD simulation. *Sensors*, Volume 8, pp. 6692-6703.
- Li, K., Zhang, Y. & Zhao, L., 2016. Outdoor thermal comfort and activities in the urban residential community in a humid subtropical area of China. *Energy and Buildings*, Volume 133, pp. 498-511.
- Liljequist, G. H. & Cehak, K., 1984. *General meteorology*. 3rd ed. Berlin: Springer-Verlag Berlin Heidelberg.

Lin, B., Li, X., Zhu, Y. & Qin, Y., 2008. Numerical simulation studies of the different vegetation patterns' effects on outdoor pedestrian thermal comfort. *Journal of Wind Engineering and Industrial Aerodynamics*, 96(10-11), pp. 1707-1718.

Lin, T., 2009. Thermal perception, adaptation and attendance in a public square in hot and humid regions. *Building and Environment*, Volume 44, pp. 2017-2026.

Lin, T. & Matzarakis, A., 2008. Tourism climate and thermal comfort in Sun Moon Lake, Taiwan. *Int. J. Biometeorol.*, 52(4), pp. 281-290.

Lin, T.-P., Matzarakis, A. & Hwang, R.-L., 2010. Shading effect on long-term outdoor thermal comfort. *Building and Environment*, 45(1), pp. 213-221.

Liu, D., Hu, S. & Liu, J., 2020. Contrasting the performance capabilities of urban radiation field between three microclimate simulation tools. *Building and Environment*, Volume 175, p. 106789.

Liu, J., Chen, J. M., Black, T. A. & Novak, M. D., 1996. E-ε modelling of turbulent air flow downwind of a model forest edge. *Boundary-Layer Meteorol*, Volume 77, p. 21-44.

Liu, J., Niu, J., Mak, C. & Xia, Q., 2017. Detached eddy simulation of pedestrian-level wind and gust around an elevated building. *Building and Environment*, Volume 125, pp. 168-179.

Liu, W. et al., 2007. Temporal characteristics of the Beijing urban heat island. *Theoretical and Applied Climatology*, Volume 87, p. 213-221.

Liu, W., You, H. & Dou, J., 2009. Urban-rural humidity and temperature differences in the Beijing area. *Theoretical and Applied Climatology*, Volume 96, p. 201-207.

Liu, Z. et al., 2020. An investigation on external airflow around low-rise building with various roof types: PIV measurements and LES simulations. *Building and Environment*, Volume 169, p. 106583.

Liu, . Z., Zheng, S. & Zhao, L., 2018. Evaluation of the ENVI-Met Vegetation Model of Four Common Tree Species in a Subtropical Hot-Humid Area. *ATMOSPHERE*, 9(5), p. 198.

Li, Y. et al., 2018. Human responses to high air temperature, relative humidity and carbon dioxide concentration in underground refuge chamber. *Build. Environ.*, Volume 131, pp. 53-62.

Lobaccaro, G. et al., 2019. Effects of Orientations, Aspect Ratios, Pavement Materials and Vegetation Elements on Thermal Stress inside Typical Urban Canyons. *International Journal of Environmental Research and Public Health*, 16(19), p. 3574.

Lobaccaro, G. & Acero, J., 2015. Comparative analysis of green actions to improve outdoor thermal comfort inside typical urban street canyons. *Urban Climate*, Volume 14, pp. 251-267.

Louka, P., Belcher, S. & Harrison, R., 2000. Coupling between air flow in streets and the well-developed boundary layer aloft. *Atmos. Environ*, Volume 34, p. 2613–2621.

Lucchese, J., Mikuri, L., de Freitas, N. & Andreasi, W., 2016. Application of selected indices on outdoor thermal comfort assessment in Midwest Brazil. *Energy Environ.*, 7(5), pp. 291-302.

Lucchese, J., Mikuri, L., de Freitas, N. & Andreasi, W., 2016. Application of selected indices on outdoor thermal comfort assessment in Midwest Brazil. *Energy Environ.*, 7(5), pp. 291-302.

Mahmoud, A. H. A., 2011. Analysis of the microclimatic and human comfort conditions in an urban park in hot and arid regions. *Building and Environment*, 46(12), pp. 2641-2656.

Mahmoud, H. & Ghanem, H., 2019. URBAN GEOMETRY MITIGATION GUIDELINES TO IMPROVE OUTDOOR THERMAL PERFORMANCE IN EGYPTIAN HOT ARID NEW CITIES. *Journal of Engineering Sciences: Assiut University*, 47(2), pp. 172-193.

Makaremi, N., Salleh, E., Jaafar, M. & GhaffarianHoseini, A., 2012. Thermal comfort conditions of shaded outdoor spaces in hot and humid climate of Malaysia. *Building and Environment*, Volume 48, pp. 7-14.

Malkawi, F. & Abu-Dayyeh, N., 2004. The condition of physical planning in Jordan 1970–1990. *Institut Francaise du Proche-Orient*, Volume 14.

Manins, P. & Sawford, B., 1979. A model of katabatic winds. *Journal of Atmospheric Science*, Volume 36, pp. 619-630.

Manni, M. et al., 2019. Exploiting selective angular properties of retro-reflective coatings to mitigate solar irradiation within the urban canyon. *Solar Energy*, Volume 189, pp. 74-85.

Masson, V., 2000. A physically-based scheme for the urban energy budget in atmospheric models. *Boundary-Layer Meteorol.*, 94(3), pp. 357-397.

- Masson, V., 2006. Urban surface modeling and the meso-scale impact of cities. *Theoretical and Applied Climatology*, Volume 84, p. 35–45.
- Masterton, J. M. & Richardson, F. A., 1979. *Humidex: a method of quantifying human discomfort*. 1st ed. Ontario: Downsview: Atmospheric Environment Service.
- Mathews, E., 1987. Prediction of the wind-generated pressure distribution around buildings. *Journal of Wind Engineering and Industrial Aerodynamics*, 25(2), pp. 219-228.
- Matias , M. & Lopes, A., 2020. Surface Radiation Balance of Urban Materials and Their Impact on Air Temperature of an Urban Canyon in Lisbon, Portugal. *Applied Sciences*, 10(6), p. 2193.
- Matzarakis, A., 2000. *MODELLING OF RADIATION FLUXES IN URBAN AREAS AND THEIR RELEVANCE TO THERMAL CONDITIONS OF HUMANS*. s.l., American Meteorological Society, pp. 163-164.
- Matzarakis, A. & Amelung, B., 2008. Physiological Equivalent Temperature as Indicator for Impacts of Climate Change on Thermal Comfort of Humans. *Advances In Global Change*, Volume 30, pp. 161-172.
- Matzarakis, A. & Helmut , M., 1996. Another kind of environmental stress: thermal stress. *WHO newsletter*, 18 January, pp. 7-10.
- Matzarakis, A., Mayer, H. & Iziomon, M. G., 1999. Applications of a universal thermal index: physiological equivalent temperature. *Int J Biometeorol*, 26 May, Issue 43, p. 76–84.
- Matzarakis, A., Rutz , F. & Mayer, H., 2007. Modelling radiation fluxes in simple and complex environments—application of the RayMan model. *International Journal Of Biometeorology*, 51(4), pp. 323-334.
- Matzarakis, A., Rutz, F. & Mayer, H., 2010. Modelling radiation fluxes in simple and complex environments: basics of the RayMan model. *International Journal of Biometeorology*, Volume 54, p. 131–139.
- Mawn, G. P., 1972. Framework for Destiny: San Francisco, 1847. *California Historical Quarterly* 51, pp. 78-165.
- Ma, X. et al., 2020. Performance of Different Urban Design Parameters in Improving Outdoor Thermal Comfort and Health in a Pedestrianized Zone. *Int. J. Environ. Res. Public Health*, Volume 17, p. 2258.

Mayer, E., 1993. Objective criteria for thermal comfort. *Building and Environment*, 28(4), pp. 399-403.

Mayer, H. & Höppe, P., 1987. Thermal comfort of man in different urban environments. *Theoretical and Applied Climatology volume*, Volume 38, pp. 43 - 49.

Meir, P., Grace, J. & Miranda, A. C., 200. Photographic method to measure the vertical distribution of leaf area density in forests. *Agricultural and Forest Meteorology*, 102(2-3), pp. 105-111.

Mei, S.-J., Luo, Z., Zhao, F.-Y. & Wang, H.-Q., 2019. Street canyon ventilation and airborne pollutant dispersion: 2-D versus 3-D CFD simulations. *Sustainable Cities and Society*, Volume 50, p. 101700.

Melbourne, W. & JouBerx, P. N., 1971. *Problems of wind flow at the base of tall buildings*. Tokyo, Int. Conf. on Wind Effects on Buildings and Structures,.

Mellor, G. & Yamada, T., 1975. A simulation of the Wangara atmospheric boundary layer data. *J. Atmos. Sci*, Volume 32, pp. 2309-2329.

Meroney, R., 1982. Turbulent diffusion near buildings. In: E. Plate, ed. *Fundamentals of Meteorology and Their Applications to Problems in Environmental and Civil Engineering*. Engineering Meteorology: Elsevier Scientific, pp. 481-525.

Meteorological Office, 1969. *Observer's handbook*. 3rd ed. London: H. M. Stationery Off.

Middel, A., Selover, N., Hagen, B. & Chhetri, N., 2016. Impact of shade on outdoor thermal comfort—a seasonal field study in Tempe, Arizona. *International Journal of Biometeorology*, Volume 60, p. 1849–1861.

Mirzaei, P. A. & Haghighat, F., 2010. Approaches to study Urban Heat Island – Abilities and limitations. *Building and Environment*, 45(10), pp. 2192-2201.

Mirzaei, P. A. & Haghighat, F., 2011. Pollution removal effectiveness of the pedestrian ventilation system. *Journal of Wind Engineering and Industrial Aerodynamics*, Volume 99, pp. 46-58.

Mirzaei, P. & Haghighat, F., 2010. A novel approach to enhance outdoor air quality: Pedestrian ventilation system. *Building and Environment*, Volume 45, pp. 1582-1593.

- Mitchell, V., Mein, R. & McMahon, T., 2001. Modelling the urban water cycle. *Environ. Model. Softw.*, 16(7), pp. 615-629.
- Monteiro, L. M. & Alucc, M. P., 2006. *Calibration of outdoor thermal comfort models*. Geneva, PLEA.
- Moonen, P. et al., 2012. Urban Physics: effect of the micro-climate on comfort, health and energy demand. *Frontiers of Architectural Research*, 1(3), pp. 197-228.
- Morakinyo, H. et al., 2020. Right tree, right place (urban canyon): Tree species selection approach for optimum urban heat mitigation - development and evaluation. *Science of The Total Environment*, Volume 719, p. 137461.
- Morakinyo, T., Dahanayake, K., Adegun, O. & Balogun, A., 2016. Modelling the effect of tree-shading on summer indoor and outdoor thermal condition of two similar buildings in a Nigerian university. *Energy and Buildings*, Volume 130, pp. 721-732.
- Morakinyo, T. E. et al., 2017. A study on the impact of shadow-cast and tree species on in-canyon and neighborhood's thermal comfort. *Building and Environment*, Volume 115, pp. 1-17.
- Morakinyo, T. E. et al., 2017. A study on the impact of shadow-cast and tree species on in-canyon and neighborhood's thermal comfort. *Building and Environment*, Volume 115, pp. 1-17.
- Morakinyo, T. E. & Lam, Y. F., 2016. Simulation study on the impact of tree-configuration, planting pattern and wind condition on street-canyon's micro-climate and thermal comfort. *Building and Environment*, Volume 103, pp. 262-275.
- Müller, N., Kuttler, W. & Barlag, A.-B., 2014. Counteracting urban climate change: adaptation measures and their effect on thermal comfort. *Theoretical and Applied Climatology volume* , Volume 115, p. 243–257.
- Muniz-Gaal, L. P., Pezzuto, C. C., de Carvalho, M. & Mota, L., 2020. Urban geometry and the microclimate of street canyons in tropical climate. *Building and Environment*, Volume 169, p. 106547.
- Murakami, S., 2006. Environmental Design of Outdoor Climate Based on CFD. *Journal of Fluid Dynamics Research*, Volume 38, pp. 108-126.

- Murakami, S. & Mochida, A., 1989. Three-dimensional numerical simulation of turbulent flow around buildings using the $k-\epsilon$ turbulence model. *Building and Environment*, 24(1), pp. 51-64.
- Murakami, S., Mochida, A. & Hibi, K., 1987. Three-dimensional numerical simulation of air flow around a cubic model by means of large eddy simulation. *Journal of Wind Engineering and Industrial Aerodynamics*, 25(3), pp. 291-305.
- Nakamura, Y. & Oke, T., 1988. Wind, temperature and stability conditions in an east-west oriented urban canyon. *Atmos. Environ.*, Volume 22, p. 2691-2700.
- Nakamura, Y. & Oke, T., 1988. Wind, Temperature and Stability Conditions in an East-West Oriented Urban Canyon. *Atmospheric Environment*, Volume 22, pp. 2691-2700.
- Ng, E., 2009. Policies and technical guidelines for urban planning of high-density cities – air ventilation assessment (AVA) of Hong Kong. *Building and Environment*, Volume 44, p. 1478-1488.
- Ng, E. et al., 2011. Improving the wind environment in high-density cities by understanding urban morphology and surface roughness: A study in Hong Kong. *Landscape and Urban Planning*, 101(1), pp. 59-74.
- Niachou, K., Livada, I. & Santamouris, M., 2008. Experimental study of temperature and airflow distribution inside an urban street canyon during hot summer weather conditions. Part II: Airflow analysis. *Building and Environment*, 43(8), pp. 1393-1403.
- Nicol, J. & Humphreys, M., 1973. Thermal comfort as part of a self-regulating system. *Build. Res. Pr.*, Volume 1, pp. 174-179.
- Nicol, J. & Humphreys, M., 2002. Adaptive thermal comfort and sustainable thermal standards for buildings. *Energy Build*, Volume 34, pp. 563-572.
- Nielsen, M., 2000. Turbulent ventilation of a street canyon. *Environmental Monitoring and Assessment*, Volume 65, pp. 396-398.
- Nikolopoulou, Marialena, 2004. *Designing Open Spaces in the Urban Environment: a Bioclimatic Approach*, Atenas: Centre for Renewable Energy Resources.
- Nikolopoulou, M., Baker, N. & Steemers, K., 2001. Thermal comfort in outdoor urban spaces: Understanding the human parameter. *Solar Energy*, Volume 70, pp. 227-235.

- Nikolopoulou, M. & Lykoudis, S., 2006. Thermal comfort in outdoor urban spaces: Analysis across different European countries. *Building and Environment*, 41(11), pp. 1455-1470.
- Nikolopoulou, M. & Lykoudis, S., 2007. Use of outdoor spaces and microclimate in a Mediterranean urban area. *Building and Environment*, 42(10), pp. 3691-3707.
- Nkemdirim, L., 1980. Cold air drainage and temperature fields in an urban environment: a case study of topographical influence on climate. *Atmospheric Environment*, Volume 14, pp. 375-381.
- Nunez, M. & Oke, T., 1977. The Energy Balance of an Urban Canyon. *Journal of Applied Meteorology*, 16(1), pp. 11-19.
- Oke, T., 1997. Urban environments. In: . W. Bailey, T. Oke & W. Rouse, eds. *The Surface Climates of Canada*. Montréal: McGill-Queen's University Press, p. 303–327.
- Oke, . T. R., Mills, G., Christen, A. & Voogt, J., 2017. *Urban Climates*. 1st ed. Cambridge: Cambridge University Press.
- Oke, T. R., 1988. Street design and urban canopy layer climate. *Energy Build.*, Volume 11, pp. 103- 113.
- Ole Fanger, P. & Toftum, J., 2002. Extension of the PMV model to non-air-conditioned buildings in warm climates. *Energy Build.*, Volume 34, pp. 533-536.
- Oliveira, S. & Andrade, H., 2007. An Initial Assessment of the Bioclimatic Comfort in an Outdoor Public Space in Lisbon. *International Journal of Biometeorology*, 52(1), pp. 69-84.
- Oshio, H., Asawa, T., Hoyano, A. & Miyasaka, S., 2015. Estimation of the leaf area density distribution of individual trees using high-resolution and multi-return airborne LiDAR data. *Remote Sensing of Environment*, Volume 166, pp. 116-125.
- Palaiologou, G., 2012. *URBAN RHYTHMS: historic housing evolution and socio-spatial boundaries*. Chile, s.n.
- Paltridge, G. W. & Platt, C., 1976. Radiative processes in Meteorology and Climatology. *Elsevier*, Volume 5, p. 334.
- Panagiotou, I., Neophytou, M. K.-A., Hamlyn, D. & Britter, R. E., 2013. City breathability as quantified by the exchange velocity and its spatial variation in real inhomogeneous urban

geometries: An example from central London urban area. *Science of The Total Environment*, 442(1), pp. 466-477.

Pantavou, K., Santamouris, M., Asimakopoulos, D. & Theoharatos, G., 2014. Empirical calibration of thermal indices in an urban outdoor Mediterranean environment. *Building and Environment*, Volume 80, pp. 283-292.

Paramita, B., Fukuda, H., Khidmat, R. & Matzarakis, A., 2018. Building Configuration of Low-Cost Apartments in Bandung—Its Contribution to the Microclimate and Outdoor Thermal Comfort. *Buildings*, 8(9), p. 123.

Park, M., Hagishima, A., Tanimoto, J. & Narita, K., 2012. Effect of urban vegetation on outdoor thermal environment: field measurement at a scale model site. *Building and Environment*, Volume 56, pp. 38-46.

Parsons, K., 2014. *Human Thermal Environments: The Effects of Hot, Moderate, and Cold Environments on Human Health, Comfort, and Performance*. 3rd ed. Boca Raton, Florida: Taylor & Francis Group.

Parsons, K. C., 2003. *Human thermal environments the effects of hot, moderate, and cold environments on human health, comfort, and performance*. 2nd ed. London: Taylor & Francis.

Paterson, D. A. & Colin, A. J., 1986. Computation of wind flows over three-dimensional buildings. *Journal of Wind Engineering and Industrial Aerodynamics*, 24(3), pp. 193-213.

Peel, M., Finlayson, B. & McMahon, T., 2007. Updated world map of the Köppen-Geiger climate classification. *Hydrol. Earth Syst. Sci.*, 11(5), p. 1633–1644.

Pendwarden, A. & Wise, A., 1975. *Wind environment around buildings*, s.l.: Building Research Establishment Digest..

Penwarden, A., 1973. Acceptable wind speeds in towns. *Building Science*, 8(3), pp. 259-267.

Perini, K. & Magliocco, A., 2014. Effects of vegetation, urban density, building height, and atmospheric conditions on local temperatures and thermal comfort. *Urban Forestry & Urban Greening*, 13(3), pp. 495-506.

Perini, K. & Magliocco, A., 2014. Effects of vegetation, urban density, building height, and atmospheric conditions on local temperatures and thermal comfort. *Urban Forestry & Urban Greening*, 13(3), pp. 495-506.

Pickup, J. & de Dear, R., 1999. An outdoor thermal comfort index (Out_SET*)– Part 1 – the model and its assumptions. *World Meteorological Organization*, pp. 284-290.

Potter, J. & de Dear, R., 2000. *Field Study to Calibrate Outdoor Thermal Comfort Index*. Geneva, Switzerland, Biometeorology and Urban Climatology at the Turn of the Millennium, pp. 315-320.

Potter, R. B., Darmame, K., Barham, N. & Nortcliff, S., 2009. “Ever-growing Amman”, Jordan: Urban expansion, social polarisation and contemporary urban planning issues. *Habitat International*, 33(1), pp. 81-92.

Priyadarsini, R., Hien, W. N. & David, C. K. W., 2008. Microclimatic modeling of the urban thermal environment of Singapore to mitigate urban heat island. *Solar Energy*, 82(8), pp. 727-745.

Radhi, H., Fikry, F. & Sharples, S., 2013. Impacts of urbanisation on the thermal behaviour of new built up environments: A scoping study of the urban heat island in Bahrain. *Landscape and Urban Planning*, Volume 113, pp. 47-61.

Ramponi, R., Blocken, B., Laura, B. & Janssen, W., 2015. CFD simulation of outdoor ventilation of generic urban configurations with different urban densities and equal and unequal street widths. *Building and Environment*, Volume 92, pp. 152-166.

Ratti, C. et al., 2002. Analysis of 3-D urban databases with respect to pollution dispersion for a number of European and American cities. *Water Air Soil Pollut*, 2(5-6), pp. 459-469.

Razak, A. A., Hagishima, A., Ikegaya, N. & Tanimoto, J., 2013. Analysis of airflow over building arrays for assessment of urban wind environment. *Building and Environment*, Volume 59, pp. 56-65.

Riain, C., Fisher, B., Martin, C. & Littler, J., 1998. Flow field and pollution dispersion in a central London street. *Environmental Monitoring and Assessment*, Volume 52, pp. 299-314.

Ricciardelli, F. & Polimeno, S., 2006. Some characteristics of the wind flow in the lower urban boundary layer. *Journal of Wind Engineering and Industrial Aerodynamics*, Volume 94, pp. 815-832.

Richards, P., Mallison, G., McMillan, D. & Li, Y., 2002. Pedestrian level wind speeds in downtown Auckland. *Wind and Structures*, 5(2-4), pp. 151-164.

Rizwan, A., Dennis, L. & Chunho, L., 2008. A review on the generation, determination and mitigation of urban heat island. *J. Environ. Sci.*, 20(1), pp. 120-128.

Robitu, M., Musy, M., Inard, C. & Groleau, D., 2006. Modeling the influence of vegetation and water pond on urban microclimate. *Solar Energy*, Volume 80, pp. 435-447.

Rohles, H., 1980. Temperature or temperament: a psychologist looks at thermal comfort. *ASHRAE Transactions*, 86(1), pp. 5-13.

Rosas, B. et al., 1980. *Measuring and modeling carbon monoxide at a high volume intersection*, Minnesota: Int. Tech. Rep. Federal Highway Administration and Minnesota Department of Transportation.

Rose-Redwood, R. S., 2005. *Commissioners' Plan of 1811*. New York: Syracuse University Press.

Rossi, F. et al., 2016. Experimental evaluation of urban heat island mitigation potential of retro-reflective pavement in urban canyons. *Energy and Buildings*, Volume 126, pp. 340-352.

Rosso, F. et al., 2018. On the impact of innovative materials on outdoor thermal comfort of pedestrians in historical urban canyons. *Renewable Energy*, Volume 118, pp. 825-839.

Rosso, F., Pisello, A. L., Cotana, F. & Ferrero, M., 2016. On the thermal and visual pedestrians' perception about cool natural stones for urban paving: A field survey in summer conditions. *Building and Environment*, Volume 107, pp. 198-214.

Ruiz, M. & Correa, E., 2015. Adaptive model for outdoor thermal comfort assessment in an Oasis city of arid climate. *Build. Environ.*, Volume 85, pp. 40-51.

Salata, F., Golasi, I., de Lieto Vollaro, R. & de Lieto Vollaro, A., 2016. Outdoor thermal comfort in the Mediterranean area. A transversal study in Rome, Italy. *Building and Environment*, Volume 91, pp. 46-61.

Salata, F. et al., 2017. Relating microclimate, human thermal comfort and health during heat waves: An analysis of heat island mitigation strategies through a case study in an urban outdoor environment. *Sustainable Cities and Society*, Volume 30, pp. 79-96.

Salata, F., Golasi, L., Vollarob, R. d. L. & Vollaro, A. d. L., 2016. Urban microclimate and outdoor thermal comfort. A proper procedure to fit ENVI-met simulation outputs to experimental data. *Sustainable Cities and Society*, pp. 318-343.

Santamouris, M., 2014. Cooling the cities ? A review of reflective and green roof mitigation technologies to fight heat island and improve comfort in urban environments. *Solar Energy*, Volume 103, pp. 682-703.

Santamouris, M., 2016. Innovating to zero the building sector in Europe: minimising the energy consumption, eradication of the energy poverty and mitigating the local climate change. *Solar Energy*, Volume 128, pp. 61-94.

Santamouris, M., Ding, L. & Osmond, P., 2019. Urban Heat Island Mitigation. In: P. Newton, D. Prasad, A. Sproul & S. White, eds. *Decarbonising the Built Environment*. Singapore: Palgrave Macmillan, pp. 337-355.

Santamouris, M., Koronakis, I., Livada, I. & Asimakopoulos, D., 1999. Thermal and air flow characteristics in a deep pedestrian canyon under hot weather conditions. *Atmospheric Environment*, Volume 33, pp. 4503-4521.

Santiago, J. et al., 2017. Evaluation of a CFD-based approach to estimate pollutant distribution within a real urban canopy by means of passive samplers. *Science of The Total Environment*, Volume 576, pp. 46-58.

Savijärvi, H. & Jin, L., 2001. Local winds in a valley city. *Boundary-Layer Meteorology*, Volume 100, pp. 301-319.

Scaperdas, A. & Colvile, R., 1999. Assessing the representativeness of monitoring data from an urban intersection site in central London, UK. *Atmospheric Environment*, Volume 33, p. 661–674.

Scaperdas, A., Colvile, R. & Robins, A., 1999. Understanding Flow Patterns at Street Canyon Intersections Using Wind Tunnel and CFD Simulations. *Transactions on Ecology and the Environment*, Volume 28, pp. 1743-3541.

Schein, A., 2016. The Relationship between Inclusive Institutions, Proximate Causes of Growth, and Economic Growth: A Case Study of the Four Mandate Territories of Lebanon, Palestine, Syria, and Trans-Jordan, 1918-1946/1948. *Journal of Economic*, March, Issue 50, p. 95–120.

Schweiker, M. & Wagner, A., 2015. A framework for an adaptive thermal heat balance model (ATHB). *Build. Environ.*, Volume 94, pp. 252-262.

- Sen, S. & Roesler, J., 2019. *Coupled Pavement-Urban Canyon Model for Assessing Cool Pavements*. Chicago, Illinois, International Airfield and Highway Pavements Conference .
- Sen, S. & Roesler, J., 2020. Wind direction and cool surface strategies on microscale urban heat island. *Urban Climate*, Volume 31, p. 100548.
- Setaih, K., Hamza, N. & Townshend, T., 2013. *ASSESSMENT OF OUTDOOR THERMAL COMFORT IN URBAN MICROCLIMATE IN HOT ARID AREAS*. Chambéry, France, 13th Conference of International Building Performance Simulation Association.
- Sharmin, T., Steemers, K. & Humphreys, M., 2019. Outdoor thermal comfort and summer PET range: A field study in tropical city Dhaka. *Energy and Buildings*, Volume 198, pp. 149-159.
- Sharmin, T., Steemers, K. & Matzarakis, A., 2015. Analysis of microclimatic diversity and outdoor thermal comfort perceptions in the tropical megacity Dhaka, Bangladesh. *Building and Environment*, 94(2), pp. 734-750.
- Sharples, S. & Bensalem, R., 2001. Airflow in courtyard and atrium buildings in the urban environment: a wind tunnel study. *Solar Energy*, 70(3), pp. 237-244.
- Sini, J., Anquetin, S. & Mestayer, P., 1996. Pollutant dispersion and thermal effects in urban street canyons. *Atmospheric Environment*, Volume 30, pp. 2659-2677.
- Sini, J.-F., Anquetin, S. & Mestayer, P. G., 1996. Pollutant dispersion and thermal effects in urban street canyons. *Atmospheric Environment*, 30(15), pp. 2659-2677.
- Siple, P. & Passel, C., 1945. Measurements of dry atmospheric cooling in subfreezing temperatures. *Proceedings of the American Philosophical Society*, 89(1), pp. 177-199.
- Skelhorn, C. P., 2013. *A Fine Scale Assessment of Urban Greenspace Impacts on Microclimate and Building Energy in Manchester*. Manchester: University of Manchester.
- Sodoudi, S. et al., 2018. The influence of spatial configuration of green areas on microclimate and thermal comfort. *Urban Forestry & Urban Greening*, Volume 34, pp. 85-96.
- Soulhac, L. et al., 2009. Flow and dispersion in street intersections. *Atmospheric Environment*, 43(18), pp. 2981-2996.

- Spagnolo, J. & De Dear, R., 2003. A field study of thermal comfort in outdoor and semi-outdoor environments in subtropical Sydney Australia. *Building and Environment*, 38(5), pp. 721-738.
- Spagnolo, J. & de Dear, R., 2003. A field study of thermal comfort in outdoor and semi-outdoor environments in subtropical. *Building and Environment*, Volume 38, pp. 721-738.
- Stadt, K. J. & Lieffers, V., 2000. MIXLIGHT: a flexible light transmission model for mixed-species forest stands. *Agricultural and Forest Meteorology*, 102(4), pp. 235-252.
- Stathopoulos, T., Wu, H. & Zacharias, J., 2004. Outdoor human comfort in an urban climate. *Building and Environment*, 39(3), pp. 297-305.
- Taesler, R. & Andersson, C., 1984. A method for solar radiation computations using routine meteorological observations. *Energy and buildings; Switzerland*, 7(4), pp. 341-352.
- Taffé, P., 1997. A qualitative response model of thermal comfort. *Build Environ*, Volume 32, p. 115–121.
- Taha, H., 1997. Urban climates and heat islands: albedo, evapotranspiration, and anthropogenic heat. *Energy Build.*, 25(2), pp. 99-103.
- Thitisawat, M., Polakit, K., Caldieron, J. & Mangone, G., 2011. *Adaptive outdoor comfort model calibrations for a semitropical region*. Louvain-la-Neuve, Belgium, Architecture & Sustainable Development : PLEA 2011, Proceedings of the 27th International Conference on Passive and Low Energy Architecture (PLEA).
- Thorsson, S. et al., 2007. Thermal Comfort and Outdoor Activity in Japanese Urban Public Places. *Environment and Behavior*, 39(5), pp. 660-684.
- Thorsson, S., Lindqvist, M. & Lindqvist, S., 2004. Thermal bioclimatic conditions and patterns of behaviour in an urban park in Goteborg. *International Journal of Biometeorology*, Volume 48, pp. 149-156.
- Todhunter, P., 1990. Microclimatic Variations Attributable to Urban-Canyon Asymmetry and Orientation. *Physical Geography*, 11(2), pp. 131-141.
- Tomah, A. N., Abed, A. & Saleh, B., 2017. Assessment of the Geographic Distribution of Public Parks in the City of Amman. *European Journal of Scientific Research*, 144(3), pp. 262-275.

Tomah, A. N., 2010. Visual privacy recognition in residential areas through amendment of building regulations. *Urban Design and Planning*, pp. 1-11.

Tominaga, Y., Akabayashi, S., Kitahara, T. & Arinami, Y., 2015. Air flow around isolated gable-roof buildings with different roof pitches: Wind tunnel experiments and CFD simulations. *Building and Environment*, 84(1), pp. 204-213.

Toparlar, Y., Blocken, B., Maiheu, B. & van Heijst, G., 2017. A review on the CFD analysis of urban microclimate. *Renewable and Sustainable Energy Reviews*, Volume 2017, pp. 1613-1640.

Tse, K. et al., 2017. Pedestrian-level wind environment around isolated buildings under the influence of twisted wind flows. *Journal of Wind Engineering and Industrial Aerodynamics*, Volume 162, pp. 12-23.

Tsichritzis, L. & Nikolopoulou, M., 2019. The effect of building height and façade area ratio on pedestrian wind comfort of London. *Journal of Wind Engineering and Industrial Aerodynamics*, Volume 191, pp. 63-75.

Tsonis, G., Ayerides, G. & Bergeles, G., 1987. Experimental and Numerical Simulation of the Wind Field over the Kythnos Wind Park. *Wind Engineering*, 11(6), pp. 325-333.

Vallati, A., Galli, G., Colucci, C. & Oclon, P., 2019. Influence of the geometrical parameters of urban canyons on the convective heat transfer coefficient. *Thermal Science*, 23(2), pp. 1211-1223.

van Hoof, J., Mazej, M. & Hensen, J. L., 2010. Thermal comfort: research and practice. *Frontiers in Bioscience*, Volume 15, pp. 765-788.

Vasilikou, C. & Nikolopoulou, M., 2020. Outdoor thermal comfort for pedestrians in movement: thermal walks in complex urban morphology. *International Journal of Biometeorology*, Volume 64, p. 277–291.

Vasilikou, C. & Nikolopoulou, M., 2020. Outdoor thermal comfort for pedestrians in movement: thermal walks in complex urban morphology. *International Journal of Biometeorology*, Volume 64, p. 277–291.

Vis, B. N., 2013. *Mapping the inhabited urban built environment : the socio-spatial significance of the material presence of boundaries through time*. leeds: University of Leeds.

Wai, K.-M., Yuan, C., Lai, A. & Yu, P. K., 2020. Relationship between pedestrian-level outdoor thermal comfort and building morphology in a high-density city. *Science of the Total Environment*, Volume 708, p. 134516.

Walther, E. & Goestchel, Q., 2018. The P.E.T. comfort index: Questioning the model. *Building and Environment*, Volume 137, pp. 1-10.

Wang, K., Li, Y., Wang, Y. & Yang, X., 2017. On the asymmetry of the urban daily air temperature cycle. *Journal of geophysical research. Atmospheres*, 122(11), pp. 5625-5635.

Wang, X. & Li, Y., 2016. Predicting urban heat island circulation using CFD. *Building and Environment*, Volume 99, pp. 82-97.

Wang, Y. et al., 2015. Effects of urban green infrastructure (UGI) on local outdoor microclimate during the growing season. *Environmental Monitoring and Assessment* , 187(12), p. 732.

Wang, y., Zhou, Y., Zuo, J. & Rameezdeen, R., 2018. A Computational Fluid Dynamic (CFD) Simulation of PM10 Dispersion Caused by Rail Transit Construction Activity: A Real Urban Street Canyon Model. *Int. J. Environ. Res. Public Health*, 15(3), p. 482.

Webb, C., n.d. Thermal discomfort in an equatorial climate. A monogram for the equatorial comfort index.. *Journal of the IHVE*, Volume 27, p. 10.

Willemsen, E. & Wisse, J. A., 2007. Design for wind comfort in The Netherlands: Procedures, criteria and open research issues. *Journal of Wind Engineering and Industrial Aerodynamics*, 95(9-11), pp. 1541-1550.

Williamson, S., 2003. *Report on wind chill temperature and extreme heat indices: evaluation and improvement projects*, Washington: Office of The Federal Coordinator For Meteorological Services And Supporting Research.

Willmott, C. J., 1981. ON THE VALIDATION OF MODELS. *Physical Geography*, pp. 184-194.

Willmott, C. & Matsuura, K., 2005. Advantages of the mean absolute error (MAE) over the root mean square error (RMSE) in assessing average model performance. *Climate Research*, Volume 30, pp. 79-82.

Wilson, J. D., 1988. A second-order closure model for flow through vegetation. *Boundary-Layer Meteorology*, 42(4), p. 371.

- Wong, N. et al., 2007. Environmental study of the impact of greenery in an institutional campus in the tropics. *Building and Environment*, Volume 42, pp. 2949-2970.
- Wu, Z. & Chen, L., 2017. Optimizing the spatial arrangement of trees in residential neighborhoods for better cooling effects: Integrating modeling with in-situ measurements. *Landscape and Urban Planning*, Volume 176, pp. 463-472.
- Xi, T., Li, Q., Mochida, A. & Meng, Q., 2012. Study on the Outdoor Thermal Environment and Thermal Comfort around Campus Clusters in Subtropical Urban Areas. *Building and Environment*, 52(1), pp. 162-170.
- Xi, T., Wang, Q., Qin, H. & Jin, H., 2020. Influence of outdoor thermal environment on clothing and activity of tourists and local people in a severely cold climate city. *Building and Environment*, Volume 173, p. 106757.
- Xu, J. et al., 2010. Evaluation of human thermal comfort near urban waterbody during summer. *Building and Environment*, 45(4), pp. 1072-1080.
- Xystrakis, F. & Matzarakis, A., 2010. *The importance of meteorological variables in the bias of Potential evapotranspiration estimates in Crete, southern Greece*. Freiburg, Germany, 7th Conference on Biometeorology.
- Yaglou, C. & Minard, D., 1957. Control of heat casualties at military training centers. *A.M.A. Archives of Industrial Health*, Volume 16, pp. 302-316.
- Yahia, M. et al., 2017. Effect of urban design on microclimate and thermal comfort outdoors in warm-humid Dar es Salaam, Tanzania. *International Journal of Biometeorology*, Volume 62, p. 373–385.
- Yahia, M. W. & Johansson, E., 2013. Influence of urban planning regulations on the microclimate in a hot dry climate: The example of Damascus, Syria. *Journal of Housing and the Built Environment*, Volume 28, p. 51–65.
- Yahia, M. W. & Johansson, E., 2014. Landscape interventions in improving thermal comfort in the hot dry city of Damascus, Syria—The example of residential spaces with detached buildings. *Landscape and Urban Planning*, Volume 125, pp. 1-16.
- Yamada, T., 1982. A numerical model study of turbulent airflow in and above a forest canopy. *J. Met. Soc. Japan*, Volume 60, pp. 439-454.

- Yang, B., Olofsson, T., Nair, G. & Kabanshi, A., 2017. Outdoor thermal comfort under subarctic climate of north Sweden – A pilot study in Umeå. *Sustainable Cities and Society*, Volume 28, p. 387–397.
- Yang, F., Lau, S. S. & Qian, F., 2010. Urban design to lower summertime outdoor temperatures: An empirical study on high-rise housing in Shanghai. *Building and Environment*, pp. 769-785.
- Yang, W., Wong, N. H. & Jusuf, S. K., 2013. Thermal comfort in outdoor urban spaces in Singapore. *Building and Environment*, Volume 59, pp. 426-435.
- Yang, X., Li, Y., Luo, Z. & Chan, P., 2017. The urban cool island phenomenon in a high-rise high-density city and its mechanisms. *Int. J. Climatol.*, 37(2), pp. 890-904.
- Yan, H. et al., 2020. The coupled effect of temperature, humidity, and air movement on human thermal response in hot–humid and hot–arid climates in summer in China. *Building and Environment*, 177(15), p. 106898.
- Yao, R., Li, B. & Liu, . J., 2009. A theoretical adaptive model of thermal comfort - Adaptive Predicted mean vote (aPMV). *Build. Environ.*, Volume 44, pp. 2089-2096.
- Yin, S., Lang, W., Xiao, Y. & Xu, Z., 2019. Correlative Impact of Shading Strategies and Configurations Design on Pedestrian-Level Thermal Comfort in Traditional Shophouse Neighbourhoods, Southern China. *Sustainability*, 11(5), p. 1355.
- Yoshida, A., Tominaga, K. & Watatani, S., 1990-1991. Field measurements on energy balance of an urban canyon in the summer season. *Energy and Buildings*, 15(3-4), pp. 417-423.
- Yu, C. & Hien, W., 2006. Thermal benefits of city parks. *Energy and Buildings*, Volume 38, pp. 105-120.
- Zajic, D. et al., 2003. *Flow and turbulence in simulated city canyons, measurements and computations*. Lodz, Poland , Fifth International Conference on Urban Climate.
- Zakhour, S., 2015. The Impact of Urban Geometry on Outdoor Thermal Comfort Conditions in Hot-arid Region. *J. Civil Eng. Architect. Res.*, 2(8), pp. 862-875.
- Zamanian, Z., Sedaghat, Z., Hemehrezaee, M. & Khajehnasiri, F., 2017. Evaluation of environmental heat stress on physiological parameters. *Journal of Environmental Health Science and Engineering*, 15(24).

Zhang, G. et al., 2007. Thermal Comfort Investigation of Naturally Ventilated Classrooms in a Subtropical Region. *Indoor and Built Environment*, 16(2), p. 148–158.

Zhang, W., Mak, C., Ali, Z. & Siu, W., 2012. A Study of the Ventilation and Thermal Comfort of the Environment Surrounding a New University Building under Construction. *Indoor and Built Environment*, 21(4), p. 568–582.

Zhao, Q., Sailor, D. J. & Wentz, E. A., 2018. Impact of tree locations and arrangements on outdoor microclimates and human thermal comfort in an urban residential environment. *Urban Forestry & Urban Greening*, Volume 32, pp. 81-91.

Zheng, S., Zhao, L. & Li, Q., 2016. Numerical simulation of the impact of different vegetation species on the outdoor thermal environment. *Urban Forestry & Urban Greening*, Volume 18, pp. 138-150.

Zhou, Q. & Zhou, L., 2020. Numerical and experimental study on wind environment at near tower region of a bridge deck. *Heliyon*, 6(5), p. 03902.

APPENDICES

Sample of the Appendices for chapter 6 – section 1.

Street grid layout C.1

Table A6. 1. Detailed microclimatic data for street grid layout C.1.

Date	Time	Wind Speed (m/s)	Air Temperature (°C)	Relative Humidity (%)	Mean Radiant Temp. (°C)	PET (°C)
		Receptor 1				
23.09.2018	06:00	0.73484	20.383	67.604	17.834	20.3
23.09.2018	07:00	0.69201	21.183	65.573	24.465	24.8
23.09.2018	08:00	0.64863	22.325	63.095	32.129	29.5
23.09.2018	09:00	0.60507	23.771	59.661	39.64	42.6
23.09.2018	10:00	0.56113	25.188	56.843	62.922	42.4
23.09.2018	11:00	0.52489	26.458	54.73	59.659	42.6
23.09.2018	12:00	0.50473	27.435	53.412	59.131	47.4
23.09.2018	13:00	0.48463	28.422	52.048	66.27	50.4
23.09.2018	14:00	0.46297	29.181	51.24	70.386	38
23.09.2018	15:00	0.44096	30	49.992	46.528	36
23.09.2018	16:00	0.42024	30.504	49.427	42.108	32.1
23.09.2018	17:00	0.40067	30.061	50.613	34.696	28
23.09.2018	18:00	0.38248	29.238	52.45	27.073	25.7
23.09.2018	19:00	0.36539	28.371	54.337	23.183	24.8
23.09.2018	20:00	0.34817	27.671	55.712	21.885	23.9
23.09.2018	21:00	0.32922	26.987	56.98	20.848	23.1
23.09.2018	22:00	0.30755	26.296	58.203	19.906	22.2
23.09.2018	23:00	0.28416	25.594	59.416	19.003	21.4
23.09.2018	00:00	0.25809	24.868	60.645	18.113	20.7
23.09.2018	01:00	0.22944	24.135	61.878	17.232	19.9
23.09.2018	02:00	0.1995	23.384	63.135	16.352	19
23.09.2018	03:00	0.1719	22.629	64.403	15.474	18.2
23.09.2018	04:00	0.15016	21.879	65.674	14.602	17.8
23.09.2018	05:00	0.13969	21.119	66.975	13.876	17.3
Date	Time	Wind Speed (m/s)	Air Temperature (°C)	Relative Humidity (%)	Mean Radiant Temp. (°C)	PET (°C)
		Receptor 2				
23.09.2018	06:00	1.2899	20.11	68.092	17.771	18.9
23.09.2018	07:00	1.2653	21.039	65.753	24.383	23.1
23.09.2018	08:00	1.2404	22.354	62.802	32.008	39.7
23.09.2018	09:00	1.2149	24.063	58.578	65.133	39.7

23.09.2018	10:00	1.1894	25.514	55.858	62.855	39.2
23.09.2018	11:00	1.1727	26.781	53.902	59.621	39.8
23.09.2018	12:00	1.1721	27.799	52.552	59.09	44.2
23.09.2018	13:00	1.1712	28.801	51.219	66.216	36.1
23.09.2018	14:00	1.1691	29.513	50.593	48.002	36.1
23.09.2018	15:00	1.167	30.304	49.446	46.427	34.6
23.09.2018	16:00	1.1658	30.829	48.835	42.012	31.1
23.09.2018	17:00	1.1659	30.301	50.186	34.632	27.5
23.09.2018	18:00	1.1678	29.389	52.211	27.029	25.3
23.09.2018	19:00	1.1714	28.459	54.223	23.167	24.1
23.09.2018	20:00	1.1755	27.717	55.673	21.87	23.1
23.09.2018	21:00	1.1784	26.994	57.003	20.831	22.1
23.09.2018	22:00	1.1791	26.264	58.282	19.886	21
23.09.2018	23:00	1.1781	25.524	59.548	18.979	20.1
23.09.2018	00:00	1.174	24.765	60.822	18.085	19.2
23.09.2018	01:00	1.166	23.999	62.097	17.2	18.3
23.09.2018	02:00	1.1544	23.219	63.391	16.316	17.5
23.09.2018	03:00	1.141	22.437	64.693	15.435	16.7
23.09.2018	04:00	1.1271	21.66	66	14.558	15.9
23.09.2018	05:00	1.1168	20.874	67.334	13.829	16.2
Date	Time	Wind Speed (m/s)	Air Temperature (°C)	Relative Humidity (%)	Mean Radiant Temp. (°C)	PET (°C)
		Receptor 3				
23.09.2018	06:00	1.6806	19.737	68.815	17.942	18.2
23.09.2018	07:00	1.6698	20.727	66.535	24.606	21.8
23.09.2018	08:00	1.6573	22.118	63.5	32.339	38
23.09.2018	09:00	1.6425	23.938	58.983	65.379	38.2
23.09.2018	10:00	1.6255	25.439	56.27	63.039	38.1
23.09.2018	11:00	1.6232	26.924	53.756	59.725	39
23.09.2018	12:00	1.6486	28.125	51.946	59.201	43.1
23.09.2018	13:00	1.6694	29.195	50.5	66.363	35.6
23.09.2018	14:00	1.683	29.948	49.806	48.234	35.6
23.09.2018	15:00	1.6946	30.539	49.244	46.704	34.4
23.09.2018	16:00	1.7062	31.083	48.585	42.275	31
23.09.2018	17:00	1.7195	30.453	50.105	34.808	27.3
23.09.2018	18:00	1.7358	29.499	52.149	27.148	25.1
23.09.2018	19:00	1.7548	28.563	54.089	23.21	23.8
23.09.2018	20:00	1.7737	27.793	55.544	21.91	22.7
23.09.2018	21:00	1.7896	27.036	56.905	20.877	21.7

23.09.2018	22:00	1.8001	26.267	58.229	19.941	20.6
23.09.2018	23:00	1.8062	25.488	59.545	19.044	19.7
23.09.2018	00:00	1.8062	24.69	60.866	18.161	18.8
23.09.2018	01:00	1.7997	23.889	62.187	17.287	17.9
23.09.2018	02:00	1.788	23.076	63.522	16.414	17
23.09.2018	03:00	1.7756	22.261	64.861	15.543	16.1
23.09.2018	04:00	1.7647	21.451	66.209	14.678	15.2
23.09.2018	05:00	1.7581	20.633	67.58	13.957	15.5
Date	Time	Wind Speed (m/s)	Air Temperature (°C)	Relative Humidity (%)	Mean Radiant Temp. (°C)	PET (°C)
		Receptor 4				
23.09.2018	06:00	3.1221	18.951	70.242	17.771	16.5
23.09.2018	07:00	3.1324	20.203	67.611	24.383	19.7
23.09.2018	08:00	3.136	21.784	64.383	32.008	24
23.09.2018	09:00	3.1337	23.797	59.459	39.525	35.4
23.09.2018	10:00	3.126	26.226	54.127	62.855	36.3
23.09.2018	11:00	3.1414	28.165	50.746	59.621	37.4
23.09.2018	12:00	3.1908	29.504	48.891	59.09	41.5
23.09.2018	13:00	3.2365	30.675	47.428	66.216	43.9
23.09.2018	14:00	3.2731	31.464	46.78	70.317	35.9
23.09.2018	15:00	3.3037	32.277	45.689	46.427	34.5
23.09.2018	16:00	3.3337	32.429	46.112	42.012	31
23.09.2018	17:00	3.3627	31.391	48.371	34.632	27.3
23.09.2018	18:00	3.3934	30.068	51.15	27.029	24.9
23.09.2018	19:00	3.427	28.911	53.501	23.167	23.4
23.09.2018	20:00	3.4604	28.001	55.182	21.87	22
23.09.2018	21:00	3.4892	27.119	56.749	20.831	20.8
23.09.2018	22:00	3.5093	26.232	58.256	19.886	19.8
23.09.2018	23:00	3.5238	25.345	59.737	18.979	18.8
23.09.2018	00:00	3.5295	24.449	61.199	18.085	17.9
23.09.2018	01:00	3.5258	23.553	62.655	17.2	16.9
23.09.2018	02:00	3.5139	22.652	64.107	16.316	15.8
23.09.2018	03:00	3.4987	21.749	65.557	15.435	15
23.09.2018	04:00	3.4832	20.85	67.021	14.558	13.9
23.09.2018	05:00	3.472	19.946	68.493	13.829	14
Date	Time	Wind Speed (m/s)	Air Temperature (°C)	Relative Humidity (%)	Mean Radiant Temp. (°C)	PET (°C)
		Receptor 5				

23.09.2018	06:00	1.954	19.353	69.547	17.812	17.7
23.09.2018	07:00	1.9451	20.456	67.125	24.437	21.2
23.09.2018	08:00	1.9347	21.931	64.012	32.087	37.1
23.09.2018	09:00	1.9223	24.146	58.223	65.192	37.9
23.09.2018	10:00	1.9078	26.139	54.172	62.899	38.1
23.09.2018	11:00	1.8996	27.771	51.512	59.646	38.9
23.09.2018	12:00	1.9056	28.877	50.188	59.116	43.1
23.09.2018	13:00	1.9118	29.948	48.883	66.251	35.9
23.09.2018	14:00	1.9172	30.464	48.922	48.058	36
23.09.2018	15:00	1.9218	31.279	47.763	46.493	34.7
23.09.2018	16:00	1.926	31.706	47.454	42.075	31.1
23.09.2018	17:00	1.9308	30.842	49.454	34.674	27.4
23.09.2018	18:00	1.9379	29.746	51.762	27.058	25.1
23.09.2018	19:00	1.948	28.725	53.834	23.178	23.9
23.09.2018	20:00	1.96	27.886	55.401	21.88	22.7
23.09.2018	21:00	1.972	27.067	56.862	20.842	21.5
23.09.2018	22:00	1.9825	26.241	58.273	19.899	20.4
23.09.2018	23:00	1.9913	25.41	59.666	18.995	19.5
23.09.2018	00:00	1.9964	24.565	61.052	18.104	18.5
23.09.2018	01:00	1.9968	23.717	62.435	17.221	17.6
23.09.2018	02:00	1.9924	22.859	63.824	16.339	16.6
23.09.2018	03:00	1.9848	22	65.214	15.461	15.7
23.09.2018	04:00	1.9754	21.145	66.616	14.587	14.8
23.09.2018	05:00	1.9679	20.283	68.032	13.86	15

Street grid layout C.2.

Table A6. 2. Detailed microclimatic data for street grid layout C.2.

Date	Time	Wind Speed (m/s)	Air Temperature (°C)	Relative Humidity (%)	Mean Radiant Temp. (°C)	PET (°C)
		Receptor 1				
23.09.2018	06:00	2.5197	19.508	69.169	17.653	28.8
23.09.2018	07:00	2.4958	20.892	65.663	57.778	33.2
23.09.2018	08:00	2.4687	23.135	59.949	62.845	36.2
23.09.2018	09:00	2.44	25.011	55.436	64.371	37.6
23.09.2018	10:00	2.4091	26.844	51.983	63.268	36.8
23.09.2018	11:00	2.3866	28.064	50.375	58.171	38.1
23.09.2018	12:00	2.3894	29.256	48.824	58.515	41.7

23.09.2018	13:00	2.3924	30.27	47.679	64.504	45.6
23.09.2018	14:00	2.3917	31.366	46.348	70.867	46.6
23.09.2018	15:00	2.3894	31.977	45.841	71.674	45.5
23.09.2018	16:00	2.3884	32.187	46.143	68.873	31.4
23.09.2018	17:00	2.3904	31.131	48.653	35.531	27.4
23.09.2018	18:00	2.3986	29.832	51.46	27.192	25.1
23.09.2018	19:00	2.4142	28.753	53.705	23.307	23.7
23.09.2018	20:00	2.4351	27.903	55.32	21.972	22.5
23.09.2018	21:00	2.4579	27.091	56.786	20.905	21.3
23.09.2018	22:00	2.4806	26.278	58.184	19.938	20.2
23.09.2018	23:00	2.5019	25.466	59.555	19.017	19.3
23.09.2018	00:00	2.5209	24.653	60.911	18.118	18.4
23.09.2018	01:00	2.5371	23.834	62.269	17.229	17.5
23.09.2018	02:00	2.5483	23.008	63.634	16.344	16.6
23.09.2018	03:00	2.5542	22.175	64.999	15.461	15.6
23.09.2018	04:00	2.5551	21.335	66.384	14.577	14.7
23.09.2018	05:00	2.5529	20.488	67.785	13.839	14.8
Date	Time	Wind Speed (m/s)	Air Temperature (°C)	Relative Humidity (%)	Mean Radiant Temp. (°C)	PET (°C)
		Receptor 2				
23.09.2018	06:00	2.4273	19.635	68.88	45.408	29.3
23.09.2018	07:00	2.4036	21.152	64.754	57.73	33.6
23.09.2018	08:00	2.378	23.176	59.848	62.81	36.1
23.09.2018	09:00	2.3506	24.973	55.577	64.328	37.6
23.09.2018	10:00	2.3211	26.748	52.237	63.218	36.7
23.09.2018	11:00	2.2984	27.854	50.912	58.126	38.1
23.09.2018	12:00	2.2971	29.059	49.274	58.479	41.7
23.09.2018	13:00	2.2965	30.077	48.094	64.466	45.6
23.09.2018	14:00	2.2933	31.22	46.612	70.827	46.5
23.09.2018	15:00	2.289	31.83	46.111	71.642	45.5
23.09.2018	16:00	2.2857	32.118	46.209	68.842	31.6
23.09.2018	17:00	2.2844	31.206	48.358	35.474	27.4
23.09.2018	18:00	2.2889	29.836	51.385	27.149	25
23.09.2018	19:00	2.2999	28.747	53.684	23.29	23.8
23.09.2018	20:00	2.316	27.899	55.312	21.957	22.6
23.09.2018	21:00	2.3343	27.091	56.779	20.887	21.3
23.09.2018	22:00	2.3532	26.284	58.175	19.918	20.3
23.09.2018	23:00	2.3711	25.477	59.541	18.992	19.4
23.09.2018	00:00	2.3873	24.67	60.89	18.09	18.5

23.09.2018	01:00	2.4009	23.858	62.241	17.197	17.5
23.09.2018	02:00	2.4101	23.038	63.598	16.308	16.6
23.09.2018	03:00	2.4143	22.213	64.954	15.421	15.7
23.09.2018	04:00	2.4139	21.381	66.329	14.533	14.8
23.09.2018	05:00	2.4107	20.543	67.721	13.792	15
Date	Time	Wind Speed (m/s)	Air Temperature (°C)	Relative Humidity (%)	Mean Radiant Temp. (°C)	PET (°C)
		Receptor 3				
23.09.2018	06:00	0.18599	20.08	68.13	17.755	22.7
23.09.2018	07:00	0.18922	21.079	65.676	25.306	27
23.09.2018	08:00	0.19191	22.397	62.959	32.162	31.3
23.09.2018	09:00	0.19438	23.881	59.377	38.658	46.7
23.09.2018	10:00	0.19608	25.544	55.892	63.353	44.2
23.09.2018	11:00	0.1963	26.879	53.611	58.248	45.1
23.09.2018	12:00	0.19614	28.228	51.34	58.576	49.3
23.09.2018	13:00	0.19415	29.136	50.357	64.57	40.1
23.09.2018	14:00	0.19222	29.778	50.165	48.767	38.4
23.09.2018	15:00	0.19069	30.292	49.882	45.224	36.3
23.09.2018	16:00	0.18988	30.912	49.037	40.877	33.2
23.09.2018	17:00	0.18996	30.433	50.143	35.63	28.6
23.09.2018	18:00	0.19109	29.494	52.078	27.266	26.1
23.09.2018	19:00	0.19318	28.536	54.086	23.336	25.1
23.09.2018	20:00	0.19591	27.764	55.577	21.998	24.1
23.09.2018	21:00	0.19908	27.022	56.939	20.935	23.3
23.09.2018	22:00	0.20242	26.279	58.248	19.974	22.4
23.09.2018	23:00	0.20548	25.534	59.534	19.058	21.6
23.09.2018	00:00	0.20818	24.785	60.809	18.166	20.7
23.09.2018	01:00	0.21044	24.027	62.092	17.285	19.8
23.09.2018	02:00	0.21202	23.258	63.39	16.407	19
23.09.2018	03:00	0.21298	22.481	64.695	15.53	18.1
23.09.2018	04:00	0.21345	21.694	66.026	14.653	17.3
23.09.2018	05:00	0.21353	20.897	67.383	13.92	18.6
Date	Time	Wind Speed (m/s)	Air Temperature (°C)	Relative Humidity (%)	Mean Radiant Temp. (°C)	PET (°C)
		Receptor 4				
23.09.2018	06:00	3.2119	18.885	70.363	17.594	14:24
23.09.2018	07:00	3.2055	20.502	66.496	57.73	04:48
23.09.2018	08:00	3.1866	22.737	61.232	62.81	00:00

23.09.2018	09:00	3.1596	24.603	56.84	64.328	19:12
23.09.2018	10:00	3.1295	26.541	53.291	63.218	12:00
23.09.2018	11:00	3.1421	28.038	51.015	58.126	02:24
23.09.2018	12:00	3.2169	29.426	49.103	58.479	14:24
23.09.2018	13:00	3.2804	30.568	47.715	64.466	09:36
23.09.2018	14:00	3.3231	31.667	46.494	70.827	07:12
23.09.2018	15:00	3.3552	32.432	45.594	71.642	14:24
23.09.2018	16:00	3.3857	32.812	45.456	68.842	14:24
23.09.2018	17:00	3.4173	31.584	48.121	35.474	07:12
23.09.2018	18:00	3.4574	30.113	51.159	27.149	00:00
23.09.2018	19:00	3.5082	28.954	53.458	23.29	09:36
23.09.2018	20:00	3.5622	28.027	55.155	21.957	00:00
23.09.2018	21:00	3.6096	27.131	56.739	20.887	16:48
23.09.2018	22:00	3.6457	26.233	58.266	19.918	16:48
23.09.2018	23:00	3.6735	25.338	59.764	18.992	16:48
23.09.2018	00:00	3.6931	24.445	61.248	18.09	19:12
23.09.2018	01:00	3.7042	23.551	62.727	17.197	21:36
23.09.2018	02:00	3.7029	22.652	64.204	16.308	21:36
23.09.2018	03:00	3.6895	21.751	65.675	15.421	19:12
23.09.2018	04:00	3.6666	20.845	67.157	14.533	21:36
23.09.2018	05:00	3.6443	19.936	68.646	13.792	21:36
Date	Time	Wind Speed (m/s)	Air Temperature (°C)	Relative Humidity (%)	Mean Radiant Temp. (°C)	PET (°C)
		Receptor 5				
23.09.2018	06:00	2.5533	19.539	69.1	17.632	29
23.09.2018	07:00	2.5284	21.116	64.799	57.762	33.4
23.09.2018	08:00	2.5015	23.202	59.718	62.832	35.9
23.09.2018	09:00	2.4728	25.024	55.395	64.356	37.6
23.09.2018	10:00	2.4419	26.829	52.019	63.25	36.6
23.09.2018	11:00	2.4187	27.878	50.903	58.155	37.8
23.09.2018	12:00	2.4194	29.037	49.415	58.502	41.4
23.09.2018	13:00	2.4208	30.049	48.25	64.491	45.5
23.09.2018	14:00	2.4186	31.288	46.513	70.853	46.5
23.09.2018	15:00	2.4152	31.916	45.958	71.663	45.5
23.09.2018	16:00	2.413	32.191	46.092	68.863	31.5
23.09.2018	17:00	2.4132	31.232	48.34	35.511	27.4
23.09.2018	18:00	2.4196	29.83	51.438	27.177	25
23.09.2018	19:00	2.4331	28.745	53.712	23.301	23.7
23.09.2018	20:00	2.4516	27.896	55.331	21.967	22.5

23.09.2018	21:00	2.4721	27.087	56.794	20.899	21.3
23.09.2018	22:00	2.4926	26.279	58.187	19.931	20.2
23.09.2018	23:00	2.5118	25.47	59.552	19.008	19.3
23.09.2018	00:00	2.5291	24.661	60.903	18.108	18.4
23.09.2018	01:00	2.5437	23.846	62.256	17.218	17.4
23.09.2018	02:00	2.5536	23.022	63.616	16.332	16.5
23.09.2018	03:00	2.5586	22.193	64.978	15.447	15.7
23.09.2018	04:00	2.5589	21.355	66.359	14.562	14.7
23.09.2018	05:00	2.5564	20.51	67.758	13.823	14.7

Street grid layout D.1.

Table A6. 3. Detailed microclimatic data for street grid layout D.1.

Date	Time	Wind Speed (m/s)	Air Temperature (°C)	Relative Humidity (%)	Mean Radiant Temp. (°C)	PET (°C)
		Receptor 1				
23.09.2018	06:00	1.1406	20.696	66.822	16.518	19.3
23.09.2018	07:00	1.1218	21.354	65.032	23.596	23.1
23.09.2018	08:00	1.1022	22.462	62.485	31.088	26.7
23.09.2018	09:00	1.0822	23.629	59.904	37.631	39.7
23.09.2018	10:00	1.0616	24.926	57.267	63.041	39.1
23.09.2018	11:00	1.0419	25.902	55.876	59.28	41.2
23.09.2018	12:00	1.0349	26.953	54.296	61.596	44.2
23.09.2018	13:00	1.0305	27.817	53.27	66.166	47.5
23.09.2018	14:00	1.0254	28.622	52.401	71.083	35.6
23.09.2018	15:00	1.02	29.365	51.555	46.065	34
23.09.2018	16:00	1.015	30.036	50.769	41.259	31.1
23.09.2018	17:00	1.0114	29.807	51.479	34.863	27.5
23.09.2018	18:00	1.0103	29.127	52.956	27.537	25.6
23.09.2018	19:00	1.0121	28.381	54.504	24.032	24.4
23.09.2018	20:00	1.0151	27.721	55.735	22.474	23.5
23.09.2018	21:00	1.0187	27.068	56.892	21.27	22.5
23.09.2018	22:00	1.0214	26.406	58.017	20.244	21.5
23.09.2018	23:00	1.0225	25.735	59.134	19.315	20.7
23.09.2018	00:00	1.0216	25.057	60.25	18.442	19.8
23.09.2018	01:00	1.0186	24.371	61.369	17.602	19
23.09.2018	02:00	1.0128	23.669	62.512	16.78	18.2
23.09.2018	03:00	1.0041	22.955	63.671	15.97	17.4

23.09.2018	04:00	0.9933	22.229	64.858	15.166	16.6
23.09.2018	05:00	0.98423	21.492	66.063	14.5	16.5
Date	Time	Wind Speed (m/s)	Air Temperature (°C)	Relative Humidity (%)	Mean Radiant Temp. (°C)	PET (°C)
		Receptor 2				
23.09.2018	06:00	0.94822	20.71	66.784	16.389	34.5
23.09.2018	07:00	0.92783	21.413	64.808	56.513	38.3
23.09.2018	08:00	0.90615	22.568	62.088	61.941	40.1
23.09.2018	09:00	0.88348	23.763	59.423	63.414	40.7
23.09.2018	10:00	0.85974	24.973	57.1	62.835	39.9
23.09.2018	11:00	0.83461	25.93	55.764	59.144	42
23.09.2018	12:00	0.8271	26.954	54.261	61.483	45
23.09.2018	13:00	0.82369	27.783	53.336	66.032	48.4
23.09.2018	14:00	0.81913	28.613	52.38	70.893	49.7
23.09.2018	15:00	0.81369	29.396	51.412	72.162	48.4
23.09.2018	16:00	0.80845	30.063	50.635	69.012	31.3
23.09.2018	17:00	0.80614	29.81	51.432	34.697	28.9
23.09.2018	18:00	0.80954	29.134	52.911	30.457	25.7
23.09.2018	19:00	0.81865	28.389	54.466	23.983	24.5
23.09.2018	20:00	0.83105	27.731	55.699	22.436	23.6
23.09.2018	21:00	0.84566	27.078	56.859	21.23	22.5
23.09.2018	22:00	0.85955	26.415	57.987	20.196	21.6
23.09.2018	23:00	0.87081	25.743	59.109	19.255	20.8
23.09.2018	00:00	0.87879	25.064	60.228	18.369	19.8
23.09.2018	01:00	0.88309	24.377	61.349	17.515	19.1
23.09.2018	02:00	0.88212	23.674	62.495	16.679	18.3
23.09.2018	03:00	0.87589	22.959	63.657	15.855	17.4
23.09.2018	04:00	0.86534	22.231	64.846	15.037	16.7
23.09.2018	05:00	0.85522	21.493	66.053	14.36	16.7
Date	Time	Wind Speed (m/s)	Air Temperature (°C)	Relative Humidity (%)	Mean Radiant Temp. (°C)	PET (°C)
		Receptor 3				
23.09.2018	06:00	0.16354	20.714	66.786	16.389	19.1
23.09.2018	07:00	0.16669	21.347	65.087	23.403	22.7
23.09.2018	08:00	0.1682	22.417	62.669	30.831	38.5
23.09.2018	09:00	0.16822	23.61	59.976	37.329	39
23.09.2018	10:00	0.16617	25.01	56.984	62.835	38.1
23.09.2018	11:00	0.161	26.03	55.48	59.144	39.9

23.09.2018	12:00	0.15966	27.086	53.921	61.483	43.1
23.09.2018	13:00	0.15933	27.9	53.076	66.032	46.7
23.09.2018	14:00	0.15891	28.687	52.281	70.893	35.2
23.09.2018	15:00	0.15892	29.351	51.681	45.784	33.7
23.09.2018	16:00	0.15929	30.035	50.862	41.038	30.9
23.09.2018	17:00	0.16086	29.795	51.567	34.697	28.5
23.09.2018	18:00	0.16502	29.117	53.012	27.42	25.4
23.09.2018	19:00	0.17171	28.368	54.552	23.983	24.2
23.09.2018	20:00	0.18002	27.706	55.78	22.436	23.2
23.09.2018	21:00	0.18889	27.053	56.935	21.23	22.2
23.09.2018	22:00	0.19741	26.398	58.049	20.196	21.2
23.09.2018	23:00	0.20444	25.735	59.154	19.255	20.4
23.09.2018	00:00	0.20974	25.065	60.258	18.369	19.5
23.09.2018	01:00	0.21323	24.386	61.366	17.515	18.8
23.09.2018	02:00	0.21433	23.69	62.503	16.679	18
23.09.2018	03:00	0.21319	22.979	63.657	15.855	17.2
23.09.2018	04:00	0.21037	22.254	64.841	15.037	16.4
23.09.2018	05:00	0.20745	21.519	66.043	14.36	16.4
Date	Time	Wind Speed (m/s)	Air Temperature (°C)	Relative Humidity (%)	Mean Radiant Temp. (°C)	PET (°C)
		Receptor 4				
23.09.2018	06:00	0.16354	20.714	66.786	16.389	21.9
23.09.2018	07:00	0.16669	21.347	65.087	23.403	26.3
23.09.2018	08:00	0.1682	22.417	62.669	30.831	30.4
23.09.2018	09:00	0.16822	23.61	59.976	37.329	46
23.09.2018	10:00	0.16617	25.01	56.984	62.835	44.2
23.09.2018	11:00	0.161	26.03	55.48	59.144	46.3
23.09.2018	12:00	0.15966	27.086	53.921	61.483	49.6
23.09.2018	13:00	0.15933	27.9	53.076	66.032	53.2
23.09.2018	14:00	0.15891	28.687	52.281	70.893	38.2
23.09.2018	15:00	0.15892	29.351	51.681	45.784	35.9
23.09.2018	16:00	0.15929	30.035	50.862	41.038	32.4
23.09.2018	17:00	0.16086	29.795	51.567	34.697	28.4
23.09.2018	18:00	0.16502	29.117	53.012	27.42	26.4
23.09.2018	19:00	0.17171	28.368	54.552	23.983	25.2
23.09.2018	20:00	0.18002	27.706	55.78	22.436	24.3
23.09.2018	21:00	0.18889	27.053	56.935	21.23	23.4
23.09.2018	22:00	0.19741	26.398	58.049	20.196	22.6
23.09.2018	23:00	0.20444	25.735	59.154	19.255	21.8

23.09.2018	00:00	0.20974	25.065	60.258	18.369	21
23.09.2018	01:00	0.21323	24.386	61.366	17.515	20.2
23.09.2018	02:00	0.21433	23.69	62.503	16.679	19.4
23.09.2018	03:00	0.21319	22.979	63.657	15.855	18.6
23.09.2018	04:00	0.21037	22.254	64.841	15.037	17.9
23.09.2018	05:00	0.20745	21.519	66.043	14.36	18.3
Date	Time	Wind Speed (m/s)	Air Temperature (°C)	Relative Humidity (%)	Mean Radiant Temp. (°C)	PET (°C)
		Receptor 5				
23.09.2018	06:00	1.4697	20.533	67.079	44.678	18.7
23.09.2018	07:00	1.4489	21.26	65.153	23.596	22.3
23.09.2018	08:00	1.4268	22.44	62.445	31.088	26
23.09.2018	09:00	1.4039	23.644	59.807	37.631	38.7
23.09.2018	10:00	1.3791	25.09	56.772	63.041	37.8
23.09.2018	11:00	1.3561	26.068	55.481	59.28	39.8
23.09.2018	12:00	1.3547	27.185	53.787	61.596	42.9
23.09.2018	13:00	1.3559	28.077	52.734	66.166	46.1
23.09.2018	14:00	1.354	28.875	51.941	71.083	35
23.09.2018	15:00	1.3504	29.58	51.237	46.065	33.7
23.09.2018	16:00	1.3464	30.243	50.501	41.259	30.8
23.09.2018	17:00	1.3444	29.933	51.349	34.863	27.4
23.09.2018	18:00	1.3479	29.213	52.867	27.537	25.4
23.09.2018	19:00	1.3572	28.435	54.45	24.032	24.2
23.09.2018	20:00	1.37	27.747	55.716	22.474	23.2
23.09.2018	21:00	1.3847	27.069	56.904	21.27	22.1
23.09.2018	22:00	1.398	26.386	58.057	20.244	21.2
23.09.2018	23:00	1.4085	25.696	59.2	19.315	20.2
23.09.2018	00:00	1.4156	25	60.34	18.442	19.4
23.09.2018	01:00	1.4188	24.296	61.483	17.602	18.6
23.09.2018	02:00	1.4165	23.577	62.649	16.78	17.8
23.09.2018	03:00	1.4084	22.847	63.828	15.97	17
23.09.2018	04:00	1.3956	22.104	65.035	15.166	16.2
23.09.2018	05:00	1.3837	21.353	66.26	14.5	16
Date	Time	Wind Speed (m/s)	Air Temperature (°C)	Relative Humidity (%)	Mean Radiant Temp. (°C)	PET (°C)
		Receptor 6				
23.09.2018	06:00	0.98915	20.119	67.726	16.389	33.8
23.09.2018	07:00	0.95898	21.087	65.201	56.513	38.2

23.09.2018	08:00	0.92576	22.498	61.93	61.941	40.1
23.09.2018	09:00	0.8909	23.878	58.874	63.414	40.8
23.09.2018	10:00	0.85457	25.239	56.39	62.835	40.2
23.09.2018	11:00	0.81936	26.294	54.967	59.144	42.3
23.09.2018	12:00	0.81217	27.422	53.323	61.483	45.4
23.09.2018	13:00	0.80992	28.297	52.375	66.032	48.8
23.09.2018	14:00	0.80482	29.19	51.335	70.893	50.1
23.09.2018	15:00	0.7976	30.029	50.259	72.162	48.8
23.09.2018	16:00	0.79009	30.725	49.455	69.012	31.6
23.09.2018	17:00	0.7862	30.298	50.578	34.697	28
23.09.2018	18:00	0.79012	29.46	52.377	27.42	25.9
23.09.2018	19:00	0.80204	28.613	54.096	23.983	24.7
23.09.2018	20:00	0.81826	27.867	55.467	22.436	23.6
23.09.2018	21:00	0.837	27.129	56.753	21.23	22.5
23.09.2018	22:00	0.8537	26.381	58.009	20.196	21.5
23.09.2018	23:00	0.86636	25.629	59.249	19.255	20.6
23.09.2018	00:00	0.87421	24.874	60.48	18.369	19.6
23.09.2018	01:00	0.87676	24.115	61.71	17.515	18.8
23.09.2018	02:00	0.8717	23.344	62.954	16.679	18
23.09.2018	03:00	0.85908	22.564	64.204	15.855	17.2
23.09.2018	04:00	0.84042	21.777	65.475	15.037	16.4
23.09.2018	05:00	0.8234	20.984	66.758	14.36	16.2
Date	Time	Wind Speed (m/s)	Air Temperature (°C)	Relative Humidity (%)	Mean Radiant Temp. (°C)	PET (°C)
		Receptor 7				
23.09.2018	06:00	1.4287	20.529	67.124	16.547	18.7
23.09.2018	07:00	1.4092	21.216	65.347	23.639	22.2
23.09.2018	08:00	1.3886	22.33	62.876	31.145	37.7
23.09.2018	09:00	1.3674	23.6	59.97	63.703	39
23.09.2018	10:00	1.3441	25.04	56.938	63.086	38.1
23.09.2018	11:00	1.3222	26.101	55.367	59.309	40.1
23.09.2018	12:00	1.3155	27.147	53.903	61.62	43.2
23.09.2018	13:00	1.3115	27.967	53.07	66.196	46.4
23.09.2018	14:00	1.3066	28.827	52.079	71.125	35.2
23.09.2018	15:00	1.3015	29.55	51.322	46.126	33.8
23.09.2018	16:00	1.2962	30.254	50.464	41.308	30.8
23.09.2018	17:00	1.293	29.927	51.361	34.899	27.4
23.09.2018	18:00	1.2944	29.206	52.881	27.562	25.4
23.09.2018	19:00	1.3008	28.43	54.458	24.043	24.2

23.09.2018	20:00	1.3105	27.745	55.719	22.482	23.3
23.09.2018	21:00	1.322	27.069	56.904	21.279	22.3
23.09.2018	22:00	1.3332	26.387	58.054	20.255	21.3
23.09.2018	23:00	1.3429	25.699	59.195	19.328	20.2
23.09.2018	00:00	1.3506	25.004	60.333	18.458	19.4
23.09.2018	01:00	1.3556	24.302	61.474	17.621	18.6
23.09.2018	02:00	1.3564	23.584	62.639	16.802	17.8
23.09.2018	03:00	1.3526	22.854	63.818	15.995	17.1
23.09.2018	04:00	1.3448	22.113	65.024	15.194	16.3
23.09.2018	05:00	1.3366	21.362	66.247	14.531	16.1
Date	Time	Wind Speed (m/s)	Air Temperature (°C)	Relative Humidity (%)	Mean Radiant Temp. (°C)	PET (°C)
		Receptor 8				
23.09.2018	06:00	0.16501	20.714	66.793	16.389	21.9
23.09.2018	07:00	0.16901	21.337	65.134	23.403	26.3
23.09.2018	08:00	0.17103	22.402	62.727	30.831	30.4
23.09.2018	09:00	0.1713	23.592	60.043	37.329	46
23.09.2018	10:00	0.16943	24.987	57.06	62.835	44.2
23.09.2018	11:00	0.16409	26.015	55.524	59.144	46.3
23.09.2018	12:00	0.16109	27.065	53.983	61.483	49.6
23.09.2018	13:00	0.15819	27.885	53.115	66.032	53.2
23.09.2018	14:00	0.15501	28.67	52.324	70.893	38.2
23.09.2018	15:00	0.15232	29.343	51.698	45.784	35.9
23.09.2018	16:00	0.15027	30.031	50.865	41.038	32.8
23.09.2018	17:00	0.14941	29.785	51.594	34.697	28.4
23.09.2018	18:00	0.1507	29.113	53.022	27.42	26.4
23.09.2018	19:00	0.15409	28.367	54.552	23.983	25.2
23.09.2018	20:00	0.15906	27.707	55.779	22.436	24.3
23.09.2018	21:00	0.16507	27.054	56.933	21.23	23.4
23.09.2018	22:00	0.1717	26.398	58.049	20.196	22.6
23.09.2018	23:00	0.17809	25.734	59.155	19.255	21.8
23.09.2018	00:00	0.18394	25.063	60.261	18.369	21
23.09.2018	01:00	0.18895	24.383	61.371	17.515	20.2
23.09.2018	02:00	0.19253	23.686	62.507	16.679	19.4
23.09.2018	03:00	0.19455	22.976	63.66	15.855	18.6
23.09.2018	04:00	0.19509	22.252	64.843	15.037	17.9
23.09.2018	05:00	0.19459	21.519	66.043	14.36	18.3

Street grid layout D.2.

Table A6. 4. Detailed microclimatic data for street grid layout D.2.

Date	Time	Wind Speed (m/s)	Air Temperature (°C)	Relative Humidity (%)	Mean Radiant Temp. (°C)	PET (°C)
		Receptor 1				
23.09.2018	06:00	0.11901	20.827	66.616	16.481	22.7
23.09.2018	07:00	0.12076	21.409	65.03	23.405	26.7
23.09.2018	08:00	0.12176	22.436	62.693	30.214	32.3
23.09.2018	09:00	0.12201	23.716	59.664	39.103	48.5
23.09.2018	10:00	0.12114	25.078	56.751	64.287	46
23.09.2018	11:00	0.11836	26.038	55.406	59.769	47.7
23.09.2018	12:00	0.11617	27.127	53.742	61.697	51.4
23.09.2018	13:00	0.11367	27.901	53.037	66.715	40.1
23.09.2018	14:00	0.11102	28.573	52.573	48.481	38.4
23.09.2018	15:00	0.10873	29.284	51.825	45.09	36.2
23.09.2018	16:00	0.10697	29.974	50.963	40.699	32.8
23.09.2018	17:00	0.106	29.737	51.666	34.767	28.8
23.09.2018	18:00	0.10635	29.083	53.066	27.688	26.6
23.09.2018	19:00	0.10769	28.353	54.561	24.134	25.5
23.09.2018	20:00	0.10982	27.705	55.762	22.55	24.5
23.09.2018	21:00	0.1124	27.067	56.89	21.327	23.7
23.09.2018	22:00	0.11515	26.429	57.974	20.285	22.9
23.09.2018	23:00	0.11769	25.782	59.054	19.346	22.2
23.09.2018	00:00	0.11994	25.129	60.131	18.465	21.4
23.09.2018	01:00	0.12182	24.466	61.215	17.62	20.7
23.09.2018	02:00	0.12311	23.786	62.324	16.797	19.9
23.09.2018	03:00	0.1238	23.094	63.45	15.986	19.1
23.09.2018	04:00	0.12401	22.389	64.607	15.184	18.4
23.09.2018	05:00	0.1239	21.675	65.778	14.52	18.9
Date	Time	Wind Speed (m/s)	Air Temperature (°C)	Relative Humidity (%)	Mean Radiant Temp. (°C)	PET (°C)
		Receptor 2				
23.09.2018	06:00	0.66976	20.858	66.584	16.35	35.8
23.09.2018	07:00	0.66117	21.466	64.862	56.376	23.7
23.09.2018	08:00	0.65023	22.517	62.416	30.006	42.6
23.09.2018	09:00	0.63692	23.81	59.336	64.598	43.2
23.09.2018	10:00	0.62089	25.06	56.793	64.086	41.4
23.09.2018	11:00	0.60191	25.999	55.485	59.612	43.2

23.09.2018	12:00	0.59417	27.025	53.987	61.583	46.5
23.09.2018	13:00	0.58878	27.824	53.18	66.566	49.3
23.09.2018	14:00	0.58271	28.596	52.395	70.521	36
23.09.2018	15:00	0.57627	29.31	51.631	44.865	34.3
23.09.2018	16:00	0.5703	29.949	50.913	40.517	31.4
23.09.2018	17:00	0.56702	29.718	51.634	34.601	27.9
23.09.2018	18:00	0.56831	29.072	53.041	27.567	25.9
23.09.2018	19:00	0.57506	28.352	54.528	24.083	24.8
23.09.2018	20:00	0.58569	27.71	55.726	22.512	23.8
23.09.2018	21:00	0.59906	27.078	56.848	21.287	22.8
23.09.2018	22:00	0.61371	26.444	57.931	20.238	22
23.09.2018	23:00	0.62776	25.8	59.01	19.287	21.1
23.09.2018	00:00	0.64038	25.149	60.085	18.393	20.2
23.09.2018	01:00	0.65094	24.489	61.165	17.535	19.4
23.09.2018	02:00	0.65798	23.814	62.269	16.698	18.6
23.09.2018	03:00	0.66093	23.125	63.39	15.873	17.8
23.09.2018	04:00	0.66006	22.423	64.542	15.057	17.1
23.09.2018	05:00	0.65717	21.714	65.707	14.381	17.2
Date	Time	Wind Speed (m/s)	Air Temperature (°C)	Relative Humidity (%)	Mean Radiant Temp. (°C)	PET (°C)
		Receptor 3				
23.09.2018	06:00	1.7412	20.818	66.665	16.51	31.2
23.09.2018	07:00	1.7123	21.496	64.697	56.547	34.6
23.09.2018	08:00	1.6813	22.644	61.916	61.515	37.8
23.09.2018	09:00	1.6486	23.9	59.011	64.854	38.6
23.09.2018	10:00	1.6142	25.1	56.664	64.331	37.3
23.09.2018	11:00	1.578	26.038	55.359	59.803	39.1
23.09.2018	12:00	1.5576	27.017	54.006	61.722	42.6
23.09.2018	13:00	1.5409	27.859	53.06	66.747	45.2
23.09.2018	14:00	1.5244	28.638	52.247	70.743	46.5
23.09.2018	15:00	1.5086	29.375	51.415	71.653	45.5
23.09.2018	16:00	1.4944	30.008	50.718	68.779	30.4
23.09.2018	17:00	1.484	29.741	51.554	34.804	28.3
23.09.2018	18:00	1.4785	29.08	53.013	30.735	25.3
23.09.2018	19:00	1.481	28.355	54.521	24.145	24.1
23.09.2018	20:00	1.488	27.714	55.72	22.559	23.1
23.09.2018	21:00	1.4985	27.08	56.844	21.335	22.1
23.09.2018	22:00	1.5108	26.442	57.932	20.296	21.2
23.09.2018	23:00	1.5231	25.793	59.017	19.358	20.3

23.09.2018	00:00	1.5342	25.137	60.099	18.481	19.5
23.09.2018	01:00	1.5435	24.473	61.186	17.639	18.7
23.09.2018	02:00	1.5489	23.792	62.296	16.819	17.9
23.09.2018	03:00	1.5496	23.1	63.423	16.011	17.2
23.09.2018	04:00	1.5459	22.394	64.579	15.212	16.4
23.09.2018	05:00	1.5403	21.681	65.75	14.551	16.1
Date	Time	Wind Speed (m/s)	Air Temperature (°C)	Relative Humidity (%)	Mean Radiant Temp. (°C)	PET (°C)
		Receptor 4				
23.09.2018	06:00	0.67332	20.856	66.588	16.35	20
23.09.2018	07:00	0.66235	21.436	64.979	23.213	24
23.09.2018	08:00	0.64828	22.504	62.465	30.006	42.6
23.09.2018	09:00	0.63123	23.81	59.338	64.598	43.2
23.09.2018	10:00	0.61076	25.053	56.817	64.086	41.4
23.09.2018	11:00	0.586	26.004	55.47	59.612	43.2
23.09.2018	12:00	0.57864	27.029	53.975	61.583	46.5
23.09.2018	13:00	0.57431	27.848	53.106	66.566	49.3
23.09.2018	14:00	0.56852	28.608	52.358	70.521	36
23.09.2018	15:00	0.56203	29.32	51.6	44.865	34.4
23.09.2018	16:00	0.5563	29.973	50.846	40.517	43.8
23.09.2018	17:00	0.55457	29.757	51.52	59.205	29.2
23.09.2018	18:00	0.55941	29.089	52.988	30.593	25.9
23.09.2018	19:00	0.5727	28.359	54.506	24.083	24.8
23.09.2018	20:00	0.59087	27.715	55.712	22.512	23.8
23.09.2018	21:00	0.612	27.081	56.838	21.287	22.8
23.09.2018	22:00	0.63376	26.445	57.924	20.238	21.9
23.09.2018	23:00	0.65342	25.8	59.006	19.287	21
23.09.2018	00:00	0.67002	25.147	60.084	18.393	20.2
23.09.2018	01:00	0.68296	24.486	61.168	17.535	19.4
23.09.2018	02:00	0.69027	23.809	62.275	16.698	18.6
23.09.2018	03:00	0.6915	23.119	63.398	15.873	17.8
23.09.2018	04:00	0.68743	22.416	64.551	15.057	17.1
23.09.2018	05:00	0.68143	21.706	65.718	14.381	17.2
Date	Time	Wind Speed (m/s)	Air Temperature (°C)	Relative Humidity (%)	Mean Radiant Temp. (°C)	PET (°C)
		Receptor 5				
23.09.2018	06:00	0.12902	20.831	66.601	16.481	22.7
23.09.2018	07:00	0.13206	21.424	64.971	23.405	26.7

23.09.2018	08:00	0.13487	22.447	62.652	30.214	32.3
23.09.2018	09:00	0.13731	23.724	59.636	39.103	48.5
23.09.2018	10:00	0.13907	25.088	56.719	64.287	46
23.09.2018	11:00	0.13993	26.046	55.38	59.769	47.7
23.09.2018	12:00	0.1373	27.139	53.708	61.697	51.4
23.09.2018	13:00	0.13414	27.908	53.016	66.715	40.1
23.09.2018	14:00	0.13142	28.579	52.557	48.481	38.4
23.09.2018	15:00	0.12933	29.282	51.834	45.09	36.2
23.09.2018	16:00	0.1274	29.973	50.968	40.699	32.8
23.09.2018	17:00	0.12527	29.743	51.649	34.767	28.8
23.09.2018	18:00	0.12315	29.085	53.059	27.688	26.6
23.09.2018	19:00	0.12022	28.355	54.555	24.134	25.5
23.09.2018	20:00	0.11772	27.706	55.759	22.55	24.5
23.09.2018	21:00	0.1158	27.068	56.885	21.327	23.7
23.09.2018	22:00	0.11466	26.43	57.97	20.285	22.9
23.09.2018	23:00	0.11425	25.783	59.051	19.346	22.2
23.09.2018	00:00	0.11438	25.129	60.129	18.465	21.4
23.09.2018	01:00	0.11489	24.466	61.213	17.62	20.7
23.09.2018	02:00	0.11566	23.786	62.322	16.797	19.9
23.09.2018	03:00	0.11664	23.094	63.448	15.986	19.1
23.09.2018	04:00	0.11778	22.388	64.606	15.184	18.4
23.09.2018	05:00	0.11872	21.674	65.778	14.52	18.9
Date	Time	Wind Speed (m/s)	Air Temperature (°C)	Relative Humidity (%)	Mean Radiant Temp. (°C)	PET (°C)
		Receptor 6				
23.09.2018	06:00	0.66879	20.749	66.722	44.552	36.4
23.09.2018	07:00	0.64977	21.423	64.844	56.376	24
23.09.2018	08:00	0.62897	22.468	62.509	30.006	42.6
23.09.2018	09:00	0.60617	23.799	59.346	64.598	43.2
23.09.2018	10:00	0.58101	25.099	56.711	64.086	41.4
23.09.2018	11:00	0.55633	26.039	55.465	59.612	43.2
23.09.2018	12:00	0.55155	27.109	53.893	61.583	46.6
23.09.2018	13:00	0.55008	27.916	53.101	66.566	50.1
23.09.2018	14:00	0.54714	28.693	52.332	70.521	36.4
23.09.2018	15:00	0.5433	29.419	51.552	44.865	34.7
23.09.2018	16:00	0.53982	30.072	50.811	40.517	31.7
23.09.2018	17:00	0.53926	29.791	51.6	34.601	28
23.09.2018	18:00	0.54339	29.124	53.006	27.567	25.9
23.09.2018	19:00	0.55484	28.387	54.5	24.083	24.8

23.09.2018	20:00	0.56999	27.727	55.717	22.512	23.8
23.09.2018	21:00	0.58715	27.078	56.859	21.287	22.8
23.09.2018	22:00	0.60419	26.429	57.963	20.238	22
23.09.2018	23:00	0.61891	25.771	59.06	19.287	21.1
23.09.2018	00:00	0.63062	25.107	60.154	18.393	20.2
23.09.2018	01:00	0.63892	24.433	61.255	17.535	19.4
23.09.2018	02:00	0.64197	23.744	62.38	16.698	18.6
23.09.2018	03:00	0.63937	23.042	63.521	15.873	17.9
23.09.2018	04:00	0.63192	22.327	64.692	15.057	17.1
23.09.2018	05:00	0.62369	21.605	65.876	14.381	17
Date	Time	Wind Speed (m/s)	Air Temperature (°C)	Relative Humidity (%)	Mean Radiant Temp. (°C)	PET (°C)
		Receptor 7				
23.09.2018	06:00	2.1439	19.746	68.385	16.51	29.4
23.09.2018	07:00	2.1276	20.984	65.093	56.547	33.4
23.09.2018	08:00	2.1066	22.688	60.993	61.515	36.5
23.09.2018	09:00	2.0826	24.348	57.23	64.854	37.7
23.09.2018	10:00	2.0558	25.832	54.595	64.331	37.1
23.09.2018	11:00	2.0327	26.859	53.365	59.803	38.9
23.09.2018	12:00	2.0434	27.907	52.104	61.722	41.8
23.09.2018	13:00	2.0552	28.843	51.061	66.747	44.5
23.09.2018	14:00	2.0612	29.686	50.218	70.743	45.7
23.09.2018	15:00	2.0634	30.45	49.394	71.653	44.9
23.09.2018	16:00	2.0647	31.042	48.892	68.779	30.6
23.09.2018	17:00	2.069	30.437	50.443	34.804	27.4
23.09.2018	18:00	2.0809	29.564	52.298	27.714	25.4
23.09.2018	19:00	2.104	28.723	53.941	24.145	24.1
23.09.2018	20:00	2.1339	27.955	55.309	22.559	22.8
23.09.2018	21:00	2.1673	27.184	56.616	21.335	21.7
23.09.2018	22:00	2.2009	26.39	57.924	20.296	20.5
23.09.2018	23:00	2.2312	25.589	59.224	19.358	19.6
23.09.2018	00:00	2.2573	24.786	60.515	18.481	18.7
23.09.2018	01:00	2.2786	23.98	61.802	17.639	17.8
23.09.2018	02:00	2.2918	23.167	63.096	16.819	17
23.09.2018	03:00	2.2963	22.35	64.39	16.011	16
23.09.2018	04:00	2.2932	21.527	65.7	15.212	15.2
23.09.2018	05:00	2.2867	20.703	67.016	14.551	14.9
Date	Time	Wind Speed (m/s)	Air Temperature (°C)	Relative Humidity (%)	Mean Radiant Temp. (°C)	PET (°C)

		Receptor 8				
23.09.2018	06:00	0.63551	20.736	66.782	16.35	20.2
23.09.2018	07:00	0.61581	21.342	65.174	23.213	24
23.09.2018	08:00	0.59321	22.421	62.692	30.006	42.6
23.09.2018	09:00	0.56793	23.785	59.398	64.598	44
23.09.2018	10:00	0.53948	25.07	56.808	64.086	42
23.09.2018	11:00	0.51015	26.031	55.492	59.612	43.9
23.09.2018	12:00	0.50742	27.101	53.917	61.583	47.3
23.09.2018	13:00	0.50862	27.913	53.11	66.566	50.1
23.09.2018	14:00	0.50752	28.691	52.338	70.521	36.4
23.09.2018	15:00	0.50514	29.421	51.545	44.865	34.7
23.09.2018	16:00	0.50338	30.102	50.725	40.517	31.7
23.09.2018	17:00	0.50575	29.804	51.563	34.601	28
23.09.2018	18:00	0.51507	29.128	52.994	27.567	26
23.09.2018	19:00	0.53403	28.389	54.494	24.083	24.8
23.09.2018	20:00	0.55787	27.728	55.714	22.512	23.8
23.09.2018	21:00	0.58383	27.079	56.858	21.287	22.8
23.09.2018	22:00	0.6089	26.429	57.961	20.238	22
23.09.2018	23:00	0.63001	25.772	59.058	19.287	21.1
23.09.2018	00:00	0.64637	25.108	60.151	18.393	20.1
23.09.2018	01:00	0.65758	24.435	61.251	17.535	19.3
23.09.2018	02:00	0.66131	23.746	62.376	16.698	18.5
23.09.2018	03:00	0.65727	23.045	63.516	15.873	17.9
23.09.2018	04:00	0.64681	22.33	64.687	15.057	17.1
23.09.2018	05:00	0.63556	21.608	65.871	14.381	17.2

Sample of the appendices for chapter 6 – section 2.

Layout 1 summer analysis.

Table A6. 5. Detailed microclimatic data for layout 1 summer analysis.

Date	Time	Wind Speed (m/s)	Air Temperature (°C)	Relative Humidity (%)	Mean Radiant Temp. (°C)	Direct Sw Radiation (W/m ²)	PET (°C)
		Receptor 1					
21.06.2018	06:00	1.5044	24.966	37.857	24.862	0	22
21.06.2018	07:00	1.4904	26.139	35.908	63.882	921.63	39.4
21.06.2018	08:00	1.4761	27.411	33.688	65.918	992.12	41.5
21.06.2018	09:00	1.4618	28.548	31.322	65.867	1032.1	42.5

21.06.2018	10:00	1.4486	29.551	28.923	64.174	1054	42.9
21.06.2018	11:00	1.4377	30.659	27.203	63.544	1058.7	43.5
21.06.2018	12:00	1.4292	31.708	25.864	71.48	1050.8	48.3
21.06.2018	13:00	1.4216	32.51	24.819	77.572	1028.7	52.2
21.06.2018	14:00	1.4148	32.853	24.96	79.272	983.51	53.4
21.06.2018	15:00	1.4077	32.978	25.472	77.614	904.31	52.6
21.06.2018	16:00	1.4002	32.736	25.986	43.361	0	36.2
21.06.2018	17:00	1.3941	32.137	26.948	33.686	0	31.9
21.06.2018	18:00	1.3852	31.295	28.131	24.839	0	27.9
21.06.2018	19:00	1.3775	30.532	29.383	23.1	0	26.6
21.06.2018	20:00	1.3702	29.703	31.93	21.621	0	25.3
21.06.2018	21:00	1.3634	28.836	33.367	20.242	0	24
21.06.2018	22:00	1.3575	27.946	34.757	18.917	0	22.7
21.06.2018	23:00	1.3522	27.037	36.604	17.624	0	21.5
22.06.2018	00:00	1.3472	26.104	39.808	16.368	0	20.3
22.06.2018	01:00	1.3429	25.744	38.686	15.99	0	19.9
22.06.2018	02:00	1.3403	25.201	38.501	15.226	0	19.3
22.06.2018	03:00	1.3365	24.752	38.726	14.681	0	18.8
22.06.2018	04:00	1.3329	24.398	39.358	14.266	0	18.4
22.06.2018	05:00	1.3287	24.446	39.154	19.613	0	19.9
Date	Time	Wind Speed (m/s)	Air Temperature (°C)	Relative Humidity (%)	Mean Radiant Temp. (°C)	Direct Sw Radiation (W/m ²)	PET (°C)
		Receptor 2					
21.06.2018	06:00	1.0316	25.06	37.652	57.245	790.43	40
21.06.2018	07:00	1.0223	26.308	35.538	63.918	921.63	41.5
21.06.2018	08:00	1.0126	27.632	33.247	65.947	992.12	43.6
21.06.2018	09:00	1.0028	28.772	30.913	65.894	1032.1	44.6
21.06.2018	10:00	0.99508	29.713	28.665	64.201	1054	44.3
21.06.2018	11:00	0.99019	30.754	27.05	63.566	1058.7	44.9
21.06.2018	12:00	0.98751	31.754	25.784	71.508	1050.8	49.8
21.06.2018	13:00	0.98568	32.545	24.758	77.607	1028.7	53.8
21.06.2018	14:00	0.9833	32.855	24.918	79.308	983.51	55
21.06.2018	15:00	0.97969	32.989	25.407	77.659	904.31	54.2
21.06.2018	16:00	0.97461	32.733	25.954	43.425	0	36.7
21.06.2018	17:00	0.96803	32.207	26.807	33.742	0	32.2
21.06.2018	18:00	0.96086	31.306	28.093	24.848	0	27.9
21.06.2018	19:00	0.95399	30.529	29.37	23.105	0	26.6
21.06.2018	20:00	0.94786	29.694	31.904	21.626	0	25.4
21.06.2018	21:00	0.94288	28.825	33.373	20.25	0	24.2

21.06.2018	22:00	0.93872	27.935	34.768	18.928	0	22.9
21.06.2018	23:00	0.93592	27.025	36.613	17.64	0	21.7
22.06.2018	00:00	0.93315	26.093	39.797	16.388	0	20.6
22.06.2018	01:00	0.93093	25.721	38.758	16.006	0	20.1
22.06.2018	02:00	0.92874	25.182	38.56	15.245	0	19.4
22.06.2018	03:00	0.92674	24.729	38.791	14.7	0	18.9
22.06.2018	04:00	0.92462	24.372	39.424	14.285	0	18.6
22.06.2018	05:00	0.92261	24.464	39.118	19.645	0	20.4
Date	Time	Wind Speed (m/s)	Air Temperature (°C)	Relative Humidity (%)	Mean Radiant Temp. (°C)	Direct Sw Radiation (W/m ²)	PET (°C)
		Receptor 3					
21.06.2018	06:00	2.7822	24.17	39.705	57.804	790.43	31.4
21.06.2018	07:00	2.7812	25.417	37.532	64.395	921.63	35.5
21.06.2018	08:00	2.7787	26.827	34.924	66.205	992.12	37.7
21.06.2018	09:00	2.7752	28.278	31.849	65.984	1032.1	39.2
21.06.2018	10:00	2.7728	29.686	28.686	64.142	1054	39.9
21.06.2018	11:00	2.772	31.181	26.413	63.287	1058.7	41.1
21.06.2018	12:00	2.7718	32.448	24.82	71.334	1050.8	45.8
21.06.2018	13:00	2.7714	33.208	23.878	77.594	1028.7	49.4
21.06.2018	14:00	2.7696	33.468	24.164	79.436	983.51	50.5
21.06.2018	15:00	2.7671	33.395	24.959	78.053	904.31	49.8
21.06.2018	16:00	2.7633	32.959	25.728	44.211	0	35.8
21.06.2018	17:00	2.7597	32.07	27.121	34.536	0	31.6
21.06.2018	18:00	2.7563	31.108	28.492	24.938	0	27.6
21.06.2018	19:00	2.7537	30.33	29.792	23.094	0	26.1
21.06.2018	20:00	2.7526	29.47	32.514	21.613	0	24.9
21.06.2018	21:00	2.7528	28.573	33.98	20.269	0	23.5
21.06.2018	22:00	2.7541	27.655	35.437	18.992	0	22.1
21.06.2018	23:00	2.7566	26.72	37.384	17.754	0	20.7
22.06.2018	00:00	2.7591	25.768	40.781	16.552	0	19.7
22.06.2018	01:00	2.762	25.417	39.443	16.123	0	19.3
22.06.2018	02:00	2.7656	24.857	39.262	15.396	0	18.7
22.06.2018	03:00	2.7677	24.404	39.489	14.854	0	18.1
22.06.2018	04:00	2.7697	24.051	40.155	14.439	0	17.8
22.06.2018	05:00	2.7708	24.069	40.03	20.028	0	19
Date	Time	Wind Speed (m/s)	Air Temperature (°C)	Relative Humidity (%)	Mean Radiant Temp. (°C)	Direct Sw Radiation (W/m ²)	PET (°C)
		Receptor 4					

21.06.2018	06:00	1.0709	24.73	38.412	57.227	790.43	40.1
21.06.2018	07:00	1.0635	25.876	36.426	63.9	921.63	40.8
21.06.2018	08:00	1.0556	27.192	34.079	65.932	992.12	42.9
21.06.2018	09:00	1.0476	28.481	31.423	65.881	1032.1	44.3
21.06.2018	10:00	1.0404	29.607	28.856	64.187	1054	44.3
21.06.2018	11:00	1.0345	30.805	26.966	63.555	1058.7	44.9
21.06.2018	12:00	1.0296	31.904	25.553	71.494	1050.8	49.9
21.06.2018	13:00	1.0251	32.701	24.53	77.59	1028.7	53.9
21.06.2018	14:00	1.0202	32.974	24.717	79.29	983.51	55.1
21.06.2018	15:00	1.0147	33.032	25.298	77.636	904.31	54.1
21.06.2018	16:00	1.0084	32.685	25.987	43.393	0	36.7
21.06.2018	17:00	1.0017	32.064	26.983	33.714	0	32.1
21.06.2018	18:00	0.99499	31.174	28.264	24.843	0	27.8
21.06.2018	19:00	0.98884	30.442	29.46	23.103	0	26.5
21.06.2018	20:00	0.98343	29.639	31.863	21.623	0	25.3
21.06.2018	21:00	0.97887	28.792	33.348	20.246	0	24.1
21.06.2018	22:00	0.97551	27.921	34.725	18.923	0	22.9
21.06.2018	23:00	0.97292	27.03	36.527	17.632	0	21.7
22.06.2018	00:00	0.97115	26.117	39.599	16.378	0	20.5
22.06.2018	01:00	0.96982	25.73	38.743	15.998	0	20
22.06.2018	02:00	0.96892	25.199	38.553	15.236	0	19.4
22.06.2018	03:00	0.96805	24.746	38.793	14.69	0	18.9
22.06.2018	04:00	0.96716	24.389	39.409	14.276	0	18.5
22.06.2018	05:00	0.96611	24.434	39.204	19.629	0	20.2

Layout 1 winter analysis.

Table A6. 6. Detailed microclimatic data for layout 1 winter analysis.

Date	Time	Wind Speed (m/s)	Air Temperature (°C)	Relative Humidity (%)	Mean Radiant Temp. (°C)	Direct Sw Radiation (W/m ²)	PET (°C)
		Receptor 1					
21.06.2018	06:00	1.3229	6.504	88.872	-1.4307	0	0.2
21.06.2018	07:00	1.3122	6.4186	88.528	3.794	0	1.4
21.06.2018	08:00	1.302	7.189	85.362	11.301	0	4.1
21.06.2018	09:00	1.2922	8.2208	80.249	16.692	0	6.4
21.06.2018	10:00	1.2825	9.0719	74.512	53.886	860.88	20
21.06.2018	11:00	1.2737	9.6269	71.844	54.927	871.33	20.9
21.06.2018	12:00	1.2668	10.037	69.686	55.449	855.26	21.5

21.06.2018	13:00	1.2613	10.377	68.459	53.94	803.71	21.2
21.06.2018	14:00	1.2566	10.492	67.369	48.085	694.78	18.8
21.06.2018	15:00	1.2522	10.291	67.698	31.341	420.66	12.6
21.06.2018	16:00	1.2477	9.7253	70.056	0.86028	0	3.4
21.06.2018	17:00	1.2432	9.1265	73.884	-0.36124	0	2.6
21.06.2018	18:00	1.2391	8.7633	76.397	-0.92194	0	2.3
21.06.2018	19:00	1.2356	8.5091	77.521	-1.3145	0	1.9
21.06.2018	20:00	1.2303	8.278	78.568	-1.6332	0	1.7
21.06.2018	21:00	1.2298	8.0189	80.326	-1.953	0	1.3
21.06.2018	22:00	1.2279	7.7818	81.023	-2.2329	0	1.1
21.06.2018	23:00	1.2273	7.5552	82.138	-2.4946	0	0.9
22.06.2018	00:00	1.226	7.3311	83.858	-2.7244	0	0.6
22.06.2018	01:00	1.2244	7.8694	81.587	-2.0688	0	1.2
22.06.2018	02:00	1.2229	7.6146	82.63	-2.4837	0	0.9
22.06.2018	03:00	1.2212	7.0671	86.237	-3.0301	0	0.4
22.06.2018	04:00	1.2193	6.6287	90.043	-3.4153	0	-0.1
22.06.2018	05:00	1.217	6.2588	93.481	-3.7307	0	-0.4
Date	Time	Wind Speed (m/s)	Air Temperature (°C)	Relative Humidity (%)	Mean Radiant Temp. (°C)	Direct Sw Radiation (W/m ²)	PET (°C)
		Receptor 2					
21.06.2018	06:00	0.89365	6.5556	88.725	-1.3514	0	0.7
21.06.2018	07:00	0.88641	6.5609	87.796	31.441	509.27	11.4
21.06.2018	08:00	0.87956	7.504	83.632	45.34	724.17	17.6
21.06.2018	09:00	0.87323	8.4794	78.948	51.242	816.96	21.1
21.06.2018	10:00	0.86743	9.2555	73.74	53.98	860.88	23.2
21.06.2018	11:00	0.86304	9.7722	71.29	55.017	871.33	24.1
21.06.2018	12:00	0.86103	10.143	69.385	55.544	855.26	24.6
21.06.2018	13:00	0.86038	10.398	68.53	20.885	0	10.4
21.06.2018	14:00	0.86015	10.47	67.672	16.564	0	9.1
21.06.2018	15:00	0.85917	10.315	67.789	9.1571	0	6.6
21.06.2018	16:00	0.8569	9.7377	70.168	0.92016	0	3.7
21.06.2018	17:00	0.85414	9.1215	74.024	-0.30784	0	2.9
21.06.2018	18:00	0.85174	8.744	76.604	-0.87305	0	2.5
21.06.2018	19:00	0.85001	8.4847	77.768	-1.2674	0	2.2
21.06.2018	20:00	0.84884	8.2513	78.827	-1.5869	0	2.1
21.06.2018	21:00	0.84878	7.9922	80.575	-1.9064	0	1.8
21.06.2018	22:00	0.84858	7.754	81.295	-2.1862	0	1.5
21.06.2018	23:00	0.84921	7.5268	82.403	-2.4477	0	1.2
22.06.2018	00:00	0.84968	7.3025	84.114	-2.6772	0	1

22.06.2018	01:00	0.85009	7.82	81.937	-2.0293	0	1.5
22.06.2018	02:00	0.85043	7.5831	82.9	-2.439	0	1.2
22.06.2018	03:00	0.85062	7.041	86.465	-2.9818	0	0.6
22.06.2018	04:00	0.85056	6.6029	90.261	-3.3657	0	0.2
22.06.2018	05:00	0.85022	6.2332	93.699	-3.6803	0	-0.2
Date	Time	Wind Speed (m/s)	Air Temperature (°C)	Relative Humidity (%)	Mean Radiant Temp. (°C)	Direct Sw Radiation (W/m ²)	PET (°C)
		Receptor 3					
21.06.2018	06:00	2.4466	6.4334	88.819	-0.4054	0	-0.4
21.06.2018	07:00	2.4458	6.2884	88.87	5.0601	0	0.6
21.06.2018	08:00	2.4454	7.0624	85.778	13.086	0	3
21.06.2018	09:00	2.4449	8.2261	79.931	52.547	816.96	14.6
21.06.2018	10:00	2.4445	9.1234	73.905	55.283	860.88	16.3
21.06.2018	11:00	2.4446	9.7432	70.952	56.236	871.33	17.1
21.06.2018	12:00	2.4464	10.173	68.698	56.855	855.26	17.7
21.06.2018	13:00	2.4485	10.479	67.687	55.424	803.71	17.5
21.06.2018	14:00	2.4509	10.404	67.399	18.391	0	6.9
21.06.2018	15:00	2.4526	10.108	68.128	10.641	0	5
21.06.2018	16:00	2.4536	9.5209	70.591	1.6508	0	2.7
21.06.2018	17:00	2.4549	8.9502	74.374	0.29794	0	2
21.06.2018	18:00	2.4569	8.6124	76.77	-0.34412	0	1.5
21.06.2018	19:00	2.4604	8.3675	77.789	-0.77164	0	1.2
21.06.2018	20:00	2.4642	8.1401	78.796	-1.1054	0	0.9
21.06.2018	21:00	2.469	7.8843	80.57	-1.4254	0	0.7
21.06.2018	22:00	2.4744	7.6481	81.212	-1.7072	0	0.4
21.06.2018	23:00	2.4802	7.4234	82.338	-1.9684	0	0.1
22.06.2018	00:00	2.4861	7.2044	84.081	-2.197	0	-0.1
22.06.2018	01:00	2.4912	7.7732	81.693	-1.6493	0	0.6
22.06.2018	02:00	2.496	7.4934	82.839	-1.9916	0	0.2
22.06.2018	03:00	2.5002	6.9423	86.531	-2.4909	0	-0.4
22.06.2018	04:00	2.5039	6.5159	90.352	-2.8628	0	-0.8
22.06.2018	05:00	2.5069	6.1596	93.762	-3.1714	0	-1.1
Date	Time	Wind Speed (m/s)	Air Temperature (°C)	Relative Humidity (%)	Mean Radiant Temp. (°C)	Direct Sw Radiation (W/m ²)	PET (°C)
		Receptor 4					
21.06.2018	06:00	0.91251	6.5673	89.066	-1.3911	0	0.7
21.06.2018	07:00	0.90645	6.5237	88.397	31.407	509.27	11.3
21.06.2018	08:00	0.90068	7.3667	84.673	45.297	724.17	17.6

21.06.2018	09:00	0.89545	8.3079	80.106	51.196	816.96	20.9
21.06.2018	10:00	0.89069	9.1151	74.721	53.933	860.88	23
21.06.2018	11:00	0.88664	9.6702	72.005	54.972	871.33	24
21.06.2018	12:00	0.88396	10.053	70.042	55.497	855.26	24.6
21.06.2018	13:00	0.88226	10.294	69.197	20.818	0	10.3
21.06.2018	14:00	0.88096	10.343	68.472	16.5	0	8.9
21.06.2018	15:00	0.87937	10.142	68.828	9.1046	0	6.4
21.06.2018	16:00	0.8773	9.5943	71.156	0.89022	0	3.6
21.06.2018	17:00	0.87524	9.0456	74.735	-0.33454	0	2.8
21.06.2018	18:00	0.87351	8.6946	77.233	-0.8975	0	2.5
21.06.2018	19:00	0.87253	8.4493	78.387	-1.2909	0	2.1
21.06.2018	20:00	0.87202	8.2254	79.414	-1.6101	0	1.9
21.06.2018	21:00	0.87231	7.9782	81.073	-1.9297	0	1.7
21.06.2018	22:00	0.87312	7.7471	81.796	-2.2095	0	1.3
21.06.2018	23:00	0.87433	7.5273	82.845	-2.4712	0	1.1
22.06.2018	00:00	0.87582	7.3114	84.471	-2.7008	0	0.9
22.06.2018	01:00	0.8773	7.7869	82.472	-2.049	0	1.5
22.06.2018	02:00	0.87878	7.5796	83.303	-2.4613	0	1.2
22.06.2018	03:00	0.88018	7.0646	86.676	-3.0059	0	0.7
22.06.2018	04:00	0.88141	6.6447	90.305	-3.3905	0	0.2
22.06.2018	05:00	0.8824	6.291	93.602	-3.7055	0	-0.1

Layout 2 different wind directions.

Wind speed values at 11:00 am maps.

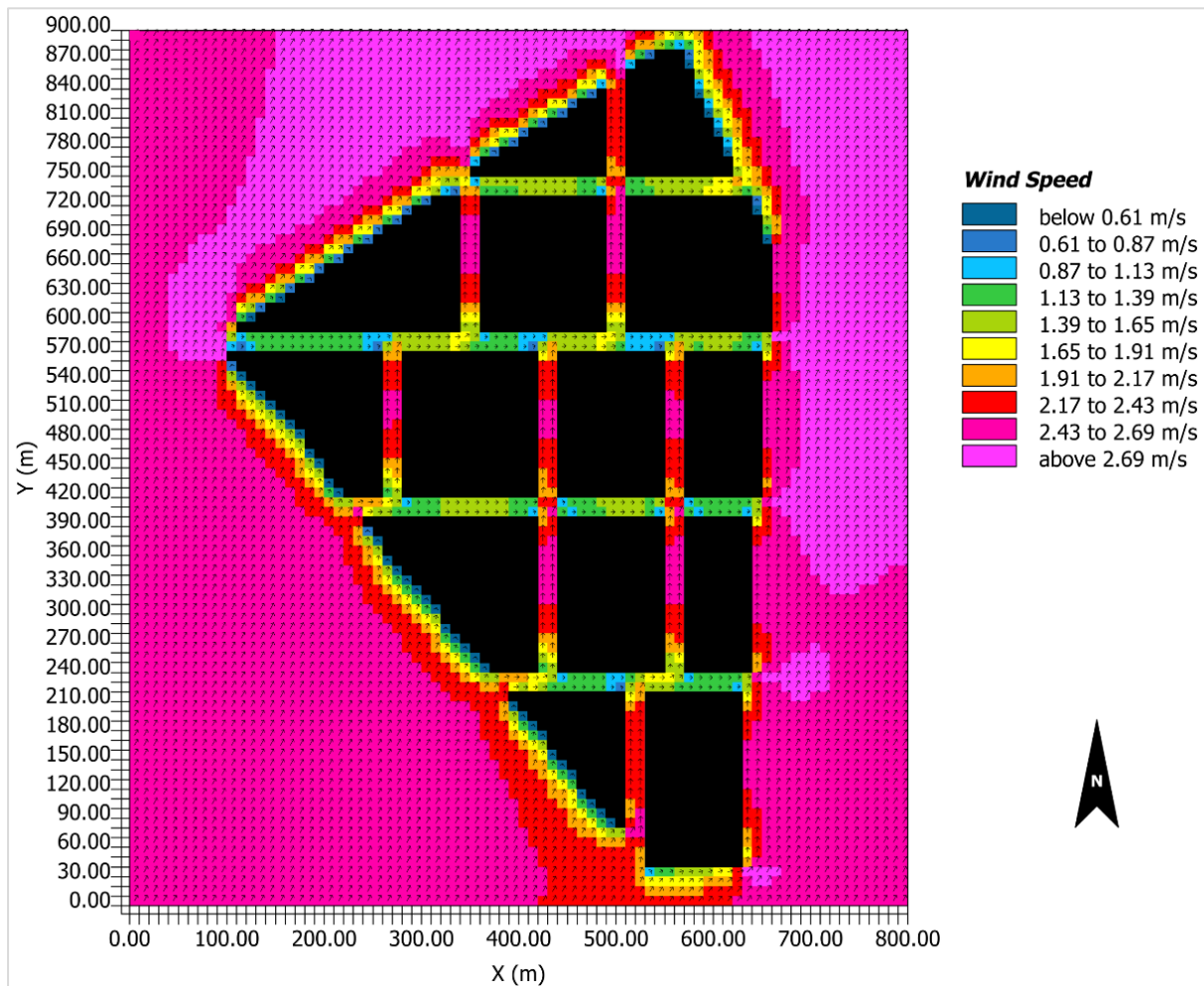


Figure A6. 1. Wind speed values for wind direction 150° at 11:00 am.

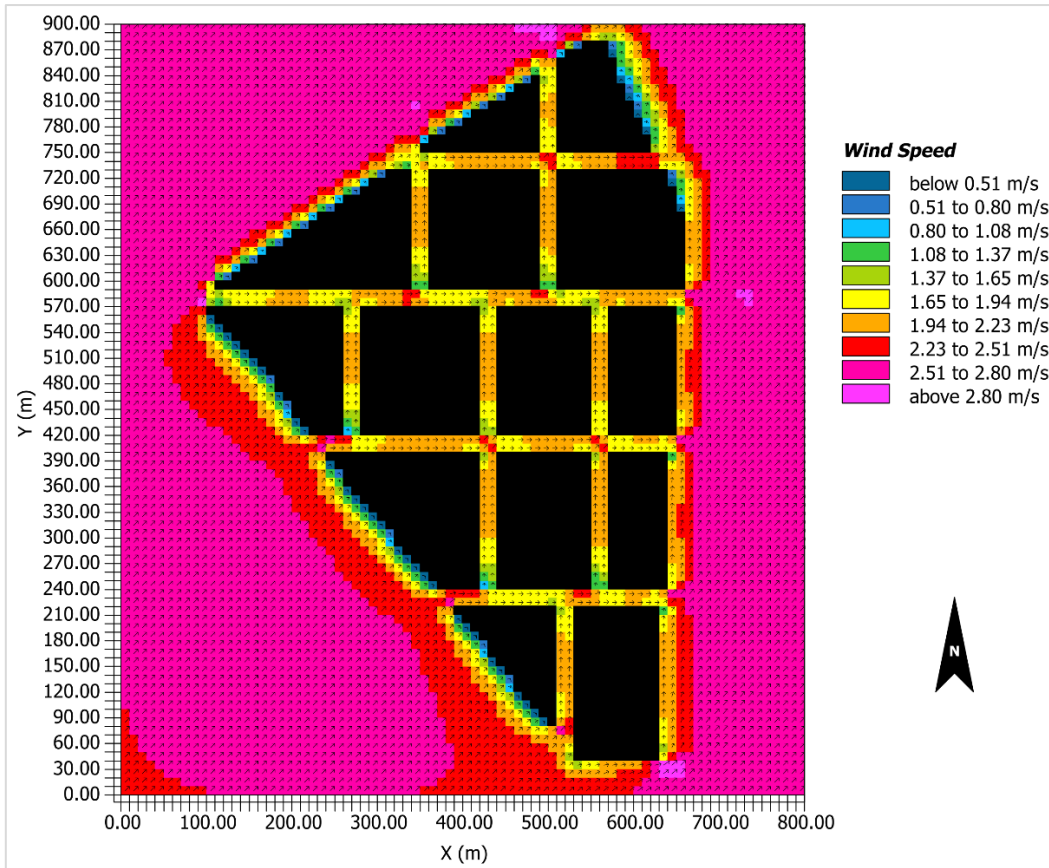


Figure A6. 2. Wind speed values for wind direction 135° at 11:00 am.

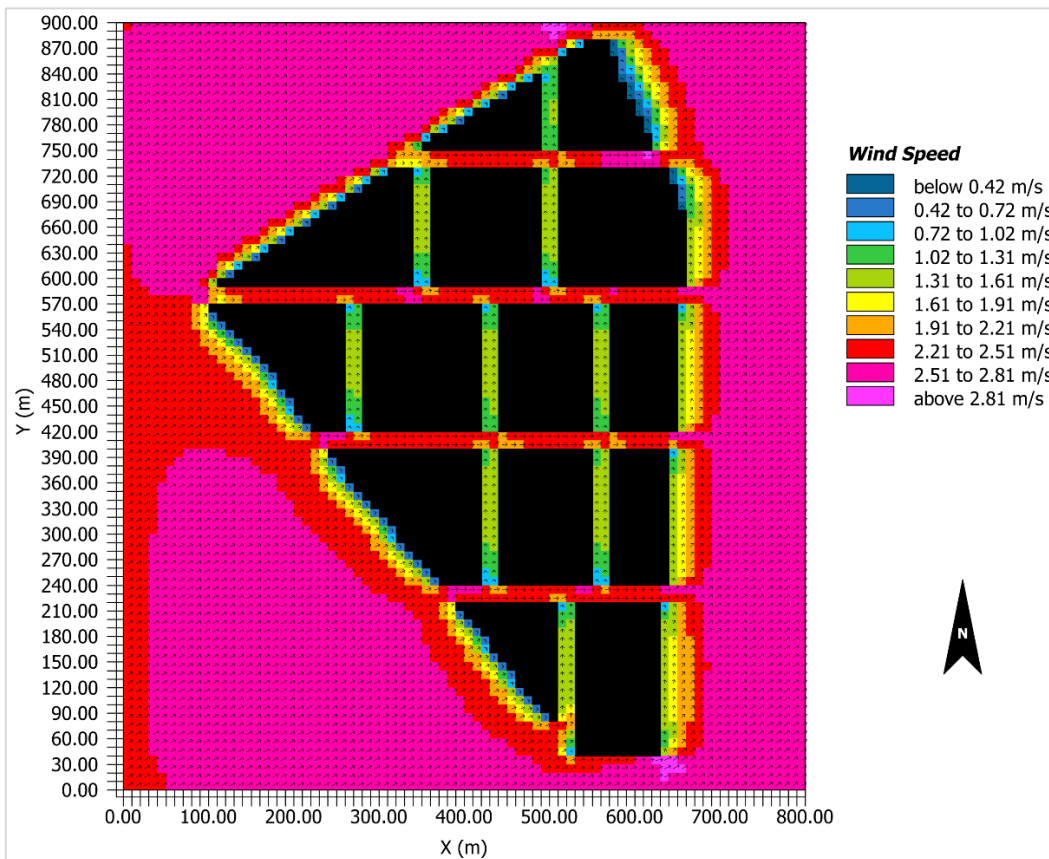


Figure A6. 3. Wind speed values for wind direction 120° at 11:00 am.

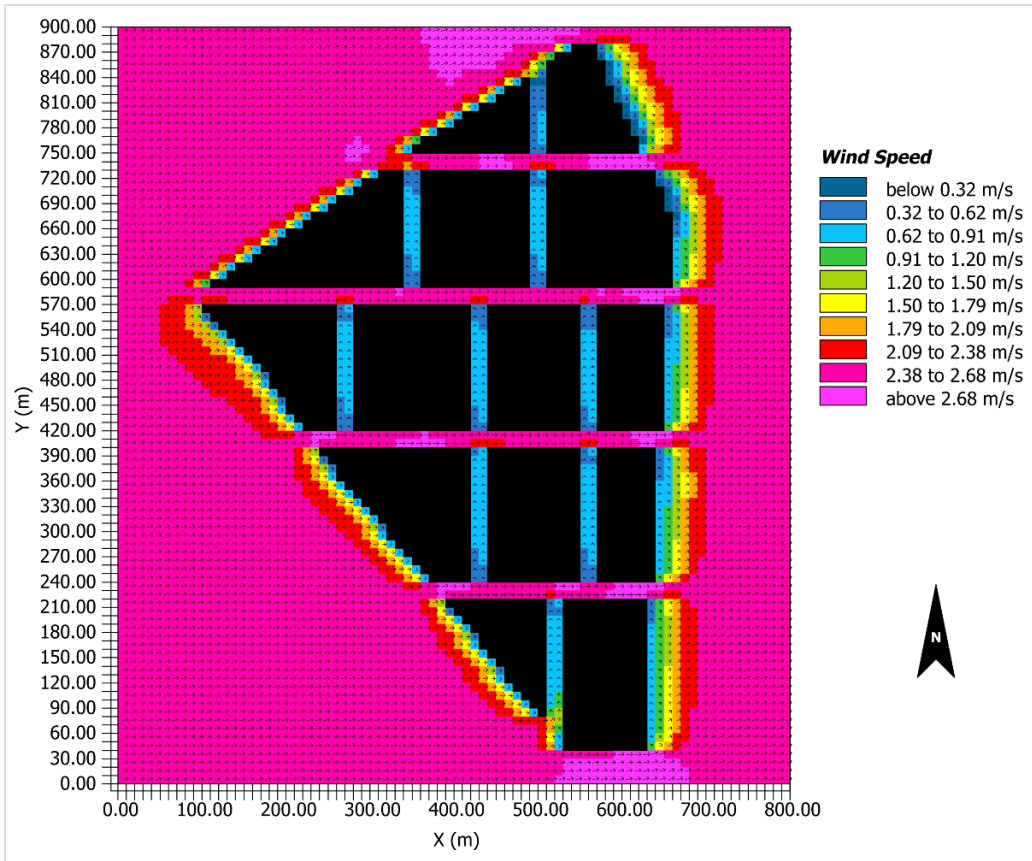


Figure A6. 4. Wind speed values for wind direction 105° at 11:00 am.

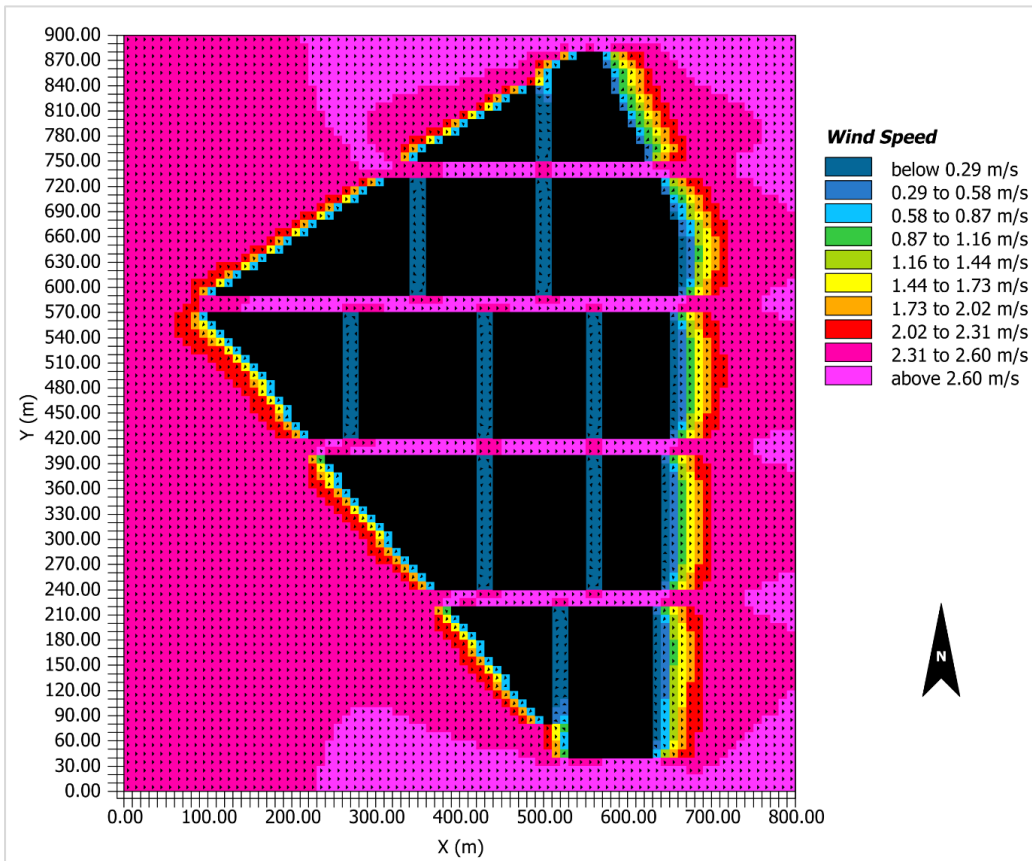


Figure A6. 5. Wind speed values for wind direction 90° at 11:00 am.

Sample of appendices for chapter 6 – section 3.

Geometrical modification - buildings pathways

Full gap Scenario wind speed maps.

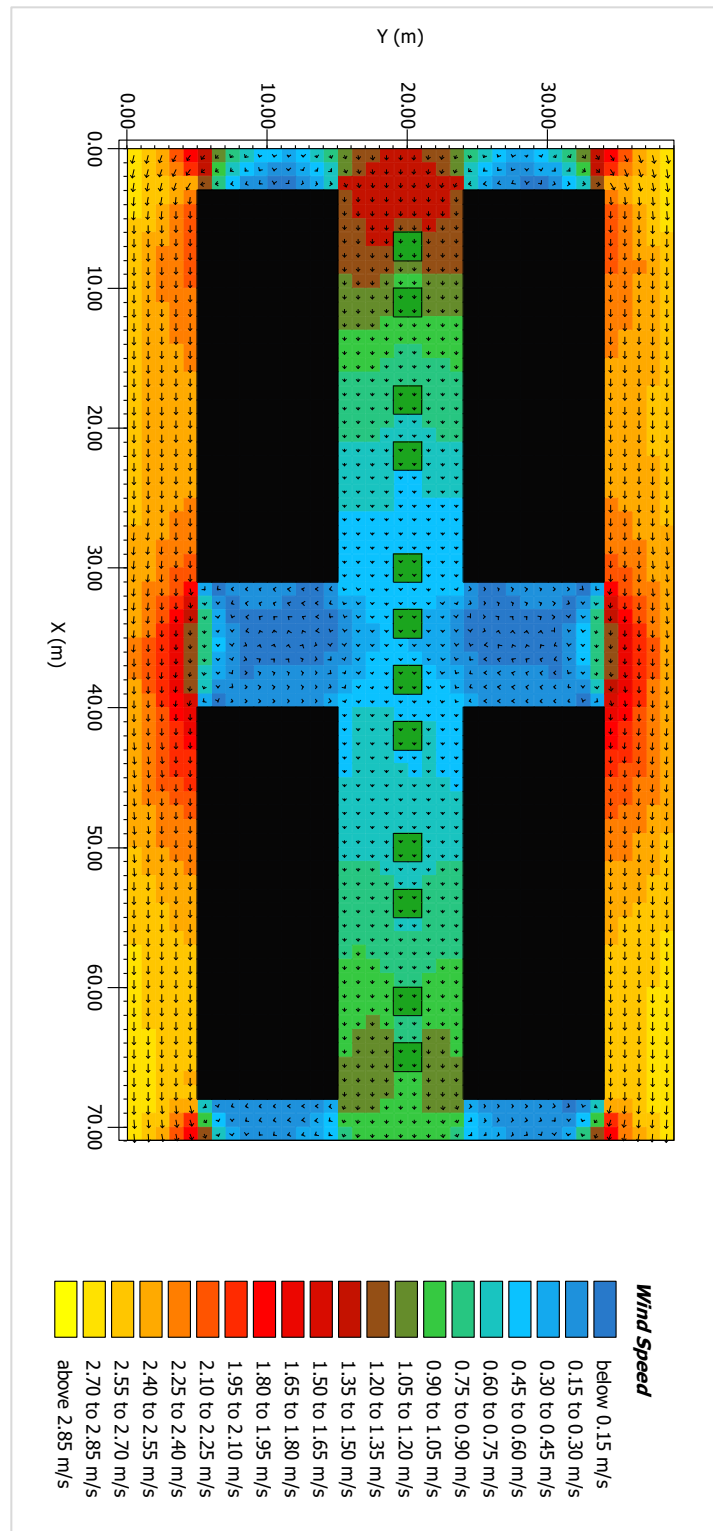


Figure A6. 6. Wind speed values for full gap scenario- At 11:00 am plan section.

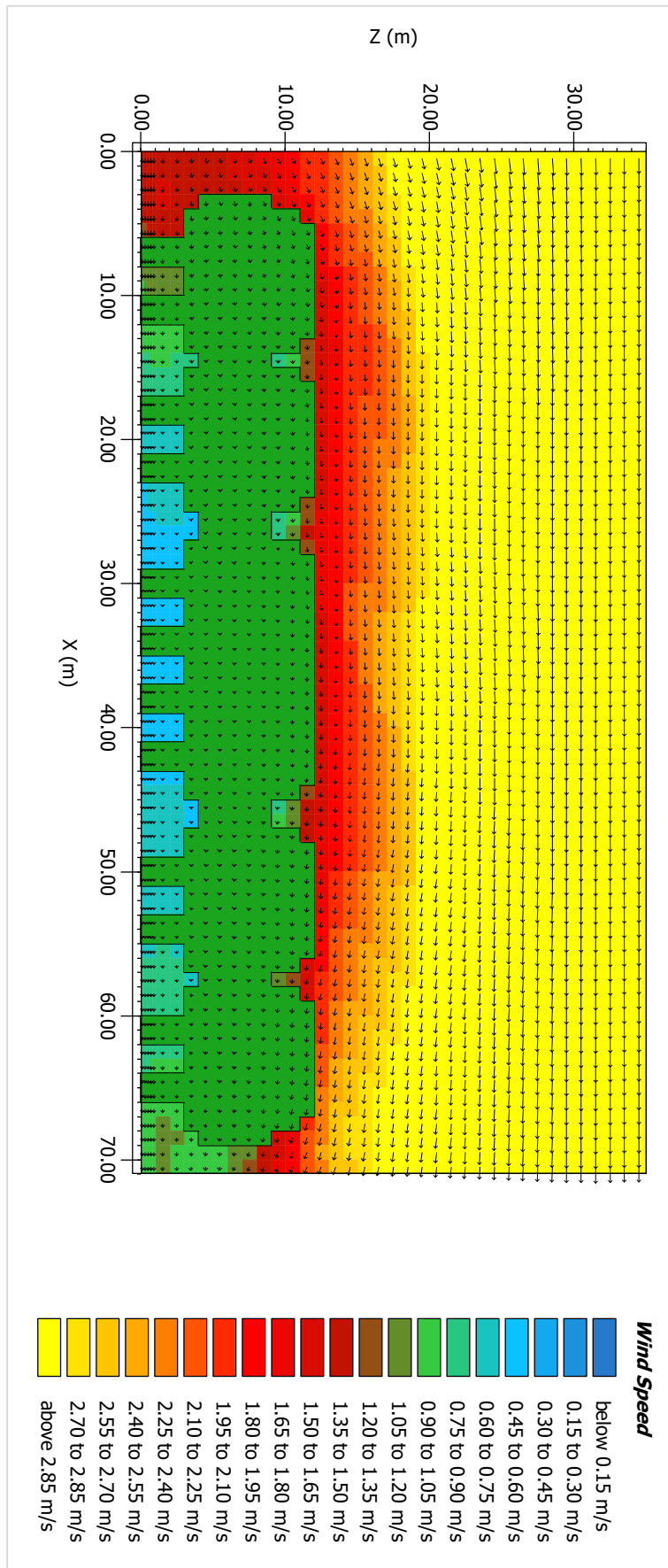


Figure A6. 7. Wind speed values for full gap scenario- At 11:00 am A-A section.

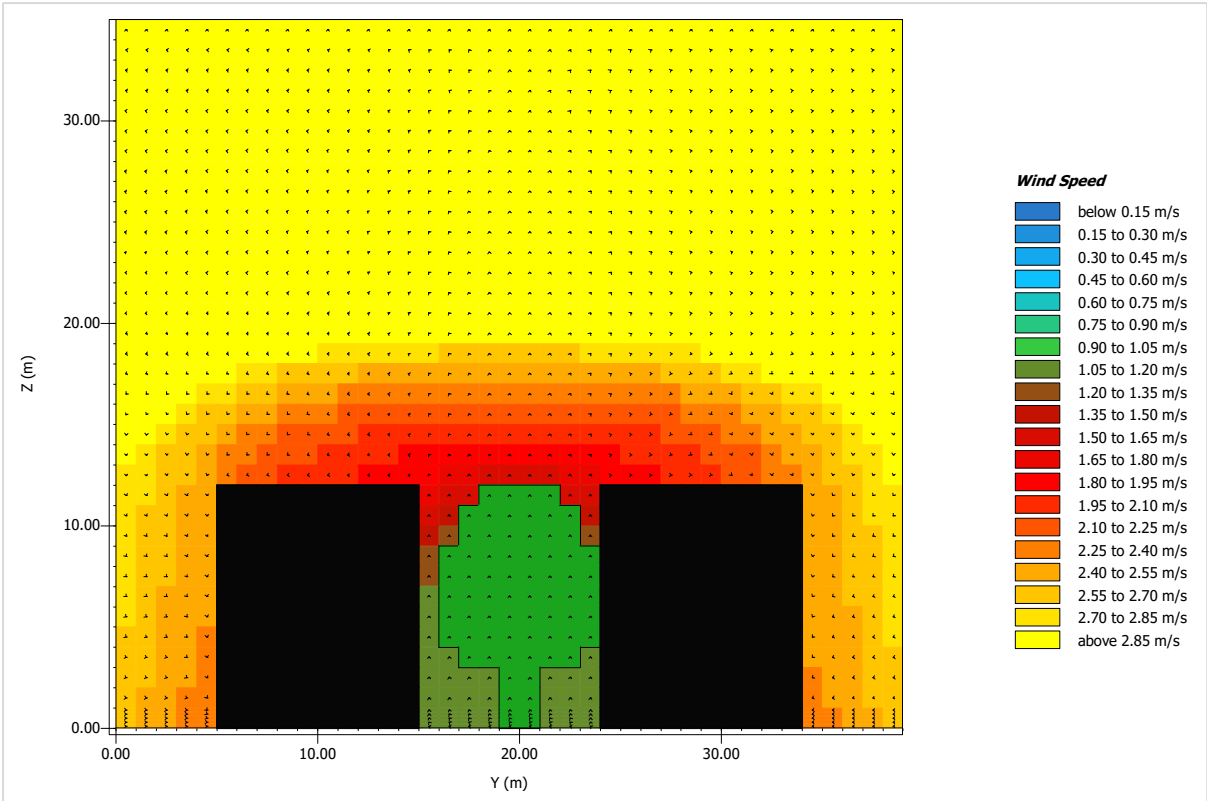


Figure A6. 8. Wind speed values for full gap scenario- At 11:00 am B-B section.

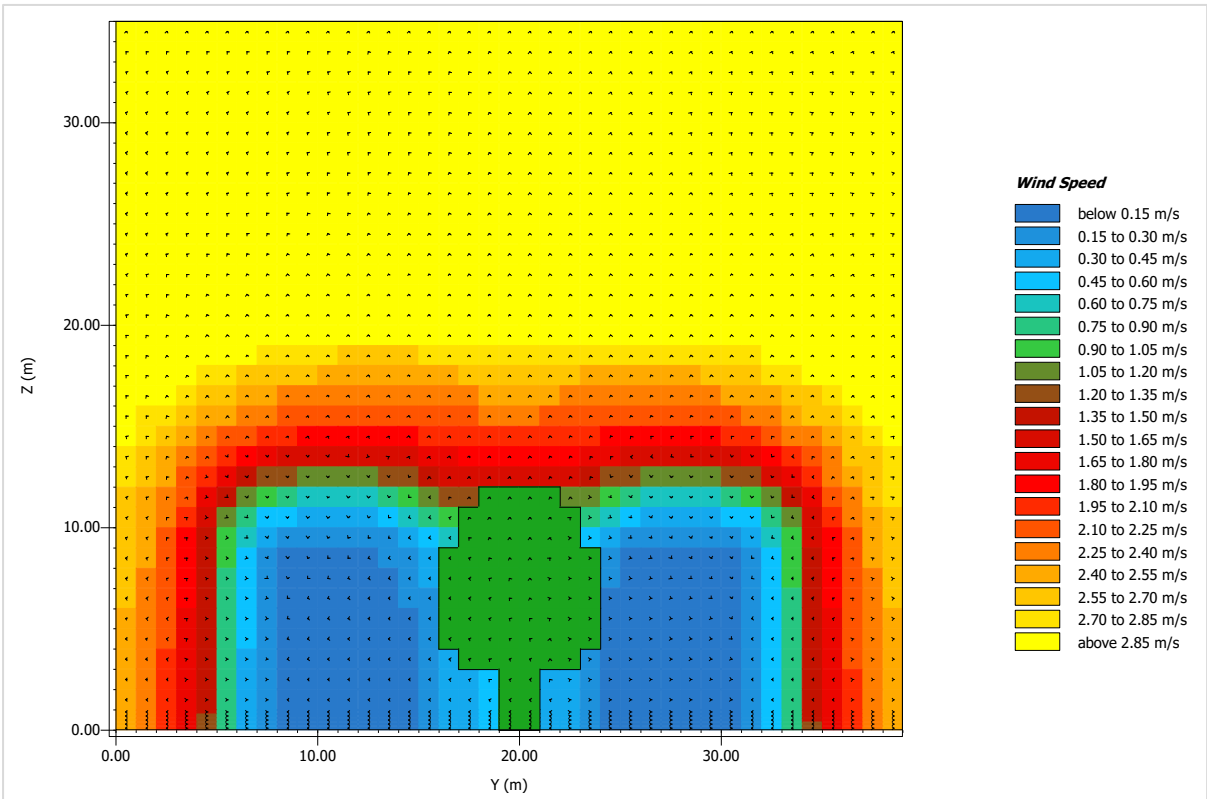


Figure A6. 9. Wind speed values for full gap scenario- At 11:00 am C-C section.

Half gap Scenario wind speed maps.

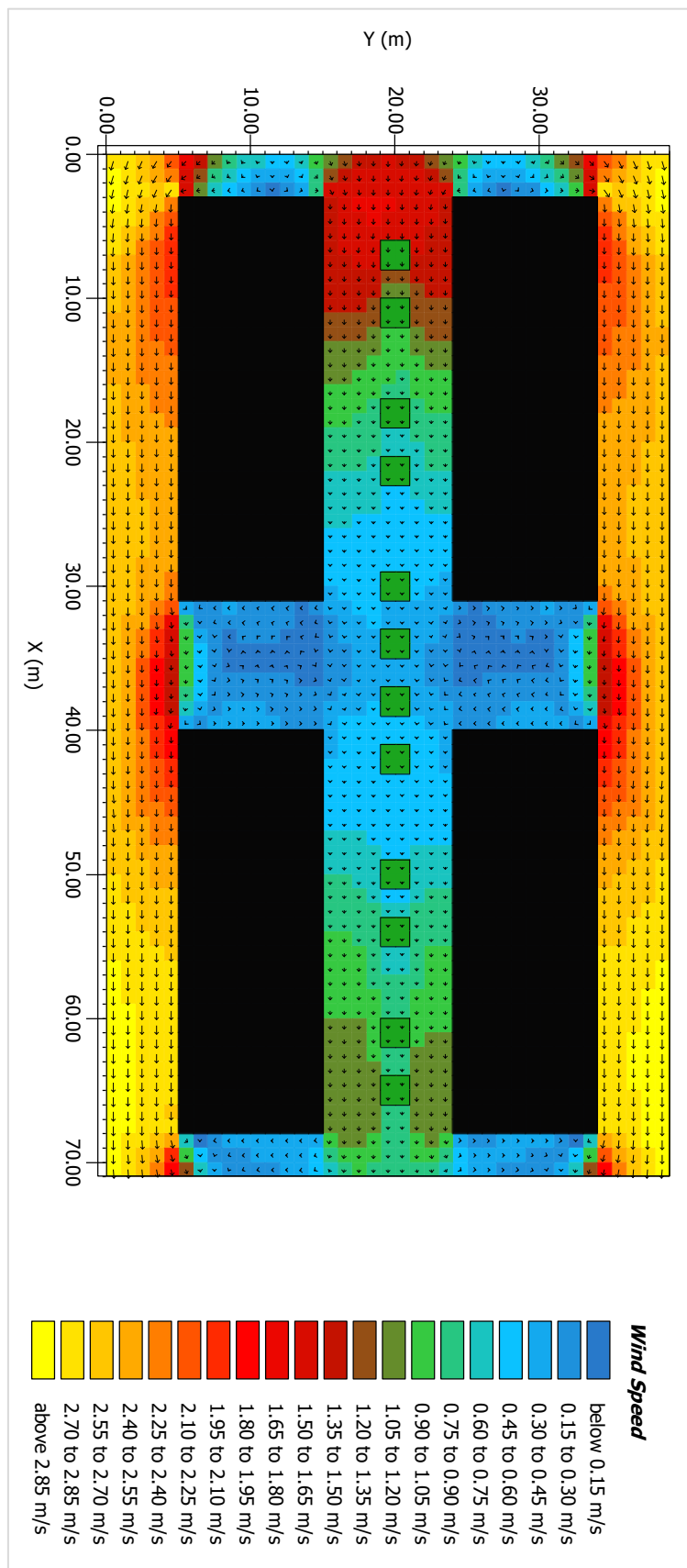


Figure A6. 10. Wind speed values for half gap scenario- At 11:00 am plan section.

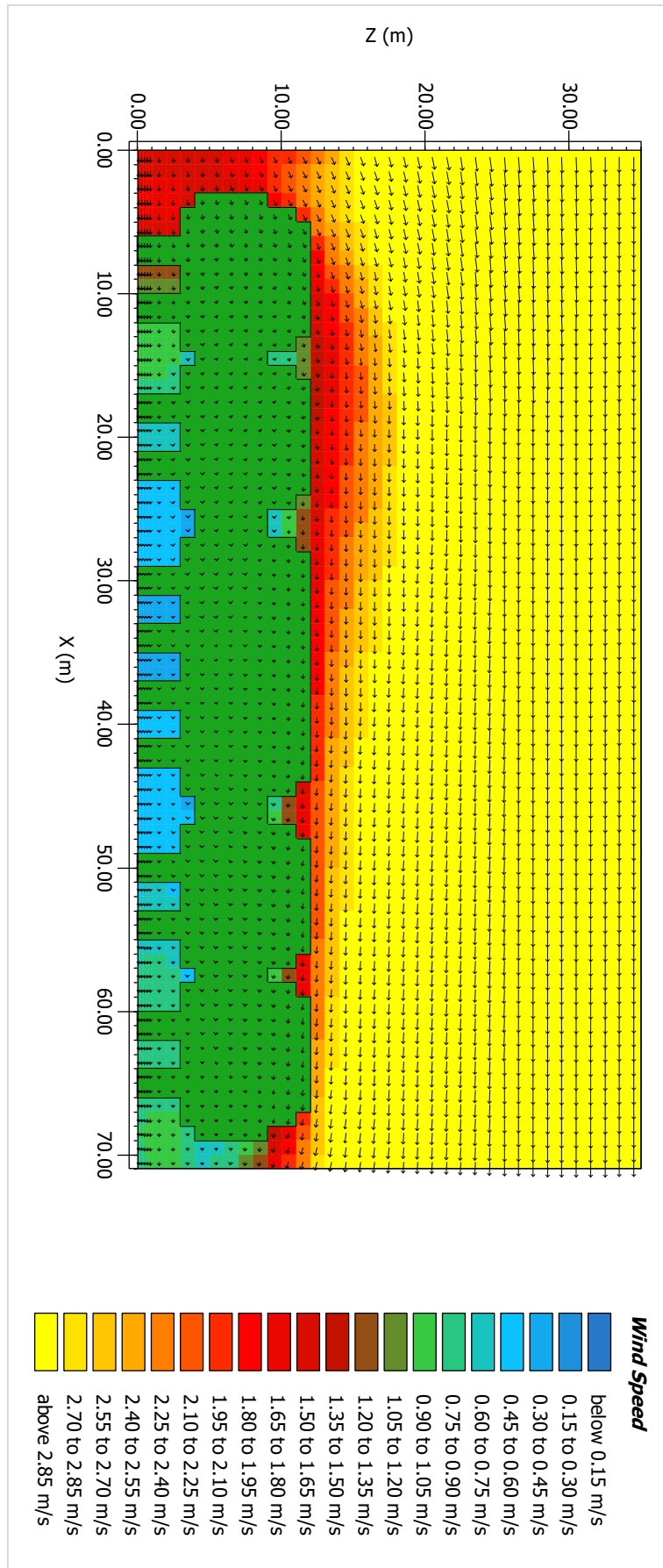


Figure A6. 11. Wind speed values for half gap scenario- At 11:00 am A-A section.

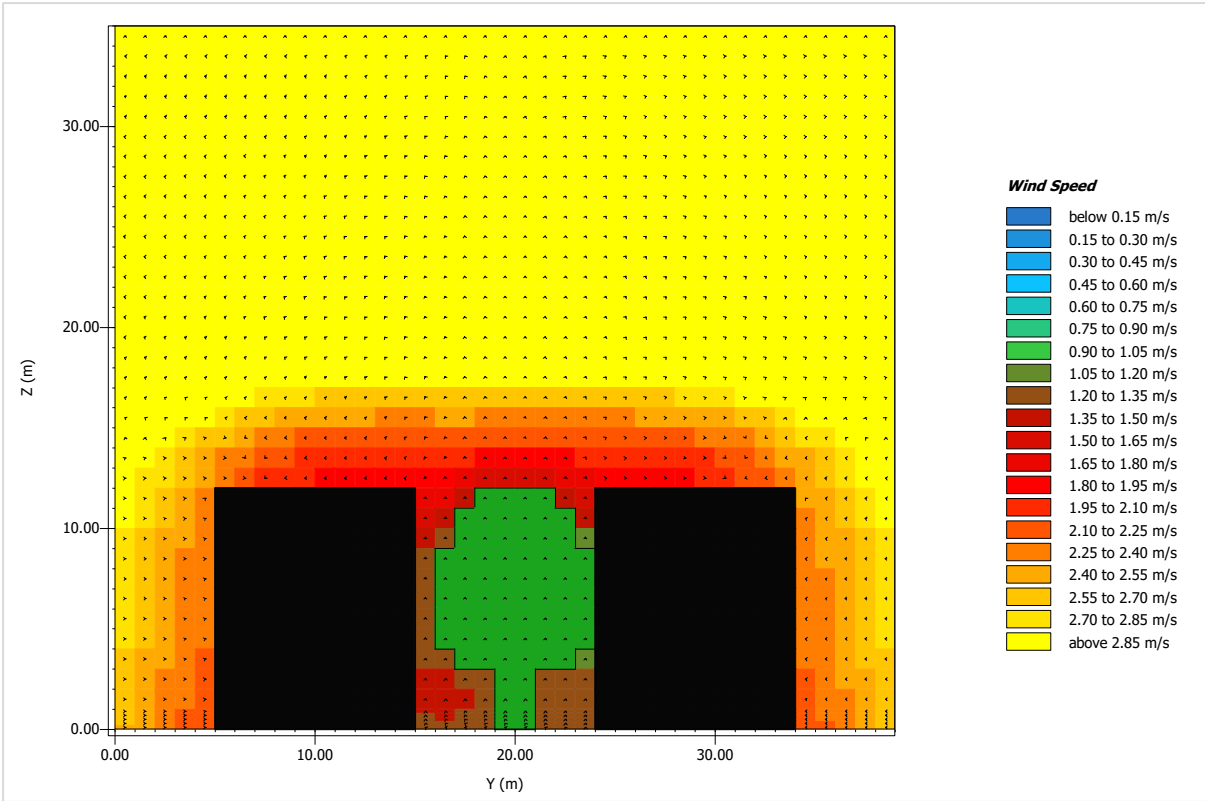


Figure A6. 12. Wind speed values for half gap scenario- At 11:00 am B-B section.

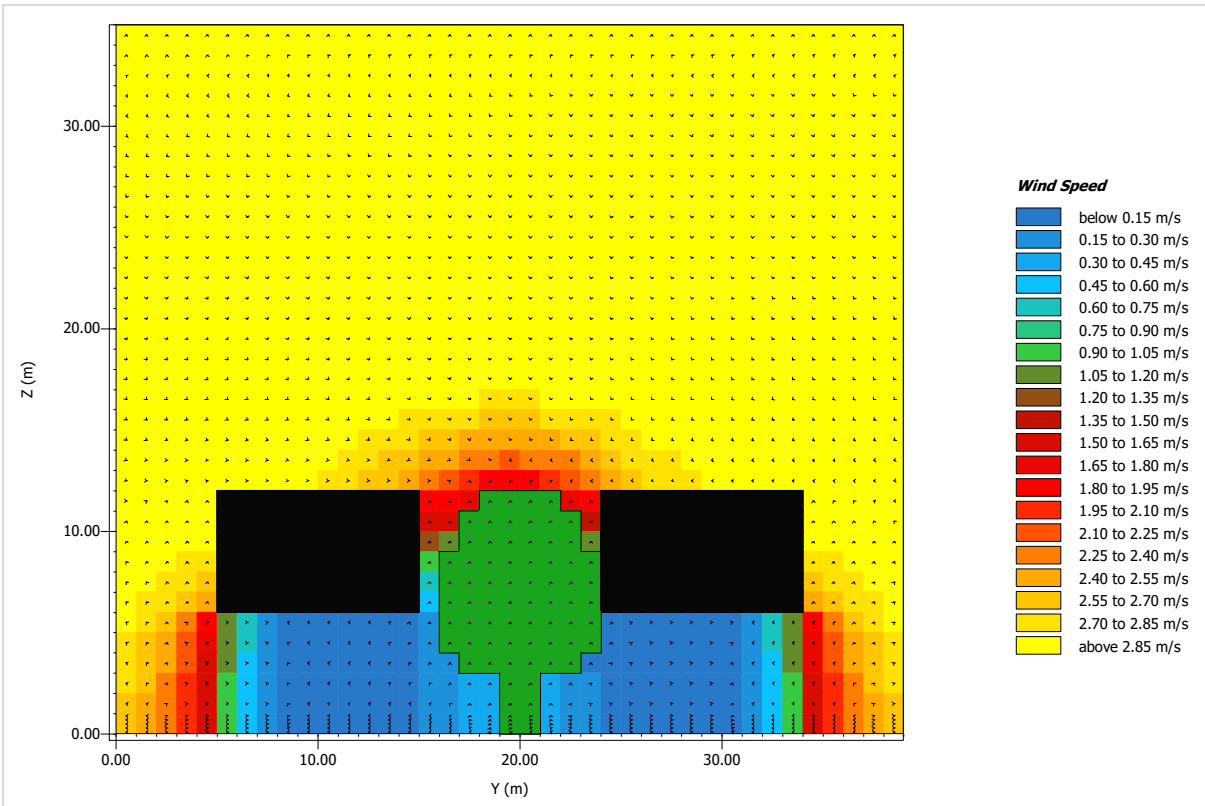


Figure A6. 13. Wind speed values for half gap scenario- At 11:00 am C-C section.

Buildings' height modifications.

12-meters buildings' height scenario- wind speed maps.

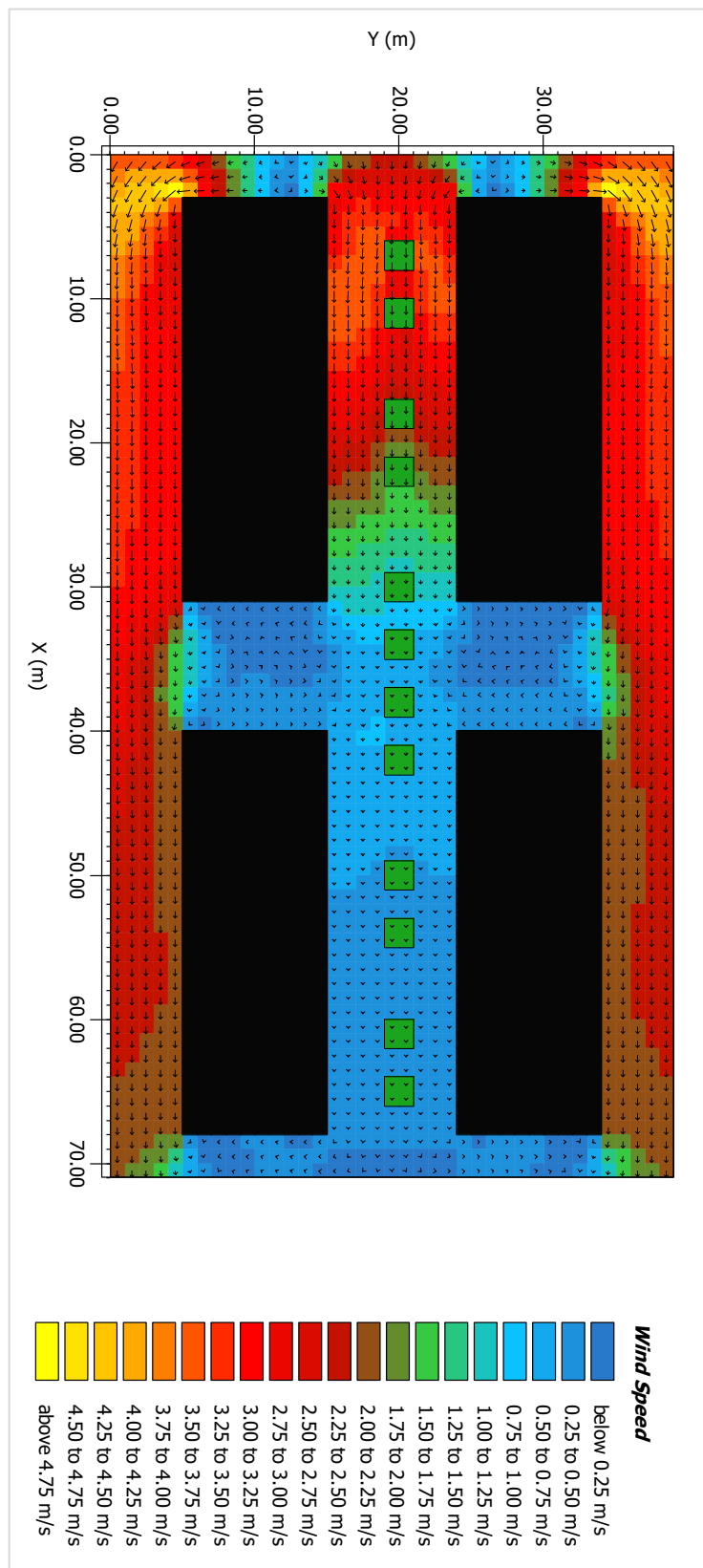


Figure A6. 14. Wind speed values for 12-meters buildings' height scenario- At 11:00 am plan section.

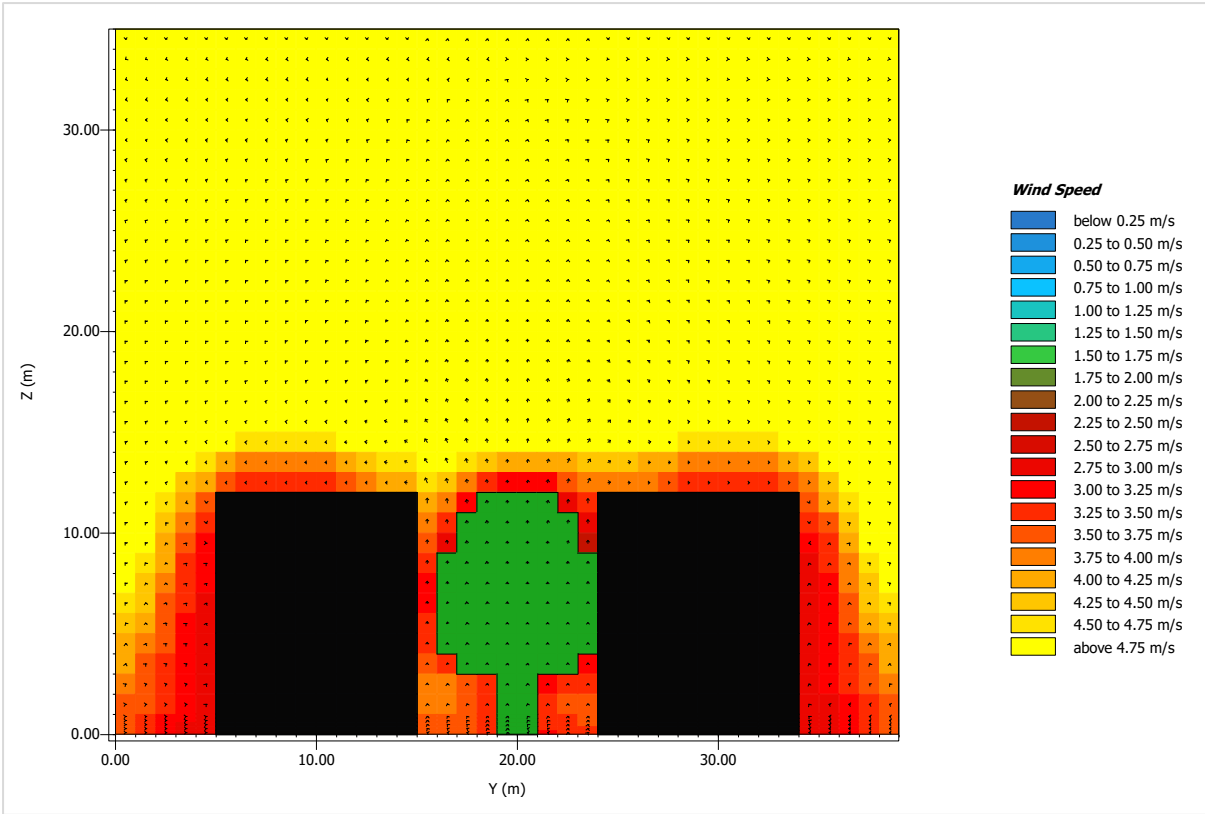


Figure A6. 15. Wind speed values for 12-meters buildings' height scenario- At 11:00 am B-B section.

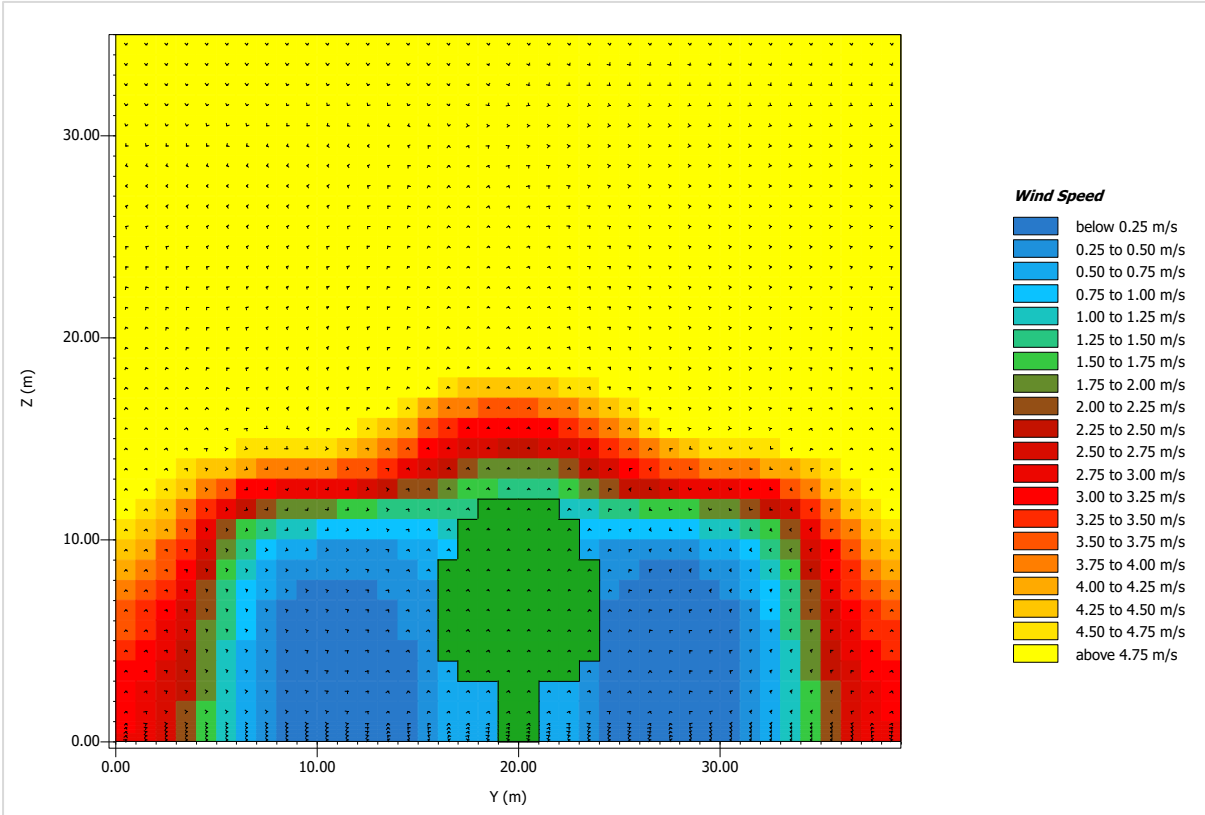


Figure A6. 16. Wind speed values for 12-meters buildings' height scenario- At 11:00 am C-C section.

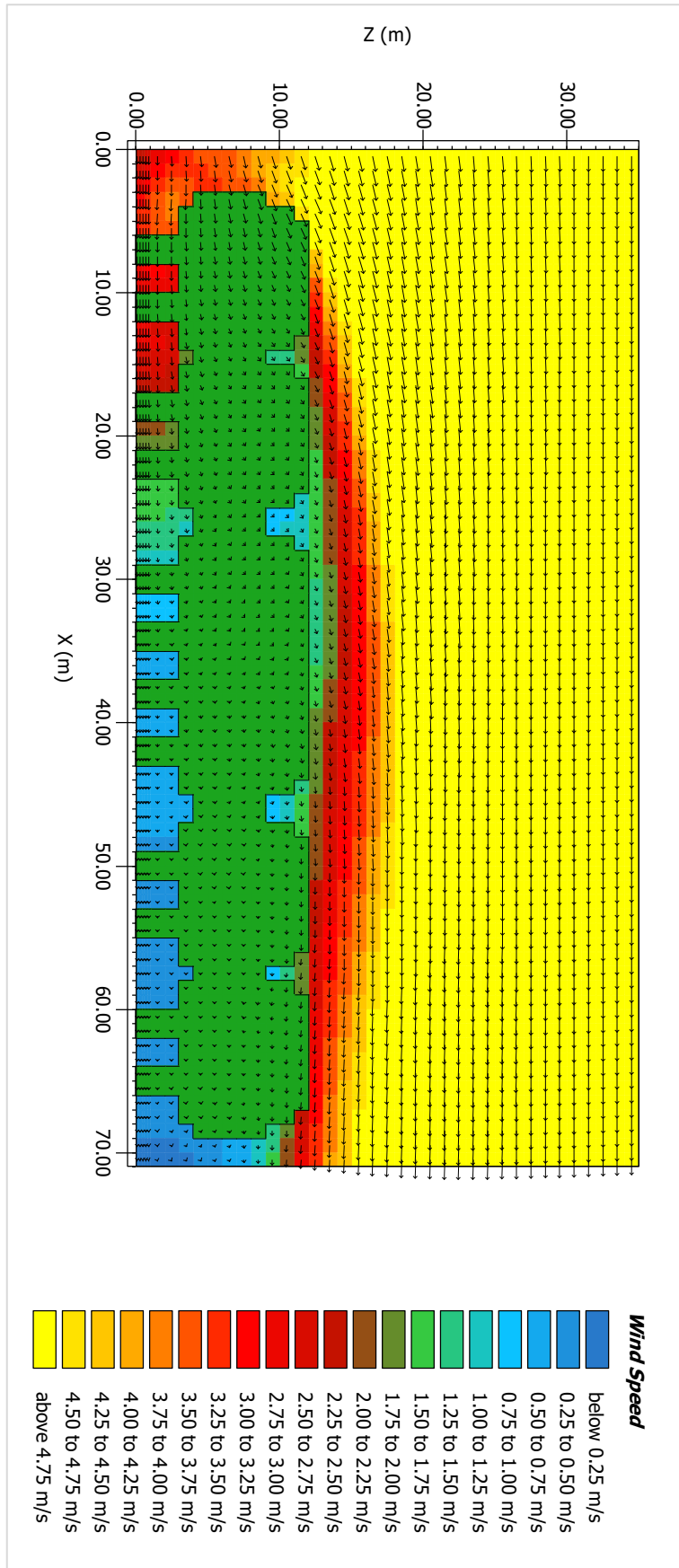


Figure A6. 17. Wind speed values for 12-meters buildings' height scenario- At 11:00 am A-A section.

18-meters buildings' height scenario- wind speed maps.

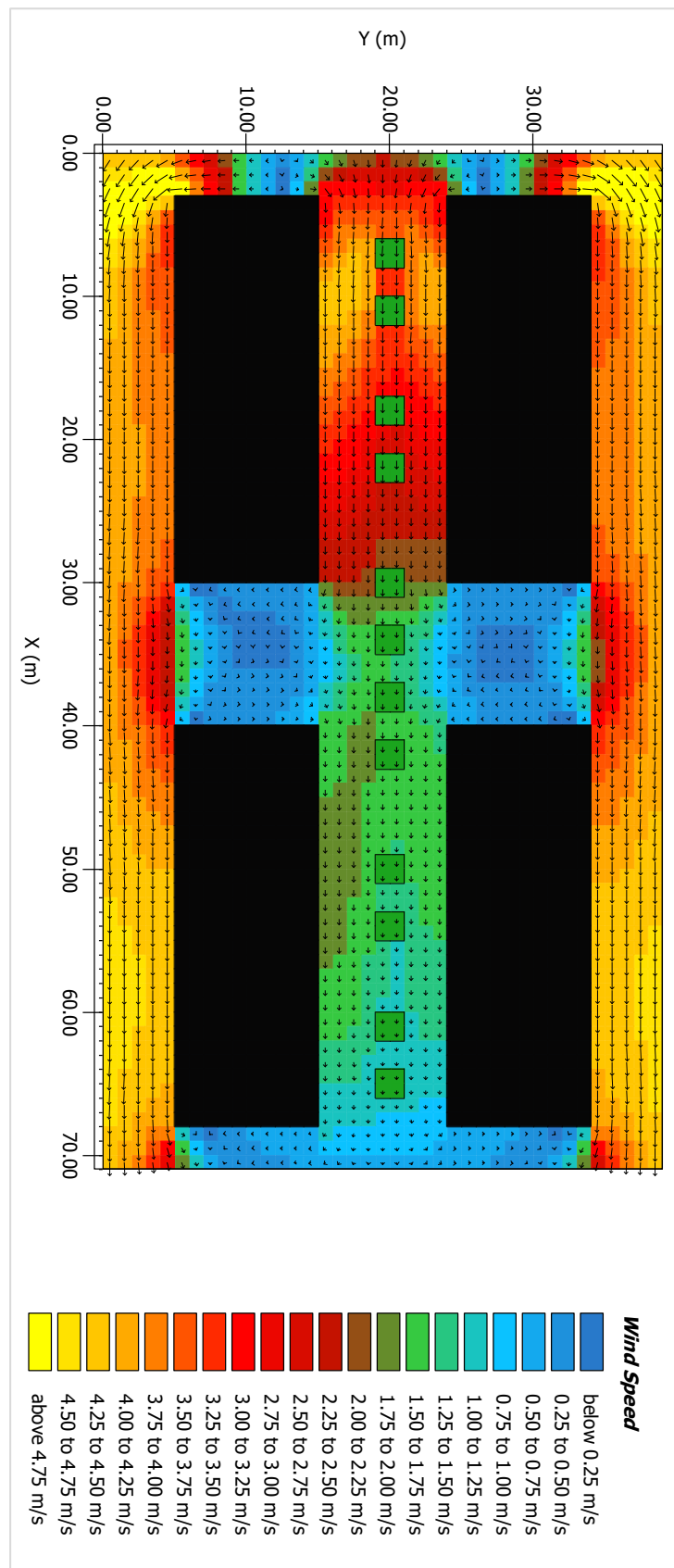


Figure A6. 18. Wind speed values for 18-meters buildings' height scenario- At 11:00 am plan section.

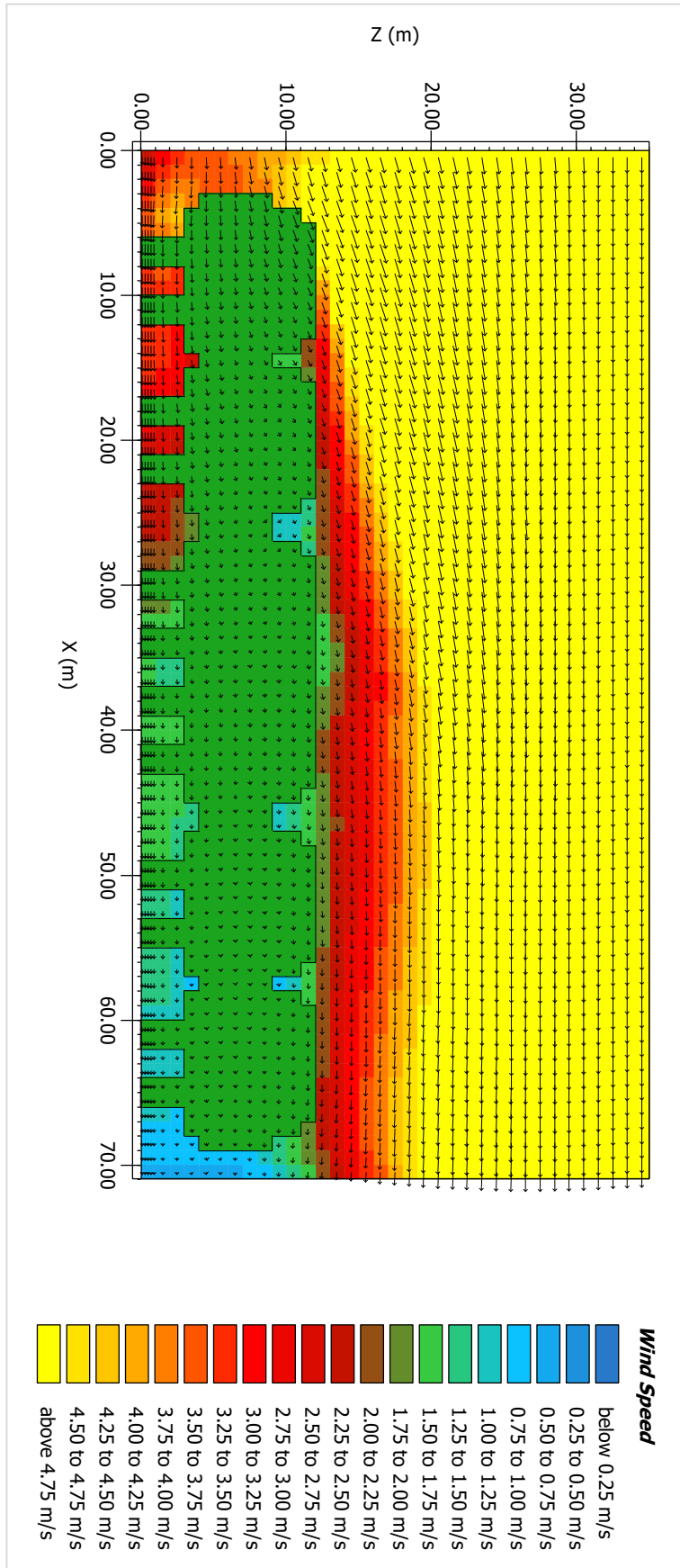


Figure A6. 19. Wind speed values for 18-meters buildings' height scenario- At 11:00 am A-A section.

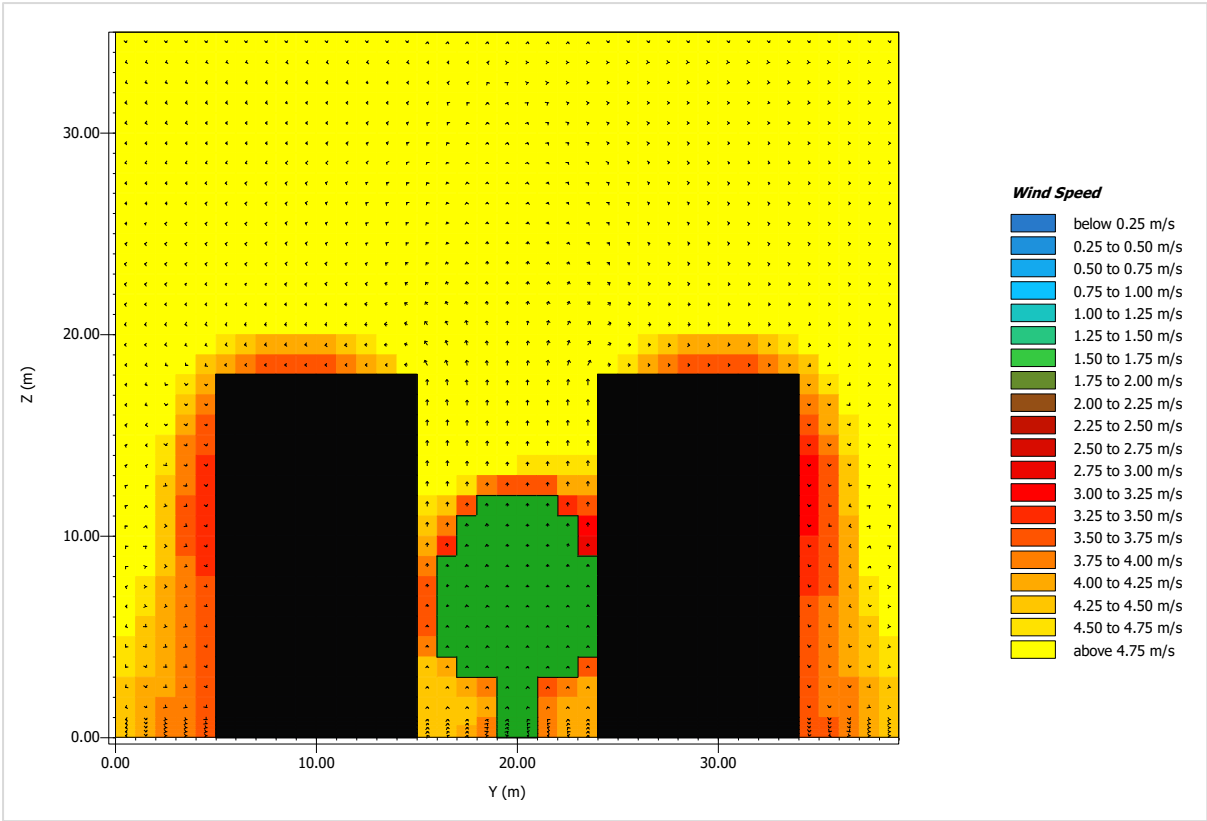


Figure A6. 20. Wind speed values for 18-meters buildings' height scenario- At 11:00 am B-B section.

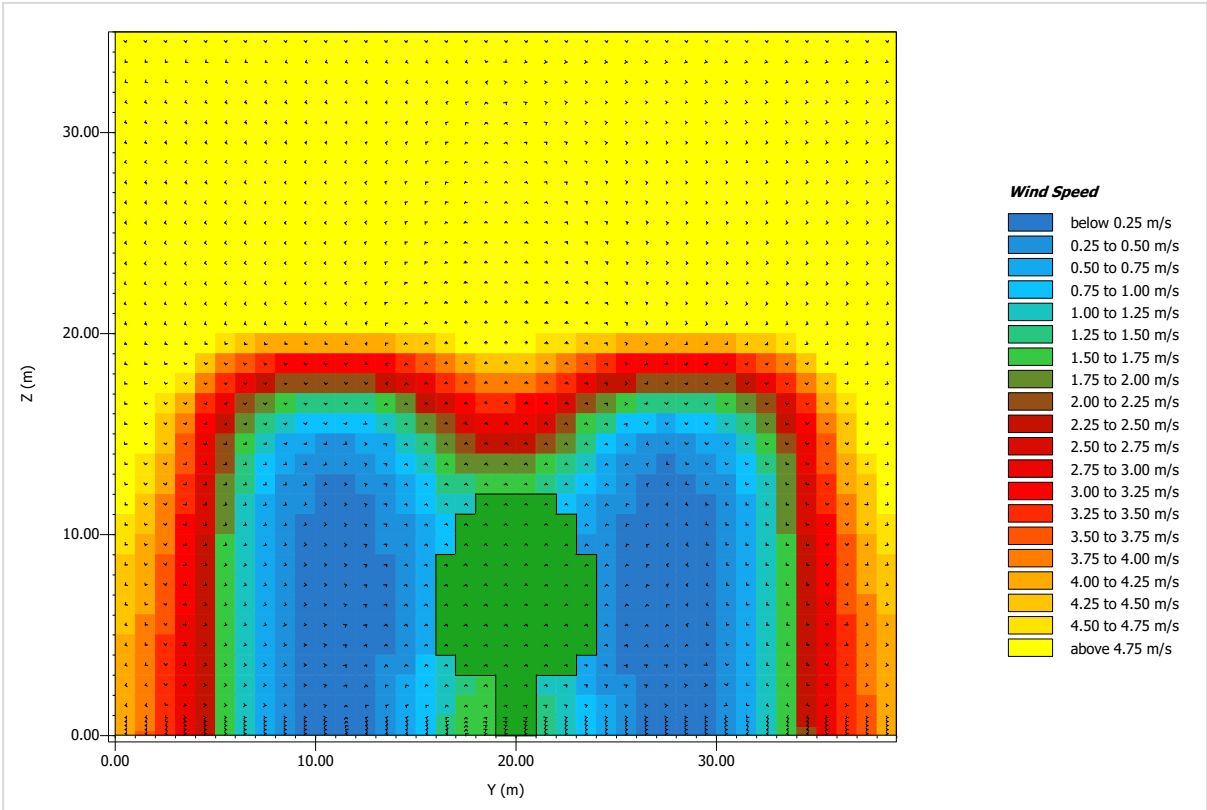


Figure A6. 21. Wind speed values for 18-meters buildings' height scenario- At 11:00 am C-C section.

18-meters buildings' height scenario- wind speed maps.

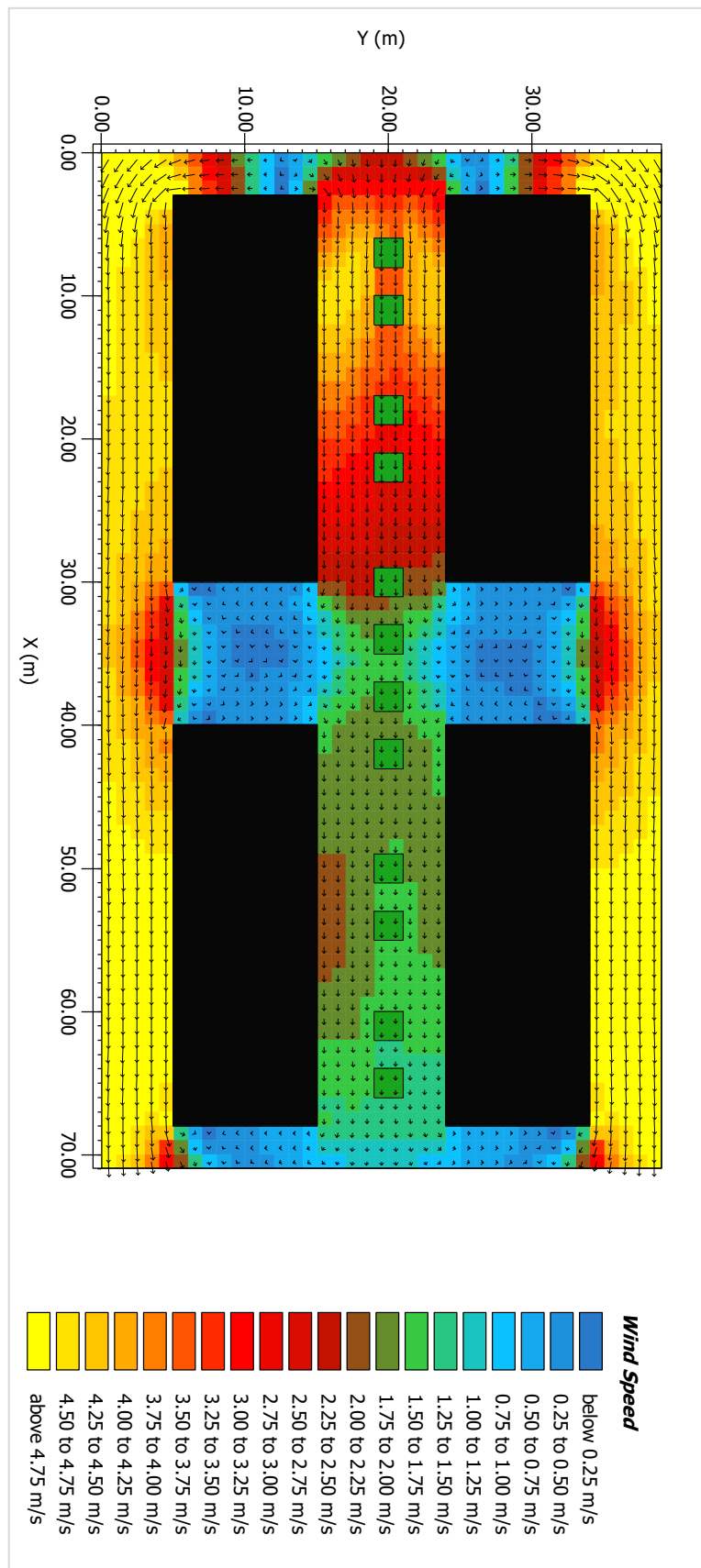


Figure A6. 22. Wind speed values for 24-meters buildings' height scenario- At 11:00 am plan section.

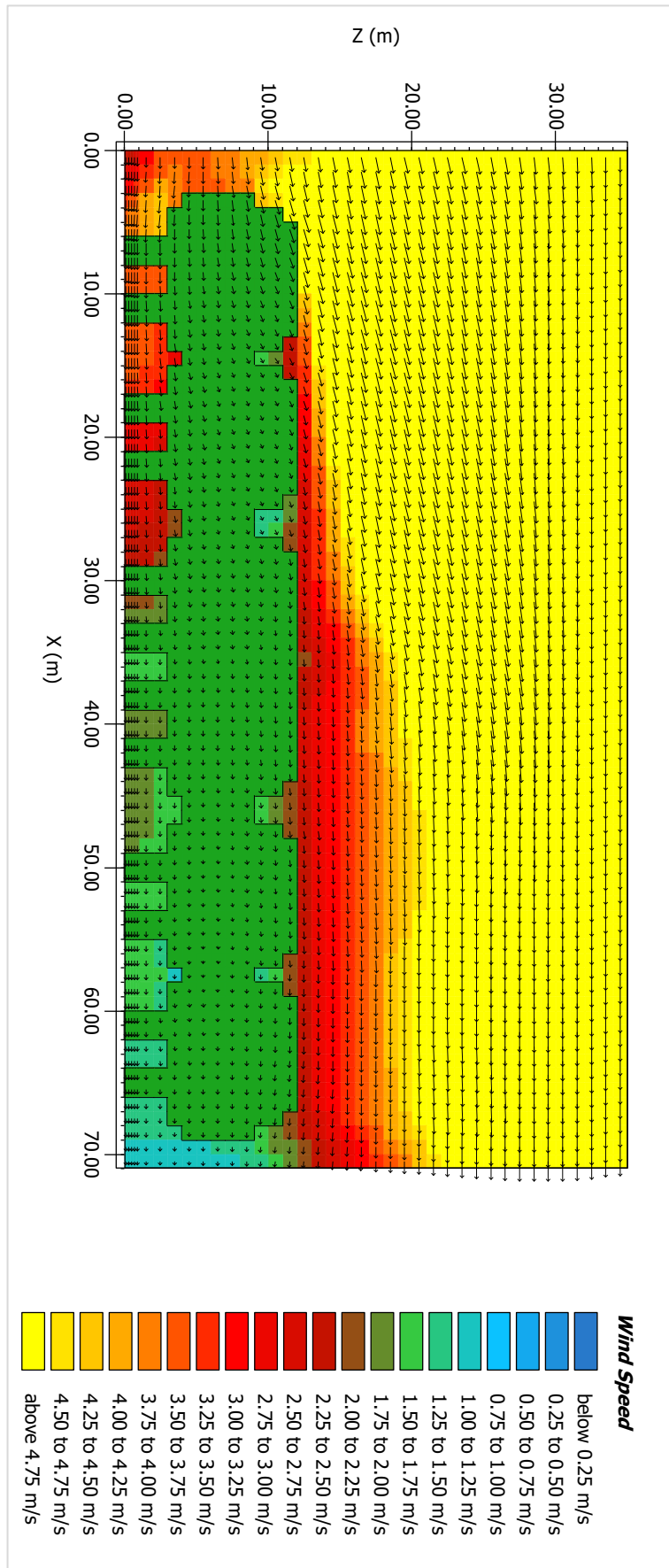


Figure A6. 23. Wind speed values for 24-meters buildings' height scenario- At 11:00 am A-A section.

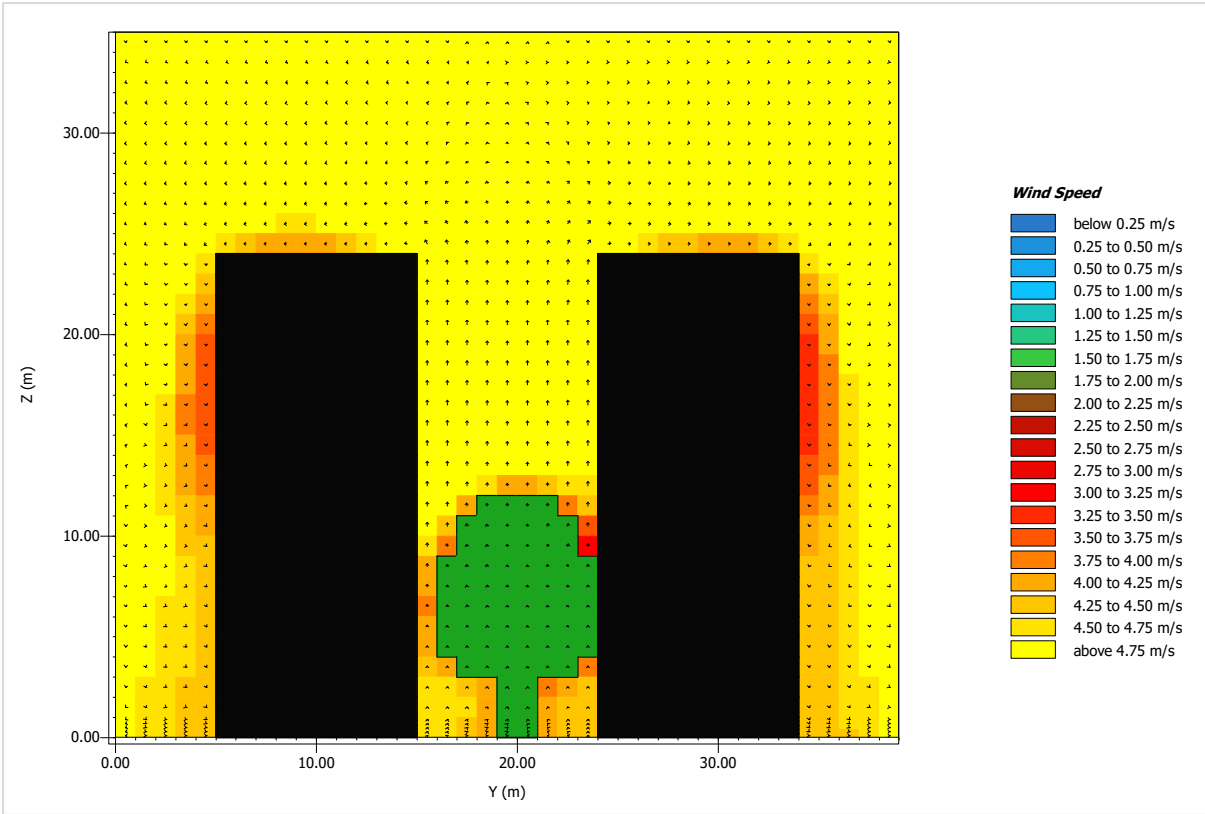


Figure A6. 24. Wind speed values for 24-meters buildings' height scenario- At 11:00 am B-B section.

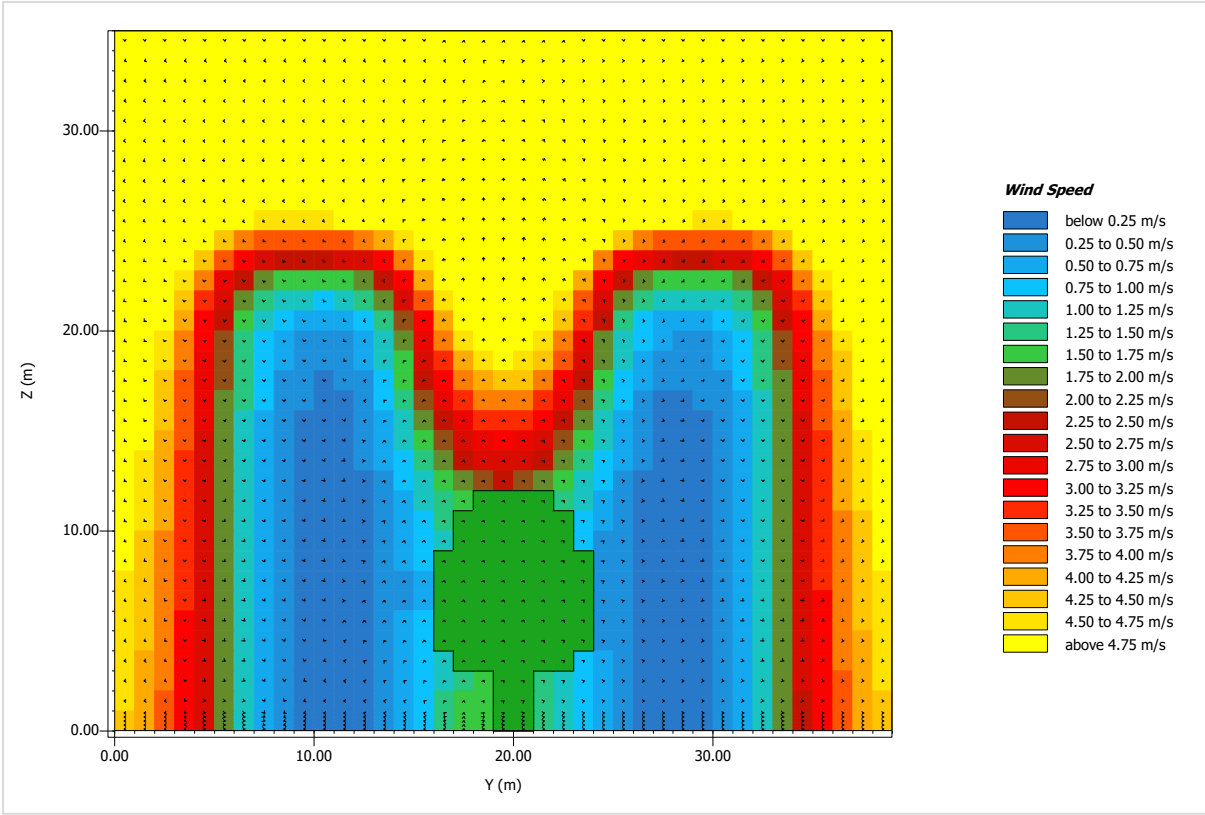


Figure A6. 25. Wind speed values for 24-meters buildings' height scenario- At 11:00 am C-C section.

Trees Leaf Area Density (LAD) modifications.

0.5 LAD scenario.

Table A6. 7. Detailed microclimatic data for 0.5 LAD scenario.

Date	Time	Wind Speed (m/s)	Air Temperature (°C)	Relative Humidity (%)	Mean Radiant Temp. (°C)	PET (°C)
		Receptor 1				
21.06.2018	06:00	1.3446	20.252	85.171	19.28	17
21.06.2018	07:00	1.383	20.699	84.66	24.883	18.8
21.06.2018	08:00	1.4157	22.146	84.216	30.083	21.9
21.06.2018	09:00	1.4443	23.575	82.264	34.843	25.1
21.06.2018	10:00	1.4775	24.551	77.225	38.357	27.3
21.06.2018	11:00	1.5289	25.502	69.627	40.26	28.8
21.06.2018	12:00	1.5953	26.604	60.697	40.045	29.4
21.06.2018	13:00	1.6628	27.689	52.243	66.185	41.6
21.06.2018	14:00	1.7254	27.78	48.55	62.636	39.9
21.06.2018	15:00	1.7802	26.53	50.378	51.097	33.4
21.06.2018	16:00	1.8195	24.181	56.876	19.04	19.4
21.06.2018	17:00	1.833	23.267	59.925	17.874	18.4
21.06.2018	18:00	1.8254	22.66	62.306	17.232	17.7
21.06.2018	19:00	1.8109	22.187	64.174	16.752	17.2
21.06.2018	20:00	1.7967	21.798	65.63	16.363	16.8
21.06.2018	21:00	1.7838	21.471	66.741	16.031	16.5
21.06.2018	22:00	1.7724	21.2	67.538	15.745	16.1
21.06.2018	23:00	1.7625	20.966	68.125	15.489	15.9
22.06.2018	00:00	1.7541	20.765	68.531	15.26	15.7
22.06.2018	01:00	1.7473	20.591	68.791	15.052	15.6
22.06.2018	02:00	1.7419	20.438	68.932	14.86	15.3
22.06.2018	03:00	1.7379	20.305	68.979	14.682	15.2
22.06.2018	04:00	1.7352	20.192	68.936	14.524	15.1
22.06.2018	05:00	1.7339	20.108	68.766	14.408	15
Date	Time	Wind Speed (m/s)	Air Temperature (°C)	Relative Humidity (%)	Mean Radiant Temp. (°C)	PET (°C)
		Receptor 2				
21.06.2018	06:00	0.96894	20.307	84.767	19.9	17.6
21.06.2018	07:00	0.97455	20.793	84.06	25.653	19.9
21.06.2018	08:00	0.97758	22.224	83.68	30.992	23.3
21.06.2018	09:00	0.97865	23.651	81.734	35.797	26.6

21.06.2018	10:00	0.98609	24.601	76.721	39.249	28.8
21.06.2018	11:00	1.0117	25.492	69.444	41.155	30.3
21.06.2018	12:00	1.0531	26.535	60.823	41.056	30.8
21.06.2018	13:00	1.0985	27.548	52.677	38.997	30.7
21.06.2018	14:00	1.1429	27.683	48.912	34.789	29
21.06.2018	15:00	1.1843	26.556	50.406	28.489	25.4
21.06.2018	16:00	1.2167	24.293	56.477	19.874	20.2
21.06.2018	17:00	1.2314	23.365	59.532	18.638	19.1
21.06.2018	18:00	1.2314	22.759	61.883	17.979	18.5
21.06.2018	19:00	1.2283	22.291	63.706	17.492	18
21.06.2018	20:00	1.2276	21.908	65.111	17.098	17.5
21.06.2018	21:00	1.2299	21.589	66.169	16.763	17.2
21.06.2018	22:00	1.2351	21.325	66.913	16.475	16.9
21.06.2018	23:00	1.243	21.098	67.45	16.218	16.7
22.06.2018	00:00	1.2534	20.905	67.804	15.987	16.3
22.06.2018	01:00	1.266	20.737	68.019	15.776	16.1
22.06.2018	02:00	1.2807	20.592	68.114	15.583	16
22.06.2018	03:00	1.2971	20.464	68.123	15.403	15.9
22.06.2018	04:00	1.3149	20.357	68.046	15.242	15.7
22.06.2018	05:00	1.3292	20.278	67.842	15.124	15.6
Date	Time	Wind Speed (m/s)	Air Temperature (°C)	Relative Humidity (%)	Mean Radiant Temp. (°C)	PET (°C)
		Receptor 3				
21.06.2018	06:00	0.76188	20.35	84.497	19.927	18
21.06.2018	07:00	0.75502	20.895	83.573	25.704	20.5
21.06.2018	08:00	0.74383	22.333	83.137	31.058	24.3
21.06.2018	09:00	0.72812	23.754	81.264	35.87	27.6
21.06.2018	10:00	0.71595	24.701	76.287	39.319	29.8
21.06.2018	11:00	0.71784	25.572	69.186	41.227	31.3
21.06.2018	12:00	0.73215	26.579	60.808	41.136	32
21.06.2018	13:00	0.74867	27.54	52.896	39.078	31.6
21.06.2018	14:00	0.76342	27.663	49.166	34.862	29.6
21.06.2018	15:00	0.77547	26.572	50.514	28.543	26
21.06.2018	16:00	0.7809	24.39	56.168	19.891	20.8
21.06.2018	17:00	0.77209	23.45	59.219	18.649	19.6
21.06.2018	18:00	0.75118	22.841	61.559	17.989	18.9
21.06.2018	19:00	0.72791	22.374	63.364	17.501	18.6
21.06.2018	20:00	0.70742	21.993	64.746	17.107	18.2
21.06.2018	21:00	0.69069	21.676	65.78	16.772	17.9

21.06.2018	22:00	0.67787	21.415	66.502	16.483	17.6
21.06.2018	23:00	0.66901	21.191	67.019	16.225	17.3
22.06.2018	00:00	0.66409	21	67.353	15.994	17.1
22.06.2018	01:00	0.66303	20.833	67.553	15.784	16.9
22.06.2018	02:00	0.66569	20.69	67.633	15.59	16.8
22.06.2018	03:00	0.67191	20.563	67.63	15.41	16.6
22.06.2018	04:00	0.68147	20.456	67.544	15.248	16.5
22.06.2018	05:00	0.69072	20.378	67.331	15.13	16.4
Date	Time	Wind Speed (m/s)	Air Temperature (°C)	Relative Humidity (%)	Mean Radiant Temp. (°C)	PET (°C)
		Receptor 4				
21.06.2018	06:00	0.62559	20.6	82.681	19.853	18.6
21.06.2018	07:00	0.60969	21.185	81.678	25.452	21.3
21.06.2018	08:00	0.59121	22.566	81.06	30.643	24.6
21.06.2018	09:00	0.56933	24.083	78.449	35.392	27.9
21.06.2018	10:00	0.5482	25.365	71.903	62.817	43.6
21.06.2018	11:00	0.53563	26.248	65.2	64.562	45.1
21.06.2018	12:00	0.53158	26.85	59.004	40.503	32.6
21.06.2018	13:00	0.52922	27.529	52.635	38.376	31.9
21.06.2018	14:00	0.52562	27.546	49.543	34.198	29.8
21.06.2018	15:00	0.5209	26.53	50.718	27.971	26.3
21.06.2018	16:00	0.51334	24.518	55.7	19.557	21.3
21.06.2018	17:00	0.49798	23.597	58.607	18.401	20.1
21.06.2018	18:00	0.47477	23.002	60.834	17.761	19.5
21.06.2018	19:00	0.44879	22.55	62.521	17.284	19.2
21.06.2018	20:00	0.42324	22.184	63.79	16.895	18.8
21.06.2018	21:00	0.39902	21.881	64.723	16.565	18.5
21.06.2018	22:00	0.37651	21.632	65.357	16.281	18.2
21.06.2018	23:00	0.35598	21.418	65.795	16.027	18
22.06.2018	00:00	0.33761	21.235	66.068	15.801	18
22.06.2018	01:00	0.32154	21.074	66.224	15.596	17.9
22.06.2018	02:00	0.30783	20.933	66.28	15.407	17.6
22.06.2018	03:00	0.29655	20.806	66.273	15.232	17.5
22.06.2018	04:00	0.2877	20.696	66.2	15.076	17.4
22.06.2018	05:00	0.28265	20.611	66.024	14.963	17.3
Date	Time	Wind Speed (m/s)	Air Temperature (°C)	Relative Humidity (%)	Mean Radiant Temp. (°C)	PET (°C)
		Receptor 5				

21.06.2018	06:00	0.84757	20.789	81.249	19.931	18.3
21.06.2018	07:00	0.81561	21.393	80.156	25.709	20.9
21.06.2018	08:00	0.78186	22.689	79.509	31.063	24.2
21.06.2018	09:00	0.74593	24.039	77.392	35.875	27.7
21.06.2018	10:00	0.71342	24.999	72.149	39.324	30
21.06.2018	11:00	0.69168	25.877	65.534	41.232	31.5
21.06.2018	12:00	0.68015	26.729	58.751	41.141	32
21.06.2018	13:00	0.67182	27.415	52.759	39.083	31.5
21.06.2018	14:00	0.66364	27.346	50.152	34.866	29.5
21.06.2018	15:00	0.65426	26.417	51.096	28.547	26
21.06.2018	16:00	0.64044	24.572	55.464	19.895	21.3
21.06.2018	17:00	0.6164	23.681	58.207	18.653	20.1
21.06.2018	18:00	0.58232	23.109	60.297	17.993	19.4
21.06.2018	19:00	0.54432	22.677	61.855	17.505	19.2
21.06.2018	20:00	0.50634	22.328	63.013	17.11	18.7
21.06.2018	21:00	0.46955	22.039	63.851	16.776	18.4
21.06.2018	22:00	0.43447	21.8	64.412	16.487	18.4
21.06.2018	23:00	0.40143	21.595	64.789	16.229	18.2
22.06.2018	00:00	0.37067	21.418	65.018	15.998	17.9
22.06.2018	01:00	0.34238	21.262	65.135	15.787	18.1
22.06.2018	02:00	0.31662	21.123	65.172	15.593	17.8
22.06.2018	03:00	0.29345	20.997	65.148	15.414	17.7
22.06.2018	04:00	0.27288	20.89	65.057	15.252	17.6
22.06.2018	05:00	0.25914	20.804	64.879	15.133	17.4
Date	Time	Wind Speed (m/s)	Air Temperature (°C)	Relative Humidity (%)	Mean Radiant Temp. (°C)	PET (°C)
		Receptor 6				
21.06.2018	06:00	1.0118	20.907	80.394	19.93	18
21.06.2018	07:00	0.97499	21.518	79.262	25.667	20.4
21.06.2018	08:00	0.93503	22.766	78.656	30.995	24
21.06.2018	09:00	0.89148	24.063	76.646	35.796	27.1
21.06.2018	10:00	0.84935	24.956	71.639	39.248	29.6
21.06.2018	11:00	0.81535	25.744	65.497	41.151	31
21.06.2018	12:00	0.79	26.537	59.147	41.043	31.5
21.06.2018	13:00	0.76803	27.196	53.455	38.983	31.1
21.06.2018	14:00	0.74676	27.212	50.733	34.779	29.4
21.06.2018	15:00	0.72525	26.366	51.404	28.492	26
21.06.2018	16:00	0.70118	24.626	55.285	19.912	21.1
21.06.2018	17:00	0.66964	23.743	57.956	18.679	19.9

21.06.2018	18:00	0.62974	23.177	59.993	18.022	19.5
21.06.2018	19:00	0.58588	22.753	61.497	17.535	19
21.06.2018	20:00	0.54153	22.411	62.605	17.141	18.8
21.06.2018	21:00	0.49803	22.128	63.399	16.807	18.5
21.06.2018	22:00	0.45607	21.894	63.921	16.519	18.3
21.06.2018	23:00	0.41612	21.693	64.266	16.262	18.3
22.06.2018	00:00	0.37853	21.52	64.463	16.032	18
22.06.2018	01:00	0.34351	21.367	64.555	15.822	18.1
22.06.2018	02:00	0.31121	21.229	64.571	15.628	17.9
22.06.2018	03:00	0.28166	21.106	64.522	15.449	17.8
22.06.2018	04:00	0.25489	21	64.411	15.288	17.6
22.06.2018	05:00	0.23661	20.914	64.221	15.171	17.9
Date	Time	Wind Speed (m/s)	Air Temperature (°C)	Relative Humidity (%)	Mean Radiant Temp. (°C)	PET (°C)
		Receptor 7				
21.06.2018	06:00	1.227	20.888	81.27	46.181	28
21.06.2018	07:00	1.1774	21.621	80.063	56.054	33.2
21.06.2018	08:00	1.1273	22.832	79.38	59.817	36.5
21.06.2018	09:00	1.0764	23.897	77.633	34.93	26.1
21.06.2018	10:00	1.0291	24.634	73.11	38.442	28.4
21.06.2018	11:00	0.98933	25.31	67.502	40.338	29.7
21.06.2018	12:00	0.95781	26.006	61.655	40.112	30.2
21.06.2018	13:00	0.93028	26.591	56.32	37.998	29.9
21.06.2018	14:00	0.90365	26.605	53.64	33.843	28.1
21.06.2018	15:00	0.87646	25.828	54.099	27.627	24.8
21.06.2018	16:00	0.84684	24.188	57.56	19.145	20.3
21.06.2018	17:00	0.81144	23.36	59.994	17.983	19.4
21.06.2018	18:00	0.76866	22.839	61.834	17.341	18.7
21.06.2018	19:00	0.72148	22.451	63.156	16.862	18.5
21.06.2018	20:00	0.67308	22.14	64.1	16.473	18.1
21.06.2018	21:00	0.62503	21.883	64.745	16.141	17.9
21.06.2018	22:00	0.57827	21.673	65.126	15.855	17.7
21.06.2018	23:00	0.53347	21.494	65.33	15.6	17.7
22.06.2018	00:00	0.49111	21.344	65.383	15.372	17.4
22.06.2018	01:00	0.45152	21.215	65.321	15.165	17.3
22.06.2018	02:00	0.4149	21.104	65.172	14.973	17.4
22.06.2018	03:00	0.38134	21.008	64.95	14.797	17.2
22.06.2018	04:00	0.35084	20.932	64.654	14.639	17.1
22.06.2018	05:00	0.32995	20.877	64.281	14.524	17.3

1.0 LAD scenario.

Table A6. 8. Detailed microclimatic data for 1.0 LAD scenario.

Date	Time	Wind Speed (m/s)	Air Temperature (°C)	Relative Humidity (%)	Mean Radiant Temp. (°C)	PET (°C)
		Receptor 1				
21.06.2018	06:00	1.3478	20.252	85.211	19.356	17
21.06.2018	07:00	1.3859	20.674	84.691	24.739	18.8
21.06.2018	08:00	1.4178	22.12	84.262	29.718	21.7
21.06.2018	09:00	1.4453	23.549	82.41	34.329	24.9
21.06.2018	10:00	1.4765	24.517	77.406	37.74	26.9
21.06.2018	11:00	1.5249	25.463	69.894	39.601	28.5
21.06.2018	12:00	1.5885	26.544	61.03	39.348	29.1
21.06.2018	13:00	1.6534	27.608	52.618	65.69	41.3
21.06.2018	14:00	1.7134	27.699	48.915	62.297	39.7
21.06.2018	15:00	1.7651	26.462	50.72	50.929	33.3
21.06.2018	16:00	1.8008	24.13	57.196	19.154	19.4
21.06.2018	17:00	1.8101	23.225	60.24	18.035	18.3
21.06.2018	18:00	1.7988	22.631	62.576	17.415	17.7
21.06.2018	19:00	1.7818	22.167	64.398	16.951	17.3
21.06.2018	20:00	1.7655	21.785	65.814	16.573	16.9
21.06.2018	21:00	1.7507	21.463	66.892	16.251	16.5
21.06.2018	22:00	1.7376	21.196	67.663	15.973	16.3
21.06.2018	23:00	1.7261	20.967	68.221	15.727	16
22.06.2018	00:00	1.7163	20.769	68.606	15.505	15.8
22.06.2018	01:00	1.7081	20.597	68.848	15.304	15.6
22.06.2018	02:00	1.7015	20.447	68.971	15.119	15.4
22.06.2018	03:00	1.6964	20.317	69	14.949	15.3
22.06.2018	04:00	1.6925	20.211	68.926	14.8	15.2
22.06.2018	05:00	1.6904	20.13	68.743	14.691	15
Date	Time	Wind Speed (m/s)	Air Temperature (°C)	Relative Humidity (%)	Mean Radiant Temp. (°C)	PET (°C)
		Receptor 2				
21.06.2018	06:00	0.92232	20.302	84.894	20.019	17.8
21.06.2018	07:00	0.93077	20.768	84.171	25.505	20.1
21.06.2018	08:00	0.93674	22.194	83.853	30.581	23.4
21.06.2018	09:00	0.94082	23.619	82.041	35.208	26.5
21.06.2018	10:00	0.95084	24.563	77.089	38.537	28.5
21.06.2018	11:00	0.97842	25.449	69.896	40.389	29.9

21.06.2018	12:00	1.0222	26.467	61.334	40.247	30.6
21.06.2018	13:00	1.0705	27.456	53.219	38.265	30.4
21.06.2018	14:00	1.1181	27.589	49.413	34.308	28.7
21.06.2018	15:00	1.1623	26.481	50.846	28.304	25.3
21.06.2018	16:00	1.1972	24.242	56.81	20.05	20.2
21.06.2018	17:00	1.2139	23.324	59.853	18.868	19.1
21.06.2018	18:00	1.2162	22.73	62.161	18.233	18.5
21.06.2018	19:00	1.2159	22.271	63.941	17.762	18
21.06.2018	20:00	1.218	21.895	65.307	17.381	17.6
21.06.2018	21:00	1.2231	21.58	66.333	17.058	17.3
21.06.2018	22:00	1.2309	21.321	67.052	16.778	17
21.06.2018	23:00	1.2412	21.099	67.56	16.531	16.7
22.06.2018	00:00	1.2538	20.908	67.894	16.309	16.4
22.06.2018	01:00	1.2685	20.743	68.09	16.106	16.2
22.06.2018	02:00	1.2851	20.601	68.168	15.92	16.1
22.06.2018	03:00	1.3032	20.476	68.159	15.749	15.9
22.06.2018	04:00	1.3227	20.376	68.048	15.597	15.8
22.06.2018	05:00	1.338	20.3	67.828	15.486	15.7
Date	Time	Wind Speed (m/s)	Air Temperature (°C)	Relative Humidity (%)	Mean Radiant Temp. (°C)	PET (°C)
		Receptor 3				
21.06.2018	06:00	0.66752	20.338	84.736	20.029	18.2
21.06.2018	07:00	0.66185	20.869	83.791	25.546	20.7
21.06.2018	08:00	0.65159	22.294	83.497	30.641	24.1
21.06.2018	09:00	0.63648	23.715	81.798	35.276	27.6
21.06.2018	10:00	0.6242	24.654	76.922	38.601	29.9
21.06.2018	11:00	0.62513	25.517	69.927	40.456	31.3
21.06.2018	12:00	0.63854	26.493	61.601	40.329	31.8
21.06.2018	13:00	0.65441	27.427	53.679	38.349	31.2
21.06.2018	14:00	0.66856	27.551	49.849	34.381	29.5
21.06.2018	15:00	0.67989	26.485	51.079	28.352	26.1
21.06.2018	16:00	0.6845	24.344	56.51	20.044	20.9
21.06.2018	17:00	0.67461	23.417	59.531	18.854	19.8
21.06.2018	18:00	0.65302	22.82	61.829	18.218	19.1
21.06.2018	19:00	0.62981	22.361	63.591	17.747	18.9
21.06.2018	20:00	0.60973	21.987	64.935	17.365	18.5
21.06.2018	21:00	0.59357	21.675	65.938	17.041	18.1
21.06.2018	22:00	0.58145	21.417	66.637	16.761	17.9
21.06.2018	23:00	0.57339	21.197	67.128	16.514	17.6

22.06.2018	00:00	0.56934	21.009	67.444	16.291	17.4
22.06.2018	01:00	0.56921	20.844	67.629	16.088	17.2
22.06.2018	02:00	0.57282	20.703	67.694	15.902	17
22.06.2018	03:00	0.58001	20.578	67.678	15.73	16.9
22.06.2018	04:00	0.59055	20.478	67.564	15.577	16.8
22.06.2018	05:00	0.60052	20.402	67.339	15.466	16.7
Date	Time	Wind Speed (m/s)	Air Temperature (°C)	Relative Humidity (%)	Mean Radiant Temp. (°C)	PET (°C)
		Receptor 4				
21.06.2018	06:00	0.50553	20.608	82.823	20.018	18.9
21.06.2018	07:00	0.49203	21.201	81.784	25.353	21.6
21.06.2018	08:00	0.47571	22.571	81.25	30.303	24.9
21.06.2018	09:00	0.45556	24.06	78.91	34.894	28.1
21.06.2018	10:00	0.43544	25.3	72.615	62.327	44
21.06.2018	11:00	0.42307	26.185	65.967	64.024	45.5
21.06.2018	12:00	0.41891	26.77	59.823	39.781	32.5
21.06.2018	13:00	0.41624	27.392	53.613	37.715	31.8
21.06.2018	14:00	0.41204	27.384	50.52	33.773	29.9
21.06.2018	15:00	0.40637	26.394	51.551	27.84	26.4
21.06.2018	16:00	0.39764	24.462	56.084	19.799	21.5
21.06.2018	17:00	0.38077	23.57	58.882	18.693	20.5
21.06.2018	18:00	0.35606	22.999	61.002	18.075	19.8
21.06.2018	19:00	0.32883	22.569	62.574	17.613	19.6
21.06.2018	20:00	0.30208	22.222	63.731	17.237	19.2
21.06.2018	21:00	0.27664	21.936	64.556	16.917	18.9
21.06.2018	22:00	0.25285	21.702	65.091	16.641	18.6
21.06.2018	23:00	0.23098	21.504	65.43	16.398	18.8
22.06.2018	00:00	0.21124	21.335	65.616	16.18	18.6
22.06.2018	01:00	0.19376	21.187	65.694	15.982	18.4
22.06.2018	02:00	0.17864	21.055	65.689	15.801	18.3
22.06.2018	03:00	0.16594	20.937	65.628	15.634	18.1
22.06.2018	04:00	0.15568	20.84	65.491	15.489	17.9
22.06.2018	05:00	0.14958	20.761	65.284	15.382	18.4
Date	Time	Wind Speed (m/s)	Air Temperature (°C)	Relative Humidity (%)	Mean Radiant Temp. (°C)	PET (°C)
		Receptor 5				
21.06.2018	06:00	0.71621	20.77	81.623	20.03	18.5
21.06.2018	07:00	0.68812	21.394	80.494	25.548	21.1

21.06.2018	08:00	0.65815	22.695	79.934	30.642	24.3
21.06.2018	09:00	0.62591	24.037	78.057	35.277	27.8
21.06.2018	10:00	0.59653	24.974	73.034	38.602	30.1
21.06.2018	11:00	0.57726	25.833	66.569	40.457	31.5
21.06.2018	12:00	0.56816	26.634	59.899	40.33	31.9
21.06.2018	13:00	0.56241	27.27	53.991	38.35	31.4
21.06.2018	14:00	0.55682	27.188	51.287	34.382	29.5
21.06.2018	15:00	0.54977	26.273	52.071	28.354	26.4
21.06.2018	16:00	0.53786	24.501	55.927	20.045	21.4
21.06.2018	17:00	0.51512	23.638	58.56	18.856	20.3
21.06.2018	18:00	0.48217	23.09	60.552	18.219	19.7
21.06.2018	19:00	0.44542	22.677	62.01	17.748	19.4
21.06.2018	20:00	0.4086	22.345	63.071	17.366	19.1
21.06.2018	21:00	0.37278	22.07	63.821	17.043	18.8
21.06.2018	22:00	0.33844	21.844	64.303	16.763	18.8
21.06.2018	23:00	0.30592	21.651	64.605	16.515	18.6
22.06.2018	00:00	0.27548	21.485	64.765	16.293	18.4
22.06.2018	01:00	0.2473	21.338	64.828	16.09	18.5
22.06.2018	02:00	0.22148	21.206	64.815	15.903	18.4
22.06.2018	03:00	0.19811	21.089	64.742	15.731	18.2
22.06.2018	04:00	0.17721	20.992	64.595	15.579	18.1
22.06.2018	05:00	0.16316	20.912	64.379	15.467	18
Date	Time	Wind Speed (m/s)	Air Temperature (°C)	Relative Humidity (%)	Mean Radiant Temp. (°C)	PET (°C)
		Receptor 6				
21.06.2018	06:00	0.93111	20.864	80.98	20.045	18.2
21.06.2018	07:00	0.89811	21.508	79.813	25.503	20.6
21.06.2018	08:00	0.86108	22.773	79.335	30.562	23.8
21.06.2018	09:00	0.8197	24.074	77.59	35.184	27.2
21.06.2018	10:00	0.77879	24.956	72.796	38.512	29.3
21.06.2018	11:00	0.74517	25.731	66.795	40.359	31
21.06.2018	12:00	0.72008	26.474	60.541	40.206	31.5
21.06.2018	13:00	0.69852	27.08	54.903	38.223	30.9
21.06.2018	14:00	0.67772	27.067	52.06	34.275	29.1
21.06.2018	15:00	0.65652	26.226	52.549	28.295	25.8
21.06.2018	16:00	0.63236	24.556	55.798	20.096	21.4
21.06.2018	17:00	0.60022	23.696	58.356	18.918	20.2
21.06.2018	18:00	0.55962	23.152	60.308	18.284	19.6
21.06.2018	19:00	0.51529	22.745	61.726	17.814	19.3

21.06.2018	20:00	0.47057	22.418	62.748	17.433	18.9
21.06.2018	21:00	0.42671	22.148	63.463	17.11	18.8
21.06.2018	22:00	0.38436	21.925	63.915	16.832	18.6
21.06.2018	23:00	0.34397	21.736	64.187	16.585	18.6
22.06.2018	00:00	0.30588	21.573	64.315	16.363	18.5
22.06.2018	01:00	0.27029	21.429	64.346	16.161	18.3
22.06.2018	02:00	0.23733	21.303	64.29	15.976	18.5
22.06.2018	03:00	0.20701	21.19	64.173	15.805	18.3
22.06.2018	04:00	0.17927	21.097	63.982	15.654	18.2
22.06.2018	05:00	0.16005	21.021	63.725	15.543	18
Date	Time	Wind Speed (m/s)	Air Temperature (°C)	Relative Humidity (%)	Mean Radiant Temp. (°C)	PET (°C)
		Receptor 7				
21.06.2018	06:00	1.1978	20.825	82.081	46.254	27.9
21.06.2018	07:00	1.1497	21.604	80.867	55.95	33.6
21.06.2018	08:00	1.1004	22.841	80.317	59.538	36.4
21.06.2018	09:00	1.0495	23.908	78.83	34.408	26.1
21.06.2018	10:00	1.0013	24.637	74.535	37.816	28.1
21.06.2018	11:00	0.95983	25.296	69.104	39.665	29.5
21.06.2018	12:00	0.92686	25.941	63.373	39.394	30.1
21.06.2018	13:00	0.89839	26.472	58.086	37.34	29.6
21.06.2018	14:00	0.87126	26.454	55.272	33.399	27.9
21.06.2018	15:00	0.84378	25.668	55.551	27.444	24.9
21.06.2018	16:00	0.81369	24.085	58.326	19.294	20.4
21.06.2018	17:00	0.77711	23.275	60.657	18.18	19.4
21.06.2018	18:00	0.73277	22.772	62.425	17.561	18.9
21.06.2018	19:00	0.68403	22.4	63.667	17.098	18.5
21.06.2018	20:00	0.63407	22.103	64.528	16.72	18.3
21.06.2018	21:00	0.58444	21.86	65.088	16.398	18
21.06.2018	22:00	0.53607	21.663	65.385	16.121	18
21.06.2018	23:00	0.48966	21.499	65.494	15.876	17.8
22.06.2018	00:00	0.44568	21.364	65.446	15.655	17.8
22.06.2018	01:00	0.40446	21.251	65.278	15.455	17.7
22.06.2018	02:00	0.36619	21.159	65	15.271	17.5
22.06.2018	03:00	0.3309	21.088	64.626	15.102	17.6
22.06.2018	04:00	0.29842	21.044	64.138	14.954	17.5
22.06.2018	05:00	0.2756	21.022	63.581	14.846	17.4

1.5 LAD scenario.

Table A6. 9. Detailed microclimatic data for 1.5 LAD scenario.

Date	Time	Wind Speed (m/s)	Air Temperature (°C)	Relative Humidity (%)	Mean Radiant Temp. (°C)	PET (°C)
		Receptor 1				
21.06.2018	06:00	1.3707	20.26	85.166	19.386	16.9
21.06.2018	07:00	1.4081	20.679	84.656	24.682	18.8
21.06.2018	08:00	1.4386	22.115	84.234	29.596	21.7
21.06.2018	09:00	1.4645	23.54	82.403	34.171	24.6
21.06.2018	10:00	1.4939	24.509	77.422	37.553	26.8
21.06.2018	11:00	1.5402	25.456	69.934	39.398	28.4
21.06.2018	12:00	1.6016	26.534	61.085	39.129	29
21.06.2018	13:00	1.6643	27.594	52.7	65.526	41.2
21.06.2018	14:00	1.7218	27.682	49.015	62.178	39.6
21.06.2018	15:00	1.7709	26.447	50.825	50.865	33.2
21.06.2018	16:00	1.8039	24.121	57.278	19.225	19.4
21.06.2018	17:00	1.8106	23.221	60.308	18.127	18.4
21.06.2018	18:00	1.7968	22.631	62.627	17.514	17.7
21.06.2018	19:00	1.7777	22.17	64.434	17.057	17.3
21.06.2018	20:00	1.7594	21.79	65.838	16.683	16.9
21.06.2018	21:00	1.7428	21.47	66.905	16.365	16.6
21.06.2018	22:00	1.7281	21.204	67.667	16.091	16.3
21.06.2018	23:00	1.7152	20.977	68.214	15.849	16.1
22.06.2018	00:00	1.7041	20.78	68.591	15.631	15.9
22.06.2018	01:00	1.6949	20.609	68.826	15.433	15.6
22.06.2018	02:00	1.6873	20.461	68.94	15.251	15.5
22.06.2018	03:00	1.6813	20.333	68.961	15.085	15.3
22.06.2018	04:00	1.6767	20.23	68.875	14.942	15.2
22.06.2018	05:00	1.6742	20.149	68.686	14.836	15.1
Date	Time	Wind Speed (m/s)	Air Temperature (°C)	Relative Humidity (%)	Mean Radiant Temp. (°C)	PET (°C)
		Receptor 2				
21.06.2018	06:00	0.90291	20.309	84.9	20.06	17.8
21.06.2018	07:00	0.9143	20.777	84.18	25.438	20
21.06.2018	08:00	0.92315	22.192	83.889	30.436	23.3
21.06.2018	09:00	0.93004	23.614	82.108	35.021	26.4
21.06.2018	10:00	0.94272	24.558	77.199	38.314	28.7
21.06.2018	11:00	0.97276	25.444	70.038	40.145	29.8

21.06.2018	12:00	1.0189	26.455	61.505	39.986	30.6
21.06.2018	13:00	1.0695	27.432	53.412	38.017	30.2
21.06.2018	14:00	1.1193	27.562	49.607	34.134	28.7
21.06.2018	15:00	1.1655	26.459	51.023	28.23	25.2
21.06.2018	16:00	1.2021	24.234	56.904	20.142	20.2
21.06.2018	17:00	1.2203	23.321	59.928	18.984	19.2
21.06.2018	18:00	1.2239	22.73	62.221	18.357	18.5
21.06.2018	19:00	1.2247	22.274	63.987	17.893	18.1
21.06.2018	20:00	1.2278	21.9	65.342	17.518	17.7
21.06.2018	21:00	1.2337	21.587	66.358	17.198	17.3
21.06.2018	22:00	1.2421	21.328	67.069	16.923	17
21.06.2018	23:00	1.2529	21.108	67.567	16.681	16.7
22.06.2018	00:00	1.2659	20.919	67.894	16.462	16.5
22.06.2018	01:00	1.2808	20.755	68.083	16.264	16.4
22.06.2018	02:00	1.2974	20.613	68.154	16.081	16.1
22.06.2018	03:00	1.3154	20.491	68.136	15.914	16
22.06.2018	04:00	1.3348	20.394	68.012	15.768	15.9
22.06.2018	05:00	1.3499	20.319	67.786	15.661	15.8
Date	Time	Wind Speed (m/s)	Air Temperature (°C)	Relative Humidity (%)	Mean Radiant Temp. (°C)	PET (°C)
		Receptor 3				
21.06.2018	06:00	0.61601	20.345	84.804	20.062	18.5
21.06.2018	07:00	0.61054	20.884	83.856	25.477	21.1
21.06.2018	08:00	0.60047	22.298	83.619	30.497	24.4
21.06.2018	09:00	0.58549	23.717	81.964	35.089	27.5
21.06.2018	10:00	0.5732	24.656	77.162	38.379	29.8
21.06.2018	11:00	0.57397	25.515	70.223	40.215	31.1
21.06.2018	12:00	0.58719	26.477	61.944	40.071	31.8
21.06.2018	13:00	0.60294	27.393	54.043	38.105	31.4
21.06.2018	14:00	0.61698	27.513	50.191	34.209	29.6
21.06.2018	15:00	0.62821	26.456	51.359	28.276	26.2
21.06.2018	16:00	0.63285	24.341	56.61	20.125	21.1
21.06.2018	17:00	0.62308	23.42	59.597	18.959	20
21.06.2018	18:00	0.60179	22.826	61.878	18.331	19.3
21.06.2018	19:00	0.5791	22.37	63.626	17.867	18.9
21.06.2018	20:00	0.55967	21.999	64.956	17.49	18.5
21.06.2018	21:00	0.54424	21.688	65.95	17.17	18.4
21.06.2018	22:00	0.53291	21.432	66.64	16.895	18.1
21.06.2018	23:00	0.52568	21.213	67.121	16.652	17.9

22.06.2018	00:00	0.52249	21.025	67.433	16.433	17.6
22.06.2018	01:00	0.52319	20.862	67.612	16.234	17.5
22.06.2018	02:00	0.52762	20.721	67.672	16.05	17.3
22.06.2018	03:00	0.53556	20.597	67.651	15.882	17.2
22.06.2018	04:00	0.5468	20.499	67.528	15.736	17
22.06.2018	05:00	0.55724	20.424	67.3	15.628	16.7
Date	Time	Wind Speed (m/s)	Air Temperature (°C)	Relative Humidity (%)	Mean Radiant Temp. (°C)	PET (°C)
		Receptor 4				
21.06.2018	06:00	0.44468	20.636	82.803	20.076	19.2
21.06.2018	07:00	0.43234	21.25	81.757	25.298	22.1
21.06.2018	08:00	0.41692	22.61	81.234	30.169	25.2
21.06.2018	09:00	0.39741	24.077	78.985	34.717	28.4
21.06.2018	10:00	0.3776	25.281	72.927	62.157	43.9
21.06.2018	11:00	0.36516	26.163	66.357	63.836	45.4
21.06.2018	12:00	0.36063	26.744	60.266	39.526	32.3
21.06.2018	13:00	0.35748	27.332	54.193	37.473	31.7
21.06.2018	14:00	0.35275	27.304	51.138	33.61	29.7
21.06.2018	15:00	0.34641	26.324	52.08	27.782	26.6
21.06.2018	16:00	0.33691	24.45	56.231	19.918	21.8
21.06.2018	17:00	0.31922	23.576	58.935	18.835	20.8
21.06.2018	18:00	0.29372	23.018	60.99	18.226	20.1
21.06.2018	19:00	0.26576	22.599	62.497	17.77	19.7
21.06.2018	20:00	0.23834	22.264	63.587	17.399	19.7
21.06.2018	21:00	0.21225	21.987	64.35	17.083	19.4
21.06.2018	22:00	0.18787	21.763	64.828	16.812	19.1
21.06.2018	23:00	0.16549	21.574	65.112	16.573	18.9
22.06.2018	00:00	0.14529	21.412	65.257	16.359	19.2
22.06.2018	01:00	0.12743	21.269	65.303	16.166	19
22.06.2018	02:00	0.11196	21.141	65.276	15.987	18.8
22.06.2018	03:00	0.098921	21.027	65.194	15.825	18.7
22.06.2018	04:00	0.08829	20.933	65.039	15.685	18.6
22.06.2018	05:00	0.081862	20.856	64.824	15.583	18.5
Date	Time	Wind Speed (m/s)	Air Temperature (°C)	Relative Humidity (%)	Mean Radiant Temp. (°C)	PET (°C)
		Receptor 5				
21.06.2018	06:00	0.65625	20.779	81.776	20.063	18.6
21.06.2018	07:00	0.63095	21.43	80.65	25.477	21.4

21.06.2018	08:00	0.6037	22.728	80.123	30.497	24.6
21.06.2018	09:00	0.57406	24.064	78.309	35.089	27.8
21.06.2018	10:00	0.54696	24.989	73.451	38.379	30.3
21.06.2018	11:00	0.52963	25.832	67.134	40.215	31.7
21.06.2018	12:00	0.52223	26.606	60.573	40.071	32.2
21.06.2018	13:00	0.51804	27.212	54.757	38.105	31.6
21.06.2018	14:00	0.51381	27.12	52.012	34.209	29.6
21.06.2018	15:00	0.50787	26.208	52.698	28.276	26.2
21.06.2018	16:00	0.49689	24.488	56.106	20.125	21.5
21.06.2018	17:00	0.47488	23.64	58.656	18.96	20.4
21.06.2018	18:00	0.44249	23.101	60.598	18.332	20
21.06.2018	19:00	0.40621	22.698	62.008	17.867	19.5
21.06.2018	20:00	0.36973	22.373	63.023	17.491	19.2
21.06.2018	21:00	0.33412	22.105	63.734	17.171	19.1
21.06.2018	22:00	0.29988	21.884	64.182	16.896	18.9
21.06.2018	23:00	0.26737	21.697	64.453	16.652	18.7
22.06.2018	00:00	0.23688	21.535	64.59	16.433	18.8
22.06.2018	01:00	0.20861	21.391	64.633	16.234	18.6
22.06.2018	02:00	0.1827	21.264	64.597	16.051	18.5
22.06.2018	03:00	0.15924	21.151	64.502	15.883	18.4
22.06.2018	04:00	0.13824	21.058	64.34	15.737	18.7
22.06.2018	05:00	0.12409	20.978	64.127	15.629	18.5
Date	Time	Wind Speed (m/s)	Air Temperature (°C)	Relative Humidity (%)	Mean Radiant Temp. (°C)	PET (°C)
		Receptor 6				
21.06.2018	06:00	0.8888	20.858	81.295	20.082	18.2
21.06.2018	07:00	0.85859	21.538	80.139	25.426	20.6
21.06.2018	08:00	0.82385	22.808	79.722	30.403	24
21.06.2018	09:00	0.7844	24.112	78.05	34.98	27.1
21.06.2018	10:00	0.74506	24.988	73.433	38.273	29.6
21.06.2018	11:00	0.71274	25.752	67.576	40.099	31
21.06.2018	12:00	0.68882	26.466	61.435	39.926	31.3
21.06.2018	13:00	0.66844	27.04	55.88	37.956	30.8
21.06.2018	14:00	0.6488	27.006	52.99	34.086	29.2
21.06.2018	15:00	0.62862	26.16	53.359	28.212	26
21.06.2018	16:00	0.60529	24.544	56.026	20.189	21.3
21.06.2018	17:00	0.57375	23.698	58.491	19.036	20.2
21.06.2018	18:00	0.53366	23.161	60.406	18.412	19.8
21.06.2018	19:00	0.48978	22.761	61.786	17.948	19.4

21.06.2018	20:00	0.44544	22.441	62.773	17.573	19.2
21.06.2018	21:00	0.4019	22.176	63.457	17.254	19
21.06.2018	22:00	0.35981	21.958	63.88	16.98	18.7
21.06.2018	23:00	0.31964	21.775	64.119	16.738	18.7
22.06.2018	00:00	0.28173	21.618	64.216	16.52	18.5
22.06.2018	01:00	0.24629	21.481	64.206	16.322	18.7
22.06.2018	02:00	0.21337	21.362	64.106	16.14	18.6
22.06.2018	03:00	0.1829	21.253	63.964	15.973	18.5
22.06.2018	04:00	0.15472	21.16	63.775	15.828	18.3
22.06.2018	05:00	0.13503	21.08	63.544	15.721	18.6
Date	Time	Wind Speed (m/s)	Air Temperature (°C)	Relative Humidity (%)	Mean Radiant Temp. (°C)	PET (°C)
		Receptor 7				
21.06.2018	06:00	1.185	20.808	82.533	46.282	27.9
21.06.2018	07:00	1.1387	21.63	81.341	55.904	33.6
21.06.2018	08:00	1.0901	22.879	80.863	59.439	36.4
21.06.2018	09:00	1.0393	23.949	79.452	34.238	26.1
21.06.2018	10:00	0.99064	24.676	75.338	37.616	28.1
21.06.2018	11:00	0.94858	25.322	70.067	39.448	29.6
21.06.2018	12:00	0.91508	25.937	64.469	39.157	30
21.06.2018	13:00	0.8863	26.435	59.275	37.113	29.4
21.06.2018	14:00	0.85905	26.391	56.424	33.237	27.7
21.06.2018	15:00	0.83162	25.593	56.584	27.374	24.8
21.06.2018	16:00	0.80153	24.056	58.708	19.38	20.4
21.06.2018	17:00	0.76471	23.255	60.95	18.289	19.4
21.06.2018	18:00	0.72003	22.758	62.687	17.678	19
21.06.2018	19:00	0.67091	22.392	63.897	17.221	18.5
21.06.2018	20:00	0.62052	22.102	64.724	16.849	18.3
21.06.2018	21:00	0.57042	21.864	65.25	16.531	18.1
21.06.2018	22:00	0.52157	21.673	65.511	16.258	18.1
21.06.2018	23:00	0.47464	21.517	65.575	16.017	17.8
22.06.2018	00:00	0.43014	21.389	65.476	15.8	17.9
22.06.2018	01:00	0.38841	21.287	65.235	15.603	17.7
22.06.2018	02:00	0.34958	21.211	64.859	15.422	17.8
22.06.2018	03:00	0.31351	21.158	64.371	15.257	17.8
22.06.2018	04:00	0.27959	21.13	63.789	15.115	17.6
22.06.2018	05:00	0.25483	21.111	63.213	15.011	17.6

Orientation scenarios.

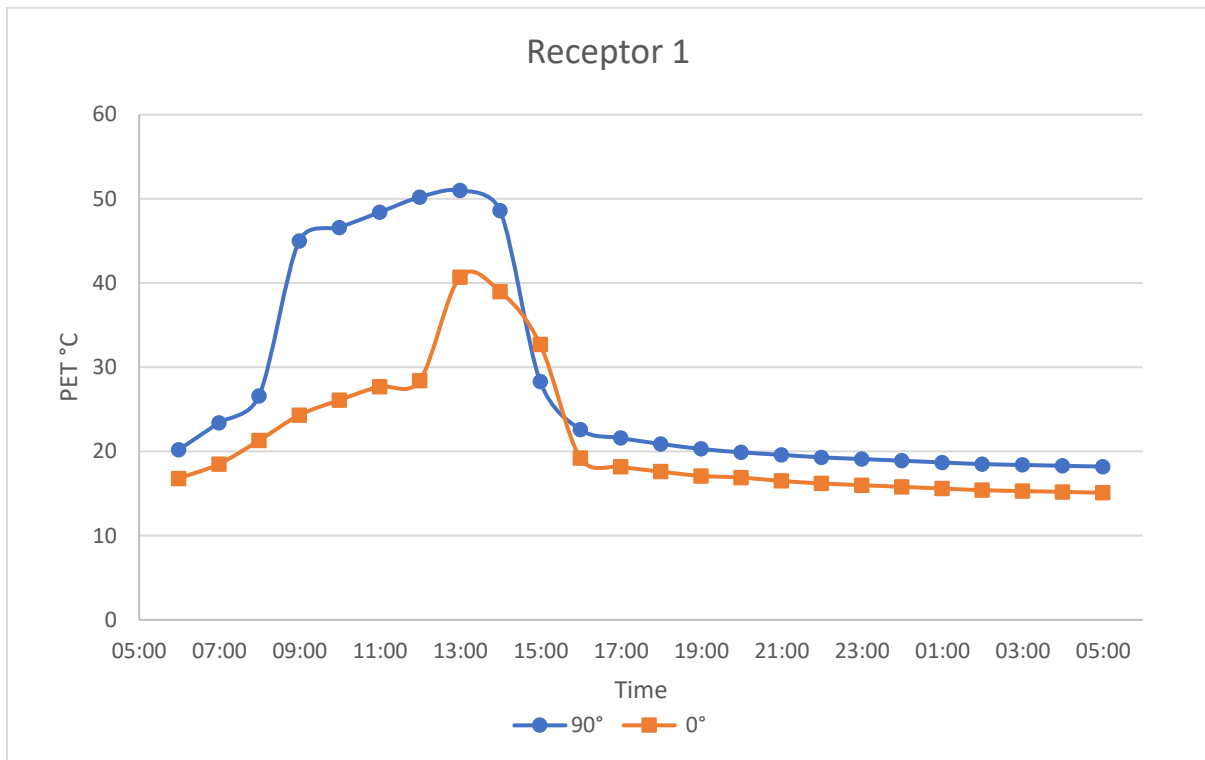


Figure A6. 26. Receptor 1 PET values comparison for 90° and 0° orientation.

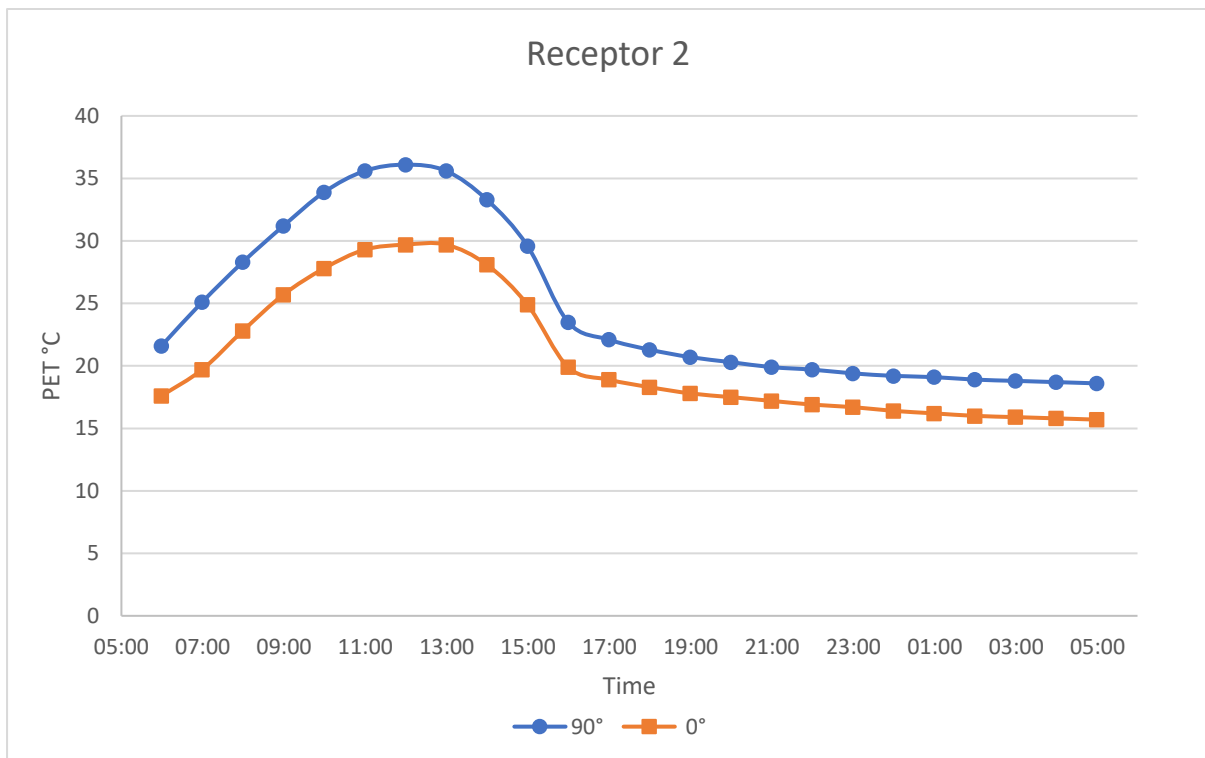


Figure A6. 27. Receptor 2 PET values comparison for 90° and 0° orientation.

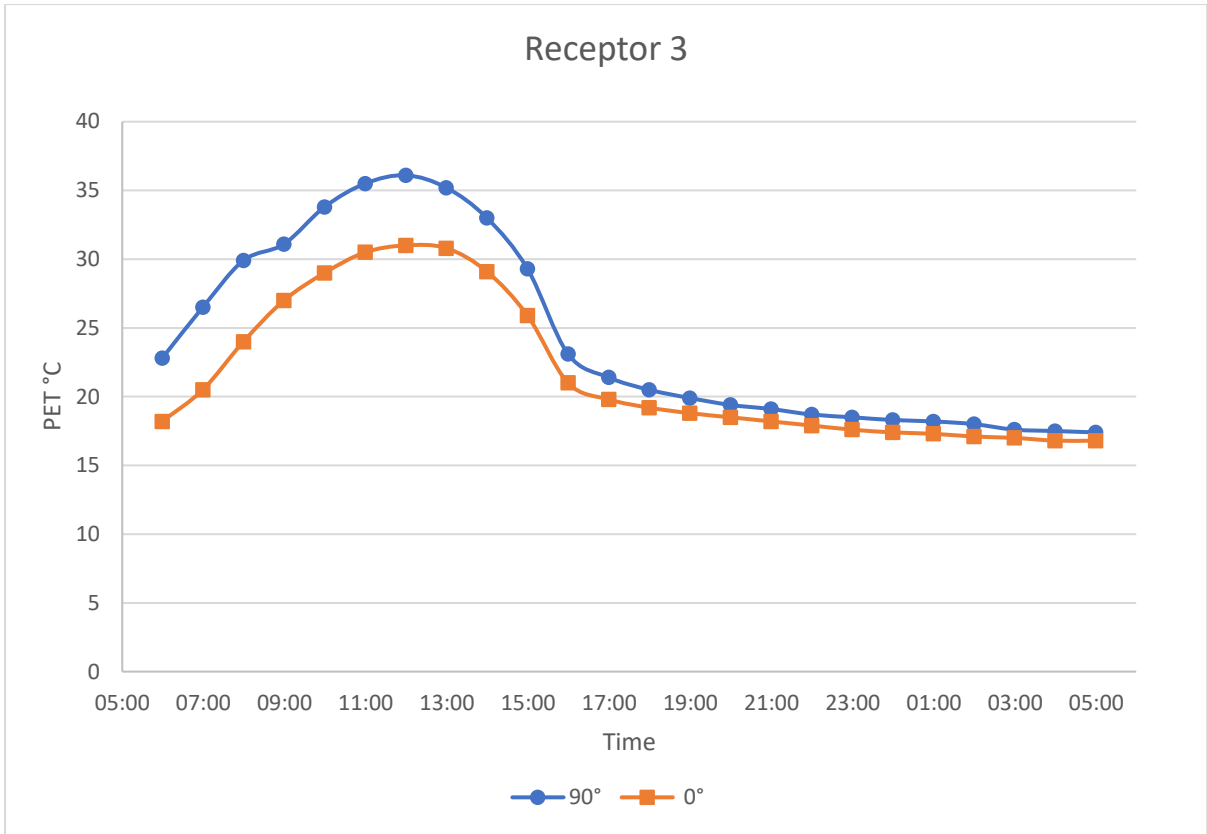


Figure A6. 28. Receptor 3 PET values comparison for 90° and 0° orientation.

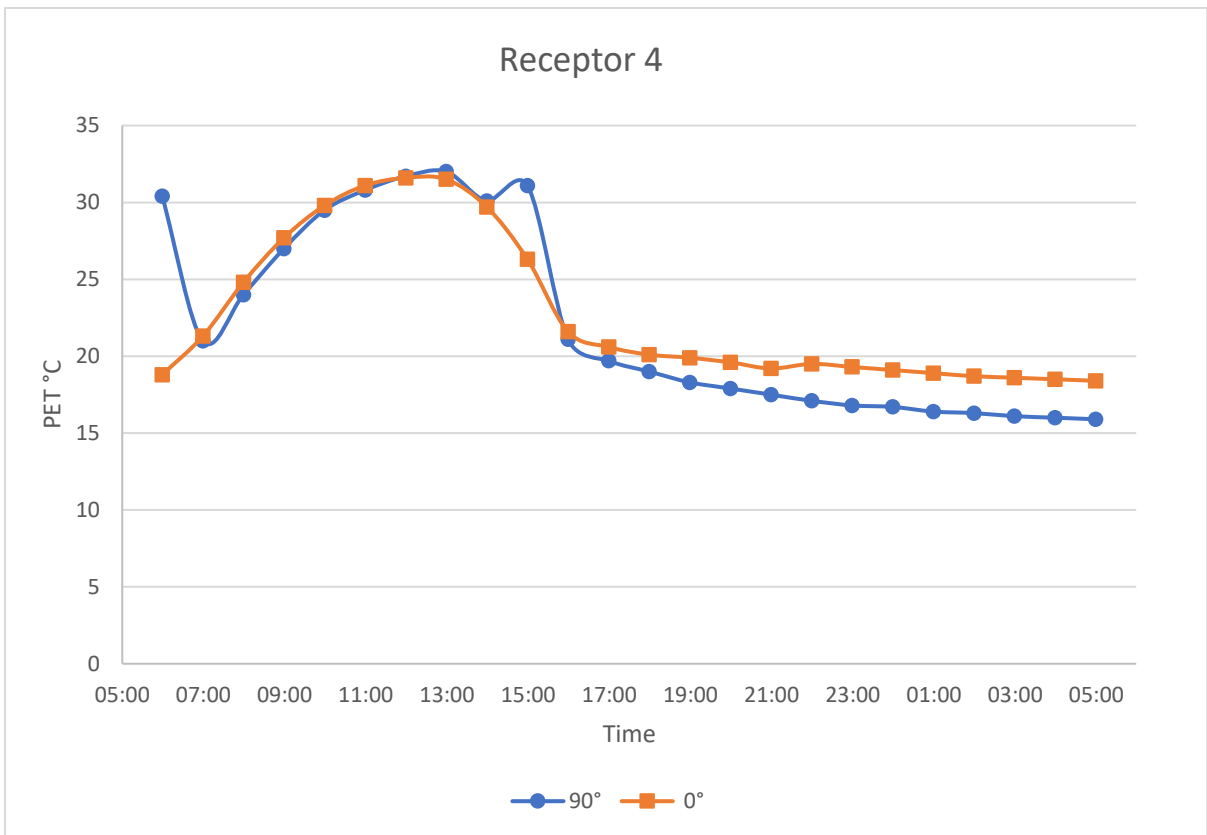


Figure A6. 29. Receptor 4 PET values comparison for 90° and 0° orientation.

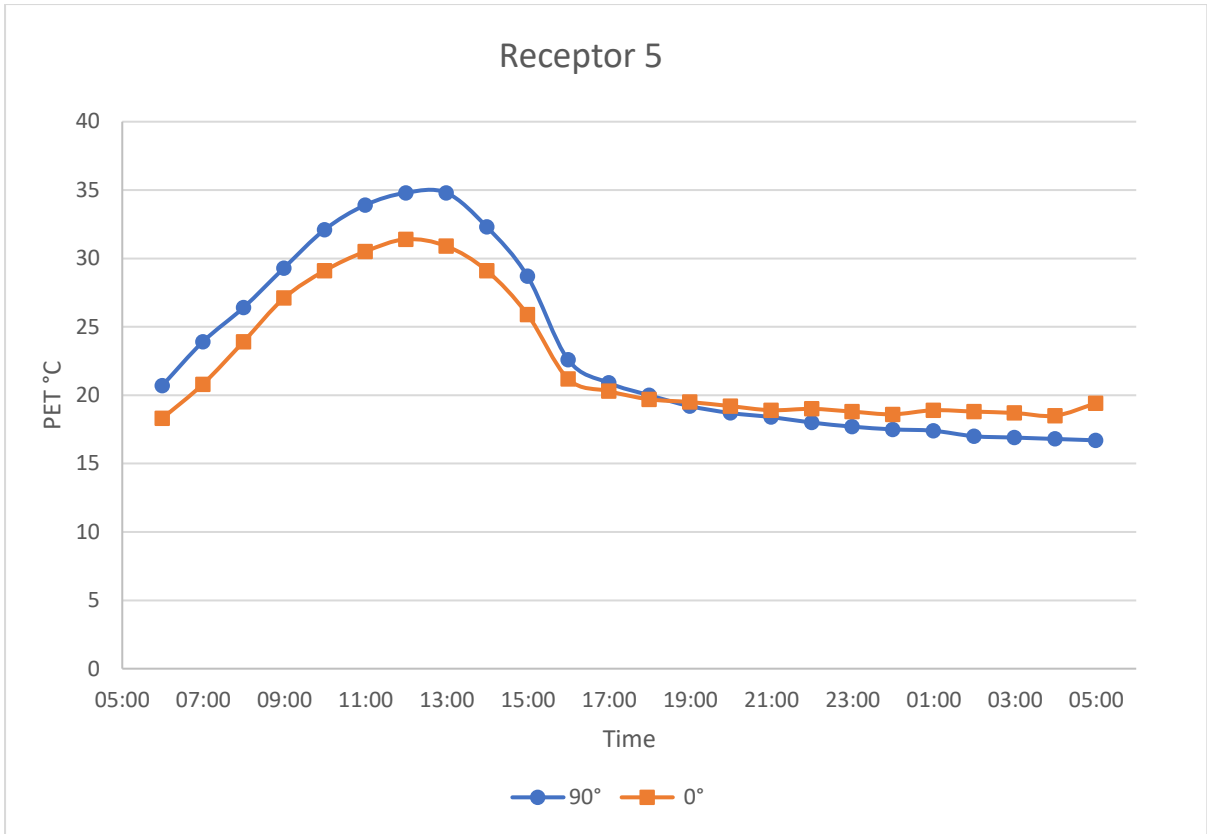


Figure A6. 30. Receptor 5 PET values comparison for 90° and 0° orientation.

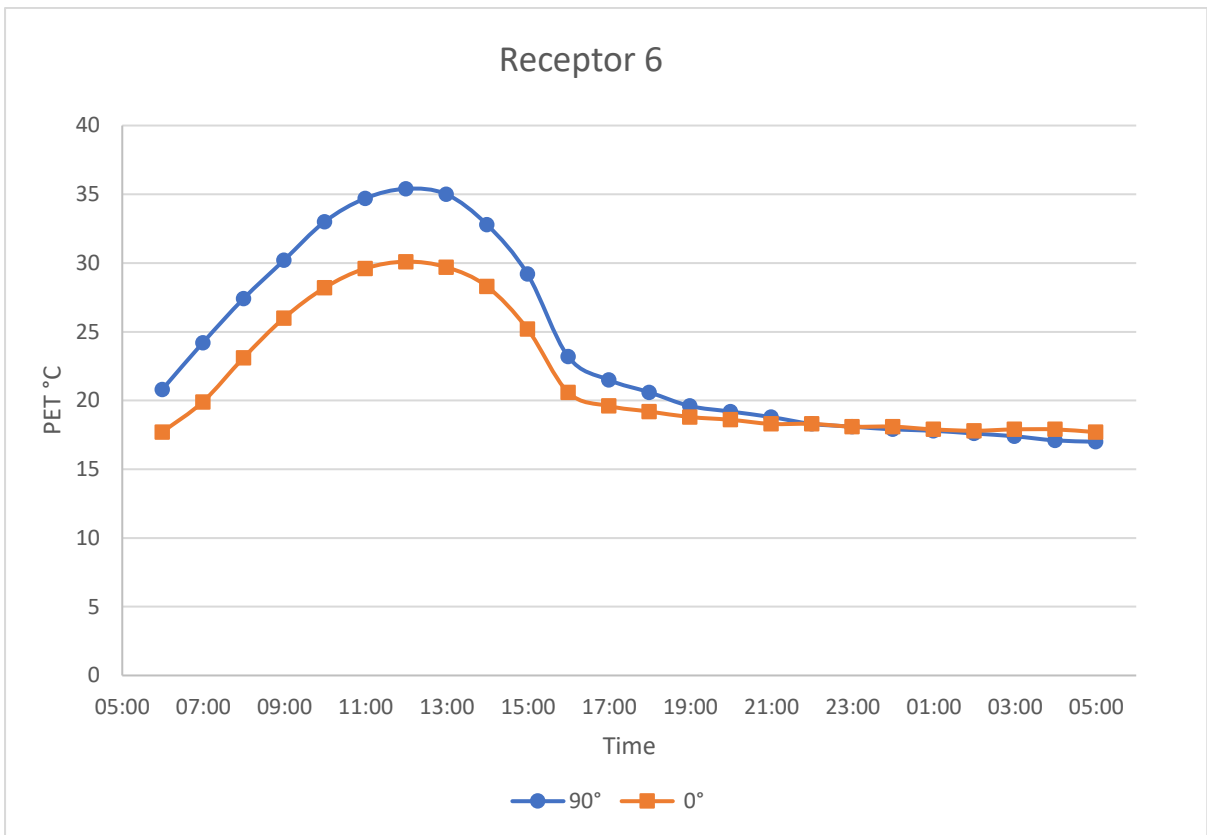


Figure A6. 31. Receptor 6 PET values comparison for 90° and 0° orientation.

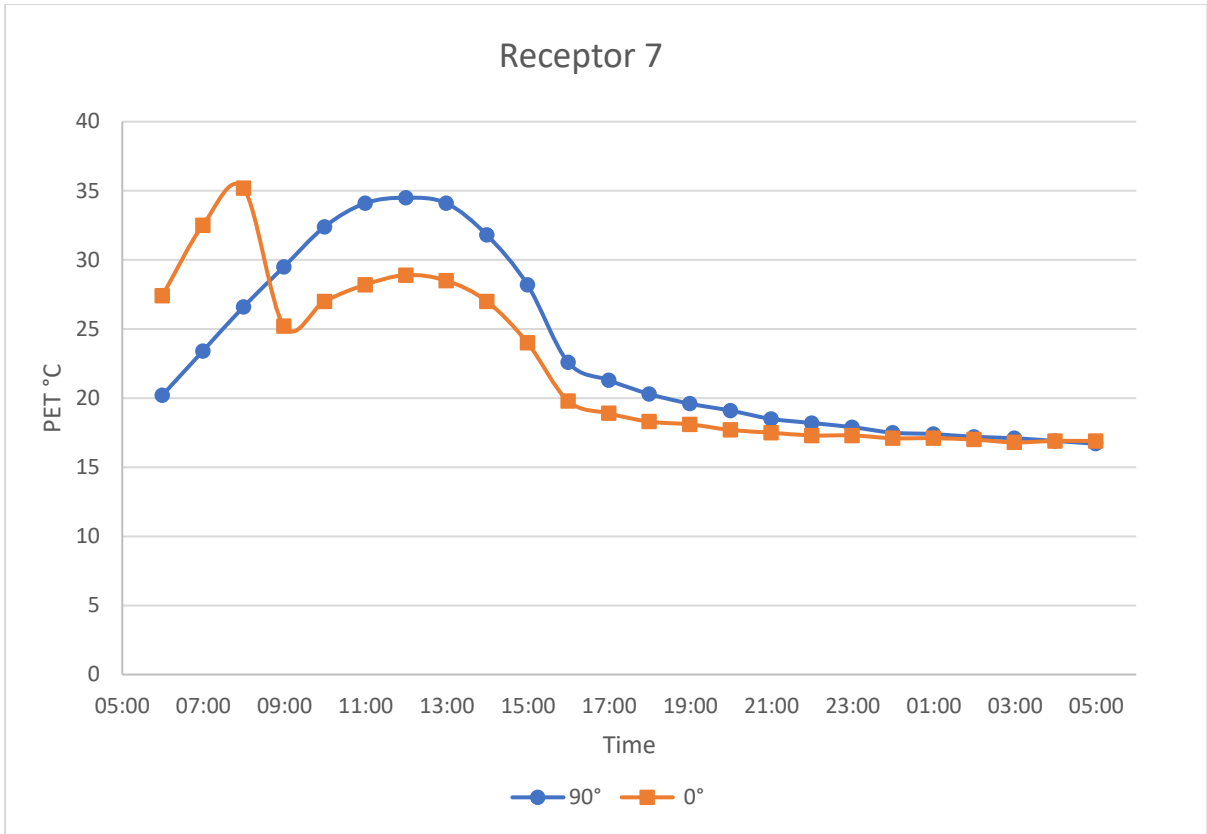


Figure A6. 32. Receptor 7 PET values comparison for 90° and 0° orientation.